ELECTROMAGNETIC INDUCTION STUDIES IN THE ITALIAN ALPS

by

SERGIO LUIZ FONTES

Thesis presented for the degree of Doctor of Philosophy
of the University of Edinburgh
1988

DECLARATION

I hereby declare that the work presented in this thesis is my own unless otherwise stated in this text, and that the thesis has been composed by myself.

Aos meus pais,
Vera e Vinicius

ABSTRACT

The Alps orogeny constitutes a challenge for a great number of geoscientists due to the intricate processes involved in the collision of the African and European plates. The research presented in this thesis is concerned with electromagnetic induction studies carried out in the Italian sector of the Alps. Audiomagnetotelluric (AMT) and magnetotelluric (MT) soundings were undertaken at a total of 14 sites; the spectral range covered was 600Hz- 100s at most sites, with longer period measurements (greater than about 3000s) made at 3 of them. The soundings were concentrated mainly in two geologically distinct regions within the Alpine orogenic belt. Cultural noise was found to pose a major obstacle to the effectiveness of the MT method in this mountainous environment. The Italian DC railway network was found to be a particularly hazardous source of electromagnetic noise in this respect. In the highly resistive environment prevailing in mountainous areas, the effect of the DC railway is enhanced due to the reduced dissipation of electromagnetic energy, relative to more conducting regions, during the diffusion process. This noise source was observed to extend beyond the Alps and it appears to affect to varying degrees most of Italy.

Various noise- reduction techniques were devised and their performance for both synthetic and noise- degraded field data are assessed and discussed in this thesis. Additionally, attempts to use the DC railway electromagnetic signal emulating a controlled source experiment have yielded reasonable geoelectrical models. The validity of these models is discussed in the light of the non-uniqueness of the inversion, aggravated in this case by the great 'lack of control' of the model parameters.

One- dimensional (1D) modelling using both the less noisy and the 'cleaned' data sets was performed by various schemes: simple approximative transformations, linearized and nonlinearized inversion, and the Monte Carlo-Hedgehog inversion. Results are compiled and discussed. Two- dimensional (2D) inversion based on the finite difference technique and a linearized inversion scheme was also performed. The 2D geoelectrical model incorporates a simplified Alpine topography and accounts for the major geological features observed in the region. Features undetected by the 1D models are revealed in the 2D model. Various aspects related to the geoelectrical structure in the region are discussed. These include the mechanisms generating an observed upper crustal conductivity anomaly and an

anomalously resistive structure at typical asthenospheric depths; their possible association either with the formation of the Alps or with remnant noise effects is critically assessed. In short, the favoured explanation for the observed low resistivity layer at depths between 1.5 and 9Km is in terms of the presence of water in pores, cracks and voids. The very tentative interpretation of the anomalously high resistivity at asthenospheric depths is associated with lateral effects of the Alpine collisional zone.

ACKNOWLEDGMENTS

I wish to deeply thank my supervisor Dr. Rosemary Hutton for having proposed the MT project. Her continuous support, encouragement and hospitality throughout my stay in Edinburgh will not be forgotten.

The friendly atmosphere and facilities provided by the Department of Geophysics were greatly appreciated. My gratitude to the members of this Department is embraced in my thanks to its Head, Professor K. Creer.

I also wish to thank all the people who participated in the fieldwork campaigns in Italy. The guidance and technical assistance provided by G. Dawes and M. Valiant in the first fieldwork campaign were invaluable. M. Meju's help during the 1986 campaign was also very much appreciated. In Italy, E. Finzi and A. Zaja helped with most of the necessary fieldwork arrangements; their hospitality during and after the campaigns is something to be remembered.

I benefited from discussions with Drs. P. Schnegg and G. Fischer, Neuchatel- Switzerland. I am indebted to Dr. P. Weidelt (Hannover-W.Germany) for the computer routine for dipole source modelling he kindly made available to me. I also acknowledge useful discussions with the various research students involved in electromagnetic induction studies, in particular T. Harinarayana and M. Meju; their friendship was very valuable to me. My warmest thanks to Ana Frankenberg for proof-reading the typescript of this dissertation.

I gratefully acknowledge the various Institutions which have funded this project. A scholarship from CNPq of Brasil provided for my maintenance and University fees. The Royal Astronomical Society (U.K.) and the Istituto di Fisica Terrestre- Universita di Padova (Italy) jointly provided for the resources for the fieldwork campaigns. The latter also made available the facilities for the 2D inversion studies presented in this dissertation. Part of the instruments used in the fieldwork campaigns were obtained through a loan from the NERC Geomagnetic Equipment Pool.

Back home, a number of persons deserve my very sincere gratitude. Dr. A.C.B. Pires, former Head of the Department of Geophysics at Observatorio Nacional (ON), for his important role in my decision to undertake this Ph.D. My brother Luiz Carlos for having diligently dealt with my personal affairs in Brasil while I was engaged in this study. My Departmental secretary, Graca Vargas- a 'Preta', for her prompt action on all matters concerning my leave from ON; her letters were always very amusing.

The good friends that I met here and my scottish- born son, Vinicius, will make my days in charming (and cold) Edinburgh forever remembered. Last but not least, I convey my deepest thanks to Vera for her love, patience and understanding; these were vital for the completion of this work.

CONTENTS

Chapter	page
1. INTRODUCTION	
1.1 General overview	1
1.2 Geology and tectonics of the Alps	4
1.3 Objectives of this study- the EM induction project	9
2. ELECTROMAGNETIC INDUCTION THEORY	
2.1 Inducing fields	11
2.1.1 MT and GDS sources	11
2.1.2 Controlled sources	12
2.2 Electromagnetic theory and Maxwell's equations	14
2.3 MT equations	16
2.3.1 Diffusion of MT fields	16
2.3.2 Induction in one- dimensional structures	17
2.3.3 Induction in two- dimensional structures	20
2.3.4 Induction in tri- dimensional structures	21
2.4 Controlled source equations	22
2.4.1 Field of an oscillating dipole- general equations	22
2.4.2 Horizontal electric dipole	24
3. DATA ACQUISITION	
3.1 Introduction	26
3.2 Instrumentation	26
3.2.1 AMT instrumentation	26
3.2.2 MT instrumentation	35
3.3 Fieldwork procedures	37
3.3.1 SPAM measurements	39
3.3.2 Band 4 measurements	41
3.3.3 Band 5 measurements	44
3.4 Fieldwork campaigns	44
4. DATA PROCESSING AND ANALYSIS	
4.1 Introduction	49
4.2 Transfer function estimations	51
4.2.1 Single input/single output system- The Cagniard response function	51
4.2.2 Two input/single output system- The tensorial impedance	54

4.3 Telluric transfer functions- Some properties and useful relations 60
4.3.1 Rotation of the impedance tensor 60
4.3.2 Polarization analysis 62
4.3.3 Dimensionality indicators 64
4.4 Magnetic transfer functions- Usual presentation 67
4.5 Mainframe processing of MT data 67
4.5.1 The window analysis program 69
4.5.2 The window averaging program 72
4.5.3 Plotting programs 74
5. NOISE IN MT MEASUREMENTS
5.1 Introduction 75
5.2 Noise souces in MT 78
5.2.1 50Hz (60Hz) form mains and related sources 78
5.2.2 Electrified fences, pipeline anticorrosion systems 79
5.2.3 DC operated railways 79
5.2.4 Wind, microseismic activity, lightning and topography 83
5.3 Regular and irregular coherent noise 85
5.3.1 Regular coherent noise 85
5.3.2 Irregular coherent noise 95
5.4 Robust estimation of impedance elements and other processing/rejection criteria 99
5.4.1 Robust estimation 103
5.4.2 Other processing/rejection criteria 106
5.5 Italian DC railways and MT measurements 108
5.5.1 The evidence 108
5.5.2 Modelling near- source fields 121
5.6 Discussion 124
6. RESULTS
6.1 Introduction 127
6.2 Asiago area 127
6.2.1 MT results 127
6.2.2 Dimensionality study 152
6.3 Cavalese area 159
6.4- Po Valley region 184

7. 1D AND 2D MODELLING STUDIES

7.1 Introduction 190

7.2 General overview 190

7.3 1D studies 195

7.3.1 Heuristic transformations 195

7.3.2 Linearized inversion- The weighted 2nd order Marquadt scheme 196 200

7.3.3 Smooth models- The Occam's inversion 203

7.3.4 Monte Carlo inversion 203

7.4 1D models for Asiago 205

7.5 2D studies 231

7.5.1 The 2D inversion algorithm 231

7.5.2 Topographic effect in the Italian Alps 232

7.5.3 2D results- Asiago area 233

7.6 Near- source modelling for the Cavalese and Po Valley soundings 258

8. INTERPRETATION AND CONCLUSIONS

8.1 Comparison of 1D and 2D model results- Asiago area 275

8.2 Interpretation of the Asiago 2D geolelectrical model 276

8.2.1 The uppermost layer- surface distortions or truly geological features 276

8.2.2 The crustal conductivity anomaly 279

8.2.3 The geoelectric structure at greater depths 283

8.3 Summary and recommendations 284

REFERENCES 286

Appendix A- Summary of the sensitivity analysis of the model parameters (2nd order Marquadt scheme) for the Asiago sites 305

Appendix B- 1D models (Monte Carlo- Hedgehog and 2nd order Marquadt schemes) for E pol and H pol polarizations- Asiago sites 327

Appendix C- Occam models (rotationally invariant, E pol and H pol responses for the Asiago sites. 343

Appendix D- Geological map of Northern Italy back cover

LIST OF FIGURES

Fig.	page
1.1 Two-dimensional evolutionary scheme of the Alps orogeny.	5
1.2 Simplified tectonic map of the Eastern Alps.	8
3.1 Simplified diagram of the short period automatic magnetotelluric system (SPAM MKII).	27
3.2 Preamplifier frequency response curves (2 SPAM versions).	29
3.3 Filter responses of 4 bands for EUIG-SPAM and NERC-SPAM.	31
3.4 Simplified flow chart of the in- field processing program.	33
3.5 Frequency response curves for the magnetic induction coils.	34
3.6 Simplified diagram of Band 4 system and preamplifier response.	36
3.7 Simplified diagram of Band 5 system.	38
3.8 FFT amplitude plots (for the 5 filters in analogue box) for all bands of NERC-SPAM.	40
3.9 Example of MT in-field results using NERC- SPAM system.	42
3.10 1D infield modelling. Bostick and Schmucker transformations for the rotationally invariant MT curves	43
3.11 Location map of all MT sites in Northern Italy.	45
3.12 Comparison of EUIG-SPAM and Neuchatel systems at LAV, Cavalese area.	47
4.1 Types of linear systems used in EM studies.	50
4.2 Main processing routines.	68
4.3 Simplified flowchart of the window analysis program.	70
4.4 Simplified flowchart of the window averaging program.	73
5.1 Examples of coherent noise (regular and irregular) observed in N. Italy- Asiago and Cavalese areas.	80
5.2 Schematic diagram of a DC railway circuit.	82
5.3 MT curves for P. di Lavaze (LAV) for distinct meteorological conditions.	86
5.4 Delay- line and notch response functions	88
5.5 Sinusoidal signals and FFT spectra used in the synthetic study.	90
5.6 Comparison of digital filtering for 50Hz noise by notch and delay-line.	92
5.7 Field example of regular coherent noise on MT data recorded at AVE, Asiago area.	93
5.8 Predicted coherence values before and after application of delay line filtering (same site of Fig. 5.7)	94

5.9 Application of MEM extension and window deconvolution techniques (examples for the synthetic study). 100
5.10 Field results recorded in MAN- Asiago, before and after the application of the MEM extension and window deconvolution techniques. 101
5.11 Field results recorded in LAV- Cavalese, before and after the application of the MEM extension technique. 102
5.12 Comparison of standard processing and robust estimation for site LAV, Cavalese area. 105
5.13 Autospectra of magnetic and electric signals and Cagniard resistivity curves automatically selected by EUIG-SPAM, band 3, site LAV. 107
5.14 Comparison of standard processing and coherence weighting processing for site LAV, Cavalese area. 109
5.15 Comparison of standard processing and processing rejecting highly coherent magnetic signals for site LAV, Cavalese area. 110
5.16 Comparison of standard processing and processing rejecting highly coherent frequency sets 111
5.17 Map of Northern Italy showing the Italian DC railway network and location of MT stations. 113
5.18 MT response curves (major and minor), azimuths and number of estimates for site LAV, Cavalese area. 114
5.19 MT response curves (major and minor), azimuths and number of estimates for site MAS, Cavalese area. 115
5.20 MT response curves (major and minor), azimuths and number of estimates for site MAN, Po Valley region. 116
5.21 Unfiltered time series recorded in LAV by the Neuchatel group. 117
5.22 Filtered time series (band 3) recorded in LAV, EUIG-SPAM equipment. 118
5.23 Ala substation experiment. 120
5.24 Horizontal electric dipole source over a homogeneous halfspace. 122
5.25 Horizontal electric dipole source over a two- layered Earth for various distances transmitter receiver (DS). 123
6.1 Asiago area map (site locations and main tectonic features). 128
6.2 MT response curves for all the sites in the Asiago area. 130
6.3 Asiago results (continuation). 139
6.4 Magnetic results for sites LAV and DAI, Cavalese area. 149
6.5 Synthetic 2D model. 153
6.6 MT responses for the 6 sites for the synthetic 2D model. 154

6.7 Dimensional weights D1 and D2 for the 6 sites for the synthetic 2D model 158
6.8 Cavalese area map. Sites are shown by bold circles. 160
6.9 MT response curves for all the sites in Cavalese area. 161
6.10 Cavalese results (continuation). 167
6.11 Polarization results for all the sites in the Cavalese area. 174
6.12 Polarization results for sites in the Asiago area. 180
6.13 MT results for site I. Mantegna in the Po Valley region. 185
7.1 Example of the influence of the starting model on the final solution of the 1D inversion using the weighted 2nd order Marquadt scheme. 206
7.2 Example of the influence of the starting model on the final solution of the 1D inversion using the Monte Carlo- Hedgehog scheme. 207
7.3 1D model results (rotationally invariant responses) for all the sites in the Asiago area. 208
7.4 Example of the influence of the starting model on the final solution of the 1D inversion using the Occam scheme. 222
7.5 Example of the influence of the Lagrange multiplier (μ) in the final solution of the 1D inversion using the Occam scheme. 223
7.6 Composite 2D section for the rotationally invariant responses- Asiago area using the 2nd order Marquadt scheme. 225
7.7 Composite 2D section for the E pol response curves- Asiago area using the 2nd order Marquadt scheme. 226
7.8 Composite 2D section for the H pol response curves- Asiago area using the 2nd order Marquadt scheme. 227
7.9 Composite 2D section for the rotationally invariant response curves (Asiago area) considering all described inversion schemes. 228
7.10 Composite 2D section for the E pol response curves (Asiago area) considering all described inversion schemes. 229
7.11 Composite 2D section for the H pol response curves (Asiago area) considering all described inversion schemes. 230
7.12 Resistivity map of Nothern Italy, including simplified topography. 234
7.13 Resistivity map of Northern Italy, neglecting any topographic feature. 235
7.14 E and H pol theoretical responses (amplitude and phase) for 4 sites in the Asiago area, when the simplified topography is included. 236
7.15 E and H pol theoretical responses (amplitude and phase) for 4 sites, when the topography is neglected. 237

7.16 Ratio of the responses topography model/flat model for sites 1 and 2 (E and H pol cases). 238
7.17 Ratio of the responses topography model/flat model for sites 3 and 4 (E and H pol cases). 239
7.18 Resistivity map of Asiago area used as starting model for the 2D inversion. 241
7.19 Observed and computes 2D responses- Asiago area. Both polarizations undertaken simultaneously. 243
7.20 2D model results for the Asiago area. Both polarizations simultaneously inverted. 248
7.21 Observed and computed responses for all sites in the Asiago area. Inversion for both polarizations undertaken independently. 249
7.22 2D model results for the Asiago area. E pol inversion results only. 254
7.23 2D model results for the Asiago area. H pol inversion results only. 255
7.24 Near- source modelling for the major response curve- site VAR using the Monte Carlo- Hedgehog scheme. 260
7.25 Near- source modelling using the Occam scheme for all the sites in Cavalese. 261
7.26 Influence of the low resistivity layer on the fitting- site MAS. 266
7.27 Examples of alternative models (horizontal electric dipole source) for two sites in the Cavalese area. 269
7.28 Near- source modelling (horizontal electric dipole source) for the major response curves Po Valley site. 272
8.1 Gravimetric- seismic model of a profile crossing the region surveyed in this study. 278
8.2 Generalized 2D cross- section of the Alpine orogeny. 280
8.3 Resistivity models of the crust and upper mantle as determined by a number of EM induction studies. 281

LIST OF TABLES

Tab	page
2.1 Classification of continuous (Pc) and irregular (Pi) geomagnetic pulsations according to their periods.	13
3.1 AMT bands for EUIG-SPAM and NERC-SPAM.	30
3.2 MT sites location.	46
7.1(a)-(b) Summary of the relevant parameters for two sites in the Asiago area using the weighted 2nd order Marquadt scheme (rotationally invariant response curves).	218
7.2 Summary of results 2D inversion for simultaneous inversion of both polarizations.	242
7.3 Summary of results of 2D inversion for the E pol direction.	256
7.4 Summary of results of 2D invwrsion for the H pol direction.	257

CHAPTER 1

INTRODUCTION

1.1 General overview

Electromagnetic (EM) induction studies provide the means by which the electrical conductivity distribution of the Earth's subsurface can be determined from measurements of natural transient electric and magnetic fields on the Earth's surface. The natural magnetic variations, which exist over a very wide spectrum of frequencies, diffuse into the Earth and induce electric currents- the telluric currents- which in turn result in secondary magnetic fields. These inductive processes are governed by two laws of classical electromagnetism- the Henry- Faraday and Biot- Savart laws. Such laws were assembled by J. C. Maxwell by the middle of last century and constitute part of the well known set of Maxwell's equation. The diffusion experienced by the magnetic and electric fields into the Earth is determined by the movement of electrons or ions in response to these fields. Depending on the mobility of these electrons or ions, which is a function of the medium, the following four types of conduction (listed in decreasing order of conductivity) can take place:

-free electrons- metals (e.g. Fe, Cu, etc)

-bound electrons- semiconductors (e.g. sulphide, graphite, etc)

-free ions- electrolytic solutions (brine)

-bound ions- ionic solids (e.g. silicates, carbonates)

EM induction studies using natural signals are performed mainly by two techniques- the geomagnetic deep sounding (GDS) and the magnetotelluric (MT) techniques. In the GDS method, the three components of the transient magnetic fields are measured and the information is used to trace anomalous structures by mapping current concentrations. The GDS method can provide reliable information about lateral variations in the conductivity structure, especially if array studies are considered. In the MT method, which was proposed independently by Tikhonov (1950) and Cagniard (1953), the time variations of orthogonal components of the magnetic and electric fields are measured simultaneously. The resulting MT response curve (usually apparent resistivity and phase values expressed as a function of the frequency) is modelled and the subsurface conductivity can thus be estimated. The MT

method can be regarded as an important mapping tool as a result of its recognized resolution and sophisticated inversion algorithms, especially when compared to other current available EM techniques for probing lower crust depths. Jones (1987) has shown a number of examples in which the MT results have played an essential role in the interpretation of areas for which seismic reflection information was equally available. Nevertheless, the MT technique can be seriously corrupted by the presence of noise, man-made or otherwise, which manifests itself by distorting the MT sounding curves. Another problem is the non-uniqueness of interpretation posed by both the finiteness of the data set and the noise content. However, non- uniqueness is a problem all other geophysical techniques face to varying degree. Fortunately, although it is a fact that all geophysical techniques have their own idiosyncratic limitations, geophysicists seem to be increasingly aware that an eclectic and intelligent use of a number of techniques as the most adequate approach for a better understanding of the Earth. As an example of this, one can take the ongoing European Geotraverse Project, which is referred to in more detail later in this introduction.

The depth of penetration of the EM induction techniques is governed by the skin depth phenomenon of electromagnetic fields.Maximumpenetration depth values for MT can reach 600-700Km, with GDS extending up to 2000Km. Therefore, these natural EM induction methods can reach greater depths than both their artificial source counterpart (at most 5Km in continental areas) and the galvanic (DC resistivity) method- about 2Km.

EM induction studies using natural signals have been carried out extensively in all sorts of geological/tectonic environments in several parts of the world. Reported applications include the study of sedimentary basins (e.g. Vozoff, 1972) ; continental and oceanic crustal/ lithospheric structures (e.g. Hutton et al., 1981, 1984; Jodicke et al., 1983; Cox, 1980; Chave and Cox, 1983, etc); mineral exploration (e.g. Strangway et al., 1973); geothermal regions (Hermance and Grillot, 1974; Devlin, 1984); etc. Reviews of such case studies can be found in previous University of Edinburgh theses (e.g. Jones, 1977; Devlin, 1984) and in a number of published papers (e.g. Hermance, 1983; Hjelt, 1986). In these published studies the MT interpretation is predominantly based on either one-dimensional (1D) inversion or two-dimensional (2D) forward modelling. Studies using two- dimensional or tri-dimensional

inversion algorithms have been very hampered to date by prohibitive computer costs.

Induction studies using artificial sources (active MT) are also becoming increasingly popular, largely due to both the high level of cultural noise observed in some parts of the world and to the intermittent nature of the natural source fields. Several applications have been reported (e.g. Goldstein and Strangway, 1975; Szarka, 1983; Schnegg and Fischer, 1984; etc) and a review considering applications to deep exploration has been given by Ward (1983). Only 1D modelling or inversion has so far been attempted in such studies. The non- uniqueness problems associated with the artificial source approach seem to be more dramatic than those faced by the natural source technique (e.g. Cox et al., 1986).

The importance of determining the conductivity structure of a particular region is very much enhanced by the fact that conductivity values are related to a number of other physical and structural parameters, namely temperature, porosity, pressure, crack content, etc (e.g. Keller and Frischknecht, 1970). Conductivity is particularly sensitive to temperature and both variables generally increase as a function of depth. Nevertheless, anomalously conductive zones observed at lower crustal/upper mantle depths seem to be a common feature in most continental regions studied (e.g. Shankland and Ander, 1983; Haak and Hutton, 1986; Adam, 1987). Such conductivity anomalies (CA) can be due to several factors; usually, they depend on the tectonical background of the region. For tectonically stable regions, the most accepted explanation for the CA is the presence of interconnected free water (0.1 % by volume or less) in active circulation and continous recharge of fluids from the upper mantle (Etheridge et al., 1983; Haak and Hutton, 1986). In tectonically active regions, it is often claimed that partial melting is a reason for CA (e.g. Shankland et al., 1981; Schwarz et al., 1984), but for partial melting to occur in 'wet' rock, temperatures greater than about 600^0C are required (Lambert and Wyllie, 1970). Besides, as suggested above, the presence of fluids in pores and cracks too may account for most observed conductive zones on active regions. Other causes and/or reported explanations include the presence of hydrated minerals (though rejected summarily by Olhoeft, 1981), carbon, CO_2, serpentinized rocks, etc.

The main subject of this thesis is the determination of the conductivity structure of the Italian Alps by use of the MT method. A number of problems related to cultural noise in this mountainous and highly resistive environment were encountered. Although such problems caused some diversion from the initial objectives of this study, they have not completely precluded the success of the MT method in revealing interesting structural aspects of the tectonic processes which have occurred in the region.

A summary of the geology and tectonics of the Alpine region, with special emphasis on the particular sector of the Alps where the MT soundings were carried out, is presented in this introduction. Section 1.3 outlines both the initial and redirected objectives of this study, and indicates how the research is to be presented in the following Chapters.

1.2 Geology and tectonics of the Alps

The Alps mountains constitute possibly one of the most geologically studied regions in the world. It is noteworthy that the ideas of continental drift proposed by A. Wegener in 1912 (cited by Dietrich ,1983) originated from geotectonic disputes about the Alps. Despite the prolific work in the region, the complex tectonic processes taking place in the Alpine belt have not as yet been fully explained. On the contrary, new questions seem to arise everyday and many conflicting results still have to be unravelled. The most recent major attempt to do so has been the conduct of the European Geotraverse (EGT). This is an international multidisciplinary project focusing on a 4000Km long north-south oriented lithospheric profile. It extends from northermost Scandinavia to North Africa and includes an Alpine segment. The data collection phase of the EGT project was scheduled for the period 1983-1987, but some very interesting preliminary results have already become available and are thus opportunely referenced throughout this Chapter.

The Alpine belt began to form in the early Jurassic with the brake-up of the supercontinent Pangaea and the movement of major plates, the climax of the deformation being reached in the Tertiary. In plate tectonic terms, The Alps consist of a continent-continent collision belt formed by the interaction of the African and Arabian plates with the Eurasian plate. The evolution of the Alpine belt is complicated because it has always consisted of a complex

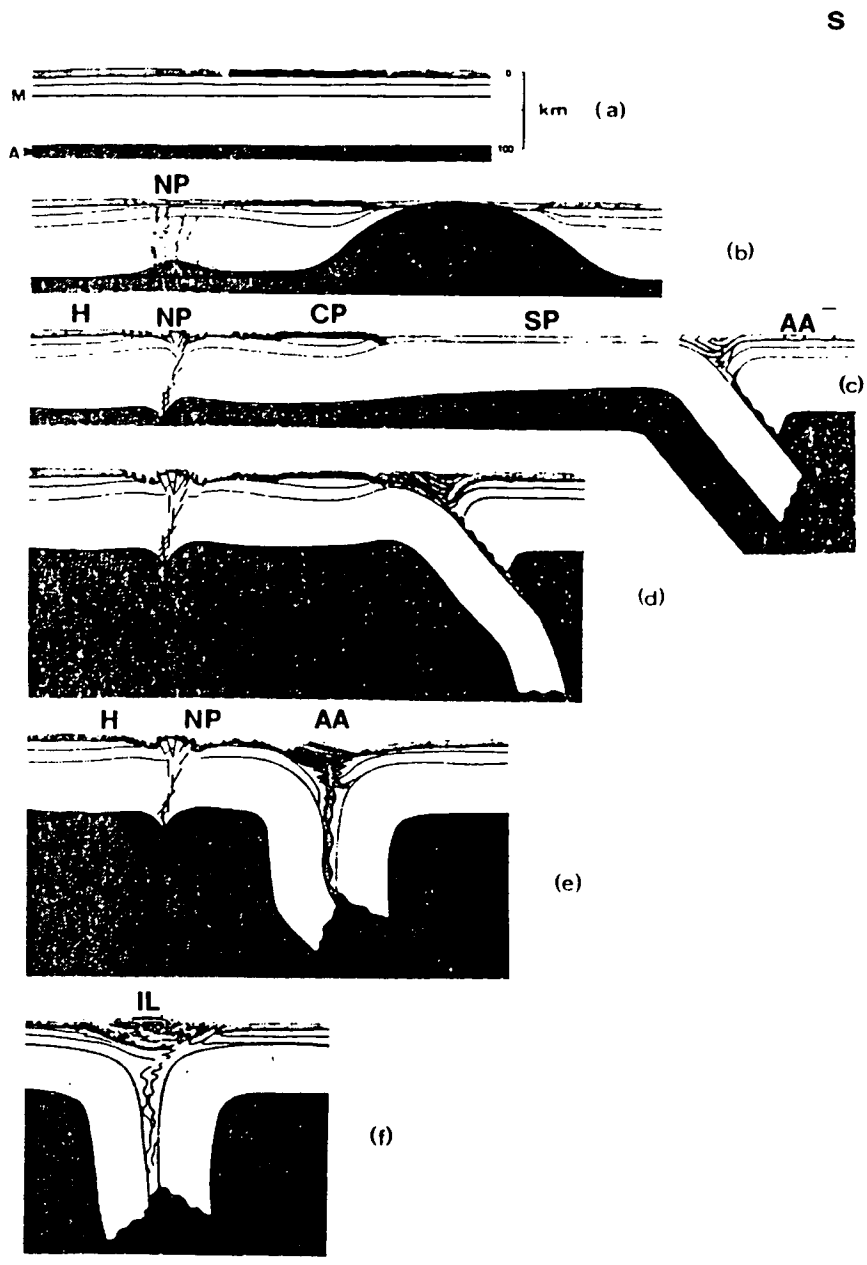

Fig. 1.1 Two-dimensional evolutionary scheme of the Alpine orogeny (after Laubscher, 1974a,b).
(a)- Initial crust-mantle system, 230my ago; (b)- Middle Jurassic ≈ 170my ago; (c)- Middle to upper Cretaceous, ≈90my ago; (d)- Lower to middle Eocene, ≈ 50 my ago; (e)- Upper Eocene, ≈ 44my ago; (f)- Pliocene, ≈ 5my ago.
NP- North Penninic domain, H- Helvetic domain, CP- Central Penninic, SP- South Penninic, AA- Austroalpine domain, IL- Insubric line. See text for further details.

system of microplates in continuous movement over a period of about 200 my. In addition, according to Laubscher (1985), the Alpine kinematics are completely inexplicable in two-dimensional sections; they represent a truly four-dimensional problem which depicts earlier stages of a 3D kinematical development preserved in certain regions.

Notwithstanding, some enlightenment of the complex Alpine belt can be achieved by a simplified 2D evolutionary scheme accounting for the major tectonic stages. Such a scheme, given by Laubscher (1974a,b), is presented in the form of cross-sections in Fig. 1.1(a)-(f). The scheme, comprising 6 stages, starts initially with a typical crust- mantle system at the end of Paleozoic (230my ago - Fig. 1.1(a)) and ends at Pliocene times (5my ago- Fig. 1.1(f)). The middle Jurassic period (170my ago-Fig. 1.1(b)) is characterized by an extensive spreading phase in which the Penninic Ocean was formed in association with minor rifting and graben formation occurring in the North Penninic realm (NP).

Fig. 1.1(c) portrays the mid-Cretaceous period (90my ago), after the maximum extension of the South Penninic Ocean had been reached. This stage is characterized by a southward directed subduction which has caused compression of the entire stack of layers forming the lithosphere. Sequences of basic/ultrabasic lavas (ophiolites) are obducted onto the Austroalpine continental margin (AA) in the south. Detachment phenomena in the southern crust are also suggested. They may have been considerably stronger than shown in Fig. 1.1(c) and may already have resulted in the formation of continental basement nappes (Laubscher, 1974b, Laubscher and Bernoulli, 1982). A secondary zone of compression is observed in the North Penninic domain, but no prominent contribution to crustal shortening has occurred because large positive and negative crustal displacements took place simultaneously.

The compressional shortening continues up to the Lower to Middle Eocene (50my ago- Fig. 1.1(d)), the South Penninic Ocean being completely consumed in the subduction process. The continuing compression has now led to a continent- continent collision which results in the formation of a steeply northward dipping subduction zone in addition to the one previously formed in the Cretaceous. Further shortening of the crustal stack can now only be accommodated by double subduction of the two zones penetrating

deeply into the asthenosphere. The Central Penninic (CP) zone has become covered with peels from the South Penninic (ophiolite) and Austroalpine (continental) domains as shown for the Upper Eocene (44my ago- Fig. 1.1(e)).

In the last stage of the Alpine orogeny, the North Penninic domain has been engulfed in the main subduction zone, and its shallow layers have been peeled off and shoved into each other to become part of the Alpine nappe system and the crustal root of the Alps. The deep structure of the Alps was more or less completed in Miocene/Pliocene times. Fig. 1.1(f) illustrates the Pliocene period. The Insubric line (IL) as seen today is a right lateral strike-slip fault which is thought to have accommodated lateral displacements between the Africa and Europa plates since the Middle Cretaceous times (Laubscher, 1983). In summary, as accepted currently by most Alpine specialists, the large-scale plate tectonic mechanism (i.e. the push of the African plate against an stationary European plate) is the fundamental driving force ultimately responsible for the formation of the Alps. In this frame, the still ongoing uplift of the Alpine mountain chain is a secondary effect due to isostatic adjustment of the intensely deformed upper lithosphere which was condiderably thickened by the plate collision process.

To complete the scenery, a simplified tectonic map of the Eastern Alps is shown in Fig. 1.2 (Dietrich, 1976). It depicts most units previously referred to and the area originally proposed for EM studies (assigned by a thick line in the Fig.) is a 200Km long North- South profile between Vicenza (in the Po Valley) and Insbruck (in the Central-Eastern Alps). This particular profile was chosen for the analysis since seismic refraction studies (Italian Explosion Seismology Group 1978, 1981) had already been undertaken along it and suggested the possibility of a doubling of the crust in the middle of the profile. More recent seismic results from the EGT (Giese, 1985, Galson and St Mueller, 1986) have indicated the presence of two 'crust- mantle' like boundaries beneath the same profile, extending beneath the Po Basin and possibly both other parts of the Southern and Western Alps and the Northern Apennines. This striking result- still subject to further scrutiny- may be associated with the large scale crustal overthrusting which is known to characterize Alpine collisional tectonics further to the north in the Central and Eastern Alps (Galson and St Mueller, 1986).

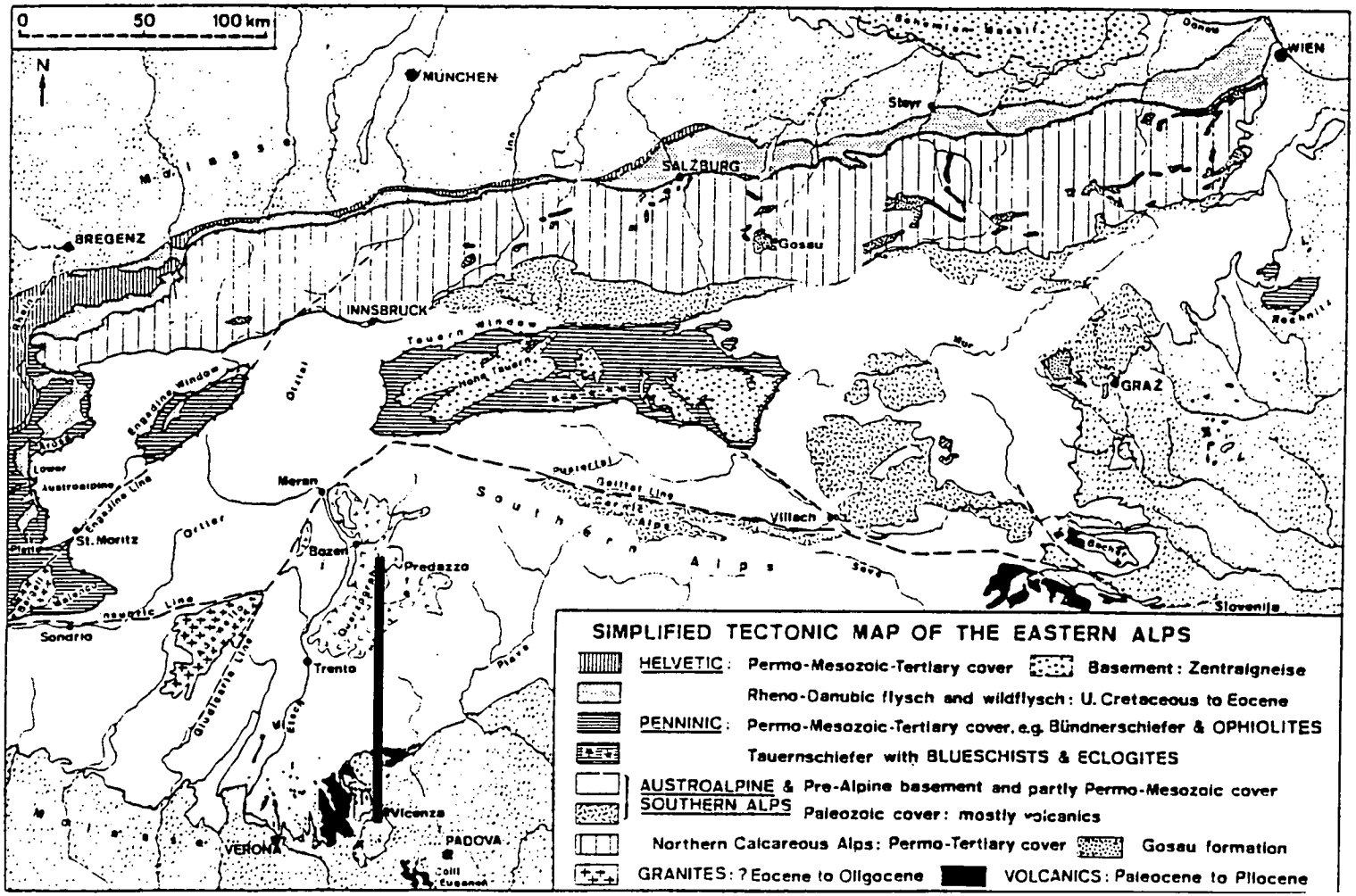

Fig. 1.2 Simplified tectonic map of the Eastern Alps (after Dietrich, 1976). Region covered by EM studies is assigned by a thick line.

1.3 Objectives of this study – the EM induction project

As already mentioned in the previous section, the EM induction project initially planned consisted of observations along a North- South traverse extending from Vicenza, through the Southern Alps, to Bolzano. The first field work campaign was designed to be a preliminary survey, from which the general pattern of the conductivity structure in the region could be gained and later used to define a more detailed survey. For this purpose, two geologically distinct areas of the profile (Cavalese and Asiago in the Trentino region) were chosen as locations in which the first set of measurements were concentrated. The Cavalese area is about 50km south of the Insubric Line and is situated in an area of active isostatic readjustment processes and crustal thickening (Progetto Finalizzato Geodinamica, 1982). It was therefore expected to depict the conductive features associated with the thickened crust. The Asiago area situated about 40Km south of Cavalese, in the main prealpine sector, was primarily expected to be of typical continental crust thickness, i.e. about 35 Km.

When magnetotelluric measurements had been carried out in these areas, it immediately became apparent that much of the data was seriously affected by noise; the sounding curves exhibiting unrealistic slopes and the apparent resistivity values were unusually high. The noise was observed to be highly coherent and thus was not eliminated by application of standard MT processing techniques (e.g. Hermance, 1973). The data corruption appeared to be more severe in the Cavalese than the Asiago area. Accordingly, much of this study was devoted to examination of the noise problem encountered at the first fieldwork sites. In the subsequent field campaigns less conventional experiments and trials were devised with the objective of revealing the nature of the noise source as well as using this very source as a possible exploratory tool. Indeed, the Italian DC railway network was eventually found to be the main source of noise in the area surveyed.

In the next 7 chapters of this dissertation most aspects generally relating to EM induction investigations and the results of the MT study in N. Italy will be reported. Chapter 2 contains the theoretical basis of EM induction methods (ultimately based on manipulations of Maxwell's equations) along with a summary of the characteristics of the natural source fields. Artificial

source methods, and more specifically, a horizontal magnetic dipole source placed in a homogeneous layered Earth are also considered. The latter was used in modelling the MT data which were severely affected by a near source- the Italian DC railway system.

In Chapter 3 the set of instruments and the fieldwork procedures used in this study are described. Details of each of the campaigns are also presented. In Chapter 4, details of the processing of the Italian data are presented and discussed under the light of some theoretical aspects of the transfer fuction estimation. Chapter 5 is devoted to the noise problem. Various sources of noise more commonly affecting MT data are cursorily described. Several noise- reduction techniques based on digital filtering are developed and applied to synthetic and field data. Evidence supporting the conclusion that the Italian DC railway system is the main noise source is provided and analysed in some detail. The processed field results are presented in Chapter 6, where an evaluation of the data quantity, quality and dimensionality is also given. The theoretical background of 1D and 2D inversion techniques and modelling of the Asiago data by various 1D schemes and 2D inversion (incorporating a simplified Alpine topography) are presented in Chapter 7. Near source modelling of the Cavalese data is also attempted in this Chapter. The interpretation of the results, the main conclusions extracted from this study and a number of suggestions for future work are presented in Chapter 8.

CHAPTER 2

ELECTROMAGNETIC INDUCTION THEORY

2.1. Inducing Fields

Electromagnetic induction studies use either natural fluctuations of the Earth's magnetic field or artificially generated electromagnetic signals to probe the Earth's geoelectric structure. The former is the main source for the magnetotelluric (MT) and geomagnetic deep sounding (GDS) techniques while the latter is used in controlled source experiments.

2.1.1 MT and GDS sources

Geomagnetic field variations in the frequency range most commonly used in MT and GDS studies (10^{3}Hz - 10^{-4}Hz) have varied origins. Despite the existence of some superposition in the frequency range of different source fields, the frequency of 1Hz is generally taken to divide the observed geomagnetic spectrum according to the nature of the source.

At frequencies below 1Hz, the natural electromagnetic fluctuations originate from the interaction between the solar wind and the Earths's main magnetic field, and its surrounding plasma coupling system. In the magnetosphere and ionosphere, these interactions basically generate current systems which are then observed as geomagnetic field fluctuations at the Earth's surface. Among these variations, magnetic storm/substorm phenomena and geomagnetic pulsations are of particular importance. Magnetic storms may last for a few days and occur once or twice a month. Despite their great variability, they seem to possess some typical features such as sudden commencement (SC), which is followed by an initial phase and a main phase. Irregularly occurring fluctuations of varied periodicities (hundreds of seconds to a few hours) are superimposed on all components. Magnetic substorms occur with greater regularity and do not exhibit all the phases normally observed in a magnetic storm. The strongest of such disturbances are confined to latitudes near the auroral zone.

Geomagnetic pulsations may exhibit a fairly regular quasi- sinusoidal character (continuous pulsation or Pc) or appear as trains of damped oscillations (irregular pulsation or Pi). Their amplitudes can range from 100nT in the auroral zones for very low frequency events to 10pT for the highest

frequencies near the geomagnetic equator (Orr, 1973). Several reviews describing the various aspects related to geomagnetic pulsations can be found in the literature, e.g., Saito (1969), Jacobs (1970) and Orr (1973). A comprehensive summary of geomagnetic fluctuations and other geomagnetic disturbances is given by Parkinson (1983- chap4). The revised classification of Pc's and Pi's (IAGA, 1973 p.12) is summarized in Tab. (2.1), where the most likely time of appearance is also given.

For frequencies above 1Hz, the main source originates from worldwide thunderstorm systems. The signals that originate from a lightning discharge are known as 'sferics'. Thunderstorms have their storm centres in Brazil, central Africa and Malaysia, and generate sferics which propagate around the planet; the ionosphere and the Earth's surface act as a wave- guide to them. The sferics source contains a very wide spectrum of frequencies, with some preferred frequencies exhibiting spectral peaks, i.e., the Schumann resonances at 8, 14, 20 and 25Hz. When the storm activity occurs far away from the MT measuring sites, the plane wave assumption (discussed later in this Chapter) holds.

Other secondary sources of signals of frequency above 1Hz originate from man- made activity. These arise mainly from electric power transmission lines and radio transmitters. Although they contribute to the background spectrum, the extent to which they may be regarded as hazardous to MT and GDS studies depends on their amplitude levels and their proximity to the observational site.

2.1.2 Controlled Sources

Utilizing a transmitter overcomes the problem of variability and unpredictability of natural signals used in both MT or GDS investigations. Such controlled source methods generally employ artificially generated dipole sources (electric or magnetic). However, the source geometry has to be taken into account whenever the transmitter- receiver distance is less than 3-5 skin depths (defined in section 2.3.2); its precise value is a function of both the dipole configuration and the receiver's azimuthal location. (Sandberg and Hohmann, 1982).

Type	Period (s)	Normal : time of appearance
Pc1	0.2-5	M D
Pc2	5-10	M
Pc3	10-45	M D
Pc4	45-150	M D
Pc5	150-600	M D E
Pc6	> 600	N
Pi1	1-40	N,M,D
Pi2	40-150	N,D
Pi3	>150	N,D

Tab. 2.1-Classification of continuous (Pc) and irregular (Pi) geomagnetic pulsations according to their periods.
M- morning, D- day, E- evening, N- night.
The comma denotes different subtypes of Pi. (From Rokityansky, 1982)

2.2 Electromagnetic Theory and Maxwell's Equations

In general terms electromagnetic theory is concerned with Maxwell's equations and their representation of the behaviour of electromagnetic fields. Maxwell assembled four equations which were established from the experiments of Coulomb, Ampere and Faraday in differential form. They are:

$$\nabla \times \mathbf{E} = -\partial \mathbf{B}/\partial t \qquad \text{(a)}$$

$$\nabla \times \mathbf{H} = \mathbf{J} + \partial \mathbf{D}/\partial t \qquad \text{(b)}$$

$$\nabla \cdot \mathbf{B} = 0 \qquad \text{(c)}$$

$$\nabla \cdot \mathbf{D} = \rho' \qquad \text{(d)} \qquad (2.1)$$

These four equations plus the equation of continuity, i.e.

$$\nabla \cdot \mathbf{J} + \partial \rho'/\partial t = 0 \qquad (2.2)$$

form a general set of interdependent equations governing all classical electrodynamic problems observed in nature. They may be simplified in the case of certain properties of the medium and/or of the boundary conditions of specific problems. The quantities expressed in Eqs. (2.1) and (2.2) in SI units are:

[B] - magnetic induction in tesla (T)

[H] - magnetic field intensity in ampere/metre (A/m)

[E] - electric field intensity in volts/metre (V/m)

[D] - electric induction in coulomb/square metre (C/m^2)

[J] - current density in ampere/square metre (A/m^2)

[ρ'] - charge density in coulomb/cubic metre (C/m^3)

The complementary constitutive equations are

$$\mathbf{D} = \varepsilon \mathbf{E} \qquad \text{(a)}$$

$$\mathbf{B} = \mu \mathbf{H} \qquad \text{(b)}$$

$$\mathbf{J} = \sigma \mathbf{E} \qquad \text{(c)} \qquad (2.3)$$

The constitutive quantities in (2.3) expressed in SI are:

[ε] - electric permittivity in farad /metre (F/m)

free space permittivity $\varepsilon_0 = 8.854 \times 10^{-12}$ F/m

[μ] - magnetic permeability in henry/metre (H/m)

free space permeability $\mu_0 = 4\pi \times 10^{-7}$ H/m

[σ] - conductivity of the medium in siemens/metre (S/m)

For complex media, e.g. anisotropic, the constitutive parameters are better expressed by tensors, and time dependence may be observed. However, for induction studies in the Earth, the following set of conditions is generally assumed to be valid.

i) The Earth is a continuous isotropic medium, ε and μ are time independent constants, with no magnetic materials present such that $\mu = \mu_0$,

ii) **E** and **B** vary harmonically with time, the explicit dependence being generally expressed as $\exp(i\omega t)$,

iii) The displacement current $\partial \mathbf{D}/\partial t$ is negligible, i.e. only conduction currents **J** are considered.

Condition (iii) may easily be shown to hold. This displacement current term was introduced by Maxwell to account for observed discrepancies in Faraday's law for high frequency phenomena. Considering (ii) and (2.3-c), the ratio between $\partial \mathbf{D}/\partial t$ and **J** is written as

$$(\partial \mathbf{D}/\partial t)/\mathbf{J} = (\omega \varepsilon E e^{i\omega t})/(\sigma E e^{i\omega t}) = \omega \varepsilon/\sigma$$

where ω is the angular frequency $\omega = 2\pi/T$. For values of resistivity $\rho = 1/\sigma < 10^5 \Omega$m and periods $T > 10^{-3}$s, it follows that

$$\omega \varepsilon << \sigma$$

Therefore, the induction processes in the Earth are adequately described by quasi- stationary fields and (2.1- b) is now

$$\nabla \times \mathbf{H} = \mathbf{J} \qquad (2.4)$$

2.3 MT equations

2.3.1 Diffusion of MT fields

Taking the curl of (2.1-a) and using (2.1-b)

$$\nabla x \nabla x E = \nabla x(\partial B/\partial t) = -\mu_0 \sigma \partial E/\partial t \qquad (2.5)$$

Applying the vector identity

$$\nabla x \nabla x E = \nabla(\nabla.E) - \nabla^2 E$$

to Eq. (2.5) will result in

$$\nabla(\nabla.E) - \nabla^2 E = -\mu_0 \sigma \partial E/\partial t \qquad (2.6)$$

However, charge does not accumulate in a conducting medium. In fact, it experiences an exponential decay given by $\exp(-\sigma t/\varepsilon)$. Consequently, ρ' vanishes very quickly for earth materials since $\sigma/\varepsilon >> 1$. Thus, (2.1-d) can be rewritten as

$$\nabla.D = 0$$

so that (2.6) reduces to the diffusion equation

$$\nabla^2 E = \mu_0 \sigma \partial E/\partial t \qquad (2.7)$$

By performing analogous operations, the magnetic field may also be shown to obey the diffusion equation

$$\nabla^2 B = \mu_0 \sigma \partial B/\partial t \qquad (2.8)$$

Therefore, the MT fields are quasi- static fields which diffuse throughout the Earth rather like a thermal diffusion process. Induction in 1- dimensional and 2- dimensional structures are considered next.

2.3.2 Induction in one- dimensional structures

A 1-dimensional or layered structure is one for which the conductivity σ varies with depth only, i.e., $\sigma=\sigma(z)$. The geomagnetic reference coordinate system in common use has the z direction pointing downwards, x is directed towards North and y towards East. In such a frame, consider a horizontal current sheet in the x direction far above the Earth's surface. This current sheet is assumed to generate a uniform incoming field (E_x, H_y) and hence it characterizes a plane wave which reaches a horizontal boundary between the air and a 1D Earth. The flat Earth approximation is valid for periods less than about a day (Srivastava, 1966). This problem requires the solution of the diffusion Eq. (2.7) in the Earth and Laplace's equation ($\nabla^2 E=0$) in the air. Since there are neither charge accumulations nor free poles allowed at the interfaces of two media, the horizontal fields involved (E_x, H_y) are subject to the well- known boundary conditions:

E_x is continuous across the interfaces,

H_y is continuous across the interfaces.

Three algorithms are known to exist for solving the induction problem in an n- layered Earth. They were given by Lipskaya (1955) (see Berdichevsky and Zhdanov, 1984 pp52-54), Wait (1954), and Keller and Frischknecht (1966). The last approach is considered here.

Assuming conditions (i)-(iii) are valid, the diffusion equation for the problem can be expressed as:

$$\partial^2 E_x/\partial z^2 = i\omega\mu_0\sigma E_x \qquad (2.9)$$

The general solution of (2.9) is

$$E_x(z) = Ae^{kz} + Be^{-kz} \qquad (2.10)$$

where

$$k = (i\omega\mu_0\sigma)^{1/2} = (1 + i).(\omega\mu_0\sigma/2) \qquad (2.11)$$

is the wavenumber. The solution (2.10) represents a combination of two plane waves diffusing upwards with amplitude Ae^{kz} and downwards with amplitude Be^{-kz}. If one takes the harmonic time dependence into account, (2.10) now

becomes

$$E_x(z) = (Ae^{kz} + Be^{-kz})\, e^{i\omega t} \tag{2.12}$$

Maxwell's Eq. (2.1a) for the problem is therefore rewritten as

$$\partial E_x/\partial z = -i\omega\mu_0 H_y$$

If the expression for electric field intensity found in (2.12) is used, the above equation becomes:

$$H_y(z) = (k/i\omega\mu_0)(Ae^{kz} - Be^{-kz})\, e^{i\omega t} \tag{2.13}$$

The ratio between the electric and magnetic field intensities can be defined as the wave impedance, or simply the impedance of the medium. For plane wave diffusion, this ratio depends only on the electrical properties of the medium at a particular frequency. The impedance has units of ohms (Ω) andfor the purpose of this problem it can be written as

$$Z(z,\omega) = E_x/H_y = \frac{i\omega\mu_0\,(Ae^{kz} + Be^{-kz}) + k\,(Ae^{kz} - Be^{-kz})}{k\,(Ae^{kz} - Be^{-kz})} \tag{2.14}$$

After some algebraic manipulation to eliminate the constants A and B and to introduce the hyperbolic function coth, the forward problem of calculating the impedance Z(0,ω) at the Earth's surface of an n- layered structure is accomplished by the recursive relation

$$Z(0,\omega) = (i\omega\mu_0/k_1)\coth\{k_1h_1 + \coth^{-1}[(k_1/k_2)\coth(k_2h_2 + \coth^{-1}(k_2/k_3 \ldots + \coth^{-1}((k_{n-2}/k_{n-1})\coth(k_{n-1}h_{n-1} + \coth^{-1}(k_{n-1}/k_n)))))]\} \tag{2.15}$$

where h_n are the layer interface depths.

A common way of expressing the Earth electric response functions is by means of both apparent resistivity (ρ) and phase (ϕ) as

$$\rho_{ij} = (\omega\mu_0)^{-1} \mid Z_{ij} \mid^2 \tag{2.16}$$

$$\phi_{ij} = \text{Arg}\ (Z_{ij}) \tag{2.17}$$

with i,j = x,y. If $Z_{ij} = E_i/H_j$ is given in MT practical units (E_x in mV/km and H_y in nT), the following well known expression is found

$$\rho_{ij} = 0.2\ T \mid Z_{ij} \mid^2 \tag{2.18}$$

where $T = 2\pi/\omega$ represents the period in seconds.

If the simplest 1D structure- the homogeneous Earth (or half- space model) is now considered, then E_x and E_y must vanish at $z \rightarrow \infty$. This condition leads to A being zero in (2.12), (2.13) and (2.14). Eq. (2.12) is now reduced to

$$E_x(z) = Be^{-kz}$$

or

$$E_x(z) = Be^{-z/\delta}e^{-i(z/\delta-\omega t)} \tag{2.19}$$

The electric field decays exponentially with depth in the Earth and the 'skin depth' $\delta = (2/\omega\mu_0\sigma)^{1/2}$ is defined as the depth at which the field amplitude is attenuated to 1/e of its surface value.

Eq. (2.14) (or 2.15) for the homogeneous medium is thus reduced to

$$Z(0,w) = i\omega\mu_0/k \tag{2.20}$$

If the value of k given by (2.11) is substituted, the above equation becomes

$$Z(0,\omega) = (\omega\mu_0/\sigma)^{1/2}e^{i\pi/4}$$

so that the phase is constant and equal to $\pi/4$ in a homogeneous medium. Examples of 1D models for field data using various inversion schemes are presented in Chapter 6.

2.3.3 Induction in two- dimensional structures

Rigorously speaking, although the conception of a homogeneously layered Earth is of significant theoretical and practical value with regard to deep induction studies, it is still a mere abstraction of reality. Indeed, 1D modelling does not provide adequate representation for quite a number of geological situations found in nature. However, in many studies substantial progress can be made if the Earth is approximated by a two dimensional model. A particular structure is called two- dimensional (or simply 2D) when its extension in one direction is greater than the skin depth of the incident field. Geological structures such as dykes, rift valleys, faults, contact zones, etc, generally fall well into this 2D classification. The 2D problem consists basically of solving Maxwell's Eqs. (2.1a) and (2.1b) for a conductivity distribution assumed invariant along (say) the x- direction, i.e. $\sigma = \sigma(y,z)$ in the same reference system described section 2.3.2. These equations are

$$\nabla \times \mathbf{E} = -i\omega\mu_0 \mathbf{H} \tag{2.21}$$

$$\nabla \times \mathbf{H} = \sigma(y,z)\mathbf{E} \tag{2.22}$$

if as before the displacement currents are neglected. Since there are no variations in the x- direction, $\partial/\partial x \equiv 0$. By expanding (2.21) and (2.22) into its components, one arrives at

$$\begin{aligned} &\partial E_z/\partial y - \partial E_y/\partial z = - i\omega\mu_0 H_x && \text{(a)} \\ &\partial E_x/\partial z = - i\omega\mu_0 H_y && \text{(b)} \\ &\partial E_x/\partial y = i\omega\mu_0 H_z && \text{(c)} \end{aligned} \tag{2.23}$$

$$\begin{aligned} &\partial H_z/\partial y - \partial H_y/\partial z = \sigma E_x && \text{(a)} \\ &\partial H_x/\partial z = \sigma E_y && \text{(b)} \\ &\partial H_x/\partial y = -\sigma E_z && \text{(c)} \end{aligned} \tag{2.24}$$

Provided that the conductivity is transversely isotropic, these two sets of equations decouple into two distinct modes which represent the H- polarization and E- polarization cases. The E- pol case (also referred in the literature as transverse electric or TE) has the electric current flowing along

the independent axis (x)- normally associated with the strike direction. It is given by the set of Eqs. (2.23b), (2.23c) and (2.24a) expressed by the triplet (E_x,H_y,H_z). H_y and H_z can be eliminated from the E- pol set and give a scalar Helmholtz equation in terms of E_x

$$\partial^2 E_x/\partial y^2 + \partial^2 E_x/\partial z^2 - i\omega\mu_0 E_x = 0 \qquad (2.25)$$

The remaining set of Eqs. (2.23a), (2.24b) and (2.24c) has the magnetic field parallel to the strike direction- the H- pol case (or transverse magnetic TM). In an analogous way, another Helmholtz equation in H_x can be obtained

$$\partial^2 H_x/\partial y^2 + \partial^2 H_x/\partial z^2 + \sigma^{-1}(\partial\sigma/\partial y.\partial H_x/\partial y + \partial\sigma/\partial z.\partial H_x/\partial z) - i\omega\mu_0\sigma H_x=0 \qquad (2.26)$$

The electric current flows perpendicular to the strike direction in the H- pol case. Thus, charge accumulation can occur at interfaces of conductivity discontinuity, resulting in field changes commonly known as the galvanic effect. This effect is frequency independent, in contrast to induction effects. Nevertheless, the conductivity is σ=0 in the non- conducting air layer, and by making the right sides of (2.24b) and (2.24c) equal to zero, the magnetic field becomes independent of both y and z, i.e., H_x remains constant at the Earth's surface irrespective of the conductivity distribution inside the Earth. As a result of this, the H pol- case is greatly simplified.

Electromagnetic induction in bodies of simple geometry can be studied analytically . For example, faults (Weaver, 1963) and dykes (Rankin, 1962) have been solved analytically. These and other analytical solutions were reviewed by Hobbs(1975). For more arbitrary conductivity configurations, the Helmholtz Eqs. (2.25) and (2.26) cannot be solved analytically and only numerical solutions can be obtained. The most common numerical procedures involve finite difference, finite element and integral equation application. They are discussed in more detail in Chapter 7.

2.3.4 Induction in tridimensional structures

While two- dimensional modelling is employed in most geophysical induction problems and can provide acceptable model fits, strictly speaking the Earth's conductivity is tri-dimensional. Maxwell's equations can also be decoupled into two modes for transversely isotropic medium (Nobes, 1986)

but no analytical solution is available. Again, numerical solutions are available employing similar numerical procedures as in the 2D case, plus other approximative techniques such as thin sheet and thick sheet analyses. The main limitation to 3D modelling to date is the prohibitive computational cost of most available algorithms.

2.4 Controlled source equations

2.4.1 Field of an oscillating dipole– general equations

A number of equations and definitions which arise in the theory of an oscillating dipole are now presented. This problem is conveniently solved by means of potential functions or other special functions such as the Hertz and the Fitzgerald vectors.

Equation (2.1c) assures that **B** is solenoidal and can therefore be expressed in terms of the curl of an arbitrary vector **A** as follows

$$\mathbf{B} = \nabla \times \mathbf{A} \tag{2.27}$$

which substituted in (2.1a) gives

$$\nabla \times (\mathbf{E} + \partial \mathbf{A}/\partial t) = 0 \tag{2.28}$$

The vector $\mathbf{E}+\partial \mathbf{A}/\partial t$ is irrotational and can therefore be obtained from another arbitrary scalar function ψ

$$\mathbf{E} + \partial \mathbf{A}/\partial t = -\nabla \psi \tag{2.29}$$

The functions **A** and ψ are respectively known as the vector and scalar potentials. Electromagnetic potentials are not unique and may be modified by a 'gauge' transformation without affecting the fields. A commonly used 'gauge' is the Lorentz condition

$$\nabla . \mathbf{A} + \mu_0 \varepsilon \, \partial \psi/\partial t + \mu_0 \sigma \psi = 0 \tag{2.30}$$

which constrains **A** and ψ in such a way that they obey the same wave Eqs. (or diffusion equations in the quasi- static approximation) as those obeyed by

the electromagnetic fields.

Hertz defined a single vector function Π to express an electromagnetic field. The vector potential **A** in term of Π is

$$\mathbf{A} = \mu_0\sigma\Pi + \mu_0\varepsilon\,\partial\Pi/\partial t \tag{2.31}$$

which also satisfies the Lorentz condition (2.21) if

$$\psi = -\,\nabla.\Pi \tag{2.32}$$

Substituting (2.31) and (2.32) in (2.29) results in

$$\mathbf{E} = \nabla\nabla.\Pi - \mu_0\sigma\partial\Pi/\partial t - \mu_0\varepsilon\partial^2\Pi/\partial t^2 \tag{2.33}$$

Applying the same vector identity as in Eq. (2.5), (2.33) becomes

$$\mathbf{E} = \nabla x\nabla x\Pi + \nabla^2\Pi - \mu_0\sigma\partial\Pi/\partial t - \mu_0\varepsilon\partial^2\Pi/\partial t^2 \tag{2.34}$$

The Hertz vector obeys the wave equation

$$\nabla^2 = \mu_0\sigma\partial\Pi/\partial t + \mu_0\varepsilon\partial^2\Pi/\partial t^2 \tag{2.35}$$

which substituted in (2.34) reduces it to

$$\mathbf{E} = \nabla x\nabla x\Pi \tag{2.36}$$

Correspondingly, the magnetic vector **B** can be written as

$$\mathbf{B} = \nabla x\mathbf{A} = \nabla x(\mu_0\sigma\Pi + \mu_0\varepsilon\,\partial\Pi/\partial t) \tag{2.37}$$

Note that by solving the wave equation (2.35) (or the diffusion equation in the quasi- static approximation), the electromagnetic fields can be determined by using (2.36) and (2.37).

2.4.2 Horizontal electric dipole

Consider an n- layered isotropic Earth's structure and a transmitter comprising an infinitesimal horizontal electric dipole dl oriented along the x-axis. Assume conditions (i)–(iii) remain valid. The differential equation for the problem in terms of the Hertz vector is (Goldstein and Strangway, 1975)

$$\nabla^2 \Pi_{ij} - k^2 \Pi_{ij} = 0 \tag{2.38}$$

where i= 0, n refer to the layer number (i=0 -> air), j = x, z and k is the wave number given by (2.11). The general solution of Eq. (2.38) is

$$\Pi_{ij} = \cos(n\phi) \int_0^\infty [f_i(m)e^{\alpha_i z} + g_i(m)e^{-\alpha_i z}] J_n(mr)dm \tag{2.39}$$

where

$$\alpha_i^2 = m^2 + k_i^2,$$
$$r^2 = x^2 + y^2,$$
$$\cos\phi = x/r,$$

$f_i(m)$ and $g_i(m)$ are functions to be determined, J_n is the Bessel function of order n, m is the separation constant and r is the distance between transmitter and receiver. It has been shown elsewhere (Sommerfeld, 1964) that only the x and z components of the Hertz vector are required in order to satisfy the boundary conditions stating the continuity of the tangential components of E and B across interfaces. As the calculations involved in the derivation of the electromagnetic fields after solution of (2.39) are very lengthy they are not developed here. The reader is referred to Keller (1968) and Scriba (1974) for the detailed derivation. The resultant field components are

$$E_x = pi\omega \left[\int_0^\infty G_1 J_0(mr)mdm + (r^2-2x^2)/r^3 \int_0^\infty (G_2-G_1)J_1(mr)dm + x^2/r^2 \int_0^\infty (G_2-G_1)J_0(mr)dm\right] \tag{2.40}$$

$$E_y = pi\omega \left[-2xy/r^3 \int_0^\infty (G_2-G_1)J_1(mr)dm + xy/r^2 \int_0^\infty (G_2-G_1)J_0(mr)dm\right] \tag{2.41}$$

$$B_x = p \left[-2xy/r^3 \int_0^\infty G_1 J_1(mr)mdm + xy/r^2 \int_0^\infty G_1 J_0(mr)m^2 dm\right] \tag{2.42}$$

$$B_y = -p\,[x^2/r^2 \int_0^\infty (G_1 J_0(mr) m^2 dm + \int_0^\infty G_3 J_0(mr) m\alpha_1 dm + (r^2-2x^2)/r^3 \int_0^\infty G_1 J_1(mr) m dm] \quad (2.43)$$

$$B_z = (py/r) \int_0^\infty G_1 J_1(mr) m^2 dm \quad (2.44)$$

where

$p = I_0 \mu_0 dl/2\pi$, I_0 is the dipole electric current,

$G_1 = r_1/(mr_1+\alpha_1)$

$G_2 = \alpha_1/k_1^2 q_1$

$G_3 = 1/(mr_1+\alpha_1)$

$r_1 = r_1(\sigma_i, d_i, \omega)$

$q_1 = q_1(\sigma_i, d_i, \omega)$

σ_i and d_i are the conductivity and thickness of the ith- layer, G_1, G_2 and G_3 are kernels of integrals. The parameters r_1 and q_1 take into account the layer structure and can be calculated recursively.

The integral terms contained in the field equations (2.40)- (2.44) are known as Hankel transforms and can be evaluated numerically by a number of algorithms. The most efficient algorithms to date are based on digital filtering techniques (Anderson, 1979). The resultant impedance elements can thus be calculated in the usual way. Forward modelling curves and inversion schemes for a horizontal electric dipole source in layered structures are presented in Chapters 5 and 7, respectively.

Other theoretical developments and associated relevant parameters concerning the processing and inversion of MT data are described in Chapters 4 and 7, respectively. A final note regarding the units of the physical quantities involved in electromagnetic induction studies is pertinent. The measured quantity is **B**, the magnetic induction vector. However, it is common practice among investigators to use **H** as the measured magnetic field, quantified with magnetic induction units. The practical units often found in the literature and used throughout this work are [H]- nT, [E]- mV/km, resistivity [ρ]- Ω.m and phase ϕ in degrees.

CHAPTER 3
DATA ACQUISITION

3.1 Introduction

This chapter deals with the acquisition of MT data in the Italian Alps during three separate fieldwork campaigns, in which a number of different instrumental systems together covering a wide spectral range, i.e., from about 500Hz up to 5000s were used. Measurements made in the audio-frequency range (512Hz- 1Hz) are usually termed audiomagnetotelluric (AMT) measurements. The lower frequency measurements are normally referred to as magnetotelluric (MT) measurements. This Chapter consists of three main sections. The first of this sections (section 3.2) describes the various instruments used in this study and their calibrations. Typical fieldwork procedure and diverse aspects of data acquisition and transfer to the mainframe computer are discussed in section 3.3. Section 3.4 presents an overview of the three fieldwork campaigns. This includes general objectives of each campaign, its site locations, and comments about the problems encountered in the course of this work.

3.2 Instrumentation

3.2.1 AMT Instrumentation

a) Data acquisition system

The Short Period Automatic Magnetotelluric System (SPAM) in its second and improved version (SPAM MKII) was used for the first time in the 1984 field campaign. This system is an updated version of an earlier system (SPAM MKI) designed by Dawes in 1981 (Dawes, 1984). Two versions of SPAM MKII which differ only in frequency range were used during the Italian project. The system which belongs to the electromagnetic induction group at Edinburgh University (EUIG-SPAM) has a spectral range of 512Hz- 8s, while the other, loaned from the National Environment Research Council (NERC) Equipment Pool (NERC-SPAM), has a spectral range of 128Hz to 32s. Both EUIG-SPAM and NERC-SPAM have their frequency ranges split into 4 equal bands (assigned the numbers 0 to 3) of 3 octaves each. The cut- off frequencies are listed in Tab. 3.1. As SPAM MKII has been described

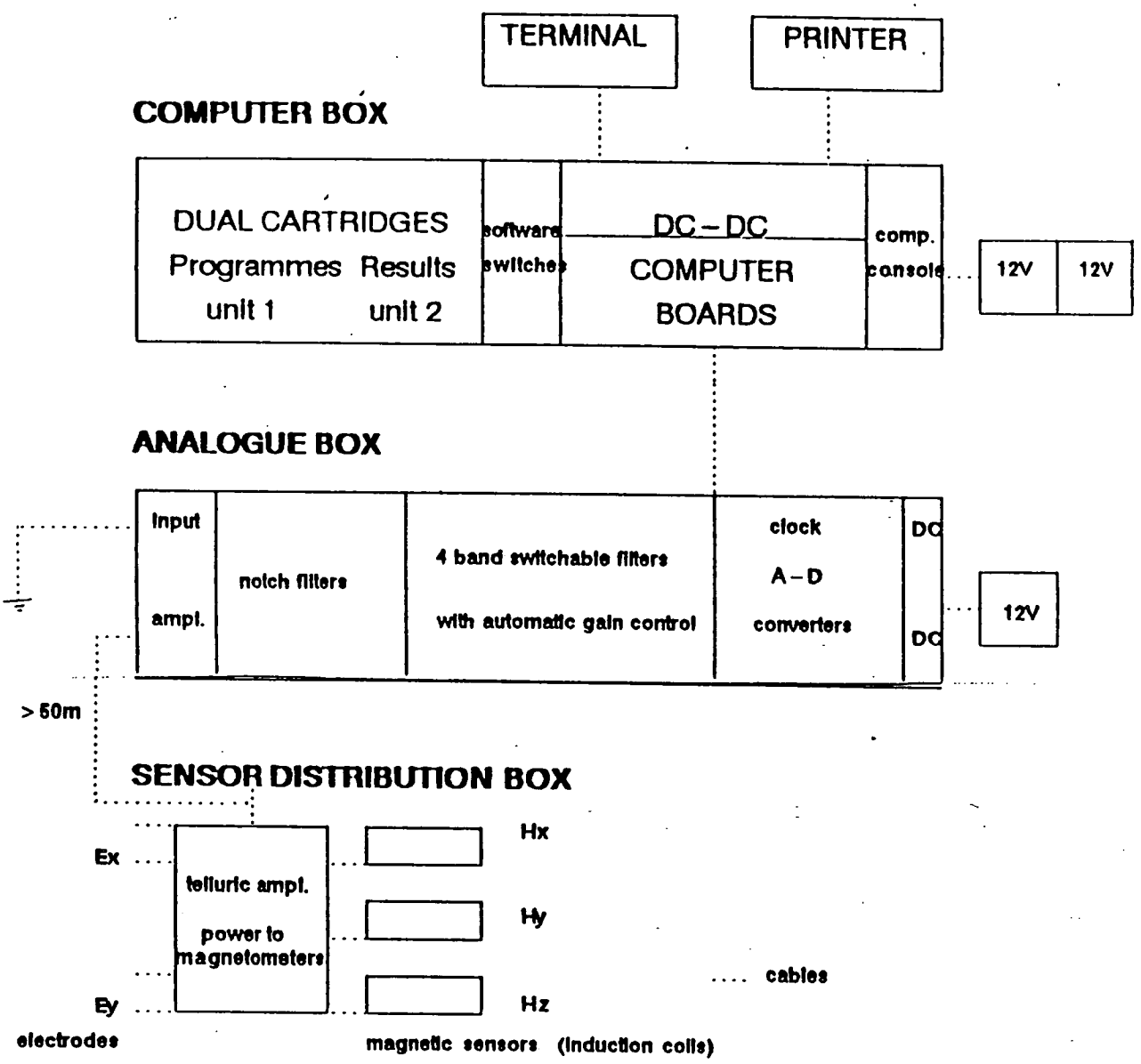

SHORT PERIOD SYSTEM (SPAM MKII)

Fig. 3.1- Simplified diagram of the short period automatic magnetotelluric system (SPAM MKII).

elsewhere (Dawes, 1984), only the main aspects of it are presented here. A block diagram of the complete system is shown in Fig 3.1. The system is composed of three subsystems disposed in three physically separated boxes, i.e., the sensor distribution box, the analogue box and the computer box.

The sensor distribution box is a unit located near the sensors which measure the 3 orthogonal components of the geomagnetic field (Hx, Hy and Hz) and the 2 orthogonal components of the telluric field (Ex and Ey). The sensor box itself contains a pair of differential amplifiers (fixed gain of 40) and band- pass filters for the telluric signals. The frequency responses of the preamplifiers for both EUIG-SPAM and NERC-SPAM (amplitude in dB) are shown in Fig. 3.2, the cut-off frequencies being 2040-1/29.5 Hz and 480-1/125 Hz, respectively. A long cable carrying both the input signal and power to the magnetometers connects the sensor and analogue boxes.

The five main sections of the analogue box are also shown in Fig. 3.1. The input magnetic and telluric signals (5 channels) are subject to identical processing in the following order:

a) Wide band filtering and preamplification. The aim of the filtering stage is the elimination of the DC level and the very high frequencies. A fixed gain of 2 (common to all channels) is also performed at this first stage. The main preamplification which is digitally controlled (manual switch operation) follows. Its gain value is the same for all channels and is in the range 1,2,4,...,128, i.e., the total gain in this board is 2**(switch value + 1). An overload detector causes an LED to flash whenever any of the five channels saturates (> ± 5V).

b) Notch filtering for 50Hz and 150Hz.

c) Band switchable filtering (combination of low pass and high pass Butterworth filters), to split the broad band range into the four frequency ranges indicated in Tab. 3.1 and Fig. 3.3, then automatic post- amplification (output gain) for optimization of the dynamic range. A fixed gain of 2 (common to all channels) is also performed at this stage. The automatically selected gains (output gain- variable for each channel) cover the same range as stated in a). The total gain for each channel through the analogue box is thus

2**(input gain number + output gain number +2).

d) Analogue to digital (A/D) conversion with an effective 19 bit dynamic range (12 bits A/D and 3 bits post- gain). The sampling rate of the signal and the

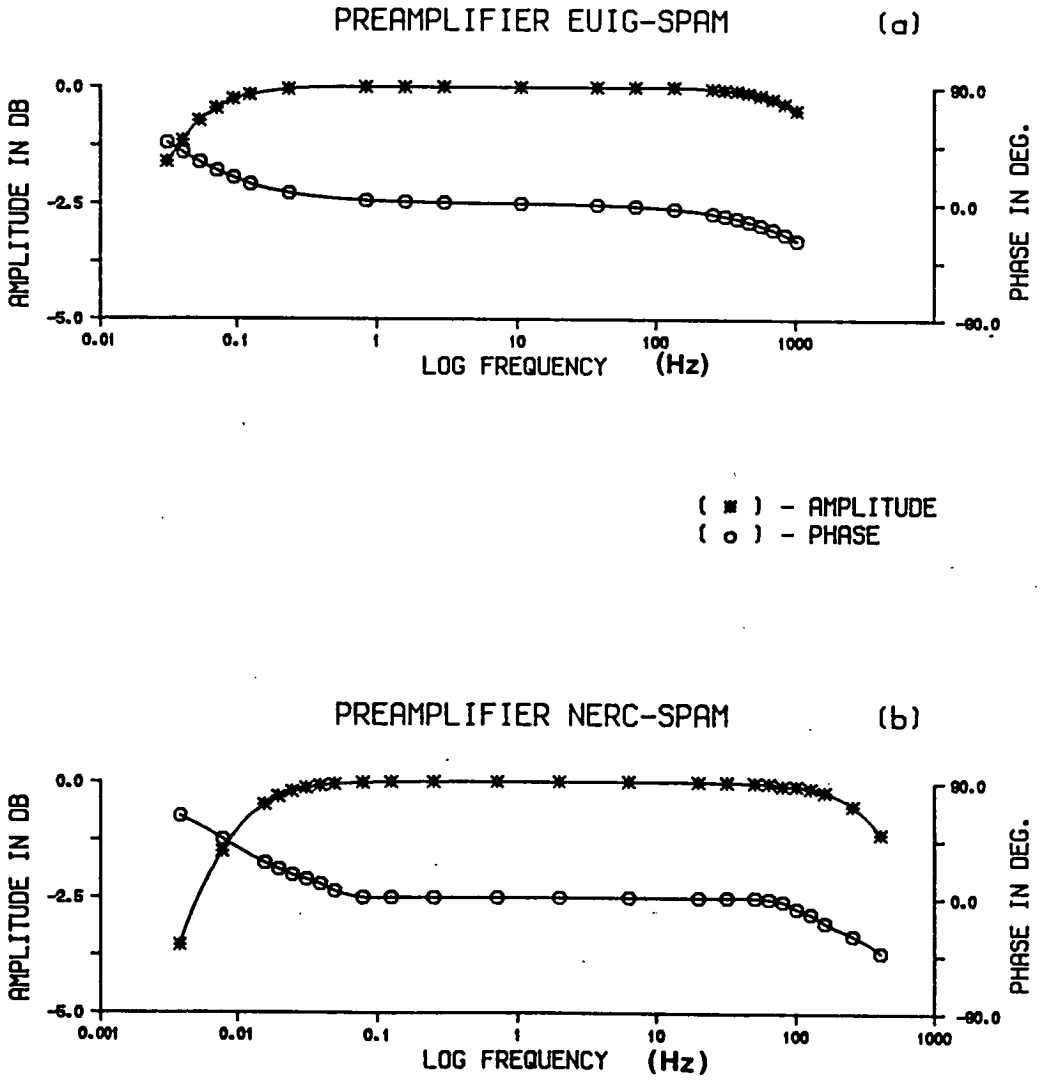

Fig. 3.2- Preamplifier frequency response curves (theoretical). Assigned values (symbols * and o) correspond to calibration values measured before the field campaigns.
(a) EUIG-SPAM curves
(b) NERC-SPAM curves

Band	EUIG-SPAM	NERC-SPAM
0	512Hz-64Hz (2048Hz)	128Hz-16Hz (512Hz)
1	64Hz-8Hz (256Hz)	16Hz-2Hz (64Hz)
2	8Hz-1Hz (32Hz)	2Hz-1/4Hz (8Hz)
3	1Hz-1/8Hz (4Hz)	1/4Hz-1/32Hz (1Hz)

Tab. 3.1 AMT bands for EUIG-SPAM and NERC-SPAM. The values in brackets are the sampling rates in Hz.

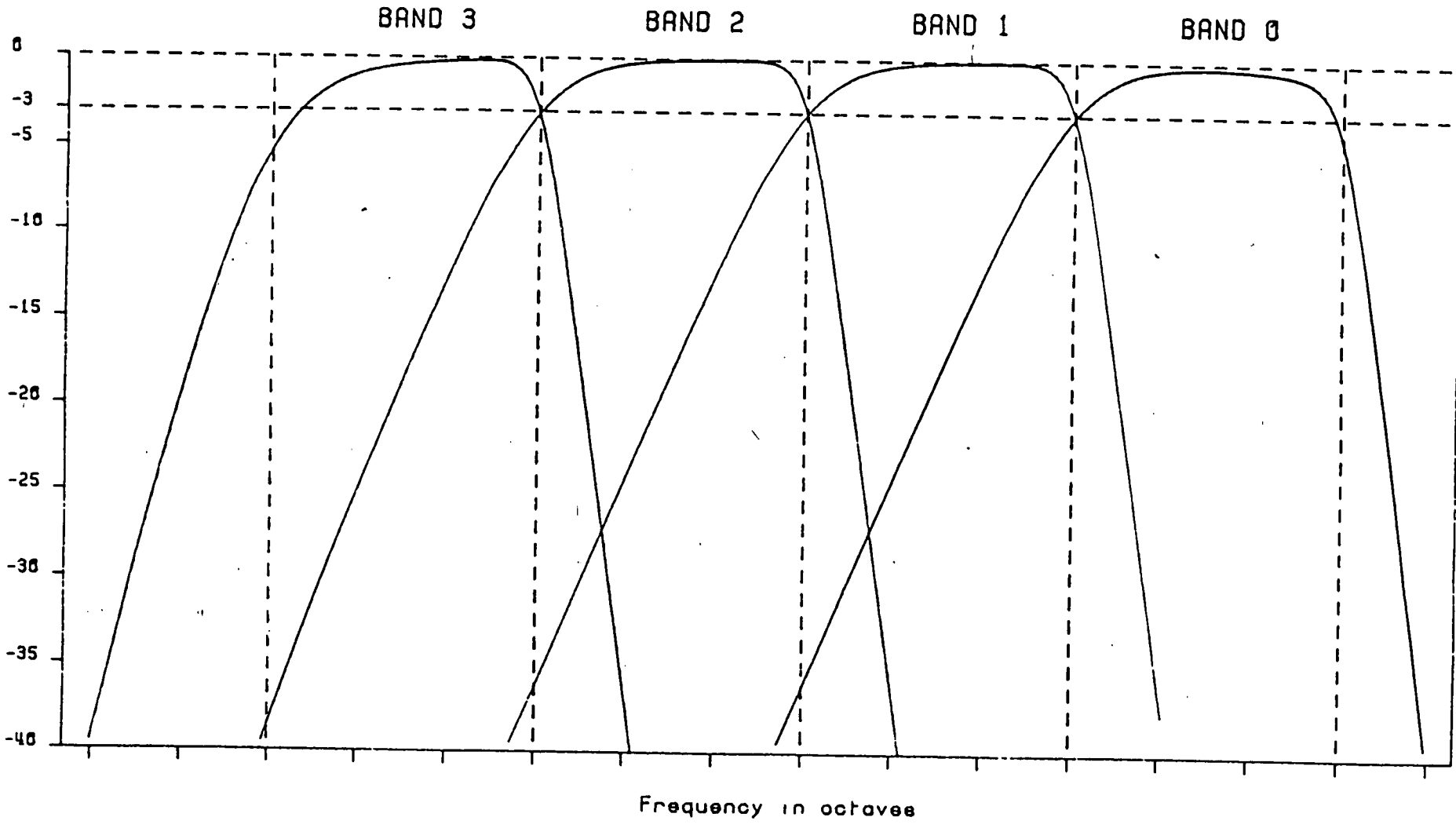

Fig. 3.3- Filter responses of 4 bands for EUIG-SPAM and NERC-SPAM. Cut-off frequencies (-3dB) given in Tab. 3.1 for the two systems.

automatic gain ranging are controlled by a crystal clock generator.

e) The DC-DC section of the analogue box contains 2 DC-DC converters such that a single 12V battery provides power to the analogue box, the sensor distribution box and the magnetic sensors.

The system in the computer box is based on the DEC LSI-11 bus architecture. It uses the LSI-11/2 processor with a 64Kb RAM. A dual TU58 cartridge unit holds the programs in unit 1 and the time series and results in unit 2. A simplified flow chart of the in- field processing program given in Dawes (1984) is shown in Fig 3.4. SPAM MKII is capable of automatically selecting AMT events (also referred as 'windows' throughout this study) on a real time basis. The selection of these events is based mainly on coherence and on the power levels of the natural signals. Full tensorial analysis is then performed and the results stacked. Listings and/or plots of individual windows or stacked results are obtainable at any time during the data acquisition. A preliminary interpretation of the results can also be made while still in the field by performing both rotations to major/minor or strike directions and by simple 1D heuristic modelling (e.g. Bostick (1977) and Schmucker (1970) transformations , which are discussed in Chapter 7). Later in the laboratory, the selected time series are transferred to a mainframe computer (Edinburgh Multi Acess System- EMAS) for more rigorous analysis. The author was involved in the development of software for both the in- field analysis and the transfer of cartridge data to EMAS. This participation consisted of writing most of the 'transfer program' and the Fortran routines for tensorial rotation and the Bostick and Schmucker transformations for in-field modelling.

b)Magnetic and telluric sensors

The magnetometers used in this study were the CM11E and CM16 induction coils supplied by Societe ECA- France. The CM16 coils are operational in the frequency range 800Hz- 3Hz, whereas the CM11E coils cover nominally the range 100Hz- 0.025Hz. These coils have very low noise characteristics- CM11E: .021- 13 pT/Hz and CM16: 2.6 x 10^{-3}- .12pT/Hz, the range of values associated with the increase in noise as the frequency decreases. Both the CM16 and CM11E frequency response curves are shown in Fig. 3.5(a)-(b).

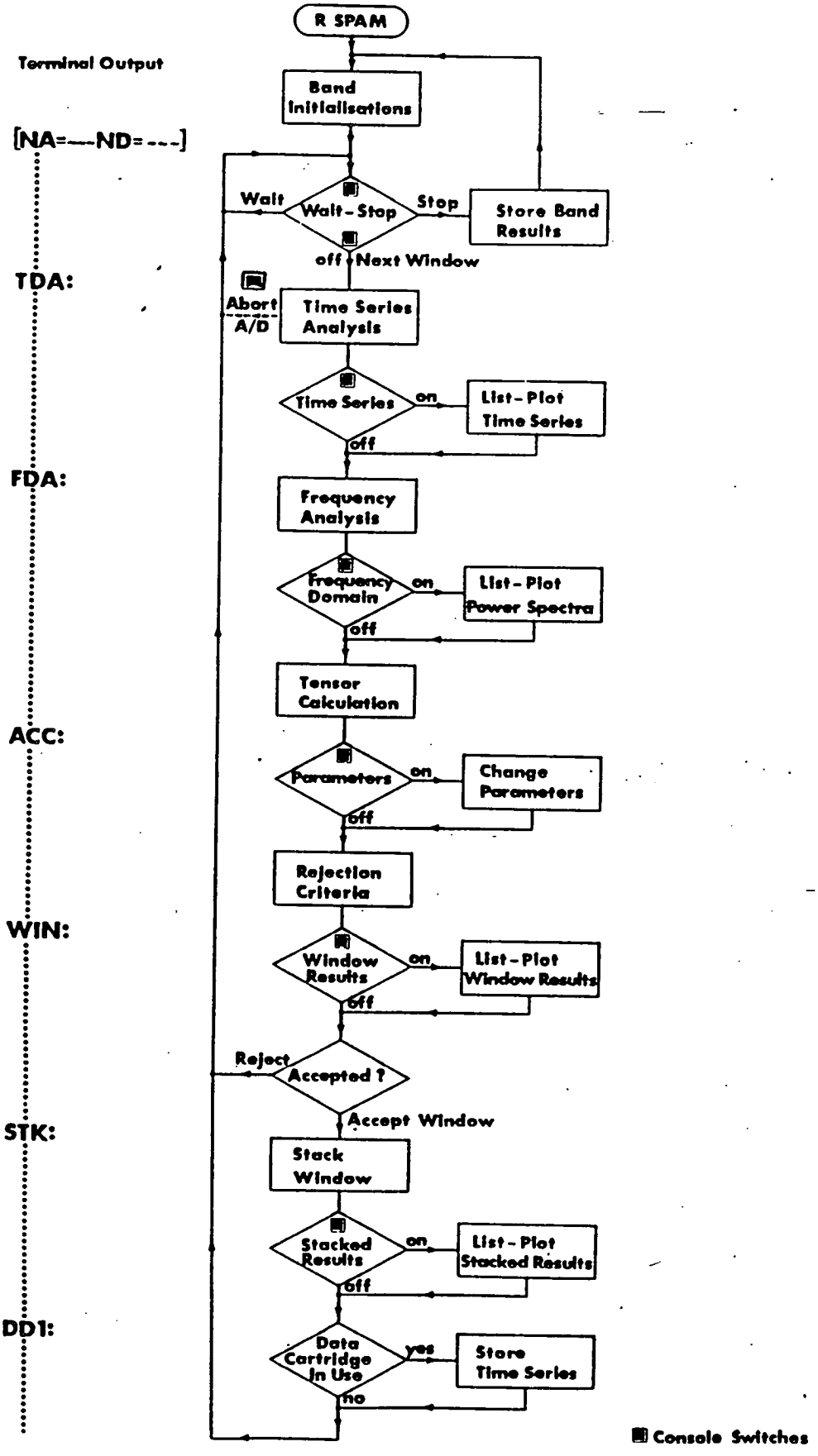

Fig. 3.4– Simplified flow chart of the in- field processing program. Main routines are written in Fortran and I/O routines in DEC machine language.

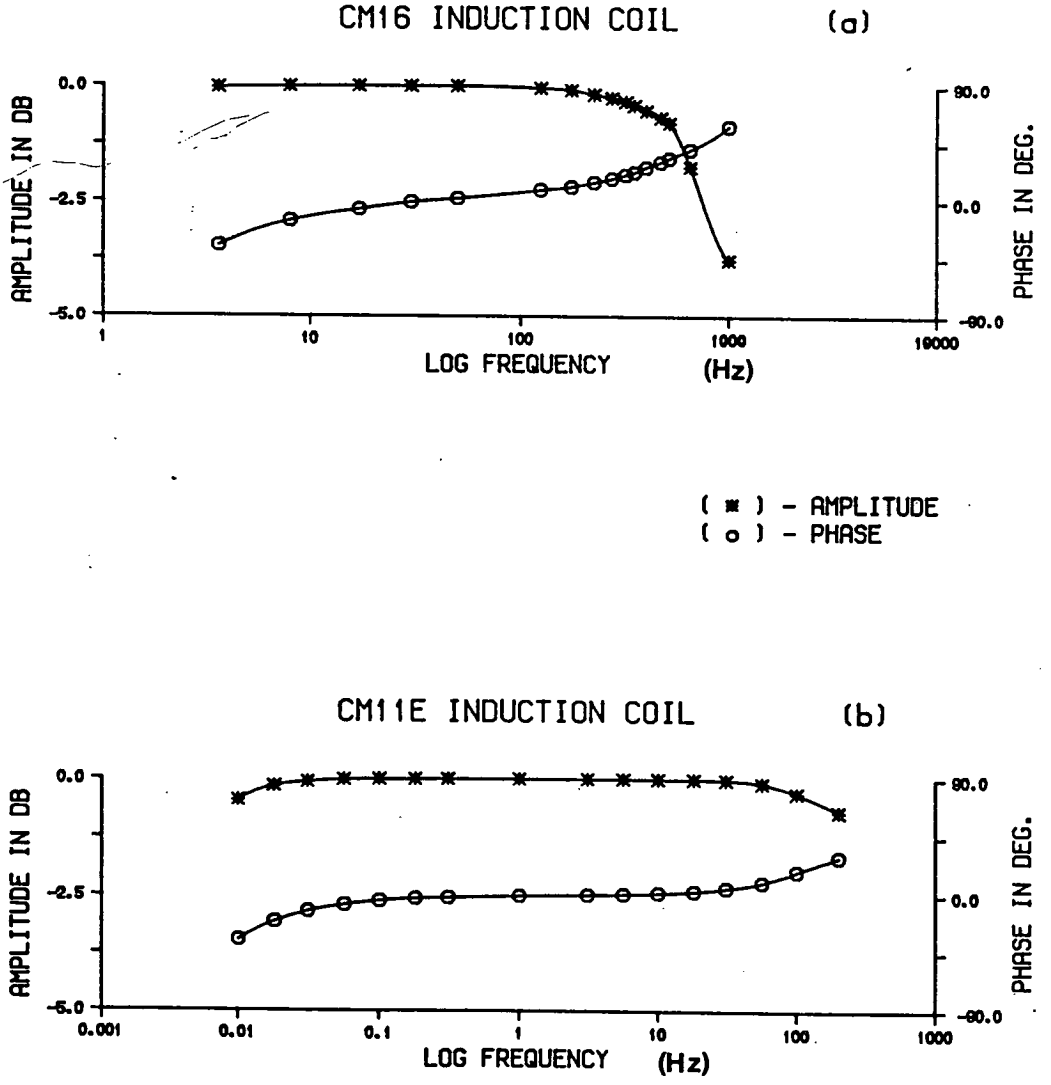

Fig. 3.5–Frequency response curves for the magnetic induction coils (measured).
(a) CM16 induction coil response.
(b) CM11E induction coil response.
Symbols (* and o) represent calibration values (last. calibration at Garchy by Devlin (1984)).

Steel probes, copper rods, $Pb-PbCl_2$ and $Cu-Cu\ SO_4$ non- polarizable electrodes were all deployed at different times during the campaigns in accordance with the results of the systematic study of electrode performance by Petiau and Dupis (1980). They showed that for frequencies higher than about 10Hz, several electrode types (including those used in this study) had similar responses and exhibited the same noise level. Howevêr, for lower frequencies, they indicated the importance of using non- polarizable electrodes due to their lower noise level, time stability and smaller temperature coefficients.

3.2.2 MT Instrumentation

Longer period measurements were performed with two distinct sets of instruments referred to as the Band 4 and Band 5 systems.

a) Band 4 system

The Band 4 system is a non- automatic long period recording system designed by Hill (1987). It operates in the frequency band 0.25Hz- 0.01Hz and is referred to as the Band 4 system to conform with the SPAM bands previously described. A block diagram of the complete system is given in Fig. 3.6(a). It is composed of three main sections: A sensor distribution box and a single box containing both an analogue section and a digital data recorder.

The sensor distribution box has a design similar to its SPAM MKII counterpart; the only distinctions are the filter cut- off frequencies of the two telluric differential preamplifiers and filter unit- 1.95Hz and 251s, and a fixed gain of 100 (Fig. 3.6(b)). It also supplies power to the magnetic sensors.

The analogue section contains five matched bandpass filters and amplifiers, with cut- off frequencies of 0.25Hz and 0.01Hz. The post gain of each channel is selected manually and has possible values of 1, 2, 4 , 10, 20 and 40.

The geologger (Valiant, 1976) is a digital data cassette recorder which performs the analogue- digital conversion for a selected number of sampling rates, e.g., 1s sampling was used for the Band 4 system . It has a dynamic range of ± 10V in 5mV digitizing steps.

The magnetic sensors are again the CM11E induction coils and as telluric sensors both Cu rods and Pb- $PbCl_2$ non-polarizable electrodes were used in this study. The author assisted in the construction of a second Band 4 system which enabled the simultaneous operation of two MT stations in the

(a)

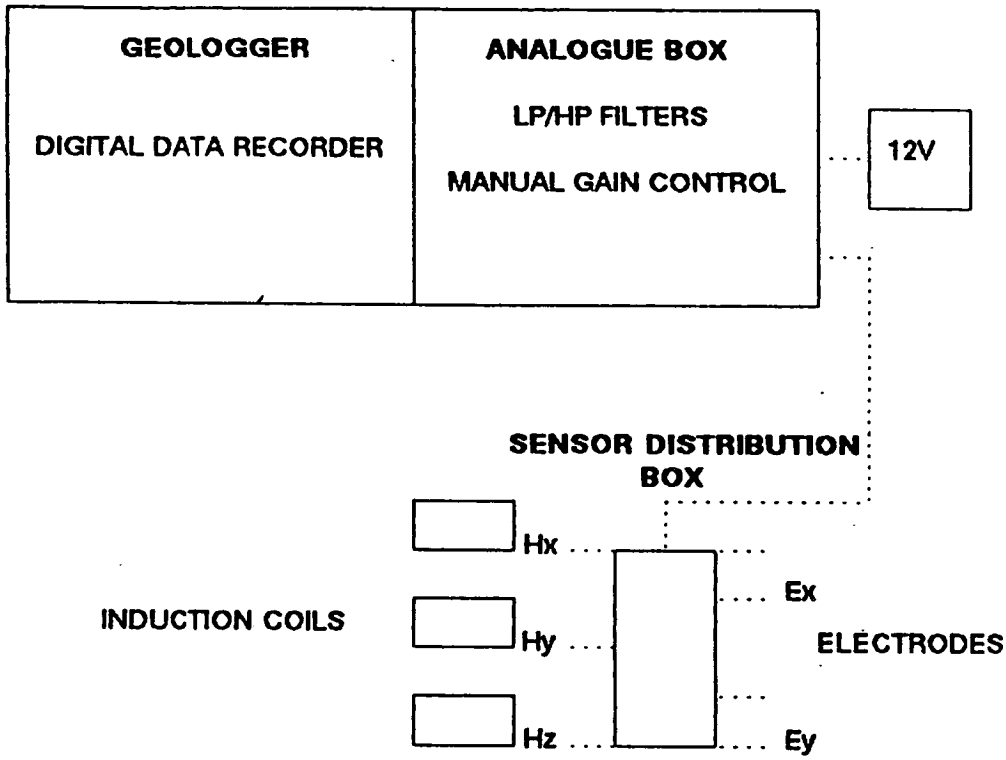

(b)

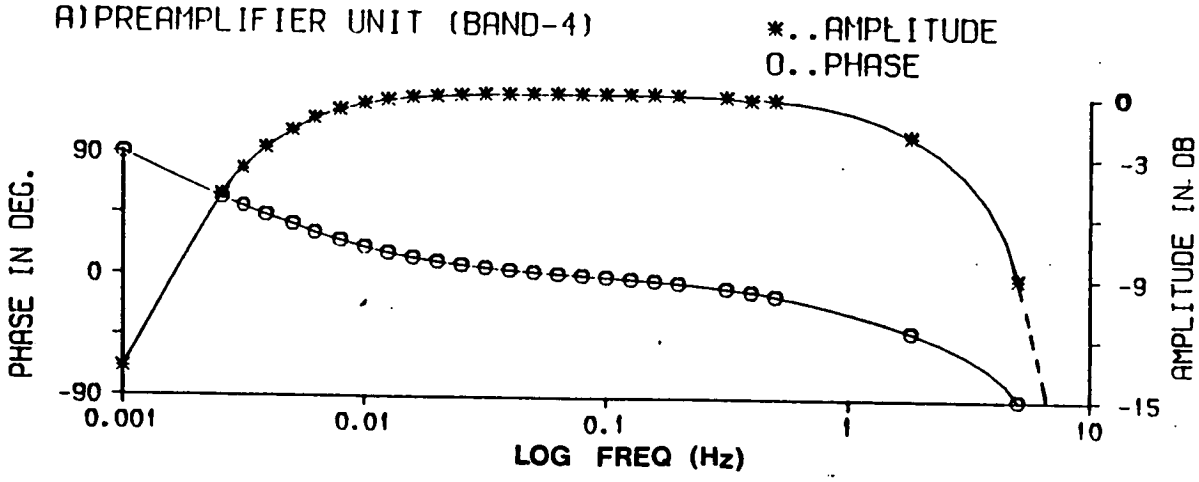

Fig. 3.6- (a) Simplified diagram of Band 4 system.
(b) Preamplifier response curve of Band 4 system (theoretical). Symbols (* and o) correspond to calibration values obtained before the field campaigns.

first fieldwork campaign.

b) Band 5 system

The Band 5 system is also a non- automatic system developed for the longer periods, i.e., 40s to DC. An EDA fluxgate magnetometer, a NERC geologger and a telluric sensor box designed by Dawes in 1986 constitute the complete Band 5 system as shown in Fig. 3.7. Fluxgate magnetometers were developed during the Second World War as airbone detectors of submarines. Nowadays, they are widely used ,e.g., in magnetic observatories and long period magnetotelluric surveys. The sensitivity of the EDA fluxgate is 10mV/nT and there is a built-in temperature compensation device which helps to control its temperature coefficient to the order of $1nT/^{0}C$. A simple description of the fluxgate principle can be found in Parkinson (1983). The fluxgate used in the Band 5 system of this study had its sensitivity increased to 50mV/nT so that the magnetic and telluric channels had identical overall responses. The telluric box contains two preamplifiers for Ex and Ey. The low pass section is a 4 pole Butterworth filter (24db/octave) with a cut- off frequency of 40s and initial amplification of 100. No high pass filtering is performed and very long period measurements (theoretically up to DC) can be carried out. The final gain is selected manually for each telluric channel from the possible values of 100 x (2, 5, 10, 20, 50 and 100). The data acquired in this study were sampled at 10s intervals and stored on cassettes by the geologger.

3.3 Fieldwork procedures

Before the fieldwork campaigns, all the instruments were calibrated and their actual response curves obtained. While it is also a good practice to recalibrate all the equipment after returning from a campaign, this has not been possible during this study due to need for the equipment for other projects. The calibration values obtained for the instruments are incorporated in the curves showing the theoretical responses (Figs. 3.2, 3.5(a)-(b) and 3.6(b)) of the 3 systems.

The first task in the field was to find suitable sites in the region to be surveyed. An AMT/MT site is ideally located in a flat area and as far away as possible of any obvious source of electromagnetic noise, e.g. power lines,

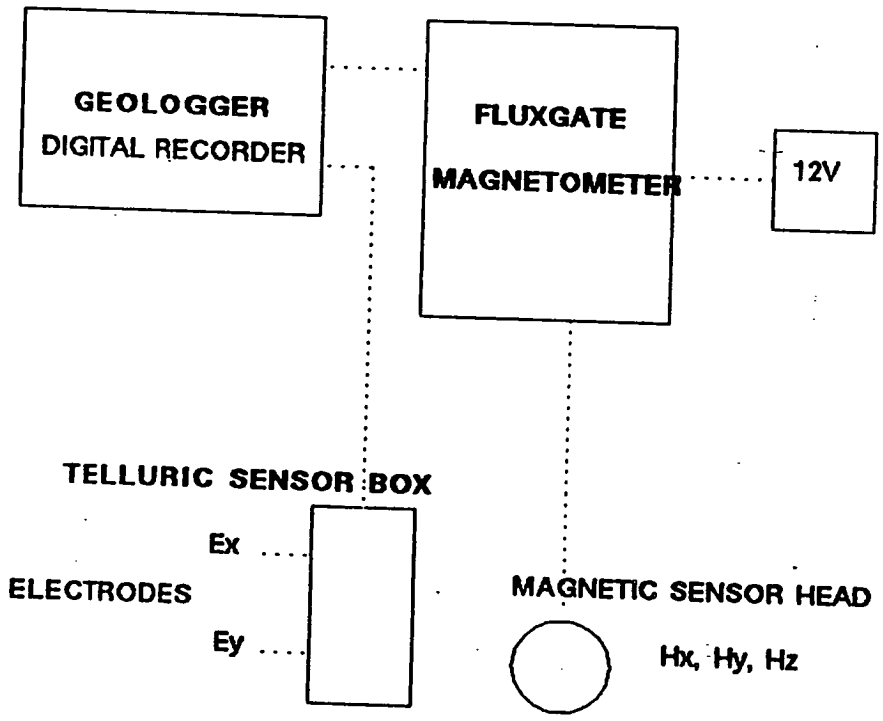

Fig. 3.7- Simplified diagram of Band 5 system.

radio frequency transmitters and repeat stations, electrified fences, etc, as well as livestock. Once a site was found, the telluric cables were usually laid out in an 'X' shape, with the exception that for the Band 5 system the two telluric channels have a common ground and thus an 'L' shape configuration was required. With electrodes spacings generally varying between 25m and 50m, telluric lines in the geomagnetic N-S (Ex) and E-W (Ey) directions were used at all stations. The electrodes were inserted into the ground and the magnetic sensors (induction coils or flux-gate sensor head) conveniently aligned and levelled. Care was taken with the installation since misalignment of the magnetic and telluric sensors affects the data accuracy. A very recent paper (Gomes- Trevino, 1987) also calls attention for a detail, also observed by Cox et al. (1970), which is concerned with the laying out of the cables. The telluric field in a non- 1D Earth (i.e. vertical magnetic field variations are observed) is non- conservative and potential differences depend on the contour described by the cable- an effect which is more pronounced for the higher frequencies. Thus the cables should ideally be layed in a straight line, but in common field practice this is seldom possible.

Specific procedures were then followed, depending on the equipment in operation, as described below:

3.3.1 SPAM measurements

All cables as illustrated in Fig. 3.1 were connected, the system was powered and some initial checks were performed to verify the proper functioning of the whole system. The latter included examination of the level of cultural noise, the correlation between the pairs of orthogonal magnetic and telluric components and the form of the signals as displayed on an oscilloscope. The correct functioning of the analogue box was tested by means of artificial signals from a pulse generator. The Figs. 3.8 illustrate one of these tests performed for all bands before starting measurements at one site. If the complete set of tests was satisfactory, the measurements were then started, generally with the higher frequency band filters, i.e. bands 0 or 1. For these bands data acquisition was more rapid and the quality of the MT curves for the particular site could therefore be assessed more readly. However, initial operation with other frequency bands could also prove advantageous since it is well known that certain types of geomagnetic activities occur preferentially during specific hours (refer to Tab. 2.1).

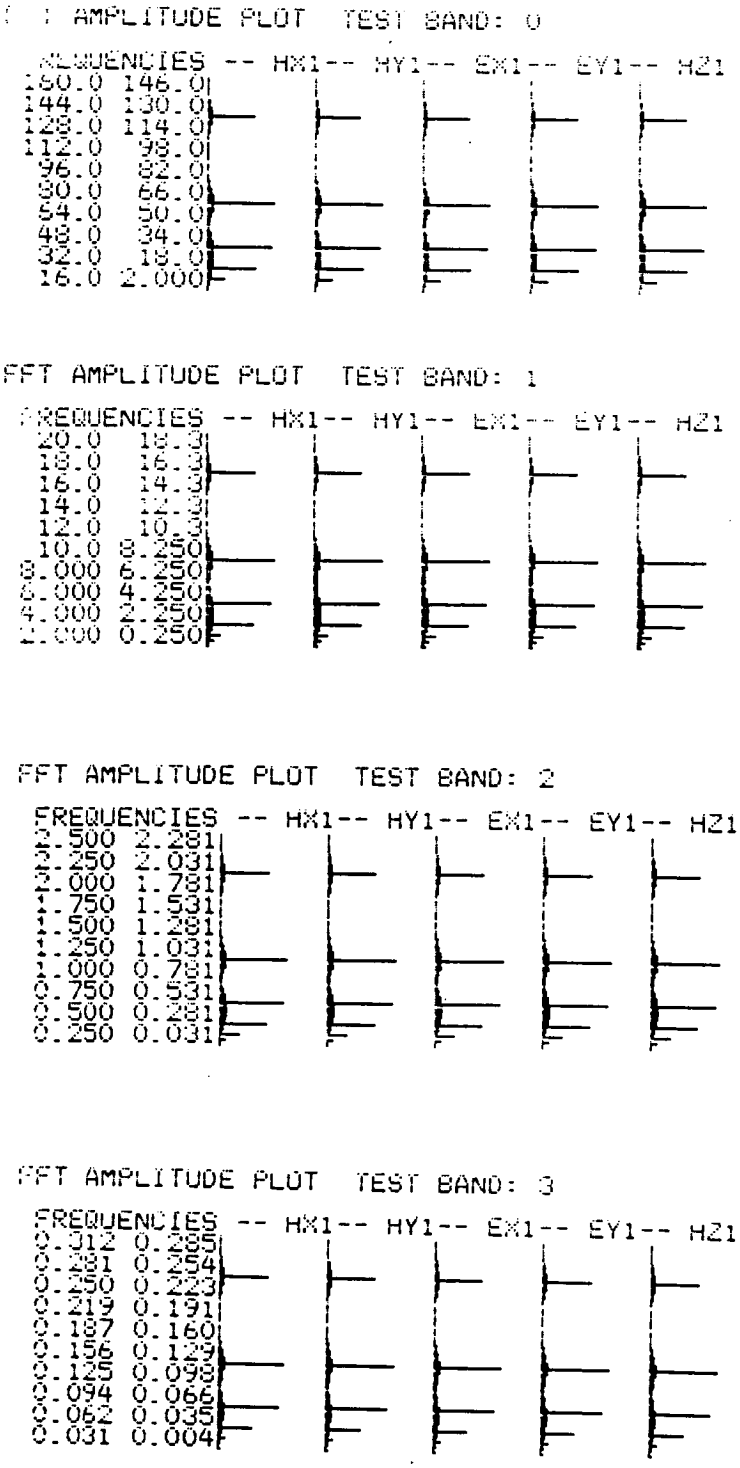

Fig. 3.8- FFT amplitude plots (for the 5 filters in analogue box) for all bands of NERC-SPAM. Generated sinusoidal signals composed of one main frequency (varying for each band) and its harmonics. Note the excellent match for all the channels and the signal amplitude attenuation, due to band- pass filtering, at the extremes of the frequency range.

By default, a data window was accepted if:

i) The average power of the magnetic signal was above 0.3pT,

ii) Four or more frequencies in the analysed window exhibited coherences higher than 0.9.

However, the criteria in force for accepting windows could be changed at any time during the course of measurements. For example. the power acceptance parameter could be altered to account for seasonal/regional variations in signal level. As discussed in detail in Chapter 5, the presence in Italy of highly coherent noise resulted in the acquisition - using such acceptance criteria- of problematic response functions.

Examples of (a) the in-field results obtained using the NERC-SPAM system- the MT curves for the various directions- and (b) the 1D heuristic models for one site in the Asiago area are given in Figs. 3.9 and 3.10, respectively. Fig 3.9 shows the apparent resistivity and phase curves for the measurement directions and the rotationally invariant responses (described in detail in Chapter 4). Skew values and the number of estimates used in the averaging are also displayed. Fig. 3.10 shows the 1D model results for the rotationally invariant curves. Both Bostick and Schmucker transformations (discussed in Chapter 7) are shown in Fig. 3.9 for the same data set.

All stored cartridge data were transferred to EMAS (mainframe) on return to the Edinburgh Department with intermediary transfers (a) onto floppy disks using a Digital Equipment Corporation (DEC) PDP minicomputer (MINC-11), (b) onto magnetic tapes and (c) to EMAS. With the more recent faster transmission speeds available for communication with EMAS, these transfer processes have now been shortened, and step (b) made redundant.

3.3.2 Band 4 measurements

The system was powered and left for tens of minutes for both the filters to settle and to allow time for the operator to select the best set of post- gains which would neither cause saturation ($>\pm$ 10V output) nor resolve insufficiently (about $\pm$ 5mV output) the recorded signals. Considering the widely variable characteristics of natural signals, a satisfactory compromise between these two factors was not easy. However, a better knowledge of the possible range of the signals was normally acquired after a few days operation at the same site, and consequently, more reasonable post- gain settings could then be selected. Each cassette stored just about 6 hours of

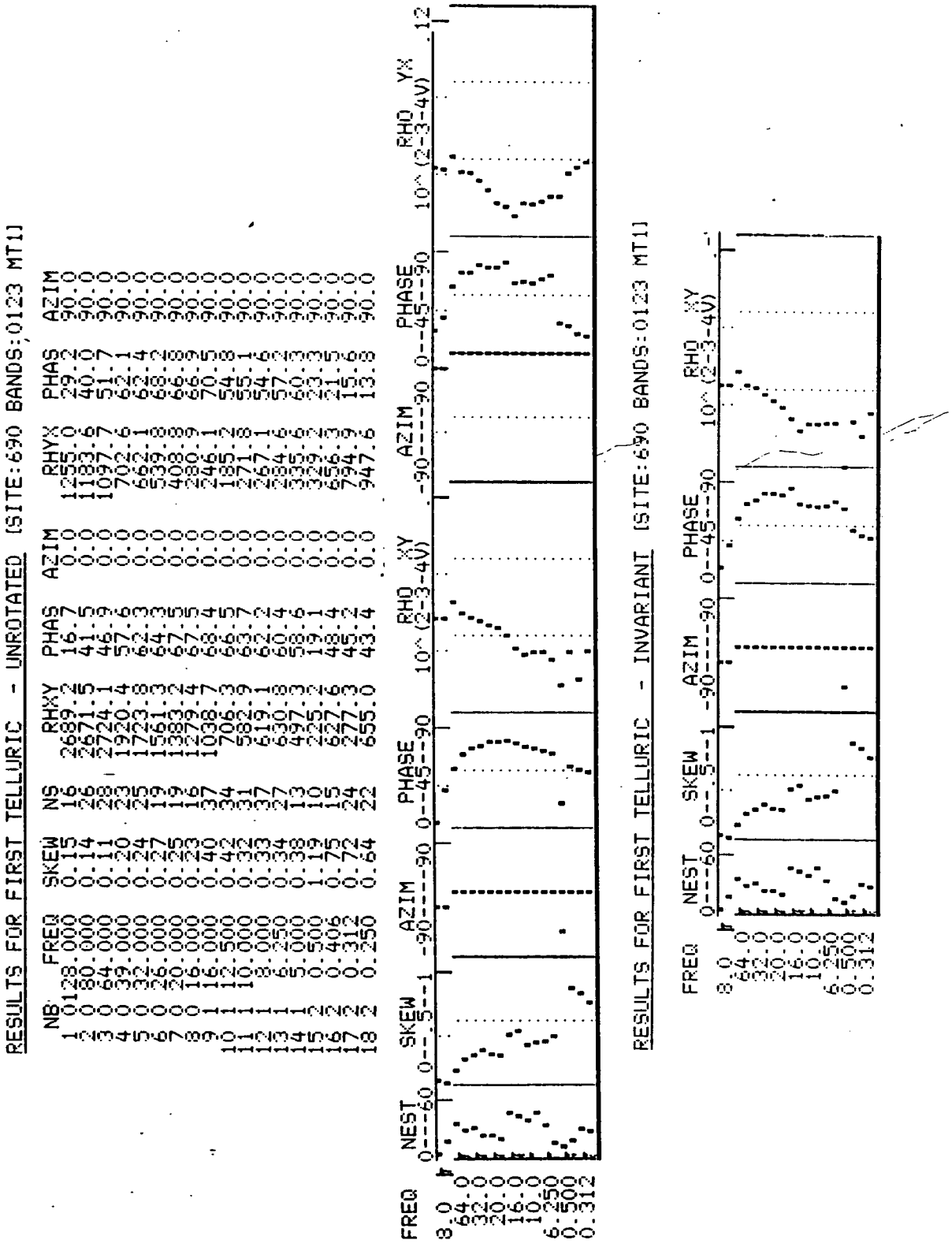

Fig. 3.9– MT infield results (apparent resistivity and phase curves, number of estimates and skew values) for the measurement directions and the rotationally invariant responses (NERC-SPAM).

*** 1-D MODELLING *** [SITE:690 BANDS:0123 MT1]

BOSTICK INVERSION [SITE:690 BANDS:0123 MT1]

NB		FREQ	NS	DINV	RHO
1	0	128.00	16	1338.	4950.6
2	0	80.00	26	1681.	2063.5
3	0	64.00	28	1866.	1378.5
4	0	39.00	23	1930.	531.8
5	0	32.00	25	2045.	414.2
6	0	26.00	19	2058.	262.4
7	0	20.00	19	2129.	217.0
8	0	16.00	16	2155.	180.2
9	1	16.00	37	1838.	95.2
10	1	12.50	34	1730.	136.1
11	1	10.00	31	2134.	178.1
12	1	8.00	37	2396.	184.6
13	1	6.25	27	2760.	183.0
14	1	5.00	13	3112.	160.5
15	2	0.50	10	5042.	53.4
16	2	0.41	15	11119.	457.6
17	2	0.31	24	10180.	358.3
18	2	0.25	22	16168.	783.3

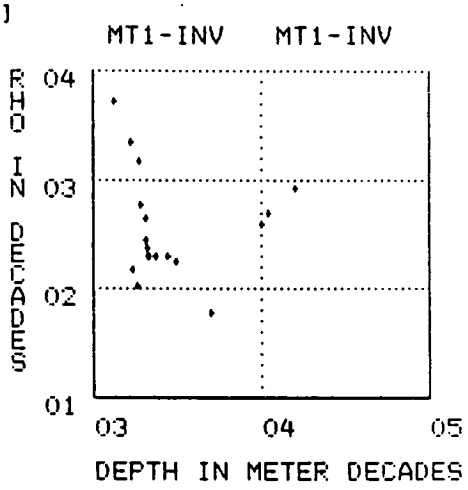

SCHMUCKER INVERSION [SITE:690 BANDS:0123 MT1]

NB		FREQ	NS	DINV	RHO
1	0	128.00	16	546.	3016.0
2	0	80.00	26	1119.	1987.3
3	0	64.00	28	1439.	1426.0
4	0	39.00	23	1696.	522.6
5	0	32.00	25	1849.	387.2
6	0	26.00	19	1923.	220.6
7	0	20.00	19	1988.	182.8
8	0	16.00	16	2010.	152.7
9	1	16.00	37	1763.	68.1
10	1	12.50	34	1522.	133.6
11	1	10.00	31	1851.	177.8
12	1	8.00	37	2067.	185.3
13	1	6.25	27	2403.	181.9
14	1	5.00	13	2783.	153.4
15	2	0.50	10	4310.	54.1
16	2	0.41	15	7409.	441.0
17	2	0.31	24	6195.	322.1
18	2	0.25	22	9444.	679.8

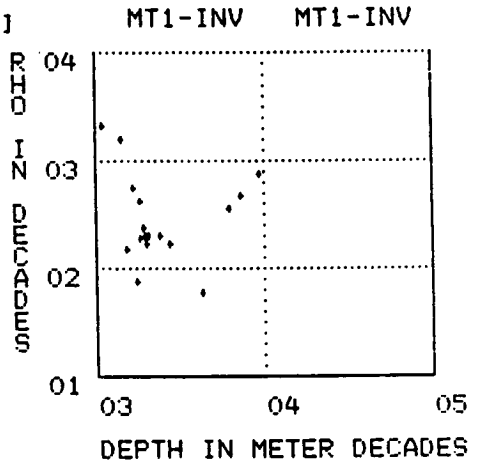

Fig. 3.10- 1D infield modelling. Bostick and Schmucker transformations for the rotationally invariant MT curves (refer to Chapter 7 for details about these transformations).

data sampled at 1s.

Finally in the Edinburgh Department's laboratory, the recorded data were more rigorously scrutinized and the events firstly selected were transferred to EMAS by means of procedures similar to those already described for the SPAM data.

3.3.3 Band 5 measurements

Since stabilization of the non-polarizable electrodes played a very important role in the Band 5 measurements, this system was not operated until there was more or less complete electrode stabilization- normally over 12 hours after installation. All necessary cables were then connected and the system powered. The whole system was left for tens of minutes for the same reasons as described for the Band 4 system. Unlike the Band 4 system however, only the telluric channels required post- amplification. Nevertheless, the same comments regarding the selection of gain settings as made for the Band 4 system also held for the Band 5 system. With a 10s sampling interval, each cassette could store over 60 hours of data. Transfer of Band 5 data to EMAS followed the shorter procedure described for the SPAM data.

3.4 Fieldwork campaigns

The first campaign, held during 3 weeks in late summer 1984, was planned as a preliminary survey. For that purpose, from the proposed 200Km long study traverse (described in the Chapter 1), two geologically distinct areas- Asiago and Cavalese, were chosen to serve as bases for the first set of measurements. A total of 12 stations covering the frequency range 512Hz-0.01Hz (EUIG-SPAM and 2 Band 4 systems) were established in this campaign, 7 of them in the Asiago area and the remaining 5 in Cavalese (see location map in Fig. 3.11). The site numbers, names and codes, along with the UTM coordinates are given in Tab. 3.2. Unfortunately, unexpected problems were experienced during this campaign. The SPAM measurements resulted in a set of unrealistic AMT curves, especially in the Cavalese area. A preliminary analysis of the Band 4 data, which was performed at the fieldwork bases by means of the MINC-11 system, also evidenced a high level of cultural noise at nearly all the sites. This, together with contingencies (equipment failure, livestock, etc) reduced the chance of recording good natural events, and

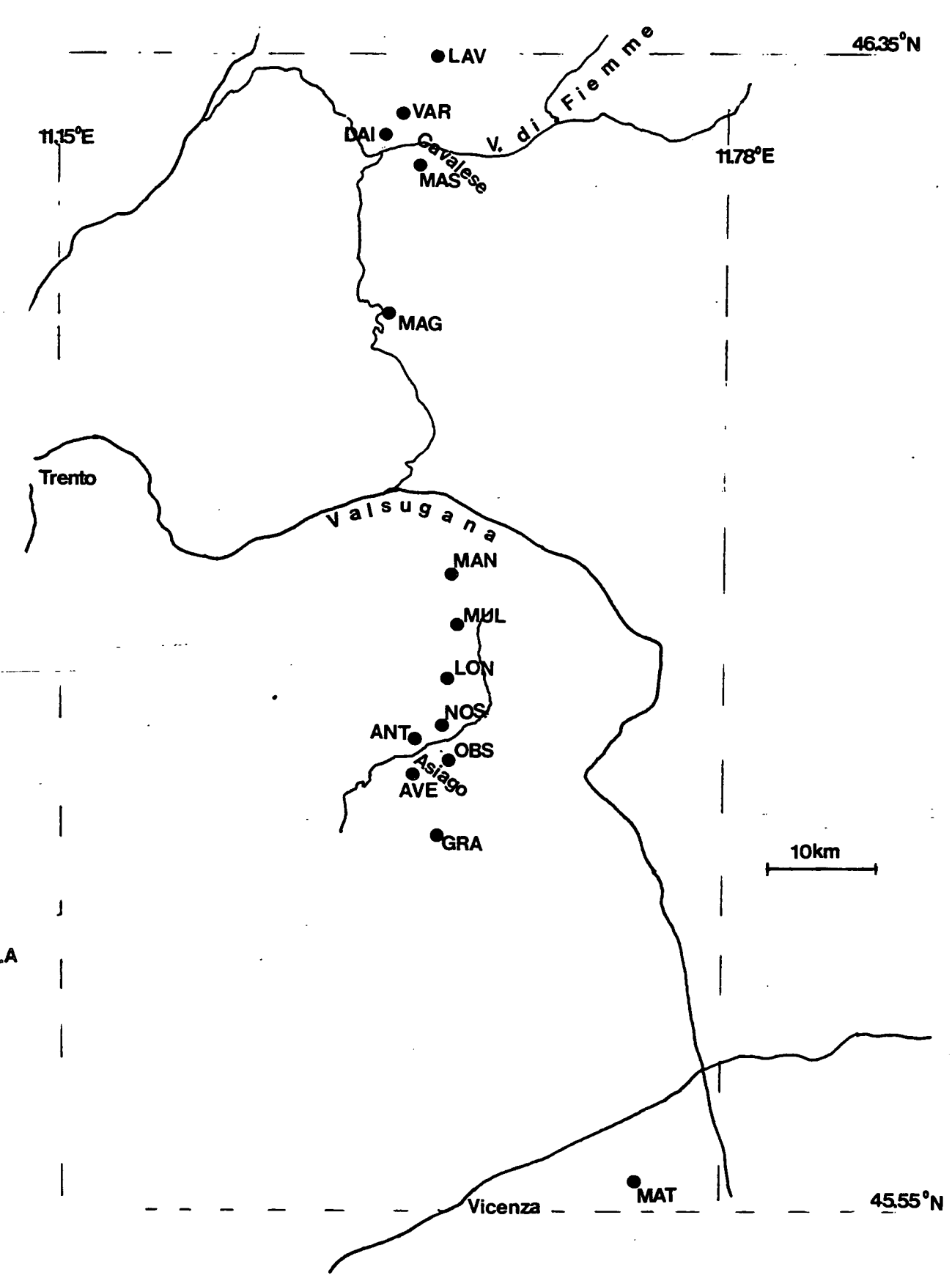

Fig. 3.11- Location map of all MT sites in Northern Italy. The sites, assigned by bold circles, are identified by the code names used throughout this study. The DC rail power substation Ala is assigned by a square.

NUMBER	NAME	CODE	UTM COORD.	SPACING (m)(proj. $N6^0.2E$)
456	Mandrielle	MAN	PR983939	--
454	Campo Mulo	MUL	PR986984	3375
455	Longara	LON	PR984883	5500
690	V.di Nos	NOS	PR963866	7275
450	C.S. Antonio	ANT	PR956865	7575
451	Observatory	OBS	PR973833	10650
453	Ave	AVE	PR951822	11950
452	Granezza	GRA	PR969763	17500

Tab. 3.2 MT sites location.

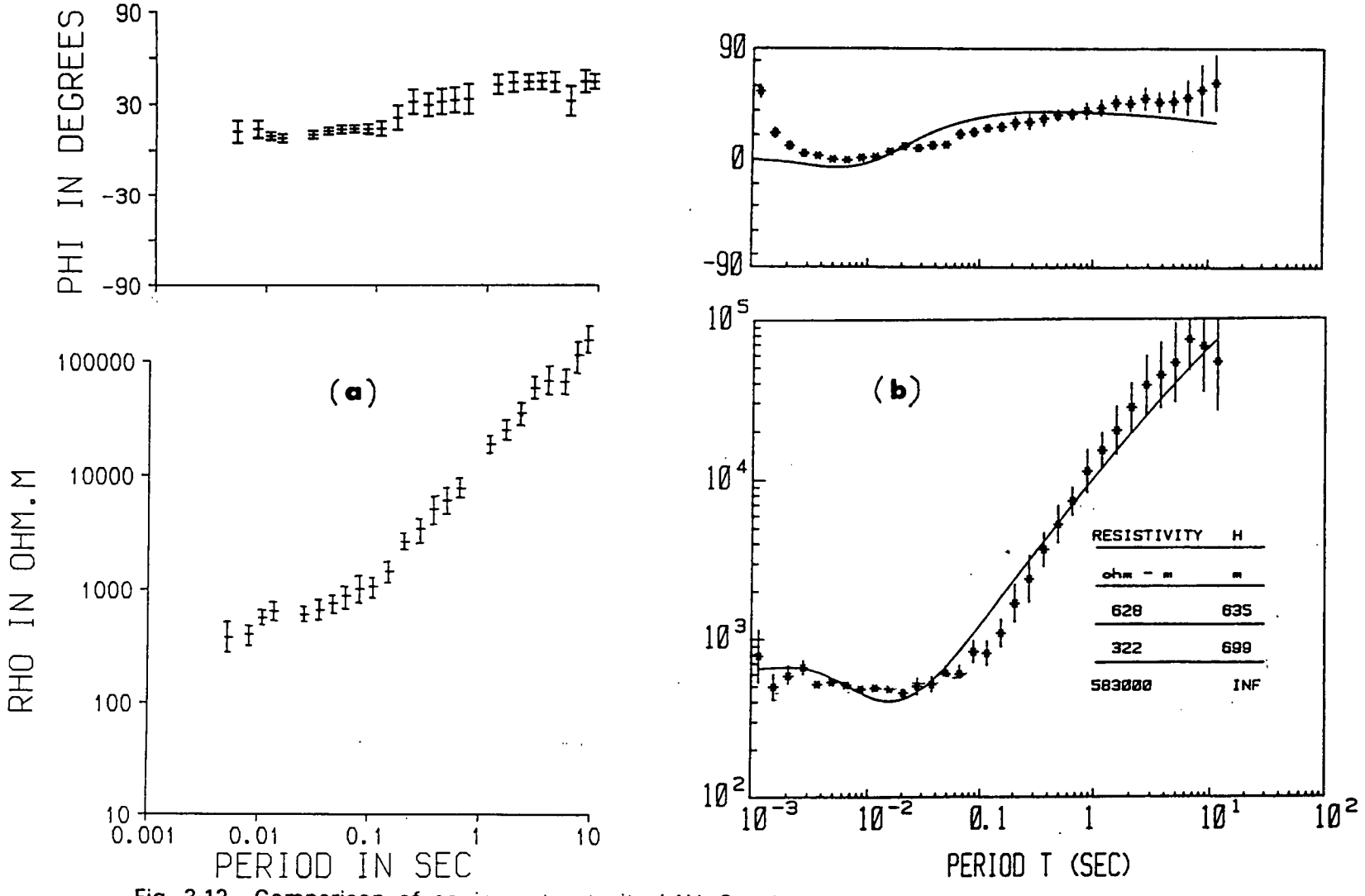

Fig. 3.12- Comparison of equipments at site LAV, Cavalese area. Rotationally invariant curves using EUIG-SPAM (a) and Neuchatel (b) systems. The ρ_a curve obtained by EUIG- SPAM exihibits slightly higher values for longer periods perhaps due to the distinct criteria employed in the data processing. EUIG- SPAM selected windows with predicted coherence > .90 for a minimum of 5 frequencies in each band, while Neuchatel equipment utilizes all the windows and uses the predicted coherences as weights during processing. Note the astonishingly high resistivity value assigned to the bottom layer of the 1D model shown in (b).

consequently, very few good quality MT curves were obtained. These facts considerably changed the subsequent course of the research programme as described below.

The second campaign was of 10 days duration and took place in late June- early July in 1985. This campaign aimed at revealing the source of the noise responsible for the unrealistic MT curves observed in 1984. Researchers from the Observatoire Cantonal- Neuchatel, Switzerland also took part in this campaign. It enabled further equipment checks through simultaneous measurements at LAV using both the Edinburgh and Neuchatel MT systems (Fig. 3.12). A controlled source experiment was planned but could not be pursued due to instrument failures. This would have provided a useful guide to the extent of the distortion. EUIG-SPAM and Band 4 measurements were repeated at three sites (LAV, MAS and GRA) using a variety of criteria for accepting data windows. The main achievement of this campaign was the determination of the main noise source as the Italian DC railway system as discussed fully in chapter 5.

In the third 12-days campaign, in early September 1986, the railway return currents were themselves monitored and NERC-SPAM and Band 5 measurements performed at 3 new sites. Details of the current measurements made at the Ala (see Fig. 3.11) power substation are given in chapter 5. An intended remote reference station located in the Po Valley region (also indicated in Fig. 3.11) was also deployed and is discussed in chapter 6.

CHAPTER 4

DATA PROCESSING AND ANALYSIS

4.1 Introduction

Processing of MT data basically consists of transforming the time-varying geoelectromagnetic fields into response functions embodying the Earth conductivity structure. This problem has been considered by many authors, some of whom are referenced in this Chapter.

For 1D Earth's structure, the Cagniard approach (given in Chapter 2 and expressed in Eqs. (2.17) and (2.18)) is followed. For a more general conductivity distribution, a 2^{nd} rank tensorial response function involving the horizontal magnetic and electric fields is usually adopted. A 3^{rd} rank tensor (i.e. which includes the vertical magnetic field) might also be chosen to express the response function. However, for complex geologic structures it leads to degenerate/ unstable solutions due to the possible collinearity of the magnetic signals, i.e., H_z is not linearly independent of H_x and H_y (Berdichevsky and Zhdanov, 1984; Chave et al., 1987).

The tensorial response function is usually estimated in the frequency domain by means of least square procedures as shown in several publications (e.g. Swift, 1967, Sims et al., 1971; Vozoff, 1972; Hermance, 1973; 1974; Gundel, 1977: Goubau et al., 1978; Kroger et al., 1983; etc). The remote reference technique (Gamble et al., 1979a,b) uses two sets of simultaneously measured signals at distinct sites to correct for bias errors introduced by locally occurring noise. This technique, by reducing the errors in cross and autospectra, is regarded as a major step in improving transfer function estimates in the frequency domain (Fischer, 1982). Time domain estimation of the Earth's response function has also been attempted (e.g. Wieladek and Ernst, 1977; Ernst, 1981; McMechan and Barrodale, 1985), but so far has failed to achieve widespread use. Other unconventional methods of response function estimation make use of the singular value decomposition technique (Jupp, 1978; Park and Chave, 1984) and an eigenstate formulation (Eggers, 1982). The use of robust statistics for estimation of magnetic transfer functions (Egbert and Booker, 1986) and power spectra, coherences and transfer functions (Chave et al., 1987) represents a promising novel trend.

This Chapter presents the theoretical background and the particularities of the frequency domain processing procedure for response function estimates adopted in this study, along with a discussion of the main time series parameters determined and flowcharts of the principal programs used in the implementation of this procedure.

4.2 Transfer function estimations

4.2.1 Single input/single output system– The Cagniard response function

While the MT problem is better defined by a more complex linear system, the single input/ single output linear system is a very useful starting model because it provides a simpler insight into the nature of the bias present in the transfer function estimates when noise is superimposed on the measured signals. The theory which describes this linear problem constitutes the basis for the estimation of the Cagniard response functions. As this theory has been considered in various text books (Jenkins and Watts, 1968, Bendat and Piersol, 1971), only its main aspects are presented in this section.

Consider the general single input/ single output linear system model given in Fig. 4.1(a). The measured input time series is x(t) and the measured output time series is y(t). They represent a stationary random process, where xn(t) and yn(t) are white noise series superimposed on both the noise– free input xs(t) and the output ys(t), respectively. The relationship between x(t) and y(t) can be described by the convolution integral

$$y(t) = \int_0^{\infty} h(\tau)(x(t-\tau)-xn(t-\tau))d\tau + yn(t) \qquad (4.1)$$

where the weighting function $h(\tau)$ embodies the dynamic characteristics of the system. The inferior limit of the convolution integral is set to zero as a condition for the physical realisability of the system. In other words, physically realisable systems can only respond to past inputs so that $h(\tau)=0$ for $\tau<0$. The Fourier transform of Eq. (4.1) is

$$Y = H (X - XN) + YN \qquad (4.2)$$

where the frequency dependence of all components is assumed. Multiplying

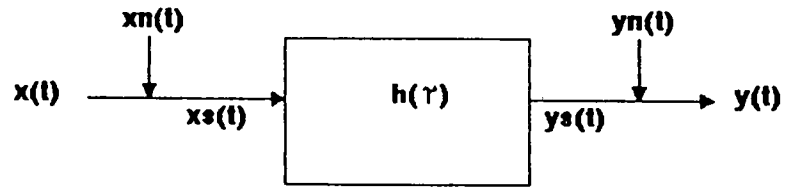

(a)

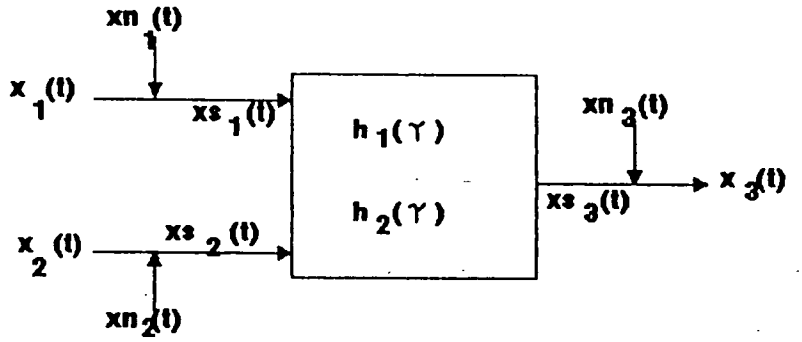

(b)

Fig. 4.1- Types of linear system used in EM studies.
(a)- Single input/ single output system
(b)- Two input/ single output system

Eq. (4.2) by the complex conjugate of the Fourier transform of the measured input series $X^*(f)$ gives

$$S_{xy} = H (S_{xx} - S_{xxn}) + S_{xyn} \tag{4.3}$$

where the S_{ij} are the cross- spectra and the frequency dependence is again assumed. If the random noise series are uncorrelated to each other and with the signals, Eq. (4.3) reduces to

$$S_{xy} = H (S_{xx} - S_{xnxn}) \tag{4.4}$$

Assume now that the measured input signal x(t) is uncontaminated by noise. Eq. (4.4) then reduces further to

$$S_{xy} = H_s S_{xx} \tag{4.5}$$

where H_s is an estimate of the noise- free response function of the problem. However, the parcel of noise on the measured signals is not really known and the response function is always estimated by (4.5). Nevertheless, the effect of noise can be qualitatively assessed if one estimates Eq. (4.5) using

$$H_s = H (S_{xx} - S_{xnxn})/S_{xx} = H S_{xsxs}/(S_{xsxs} + S_{xnxn}) \tag{4.6}$$

Hence, the response function H_s is downward biased by random noise on the input signal. Note that the presence of noise on the output signal does not affect H_s. Alternatively, another estimate of H can be obtained by multiplying Eq. (4.2) by Y^*. This gives

$$S_{yy} = H S_{yx} + S_{ynyn} \tag{4.7}$$

Assuming that there is no noise in the measured output signal, Eq. (4.7) reduces to

$$S_{yy} = H'_s S_{yx} \tag{4.8}$$

Repeating the procedure as above, it can be demonstrated that H'_s is upward biased by noise on the measured output but is unaffected by noise on the measured input signal.

Coherence functions

The level of noise present in the measurements can be assessed by the coherence between the input and output series. The ordinary coherence function is defined as

$$\gamma^2_{xy} = |S_{xy}|^2 / S_{xx}.S_{yy} \qquad (4.9)$$

and is a real quantity. Note that the frequency dependence is assumed throughout. Another less frequently used quantity

$$\gamma_{xy} = S_{xy}/(S_{xx}.S_{yy})^{1/2}$$

is the complex- valued coherency function. The coherence function satisfies the limits $0 \leqslant \gamma^2 \leqslant 1$. For totally correlated signals, this function is $\gamma^2_{xy}=1$. Conversely, $\gamma^2_{xy}=0$, for completely uncorrelated x(t) and y(t) series. The coherence function, like the transfer function, is also biased by the presence of noise on input and/or output series.

Cagniard response functions

Both Eqs. (4.5) and (4.8) can be used to estimate the Cagniard impedances defined in Chapter 2

$$E_3 = Z_{xy}H_2 \qquad (a)$$

$$E_4 = Z_{yx}H_1 \qquad (b) \qquad (4.10)$$

where the indices for the field components i=1,..., 4 stands for $H_x(f)$, $H_y(f)$, $E_x(f)$ and $E_y(f)$, respectively. Analogously, $H_x(f).H_x(f)=S_{11}$, $H_x(f).H_y(f)=S_{12}$, ...etc. Multiplying Eq. (4.9-a) by H_2^* yields

$$S_{23} = Z_{xy}S_{22} \qquad (4.11)$$

or by E_3^*

$$S_{33} = Z_{xy} S_{32} \tag{4.12}$$

From the discussion presented earlier in this section, the estimate of Z_{xy} given by (4.11) will be biased downwards by random noise on the magnetic channel and the estimate given by (4.12) will be upward biased by random noise on the telluric signal. It is generally observed that the magnetic field is frequently less disturbed than the electric field. Therefore, Z_{xy} is usually estimated by (4.11). For the same reason, the estimate of Z_{yx} (Eq. (4.10-b)) is normally given by

$$Z_{yx} = S_{14}/S_{11} \tag{4.13}$$

4.2.2 Two input/single output system- The tensorial impedance

The most general two input/ single output system is well described by Bendat and Piersol (1971,p.147ff). This system is schematically represented in Fig. 4.1(b) and is briefly outlined below. The measured inputs are $x_1(t)$ and $x_2(t)$ and the measured output is $x_3(t)$. All measured signals comprise noise-free components ($xs_1(t)$, $xs_2(t)$ and $xs_3(t)$) and random series ($xn_1(t)$, $xn_2(t)$ and $xn_3(t)$). The expression relating x_1, x_2 and x_3 is given by the convolution

$$x_3(t) - xn_3(t) = \int_0^\infty h_1(\tau)(x_1(t-\tau)-xn_1(t-\tau))d\tau + \int_0^\infty h_2(\tau)(x_2(t-\tau)-xn_2(t-\tau))d\tau \tag{4.14}$$

where the inferior limits of the integrals are zero as in (4.1). The Fourier transform of (4.14) is

$$X_3 - XN_3 = H_1 (X_1 - XN_1) + H_2(X_2 - XN_2) \tag{4.15}$$

the frequency dependence being dropped throughout. The response functions H_1 and H_2 can be estimated in terms of the auto- and cross- spectral functions of the signals as for the single input- single output system. Again the noise series are assumed uncorrelated both to each other and to the signals. Multiplying (4.15) by the complex conjugate of either of the two input series results in

$$S_{13} = H_1 (S_{11} - S_{n1n1}) + H_2 S_{12} \quad (a)$$
$$S_{23} = H_1 S_{21} + H_2 (S_{22} - S_{n2n2}) \quad (b) \qquad (4.16)$$

where the subscript x is dropped throughout (i.e. $S_{13} = S_{x1x3}$, $S_{n1n1} = S_{xn_1xn_1}$, ...etc). Eqs. (4.16) can be solved for either H_1 or H_2. The solution for H_1 is written

$$H_1 = \frac{S_{13}\left(1 - \dfrac{S_{12}S_{23}}{S_{13}(S_{22}-S_{n2n2})}\right)}{(S_{11}-S_{n1n1})\left(1 - \dfrac{|S_{12}|^2}{(S_{11}-S_{n1n1})(S_{22}-S_{n2n2})}\right)} \qquad (4.17)$$

However the noise contribution is not known and the calculated estimate of H_1 is derived from the measured powers.

$$H_1 = \frac{S_{13}\left(1 - \dfrac{S_{12}S_{23}}{S_{13}S_{22}}\right)}{S_{11}\left(1 - \dfrac{|S_{12}|^2}{S_{11}S_{22}}\right)} \qquad (4.18)$$

Therefore, H_1 (and similarly H_2) has an unknown bias error. The noise level of a two input- single output system can be assessed by the multiple coherence (or predicted coherence) given by the expression (Jenkins and Watts, 1968, p.487)

$$\gamma^2_{312} = \frac{S_{11}\,|S_{23}|^2 + S_{22}\,|S_{13}|^2 - 2\,\mathrm{Re}(S_{12}S_{23}S_{31})}{S_{33}(S_{11}S_{22} - |S_{12}|^2)} \qquad (4.19)$$

It can be shown that γ^2_{312} can be expressed in terms of auto- powers of the output noise and signal as (Bendat and Piersol, 1971, p.160-161)

$$\gamma^2_{312} = 1 - S_{n3n3}/S_{33} \qquad (4.20)$$

The predicted coherence is real and also bounded by the inequality $0 \leqslant \gamma^2_{312} \leqslant 1$. Partial coherences can also be defined to express the degree of coherence between one single input (either x_1 or x_2) and the output x_3. Their definitions in terms of ordinary and predicted coherences are

$$\gamma^2_{31.2} = (\gamma^2_{312} - \gamma^2_{32})/(1 - \gamma^2_{32}) \quad (a)$$
$$\gamma^2_{32.1} = (\gamma^2_{312} - \gamma^2_{31})/(1 - \gamma^2_{31}) \quad (b) \qquad (4.21)$$

where $\gamma^2_{31.2}$ is the partial coherence between the input $x_1(t)$ and the output $x_3(t)$, the effect of $x_2(t)$ being removed. $\gamma^2_{32.1}$ is similarly defined.

All coherence functions are biased by the presence of noise. Expressions for estimating the bias in ordinary functions as a function of the number of degrees of freedom (i.e. number of available estimates)are given by Carter et al. (1973). Bias estimates for predicted coherence functions can be found in White (1973). Travassos (1987) has shown that the bias errors for $\gamma^2_{ijk} > 0.85$ are always less than 10% for any number of estimates.

The tensorial impedance

More general Earth conductivity structures are not adequately described by the Cagniard impedance. Two-dimensional or three-dimensional Earth structures are conventionally expressed by the second rank tensorial impedance. The horizontal electric field time variations are given by the convolution of this tensorial impedance with the horizontal magnetic field. Its expression in the frequency domain is

$$\mathbf{E}(f) = \mathbf{Z}(f)\mathbf{H}(f) \qquad (4.22)$$

or in an expanded form as

$$\begin{bmatrix} E_x \\ E_y \end{bmatrix} = \begin{bmatrix} Z_{xx} & Z_{xy} \\ Z_{yx} & Z_{yy} \end{bmatrix} \begin{bmatrix} H_x \\ H_y \end{bmatrix} \qquad (4.22)'$$

The assumed linear coupling between the electric and magnetic field is actually not proven but is widely adopted as a practical tool by MT workers (Rokityanski, 1982). The vertical magnetic component Hz is also assumed to be linearly coupled with the horizontal magnetic components, viz

$$H_z(f) = A(f).H_x(f) + B(f).H_y(f) \qquad (4.23)$$

where the pair (A,B) are referred to as the 'tipper' due to their vertical tipping operation on the horizontal magnetic field. For a purely 1D Earth, the diagonal elements of Z are zero and $Z_{xy} = -Z_{yx}$, i.e. the Cagniard estimates. No 'tipping' occurs in strictly 1D situations and thus A=B=0. It is shown later in this section that if two-dimensional structures are involved, a simple rotation operation for the structural strike direction can be performed and the diagonal elements set to zero. Note that (4.22) represents a combination of two linear systems of type two input-single output. Various methods for solving (4.22) (and by extension (4.23)) have been reported in the literature and a few of them have been reviewed by Hermance (1973). The use of two independent sets of records for estimating the tensor elements has been proposed by Cantwell (1960) and Bostick and Smith (1962) using different procedures. In practice however, measured data inevitably contain errors and a more realistic relationship between E and H is written

$$\mathbf{N} = \mathbf{E} - \mathbf{Z}\,\mathbf{H} \qquad (4.24)$$

where **N** is the total error due to noise in all the channels. Minimization of the mean value of $|N_x|^2$ and $|N_y|^2$ by least squares analysis and cross spectral techniques can be performed either on M independent record sets or an one single record set.

Consider the pair (C,D) representing any two components of the horizontal fields (H_x, H_y, E_x, E_y). Thus, 6 distinct combinations are possible for the pair (C,D). A common choice for (C,D) is (H_x,H_y) (Vozoff, 1972). In this choice the magnetic fields are regarded as noise- free and the noise on the electric signals are minimized. The estimator Z^H representing the tensor elements Z_{xx}, Z_{xy}, Z_{yx} and Z_{yy} is concisely written as

$$Z^H = [\,E\,H\,]\,[\,H\,H\,]^{-1} \tag{4.25}$$

where **[C D]** is the average spectral density matrix for the fields **C** and **D**, defined as by (Jenkins and Watts, 1968)

$$[C\,D\,] = \begin{bmatrix} \langle C_x D^*_x \rangle & \langle C_x D^*_y \rangle \\ \langle C_y D^*_x \rangle & \langle C_y D^*_y \rangle \end{bmatrix} \tag{4.26}$$

where the < > symbol indicates a spectral average either over M independent narrow bands of frequencies (M independent record sets) or over frequency bands with each band including many ,say M, Fourier harmonics (one single record set). Note that the magnetic transfer function (Eq. 4.23) can also be estimated by an identical procedure and the tipper values (A,B) obtained by 3 combinations of a pair (C,D) from the set (H_x, H_y, H_z), again usually (H_x, H_y). Sims et al. (1971) have analysed all 6 possible solutions. They have shown that the two estimates using the pair (E_y,H_x) and (E_x,H_y) are unstable for a 1D Earth or strongly polarized fields. By using arguments similar to those discussed in section 4.2.1 (i.e. by assuming a unidimensional Earth), they have also shown that two estimates -the ones given by the pairs (E_x,E_y) and (E_x,H_x), are biased upwards by noise on the electric field while the two remaining estimates (pairs (H_y,E_y) and (H_x,H_y)- the estimate given by (4.25))- are downward biased by noise on the magnetic channels.

Several bias- reducing techniques have been reported in the literature, probably all of them assuming noise and signals uncorrelated. Sims et al. (1971) have proposed the averaging of the 4 stable estimates as a suitable 'final' estimate. Larsen (1980) has shown that Z must lie between Z^H and Z^E and derived averaged estimates by weighting Z^H and Z^E as a function of both the relative noise level between E and H and the source direction. The use of the geometric mean of Z^H and Z^E and averaging of their associated errors has been suggested by Filloux (1977). Hermance and Pedersen (1980) have proposed either the geometric mean or arithmetic mean of Z^H and Z^E depending on the signal to noise ratio. Elsewhere (Kroger et al., 1983) bias errors have been estimated as functions of the signal-to-noise ratio and of an

interference impedance; the latter is the impedance of the assumed known noise contributions. Kao and Rankin (1977) have described an iterative scheme for reduction of bias errors by assuming that the noise exists in the autopowers only. Under the same assumption, Goubau et al. (1978) have presented two closely related methods in which the impedance element estimates are expressed entirely in terms of crosspowers. However, their methods fail if the Earth is 1D or if the sensors are aligned in the strike direction in 2D situations. Despite such publications of sophisticated methods for tensor element estimation, their estimation through Z^H is probably still the preferred one among MT workers. Analysis undertaken by the author of all possible estimates for the Italian data suggested that this latter estimate was the one with the least scatter. It corroborates both previous Ph.D. studies by the Edinburgh induction group (Rooney, 1976; Jones, 1977; Devlin, 1984; Sule, 1985; etc) and the generally observed fact that the magnetic signals are less affected by noise than the electric signals. It is noteworthy that all the above methods of tensor element estimation tend to suffer from an inherent handicap- the noise in the measured signals is , in the strict sense, not known. Undoubtedly, a major step to circumvent this lack of information has been the proposal of the remote reference technique by Gamble et al (1979a,b). Provided that i) the noise at the measuring station is incoherent with the noise at the reference station and ii) the noise at the measuring station is incoherent (with the measured signals), truly bias- free impedances can be estimated by this technique. Although either the magnetic or the electric signals can theoretically be used remotely as references, the magnetic channels have been more often applied due to their already alluded lower level of noise. Unfortunately, the use of the remote reference technique can be costly as it does requires the simultaneous operation of two sets of equipment and accurate time synchronization between them.

The assumptions underlying the above approaches for estimating Z are data stationarity and a Gaussian distribution of the signals and the superposed random noise. The existence of slowly varying spectra is also an additional requirement for frequency band averaging of the auto- and cross spectra involved in the estimates of Z. These estimates are statistically optimal if the assumptions are fulfilled (Graybill, 1976, p.173ff). However, the presence of a small fraction of non-Gaussian noise ('outliers') in measured data is not

uncommon and may distort the estimates in an unpredictable way. As large amplitude coherent outliers were observed in the Italian data, techniques to reduce their effect on the estimates are discussed in Chapter 5. Estimates of Z which exceeds the mean value by about ± 2 standard deviations are also rejected by the processing software utilized (see section 4.3). Elsewhere (Chave et al., 1987; Egbert and Booker, 1986) the use of robust statistics has been applied to transfer function estimations and related parameters. Their approaches are reported to be effective for data containing up to about 25% of outliers. Rousseeuw (1984) has proposed a robust method, called least median of squares regression, which can account for data 50% contaminated by outliers. This apparently very attractive method has yet to be exploited by MT workers. By using medians and median absolute residuals in place of arithmetic means and standard deviations, a simple robustification scheme has been incorporated in the processing of the Italian data, as presented and discussed in Chapter 5. While there is some controversy regarding which of the robust methods is optimal, there is a general consensus among statisticians that almost any robust method is better than none at all (Chave et al., 1987).

4.3 Telluric transfer functions– Some properties and useful relations

4.3.1 Rotation of the impedance tensor

After Z has been estimated in the original x,y coordinate system, it can be rotated to any other system x′,y′ through an angle θ. This rotation enables the determination of the tensor elements in the direction of the structural strike of a two–dimensional anomaly. The Cartesian rotation matrix R (clockwise direction) is

$$\mathbf{R} = \begin{bmatrix} \cos\theta & \sin\theta \\ -\sin\theta & \cos\theta \end{bmatrix} \tag{4.27}$$

which when applied to Eq. (4.22′) gives

$$\mathbf{E}' = \mathbf{R}.\mathbf{E} = \mathbf{R}.\mathbf{Z}.\mathbf{H} = \mathbf{R}.\mathbf{Z}.\mathbf{R}.^{-1}\mathbf{H}' = \mathbf{Z}'.\mathbf{H}'$$

so that the rotated tensor Z′ is

$$Z' = R.Z.R^{-1} \qquad (4.28)$$

and E', H' are the field vectors in the rotated direction. Note that the loci of the elements of Z' are more generally elliptical. Expanding Eq. (4.28), each element of the rotated tensor can be expressed in terms of the unrotated elements as

$$\begin{aligned}
Z'_{xx}(\theta) &= 0.5[\, Z_{xx}+Z_{yy}+(Z_{xx}-Z_{yy})\cos 2\theta+(Z_{xy}+Z_{yx})\sin 2\theta \,] && \text{(a)}\\
Z'_{xy}(\theta) &= 0.5[\, Z_{xy}-Z_{yx}+(Z_{xy}+Z_{yx})\cos 2\theta-(Z_{xx}-Z_{yy})\sin 2\theta \,] && \text{(b)}\\
Z'_{xx}(\theta) &= 0.5[-Z_{xy}+Z_{yx}+(Z_{xy}+Z_{yx})\cos 2\theta-(Z_{xx}-Z_{yy})\sin 2\theta \,] && \text{(c)}\\
Z'_{xx}(\theta) &= 0.5[\, Z_{xx}+Z_{yy}-(Z_{xx}-Z_{yy})\cos 2\theta-(Z_{xy}+Z_{yx})\sin 2\theta \,] && \text{(d)}
\end{aligned} \qquad (4.29)$$

The principal axis of Z are values of θ which both maximize $Z'_{xy}(\theta)$ and minimize $Z'_{yx}(\theta)$. The values of θ_s satisfying this condition can be calculated by computing Z_{ij} through incremental steps of θ. Alternatively, Swift (1967) has suggested an analytical technique in which θ_s is determined as the value of θ which maximizes the function

$$|Z'_{xy}|^2+|Z'_{yx}|^2$$

Differentiating this expression with respect to θ and equating it to zero results in

$$\theta_s = 1/4\tan^{-1}\frac{(Z_{xx}-Z_{yy})(Z_{xy}+Z_{yx})^*+(Z_{xx}-Z_{yy})^*(Z_{xy}+Z_{yx})}{|Z_{xx}-Z_{yy}|^2-|Z_{xy}+Z_{yx}|^2} \qquad (4.30)$$

For a purely 2D Earth $Z'_{xx}(\theta_s)$ and $Z'_{yy}(\theta_s)$ are zero. This leads to the definition of major and minor apparent resistivities written as

$$\begin{aligned}
\rho_{max} &= 0.2T|Z'_{xy}|^2 && \text{(a)}\\
\rho_{min} &= 0.2T|Z'_{yx}|^2 && \text{(b)}
\end{aligned} \qquad (4.31)$$

The ratio of ρ_{max} to ρ_{min} gives a measure of the anisotropy at the observation site. The anisotropy is obviously 1 for 1D situations and increases as the conductivity discontinuity of a 2D structure is approached.

The degree of anisotropy can therefore be useful as a dimensionality indicator. It can be easily shown that θ_s+90^0 also satisfies (4.30) resulting in possible ambiguous association of ρ_{max} and ρ_{min} with the E-pol and H-pol cases described in Chapter 2. Sims and Bostick (1969) have shown that for a general Earth structure the complex values Z_1 and Z_2

$$Z_1 = Z_{xy} - Z_{yx} \tag{4.32}$$

$$Z_2 = Z_{xx} + Z_{yy} \tag{4.33}$$

are rotationally invariant. Another such invariant is Z_3 given by

$$Z_3 = Z_{xx}Z_{yy} - Z_{xy}Z_{yx} \tag{4.34}$$

Apparent resistivity formulae derived from Z_2 and Z_3 are frequently found in the literature (e.g. Berdichevsky and Dimitriev, 1976; Ranganayaki, 1984). They are written

$$\rho_{i1} = 0.2T\left| \; Z_1/2 \; \right|^2 \tag{4.35}$$

$$\rho_{i2} = 0.2T\left| \; (Z_3)^{1/2} \; \right|^2 \tag{4.36}$$

For 1D inversion either ρ_{i1} or ρ_{i2} are possibly superior to ρ_{max} and ρ_{min} (or ρ_{xy} and ρ_{yx}) because they are unique for each site irrespective of the complexity of the Earth structure.

4.3.2 Polarization analysis

Polarization characteristics can be used to investigate the nature of the source fields, e.g. polarization studies of geomagnetic pulsations are one of the means by which information about the source, the mode of propagation and ionospheric properties can be acquired. Furthermore, transfer function estimates are dependent on the degree of polarization of the electromagnetic signals, as indicated earlier in section 4.2.2 and investigated by Lienert (1980). Polarization characteristics of an electromagnetic field can be obtained through the cross spectral matrix (Fowler et al., 1967; Jones, 1979)

$$J = \begin{bmatrix} \langle J_x^* J_x \rangle & \langle J_x^* J_y \rangle \\ \langle J_y^* J_x \rangle & \langle J_y^* J_y \rangle \end{bmatrix} \tag{4.37}$$

with J representing either the magnetic or electric signals and the matricial notation as in Eq. (4.25). The degree of polarization R is given by the ratio between the polarized power and the total power. The expression for R, in terms of the determinant and the trace of (4.37) is:

$$R = \left(1 - \frac{4 \det [J]}{tr^2[J]}\right)^{1/2} \tag{4.38}$$

For a completely polarized signal, det[J] = 0 and R=1. Conversely, for a completely unpolarized signal, $J_{xy}=J_{yx}=0$ and R=0.

An expression relating the easily misleading concepts of polarization and ordinary coherence (defined by Eq. 4.9) of components of either the magnetic or electric signals is (Jones, 1979)

$$1-R^2 = \frac{4 J_{xx}J_{yy} (1 - \gamma^2_{xy})}{(J_{xx} + J_{yy})^2} \tag{4.39}$$

which assures $R^2 \geq \gamma^2_{xy}$, the equality holding only for $J_{xx}=J_{yy}$.

Time variations in the polarization of both the source magnetic fields H_x and H_y and the electric fields E_x and E_y can be represented by polarization ellipses (Bennet and Lilley, 1972). These polarization ellipses are mutually perpendicular for plane waves diffusing in a horizontally layered homogeneous medium (Kaufman and Keller, 1981). The polarization angle, the direction of the major axis of the field ellipse (counted clockwise from the x axis), for either E or H is given by

$$\Theta = (1/2)\tan^{-1}\{(2 \, Re[J_{xy}])/(J_{xx} - J_{yy})\} \tag{4.40}$$

4.3.3 Dimensionality indicators

A careful study of the geolectrical structural dimensions is an important step towards a meaningful interpretation of MT data. Apart from anisotropy defined in section 4.3.1, a number of other parameters are used in determining the dimensionality of the Earth. These parameters provide means of assessing the predominant dimension of the various individual 1D, 2D and 3D contributions present at the observed site. The appropriateness of presenting them in this Chapter is due to the fact that most indicators make use of the rotational properties of the tensor elements presented in section 4.3.1. Moreover, they are estimated by the processing routines used in this study and described later in this Chapter.

(a) Skew

The most frequently used dimensionality indicator is the skew, which is defined by the ratio of the magnitudes of the rotationally invariants Z_2 and Z_1 (expressed by (4.33) and (4.32), respectively), i.e.

$$S = |Z_2/Z_1| = |(Z_{xx}+Z_{yy})/(Z_{xy}-Z_{yx})| \qquad (4.41)$$

which is therefore a rotationally invariant real quantity. The skew, by definition, is zero for purely 1D and 2D structures as $Z_{xx}=Z_{yy}=0$ in both cases. The skew is thus an indicator of 3D structures. However, the skew is seldom equal to zero both because the existence of a pure 1D or 2D Earth is an abstraction and because noise is always present in actual data. The choice of an upper limit of the value of S for which a real structure can be defined as tridimensional is not clear (Kao and Orr, 1982) and distinct limits have been set by different authors (e.g. 0.4, 0.12 and 0.5 in Reddy et al. (1977), Ting and Hohmann (1981) and Park et al. (1983), respectively). Moreover, the skew is also zero for measurements made on a plane of symmetry of a 3D structure (Word et al., 1971; Ting and Hohmann, 1981).

(b) Tipper

The tipper complex coefficients A and B (the single station vertical magnetic field transfer function) are defined in Eq. (4.23) and are estimated through the procedure detailed in section 4.2.2. The vertical magnetic field transfer functions are also helpful in determining the structural strike direction (e.g. Vozoff, 1972). The magnitude of the tipper is given by

$$T=(A^2+B^2)^{1/2} \tag{4.42}$$

For 1D structures, T=0 as A=B=0 and no 'tipping' of the horizontal magnetic components occur. For a 2D Earth, with strike in the x-direction, A=0. Hence, tipper can be qualitatively used to identify 2D effects. Jupp and Vozoff (1976) have defined the tipper skew as

$$t_s = 2T^{-2}(\mathrm{Re}(A)\ \mathrm{Im}(B) - \mathrm{Im}(B)\ \mathrm{Re}(B)) \tag{4.43}$$

For 2D structures t_s is zero. The quantities T and t_s are rotationally invariant. However. despite their apparent usefulness as dimensionality indicators, the use of these parameters is not frequently reported in the literature.

(c) Eccentricity and ellipticity

The major and minor axes (M_1 and M_2) of the $Z'(\theta)$ ellipse are related to the principal directions θ_0 and (θ_0+90^0) and are given by

$$M_1 = (Z'_{xy}(\theta_0)+Z'_{yx}(\theta_0))/2 \qquad \text{(a)}$$
$$M_2 = (Z'_{xx}(\theta_0)-Z'_{yy}(\theta_0))/2 \qquad \text{(b)} \tag{4.44}$$

The eccentricity of the rotation ellipse can be defined as by Word et al. (1971)

$$\beta(\theta) = (Z'_{xx}(\theta)-Z'_{yy}(\theta))/(Z'_{xy}(\theta)+Z'_{yx}(\theta)) \tag{4.45}$$

where Z'_{ij} are the rotated (through an angle θ) tensor elements. The eccentricity is clearly dependent upon the rotation angle. For a 2D structure, $\beta(\theta_0)=0$. The ellipticity is defined as the ratio of minor to major axes of the rotation ellipse (Word et al., 1971)

$$\beta_0 = \beta(\theta_0) = m_2/m_1 \tag{4.46}$$

so that nonzero values for $|\beta_0|$ may thus indicate tridimensionality. Some MT investigators seem sceptical about the usefulness of β_0 as a 3D indicator (e.g. Hermance, 1982; Beamish, 1986).

(d) Dimensional weights

In an attempt to quantify simultaneously the relative 1D, 2D and 3D structural contributions at an observed site, Kao and Orr (1982) defined a set of three normalized dimensional weights D1, D2 and D3 (and D3') as

$$\begin{aligned} D1 &= |Z_1|/C && \text{(a)} \\ D2 &= |M_1|/C && \text{(b)} \\ D3 &= |Z_2|/C && \text{(c)} \\ D3' &= |M_2|/C && \text{(d)} \end{aligned} \qquad (4.47)$$

where the numerators are previously defined parameters and

$$C = |Z_1| + |M_1| + (|Z_2| + |M_2|)/2$$

(e) Weidelt constraints

Weidelt (1972) has proposed a set of 19 inequalties to be obeyed by the data as a necessary condition for the existence of a 1D model fitting the data. More recently, Weidelt (1986) has taken his arguments further and has proposed a set of 4 inequalities as necessary and sufficient conditions for the existence of a unidimensional model fitting the data. These 4 inequalities are

$$\begin{aligned} &[(h_2/\omega_2 - h_1/\omega_1)/(\omega_2-\omega_1)] < 0 && \text{(a)} \\ &[(g_2 - g_1)/(\omega_2-\omega_1)] < 0 && \text{(b)} \\ &|[(c_2c_1)/(\omega_2-\omega_1)]|^2 < (h_1h_2)/(\omega_1\omega_2) && \text{(c)} \\ &|[(\omega_2c_2-\omega_1c_1)/(\omega_2-\omega_1)]| < g_1g_2 && \text{(d)} \end{aligned} \qquad (4.48)$$

where the indices 1, 2 are associated with two distinct frequencies and c is the Schmucker transfer function (Schmucker, 1970) defined in SI units as

$$c(\omega) = E_x(\omega)/i\omega\mu_0H_y(\omega) = g(\omega)-ih(\omega) = |c(\omega)|\exp(-i\psi(\omega)) \qquad (4.49)$$

The relationship between c and the frequently used impedance Z, apparent resistivity ρ_a, and phase ϕ is

$$Z = i\omega\mu_0c$$

$$\rho_a = \omega\mu_0 |c|^2$$

$$\phi = 90^0 - \psi$$

The dimensionality indicators for the Italian data are discussed in Chapter 6.

4.4 Magnetic transfer functions– Usual presentation

The magnetic transfer functions, defined by Eq. 4.24 and solved as described in section 4.2, are normally presented in form of real (or in-phase) and imaginary (or quadrature) induction vectors (e.g Banks, 1973), where the length of the real vector is

$$((\text{Re } A)^2 + (\text{Re } B)^2)^{1/2} \tag{4.50}$$

and its azimuth is

$$\tan^{-1} (\text{Re } B/ \text{ Re } A) \tag{4.51}$$

Similar expression define the imaginary vector. The real induction vector is much larger than the imaginary vector for large deep conductors but the latter may be large for near surface anomalies (Hutton, 1976). At a particular observational point, the angle θ made by the variation vector with the downward vertical can be expressed as a function of the components of the magnetic field variation of a particular event (e.g. bay, substorm , etc) as (Parkinson, 1962)

$$\tan\theta = (\Delta H_x^2 + \Delta H_y^2)^{1/2}/\Delta H_z \tag{4.52}$$

4.5 Mainframe processing of MT data

The processing of the Italian MT data on EMAS has been performed by the three main FORTRAN programs illustrated in Fig. 4.2. The basic processing routines composing the window analysis and window averaging programs were originally implemented by Rooney (1976). Dawes has written the

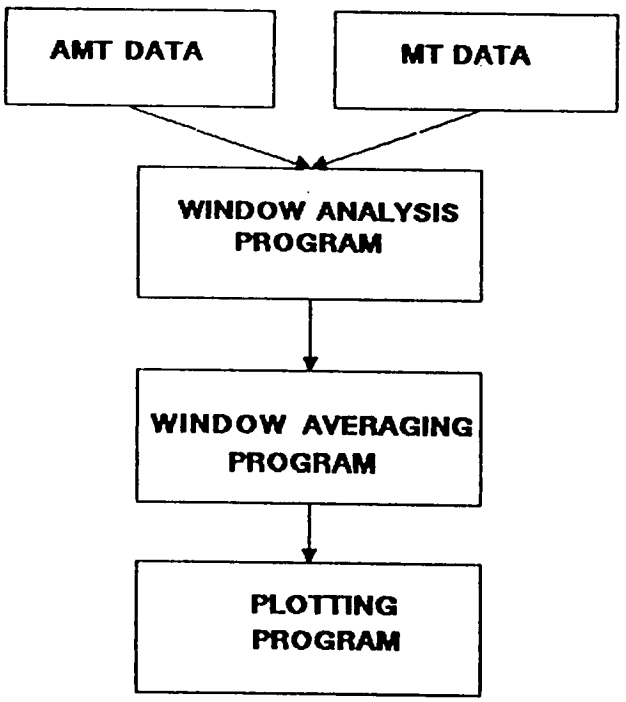

MAINFRAME PROCESSING OF AMT/MT DATA
(MAIN PROGRAMS)

Fig. 4.2- Main processing routines.

plotting program and has introduced a number of modifications to the whole package (e.g. Dawes, 1980), mainly to account for updates made in the hardware, since its initial implementation over 10 years ago. The basic processing is common to all bands (bands 0–5) with minor differences to account for different instrumental response functions and storage data formats. The remainder of this section describes in some detail the most important features of the programs within the standard package. The main software additions made by the author for processing the Italian data are reported in Chapter 5.

4.5.1 The window analysis program

A simplified flowchart of the window analysis program is shown in Fig. 4.3. For convenience of description, the program has been split into its main part and the main analysis routine. The main program has a managing function. It reads in various parameters which provide scaling factors and correction tables. Typical parameters are site number, frequency band, sampling frequency, telluric lengths, etc. Time series events (normally referred to as windows in this study) are read and individually treated by the analysis routine. As pointed out in Chapter 3, these windows are either real–time selected by SPAM MKII (bands 0–3) or visually selected using the MINC/LSI (bands 4–5).

Data reduction and conditioning

Data reduction and conditioning is the first step in the analysis routine. It consists of the following stages:

- The time series have their trend removed. A polynomial of maximum order 2 is fitted to the signals and the residuals are calculated. For AMT frequencies a zero order polynomial (i.e. the mean value) is normally sufficient as no major trend is present. For MT frequencies, a linear trend removal is suitable in most cases.
- Prewhitening is performed if required. However, it is seldom necessary due to the generally random nature of the residuals.
- Normalization performs a scaling by dividing the residuals by its standard deviation. This operation is not fundamental and is useful mainly when comparing spectra from various components.
- Tapering is undertaken to reduce the spectral leakage introduced by estimating the spectra from a finite length of data. The simplest tapering may

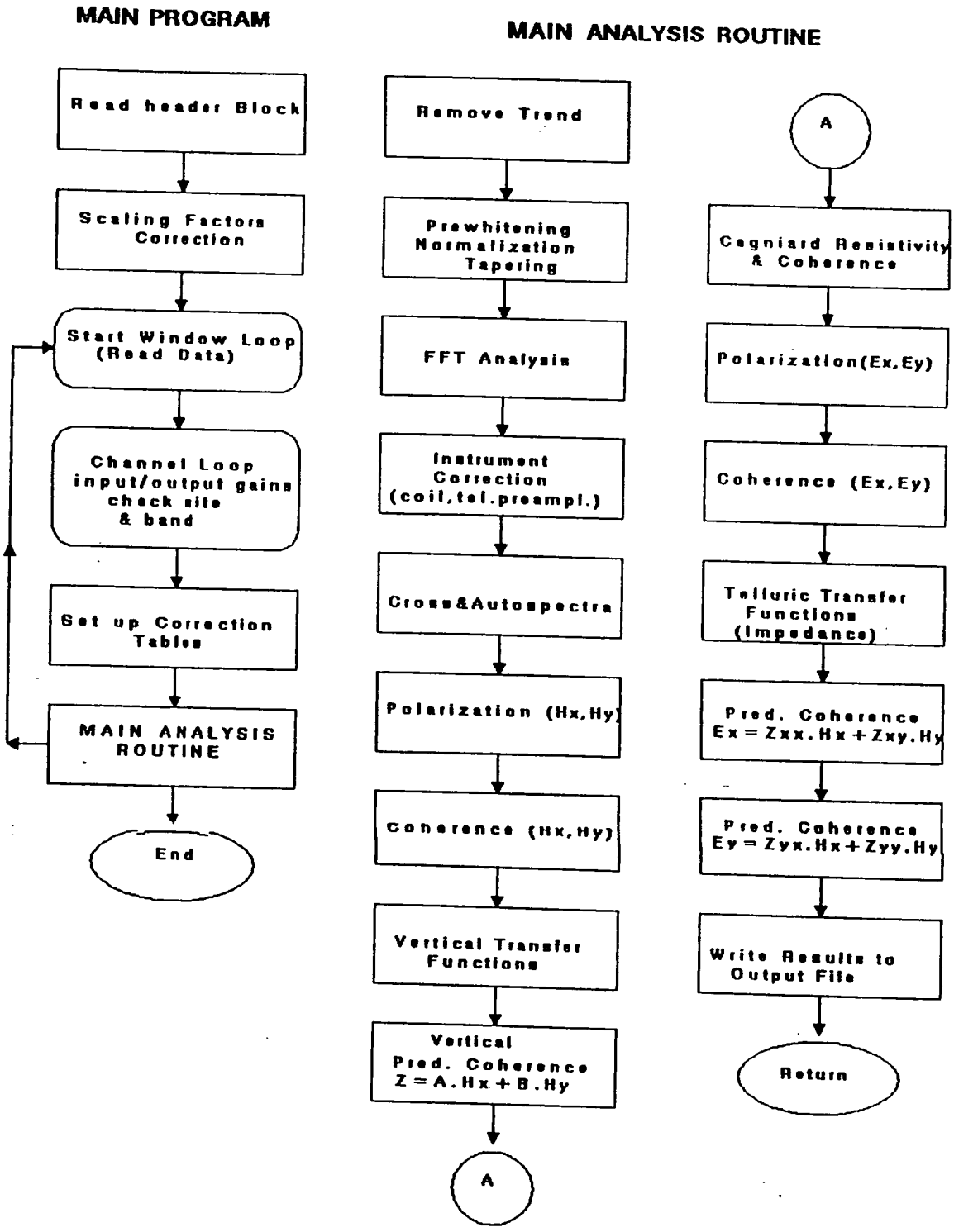

MAINFRAME PROCESSING OF AMT/MT DATA

Fig. 4.3- Simplified flowchart of the window analysis program.

be viewed as a multiplication of a record of length T by a window (observe the different meaning for window in this context) having a rectangular shape. This window is real and its time domain expression is u(t)=1 for $|t| < T/2$ and u(t)=0 elsewhere. It is easily shown that the rectangular window is not a suitable choice as U(w) exhibits side lobes which severely distort the spectra (see for instance Kanasewich, 1985, p.118ff). One remedy is to apply another window which tapers off gradually at both ends of the measured data. Various types of window have been suggested in the literature as reviewed by Harris (1978). Tapering in the present analysis routine is undertaken by a cosine tapered window applied to the first and last 10% of the residuals. The cosine taper window, also referred to as a Tukey window, is expressed for finite Fourier transformation as (Kanasewich, 1985, p.120)

$$u(n) = \begin{cases} 1/2(1 + \cos(\pi(n+L)/K) & -(L+K) < n < -L \\ 1 & -L < n < L \\ 1/2(1 + \cos(\pi(n-L)/K) & L < n < L+K \end{cases} \quad (4.53)$$

where 2L=N is the number of samples and K set to 10% of N.

Fourier Transform, response correction and cross-spectra estimations

The data is Fourier transformed by a routine based on the algorithm of Cooley and Tukey (1965). The harmonics are then corrected for the appropriate instrumental response curves for the magnetic and electric sensor systems. Cross- and autospectra are estimated through the averaging processes described in (4.26) for sub- bands of frequencies within a particular band. The centre frequencies for each sub- band are equi-spaced on a log-frequency scale. The objective of the averaging procedure for each individual record set is the reduction of the variance of each estimate by increasing the number of degrees of freedom associated with the estimate.

Time series parameters and transfer functions estimates

The final step in the routine analysis comprises the estimation of several time series parameters, namely the ordinary and predicted coherences, the polarization of magnetic and electric signals and the magnetic and telluric transfer functions (including the Cagniard apparent resistivity and phase curves). All these estimates are written onto an output file, with no rejection of bad estimates at this stage.

4.5.2 The window averaging program

Cross- and autospectral estimates, transfer functions and coherence results obtained in the first stage are read in by the window averaging program, shown in the flowchart in Fig. 4.4. Before averaging, the transfer functions are scrutinized and the following set of criteria for rejection of bad estimates are employed:

1)- The power rejection test which is aimed at rejecting estimates in which the energy content of the magnetic signals is below a certain level. This level is in general terms dictated by both the instrumental noise and the geomagnetic spectrum, allowing for some seasonal and regional variations. As well known from source field studies, the power level is frequency dependent. For this reason, in this study the set of values (1, 4, 3, 4, 10, 5000) x 10^{-4}nT were chosen for the bands 0-5, respectively. The observed signals power level was generally found to be high and on the average less than 5% of the estimates in the various bands were rejected on the basis of this 'power' criterion.

2)- The coherence rejection test by which each frequency set uses the maximum of the mean predicted coherence and 0.7 as the minimum acceptable predicted coherence. Rejection of data based on coherence levels is a widespread practice among MT workers, but no universally acceptable level is adopted. Some authors use weighted averages instead, with the coherences values (or functions based on them) as weights (Fischer, pers. com.; Stodt, 1983). This latter procedure was attempted for the Italian data, but showed no sign of improvement when compared to estimates based on rejection on coherence grounds; an example in shown in Chapter 5. For the Italian data, coherence estimates exhibited wide variability, and conspicuosly the highest coherence values were normally not related to natural signals, as discussed in more detail in Chapter 5.

3)- The sign rejection test in which the preferred sign of the off-diagonal elements is determined for each frequency set. Only values having the preferred sign are accepted and the tensor elements are averaged under the assumption that they are log-normally distributed (Bentley, 1973). The magnetic transfer function estimates are linearly averaged. The sign rejection criteria is designed mainly to protect the average phase as it avoids tensor elements lying in distinct quadrants in the complex plane.

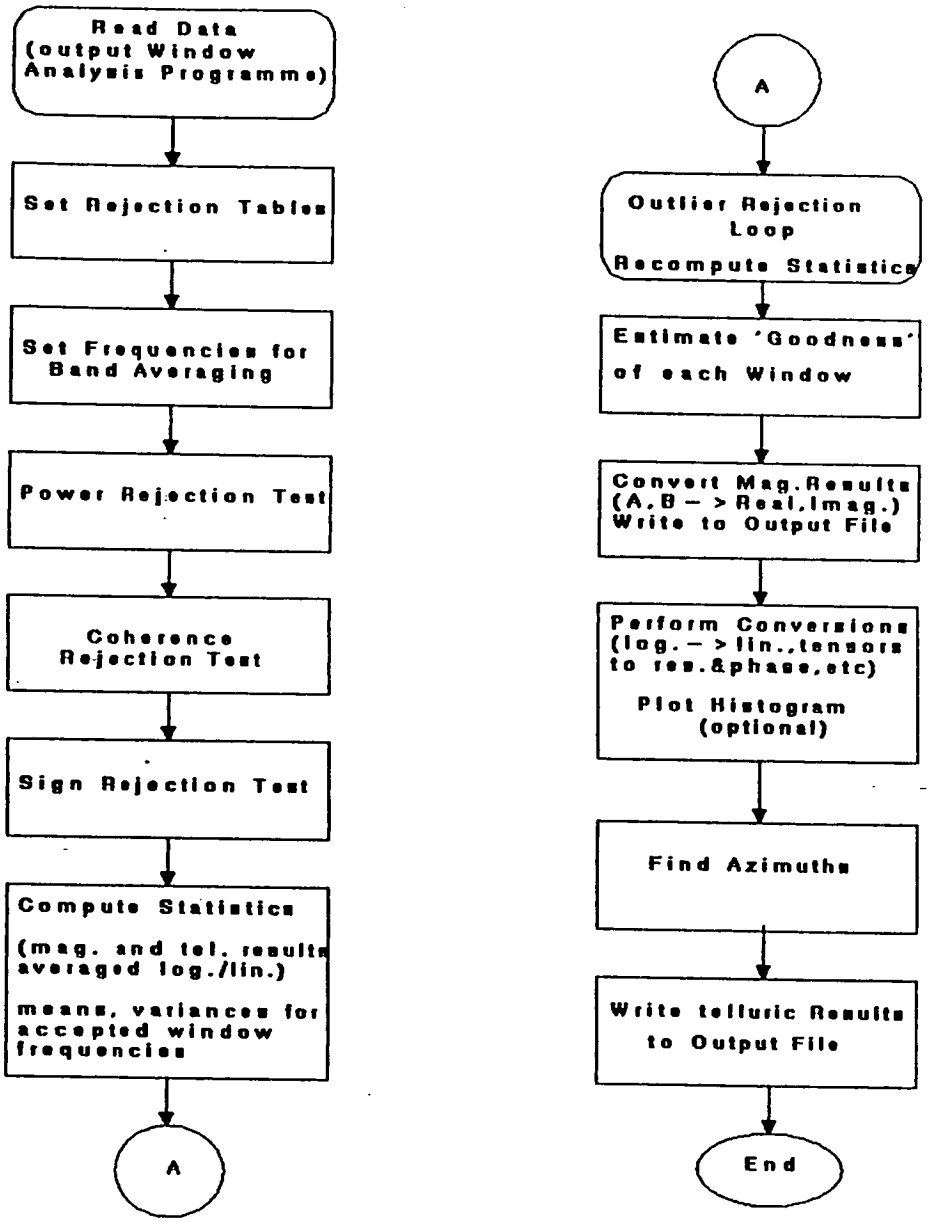

MAINFRAME PROCESSING OF AMT/MT DATA

Fig. 4.4– Simplified flowchart of the window averaging program.

4) The outlier rejection loop test by which tensor elements estimates exceeding ± 2.2 standard deviations from the mean values are rejected and new mean values and errors are calculated for each frequency set. The whole process is repeated once more and the final statistics is thus performed.

In fact, a further constraint was imposed on the 'selection procedure' before performing the final statistics. The selection of frequency sets in the program is made independently for the two orthogonal measurement directions, so that the number of estimates is generally different for each direction. The additional constraint was that only the events selected simultaneously in both directions were considered for the final statistics. This procedure provides a physical constraint when rotating the reponses for determination of the principal directions as the polarization directions involved are internally consistent. In most cases, the enforcement of this latter constraint resulted in minor differences between the new results and the results obtained with the independent selection. However, more pronounced differences could be noted when the number of estimates was very small.

4.5.3 - Plotting programs

The impedance estimates are converted to apparent resistivity and phase curves, with the plotting program utilizing the Calcompics graphic package. The plots comprise the integrated results for all bands for the measurement directions, major and minor directions and the rotationally invariant results. Skew values, the number of estimates and the azimuths are also plotted over the whole frequency range. Other pertinent results such as dimensionality indicators, Weidelt constraints, polarization ellipses, and tensor elements rotated for a particular direction are optionally calculated and plotted. Plots of time-series and cross spectra can also be obtained by other available routines.

CHAPTER 5

NOISE IN MT MEASUREMENTS

5.1 Introduction

Man-made noise can be a major obstacle to the effective application of the MT method in studies of the electrical structure of certain regions of the Earth's crust. Noise can be defined as that portion of the measured electric and magnetic data which is neither induced nor homogeneously induced, and which thus does not fulfil the plane wave assumption required by the magnetotelluric method. The non-induced part can exist in the recordings of both magnetic and electric fields, the noise in the magnetic field being independent of that in the electric field, i.e. incoherent or random MT noise. Noise due to inhomogeneous induction is essentially that of a nearby source (i.e. < 3 skin-depths away) and therefore the electric and magnetic fields are related to each other, i.e. coherent noise. Both categories of noise may occur either singly or in combination, exhibiting variable amplitude and frequency of occurrence, and they may be generated by a great number of sources.

Incoherent noise may sometimes have its origin in the data acquisition system itself, may be caused by moving vehicles which produce magnetic disturbance or arise from natural disturbances such as wind or microseismic activity. Several investigators have assessed the biasing of the transfer function estimations introduced by incoherent noise (e.g. Sims et al., 1971; Goubau et al., 1978; Pedersen and Svennekjaer, 1984). If severe surface distortions are not present, and some care is exercised during acquisition and processing of data contaminated only by random noise in a single site study, one can generally get an interpretable set of resistivity and phase curves.

Coherent noise in MT signals is also due to various sources and the literature concerned with the problems caused by these noise sources is considerable. For example, the noise signatures of various man-made disturbances have been reviewed by Herman (1979). The stray currents observable in the vicinity of DC operated railways and their influence in masking the natural electromagnetic signals have been discussed by Kovaleskiy et al. (1961), Jones and Keller (1966), Chaize and Lavergne (1970), Linington (1974), Yanagihara (1977) ,etc. Besides the railway noise problem,

Adam et al. (1986) have reported on their experience of various other noisy signals in magnetotelluric data recorded in the highly resistive and mountainous Eastern Alps. These include signals from an unbalanced power network and from pipeline anticorrosion currents. A recent comprehensive review of man-made electromagnetic noise sources has been given by Menvielle and Szarka (1986).

Processing of MT signals degraded by coherent noise poses a formidable task as the natural and man-made signals are indistinguishable. With the advent of more sophisticated acquisition systems possessing comprehensive real-time analysis capabilities, a clear indication of the presence of coherent noise may only be noticed after the processing of the data. For example, the apparent resistivity and phase curves obtained may exhibit unrealistic slopes or provide unreasonable Earth's models. Nevertheless, on scrutiny of the original time series the noisy segments or spikes may be located on amplitude considerations, if the noise amplitude is considerably higher than the natural signals. The discussion which follows is restricted to this situation. It is useful to distinguish between two types of coherent noise according to whether it occurs regularly or irregularly.

The general objective of the present study is the assessment of the effectiveness of various digital filtering techniques to remove regular and irregular coherent noise from the recorded magnetotelluric signals. The analysis is performed both on synthetic data and on noisy field data recorded in Asiago and Cavalese. The use of a particular type of noise (from the DC operated railways) as a geophysical tool is also examined. Firstly, an individual description of the main noise sources (man- made and natural) known to MT workers is presented, with particular emphasis to those sources which are known to have handicapped effective MT surveys in Italy. Secondly, the reduction of regular coherent noise by the application of notch and delay-line filters are compared. Thirdly, coherent 'spike' noise signals of regular or irregular character are detected on amplitude grounds and reduced by two distinct approaches. In one, the data set is divided into 'contaminated' and 'uncontaminated' segments and the uncontaminated segments are extended to replace the contaminated segments by means of the maximum entropy method. The second approach assumes that the data set is convoluted with a combination of rectangular windows such that the

contamination by the 'spike' noise is reduced. The resulting spectral distortion is attenuated by a deconvolution operation.

Finally, the set of evidence which has led to the indication of the Italian DC railway network as the main man- made noise source in this study is presented. Then, as an alternative to the digital filtering techniques, the use of this noise source as an exploratory tool is suggested, along with a discussion of the assumptions made, and the limitations and difficulties faced by this attempt.

A final introductory remark is due here. This Chapter has resulted mainly from the fusion of two papers in which the author has participated: Fontes et al. (1987) and Schnegg et al. (1986)- to be referred to as papers 1 and 2, respectively. Paper 1 was initially presented at the 8th Workshop on Electromagnetic Induction in the Earth and Moon, Neuchatel- Switzerland, 1986 and is now in press. This paper made use of noisy data recorded in N. Italy, S. Scotland and Milos- Greece to illustrate the various noise- reduction techniques presented later in this Chapter. In this dissertation, however, the examples have been restricted to the Italian data and an extended discussion of noise sources is presented together with more detailed mathematical derivations. In addition to the procedures discussed in paper 1, a simple robust scheme for estimating the impedance elements and a number of alternative criteria for rejecting frequency sets during processing is reported here. The author, unless otherwise stated, wrote all the computer routines necessary to implement these noise- reduction techniques. Paper 2 resulted from a collaborative study involving the Edinburgh, Neuchatel and Padua MT groups and was also presented at the same Workshop in Neuchatel. The author's contribution to the paper at that time was the application of the MEM extension technique (discussed later in this Chapter) to data contaminated by noise due to the Italian DC railway network. The present study also includes a near- source inversion scheme which differs from that previously proposed in paper 2 by the Swiss authors. The resulting new Earth models, presented and discussed in Chapter 7, seem more reasonable than those previously reported at the Neuchatel Workshop.

5.2 Noise sources in MT

The quality of an MT survey depends by and large on the noise level of the region to be surveyed. It is clear that the concept of noise is intrinsically related to the geophysical method employed, e.g., the natural electromagnetic signals are regarded as noise when probing the Earth by means of controlled source or DC resistivity methods. Noise in MT measurements may be classified in various ways. It is convenient here to classify it according to whether its origin is man- made (cultural noise) or natural (e.g. wind, microseismic activity, topography, etc). Man- made noise can be sensed directly (or possibly indirectly- see Fraser- Smith (1979) for a discussion about magnetospheric current distortions by man- made activities) almost everywhere on the planet, and in particular in highly urbanized Europe. For this reason, a better understanding of the noise source characteristics seems to be vital for a sucessful MT campaign carried out in noisy environments. Additionally, this better understanding might also contribute to the use of the noise sources as an exploratory tool, as shown in previous works (Heinrich and Junge, 1984; Szarka, 1983; Hoogervorst, 1979; etc) and as attempted in this work.

5.2.1 -50Hz (60Hz) from mains and related sources

Noise from electric power transmission lines is by far the most common man- made noise source. Galvanic contact, inductive coupling (and to a lesser extent capacitive coupling) are the main interactions responsible for the propagation of electromagnetic radiation into the Earth. The incorporation of notch filters in the MT acquisition systems is shown to cope perfectly well with any level of 50Hz signal superposed on natural signals, provided that the 50Hz has a pure sinusoidal character and that no systematic fluctuation in the network frequency is observed. However, departure from a purely sinusoidal character seems to be the rule rather than the exception. For moderate levels of contamination by 50Hz of a more general character (e.g. square pulses), the manifestation of odd harmonics can also be filtered out by notches, provided that a sufficient number of notches is available in the acquisition system. The higher the level of the 50Hz disturbance, the larger the number of notches required by the acquisition system. A comparative study of the notch and the delay- line filters in removing the

50Hz signals from both synthetic and field observations is presented in the section 5.3.

A few other types of noise are related to mains power supply. One of them is the so called unbalanced power network (Adam et al., 1986). This type of noise is basically generated by sudden fluctuations in the mains voltage, and is normally associated with major variations in the demand for electricity. The presence of 'TV noise', also reported by Adam et al. (1986) has been observed mainly in band 4 measurements during the Italian fieldwork. It occurs typically at sites near small villages, and predominantly early in the evening.

5.2.2 – Electrified fences, pipeline anticorrosion systems

Noise due to electrified fences has been observed in some sites near farms in Southern Scotland (Paper 1). An artificial signal with repeat frequency of 0.8Hz was present throughout three different recording frequency bands (bands 0, 1 and 2 of the NERC-SPAM system, already described in Chapter 3). Elsewhere a repeat frequency of 2Hz from this same type of noise source has been reported (Menvielle and Szarka, 1986). Non electrified wire fences (and buried pipelines) are also a source of disturbance when they are connected to the ground.

There are two main types of anticorrosion methods applied to pipelines, another man-made source of noise. The first one involves pipelines connected directly (or by means of a rectifier) to rails; the currents that flow will depend on train traffic. The second type of anticorrosion method applies a rectifier supplied from the network, and the current intensity is controlled by a desired voltage difference between the pipeline and the soil (Brasse and Junge, 1984). In Italy, a dominant regular 100Hz coherent noise signal recorded at a site in the Asiago (Fig. 5.1(a)) area fits well the latter description and might be ascribed to a corrosion protection system. Confirmation of this hypothesis is not available. The reduction of this type of noise is discussed in section 5.3.

5.2.3 – DC operated railways

Electromagnetic disturbance due to DC operated railway systems has for long been known by scientists involved with the installation and operation of permanent magnetic observatories. The literature on this is extensive and has been already partially reviewed in this Chapter. A very simple schematic diagram of a DC railway circuit is shown in Fig. 5.2. The power substations A

Fig. 5.1- Examples of coherent noise (regular and irregular) observed in N. Italy- Asiago and Cavalese areas (EUIG-SPAM system).
(a)- Time series for band 0, site AVE.
(b)- Time series for bands 2 and 3, site LAV.
Digitizing rates (freq. sampl.) and cut- off frequencies for bandpass filtering (bandwidth) are indicated for each window.

REGULAR NOISE (a)

FREQ.SAMPL.=2048Hz BANDWIDTH=512-64Hz

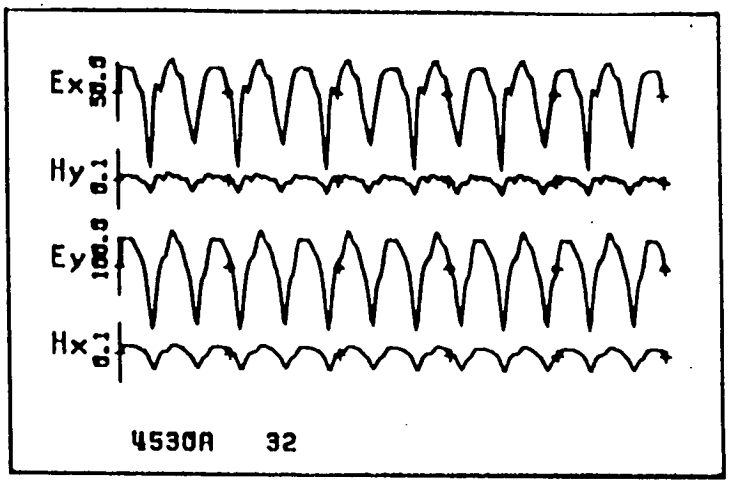

IRREGULAR NOISE (b)

FREQ.SAMPL.=32Hz BANDWIDTH=8-1Hz

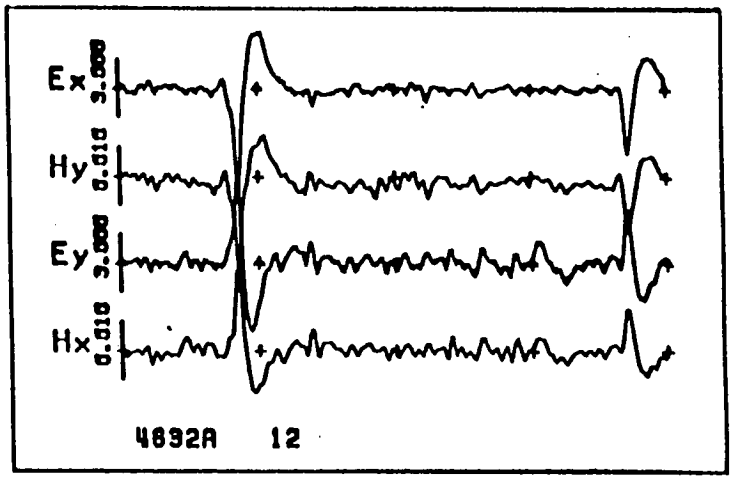

FREQ.SAMPL.=4Hz BANDWIDTH=1-0.06Hz

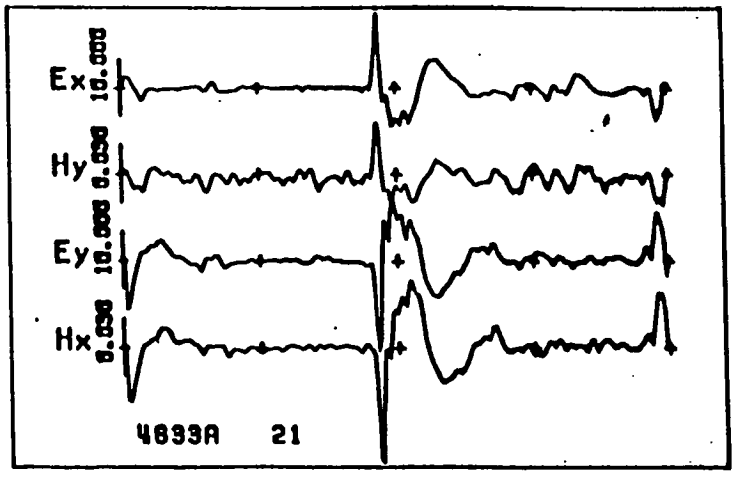

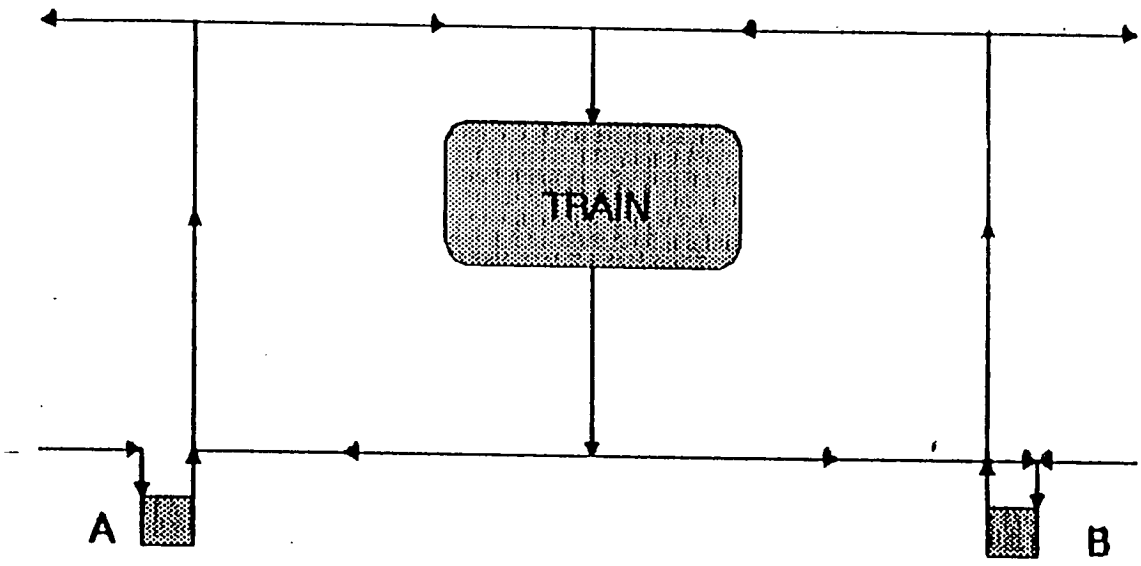

Fig. 5.2– Schematic diagram of a DC railway circuit between two power stations A and B. The arrows indicate the current directions.

and B provide the necessary energy to move the train. The arrows in the diagram indicate the current path. The current is transferred to trains through the catenary and it returns to A and B through the rails. If there were no leakage of current to the ground between A and B, the electromagnetic disturbance would be very localized as the current in the catenary and rails have contrary directions and cancel each other out. However, as rail and ground are at different potential, and insulation is generally not so good, a considerable amount of current may leak into the ground. Strong electromagnetic fields are thus generated, the intensity being generally greater for larger distances between power substations (Yanagihara, 1977). To generate sufficient power to move the trains, large electric currents are normally involved. In Italy for example, the trains run at a relatively low voltage (3000V DC) when compared to the German or Swiss' systems (25000V AC). Thus, the required current is proportionally much larger in the Italian case. Indeed, return currents measurements made at one Italian substation (discussed later in this Chapter) exhibited amplitudes around 1500 A. The extent of the area under the influence of this type of noise is obtained by taking into account the relevant skin- depth. Consider the Italian case again and assume a realistic top resistivity layer of 1000Ωm for the Italian Alps. For a period of 1s, the skin- depth is δ = 50Km. It is well established in the literature (e.g. Goldstein and Strangway, 1975; Sandberg and Hohmann,1982) that a distance of at least 3 skin- depths from any source is required for the plane wave assumption to be valid. In the example given, a distance of 150Km on either side of the railway track would thus be within the near-source zone. Due mainly to its both highly coherent character and irregular occurrence (see Figs. 5.1(b)), the noise from the DC railway network has been the major problem for MT surveys in Italy. The use of this noise as a controlled EM source for electrical conductivity studies in the Italian Alps is discussed in section 5.4.

5.2.4 Wind, microseismic activity, lightning and topography

This section is devoted to some of the most frequently observed noise sources of natural origin. Noise on MT measurements caused by the direct (or indirect) action of the wind on magnetic sensors, electrodes and cables has seldom been described in the literature. Nevertheless, the appearance of this type of noise is easily understood. According to Faraday's law, electric

currents are induced in a conductor moving in a magnetic field. Indeed, vibration in cables and coils introduced by either direct wind or by ground movements due to the wind's action on nearby trees may generate spurious electromagnetic signals observed mainly at frequencies around the 'dead band' ,i.e., around 1Hz (Strangway et al., 1973, A. Jones, pers. comm.). A microphonic noise effect may additionally arise on the cables at metal to metal contacts along the wire (Kaufmann and Keller, 1981).

Noise due to microseismic activity is not well known, perhaps because it is very difficult to distinguish it from the natural signal. This type of noise is expected to occur more often in tectonically active areas, where tectonomagnetic and tectonoelectric effects have been reported (see for instance Johnston, 1987, for a recent review on the subject).

The noise due to microseismic activity bears a close resemblance to that produced by wind. It occurs more often in tectonically active areas, most of the power being again concentrated at frequencies around 1Hz.

The effect of varying topography on MT measurements is well established in the literature and some reference to it can be found in Chapter 7. Electric currents flowing perpendicular to the strike direction (H- pol case) are distorted by topographic features in the region of measurement. The associated resistivity curves are upward biased in the frequency range affected by the topography (as will be shown in Chapter 7). As intuitively expected, the effect of topography is less pronounced the more one moves away from any topographic feature.

These natural noise sources are present everywhere with varying degrees of intensity. An MT survey may prove impossible under severe conditions of wind or microseismic activity since the natural signal may risk being outweighed by noise. However, for moderate levels of activity, the best remedy is to avoid the proximity of deep- rooted trees when choosing a site, and to set coils as far apart as possible. The latter procedure is in the hope that the noise in the magnetic channels may thus be uncorrelated.

Lightning activity, though a major natural source of MT signals as described earlier in Chapter 2, is a source of noise when occurring close to the observational site, i.e. local lightning. Noise signals are introduced mainly into the electric field observations by ground discharge current from direct lightning strikes. Unlike some other natural manifestations, e.g. earthquakes,

lightning strokes hardly ever occur twice at the same location. The varying position of this nearby source will normally produce very scattered MT curves as shown for example, by the MT curves obtained for the site Lavaze on days of visible thunderstorm activity (Fig. 5.3(a)) and fine weather conditions (Fig. 5.3(b)). The two curves differ remarkably, and the results obtained on the day of atmospheric activity exhibit large error bars. It is thus inadvisable to undertake MT soundings under intense nearby thunderstorm activity as the results will be unreliable and the risk of equipment damage is very high.

In addition to a number of man- made noise sources, Alpine topography is shown in Chapter 7 to contribute moderately to the final form of the MT curves. Surface inhomonegeities are also known to distort the MT curves (Berdichevsky and Dmitriev, 1976; Larsen, 1977). An account of this type of distortion in the Italian data is also given in Chapter 8.

5.3 Regular and irregular coherent noise

5.3.1 Regular coherent noise

Usually, MT field data acquisition systems incorporate notch filters which remove the 50Hz (or 60Hz) noise and its harmonics from power-lines with varying levels of success. The main concern here is with the regular coherent noise which was not eliminated during acquisition time. Such noise is highly coherent and since in-field data selection is generally based on minimum coherence levels (Pedersen, 1986), apparently excellent MT responses result as shown later in examples observed in data sets recorded in Italy. To reduce such regular coherent noise, two digital filtering techniques have been used, namely the notch and the delay-line filters.

5.3.1(a) The notch filter

The notch filter is well known to geophysicists involved in the acquisition and processing of data. The outline which follows is based on the discussion by Kanasewich (1985, pp.247-252). The description of its digital formulation may easily be given in the z domain. Let

$$z = e^{-iw} \tag{5.1}$$

Each point on the unit circle $|z|=1$ represents an infinitely long sinusoidal oscillation with frequency $f=w/2\pi$, where w is the angular frequency. The z transform of the notch filter impulse response can be written as

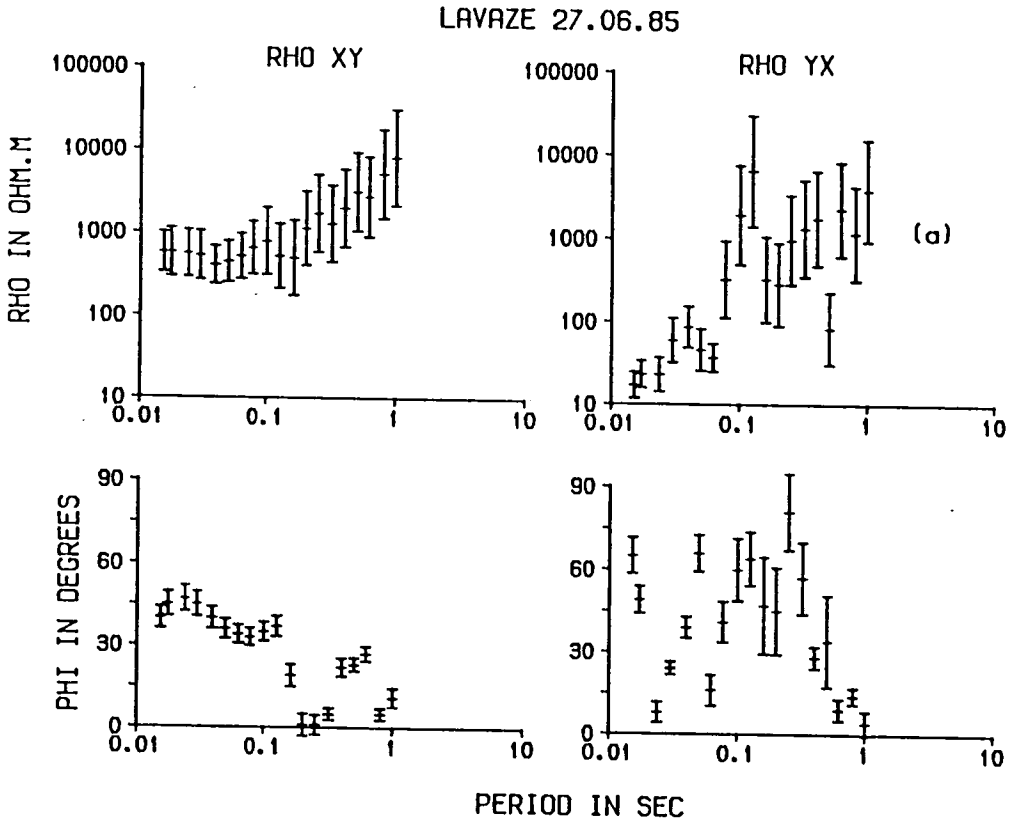

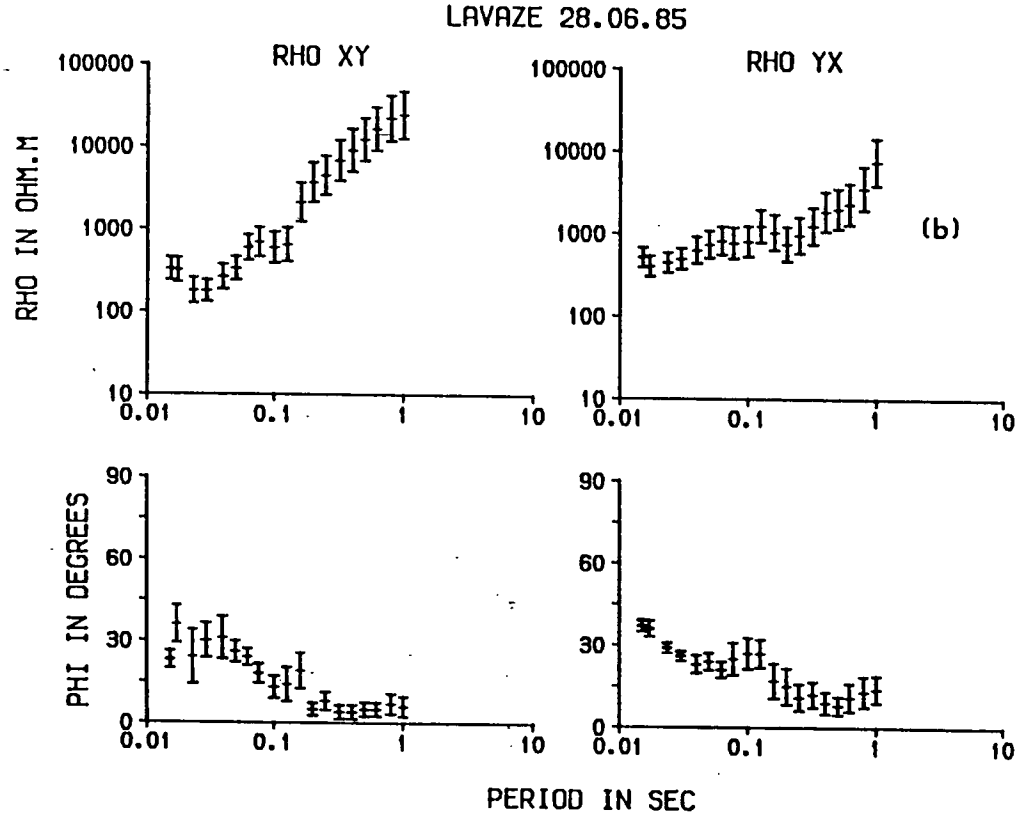

Fig. 5.3- MT curves for P. di Lavaze (LAV) for distinct meteorological conditions.
(a)- Visible thunderstorm activity
(b)- Fine weather

$$W(z) = G\ (z-z_z)(z-z_z^*)/(z-z_p)(z-z_p^*) \qquad (5.2)$$

where z_z is the point on the unitary circle associated with the frequency to be rejected, z_z^* is its complex conjugate. z_z and z_z^* are the 'zeros' of Eq. (5.2). z_p is a point of radius r_p located just outside the unitary circle and z_p^* is its complex conjugate. z_p and z_p^* are the 'poles' of Eq. (5.2). G is a constant for normalizing the filter response gain to unity for a particular frequency, usually the Nyquist frequency.

The value chosen for r_p gives a compromise between sharpness of the filter and length of the impulse response. Thus if r_p is very close to 1 (say r_p=1.001), the filter produces a very sharp cut-off response but it requires a signal of long duration for the filter to become effective. The Fig. 5.4(a) illustrates the response function W(z) for r_p=1.02.

5.3.1(b) The delay-line filter

The delay-line filter (Comb filter) was first applied to MT data by Schnegg et al. (1980). Its impulse response in the Z domain is

$$W(z) = 1 - z^n \qquad (5.3)$$

which has n zeros equally spaced on the unitary circle at locations given by

$$Z_z = e^{i2\pi z/n} \qquad ,z=0,1,2,...,(n-1) \qquad (5.4)$$

Z_0 corresponds to the fundamental frequency to be filtered, e.g. 50 Hz , and $Z_1,...,Z_n$ are all the higher harmonics up to the Nyquist frequency. The corresponding linear difference equation for this filter is

$$y(t)=x(t)-x(t-n) \qquad (5.5)$$

where x(t) is the sampled signal at time t. The desired delay n is the ratio between the sampling frequency f_s (in Hz) and the frequency associated with the signal to be rejected f_r, i.e. n= f_s/f_r.

It is easily verified that W(z) in Eq. (5.3) (see also Fig. 5.4(b)) has variable amplitude with its maximum value reaching 2 at all the frequencies midway between two harmonics (or zeros of W(z)). Fortunately, this undesirable behaviour does not lead to any serious problem when this filter is applied to MT data since both magnetic and electric signals (or their spectra) are affected equally.

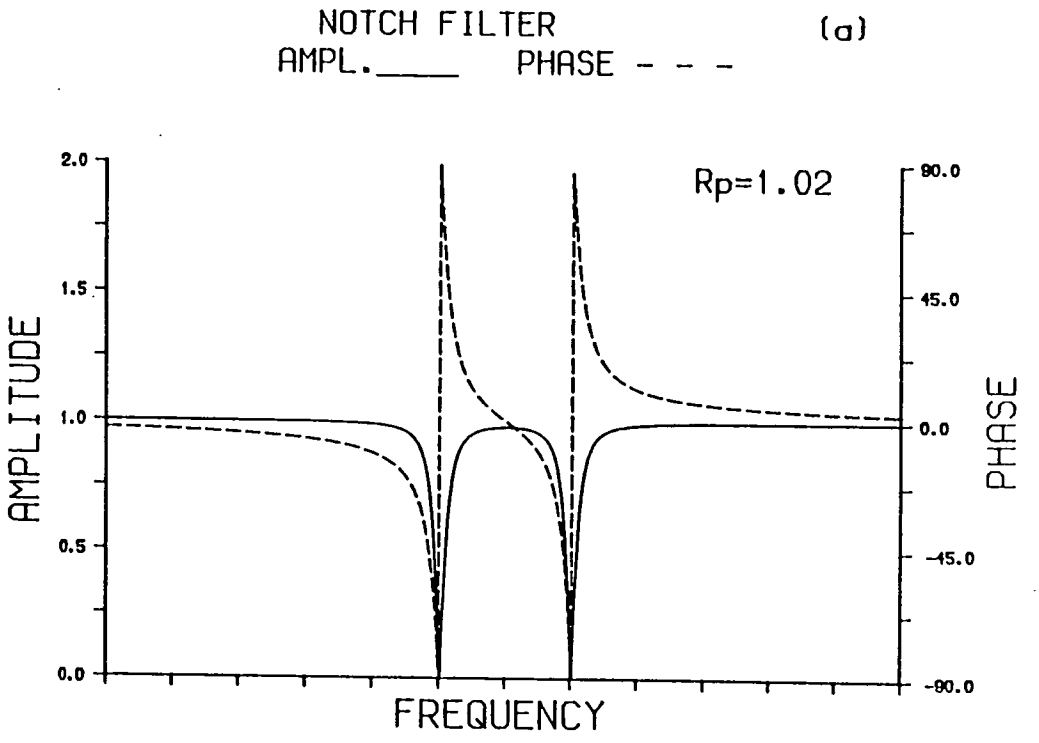

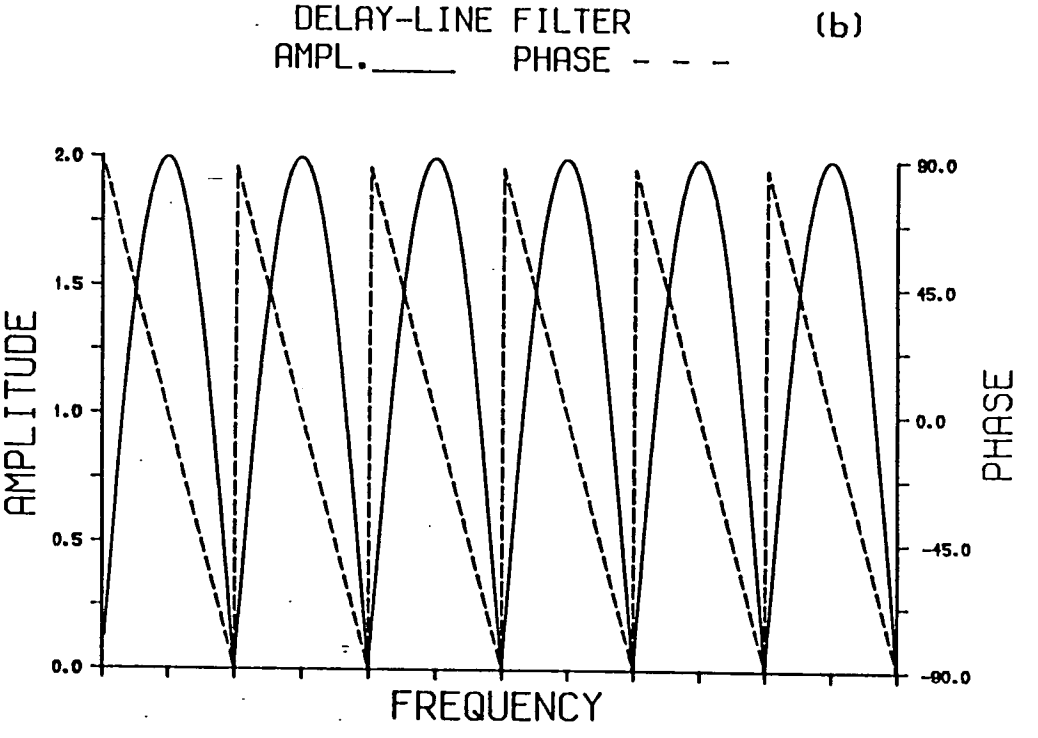

Fig. 5.4- Filter response functions
(a)- Notch filter (amplitude and phase). Minima in the amplitude response (discontinuity in the phase response) occur at ± frequency to be notch filtered.
(b)- delay- line filter (amplitude and phase). Minima in the amplitude response (discontinuity in the phase response) occur at the fundamental frequency to be filtered out and all its higher order harmonics.

5.3.1(c) Applications

A comparison of the notch and the delay-line filtering techniques applied to a synthetic sinusoidal signal sampled at 1/1600s and composed of four unitary amplitude sinusoids of frequencies 100Hz, 219Hz, 375Hz and 563Hz is presented in Figs. 5.5(a)-(c) and 5.6(a)-(b). The signal and its FFT spectrum are given in Fig. 5.5(a). In Fig. 5.5(b) the same signal corrupted by a 50Hz sinusoidal noise of amplitude 4 times that of each individual sinusoid, and its respective spectrum are shown. The same synthetic signal as before, but 'corrupted' by non-sinusoidal noise, and its spectrum are depicted in Fig. 5.5(c). It is shown that unlike the 50Hz sinusoidal noise, the 50Hz non-sinusoidal noise resulted in a spectrum presenting several odd harmonics of 50 Hz. The spectra resulting from the application of both the notch and the delay- line filters to the corrupted signal of Fig. 5.5(b) are shown in Fig. 5.6(a). From these examples, it is clear that the notch filter is more effective in removing pure sinusoidal noise from the data (in this case a 50Hz signal with no harmonics), The delay-line filter on the other hand, may remove along with the noise, valid components of the signal, e.g. the 100Hz sinusoid has been removed in this particular example. In Fig. 5.6(b), the spectra resulting from the application of both the notch and the delay- line filters to the 'corrupted' signal of Fig. 5.5(c) are presented. In this situation the delay-line filter appears to be more effective than the notch filter in removing the non-sinusoidal noise. Note, however, that the 100Hz is again absent and that the spectral components have their amplitudes changed as a result of the variable gain response for the delay- line filter mentioned earlier in section 5.3.1(b).

The application of the delay-line filter to real data is shown in Fig. 5.7(a)-(b). A dominant regular 100Hz coherent noise signal of amplitude greater than 100 mV/Km in the electric channels completely masks the natural signal in data recorded in Asiago (Fig. 5.7(a)). The delay-line filtered data window (256 samples per channel) corresponding to Fig. 5.7(a) is shown in Fig. 5.7(b). The respective rotationally invariant apparent resistivity and phase curves obtained after processing 60 data windows are shown in Fig. 5.7(c). The effect of filtering in the (1/512- 1/64s) band results in better continuity of the MT response with the values found for the undisturbed adjacent frequency band. Besides, the values for the predicted coherence before and after delay-

Fig. 5.5– Synthetic study.
(a) Synthetic example of 'pure' signal (time series and FFT spectrum) sampled at 1600Hz and composed by four unitary amplitude (arbitrary units) sinusoids of frequencies 100Hz, 219Hz, 375Hz and 563Hz.
(b)– Same signal of (a) superposed by a 50Hz sinusoidal 'noise' of amplitude 4 times that of each individual sinusoid.
(c)– Same signal of (a) superposed by a 50Hz square pulse 'noise' of amplitude 4 times that of each individual sinusoid.

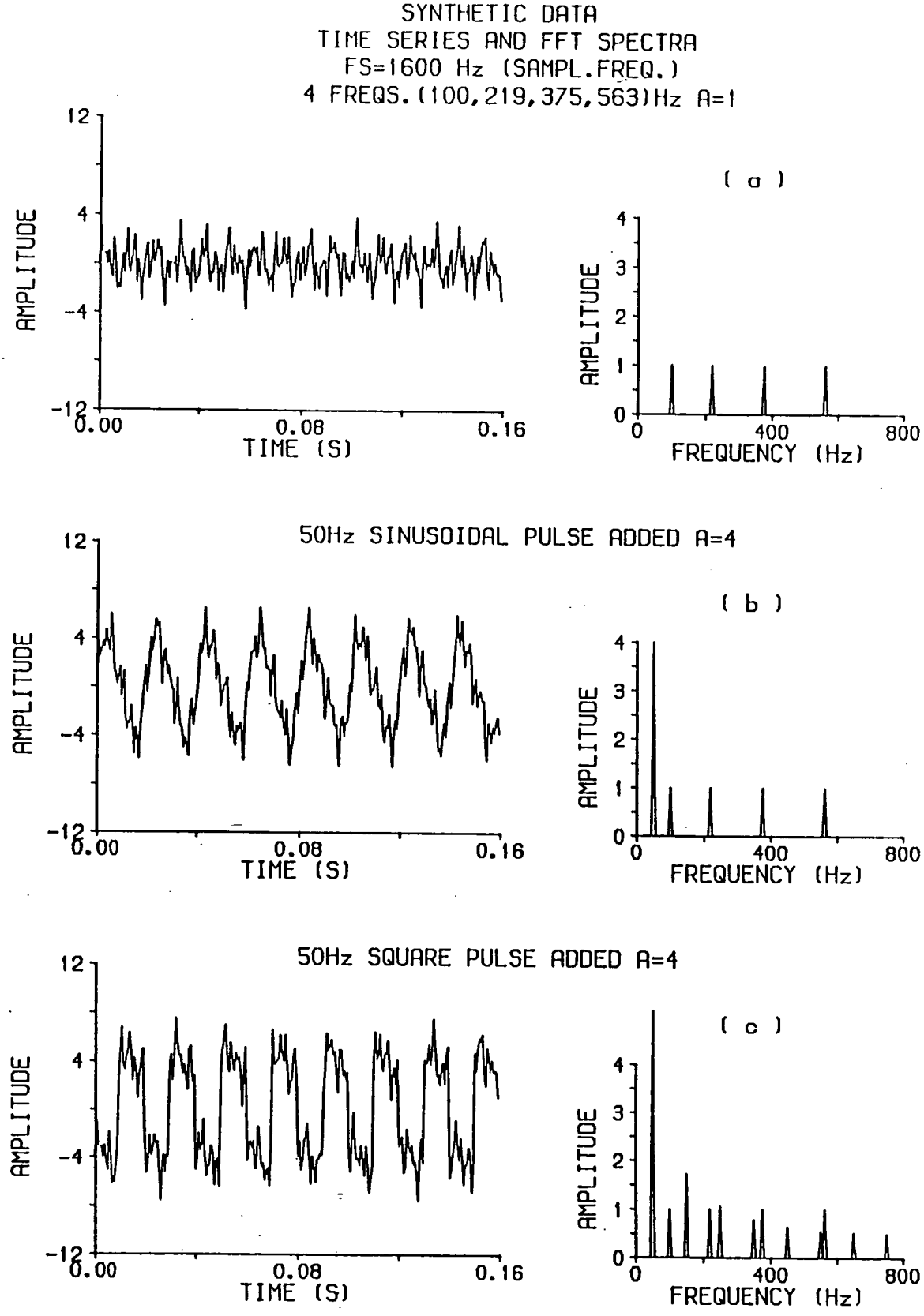
SYNTHETIC DATA
TIME SERIES AND FFT SPECTRA
FS=1600 Hz (SAMPL.FREQ.)
4 FREQS.(100,219,375,563)Hz A=1
(a)
AMPLITUDE
TIME (S)
FREQUENCY (Hz)
50Hz SINUSOIDAL PULSE ADDED A=4
(b)
50Hz SQUARE PULSE ADDED A=4
(c)

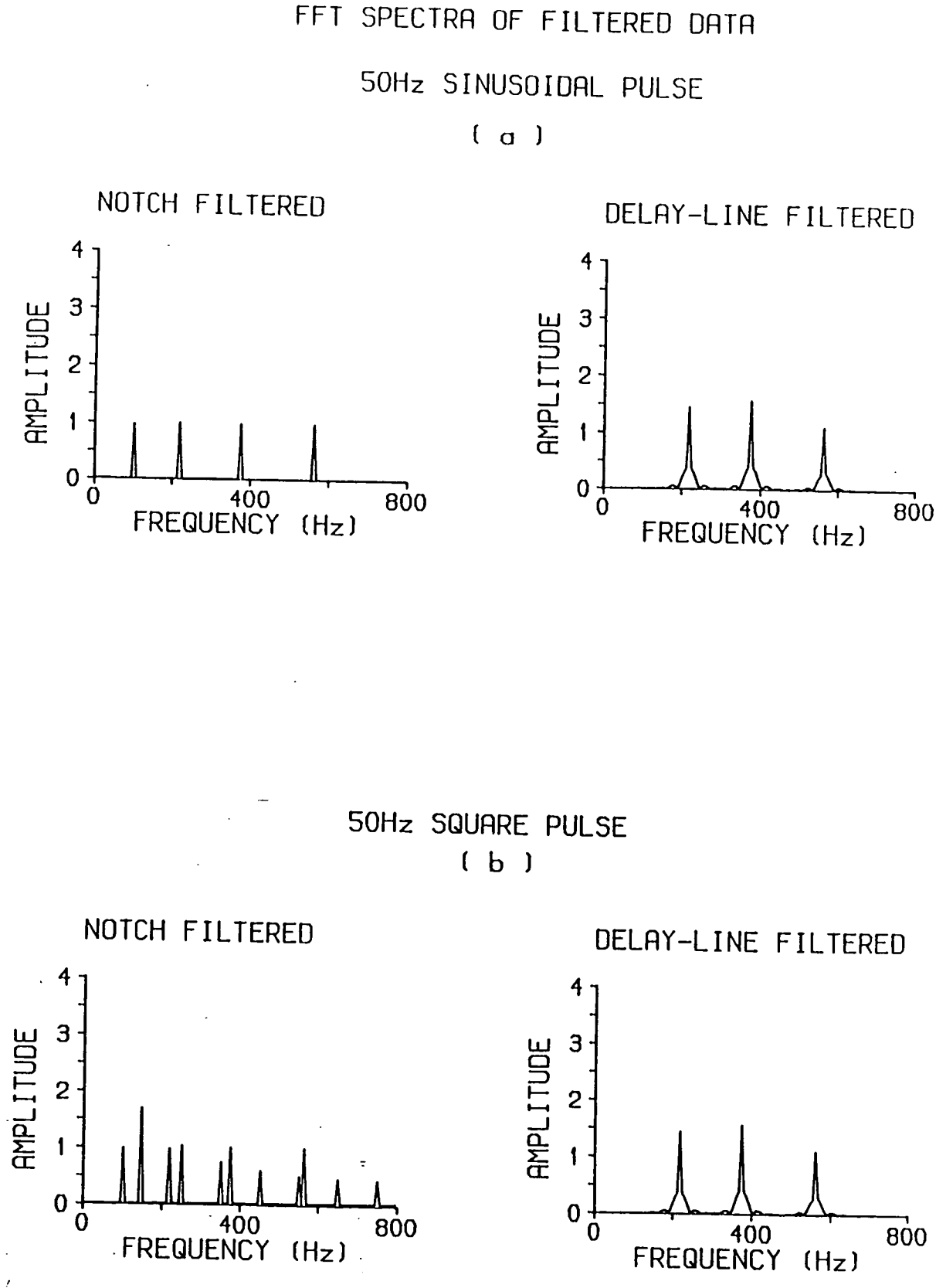

Fig. 5.6- Comparison of digital filtering for 50Hz noise by notch and delay-line.
(a)- FFT spectra of 50Hz sinusoidal 'noise' filtered by notch and delay- line.
(b)- FFT spectra of 50Hz square pulse 'noise' filtered by notch and delay- line.

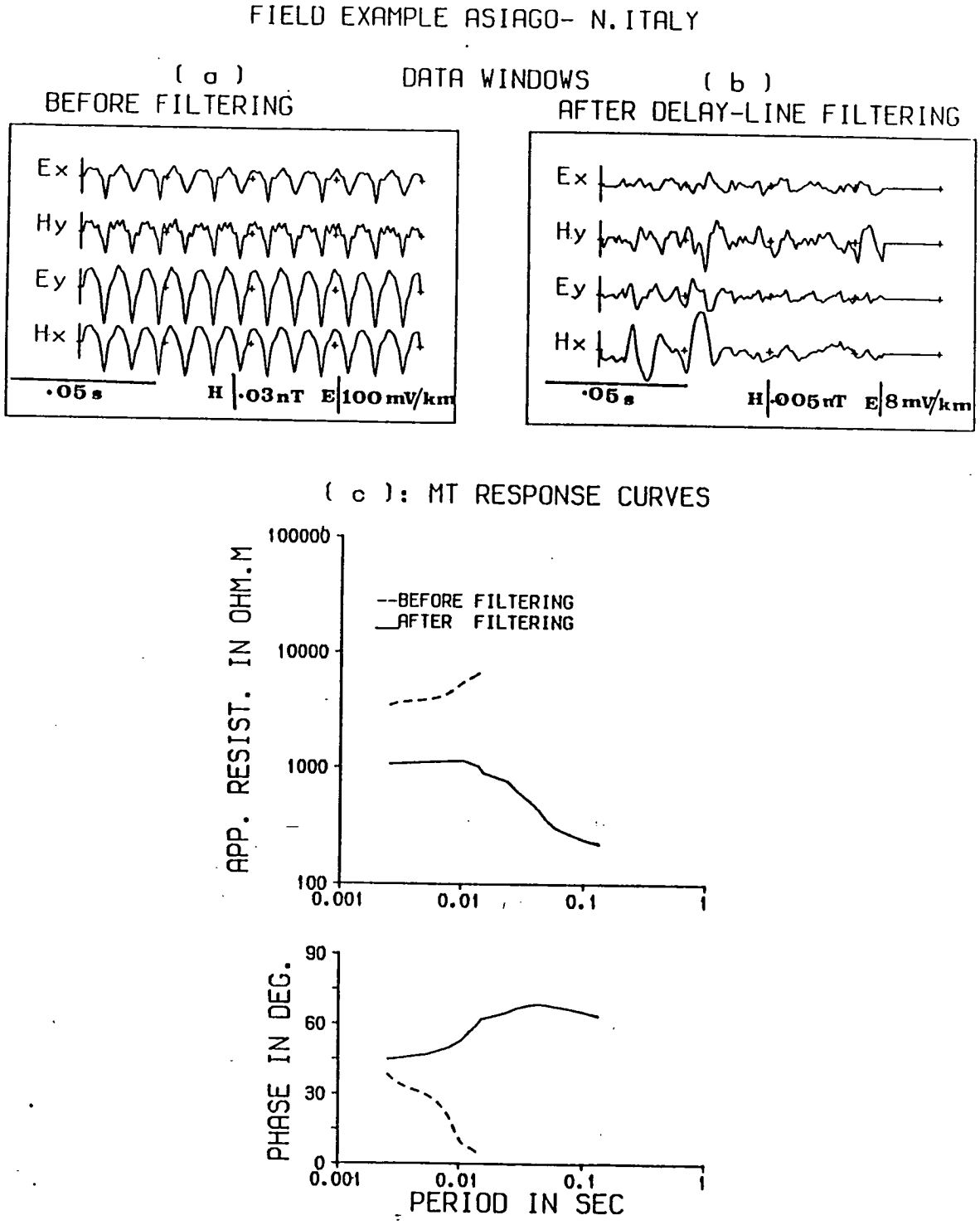

Fig. 5.7- Field example of regular coherent noise on MT data recorded in Ave, Asiago area.
(a)- Magnetic (nT) and electric (mV/Km) signals for a recorded data window.
(b)- Same data window after delay- line filtering. Note the different amplitude scales used for the electric and magnetic signals.
(c)- MT response curves (averaging of 60 data windows) for the invariant before and after application of delay-line filtering (.005s-.01s).

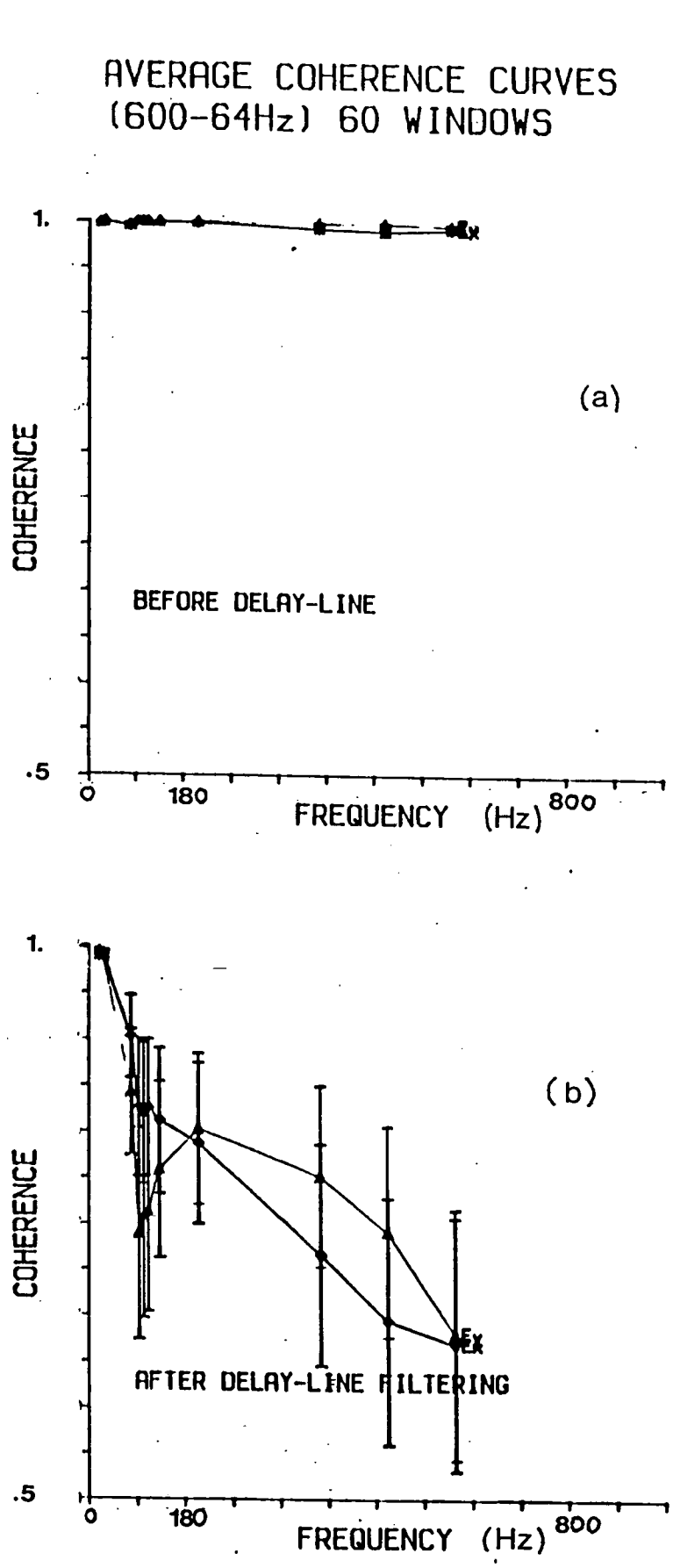

Fig. 5.8- Predicted coherence values before (a) and after (b) application of delay line filtering (same site of Fig. 5.7)

line filtering (Fig. 5.8) suggest that the results would certainly improve even further if the data were delay- line filtered prior to automatic selection.

5.3.2 Irregular coherent noise

Irregularly occurring coherent noise in recorded MT signals is only recognizable if its amplitude exceeds the natural signal. The primary difficulty in this situation is the establishment of a discrimination level between good signal and noise. Whatever the criterion adopted, the detection of noise-contaminated segments of a data window must therefore be based on amplitude levels. In the present study, each data window has been sub-divided insuch a way that 16 partial variances have been estimated and highly coherent segments with unexpectedly high variance values have been disregarded. As gaps result in some data windows, two approaches have been examined for processing these particular data windows- use of the maximum entropy method for extending good data to the rejected segments and use of a window deconvolution scheme.

5.3.2(a) The maximum entropy extension

The maximum entropy method (MEM) was proposed by Burg (1967, 1972, 1975) and since then has been utilized as an important tool in spectral analysis. Its improved spectral resolution compared to most traditional methods is well known, more especially when periods of interest are comparable to data sample lengths. Indeed, the main virtue of the method proposed by Burg is that, unlike the other methods derived from Blackman and Tukey (1949, 1958), no assumption is made for the data structure outside the measured interval. Among all possible spectra, the maximum entropy spectral analysis is based on choosing the spectrum which corresponds to the most random or the most unpredictable time series whose autocorrelation functions (defined later in this section) agree with the known values. In the present study, the potentiality of MEM as a predictive technique is explored. In fact, the potentiality of this technique has already been investigated by Ulrych and Clayton (1976) using synthetic data. Wiggins and Miller (1972) have successfully employed a predictive noise reduction technique, derived from Burg's method, to seismological data. The scheme now proposed differs in some aspects from the Wiggins and Miller technique and the steps necessary for its implementation are outlined here. Consider a non-deterministic time series

s_t , t=1,...,N

Then

$$s_t = \sum_{k=1}^{\infty} a_k e_{t-k} \tag{5.6}$$

is its infinite moving average (MA) representation, where $a_0=1$ and e_t is a white noise process.

Whether or not a_t is a minimum delay wavelet, it is always possible to convert an MA process to an autoregressive process (AR) (Robinson , 1964, 1967)

$$s_t = \sum_{k=1}^{\infty} p_k s_{t-k} + e_t \tag{5.7}$$

the main advantage being that AR parameters are easier to estimate (Ulrych and Clayton, 1976). For practical applications the number of parameters to be estimated must be finite and the forward prediction error (EF) may be written as

$$EF_t = \sum_{k=0}^{M} a_k s_{t-k} , \qquad a_0=1 \qquad a_i=-p_i \ ,i=1,...,M \tag{5.8}$$

and the backward prediction error (EB) as

$$EB_t = \sum_{k=0}^{M} a_k s_{t+k} \tag{5.9}$$

Minimizing the residual sum of squares EF_t^2 (or EB_t^2) with respect to the coefficients a_k's result in the M+1 equations

$$\sum_{k=0}^{M} r(m-k)a_k = \begin{cases} P_M \ ,m=0 \\ 0, \ m=1,2,...,M \end{cases} \tag{5.10}$$

where r is the autocovariance function, with discrete representation given by

$$r(u) = \sum_{t=1}^{N-u} s_t s_{t+u}$$

P_M is the prediction error power in both directions

$$P_M = \sum^{N}_{t=1}(EF_t^2 + EB_t^2) \tag{5.11}$$

The set of Eqs. (5.10) can be solved in several ways. Burg solved them in a recursive way by manipulating the two sets of Toeplitz matrices formed when Eqs. (5.10) are written for two consecutive orders of the AR process, say orders M-1 and M. The coefficients $a_k(M)$ are

$$a_k(M) = a_k(M-1) + c(M).a_{M-k}(M-1) \text{ ,k=0, 1,...,M} \tag{5.12}$$

and P_M is

$$P_M = P_{M-1}(1-c_M) \tag{5.13}$$

where $a_M(M-1)=0$. The value of c(M) in Burg's approach is obtained by minimizing P_M (Eq. 5.11) at each recursive step, with EF_t and EB_t expressed after substitution of Eq. (5.12) in Eqs. (5.8) and (5.9). Unlike their use in the frequently adopted Levinson recursive method (Levinson, 1947), autocovariance estimations are not required and c(M) is expressed by

$$c(M) = -2\sum^{N}_{t=1}EF_t(M-1).EB_{t-1}(M-1)/\sum^{N}_{t=1}[EF_t^2(M)+EB^2_{t-1}(M-1)] \tag{5.14}$$

All the necessary equations required for implementation of the algorithm have been presented. Only the determination of the final order M of the AR process remains to be decided. A number of empirical criteria for choosing the value of M have been proposed (Akaike, 1969a,b, 1976; Parzen, 1976; Wang Ding-yi et al., 1982 ; etc). Among them, the most widely used criterion is the Akaike's (1969) final prediction error FPE given by

$$FPE_m = P_m\ (n+m+1)/(n-m-1) \tag{5.15}$$

The optimal AR order m is then determined by the minimum value of FPE_m for m=1, 2,....

More recently, new algorithms using least squares solutions of Eq. (5.10) have been proposed (Barrodale and Erickson, 1980; Marple, 1980). The author's experience of the Barrodale and Erickson algorithm for computing geomagnetic spectra (Fontes and Figueiredo, 1980, 1981) has indicated that in general it is marginally better than Burg's algorithm but involves extra

computational time. The Burg algorithm has been preferred in this study for both its simplicity and stability relative to these more recent methods.

The noise reduction scheme based on the MEM extension of good segments of a data window comprises the following steps:

(i)- Noise- contaminated segments are rejected, the criterion being a partial variance exceeding 3-4 times the average variance for the particular site;

(ii)- EF_t and EB_t are estimated for the non-contaminated subsets of a data window using the Burg algorithm and the FPE criterion (Eq. (5.15)) for controlling the order of the process M;

(iii)- The gaps in the data window are filled with values obtained by averaged forward and backward predictions;

(iv)- Transfer functions of 'cleaned' data windows are estimated in the frequency domain in the conventional way.

5.3.2(b) The window deconvolution technique

In this scheme the gaps created by the deletion of the noisy segments are not filled, i.e. zero signal level is assumed. It implies that the signal s_t is multiplied by a window W_t

$$W_t = \begin{cases} 1\,, & \text{noise-free data} \\ 0\,, & \text{noise-contaminated data} \end{cases} \qquad (5.16)$$

or in the frequency domain

$$S_w(w) = S(w) * W(w)$$

with power spectra representation

$$PS_w(w) = PS(w) * PW(w) \qquad (5.17)$$

The distortion introduced by W_t can be attenuated by deconvolving $PS_w(w)$ with $PW^{-1}(w)$

$$PS_w(w) * PW^{-1}(w) \qquad (5.18)$$

The inverse $PW^{-1}(w)$ can be calculated by means of a spiking filter operation as described by Robinson (1967). Spiking filter computer routines are listed in Silvia and Robinson (1979).

5.3.2(c) Applications

In Fig. 5.9(a)-(b), the application of both the MEM extension and the window deconvolution techniques for the same synthetic data used in the examples of section 5.3.1(c) are demonstrated. Two distinct levels of contamination by spike noise are considered. The FFT spectrum for the series in which 25% of its length is contaminated by irregularly occurring spike noise is given in Fig. 5.9(a). This figure also shows the FFT spectrum estimated for the time series with spike segments replaced by zeros (the 'zeroed' series) and the spectra obtained after spike removal by the MEM extension and the window deconvolution techniques. Similarly, the results for the 35% contaminated signals are given in Fig. 5.9(b). By comparing the spectra in Fig. 5.9, one can see that the MEM extension technique recovers the FFT amplitudes of the original series (Fig. 5.5(a)) for both levels of contamination. While the window deconvolution technique can recover the peaks amplitudes when compared to the 'zeroed' series spectrum, it does not remove completely the additional noise in other portions of the spectrum.

In Fig. 5.10, the MEM extension and the window deconvolution techniques are compared for field data from Asiago. This comparison suggests equivalent performance. The application of the MEM extension technique to field data from Cavalese (Fig. 5.11) seems to indicate that only part of the noise fraction has been sucessfully removed from this highly disturbed site. The noise in both cases was found to be due to the leakage of currents from the DC electric railway system. This will be justified in section 5.6.

5.4 Robust estimation of impedance elements and other processing/ rejection criteria

This section summarizes a number of procedures designed to tackle the coherent noise problem observed in Italy. All these procedures are exemplified by using one of the most affected data sets recorded in the Cavalese region- the site Lavaze (LAV). This site was chosen both because a great quantity of data has been collected there and because it has served as a test site for a number of experiments and a comparison of instruments (Chapter 3). Furthermore, LAV is a typical site for the entire Cavalese area,

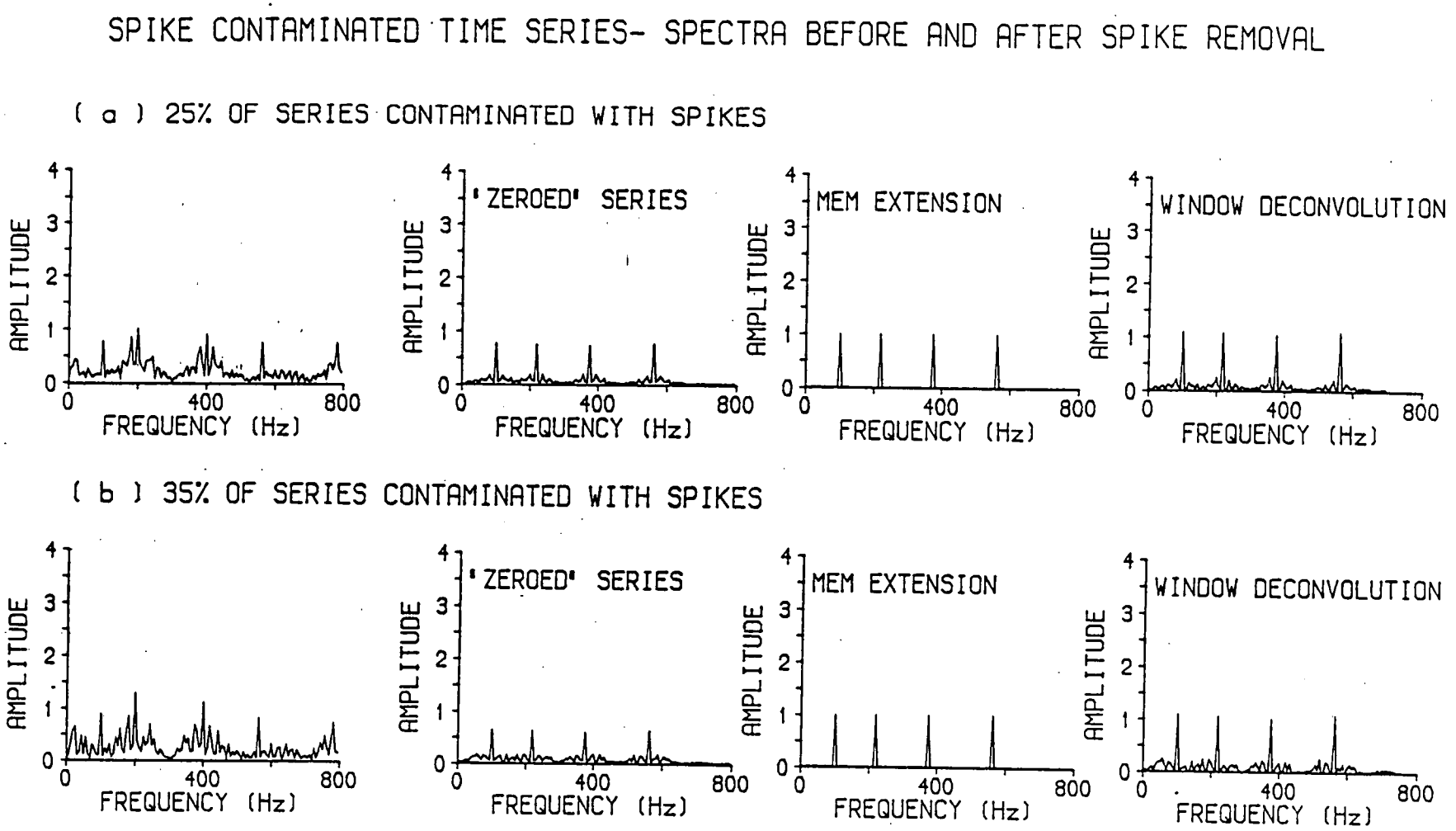

Fig. 5.9- Application of MEM extension and window deconvolution techniques to the same synthetic signal of Fig. 5(a) in which 25% and 35% of its length is contaminated by spike 'noise' signals of irregular occurrence.
(a)- FFT spectrum of spike added time series (25% case), and the FFT spectra after spike removal by 'zeroed' series, MEM extension and window deconvolution techniques.
(b)- Same as (a) for 35% spike noise added.

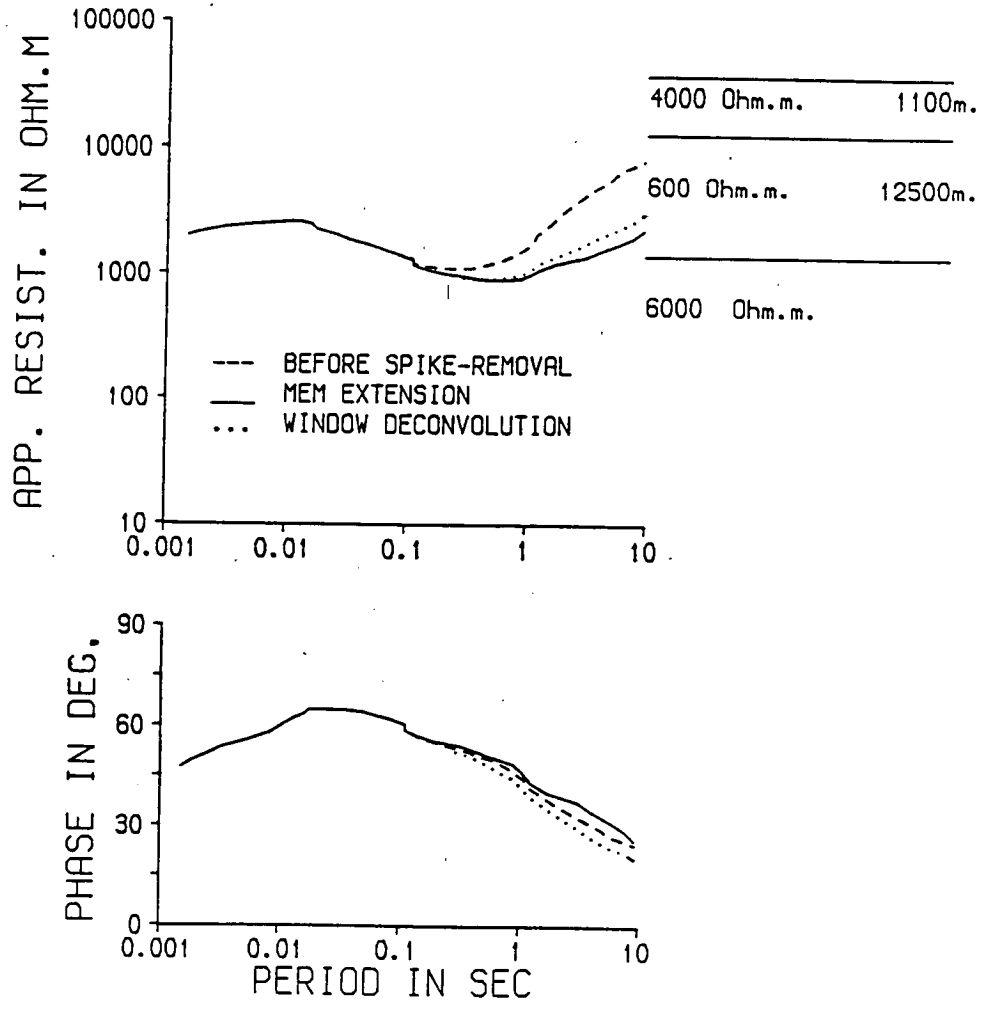

Fig. 5.10- Field results recorded in MAN- Asiago, before and after the application of the MEM extension and window deconvolution techniques: MT response curves and 1D model for the filtered response.

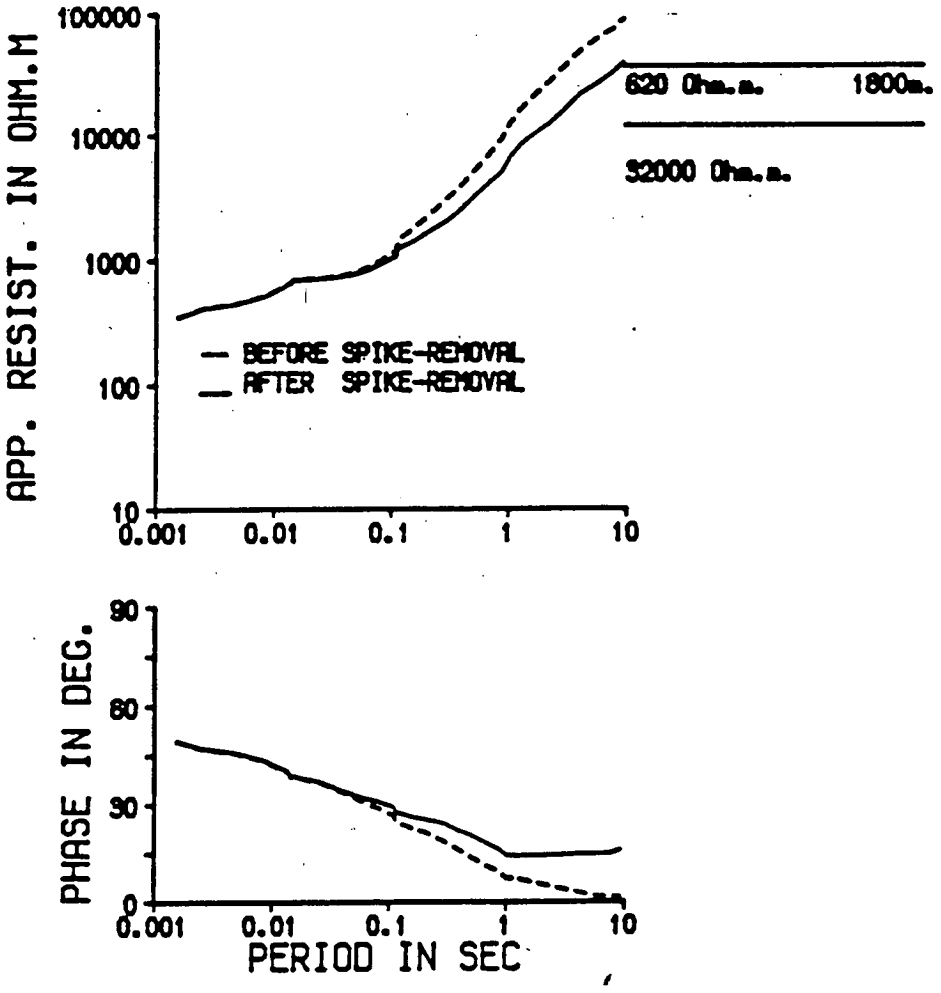

Fig. 5.11- Field results recorded in LAV- Cavalese, before and after the application of the MEM extension technique (0.2s-10s): MT response curves and 1D model for the filtered response.

according to the MT responses obtained in this study (this is shown in full in Chapter 6).

5.4.1 Robust estimation

The use of some statistical parameters to describe the characteristics of a data set are so widespread that it is frequently forgotten that the two well known statistics, sample mean (as an estimation for location) and standard deviation (as an estimation for scale), only characterize samples drawn from a normal distribution. Sample, location and scale are common statistical jargon.In the context of time series analysis, sample can be defined as a measured finite set of a continuosly varying physical process; location expresses the average value of a sample and scale is the measure of dispersion around the location. For normally distributed data (sample), the mean and the variance are the best estimators of location and scale, respectively. In the case of data sets that are either non- normally distributed or that contain outliers, these estimators can be very biased, as illustrated in various statistical textbooks (e.g. Hampel et al., 1986, Rousseuw and Leroy, 1987). Therefore, both the prior knowledge of the distribution followed by the data and the use of statistics which do not produce estimates that are overly influenced by a small number of outliers- the so called robust statistics, is recommended. These statistics are robust in the sense that they are not optimal for any particular distribution, but are resistant to the presence of a number of outliers in the data set. MT data is believed to be log- normally distributed (Bentley, 1973), but by no means free from contamination by outliers. By assuming in principle that the coherent noise in Italy has an outlier character, it seemed worthwhile to verify whether the application of simple robust statistics would cause any improvement in the curves observed in the Cavalese area. The main motivation comes from the fact that the filtering techniques described in the earlier sections of this Chapter have shown very limited success when applied to curves from Cavalese.

A general class of robust estimates for location is often referred to as a trimmed mean. An expression for the α- trimmed mean is

$$x_\alpha = \begin{cases} 1/(n(1-2\alpha)[\sum_{k+2}^{n-k-1} x_i + (1-k-n\alpha)(x_{n+1} + x_{n-k})] & \\ & (\text{for } k+2 \leqslant n-k-1) \\ 0.5(x_{k+1} + x_{n-k}) & (\text{otherwise}) \end{cases} \qquad (5.19)$$

where

(i) α ($0 < \alpha < 0.5$) is the fraction of the observation trimmed at each end of an ordered data set $x_1, x_2, \ldots, x_k$;

(ii) $k=n\alpha$ is the largest integer $\leqslant n\alpha$.

As special cases trimmed means include the extremes values of α, i.e. the ordinary arithmetic mean ($\alpha=0$) and the median ($\alpha=0.5$). The choice of α is dependent on the degree of protection against outliers one requires. As a robust estimate of scale, the median absolute deviation (MAD), is the counterpart of the median as the most robust estimator for location, and is defined by

$$\text{MAD} = \text{median} \left| x_i - \text{median}\,(x_i) \right| / c_{\text{MAD}} \qquad (5.20)$$

where c_{MAD} is a normalizing factor to make MAD a bias-free estimate of the standard deviation (Kleiner and Graedel, 1980). For a large number of estimates, $c_{\text{MAD}} = 0.6745$. Both median and MAD were used in this study in the averaging stage of the tensor elements estimates and error bars, respectively. In Fig. 5.12, the results of this procedure are compared against the standard processing for the data set measured in LAV. It can be observed that the the results for both techniques do not exhibit any appreciable difference, which in turn suggests that the DC railway noise signals cannot be considered as outliers, i.e. they are not a small fraction of the data. As further evidence of the latter statement, the median and the arithmetic mean values in this example were found to be in very close accordance and the distribution of the estimates for various frequency sets has shown no pronounced skewness and exhibited a fairly normal (phase curves) / log-normal (ρ curves) character. These results, though based on very simple robust techniques, are nevertheless useful in that they suggest that even more sophisticated robust techniques may not succeed in this situation. In any case, it appears to the author that the least median of squares method - LMS (Rousseeuw, 1984) should be adapted to the MT problem and applied to the Italian data. Rousseeuw's method is proven to be resistant to up to 50%

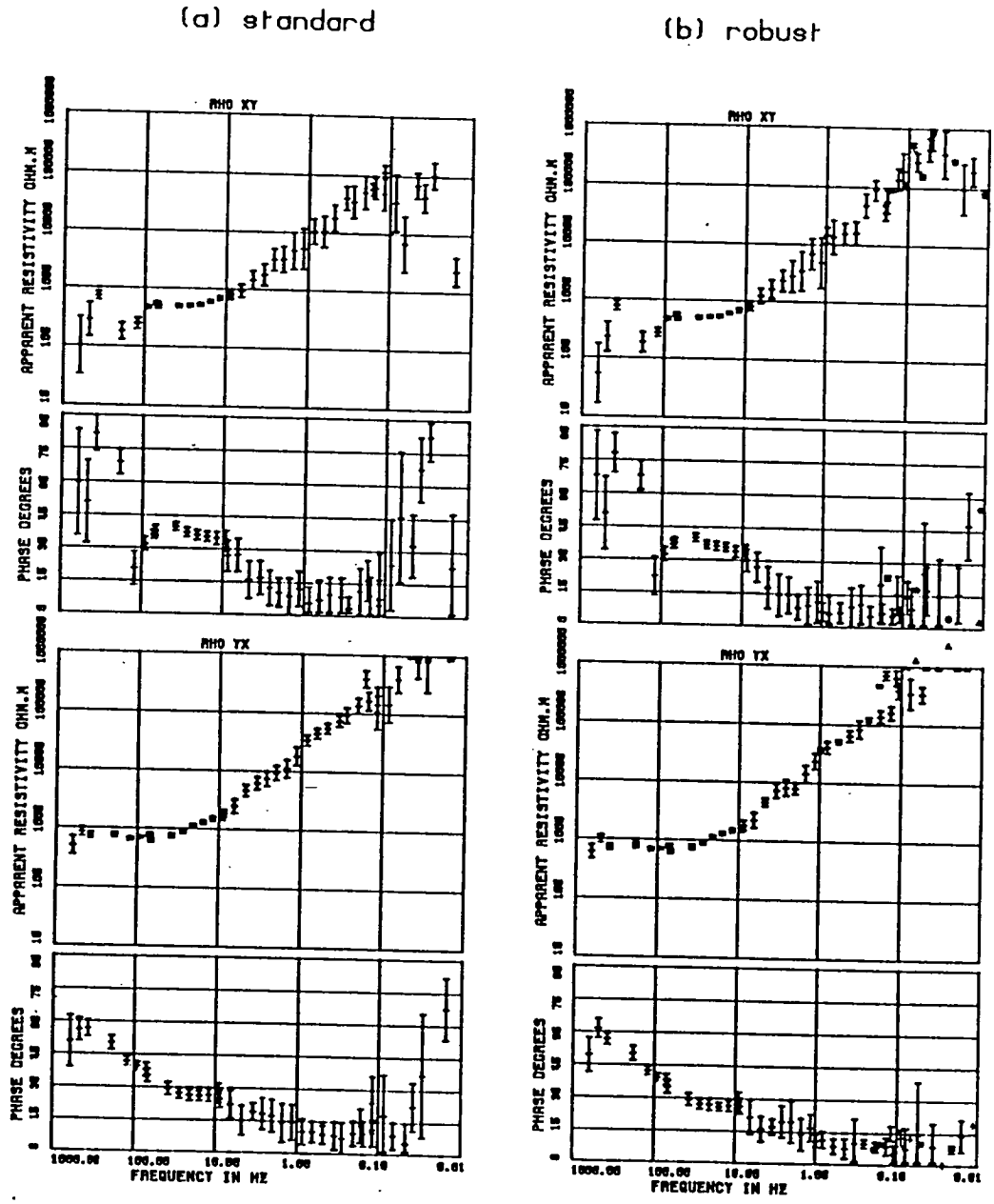

Fig. 5.12- Comparison of standard processing and robust estimation for site LAV, Cavalese area.
(a)- standard processing response curves
(b)- robust estimation response curves

of outliers, certainly the maximum any method can achieve as, above that, the choice of 'good' and 'bad' data clearly becomes a question of semantics. It is noteworthy, however, that if the data set is essentially (log-)normally distributed, all the trials with robust methods, including the LMS method, are bound to be ineffective.

5.4.2 Other processing/rejection criteria

(1)- Individual analysis of accepted windows

A type of coherent noise observed on Milos (paper 1) was observed to have an intermittent character and the accepted windows could be clearly separated (through individual selection) into two groups, one of which contained the noise- degraded sets and the other the assumed noise- free windows. The noise in the Milos case was found to coincide with the opening and closure of the valves on the test wells of a geothermal power station.

In order to investigate whether the noise in Italy had the same intermittent character as in Greece, the responses for each window were displayed in plots, as exemplified in Fig. 5.13. The Fig. illustrate the results of 15 accepted windows (band 3, EUIG-SPAM) for the site LAV. These results consist of Cagniard resistivity curves (ρ_{xy} and ρ_{yx}) and smoothed autospectra for the magnetic (H_x, H_y) and electric (E_x, E_y) components. Though the signal power content exhibits some level of variability for distinct windows, the resultant Cagniard curves do not show appreciable differences. Therefore, unlike in the Greek case, it doesn't seem feasible to reduce the noise in the Italian data by selecting 'adequate' windows. Moreover, the same was observed for all other noise- affected sites and the individual selection approach has had very limited use in this study.

(2)- Weighting on coherence

Most MT workers base the selection of data sets on coherence levels observed in the signals (Pedersen ,1986). Nevertheless, Stodt (1983) has proposed a weighted least square procedure which uses the coherence estimates as weights. A similar approach was applied in this study and all the estimates were averaged by using the following normalized weight

$$(1/coh^2)/(\Sigma\ 1/coh^2) \qquad (5.21)$$

where 'coh' is the predicted coherence of a particular frequency set and the

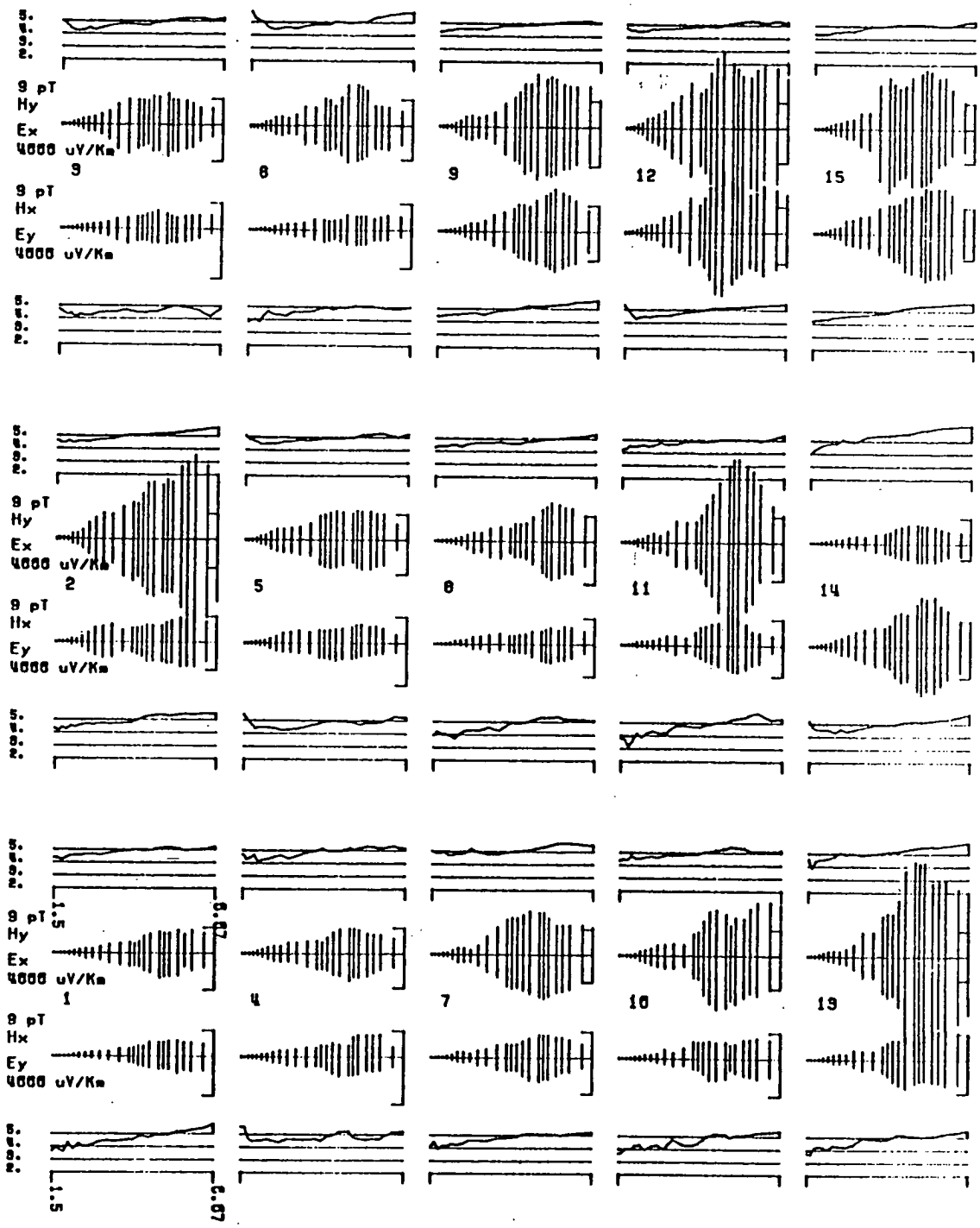

Fig. 5.13- Autospectra of magnetic and electric components and Cagniard resistivity curves for 15 windows automatically selected by EUIG- SPAM, band 3, site LAV. Frequency is the abcissae for each window (1.5Hz- 0.07Hz range). The Cagniard resistivity curves are given in Ωm (10^2- 10^5 range). The average signal intensity is given in pT (magnetic) and μV/Km (electric).

summation considers all available estimates. The comparison of the standard processing (frequency sets with predicted coherences > 0.90) and this weighted procedure is illustrated in Fig. 5.14. No significant difference is observed.

(3)– Rejecting highly coherent magnetic signals

Theoretically, the inducing orthogonal magnetic components should be completely uncorrelated. In practice, however, it seldom happens and one has to be contented with a certain acceptable level of coherence of the magnetic components. Nevertheless, the presence of highly coherent magnetic signals may result in unstable estimations of transfer functions (Kaufmann and Keller, 1981, pp483). Thus, the frequency sets with coherences (H_x, H_y) greater than 0.90 were not considered for the final averaging. As an example, the same site LAV is used and the results are shown in Fig. 5.15. The comparison between the standard processing response (Fig. 5.15(a)) and the response after including this extra criterium (Fig 5.15(b)) does not show any noticeable difference between the two sets of responses.

(4)– Rejecting highly coherent frequency sets

The natural signals (i.e. the orthogonal components of the magnetic and telluric signals) should ideally be highly coherent but, in practical terms, the level of coherence (measured by the predicted coherence function) generally considered acceptable is > 0.90. As the artificial signals are themselves highly coherent in the Italian case, the idea of rejecting the frequency sets exhibiting predicted coherences greater than say 0.95 seemed attractive, given that by doing so one might eliminate the noise. However, the use of 0.95 as the maximum acceptable coherence resulted in a massive rejection of estimates. The limit was thus increased to 0.98. The result of this trial, once more for the site LAV, is shown in Fig. 5.16. This time the only observable change is a slight increase in the scatter of the responses , especially in bands 3 and 4.

5.5 Italian DC railways and MT measurements

5.5.1 The evidence

Some magnetotelluric soundings (512Hz– 100s) undertaken in Northern Italy have resulted in unexpectedly high and unrealistic apparent resistivities at the longer periods. It was clear from the form of the apparent resistivity

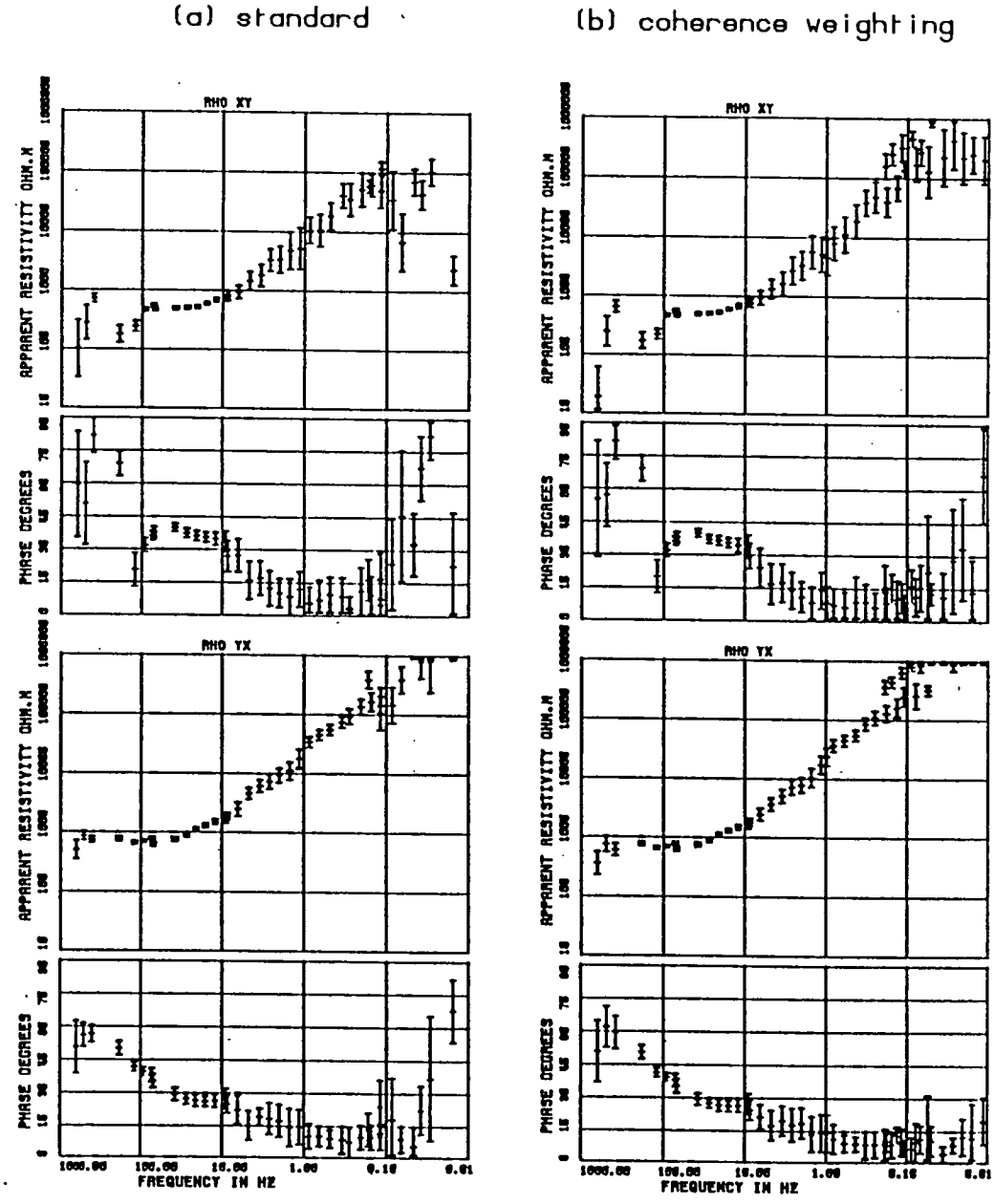

Fig. 5.14- Comparison of standard processing and coherence weighting processing for site LAV, Cavalese area.
(a)- standard processing
(b)- weighting on coherence

(a) standard (b) coherent mag. signal rej.

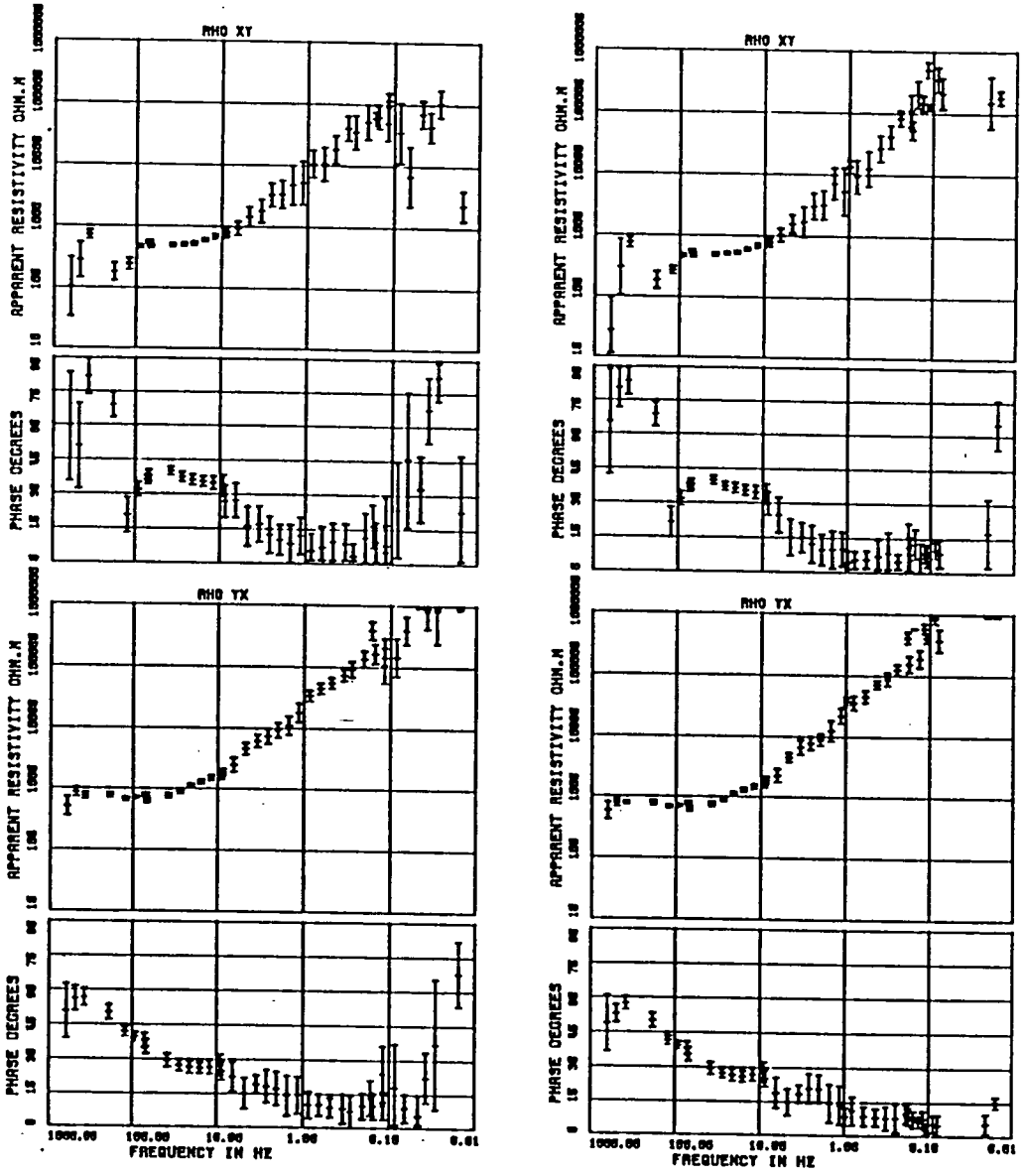

Fig. 5.15- Comparison of standard processing and processing rejecting highly coherent magnetic signals for site LAV, Cavalese area.
(a)- standard processing
(b)- rejecting highly coherent magnetic signals

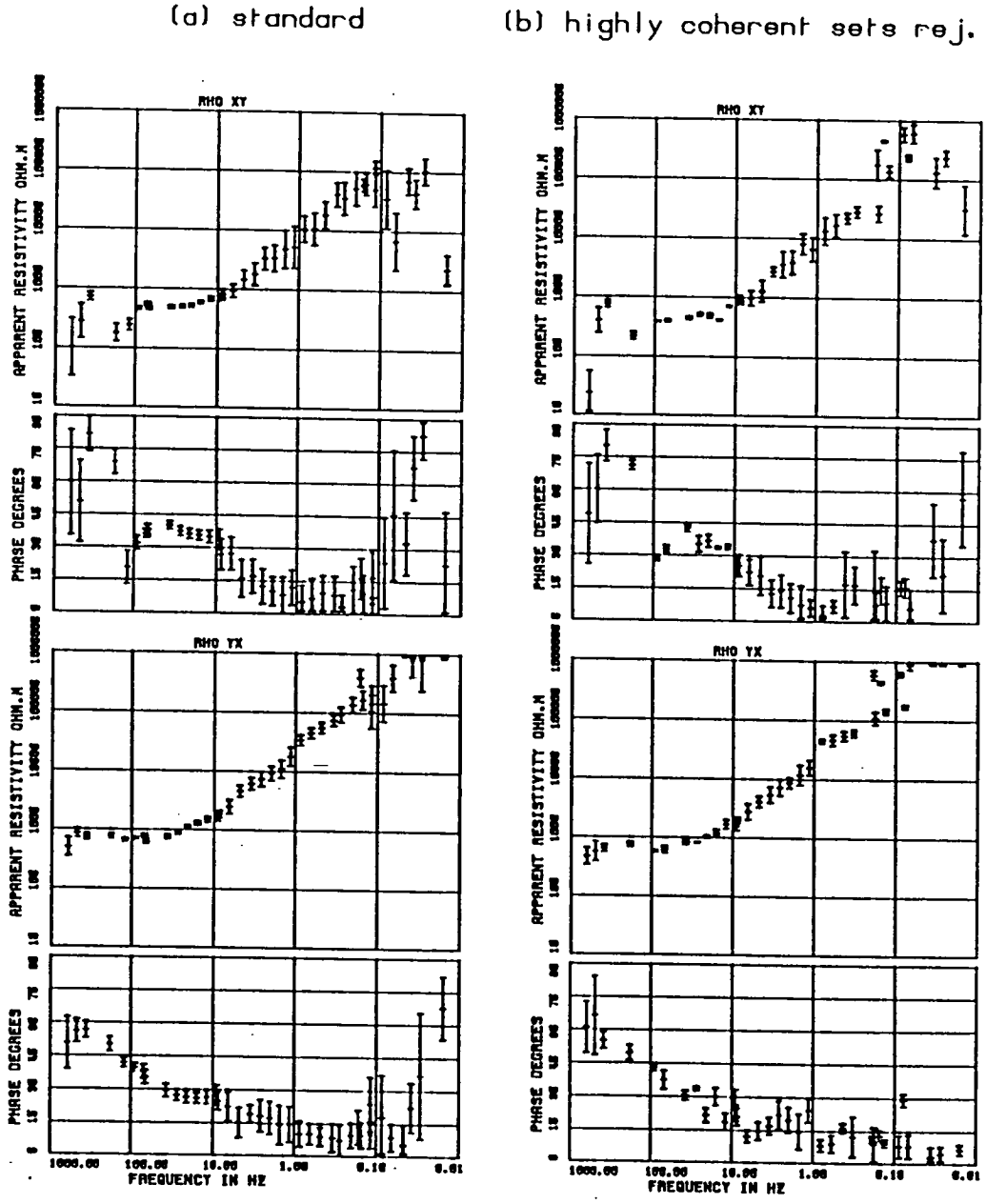

Fig. 5.16- Comparison of standard processing and processing rejecting highly coherent frequency sets
(a)- standard processing
(b)- rejecting highly coherent frequency sets

curves that the data were contaminated by near- field sources. This section is concerned with the evidence which led to the determination of the man-made origin of the signals- the Italian DC railways. For easy reference, a map of Northern Italy containing the DC railway network and some MT stations is given in Fig. 5.17. Figs. 5.18, 5.19 and 5.20 show MT response curves (major and minor) for the sites Lavaze (assigned LAV in Fig. 5.8) and Mas di Saugo (MAS) in the Cavalese area, and Mantegna (MAT) in the Po Valley region, respectively. It can be seen that for the observed resistivities of 600-1000Ωm (Figs. 5.18 and 5.19) for the period range .001s- .01s are compatible with upper crustal resistivities in other continental regions (Hjelt, 1986). Due to the more conductive nature of the Po Valley region, acceptable MT responses extend by an extra decade (i.e. up to 1s) at the site MAT. However, for longer periods both the slope and the extreme apparent resistivity values (particularly for the Cavalese sites) are indicative of near- source fields (Goldstein and Strangway, 1975). As implied by the distances between these 3 stations, the noise source is detectable over a large area in Italy and extends beyond the mountainous region.

The examination of both the unfiltered and filtered time series provides a second piece of evidence. Unfiltered time series for LAV recorded by the Neuchatel group exhibited step- like signals superposed on each MT trace (Fig. 5.21). Filtered time series for the same site recorded using the Edinburgh equipment (Fig. 5.22) displays exceptionally coherent and abnormally high amplitude spike- like signals in bands 2 and 3. Similar signal waveforms have been previously reported in the literature to be associated with stray currents from DC railways (Jones and Kelly, 1966; Mikerina, 1962; Chaize and Lavergne, 1970; etc).

A third piece of evidence is perhaps given by the azimuth values, also seen in Figs. 5.18, 5.19 and 5.20. Under normal circumstances, the azimuth indicates the preferred direction of the current flow at the sounding site. One can notice, especially at MAS in the Cavalese area, that the azimuth values experience remarkable change in direction which coincide with the abrupt change in the form of the MT responses.

Return current measurements and their FFT spectrum at the power substation Ala (assigned with a circle in Fig. 5.17) are shown in Fig. 5.23(a)-(b) Currents with amplitudes up to more than 1000 A are observed to have

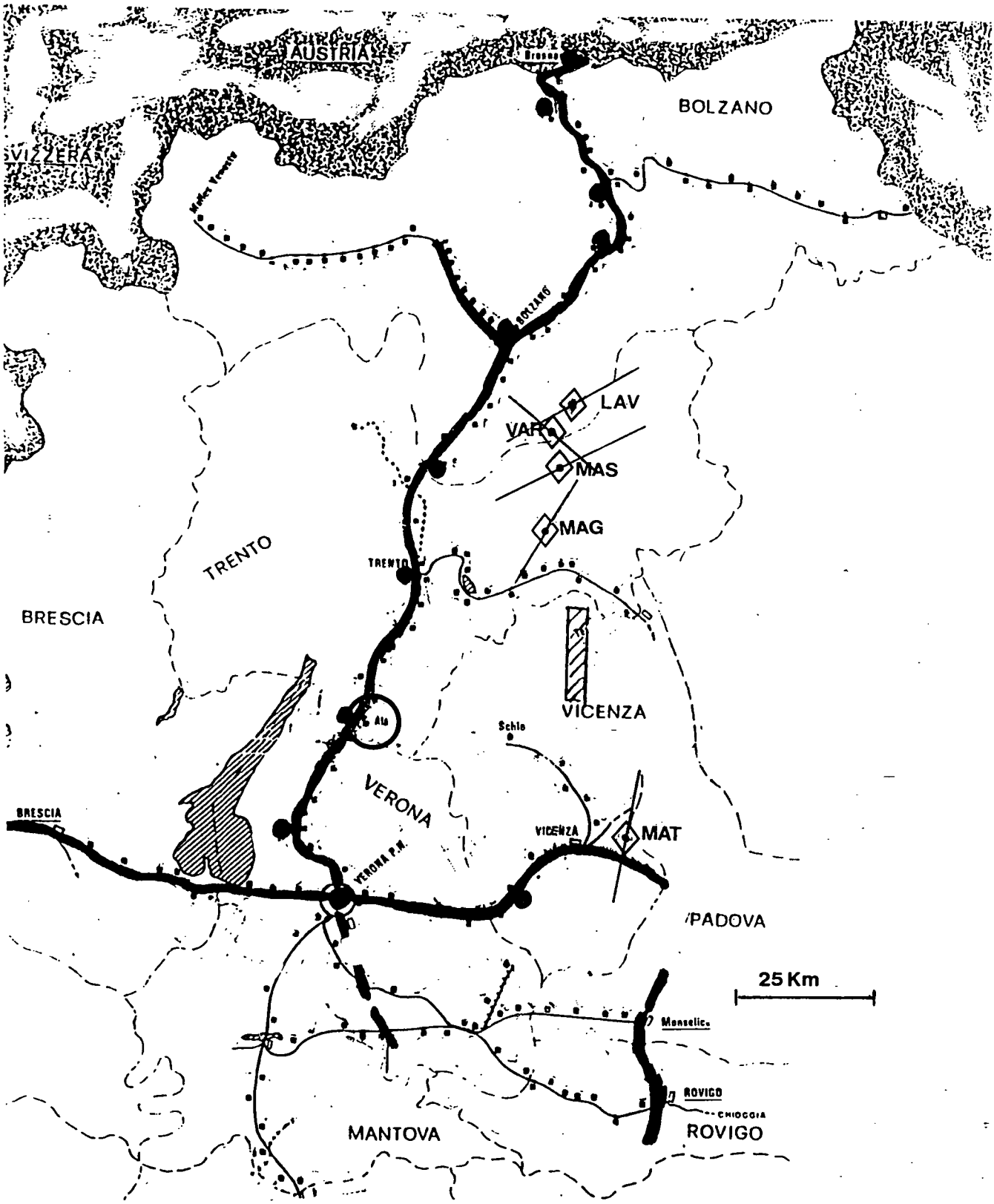

Fig. 5.17- Map of Northern Italy showing the Italian DC railway network (thick line), location of some MT stations (diamonds) and Ala substation (open circle). The Asiago profile (hachured area) and other substations (bold circles) are also indicated in the Fig. Azimuths for the major curves (average values for the noise affected bands) are shown for the Cavalese and Po Valley soundings.

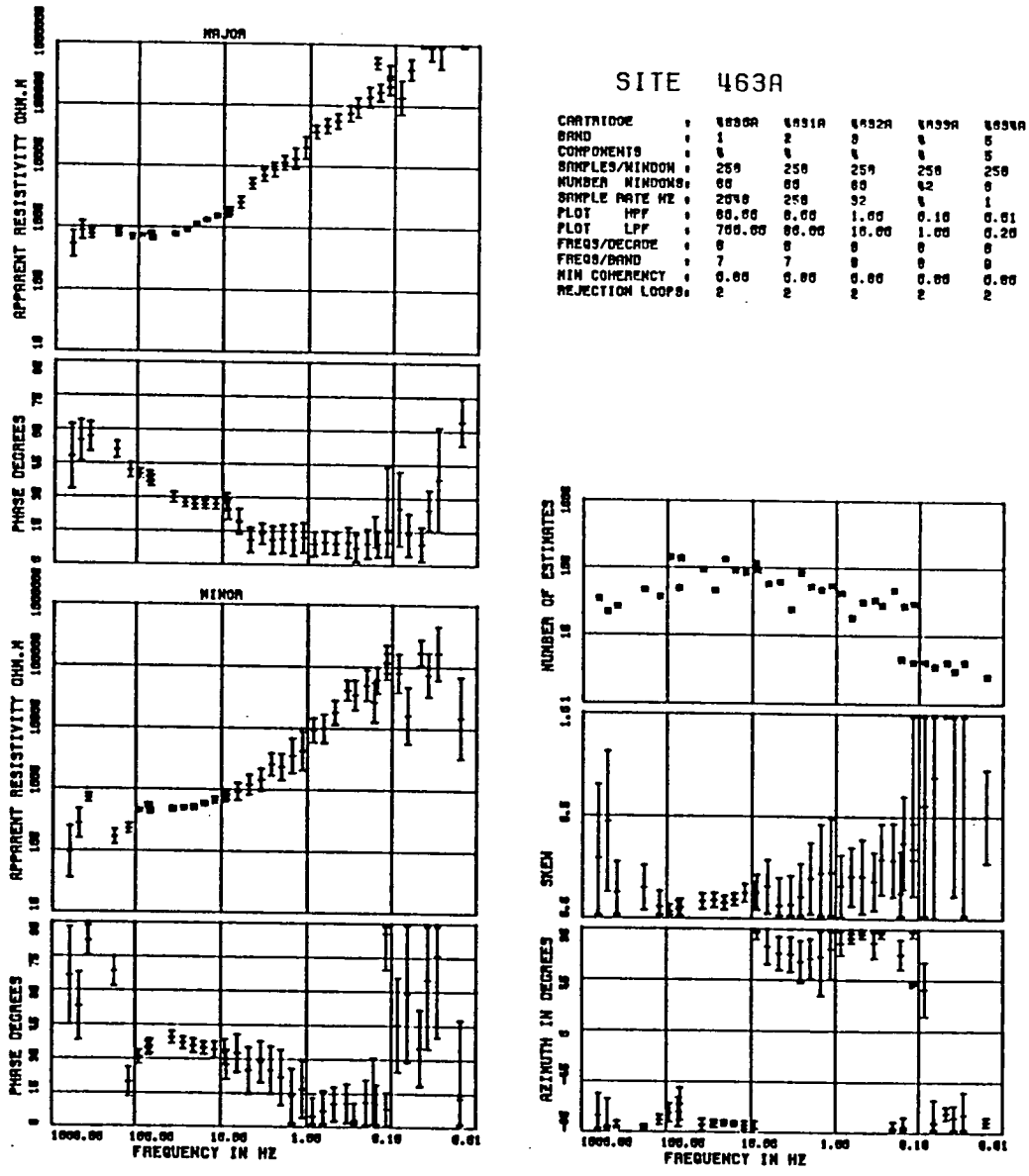

Fig. 5.18- MT response curves (major and minor), azimuth, skew and number of estimates for site LAV, Cavalese area.

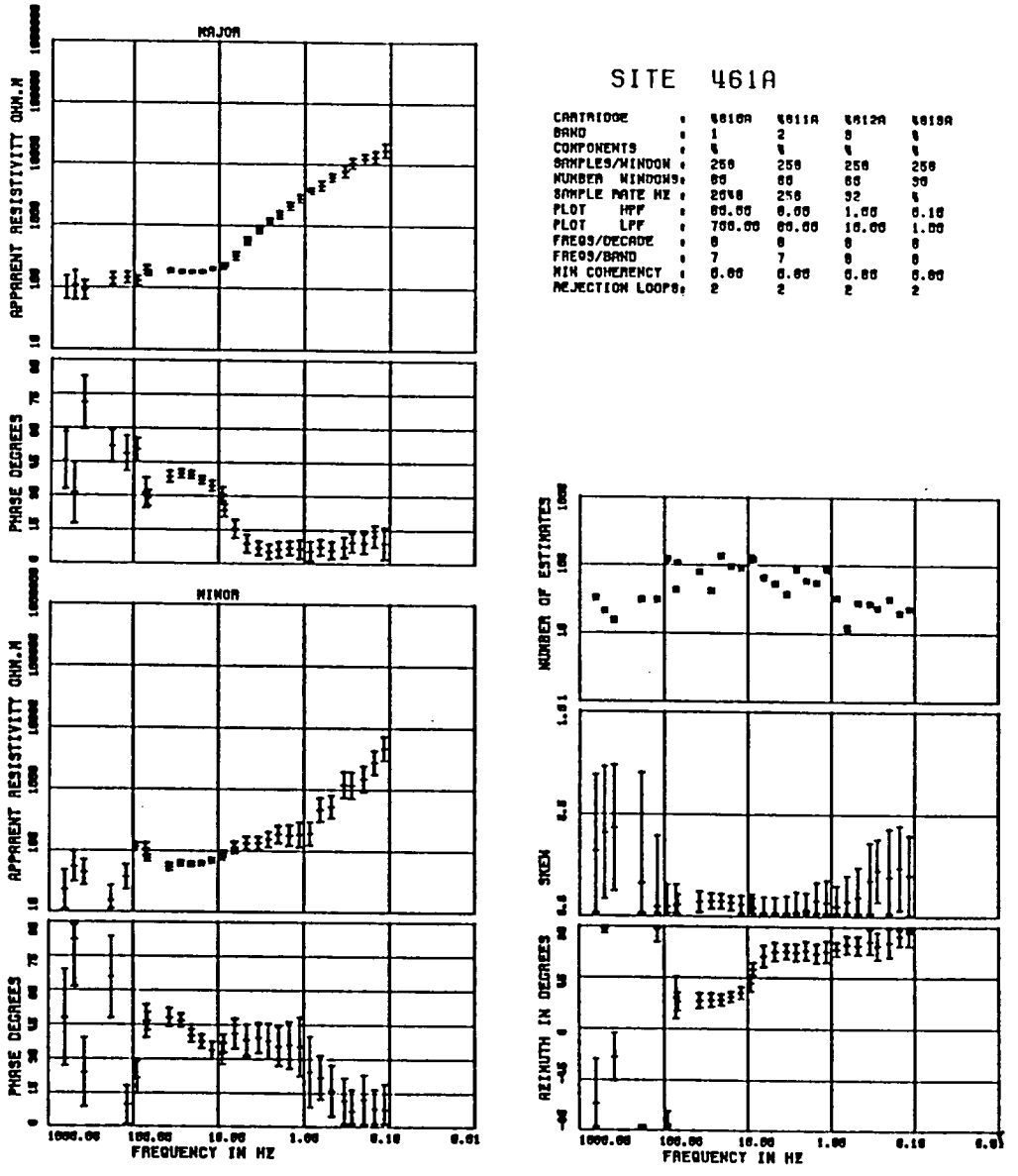

Fig. 5.19– MT response curves (major and minor), azimuth, skew and number of estimates for site MAS, Cavalese area.

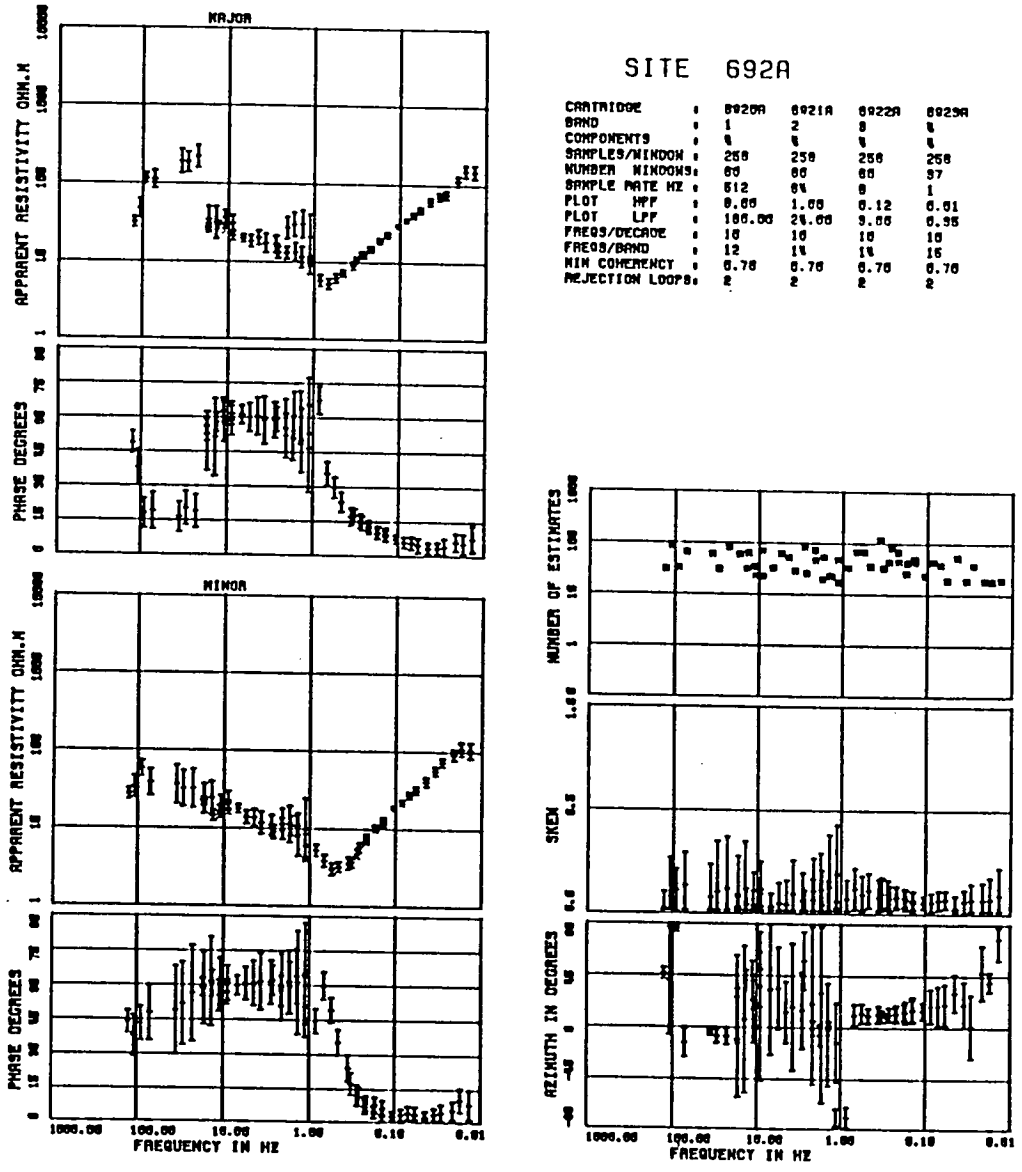

Fig. 5.20– MT response curves (major and minor), azimuth, skew and number of estimates for site MAT, Po Valley region.

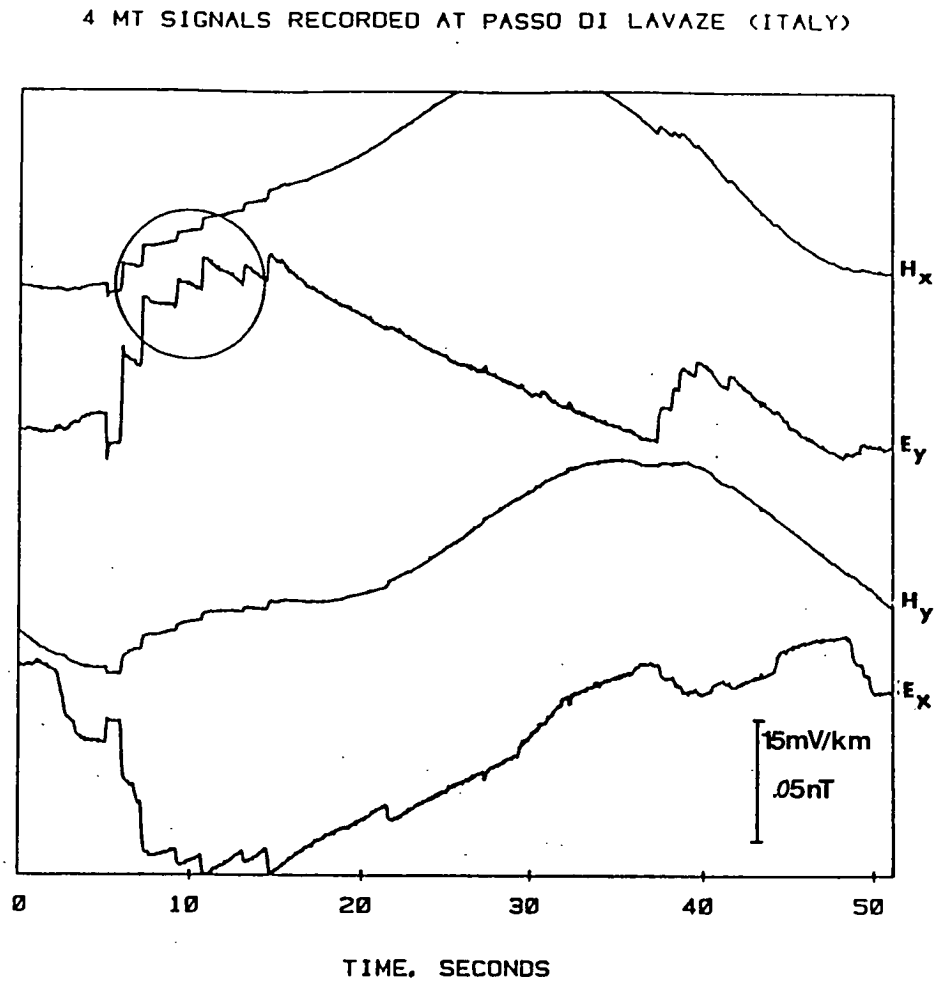

Fig. 5.21– Unfiltered time series recorded at LAV by the Neuchatel group.

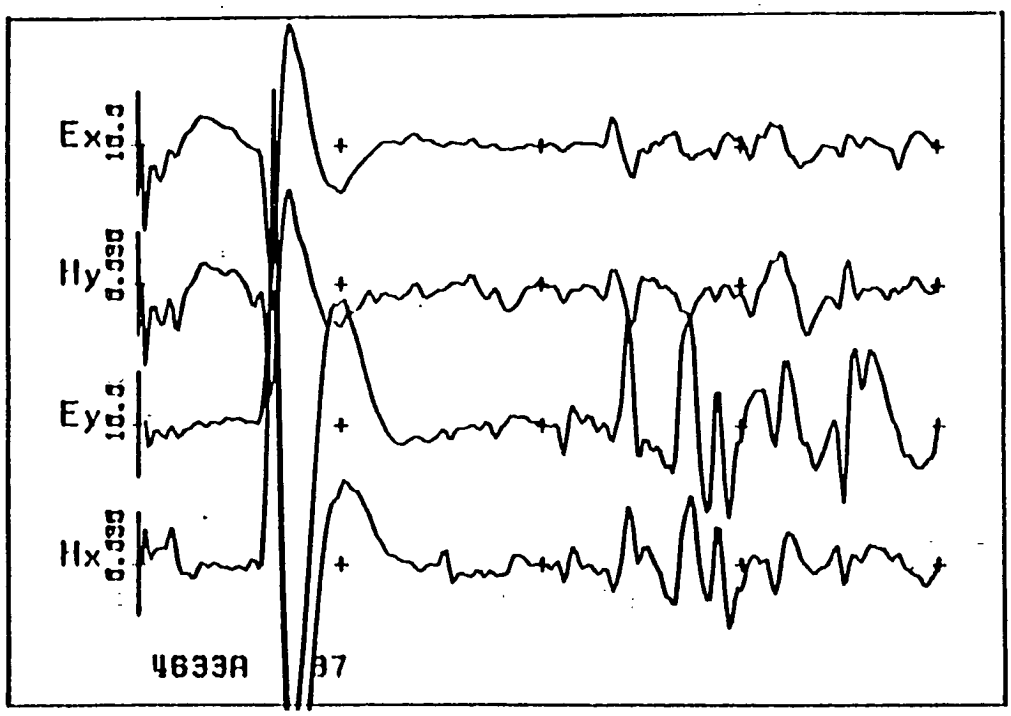

Fig. 5.22- Filtered time series (band 3) recorded at LAV, EUIG-SPAM system. Magnetic signals (H_x and H_y) in nT and electric signals (E_x and E_y) in mV/Km.

continuous fluctuations of varied (including step- like) forms- Fig. 5.23(a). These can be associated with the variation in the power demand which occurs when locomotives draw more or less power, at the start of their movement or at nearly constant speed, respectively. The rather smooth record section around noon corresponds to the period when no trains were on the line and railwork repairs were undertaken. The inspection of the FFT spectrum of the band- passed return current fluctuations (Fig. 5.23(b)) suggests that the energy content is primarily above 200s. Unfortunately no single frequency dominates or can be regarded unequivocally as representative of the railway network. Had either been the case, a simple filtering operation would enable the MT data to be corrected for the railway noise. One attempted to make MT measurements near the Ala power station simultaneous with the railway current monitoring, but this was unsuccessful due to great difficulty in finding a satisfactory site. The rough topography of the region and an unexpected localized noise (found later to be due to a pipeline system) rendered the only practicable site problematical. Had this experiment been successful, it would have certainly provided the most conclusive support for the hypothesis that the Italian DC railway system is the main source of electromagnetic disturbance in Italy.

The combination of the features exhibited by the noisy signals such as stability, permanence, detectability over a large area and major effect on periods greater than 1s rules out many of the more common noise sources (e.g. the mains frequency and its harmonics, lightning discharges, etc). Moreover, it is known that other MT workers in Italy have experienced similar near- field problems in the same frequency range (Hutton et al., 1985; Dupis, priv. comm.; Watts, priv. comm.) but to a lesser extent. However, Dupis et al. (1972) seemed unaware of this noise problem. An inspection of their MT curves for sites in the Po Valley region show identical behaviour to site MAT (Fig. 5.20).

All the evidence points towards the Italian DC railway network as a major obstacle to the successful application of the MT technique in much of Italy. Long period measurements (200s -4000s) made at sites in the Cavalese, Asiago and Po Valley regions (results to be discussed in Chapter 6) seem to indicate that, due to the generally high level of noise observed, the use of the remote reference technique and very long field campaigns (say a couple of

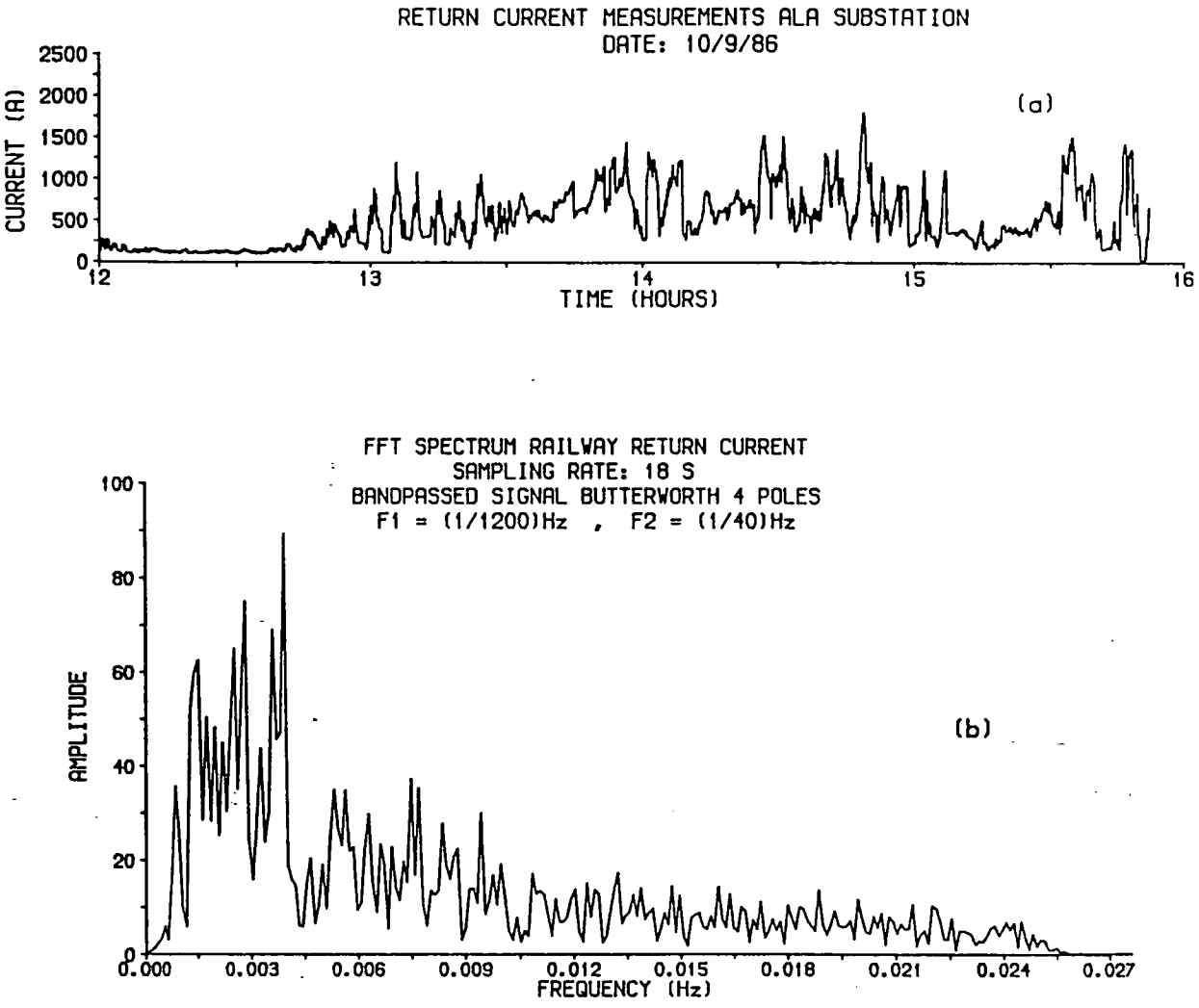

Fig. 5.23- Ala substation experiment.
(a)- Return current measurements
(b)- FFT spectrum of return current time fluctuations. Bandpassed signal.

months or more) are essential.

5.5.2 Modelling near- source fields

The use of the DC railway stray currents to provide geophysical information about the conductivity structure in N. Italy is justified in this section. However, unlike a normal controlled source method, both the source signal and the transmitter- receiver distance are not known precisely. Another complicating factor is the fact that both the natural and artificial signals are expected to contribute to the observed response curves. Evidently, the lack of any information regarding the superposed natural and man-made signals makes this a rather difficult task. Nevertheless, the problem is tentatively approached by making the following assumptions:

(1)- The DC railway source is dominant over the natural signals for longer periods (i.e. > 1s in the Cavalese area or > 10s for the Po Valley area),

(2)- The source signal can be represented by an oscillating horizontal electric dipole,

(3)- The railway current leaks occur at stationary points along the railway track.

Assumption (1) is perhaps reasonably realistic for periods around the dead band due to the very reduced intensity of the natural signals. Although this is normally not the case for longer periods (say >10s), two facts seem to lend some support to this assumption outside the dead band. Firstly, there is the very high level of coherence of the signals, seldom found in nature. The second fact was the strikingly fast rate of acceptance of the data windows by the automatic system SPAM. For instance, for band 3 measurements (using both EUIG and NERC- SPAM's), the data acquisition times were always less than a third of typical recording times in other regions, as judged by the author's personal experience in the Highlands of Scotland and by that of members of EUIG in other campaigns.

The return current spectrum (Fig. 5.23(b)) indicates a wide- band of signals, so that an oscillating dipole is an appropriate source choice. The striking similarity between the MT curves in Figs. 5.18, 5.19 and 5.20 and the curves for a horizontal electric dipole source over both a homogeneous and a two- layered Earth (Figs. 5.24 and 5.25) seem to justify assumption (2). Figs. 5.24(a)-(b) shows curves for two different half- space models (10Ωm and 1000Ωm, respectively) for various transmitter- receiver distances (DS). Fig.

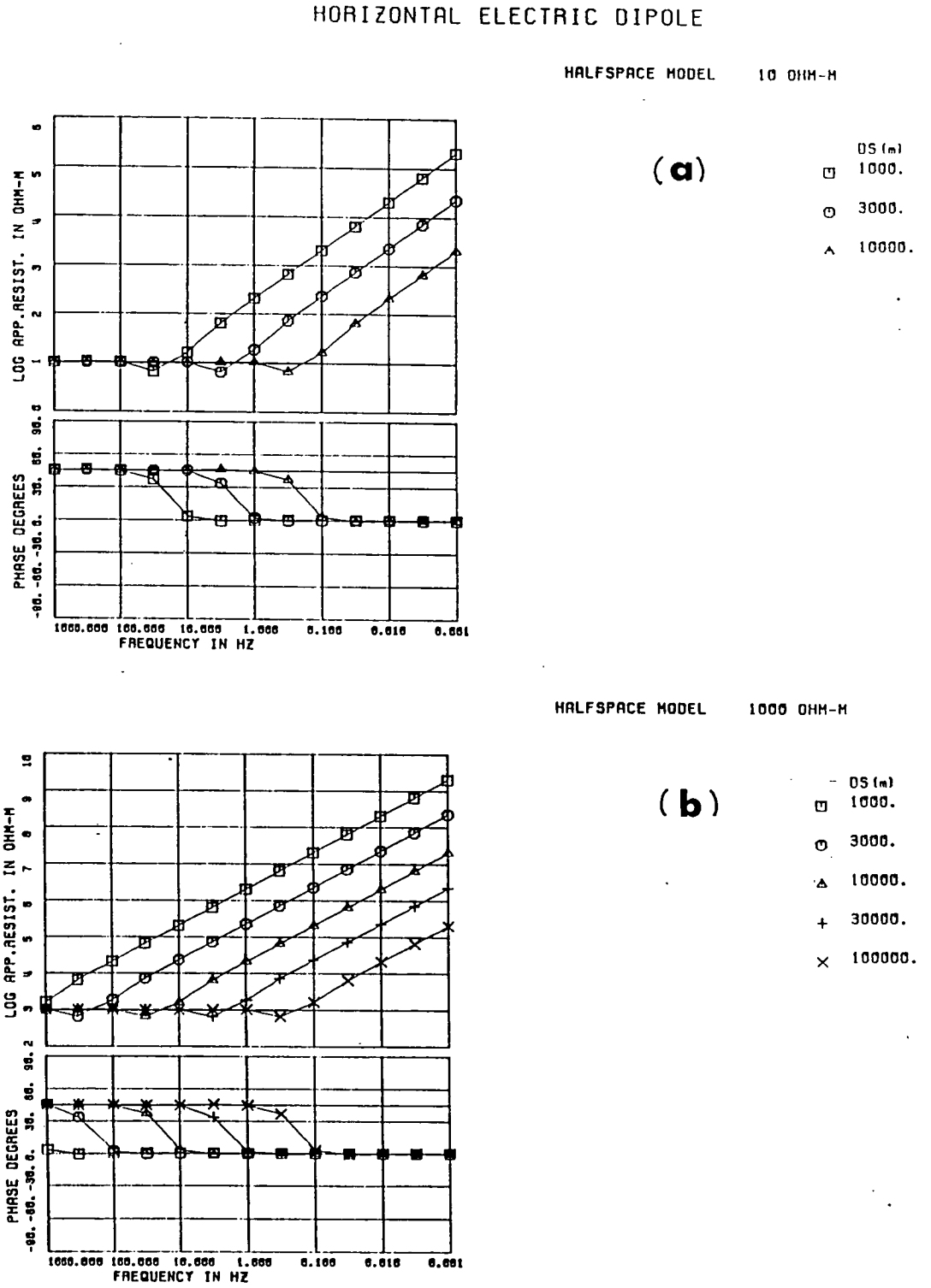

Fig. 5.24- Horizontal electric dipole source over a homogeneous halfspace ((a)- 10Ωm, (b)- 1000Ωm) for various distances transmitter- receiver (DS).

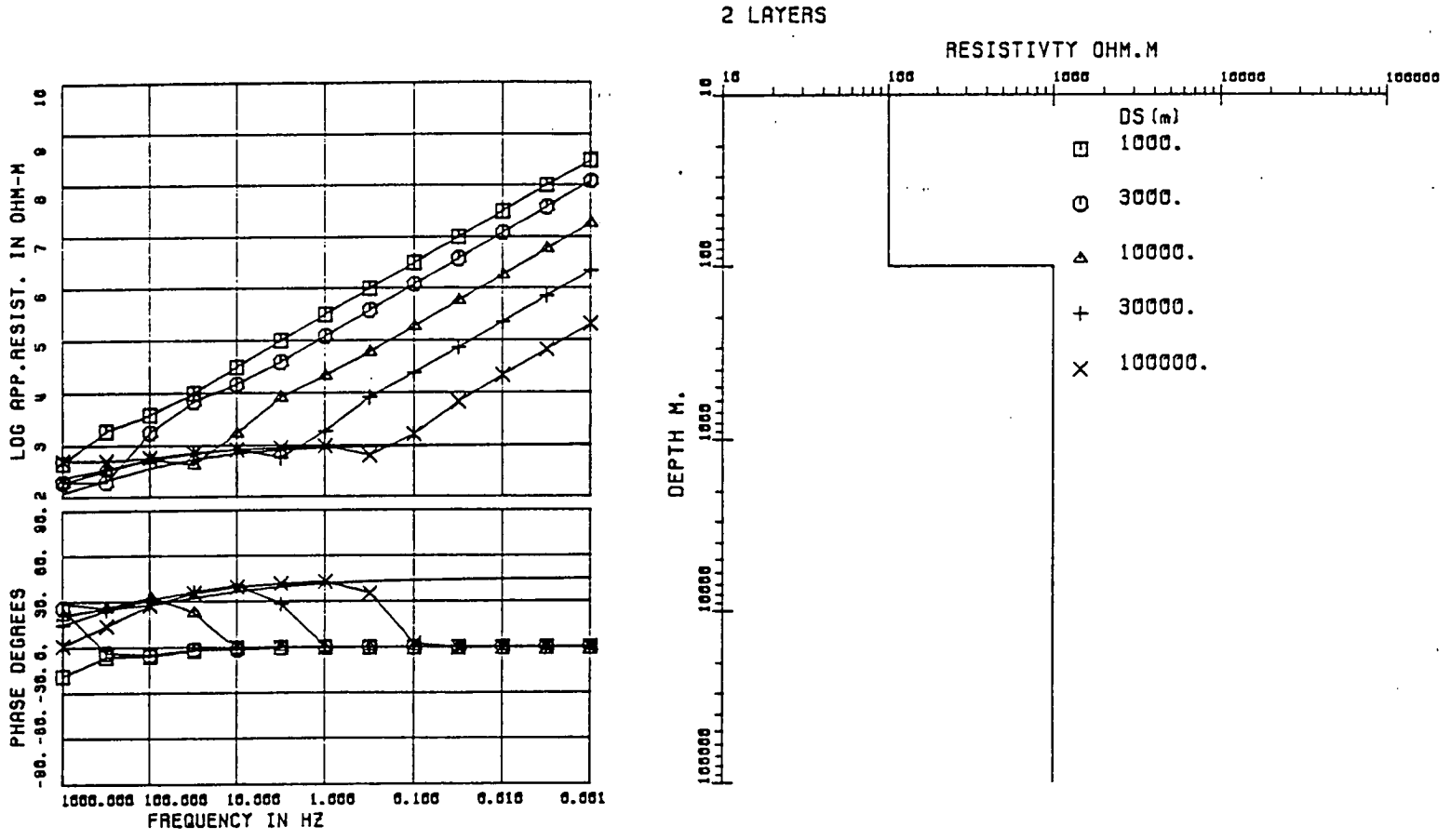

Fig. 5.25- Horizontal electric dipole source over a two- layered Earth for various distances transmitter- receiver (DS).

5.25 shows similar curves for a two- layered Earth, again for various transmitter- receiver distances. It can be observed that the departure from the corresponding MT curves (constant apparent resistivity curve and phase of 45 degrees for the homogeneous Earth) is a function of DS.

Assumption (3) seems justified by the very well defined azimuths at the three observational sites (Figs. 5.18, 5.19 and 5.20) used as examples in this section. It suggests that the current leakage is not associated with the train position along the track given that this would lead to an erratic azimuth. Hoogervorst (1979) came to a similar conclusion by observing time independent potential gradients in resistivity surveys in the vicinity of a DC railway.

The transmitter- receiver distance (DS) is treated as an unknown parameter to be determined by the 1D near-source inversion schemes used in this study- both modified versions of the Monte Carlo and Occam techniques, discussed in detail in Chapter 7.

The resulting geoelectric models for the data sets under the influence of the Italian DC railway network (the three sites shown in section 5.2.1 plus two other sites in the Cavalese region) are presented in Chapter 7. Their validity in the light of all constraints and limitations posed by the uncertainties of this modelling exercise, are also discussed in Chapter 7.

5.6 Discussion

When man-made noise reaches high levels, as observed in data sets from N. Italy, the notch filters normally incorporated in MT data acquisition systems are inadequate since large amplitude non-sinusoidal noise sources can produce very high order harmonics in the data. Additional notch filters could be included either in the acquisition systems or alternatively, be applied to the data during processing. The latter option should only be considered when hardware limitations have resulted in inadequate notch filtering. Otherwise the data resolution may be considerably reduced due to practical limitations in the dynamic range of the recording device. The delay-line filter has been shown to be more effective than the notch filter since the main noise source frequency and all its harmonics (odd and even) are completely eliminated by it. Unlike the notch filter, which is applied either to analog or

digital signals, delay- line filtering is more generally applicable to digital signals. It thus appears advantageous to incorporate an optional delay-line filter in real time data analysis systems.

In frequency domain processing of MT data, the presence of a single spike noise can contaminate the whole spectrum. Simply deleting the spikes can cause leakage from this portion to the uncontaminated portion of the data set. The maximum entropy method used as a predictive technique has been applied to this problem. When applied to field data of which > 30% have been contaminated by spike noise (paper 1), the technique has proved effective in producing acceptable resistivity and phase curves. Nevertheless, when applied to data sets from Cavalese, the MEM technique was only partially successful.

The window deconvolution technique presented in this study attenuates the noise effects simply by deleting the noise-contaminated segments of a data window. The application of this technique to synthetic and field data showed that it was in good agreement with the MEM extension technique, but it did not represent any significant improvement over the simple replacement of the spike segments by zero. Its only advantage is its ease of implementation in the data processing.

No claim is made that all man-made noise can be eliminated by the digital filtering techniques discussed above, nor is it certain that all the superposed noise has been removed from the field examples presented in this study. Filtering itself may introduce noise and should thus always be applied with great care. In some cases, as exemplified in paper 1 (see also Dawes, 1985), the monitoring of filtered and/or unfiltered signals (e.g. by chart recorders), may provide the clues for determining the source of noise present, and thus helping to choose the most suitable approach for dealing with the noise problem.

The additional set of rejection criteria presented in section 5.4.2 has failed to produce any significant change on a data set believed to be heavily affected by the DC railway noise signals, and has therefore not been applied to other noise degraded data.

Alternatively, the use in MT studies of robust statistical techniques more sophisticated than the one exemplified in this Chapter is a very recent research topic (Egbert and Booker, 1986; Chave et al., 1987). Although their

robust estimations may not cope with noise content of over about 20% of the total signal, they very possibly represent the most convenient approach to be taken when processing MT data not severely contaminated by noise. Following the same lines, the robust method proposed by Rousseeuw (1984 op. cit.) might be even more effective than these more recent methods for MT data sets badly contaminated by noise. Rousseeuw's method may account for noise content as high as 50%, which is very likely to occur in Italy. A decision about the best approach to be taken for a particular data set can perhaps be gained by producing a number of statistical parameters which are considered in the so called exploratory data analysis techniques (e.g. Kleiner and Graedel, 1980).

The effectiveness of the use of the noise in Italy as an exploratory tool is discussed in Chapter 7.

CHAPTER 6

RESULTS

6.1 Introduction

The processed results of the AMT/MT data from all the observational sites are presented in this Chapter. For convenience, the Asiago, Cavalese and Po Valley regions are considered separately, according to their geology and tectonic history. The results are presented in plots containing apparent resistivity and phase curves for 1) the measurement directions, 2) the major and minor directions, 3) the E pol and H pol directions and 4) the rotationally invariant responses. Additional parameters, e.g. the azimuths of the major, the number of estimates, the skew values and the dimensionality weights are also presented in these plots, along with ancillary information related to the processed results of the particular site. The processing of the noisy MT/AMT data was performed by using the techniques discussed in Chapter 5; the particular technique adopted is indicated in each case. Prior to the analysis of the dimensional weights for the actual data in the Asiago area, these weights are assessed for a pure 2D situation. Whenever available (i.e. for most bands 4 /5 and a very few AMT recordings), the magnetic transfer function results were very noisy, exhibiting generally sufficient scatter to make them unsuitable for any reliable interpretation, as shown in two examples presented later in this Chapter.

6.2 Asiago area

6.2.1 MT results

Asiago and its surroundings are part of a tectonic unit referred to as the main prealpine region of the Venetian platform. The entire region has been subject to articulated deformation with increasing energy. The main compressional efforts were due to a SSE-NNW northward movement of the 'Adriatic microplate' (Zanferrari et al, 1982). The 8 MT sites in Asiago are irregularly spaced in an 18Km traverse, roughly disposed in the North-South direction as shown in the detailed map of Fig. 6.1. This Fig. also presents the main tectonic structures in the region. The MT results for all sites are shown in Figs. 6.2 (a)-(h) and Figs. 6.3 (a)-(h). Figs. 6.2(a)-(h) contain some of the

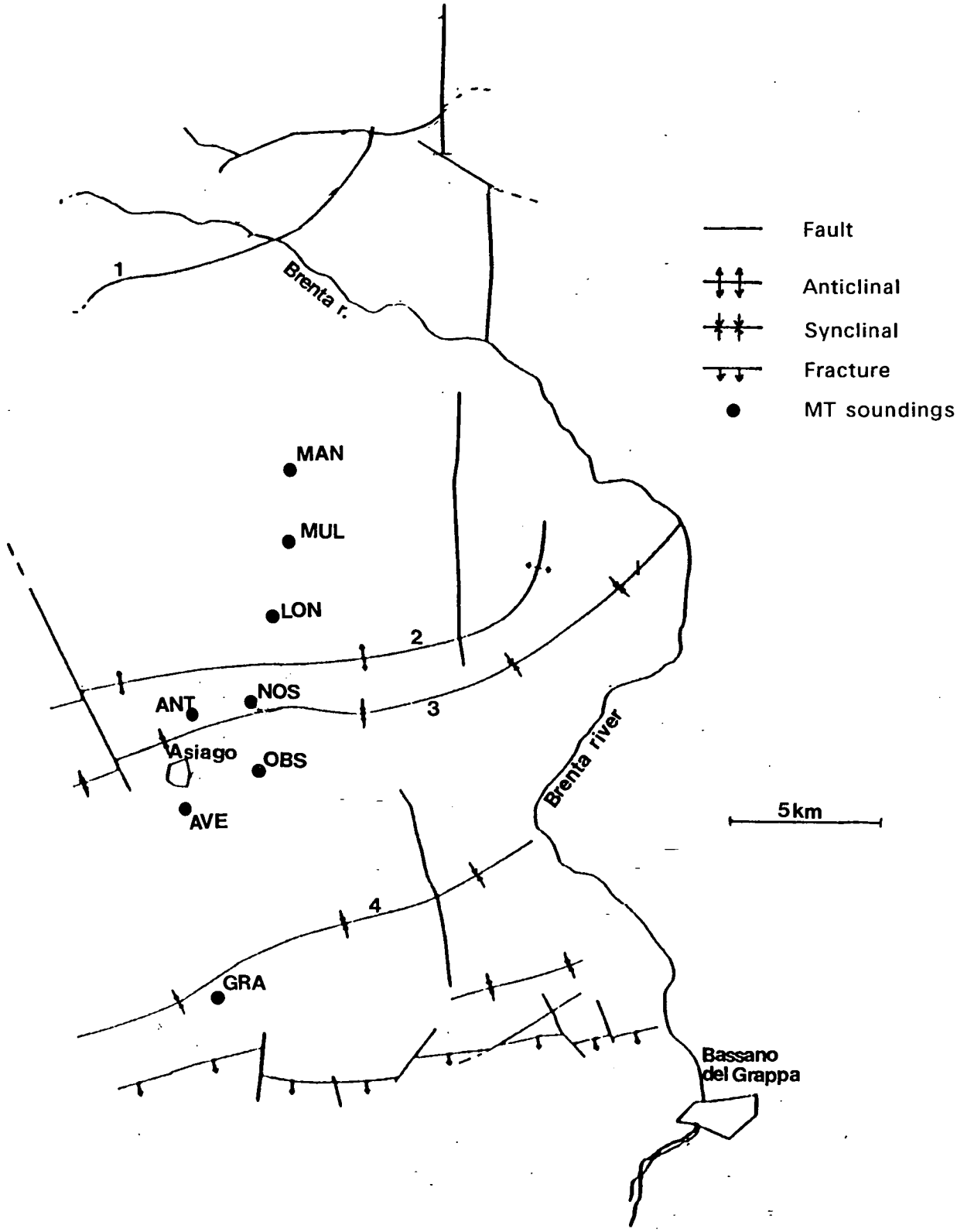

Fig. 6.1- Asiago area map. Sites are assigned by bold circles. The main tectonic features (e.g. faults, flexures, etc) are assigned by numbers and are as follows (De Zanche et al., 1981 and Gatto et al., 1981) :
(1) Valsugana line; (2) M. Lissier anticlinal; (3) Galio synclinal; (4) Granezza synclinal.

main results of processing, i.e. the apparent resistivity and phase curves (response curves, for short) for the measurement directions x and y (assigned 'xy' and 'yx', respectively), the response curves rotated for the major and minor directions and the response curves rotated for the E pol and H pol directions. The rotationally invariant response curves, the azimuth values for the major, the skew values the number of estimates used for each frequency set, the dimensional weights, along with a table containing additional information (i.e. the number of frequency sets accepted per band, minimum coherence for accepted sets, etc) are all presented in the Figs. 6.3 (a)–(h). The processing of the data shown in these two sets of Figs. included the following of the techniques described in Chapter 5:

1) Delay-line filtering applied to band 0 data of sites 452- GRA and 453- AVE; the improvement achieved in site AVE after delay-line filtering was shown in Chapter 5.

2) Maximum entropy extension technique applied to band 3 data of sites GRA and 456- MAN. Station MAN was used in Chapter 5 to illustrate the application of the MEM extension technique.

All the other sites/ bands followed the standard processing techniques described in Chapter 4.

As seen from the curves in Figs. 6.2, the sites GRA and 690- NOS cover the largest frequency range while the sites 450- ANT and 451- OBS show the smallest range. Site GRA includes band 4 measurements and therefore the response is available up to about 100s. Site 690 includes band 5 measurements and the response curve extend up to around 3000s. Sites ANT and OBS were found to be very noisy for measurements in the lowest frequency bands (2 to 4) and were thus abandoned before completion. The high level of noise observed in Band 4 measurements at all other sites were laboriously scrutinized but unfortunately, due to a generally high level of man-made noise and other secondary factors already reported in Chapter 3, this did not lead to results suitable for interpretation. Nevertheless, the long period results for site 690 indicate a levelling off around 1000Ωm of the apparent resistivity values and show signs of a downwards trend to a more conductive structure, which makes the results in this area conform with observed deep conductivity structures in other parts of the world (see for instance Hjelt (1986) for a recent review of case studies). To a certain extent,

Fig 6.2(a)-(h)- MT response curves for all the sites in the Asiago area. The responses comprise apparent resistivity (Ωm) and phase (degrees) curves for i) the measurement directions x and y (indicated xy and yx, respectively), ii) the major and minor directions and iii) the E and H pol directions (76^0NE). See text for further details.

MT RESPONSE CURVES SITE 456 MANDRIELLE

(a)

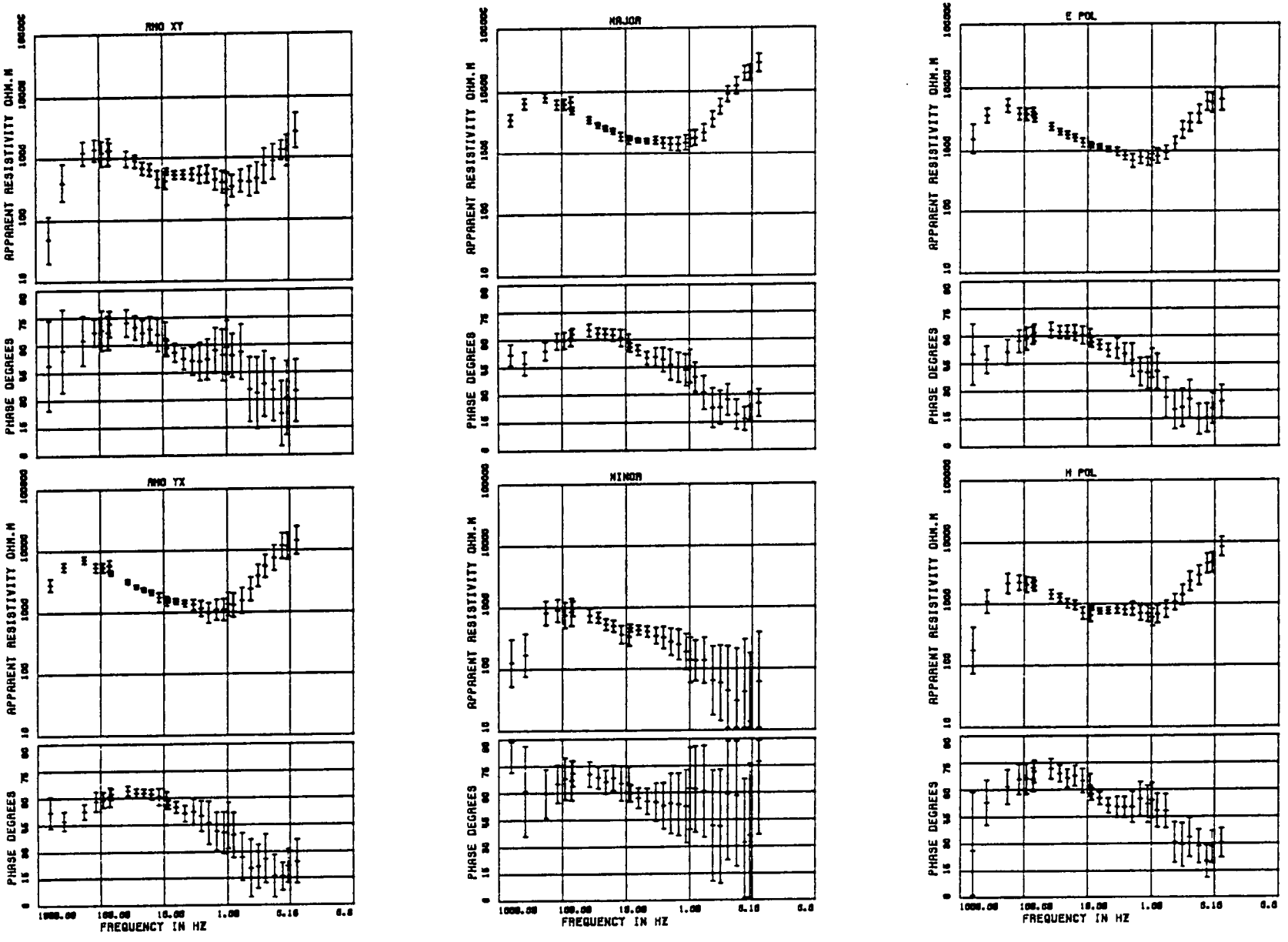

MT RESPONSE CURVES SITE 454 C. MULO

(b)

MT RESPONSE CURVES SITE 455 LONGARA

(c)

MT RESPONSE CURVES SITE 690 V. DI NOS

(d)

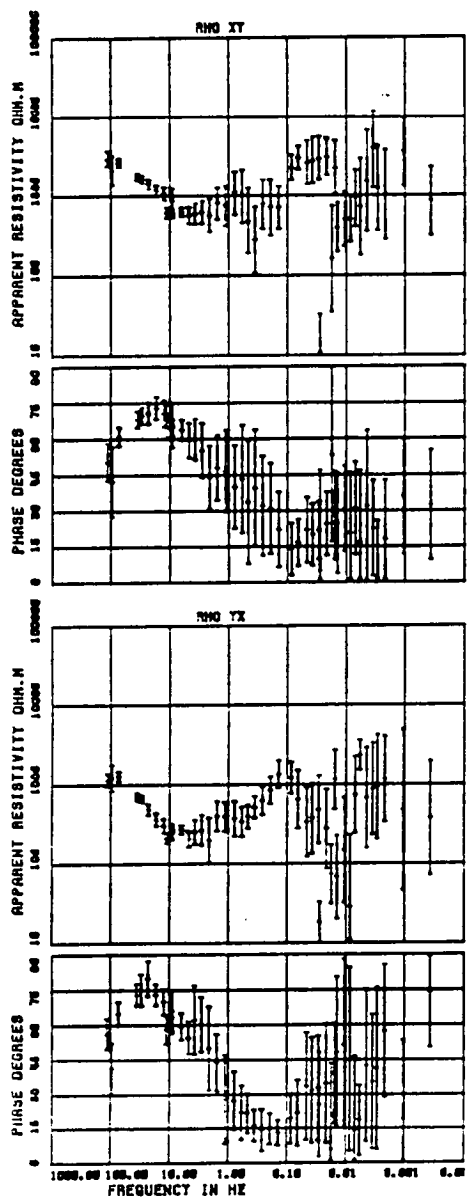

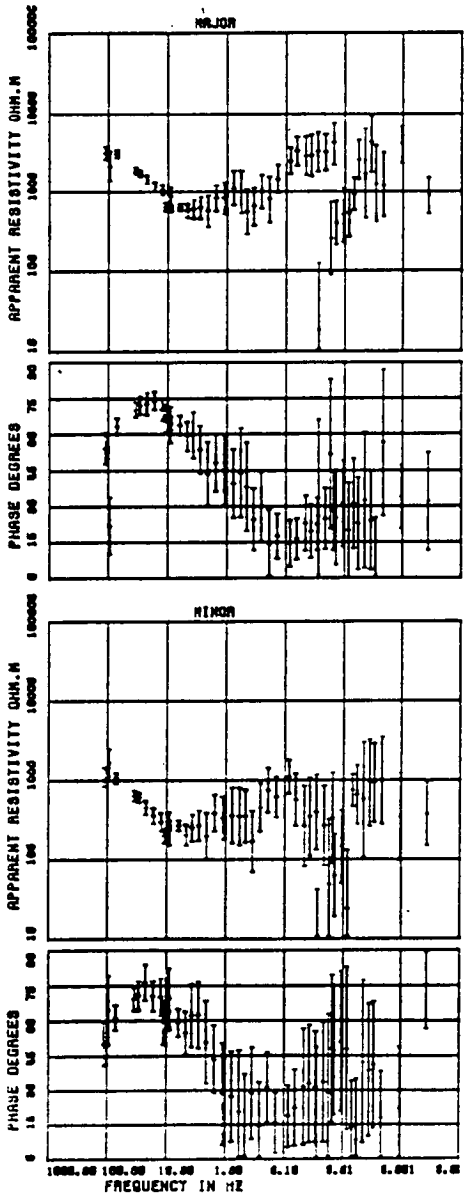

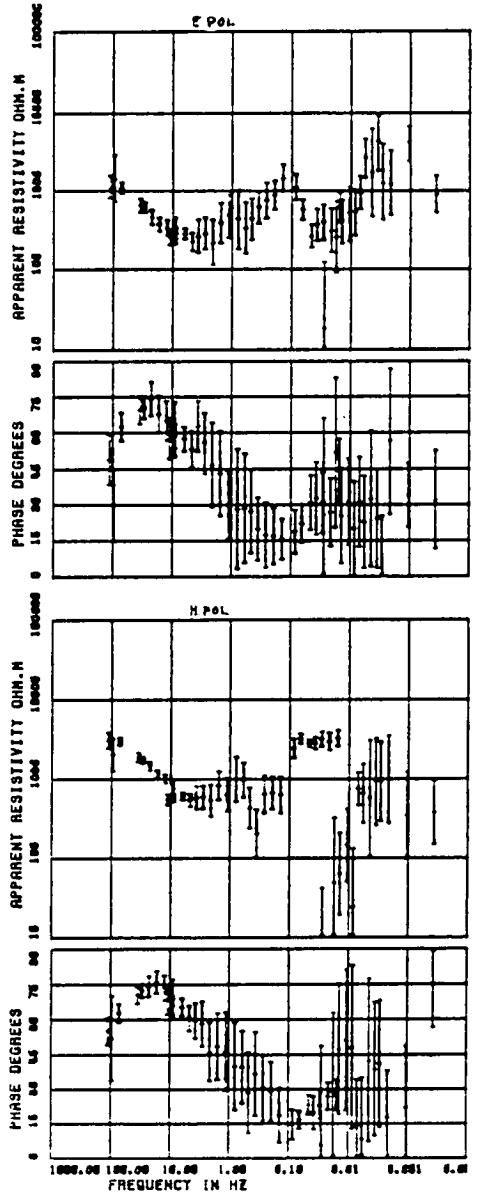

MT RESPONSE CURVES SITE 450 C.S. ANTONIO

(e)

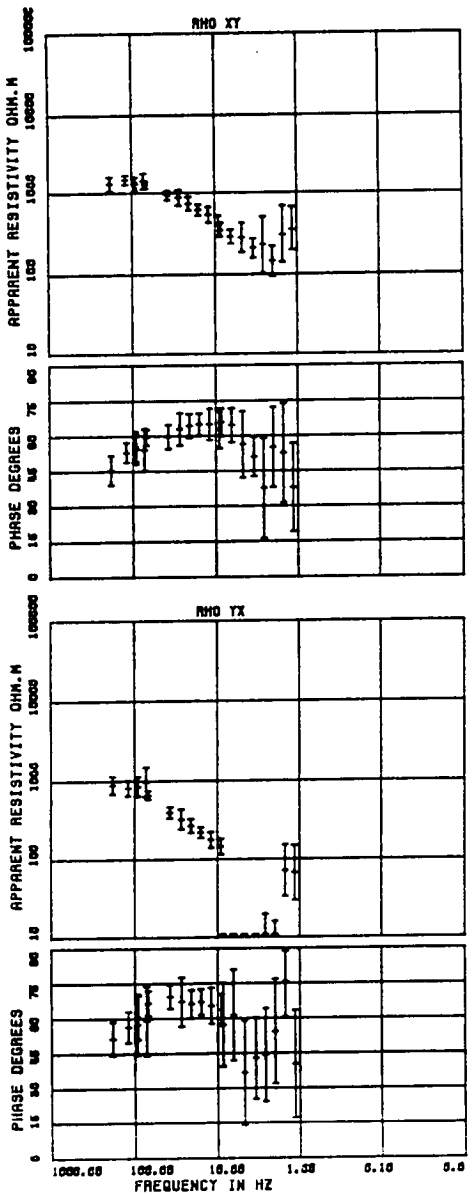

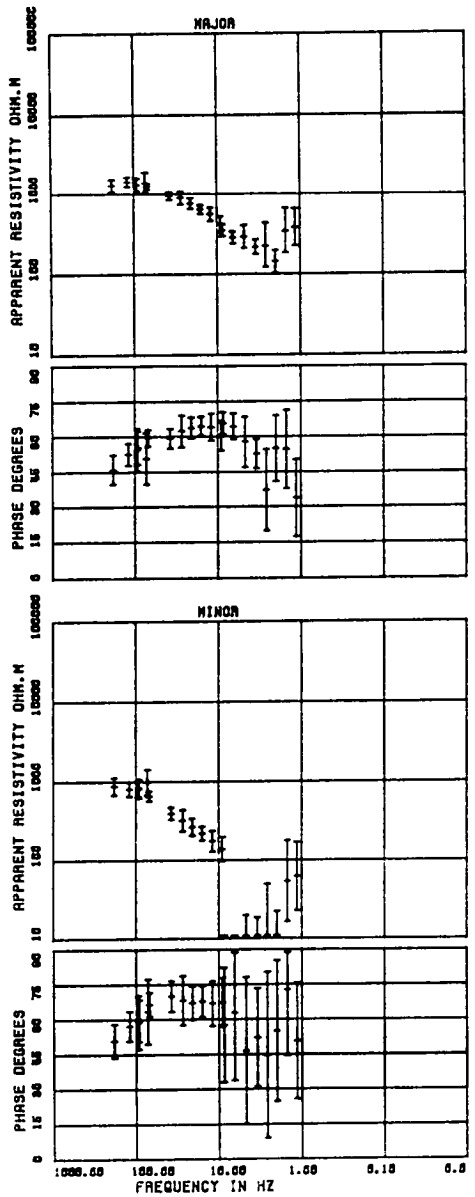

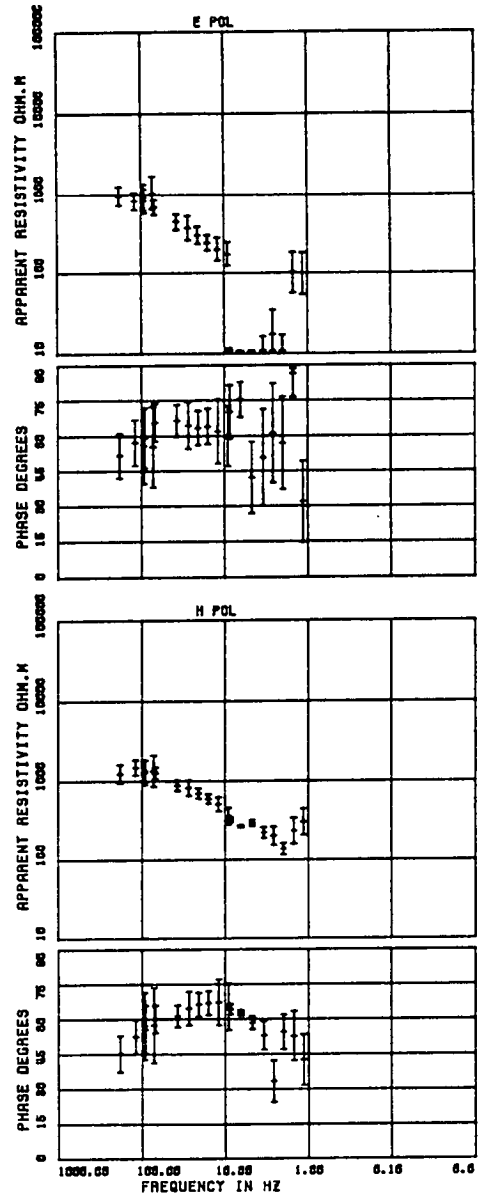

MT RESPONSE CURVES SITE 451 OBSERVATORIO

(f)

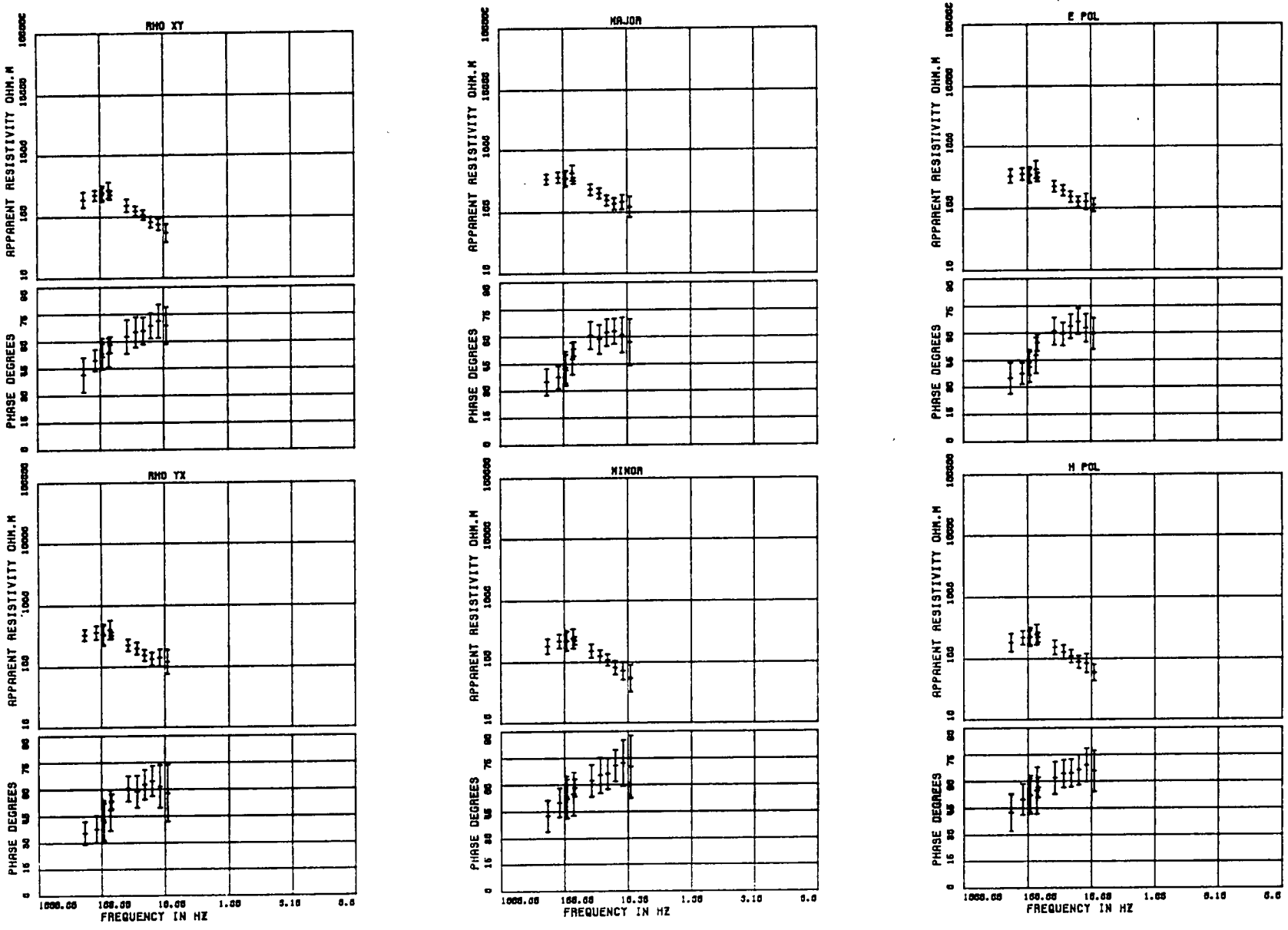

MT RESPONSE CURVES SITE 453 AVE

(g)

MT RESPONSE CURVES SITE 452 GRANEZZA

(h)

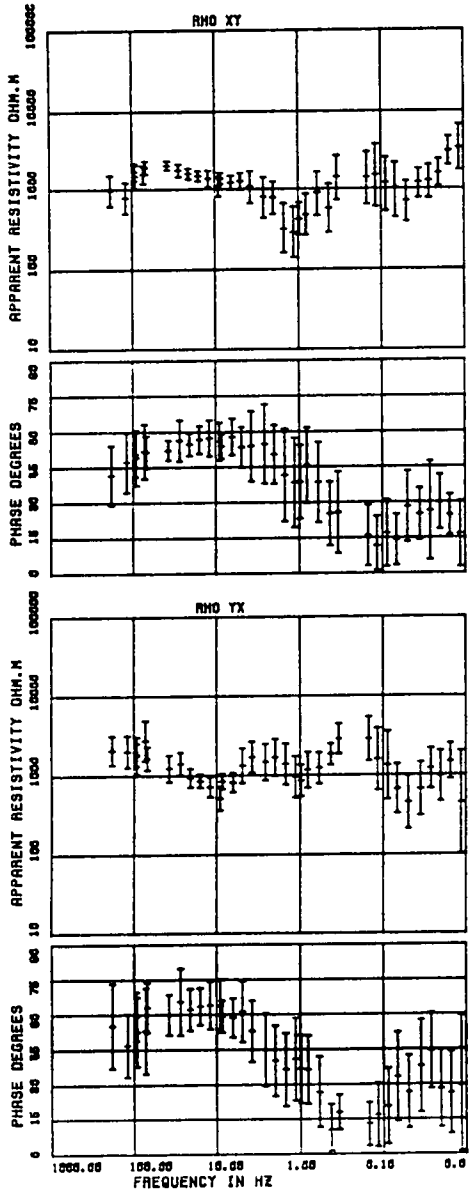

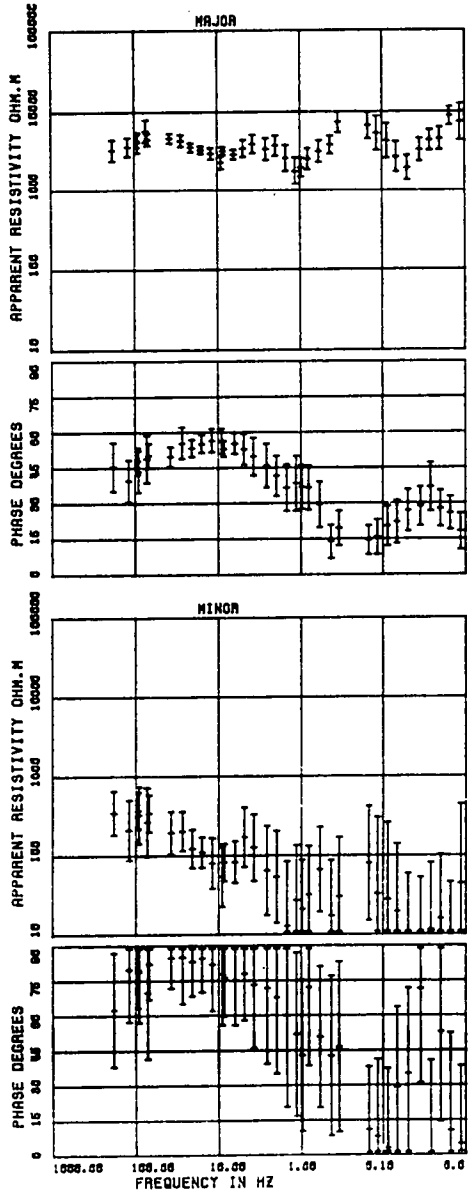

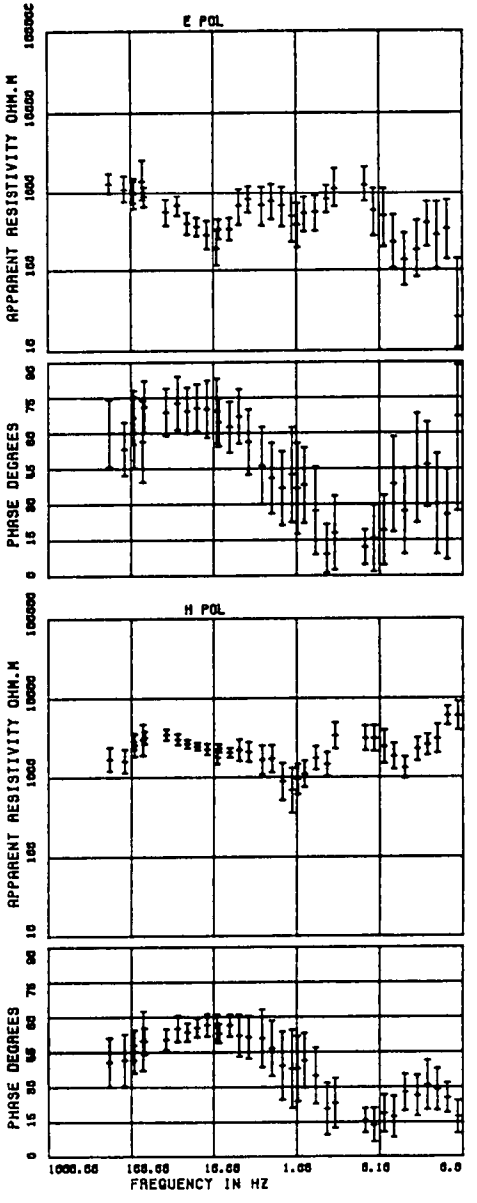

Fig. 6.3(a)-(h)- Asiago results (continuation). MT response curves (rotationally invariant) for all the sites, number of estimates used for averaging in each frequency set, azimuth values for the major direction, skew and dimensional weights values. Auxiliary information related to the processing (e.g., number of samples per window, cut- off frequencies for high and low pass filters, etc) are also displayed at the top of each of the Figs.

SITE : 456A

	4560A	4561A	4562A	4563A
CARTRIDGE	1	2	3	4
BAND	4	4	4	4
COMPONENTS	256	256	256	256
SAMPLES/WINDOW	60	60	60	5%
NUMBER WINDOWS	2048	256	32	4
SAMPLE RATE HZ	0.00	1.00	0.12	0.01
PLOT HPF	0.00	100.00	20.00	9.00
PLOT LPF	0	0	0	0
FREQS/DECADE	7	7	0	11
FREQS/BAND	0.00	0.00	0.00	0.00
MIN COHERENCY	2	2	2	2
REJECTION LOOPS				

(a)

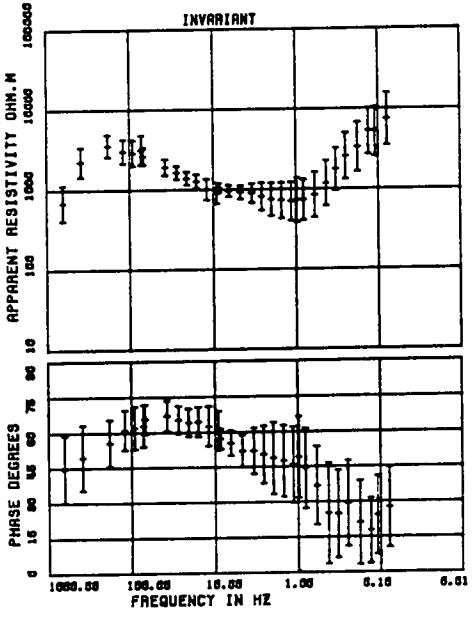

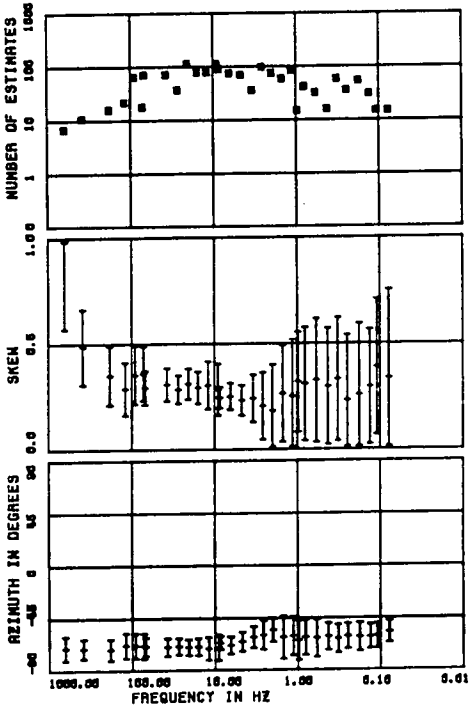

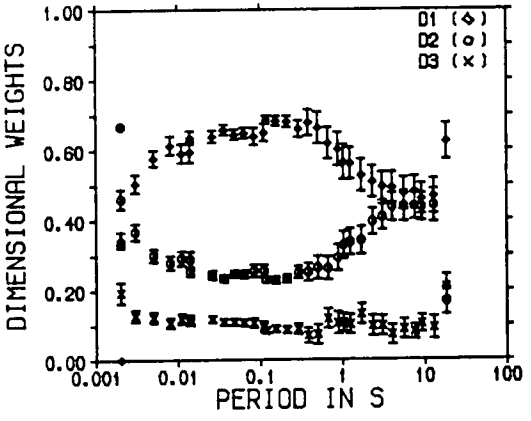

SITE : 454A

CARTRIDGE :	454GA	454HA	454JA	454KA
BAND :	1	2	3	4
COMPONENTS :	4	4	4	4
SAMPLES/WINDOW :	256	256	256	256
NUMBER WINDOWS:	30	60	60	60
SAMPLE RATE HZ :	2048	256	32	4
PLOT HPF :	0.00	1.00	0.12	0.01
PLOT LPF :	0.00	100.00	24.00	3.00
FREQS/DECADE :	8	8	8	8
FREQS/BAND :	4	8	8	8
MIN COHERENCY :	0.80	0.80	0.80	0.80
REJECTION LOOPS:	2	2	2	2

(b)

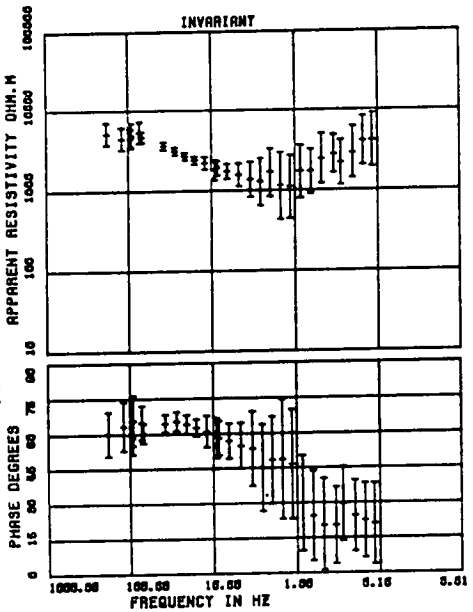

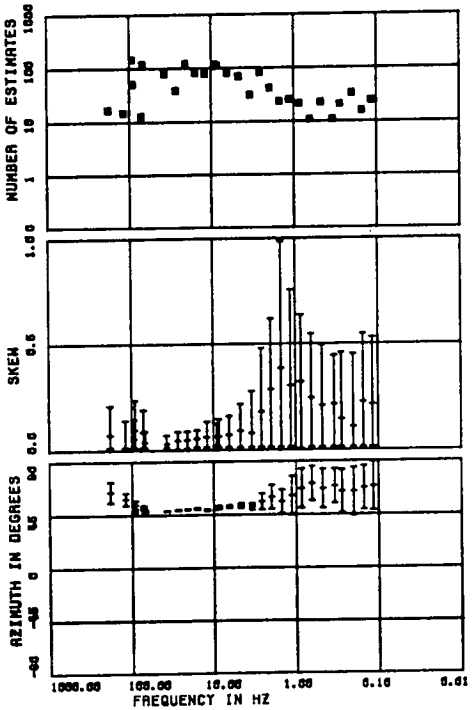

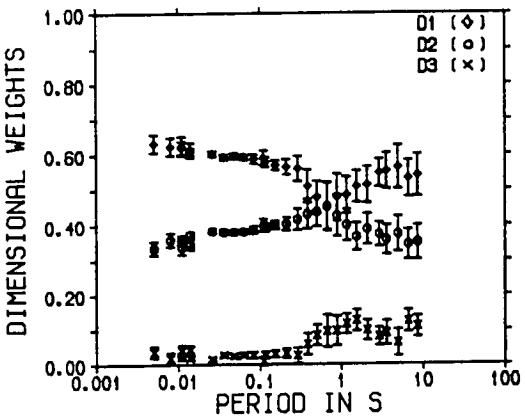

SITE : 455A

	4551A	4552A	4553A
CARTRIDGE	2	3	4
BAND	4	4	4
COMPONENTS	256	256	256
SAMPLES/WINDOW	30	60	61
NUMBER WINDOWS	256	32	4
SAMPLE RATE HZ	1.66	6.12	6.61
PLOT HPF	166.66	24.66	3.66
PLOT LPF	6	6	6
FREQS/DECADE	8	8	8
FREQS/BAND	6.66	6.66	6.66
MIN COHERENCY	2	2	2
REJECTION LOOPS			

(c)

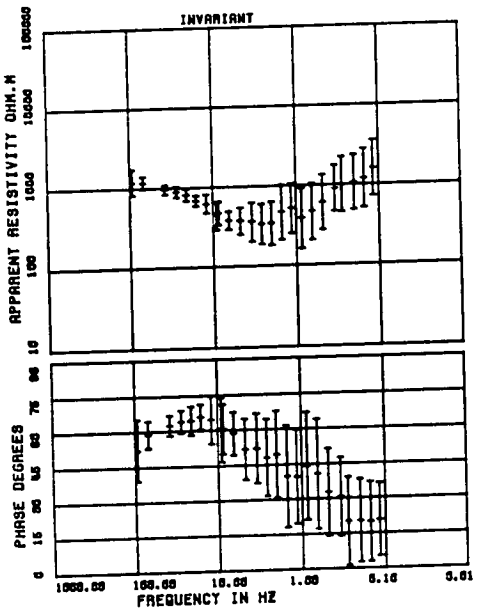

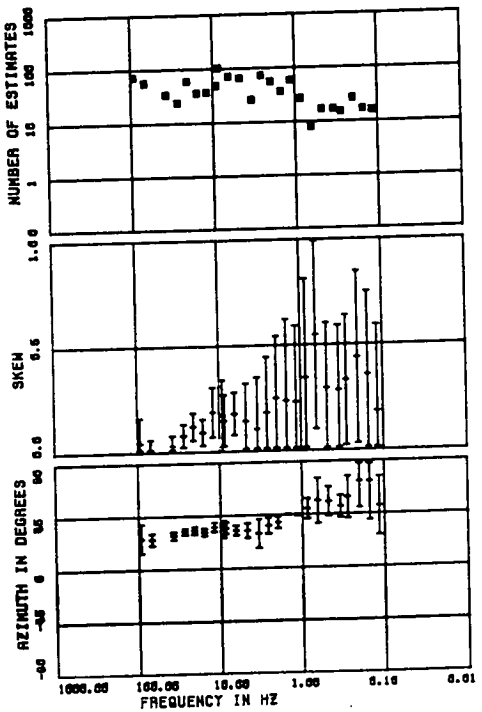

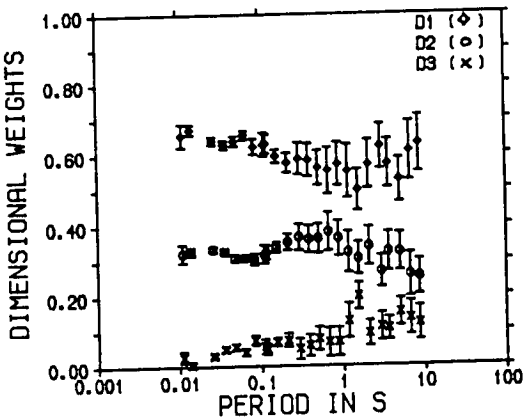

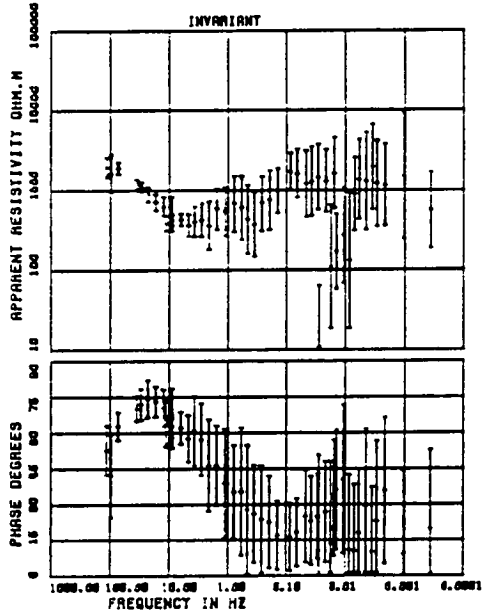

SITE 690A

CARTRIDGE :	6960A	5961A	5962B	5963B	6964A	6965A
BAND :	1	2	3	4	4	5
COMPONENTS :	4	4	4	4	4	4
SAMPLES/WINDOW :	256	256	256	256	256	256
NUMBER WINDOWS:	46	46	52	114	24	6
SAMPLE RATE HZ :	512	64	8	1	0	0
PLOT HPF :	8.66	1.66	0.12	0.01	0.002	0.0002
PLOT LPF :	128.66	12.66	1.66	0.16	0.033	0.0046
FREQS/DECADE :	8	8	8	8	16	16
FREQS/BAND :	9	9	7	7	13	13
MIN COHERENCY :	0.75	0.75	0.75	0.75	0.75	0.75
REJECTION LOOPS:	2	2	2	2	2	2

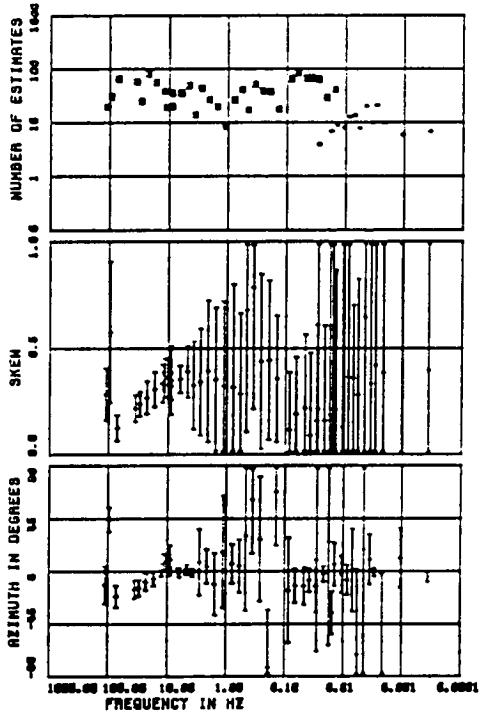

(d)

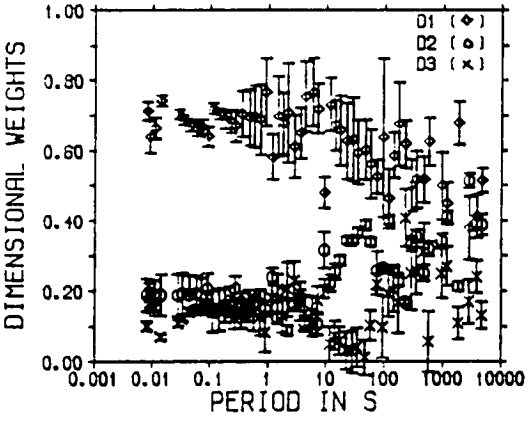

SITE : 450A

CARTRIDGE	4500A	4501A	4502A
BAND	1	2	3
COMPONENTS	4	4	4
SAMPLES/WINDOW	256	256	256
NUMBER WINDOWS	66	66	53
SAMPLE RATE HZ	2048	256	32
PLOT HPF	0.00	1.00	0.12
PLOT LPF	0.00	100.00	24.00
FREQS/DECADE	8	8	8
FREQS/BAND	4	8	8
MIN COHERENCY	0.00	0.00	0.00
REJECTION LOOPS	2	2	2

(e)

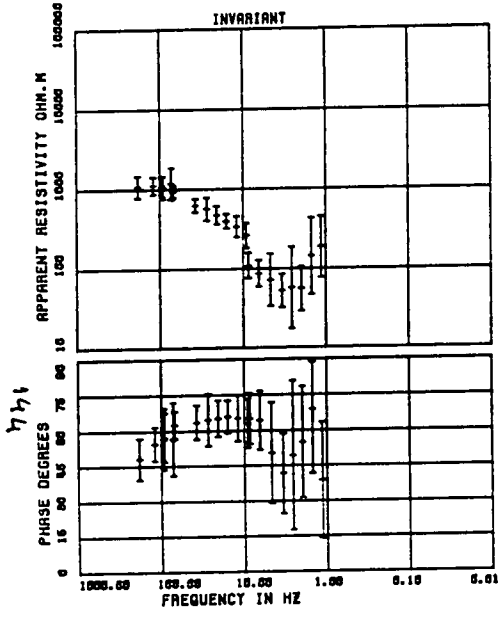

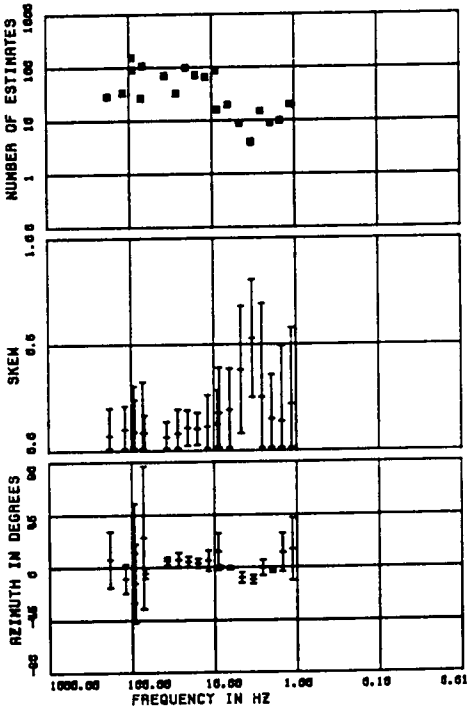

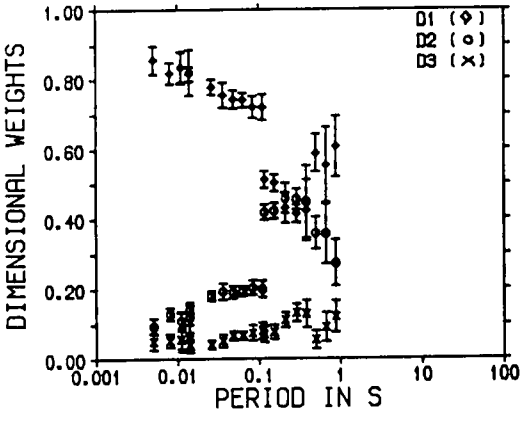

(f)

SITE : 451A

CARTRIDGE	:	4516A	4511A
BAND	:	1	2
COMPONENTS	:	4	4
SAMPLES/WINDOW	:	256	256
NUMBER WINDOWS	:	96	88
SAMPLE RATE HZ	:	2048	256
PLOT HPF	:	0.00	1.00
PLOT LPF	:	0.00	100.00
FREQS/DECADE	:	8	8
FREQS/BAND	:	4	8
MIN COHERENCY	:	0.00	0.00
REJECTION LOOPS	:	2	2

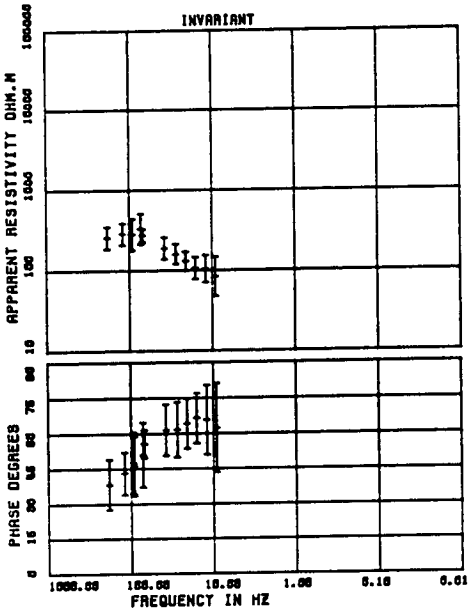

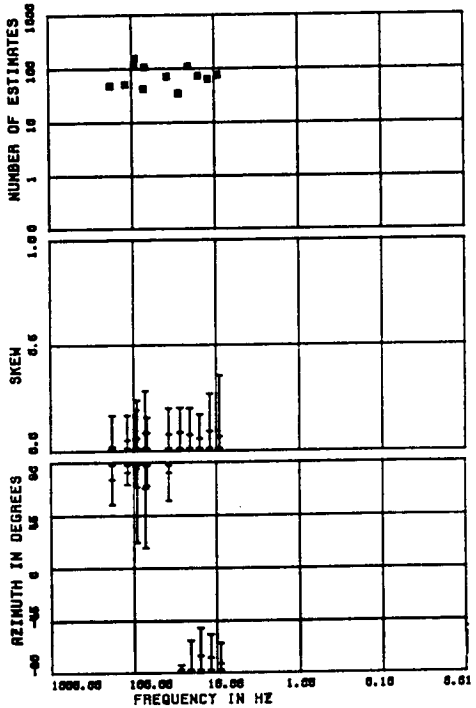

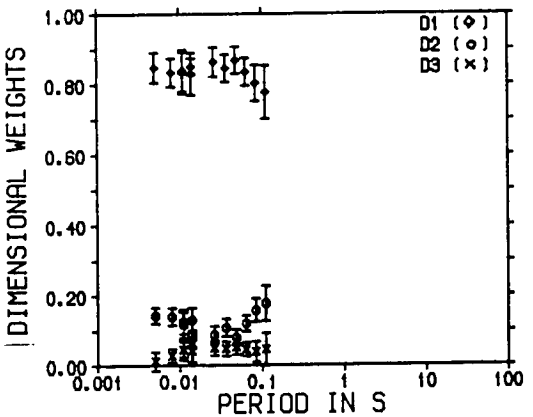

(g)

SITE : 453A

		4530A	4531A	4532A	4533A
CARTRIDGE	:				
BAND	:	1	2	3	4
COMPONENTS	:	4	4	4	4
SAMPLES/WINDOW	:	256	256	256	256
NUMBER WINDOWS	:	80	80	36	80
SAMPLE RATE HZ	:	2048	256	32	4
PLOT HPF	:	0.00	1.00	0.12	0.01
PLOT LPF	:	0.00	100.00	24.00	3.00
FREQS/DECADE	:	8	8	8	8
FREQS/BAND	:	7	7	8	11
MIN COHERENCY	:	0.00	0.00	0.00	0.00
REJECTION LOOPS	:	2	2	2	2

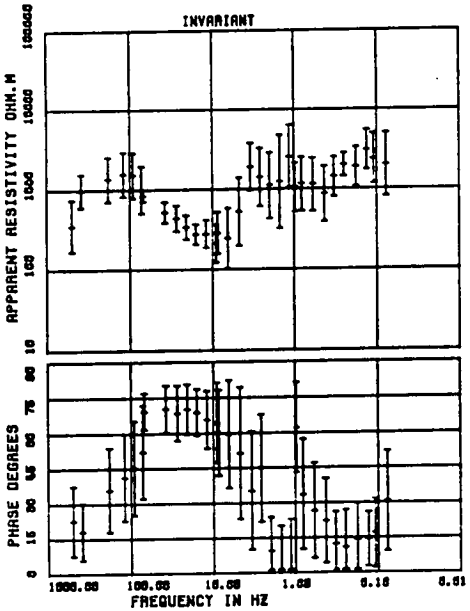

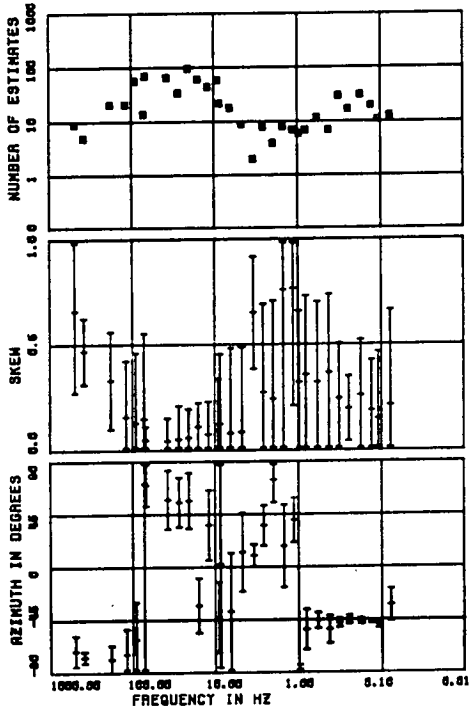

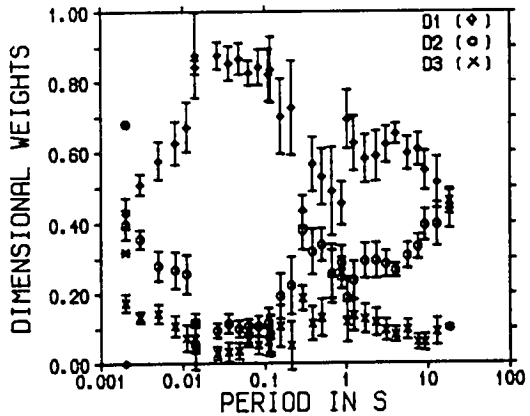

SITE : 452A

CARTRIDGE	4520A	4521A	4522A	4523A	452
BAND	1	2	3	4	5
COMPONENTS	4	4	4	4	4
SAMPLES/WINDOW	256	256	256	256	102
NUMBER WINDOWS	59	60	86	48	24
SAMPLE RATE HZ	2048	256	32	4	1
PLOT HPF	8.88	1.88	0.12	0.01	0.0
PLOT LPF	0.00	100.00	24.00	3.00	0.5
FREQS/DECADE	8	8	8	8	8
FREQS/BAND	4	8	8	5	10
MIN COHERENCY	0.80	0.80	0.80	0.80	0.8
REJECTION LOOPS	2	2	2	2	2

(h)

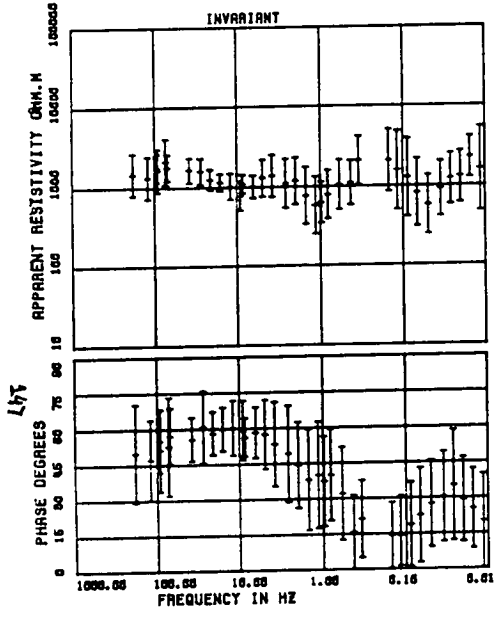

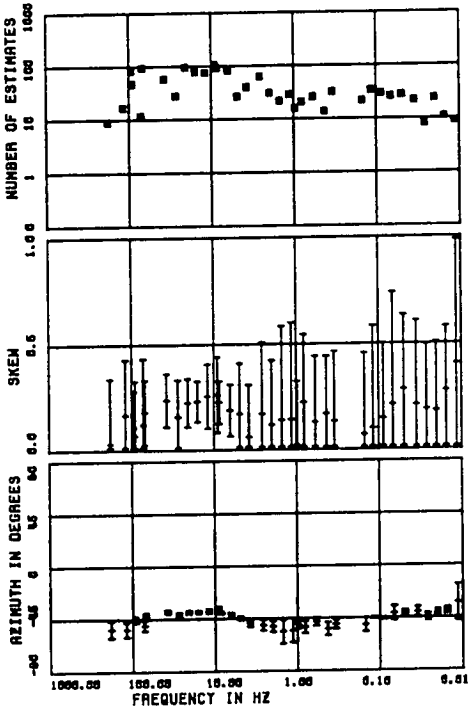

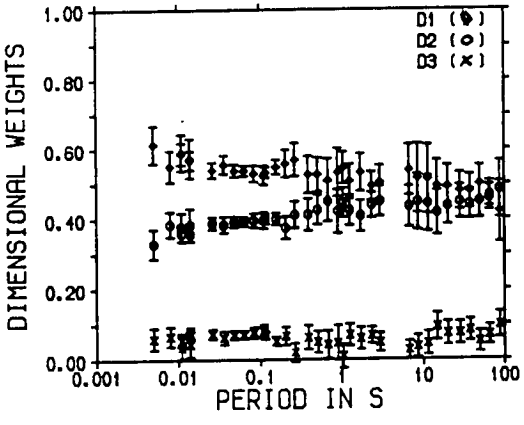

this site alone, lends support to the plausibility of the results obtained for the other sites in this region and therefore contributes to the credibility of the modelling studies presented in Chapter 7.

As expected from young mountainous formations, the whole region is resistive, with the apparent resistivity values at high frequencies (i.e. corresponding to shallow depths) over 1000Ωm at half of the sites. The northernmost sites (Figs. 6.2(a)-(b) and Figs. 6.3(a)-(b)) and the southernmost site (Fig. 6.2(h) and Fig. 6.3(h)) exhibited the highest apparent resistivity values of the profile, while the central sites (Figs. 6.2(c)-(g) and Figs 6.3(c)-(g)) exhibited lower apparent resistivity values.

The localized complex fault system observed in the region (shown in Fig. 6.1), along with the well known ambiguity of the azimuth determinations when the tipper information is not available (actually only available for 2 sites in the Cavalese area, Lavaze (LAV) and Daiano (DAI), as illustrated in Figs. 6.4(a)-(b)), make the unequivocal relation between estimated azimuths and the geological strike a rather difficult task. Moreover, the conventional method of strike determination described in Chapter 4 has been shown to be biased towards the local strike (Zhang et al ,1987) Some suggestions/rules for strike determination can be found elsewhere (e.g. Gamble et al, 1982; Wannamaker et al, 1984; Zhang et al, 1987). Nevertheless, these authors tend to reckon that the regional strike can only be uniquely determined by additional constraint- either from geological considerations or from tipper strikes. For 1D studies, to be presented in Chapter 7, this difficulty is circumvented by modelling the rotationally invariant response curves. In addition, the response curves rotated to a regional strike direction (E-pol and H-pol) are also considered in these 1D modelling studies. The adopted strike (76^0E), used also in the 2D studies treated in Chapter 7, is the regional strike posed by the Alpine belt and given by the average direction of the Insubric Line (described in Chapter 1) in this region.

The general pattern observed in all the responses of the region (perhaps more quickly assessed by looking at the invariant curves in Figs. 6.3 and disregarding a weathered superficial layer not well characterized in the frequency range 500Hz- 100Hz), suggests a gross 3 layered structure which exhibits a resistive top layer, an intermediate relatively conductive layer and a resistive basement. As can be depicted from the response curves shown in

Fig. 6.4- Magnetic results for sites LAV (a) and DAI (b) in the Cavalese area. Real and imaginary parts of the magnetic transfer functions and respective azimuths. Number of estimates per frequency are also shown in the Fig.

(a)

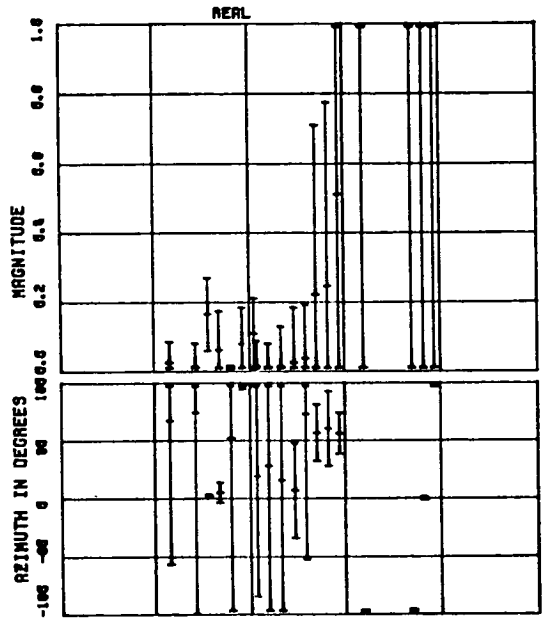

SITE 580A LAV

CARTRIDGE :	5801A	5802A	5803A
BAND :	2	3	4
COMPONENTS :	6	6	6
SAMPLES/WINDOW :	256	256	256
NUMBER WINDOWS :	72	84	24
SAMPLE RATE HZ :	256	32	4
PLOT HPF :	0.06	1.00	0.10
PLOT LPF :	60.00	10.00	1.00
FREQS/DECADE :	8	8	8
FREQS/BAND :	7	8	8
MIN COHERENCY :	0.60	0.60	0.60
REJECTION LOOPS :	2	2	2

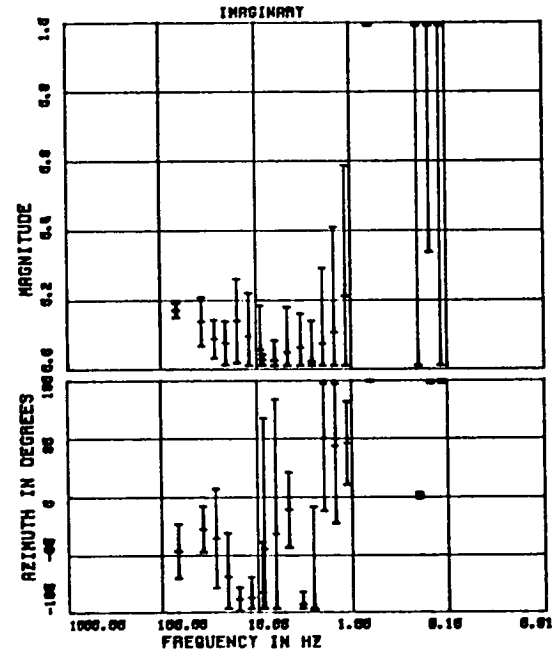

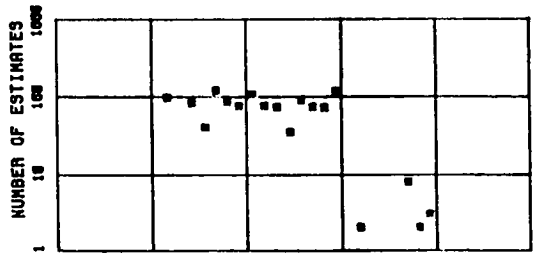

(b)

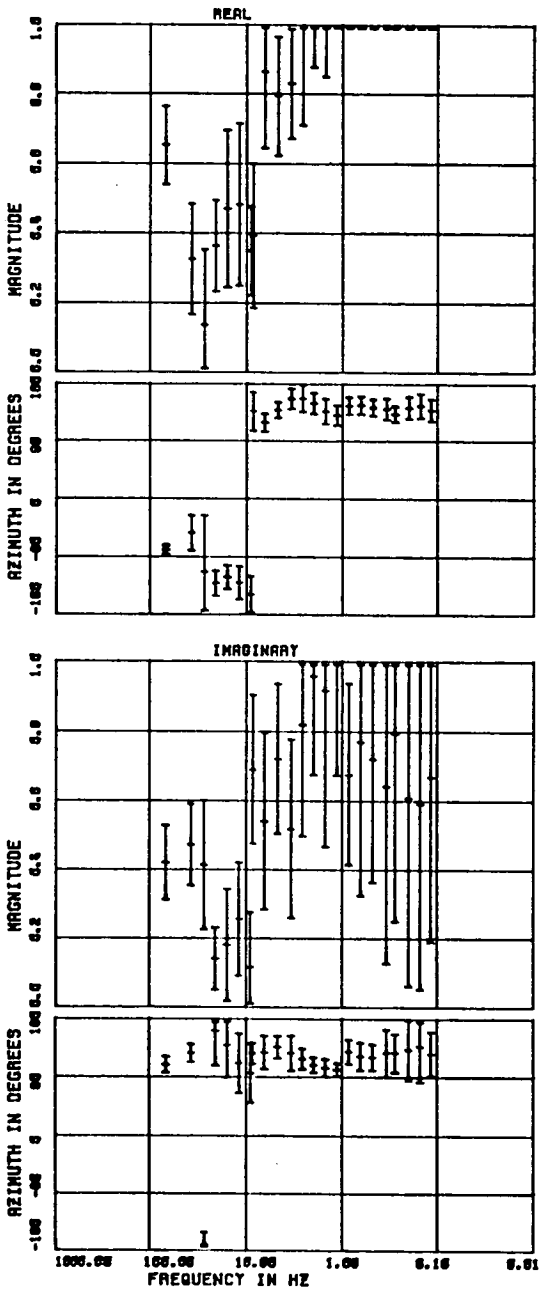

SITE : 581A DAI

CARTRIDGE :	5811A	5812A	5813A
BAND :	2	3	4
COMPONENTS :	5	5	5
SAMPLES/WINDOW :	256	256	256
NUMBER WINDOWS :	6	6	6
SAMPLE RATE HZ :	256	92	4
PLOT HPF :	0.05	1.00	0.10
PLOT LPF :	80.00	10.00	1.00
FREQS/DECADE :	8	8	8
FREQS/BAND :	7	8	8
MIN COHERENCY :	0.00	0.00	0.00
REJECTION LOOPS :	2	2	2

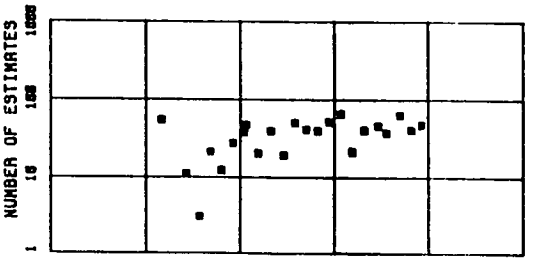

Figs. 6.2 and 6.3, the overall data quality cannot be regarded as high. Nevertheless, no major inconsistency is observed in the data sets. However, both the limited number of stations and the small extension of the profile are obvious obstacles to a bold interpretation of the conductive structure in the region.

6.2.2 Dimensionality study

Before analysing in detail the values of the dimensionality indicators for actual data from Asiago, the dimensional weights (described in Chapter 4- Eqs. 4.47) were computed for 6 hypothetical sites of the synthetic 2D Earth shown in Fig. 6.5. This 2D model, chosen for bearing a possible resemblance with the actual structure in this region, was computed for 20 frequencies in the range $1000-10^{-2}$Hz using the Jupp and Vozoff (1977) code (described in some detail in Chapter 7). The tensor elements, derived from the E and H pol impedance response curves, were then used in the estimation of the dimensional weights. The E pol and H pol response curves for all the sites are summarized in Figs. 6.6(a)-(c). It can be observed that the sites further away from the 2D discontinuity (e.g. sites 1,2 and 6) have E pol and H pol responses almost identical suggesting a 1D structure, while at the remaining sites (3 , 4 and 5) there is a clear mismatch, indicating nearby lateral discontinuities. The resulting dimensional weights D1 and D2 for all the sites are shown in Fig 6.7. They indicate that for sites 1, 2 and 6 located far away from the conductivity discontinuity, the 2D effects are negligible, and in conformity with the analysis of the E pol and H pol curves. Hence D1 is nearly 1 and consequently D2 is nearly 0 throughout the whole frequency range. As expected, the closer to the discontinuities, the larger the 2D contribution is and so larger is D2. For instance, site 4, at the centre of the 2D anomaly, is the most affected site, with larger values of D2 especially at the longer periods. It is interesting to note that the values of D1 are always larger than D2 at all the sites. This indicates that the 1D feature is still dominant throughout the profile. Tri- dimensionality indicators (i.e. skew and D3) are naturally zero for pure 2D situations and could not be assessed by this study. The full validity of this synthetic study is further limited by the fact that anisotropy (either in the rock fabrics or due to folded Earth structure) has also been neglected, and anisotropy may play an important role in the nappes structure found in the Alps. Nevertheless, in real situations, it is

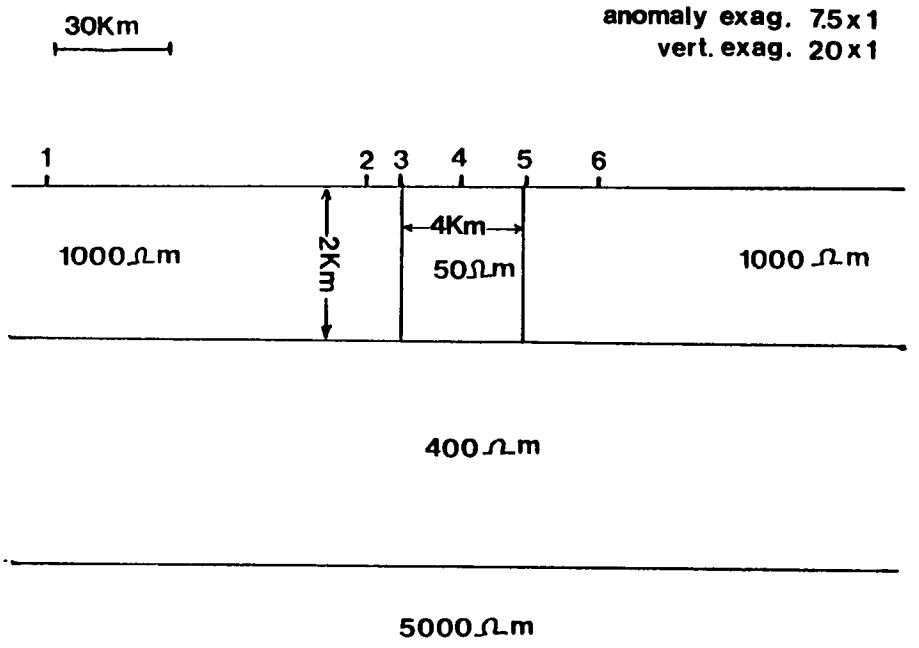

Fig. 6.5- Synthetic 2D model. The sites are assigned in the Fig. and their relative distances to the lateral discontinuity are given in K m.

Fig 6.6(a)-(c)- MT responses for the 6 sites for the synthetic 2D model of Fig. 6.5.

STATION 1

(a)

E POL (∞)
H POL (+)

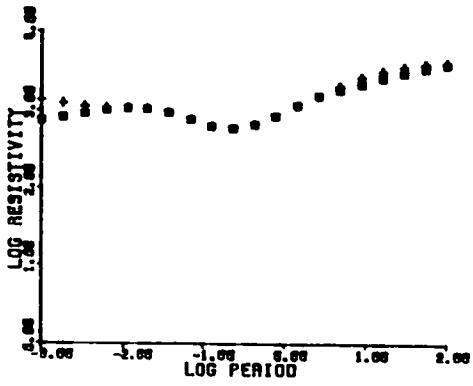

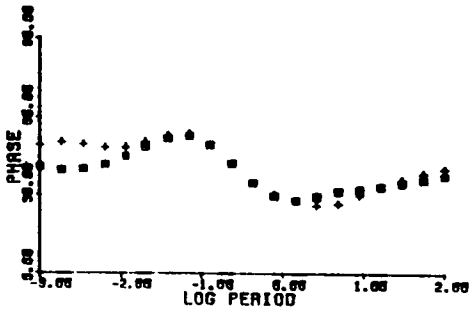

STATION 2

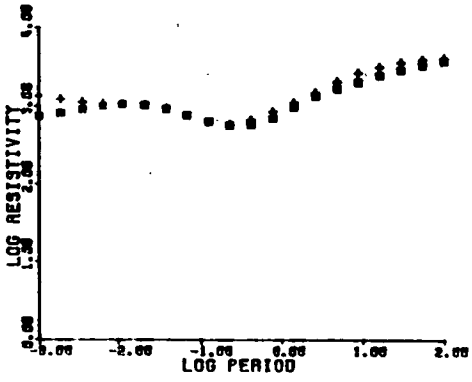

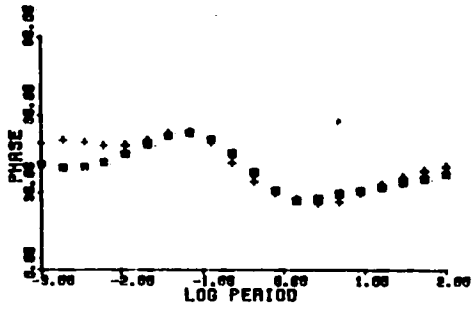

STATION 3

(b)

E POL (▫)
H POL (+)

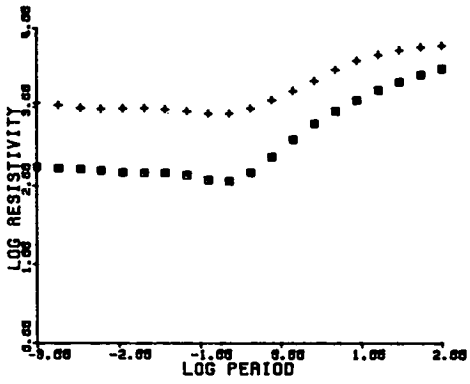

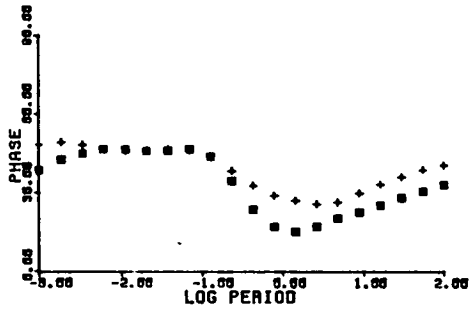

STATION 4

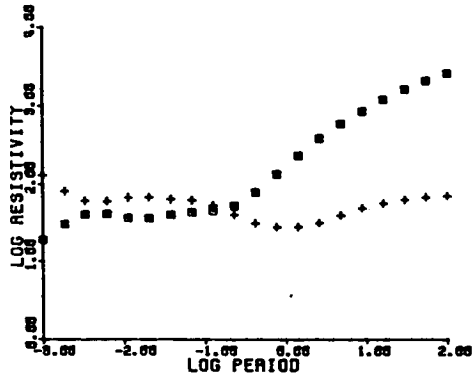

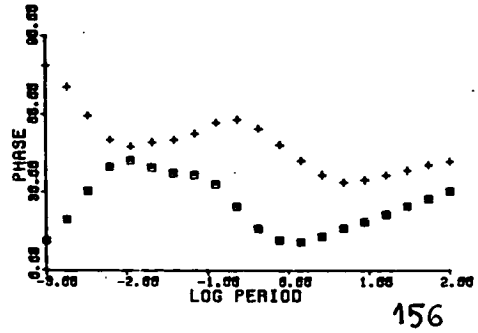

STATION 5

(c)

E POL (□)
H POL (+)

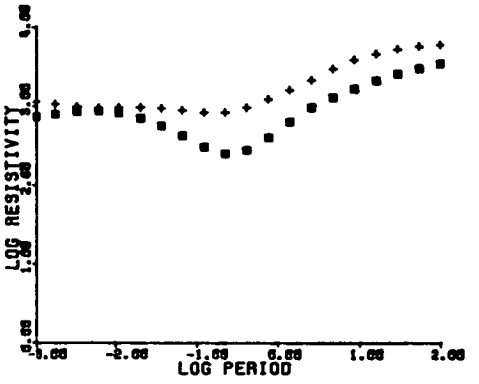

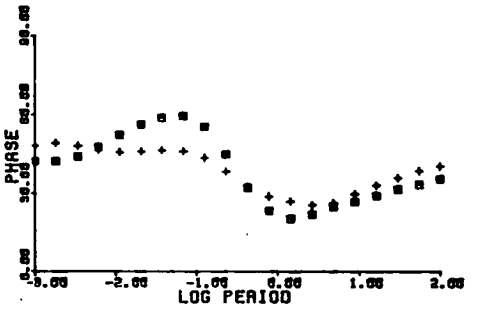

STATION 6

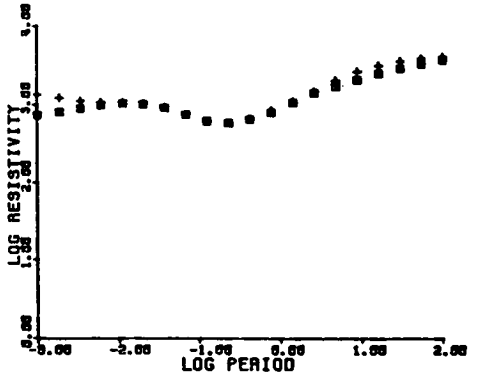

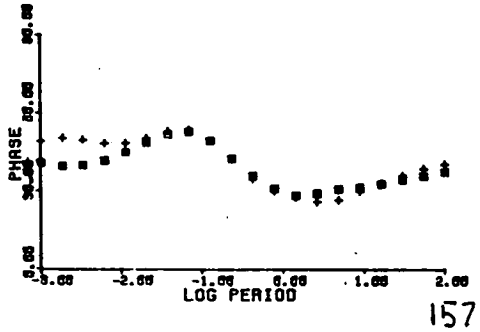

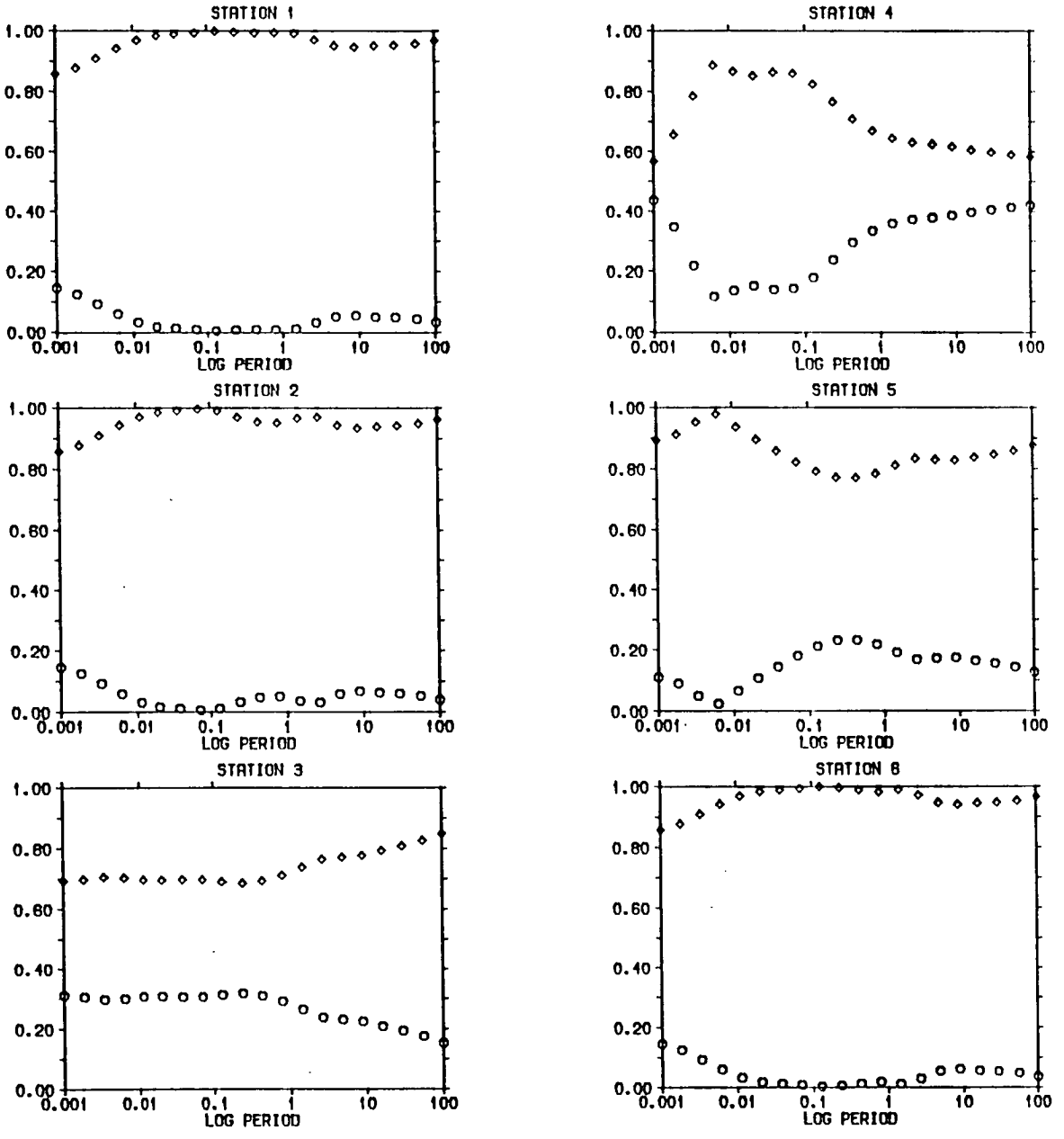

Fig. 6.7- Dimensional weights D1 and D2 for the 6 sites for the synthetic 2D model of Fig. 6.5.

usually difficult to distinguish between anisotropy and lateral inhomogeneities. As a result, it is a common practice to neglect anisotropy effects in most 2D studies. The use of the Weidelt's constraints was also attempted in this 2D synthetic study, but all the sites failed the fourth constraint (Eq. 4.48(d)) imposed on the response curves. In other words, applications of this constraint confirmed that the data at all the sites were, in a strict sense, 2D, rather than 1D. However, the Weidelt's constraints were verified to be obeyed when checked for a pure 1D situation.

The dimensional weights computed for Asiago (Figs. 6.3(a)-(h)) show that D1 is the overall largest parameter for all sites and they suggest a dominant 1D structure in this area. The 2D contribution (given by D2) varies considerably from site to site, but it is generally higher for lower frequencies and at the extremities of the profile. Tri- dimensional effects seems to be very minor all through the profile and for the whole frequency range. The use of the skew values (also in Figs. 6.3(a)-(h)) as a reliable tridimensional indicator has been questioned in the literature (see discussion in section 4.3). Nevertheless, the skew values are generally lower than 0.4 for most sites and frequencies. This seems to corroborate the results exhibited by the dimensional weights and to suggest that 3D contributions are small (if not negligible) in this region. It is thus reasonable to assume that the 1D studies (presented in Chapter 7) represent the general conductivity structure of the region, while the 2D results (also presented in Chapter 7) 'refine' these 1D model results.

6.3 Cavalese area

This region is dominated by volcanic detrital Permo- Scynthian rocks with sedimentary slabs observed along the Insubric Line. Despite being located in the same Venetian platform, this region is marked by a more general uplift of varying intensity, linked basically to isostatic readjustment processes within the Alpine range with Cretaceous- Paleogenic tectogenesis (Zanferrari et al, 1982).

A location map showing the sites in this region is given in Fig. 6.8. The MT results for the 5 sites in the region are shown -as for the Asiago sites- in Figs. 6.9(a)-(e) for the measurement directions x, y, the major and

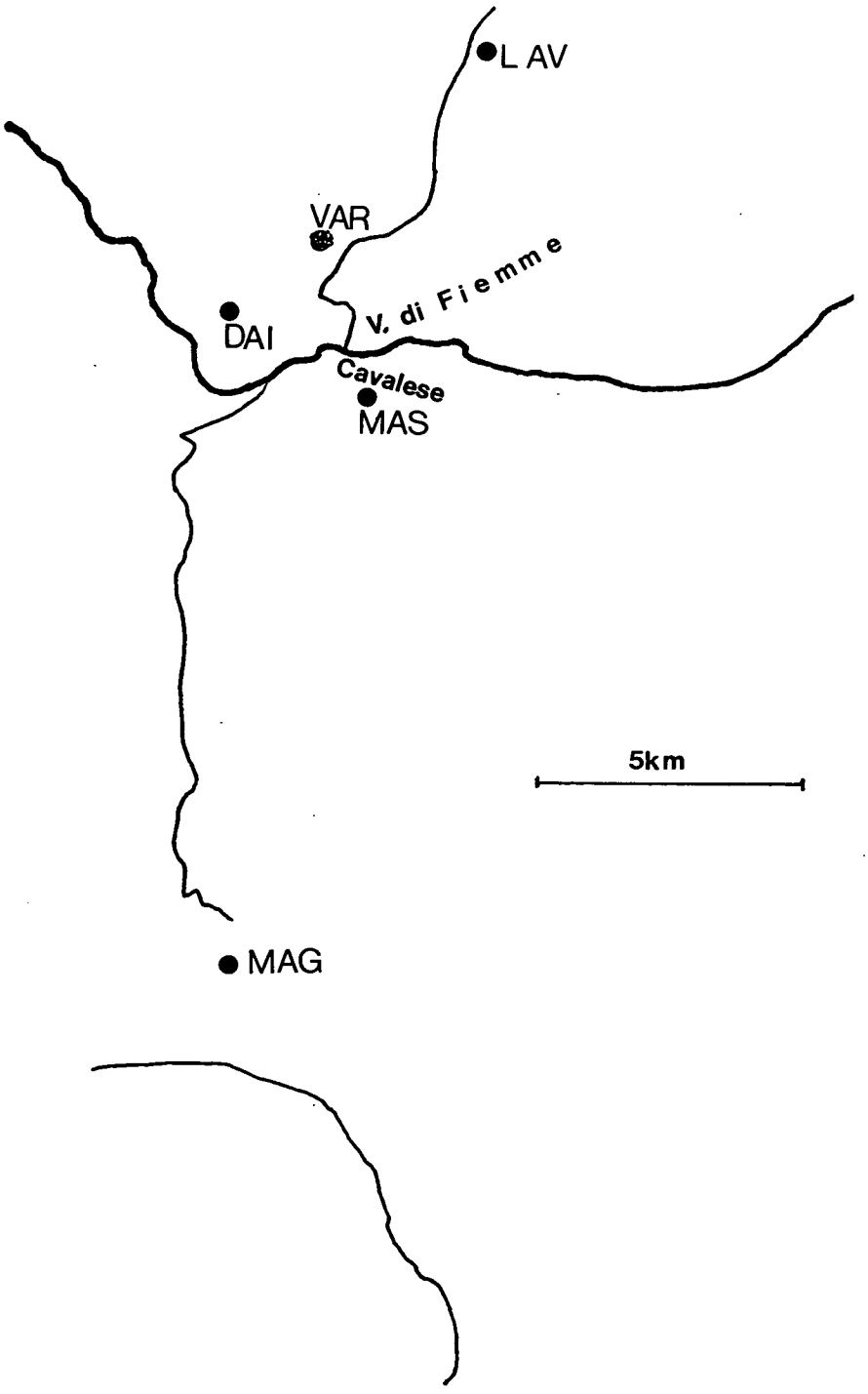

Fig. 6.8- Cavalese area map. MT sites are assigned by bold circles.

Fig. 6.9(a)-(e)- MT response curves for all the sites in Cavalese area. See legend of Fig. 6.2.

MT RESPONSE CURVES SITE 463 P. LAVAZZE

(a)

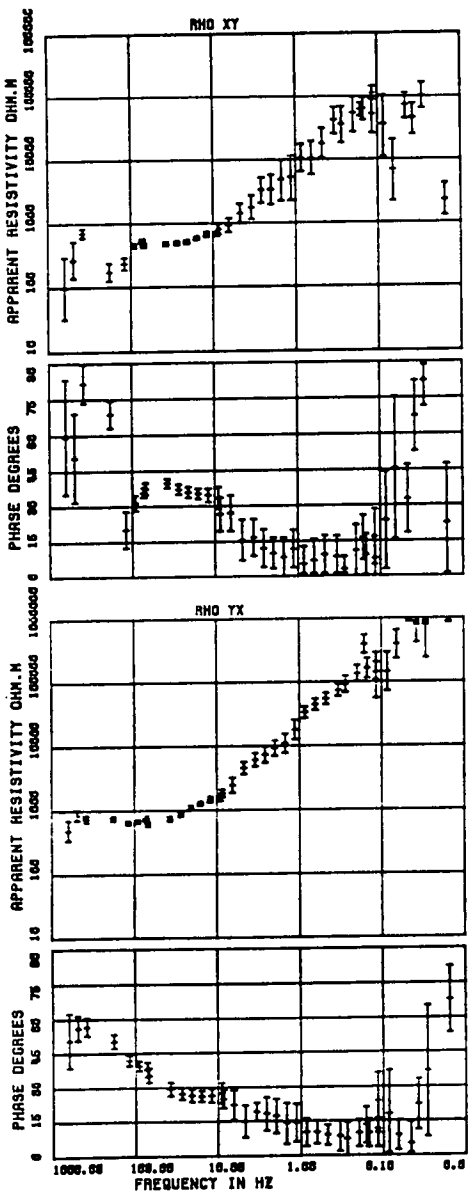

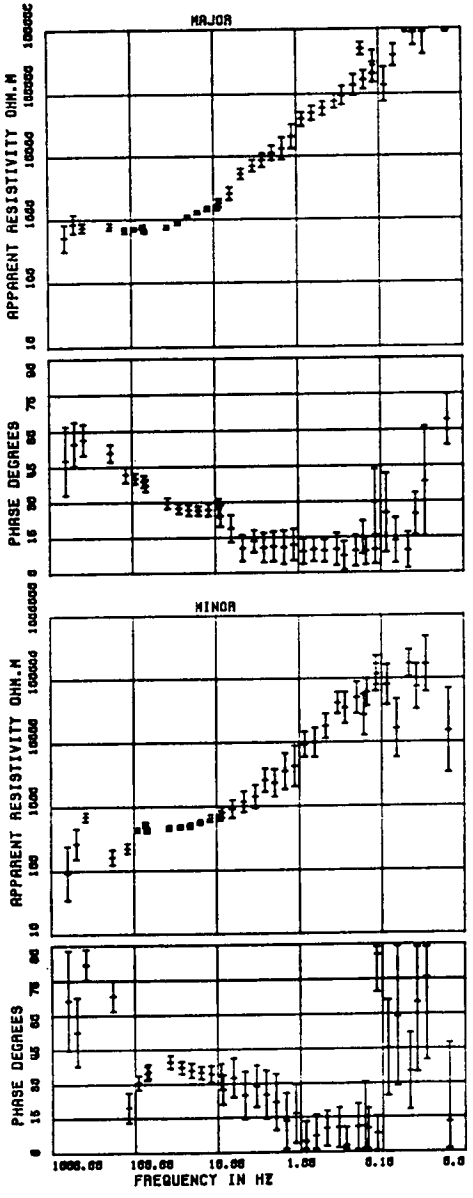

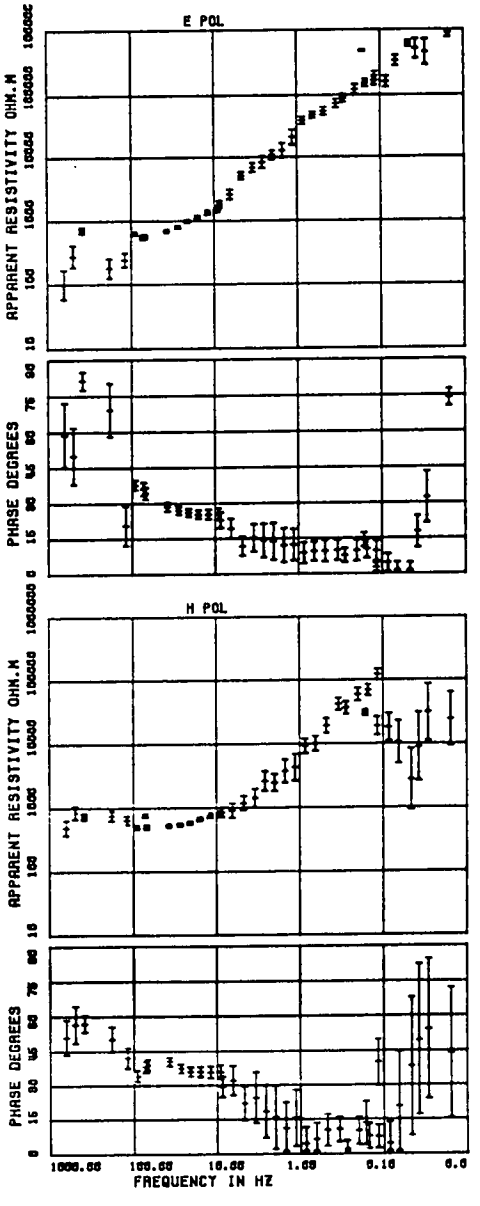

MT RESPONSE CURVES SITE 581 DAIANO

(b)

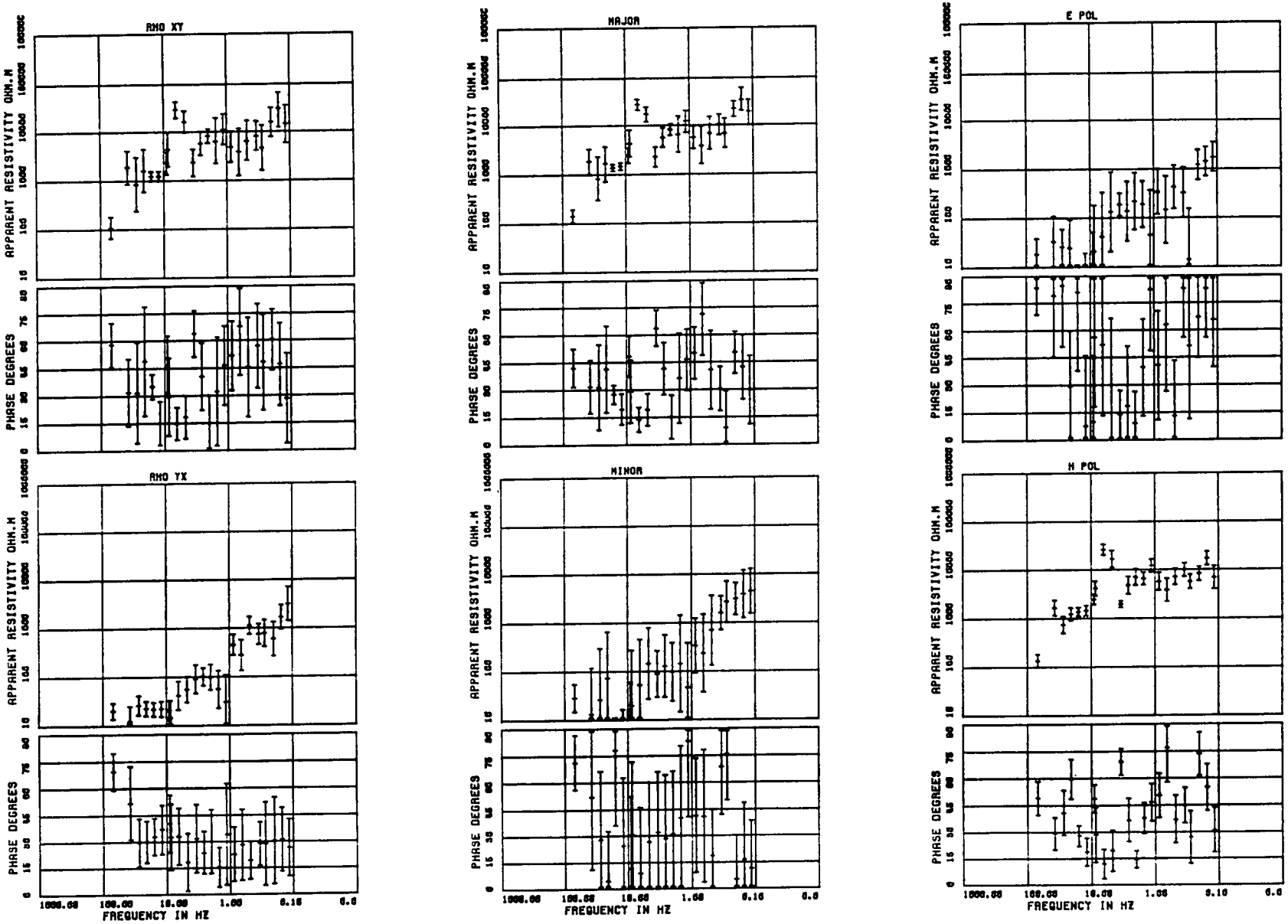

MT RESPONSE CURVES SITE 460 CALVELLO

(c)

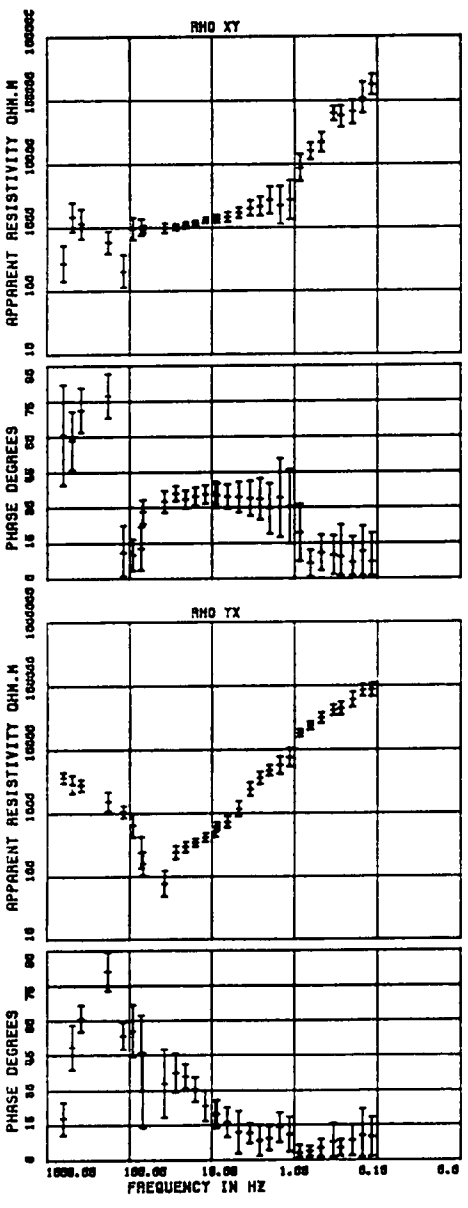

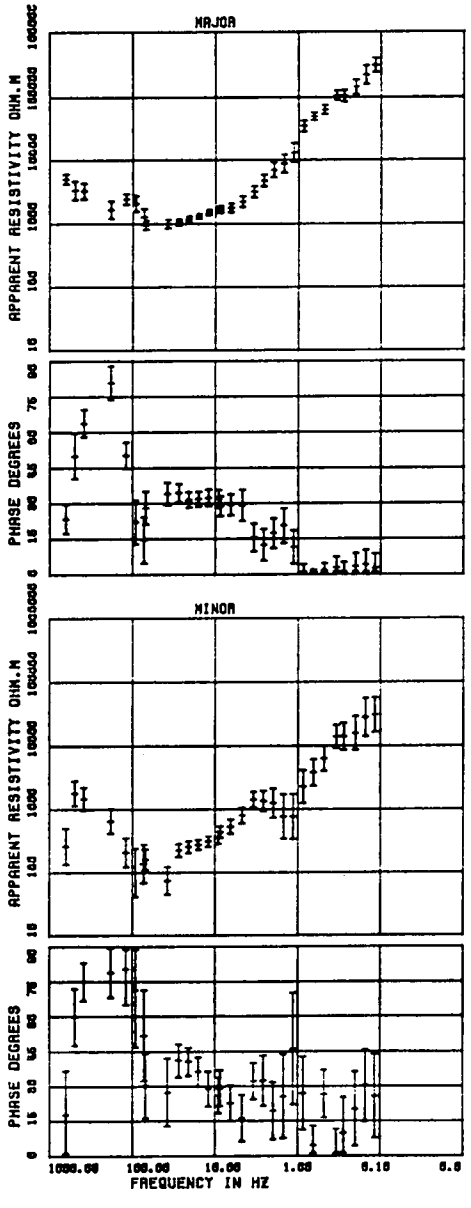

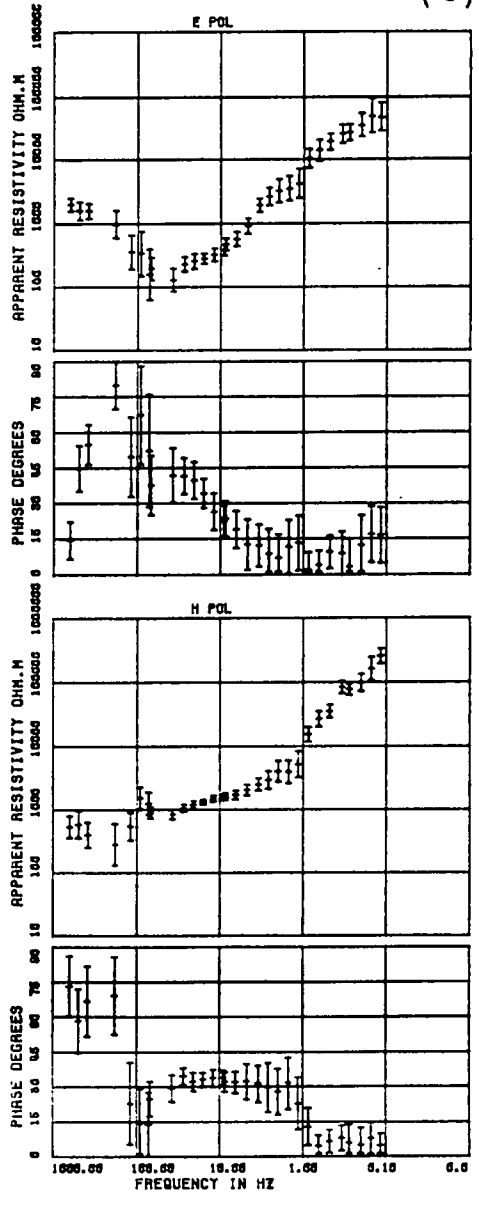

MT RESPONSE CURVES SITE 461 MAS DI SAUGO

(d)

MT RESPONSE CURVES SITE 462 P. MANGHE

(e)

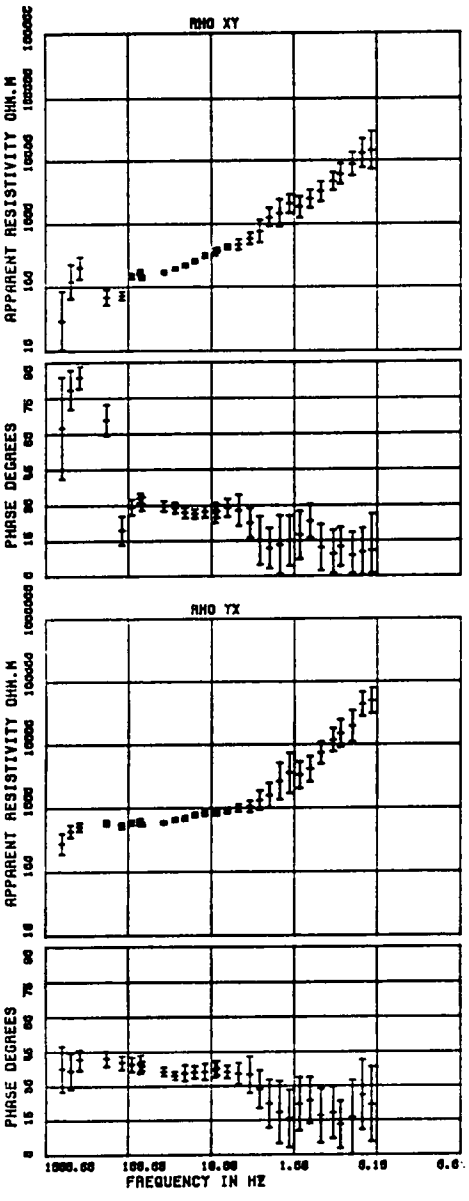

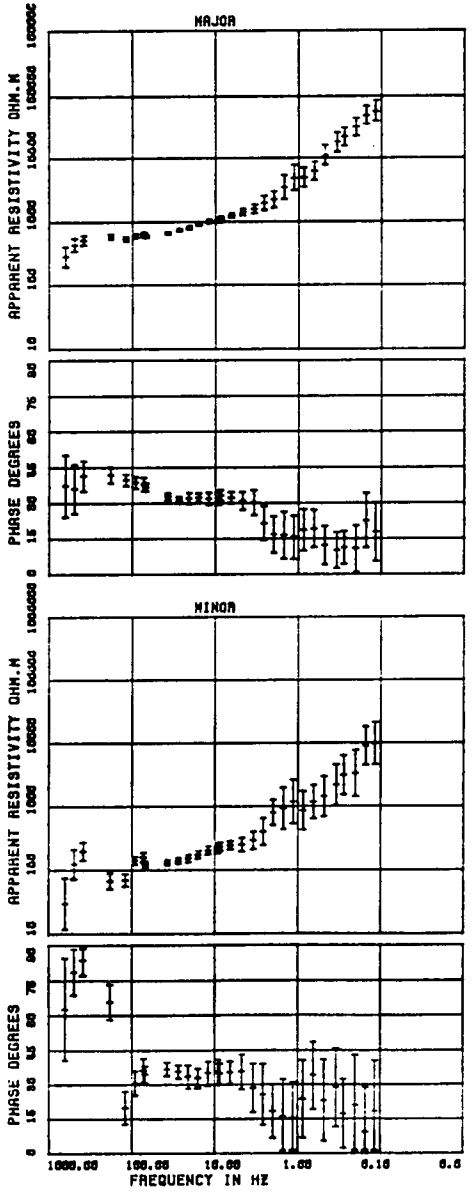

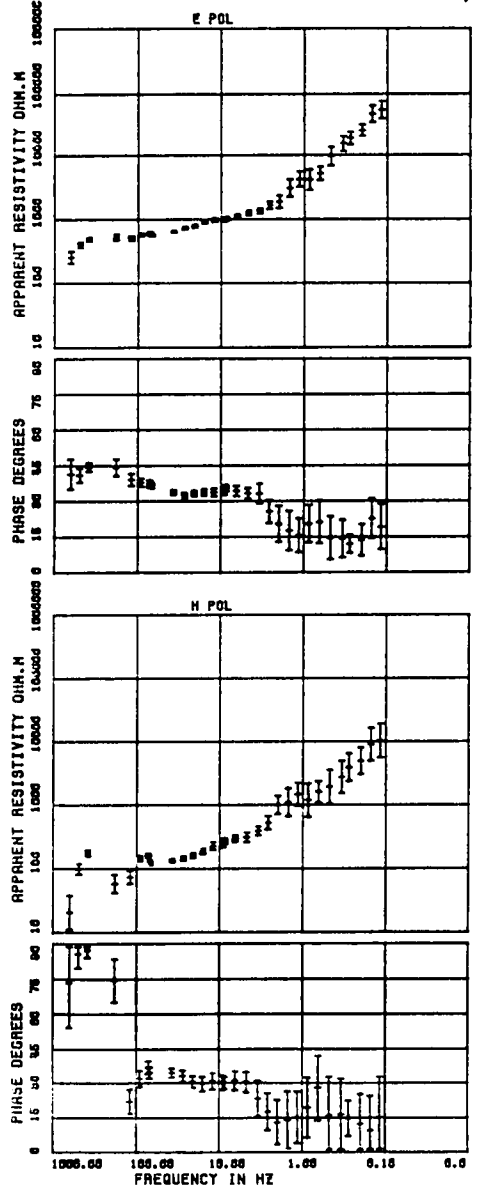

Fig. 6.10(a)-(e)- Cavalese results (continuation). See legend of Fig 6.3.

SITE 463A

(a)

CARTRIDGE :	4636A	4631A	4632A	4633A	4634A
BAND :	1	2	3	4	5
COMPONENTS :	4	4	4	4	5
SAMPLES/WINDOW :	256	256	256	256	256
NUMBER WINDOWS:	66	66	66	42	8
SAMPLE RATE HZ :	2048	256	32	4	1
PLOT HPF :	66.66	8.66	1.66	6.16	6.61
PLOT LPF :	766.66	66.66	16.66	1.66	6.26
FREQS/DECADE :	6	6	6	6	6
FREQS/BAND :	7	7	6	6	6
MIN COHERENCY :	6.66	6.66	6.66	6.66	6.66
REJECTION LOOPS:	2	2	2	2	2

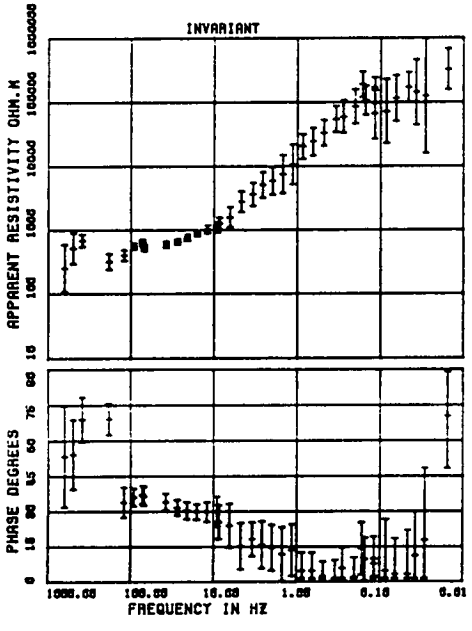

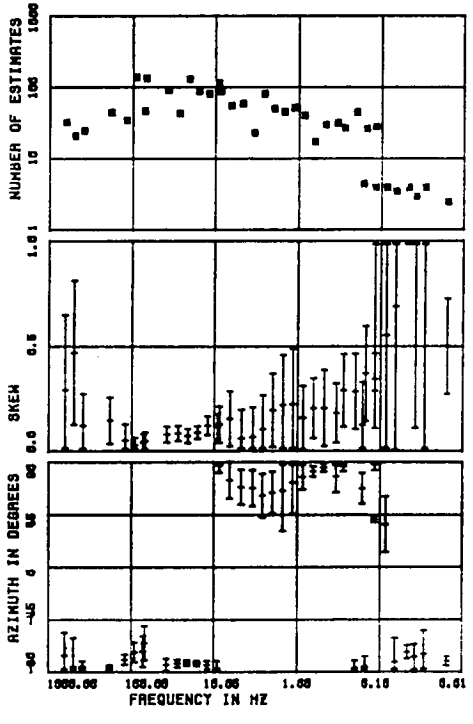

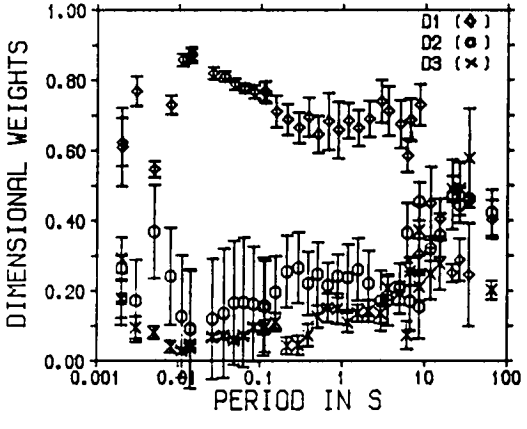

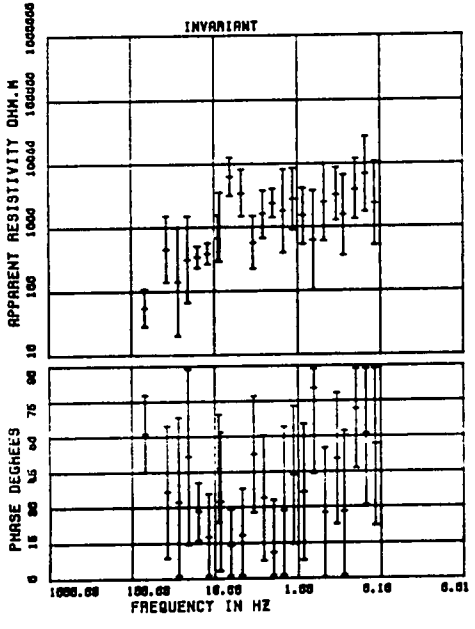

SITE 581A

CARTRIDGE :	581A	582A	583A
BAND :	2	3	4
COMPONENTS :	5	5	5
SAMPLES/WINDOW :	256	256	256
NUMBER WINDOWS:	48	48	48
SAMPLE RATE HZ :	256	32	4
PLOT HPF :	6.66	1.66	0.16
PLOT LPF :	66.66	16.66	1.66
FREQS/DECADE :	6	6	6
FREQS/BAND :	7	8	8
MIN COHERENCY :	6.66	6.66	6.66
REJECTION LOOPS:	2	2	2

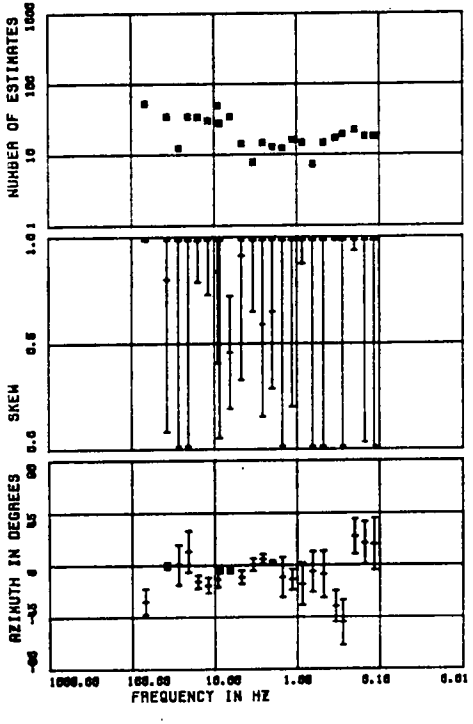

(b)

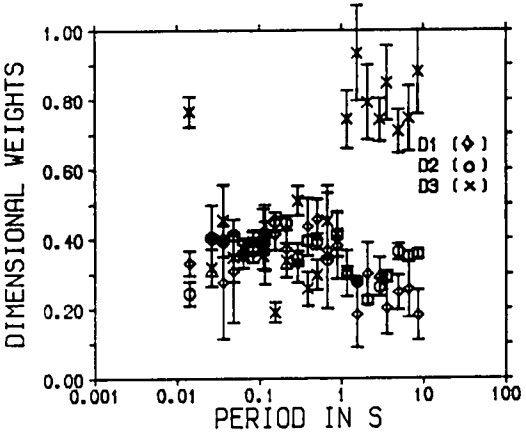

(c)

SITE 460A

CARTRIDGE	:	4600A	4601A	4602A	4603A
BAND	:	1	2	3	4
COMPONENTS	:	4	4	4	4
SAMPLES/WINDOW	:	256	256	256	256
NUMBER WINDOWS	:	66	166	66	36
SAMPLE RATE HZ	:	2048	256	32	4
PLOT HPF	:	66.66	6.66	1.66	6.16
PLOT LPF	:	766.66	66.66	16.66	1.66
FREQS/DECADE	:	8	8	8	8
FREQS/BAND	:	7	7	8	8
MIN COHERENCY	:	6.66	6.66	6.66	6.66
REJECTION LOOPS	:	2	2	2	2

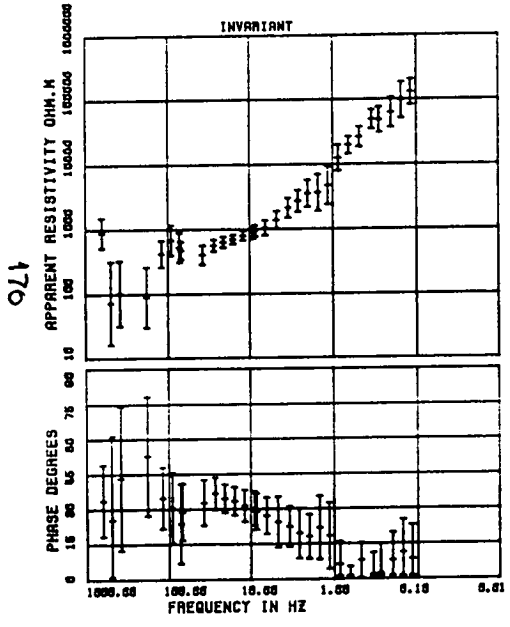

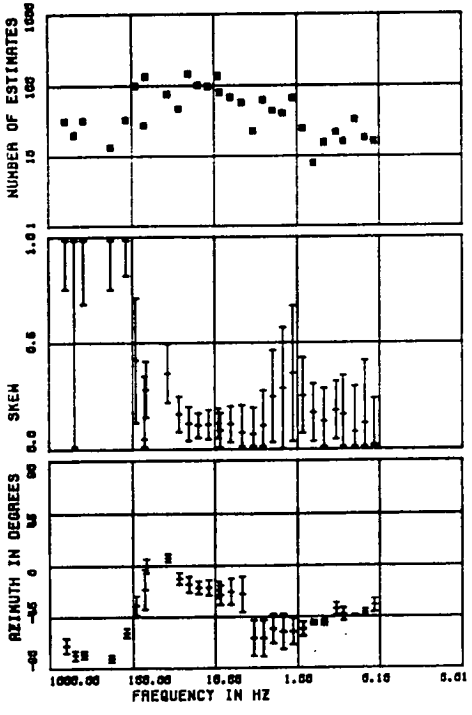

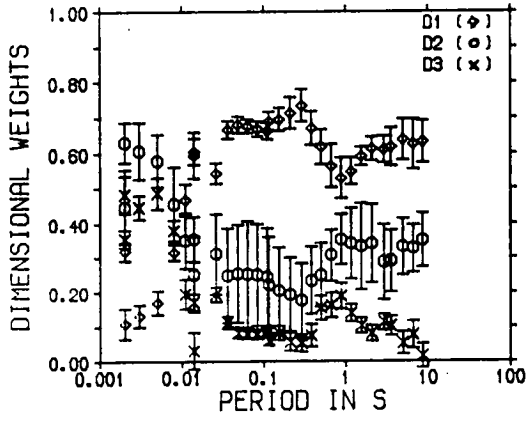

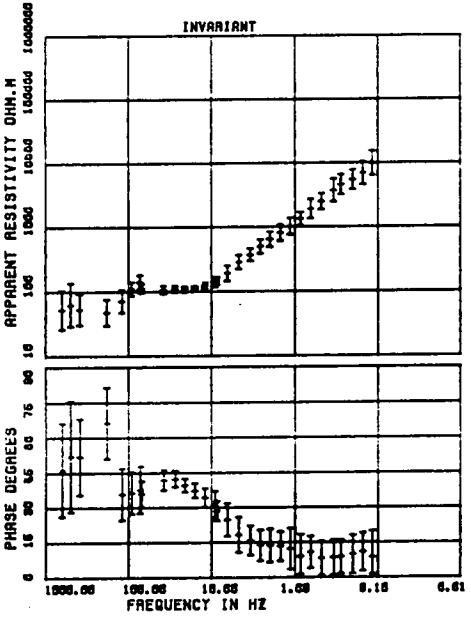

SITE 461A

CARTRIDGE	4616A	4611A	4612A	4613A
BAND	1	2	3	4
COMPONENTS	4	4	4	4
SAMPLES/WINDOW	256	256	256	256
NUMBER WINDOWS	60	60	60	30
SAMPLE RATE HZ	2048	256	32	4
PLOT HPF	60.00	6.00	1.00	0.10
PLOT LPF	700.00	60.00	10.00	1.00
FREQS/DECADE	8	8	8	8
FREQS/BAND	7	7	8	8
MIN COHERENCY	0.80	0.80	0.60	0.80
REJECTION LOOPS	2	2	2	2

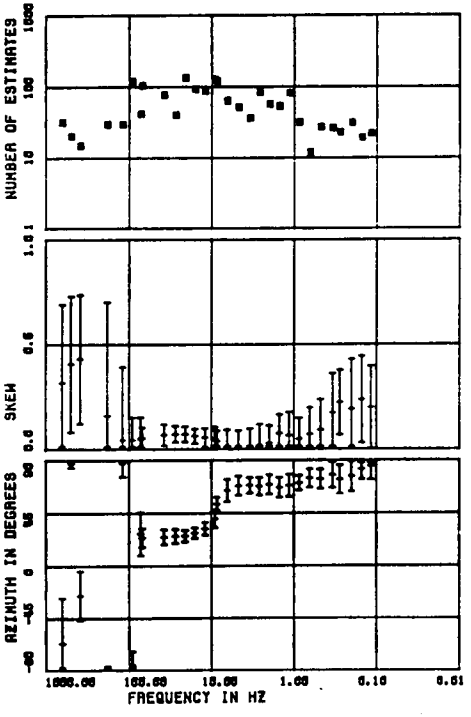

(d)

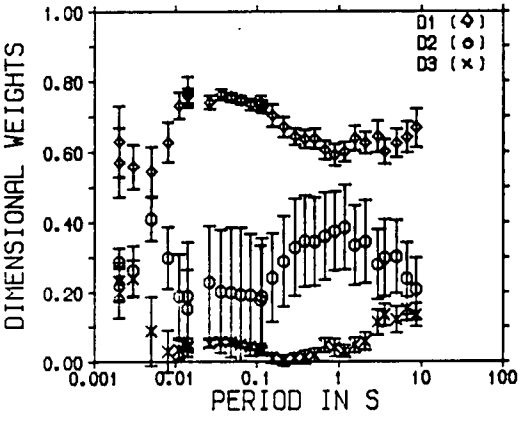

SITE 462A

CARTRIDGE	4628A	4621A	4622A	4623A
BAND	1	2	3	4
COMPONENTS	4	4	4	4
SAMPLES/WINDOW	256	256	256	256
NUMBER WINDOWS	60	60	60	30
SAMPLE RATE HZ	2048	256	32	4
PLOT HPF	60.00	8.00	1.00	0.10
PLOT LPF	700.00	60.00	10.00	1.00
FREQS/DECADE	8	8	8	8
FREQS/BAND	7	7	8	8
MIN COHERENCY	0.80	0.80	0.80	0.80
REJECTION LOOPS	2	2	2	2

(e)

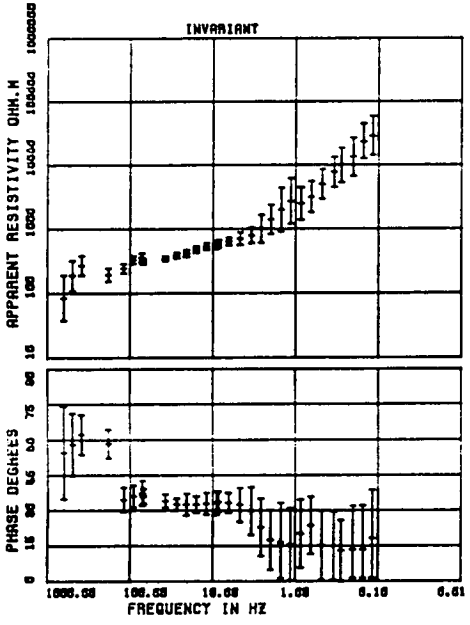

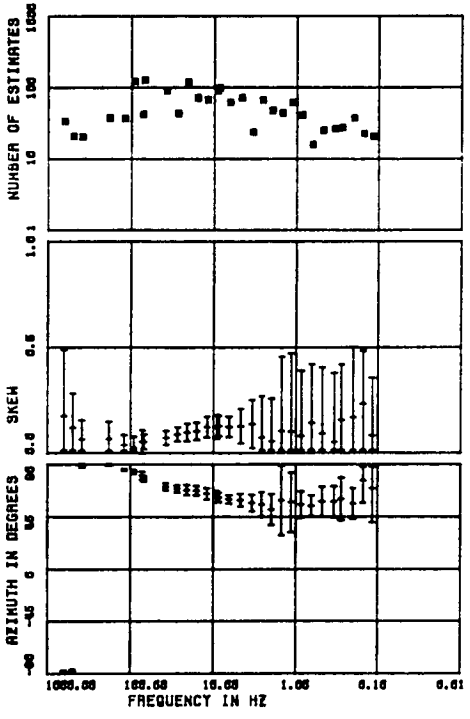

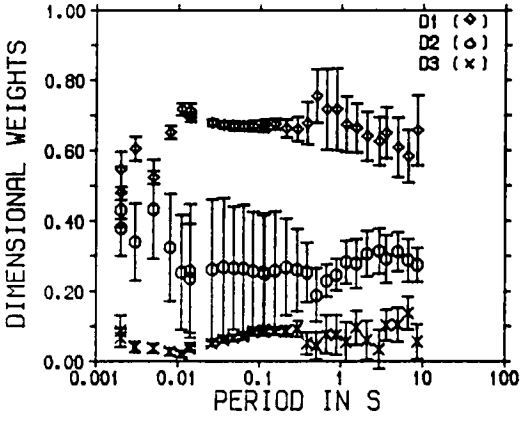

minor directions and E and H pol directions. The Figs. 6.10(a)-(e) present the rotationally invariant curves, number of estimates, skew and dimensional weights values. All the curves were processed by means of the standard procedure described in Chapter 4, since the use of filtering techniques proved ineffective at removing convincingly the coherent spike noise observed in all sites in this region; this was exemplified in Chapter 5. In considering the observed distinctive features of the Daiano responses (Figs. 6.9(b)- 6.10(b)), the fact that no coherence rejection criterion was enforced while data was acquired at this location must be born in mind since they possibly contain greater contribution from natural (unfortunately with low coherences) signals. As can be observed from the Figs. 6.9 and 6.10, only band 0 (though very scattered for most sites) and partly band 1 results can possibly be regarded as plausible for a natural MT survey. One can also observe from most of Figs 6.10 that the azimuths tend to experience abrupt changes coincident with the start of the dubious portion of the curves. The characteristics of the curves for the remaining bands (e.g. the steep slopes and unrealistically high apparent resistivity values) strongly indicate that the sites are located within a near- field source region, with the azimuths values possibly associated with the source's current direction. Curves showing the magnetic and telluric field polarizations (Figs. 6.11(a)-(e)) for a number of frequencies in each band reveal telluric fields generally more strongly polarized than their magnetic counterparts, and in one case only (Fig. 6.11(d))- change in the telluric polarization direction from band 1 to band 2 which might be associated with a change of source fields. Nevertheless, these results seem not to be unevoquivocal indicators of abnormality as the polarization ellipses for 'unsuspicious' sites in the Asiago area (Figs. 6.12(a)-(c)) show similar polarization patterns. The facts and inferences which have led to the conclusion that the Italian DC railway network as this near- source have been reported in Chapter 5. Hence, a near-source modelling (also referred to as active MT modelling) has been attempted in this study and the results are presented in Chapter 7. Site LAV (Figs. 6.9(a)- 6.10(a)) includes band 4 measurements. Band 5 measurements carried out at site DAI, situated roughly at the centre of the profile in this region, were found to be dominated by very strong and coherent electric signals, with no magnetic counterpart. It may be significant that the dimensional weights and skew values (shown in Figs. 6.10)

Fig. 6.11(a)-(e)- Polarization results for all sites in Cavalese area. Polarization ellipses for the telluric and magnetic signals are shown for a number of frequencies log- equally spaced within each band. The directions are given by the angles, with 0^0 associated with the magnetic North, and $+90^0$ and -90^0 indicating the magnetic East and West, respectively. The magnetic declination in the region during the survey period was about 2^0W. The ellipses are drawn by using all the events for a particular frequency; the amplitudes (for each direction) are normalized with respect to the total number of events.

POLARIZATION PLOTS

(a)

POLARIZATION PLOTS

(b)

4601A
MAGNETIC
TELLURIC
-90
0
90
69.3
37.8
27.5
20.9
16.0
12.0
9.11

4600A
MAGNETIC
TELLURIC
-90
0
90
639.
500.
388.
184.
120.
91.8
72.0

4603A
MAGNETIC
TELLURIC
-90
0
90
0.863
0.648
0.481
0.343
0.281
0.202
0.152
0.117

4602A
MAGNETIC
TELLURIC
-90
0
90
8.66
6.49
4.73
3.44
2.62
2.00
1.50
1.14

(c)

POLARIZATION PLOTS (P)

4621A
MAGNETIC
TELLURIC
-90
0
90
4620A
MAGNETIC
TELLURIC
-90
0
90
4623A
MAGNETIC
TELLURIC
-90
0
90
4622A
MAGNETIC
TELLURIC
-90
0
90

(e)

Fig. 6.12(a)-(b)- Polarization results for sites MUL, AVE and GRA in the Asiago region. See legend of Fig. 6.11.
The strong polarization observed for both the telluric and the magnetic signals (band 0 data) at site AVE (Fig. 6.12(b)) is caused by the 100Hz noise signal already mentioned in Chapter 5.

POLARIZATION PLOTS

(D)

POLARIZATION PLOTS

(b)

POLARIZATION PLOTS

(c)

are indicative of a predominant 1D structure in this region.

It is interesting to consider at this stage why the effect of the DC railway network appears more intense in the Cavalese than in the Asiago areas. A combination of two facts may shed some light on this question. Firstly, the relatively conductive layer observed in Asiago area, if present in the Cavalese area, is likely to be at greater depths. Thus, with a thicker upper resistive layer around Cavalese, the electric signals would be enhanced and capable of detection over larger distances (by skin depth considerations). The second fact is concerned with the operation of the DC railway network in Italy itself. The Italian network is operated either by governmental or by private companies. According to technicians operating the railway power substation in Ala, the privately run segment (which includes Cavalese area) has poorer rail insulation and as a result, more current leakages to the ground can be expected. A systematic study to check the veracity of the latter statement is beyond the scope of this work.

6.4 Po Valley region

This region is characterized tectonically by a prevailing lowering relative to the prealpine region. In this study observations were made at only 1 site, situated between Padua and Vicenza.

The results are summarised in Figs. 6.13(a)-(c). One can observe an apparently two-layer Earth, followed by a typical near-source effect similar to that observed in Cavalese. The more conductive nature of this region results in the dominance of the near- field source effects at lower frequencies than at sites in the Cavalese area. Again the dimensionality indicators (Fig. 6.13(b)) suggest a remarkably predominance of 1D features, a result corroborated by the great isotropy observed in all response curves (Fig. 6.13(a)) at this site. The polarization ellipses for all the bands (Fig. 6.13(c)) are once more ineffective in providing any convincing evidence leading to an artificially originated source field. As with the Cavalese data, near-source modelling has been attempted for this site and results are discussed in Chapter 7.

As mentioned briefly in Chapter 3, it was originally intended that this Po Valley station would serve as remote reference for band 5 measurements

Fig. 6.13- MT results for site I. Mantegna in the Po Valley region.
(a)- See legend of Fig. 6.2.
(b)- See legend of Fig. 6.3.
(c)- See legend of Fig. 6.11.

MT RESPONSE CURVES SITE 692 I. MANTEGNA

(a)

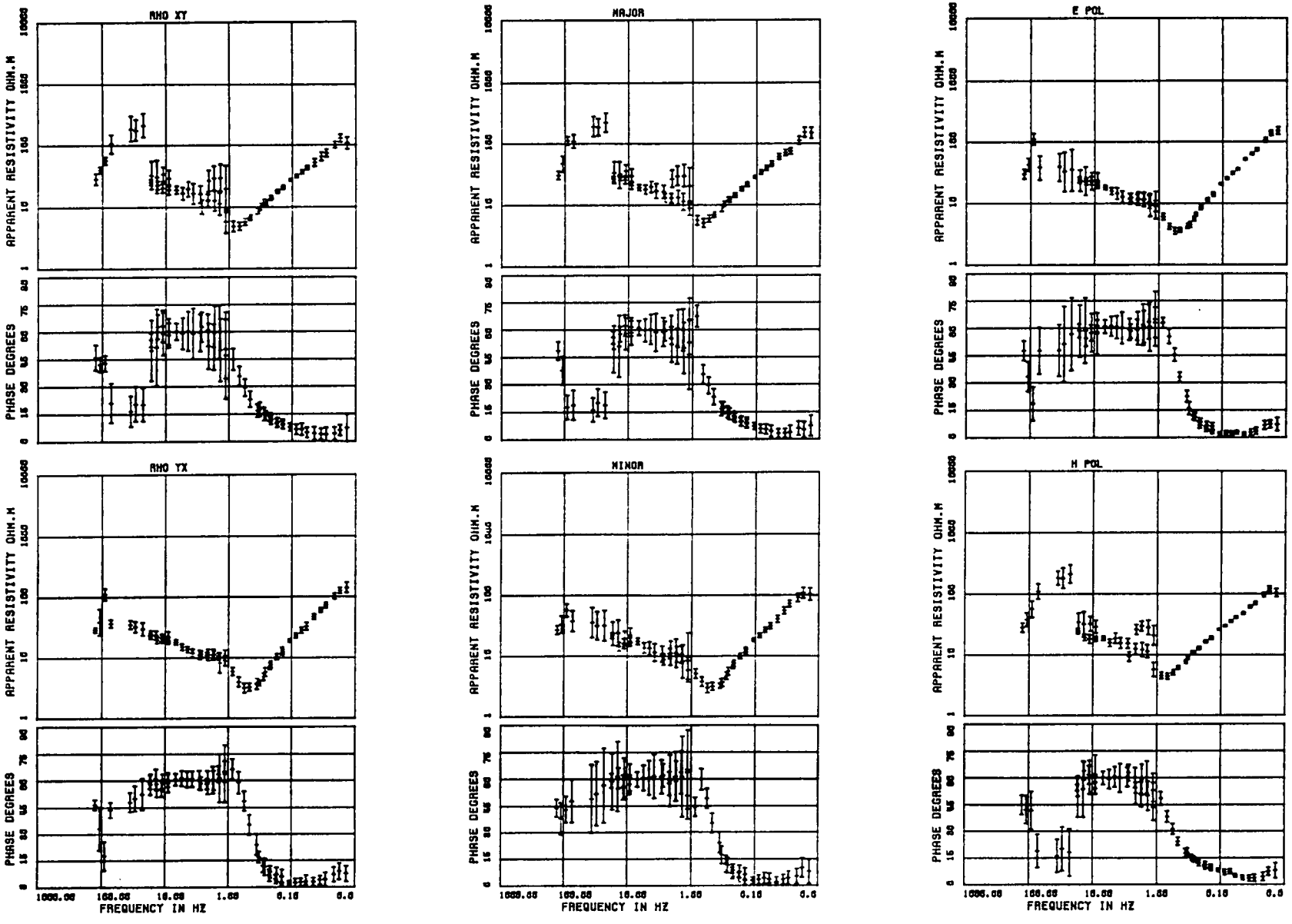

(b)

SITE 692A

CARTRIDGE :	8920A	8921A	8922A	8923A
BAND :	1	2	3	4
COMPONENTS :	4	4	4	4
SAMPLES/WINDOW :	256	256	256	256
NUMBER WINDOWS:	60	60	60	37
SAMPLE RATE HZ :	512	64	8	1
PLOT HPF :	8.00	1.00	0.12	0.01
PLOT LPF :	100.00	24.00	3.00	0.35
FREQS/DECADE :	10	10	10	10
FREQS/BAND :	12	14	14	15
MIN COHERENCY :	0.70	0.70	0.70	0.70
REJECTION LOOPS:	2	2	2	2

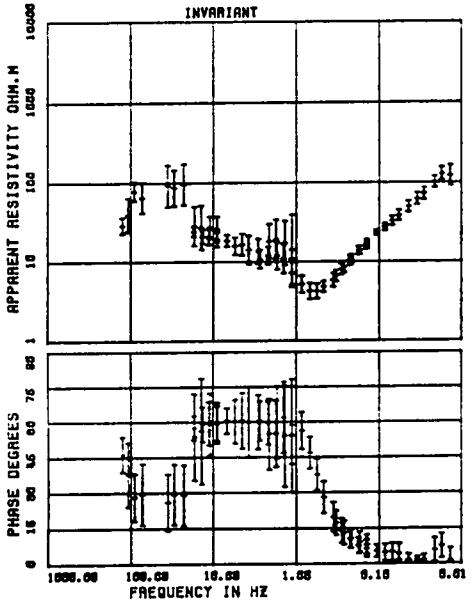

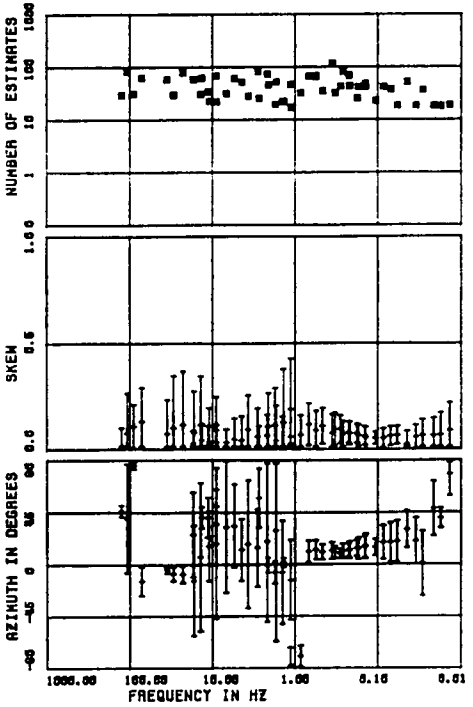

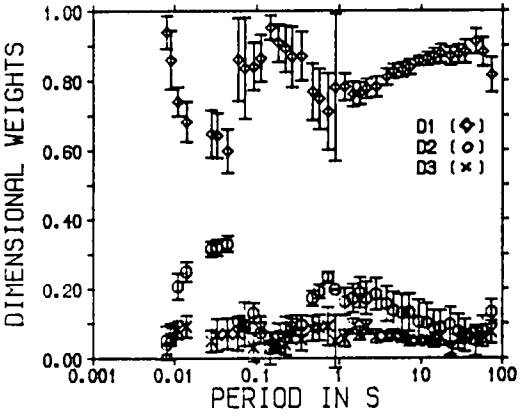

POLARIZATION PLOTS

(c)

undertaken simultaneously at Asiago and Cavalese areas. However, the highly coherent nature of the noise signal in this region (for instance, band 3 measurements with NERC-SPAM system exhibited 12 frequency sets (out of possible 12) with predicted coherences > 0.95 for nearly all recorded windows!) did not recommend the use of this station as a remote station. The reasons for not using another station as reference are discussed below.

The two main assumptions underlying the remote reference technique were given in section 4.2.2 and are briefly reiterated here. The first of these assumptions requires that the noise at the measuring site be independent of the noise at the remote site. This condition may be satisfied even for the Italian data, provided that the noise fields originating from the DC railway network are not syncronized for stations very far apart. The second assumption states that the noise at the measuring station must be incoherent. This latter assumption is clearly violated in the Italian case. Nevertheless, Kroger et al (1983) have produced estimates in which this last assumption can be relaxed, the condition being that the remote site is much less contaminated by noise than the measuring site. None of the 3 simultaneously recorded sites in Italy fulfilled this less restrictive requirement. Moreover, in view of the limited extent of available data (3 recording days in the Po Valley site and 4 days in Cavalese) it was not considered worthwhile to develop the necessary software for remote reference analysis, for this study.

CHAPTER 7

1D AND 2D MODELLING STUDIES

7.1 Introduction

This Chapter details the various mathematical modelling methods employed in this study and the results of their applications to the Italian data. A general overview of the modelling problem in electromagnetic induction studies is given in the following section. 1D and 2D modelling techniques and the results achieved with them for the Asiago area are presented in sections 7.3, 7.4 and 7.5. Near field modelling of data observed at both the Cavalese and Po Valley areas is discussed in the last section of this Chapter.

7.2 General overview

In general terms, the main aim in geophysics is the extraction from measured data of reliable information about a particular physical property of the Earth. For example, in electromagnetic induction studies, the two main objectives are to reveal the spatial distribution of the parameters describing the Earth's conductivity structure and to unravel possible geological and tectonic processes associated with this conductivity structure. The aim of this Chapter is to achieve the first of these objectives. Some mathematical modelling is therefore performed by means of forward or inverse procedures. The second objective is generally better accomplished by reuniting the pertinent geological and geophysical information available for the surveyed area and is presented in Chapter 8.

Forward modelling

The forward solution for the 1D problem in MT has a simple analytical description which has been presented in Chapter 2. The use of substitute conductors for MT response estimates (e.g. Schmucker and Niblett- Bostick transforms), also referred to as approximate heuristic methods of inversion (Rokityanski, 1982), provide very useful insight for the interpretation of 1D structures. They are described in detail in the following section. Other EM problems require a numerical approach, which is usually based on the use of Hankel transforms (including the 1D controlled source models also described

in Chapter 2) and is an active field of research. In a vast majority of cases, the MT forward solutions for 2D and 3D structures can only be tackled by either analogue models or by solving numerically the differential equations (E-pol and H-pol cases for 2D situations, derived in Chapter 2) governing the problem. Analogue modelling is particularly useful for very complex 2D or 3D situations, despite practical problems of modelling intermediate conductivity contrast (Kaikonnen, 1983). Published examples of analogue modelling include faults and dykes (Dosso, 1966), electromagnetic induction studies in Canada: Vancouver Island region (Nienaber et al., 1979) , subducting plates in the Juan de Fuca Plate region (Dosso and Nienaber, 1986), and Australia: sedimentary basins in Tasmania region (Dosso et al., 1985). The most frequently used numerical methods for 2D and 3D problems are:

1- The finite difference method (e.g. Jones and Pascoe, 1971; Jones, 1973; Brewitt-Taylor and Weaver, 1976 , 1986) which requires a spatial discretization- all the derivatives involved in the differential equations and boundary conditions are expressed by difference approximations and associated to a chosen rectangular grid structure.

2- The finite element method (e.g. Reddy and Rankin, 1975; Kisak and Silvester, 1975; Kaikkonen, 1977, 1983; Wannamaker et al., 1987) in which the the continuous medium is approximated by a more flexible mesh structure (rectangles which can be subdivided in 2 or 4 triangles) and the total electromagnetic energy functional within each element of the mesh is minimized. The extra flexibility allows a more exact representation of complex geologies and topography, in comparison with the finite difference method. Problems of accuracy especially at low frequencies result from the limited precision of computers. Although most finite element programs suffer from this drawback, Wannamaker et al. (1985, 1987) have proposed an algorithm which seems to overcome these accuracy limitations by decomposing the electromagnetic fields in and around an inhomogeneity into primary and secondary components (Hohmann, 1983). The former represent the fields in the 1D host when the inhomogeneity is absent, while the secondary component results from the inhomogeneity itself. Greater accuracy is then achieved by solving directly the secondary variations of the field. Their program was adapted by the author for running on EMAS (Amdahl 470 V/8 machine) and then used in this study for preliminary qualitative 2D modelling

and assessment of the distortions due to topography on the Italian MT reponses. It was found to be about 20% slower than the finite difference code by Brewitt-Taylor and Weaver (1976) when running a quarter space model.

3- The integral equation method (e.g. Coggon, 1971; Weidelt, 1975; Wannamaker et al., 1984) uses Green functions and reduces the differential equations to a system of integral equations within the domain of the inhomogeneity. The reader is referred to Hohmann (1983) for a review of formulations and computational procedures involving integral equation methods. This method is computationally more efficient than the two former methods and is consequently more suitable for 3D studies.

4- Thin sheet modelling is a fast growing research topic and has become a very viable way of treating surface inhomogeneities (Chave and Booker, 1987). It has been used mainly for 3D studies. The most recent publications concerned with thin sheet analysis include the works of Ranganayaki and Madden (1980), Dawson (1983), McKirdy and Weaver (1984) and McKirdy et al. (1985). The method basically assumes the inhomogeneities to be confined to a small area (or a thin sheet) of the total region modelled. In other words, the depth of penetration of the electromagnetic waves must be much greater than the thickness of the sheet.

Another common method is the transmission surface analogy (Wright, 1970; Swift, 1971; Ku et al., 1973, Brewitt- Taylor and Johns, 1980; etc) in which the medium is substituted by an equivalent electrical network. Hybrid methods combining the finite element and integral equation approaches (Best et al., 1985) or the finite element technique and analytical solution (Yegorov et al., 1983) are also in use.

The natural procedure for forward modelling is a trial-and-error process involving an unpredictable number of forward models until the investigator is satisfied with the overall fit between measured data and mathematical model. While several inversion schemes as described below have been developed for the 1D problem, interpretation of most 2D (and all 3D) structures is still performed through forward modelling.

Inversion techniques

Geophysical inversion is basically an attempt to fit the response of an idealized Earth model to a finite set of actual observations. For the 1D

magnetotelluric inversion problem, the simplicity of forward modelling is overshadowed by the fact that the relationship between the observed quantities and the unknown conductivity profile is nonlinear. Parker (1983) has discussed this point as well as the existence, the uniqueness and the construction of solutions. The existence and uniqueness of models for various types of ideal data have been well established (e.g. Bailey, 1970; MacBain and Bednar, 1986). However, for inaccurate real data, only the necessary and sufficient conditions for existence of solutions have been substantiated (e.g. Weidelt, 1972, 1986; Parker, 1980). As to the solution uniqueness for actual data, an infinite number of solutions exist if one does (Parker, 1983). Furthermore, when 1D models do not fit the data exactly, the model with the smallest least squares error (or misfit χ^2) always consists of a set of infinite delta functions in conductivity- the Parker's D+ case. However, as D+ models are clearly unrealistic in most geological situations, it is common to relax the fit to some extent, i.e. to allow for a larger misfit χ^2. Despite the difficulties imposed by nonlinearity and nonuniqueness, many 1D inversion schemes have been reported in the literature and the COPROD Program (1979) has compared the results of a number of them when applied to a data set from Newcastleton (Jones and Hutton, 1979). The models derived from these various schemes can be classified as either discontinous (parametric) or continuous (smooth) solutions. Examples of discontinuous solutions have been described by Jupp and Vozoff (1975), Larsen (1981), Fischer and Le Quang (1981), In essence, these discontinous schemes search iteratively for a simple model comprising a small number of homogeneous layers by means of minimizing the misfit through a linearized least squares system. A very readable tutorial on least squares inversion has been published by Lines and Treitel (1984). The Monte Carlo solution proposed by Jones and Hutton (1979) can also be included in the category of discontinuous solutions. However, unlike the other solutions, no linearization is performed in this case. Both a modified version of this Monte Carlo inversion and the inversion proposed by Jupp and Vozoff (1975) were utilized in this study; they are described in more detail in the following section.

Most inversion schemes categorized as continuous conductivity solutions are basically variants of the work of Backus and Gilbert (1967), e.g. Parker (1970, 1977), Oldenburg (1979) and Hobbs (1982). In this category the

works of Marchisio and Parker (1984), Constable et al. (1987) and Smith and Booker (1986) can also be included. These latter schemes search for the smoothest model fitting the data within some prescribed value of χ^2. The scheme proposed by Constable et al. (1987), referred to as Occam's inversion, was also used in this study and is briefly described in section 7.3.3.

Examples of 2D inversion schemes have been given by Jupp and Vozoff (1977), Zhdanov and Gobulev (1983), Jiracek et al. (1986) and Hill (1987). All these 2D solutions have used an approach similar to those of the 1D discontinuous solutions described above. Normally, a limited parameterization, i.e. a relatively small number of conductive blocks, is used. The values of the parameters are adjusted until a reasonable fit is reached. Linearized least squares fitting is employed in all these schemes. The 2D algorithm proposed by Jupp and Vozoff (1977) was used in this study and is described in more detail later in this Chapter. A 3D inversion scheme has been reported by Weidelt (1985). Despite the progress already attained, the application of 2D (and especially 3D) inversion schemes is still rare. This is so mainly due to the high computational costs involved in running most of the current schemes. However, it is probable that a combination of both more efficient algorithms and faster processors will soon make such inversions more widespread.

Inversion schemes for controlled source (or active) MT data can be undertaken using any of the 1D inversion schemes, provided the source is about 3 skin depths away as discussed earlier in Chapter 2. Near- source field inversion was attempted by Cox et al. (1986). In an EEC project carried out in Milos- Greece in 1986 involving induction groups of various countries, German investigators have reported the use of a hybrid natural/active MT inversion scheme (Hutton, pers. comm.). Two inversion schemes utilizing the Italian DC railway network as the electromagnetic source (transmitter) are reported later in this Chapter. They are based on the modified Monte Carlo (Jones and Hutton, 1979) and Occam's inversion (Constable et al., 1987) schemes.

7.3 1D studies

7.3.1 Heuristic tranformations

The approximate inversions used in this study were the Schmucker and Niblett- Bostick transformations. The Schmucker transformation (Schmucker, 1970) defines the thickness d^* of the resistive top layer (i.e. the depth to a perfect substitute conductor) as a function of the apparent resistivity ρ_a and phase ϕ by the expression

$$d^* = (\rho_a/\mu_0\omega)^{1/2}\sin\phi \tag{7.1}$$

The related expression for the transformed apparent resistivity ρ^* is

$$\rho^* = 2\rho_a\cos^2\phi \tag{7.2}$$

The Niblett transformation (Niblett and Sayn-Wittgenstein, 1960) and the Bostick transformation (Bostick, 1977) were shown to be equivalent by Jones (1983). The expressions for depth d_{NB} and the transformed apparent resistivity ρ_{NB}, also as a function of ρ_a and ϕ, are

$$d_{NB} = (\rho_a/\mu_0\omega)^{1/2} \tag{7.3}$$

$$\rho_{NB} = \rho_a[(\pi/2\phi)-1] \tag{7.4}$$

All the transformations (Eqs. 7.1-7.4) are given in S.I. units. Schmucker (1987) has compared the expressions of these transformations. His studies on synthetic data by means of plots of $\rho^*(d^*)$ and $\rho_{NB}(d_{NB})$ have shown comparable results and they indicated that both approximations perform best for structures that increase their conductivity with depth. Elsewhere (Dekker, 1983), a comparison of these techniques for field data has suggested that the Niblett- Bostick transformation performed better when the phase information was unreliable. Hence, this was the transformation adopted in this study and it was used as a basis for more sophisticated 1D inversions. Results are presented later in this Chapter.

7.3.2 Linearized inversion – The weighted 2nd order Marquadt scheme

The 1D linearized inversion used in this study has been fully described elsewhere (Jupp and Vozoff, 1975a). Hence only the main aspects of this scheme are outlined in this section.

Let the n observations of a general set of Earth data be represented by the vector

$$\mathbf{y} = (y_1, y_2, \ldots, y_n)^T \tag{7.5}$$

For MT data, y_i is the apparent resistivity or phase at the i^{th} period. Let the model response be represented by the vector

$$\mathbf{f} = (f_1, f_2, \ldots, f_n)^T \tag{7.6}$$

Assume that this model is a function of p parameters which are the elements of the vector x, i.e.

$$\mathbf{x} = (x_1, x_2, \ldots, x_p)^T \tag{7.7}$$

In fact, each element in (7.6) is a function of **x** and (7.6) can be rewritten as

$$\mathbf{f(x)} = (f_1(\mathbf{x}), f_2(\mathbf{x}), \ldots, f_n(\mathbf{x}))^T \tag{7.8}$$

The basic strategy in an inversion scheme is to determine values of **x** so that the functional **f(x)** matches the observed set **y** in some sense, by minimizing well known error parameters such as the misfit χ^2 or the root mean squares relative error (rms) between model and data. The misfit χ^2 is defined as

$$\chi^2 = \sum_{i=1}^{n} (y_i - f_i)^2 / \sigma_i^2$$

where σ_i is the error associated to the ith datum y_i. The rms error can be defined as

$$E(\mathbf{x}) = \{(1/n) \sum_{i=1}^{n} [(y_i - f_i)^2 / y_i^2)]\}^{1/2}$$

One of these error parameters (Jupp and Vozoff utilize the rms error) can be iteratively minimized by using the Gauss- Newton method. In this method, an initial estimate $\mathbf{x}^0$ generates an initial model response $\mathbf{f}^0$. The model response **f** can be represented by a Taylor expansion about $\mathbf{x}^0$ as

$$\mathbf{f}(\mathbf{x}^0+\delta\mathbf{x}) = \mathbf{f}^0 + \mathbf{J}\delta\mathbf{x} + \mathbf{R}(\mathbf{f},\delta\mathbf{x}) \tag{7.9}$$

where **J** is the n x p Jacobian matrix of partial derivatives of the vector function **f(x)** with respect to the parameters x_j, $\delta\mathbf{x}=\mathbf{x}-\mathbf{x}^0$ and **R** contains the higher order terms of the Taylor expansion. If **f(x)** is assumed to be linear (or the initial model response is very close to the sought model response), then **R(f, δ)** is zero (or negligible). This assumption is referred to as local linearization. In the iterative process, the initial value $\mathbf{x}^0$ is changed by an amount **δx**, which is calculated by a standard linear least-squares procedure as follows:

Let **e** represent the error vector expressing the difference between the model response **f** and the observed data **y**:

$$\mathbf{e} = \mathbf{y}-\mathbf{f} \tag{7.10}$$

Assuming **R** = **0** in (7.9) and combining it with (7.10), results in

$$\mathbf{e} = \mathbf{y} - \mathbf{f}^0 - \mathbf{J}\delta\mathbf{x} \tag{7.11}$$

Defining the discrepance vector **g** as $\mathbf{y}-\mathbf{f}^0$, (7.11) can be rewritten as

$$\mathbf{e} = \mathbf{g} - \mathbf{J}\delta\mathbf{x} \tag{7.12}$$

The least squares procedure can be accomplished by differentiating the total squared error $S = \mathbf{e}^T\mathbf{e}$ with respect to **δx**. This results in

$$\mathbf{J}^T\mathbf{J}\delta\mathbf{x} = \mathbf{J}^T\mathbf{g} \tag{7.13}$$

which are the so called normal equations due to the geometric property that the vector **e** is perpendicular, or normal to the Jacobian matrix **J**. Solving

(7.13) for the parameter change vector $\delta\mathbf{x}$ gives the so-called Gauss- Newton solution

$$\delta\mathbf{x} = (\mathbf{J}^T\mathbf{J})^{-1}\mathbf{J}^T\mathbf{g} \qquad (7.14)$$

All the development described so far is a straightforward least squares procedure. The results are general and applicable for 1D as well as 2D/3D inversion schemes. Unfortunately though, solutions of (7.14) can be unstable if the matrices involved are not well conditioned (Jackson ,1972). For instance, problems arise when the matrix $\mathbf{J}^T\mathbf{J}$ is nearly singular, or has a reduced number of degrees of freedom caused by random errors present in the actual data. The latter will affect the rank of **J**, implying a rank always $<\min(n,p)$. In the Jupp and Vozoff scheme, both generalized matrix inversion and singular value decomposition (Lanczos, 1958, 1961) are employed to overcome rank deficiency, numerical inaccuracies and to individually assess the importance of each model parameter. Generalized matrix inversion determines a unique $\delta\mathbf{x}$ which minimizes

(i) $|\mathbf{g}-\mathbf{J}\delta\mathbf{x}|$
(ii) $|\delta\mathbf{x}|$

The matrix **J** can be decomposed into a product of three matrices

$$\mathbf{J}=\mathbf{U}\,\mathbf{S}\,\mathbf{V}^T \qquad (7.15)$$

where **U** is an n x p matrix whose columns contain p of the total of n orthonormal 'observation' eigenvectors $\mathbf{u}_i$ and **V** is a p x p matrix containing the p orthonormal 'parameter' eigenvectors $\mathbf{v}_i$. Both $\mathbf{u}_i$ and $\mathbf{v}_i$ matrices satisfy the relation

$$\mathbf{J}\,\mathbf{J}^T(\mathbf{u}_i,\mathbf{v}_i) = s_i^2(\mathbf{u}_i,\mathbf{v}_i)\ ,i=1,\ldots,n \text{ but } \lambda_{p+1}=\ldots=\lambda_n=0.$$

S is a p x p diagonal matrix containing the non- null singular values- at most p in number- $+s_i$ (the square roots of the eigenvalues s_i^2) with $s_1>s_2>\ldots>s_p$. The model parameters are thus classified as important, unimportant and

irrelevant, according to their associated singular values. For instance, a model parameter with singular value zero is said to be irrelevant as it has no influence in the model response. The remaining model parameters are split into important and unimportant according to whether their singular values are, respectively above or below a certain threshold. To avoid instabilities in the solutions caused by irrelevant and unimportant model parameters, these parameters are damped or truncated by a number of methods. The two most consecrated approaches are the Marquadt- Levenberg or 'ridge regression' method (Marquadt, 1963) and the Singular Value Truncation technique (e.g. Madden, 1972). The Jupp and Vozoff scheme employs a third approach which combines these two known techniques. The Jacobian J is multiplied by a p x p damping diagonal matrix $\mathbf{T}^{(N)}$ of entries t_i (called 'damping factors') written as

$$t_i^{(N)} = \begin{cases} k_i^{2N}/(k_i^{2N}+\mu^{2N}) & i=1,\ p \\ 0 & i>p \end{cases} \qquad (7.16)$$

where $k_i=s_i/s_1$ is the normalized singular value and $\mu=\nu/s_1$ is a relative threshold, with ν being a Lagrange multiplier which controls the size and direction of $\delta\mathbf{x}$ in the Marquadt- Levenberg method (Lines and Treitel, 1984). Eq. (7.16) actually embodies both the singular value truncation and Marquadt-Levenberg methods, since Jupp and Vozoff (1975a) have shown that $\mathbf{T}^{(1)}$ corresponds to the latter while $\mathbf{T}^{(\infty)}$ defines the truncation method. A suitable choice of $\mathbf{T}^{(N)}$ is dictated by the nature and quality of the actual data. In the present study, $\mathbf{T}^{(2)}$ was chosen as the damping matrix, as suggested by Jupp and Vozoff (1975b). This choice can be referred to as second order Marquadt damping. Additionally, a form of scaling can be beneficially used to speed the convergence of the iterative process (Smith and Shanno, 1971). A diagonal matrix D is found such that $\mathbf{J}\,\mathbf{D}^{-1}$ places 'ones' along the main diagonal of the scaled matrix $(\mathbf{J}\,\mathbf{D}^{-1})^T(\mathbf{J}\,\mathbf{D}^{-1})$. The element d_i of D is the r.m.s. of the values of the elements in the ith column of the unscaled Jacobian matrix J. The resulting solution $\delta^{(D)}$ must then be rescaled, i.e.

$$\delta = \mathbf{D}^{-1}\delta^{(D)}.$$

The Jupp and Vozoff code performs inversion of MT and DC resistivity data either independently or jointly. The program requires both the specification of the number of layers and a starting model. The initial $\mathbf{x}^0$ contains the logarithms of the layer resistivities and thicknesses. The use of 'log' values is a simple way of restricting the acceptable models of the mathematical model space to physically meaningful models involving only positive values of resistivity and thicknesses. A solution is normally reached after a number of iterations, depending on how close the starting model is to a sought solution (or perhaps simply a minimum in the parameter space). In any case, because of the constraint imposed by the local linearization assumption, the inversion scheme confines the search to a limited region of the model space in the vicinity of the starting model. The analysis of the parameter matrix **V** along with the damping factors t_i provides a means for assessing the importance and the resolution of the parameters involved in the modelling. In short, the product

$$|V_{ij}|\,t_i \tag{7.17}$$

is close to 1 if the parameter is relevant or, conversely, close to zero if the parameter is unimportant. Values around 0.5 are called 'threshold parameters'. In the implementation of this code to the Italian data, the response curves were weighted by using relative resistivity and phase errors.

7.3.3 Smooth models– Occam's inversion

The Occam inversion, proposed and fully described by Constable et al. (1987), is only briefly outlined here. This technique, for philosophical reasons, was named Occam after in the fourteenth century William of Occam wrote that

'it is vain to do with more what can be done with fewer'

(from Russell, 1946).

The concept of simplicity contained in Occam's statement has since become a major principle guiding scientific work in all branches of Science. The Occam inversion searches for the smoothest model which fits the data within a certain tolerable error or misfit. This is accomplished by minimizing

the model's roughness, the converse of smoothness, defined for continuous profiles by the integral of the squared first or second derivative with respect to depth:

$$R_1 = \int (dm/dz)^2 dz \qquad \text{(a)}$$

or

$$R_2 = \int (d^2m/dz^2)^2 dz \qquad \text{(b)} \qquad (7.18)$$

where m(z) is either resistivity or log resistivity. The scheme simultaneously minimizes the roughness of the model and the misfit between model and data. An identical formulation, described by Twomey (1977, p.122-144), has been referred to as constrained linear inversion. Denoting the vector of dimension p representing the model parameter by **m**, the vector of the n observed data by **y** and the functional expressing the model response by **f(m)**, an unconstrained functional U which relates the roughness and misfit can be written in matrix notation as

$$U = |\boldsymbol{\mu m}|^2 + \nu^{-1}\{|\mathbf{Wy} - \mathbf{Wf(m)}|^2 - X_*^2\} \qquad (7.19)$$

where the first term on the right is the roughness and the second the misfit, weighted by the Lagrange multiplier ν^{-1}. $\boldsymbol{\mu}$ is a n x n matrix which expresses 7.18(a) discretely. **W** is a n x n diagonal matrix containing the inverse of the error estimate associated with each datum of **y**. X_*^2 is a value regarded as acceptable for a realistic misfit, adequately chosen not to be too close to the smallest achievable value since the resulting model, for MT problems, would then be a series of delta functions (Parker, 1980). If the noise in the data is gaussian the expected value of X^2 is just n, the number of data points in the response curves. In Occam's inversion scheme, Eq. (7.18) is minimized iteratively by assuming a local linearization for **f** around a starting model $\mathbf{m}^0$, much in the same way as in the procedure followed in the Jupp and Vozoff scheme and expressed in Eq. (7.9). Under this approximation, the model parameter $\mathbf{m}_{k+1}$ relative to the k+1 iteration which minimizes U is given by

$$\mathbf{m}_{k+1}(\nu) = [\nu\boldsymbol{\mu}^T\boldsymbol{\mu} + (\mathbf{WJ}_k)^T\mathbf{WJ}_k]^{-1}(\mathbf{WJ}_k)^T\mathbf{Wy}_k \qquad (7.20)$$

where **J** is the Jacobian matrix, as before, and $\mathbf{y}_k$ is a modified data vector given by

$$\mathbf{y}_k = \mathbf{y} - \mathbf{f}(\mathbf{m}_k) + \mathbf{J}_k\mathbf{m}_k \tag{7.21}$$

Unlike most traditional inversion schemes, including Jupp and Vozoff's, no damping or truncation is performed in the Occam inversion scheme. Instead, by using (7.20), the true misfit of the model $\mathbf{m}_{k+1}(\nu)$

$$X_{k+1}(\nu) = \left|\mathbf{W}\mathbf{y} - \mathbf{W}\mathbf{f}(\mathbf{m}_{k+1}(\nu))\right| \tag{7.22}$$

is calculated for several values of ν by means of a 1-D linear search until $X_k(\nu)$ is minimized or equals X_*. It is possible that more than one value of ν can be selected in this process. That being the case, the largest value of ν ought to be selected as it causes the roughness to be least. It may be shown that if this scheme converges, it will solve the minimization of the nonlinear functional, and therefore, provided the minimum is unique, the final answer should be independent of the starting model (Constable et al., 1987). The computer program used in this study was implemented by Meju (pers. comm.) and is described in more detail in his contemporary Ph.D. thesis. It used as the starting model either one based on the Bostick transformation of the MT curves, described earlier in this section, or one in which a uniform conductivity was considered for all layers. The number of layers was fixed and equal to half the number of data points. The thickness of each layer was also fixed at equal increments on a logarithm scale from the minimum to the maximum penetration depths (given by the extremal depth values of the Bostick transformation). Additionally the author modified the Occam's code to invert controlled source (active MT) responses. This was performed by incorporating an appropriate forward routine which solves analytically the near source problem (either a horizontal magnetic dipole or a horizontal electric dipole as source) in a layered Earth structure. This forward routine, written by Weidelt (pers. comm.), computes the Hankel transforms associated with this problem by means of the digital filter method described by Anderson (1979, 1982).

7.3.4 Monte Carlo- Hedgehog inversion

The Monte Carlo- Hedgehog inversion scheme used in this study has been modified from the Monte Carlo scheme fully described elsewhere (e.g. Jones, 1977, Jones and Hutton, 1979) and in which a starting model parameters vector $\mathbf{x}^0$ is perturbed in a random way and the model response $\mathbf{f}(\mathbf{x}^0)$ is compared against the actual response $\mathbf{y}$. The acceptability of any randomly generated model is set to be within 95 per cent confidence limits and the measure of the misfit of the ith model is given by the expression

$$\Psi = \sum(\log\rho-\log\rho_i)^2 + (\phi-\phi_i)^2 \qquad (7.23)$$

where $\mathbf{y}$ and $\mathbf{f}(\mathbf{x})$ are expressed in terms of apparent resistivities ρ and phases ϕ. The summation is carried out over all frequencies, i.e. the n data points. The use of logarithms follows from an assumed log-normal apparent resistivity distribution (Bentley, 1973).

The scheme is iterative with a large number of random models being generated and the best models selected after each iteration. The search for models in the model space is obtained by using previous models. In a given iteration, the kth layer of the new model response is

$$h'_k = h_k\ 10^{r_k} \qquad \text{(a)}$$
$$\rho'_k = \rho_k\ 10^{r_j} \qquad \text{(b)} \qquad (7.24)$$

where the model parameters vector $\mathbf{x}^k$ is expressed in terms of the layer thickness h_k and the layer resisitivity ρ_k, and r is a normalized gaussian distributed (with zero mean) random number. However, the code utilizes only the random numbers comprised between −1 and +1 (68 per cent of a normal distribution), so that all the h'_i and ρ'_i are between a tenth and ten times the original model parameter, i.e. h'_i is between $h_i/10$ and $10h_i$. The randomly generated layer thickness h'_k is further constrained by a natural condition that $h'_k > h'_{k-1}$. This condition was observed to increase the computing time very substantially whenever a very thin layer was implied by the data structure.

One version of the above code used in this study (version 1) is a modification of the original code in the sense that it incorporates a Hedgehog technique (e.g. Keiris-Borok and Yanovskaja, 1967), in which a search is

conducted in an organized manner around some satisfactory initial model. Such a procedure can speed up the solution considerably. Version 1 has the following practical features: the number of layers of the model is specified and layer resistivities and thicknesses (including extremal bounds) assumed for the starting model. In each iteration, 50 random models within the bounds are generated and the 20 best models selected are put in an order table, with the best fitting one at the top. These selected models are then averaged and the mean values and associated standard deviations used to form a new starting model and bounds for another iteration. After each iteration, the order table is updated and at the end of 20 iterations, the best 20 models give a range of acceptable models , and hence some indication of nonuniqueness of the 1D inversion.

The main merit of this modified inversion scheme is that no linearization is performed at any stage of it. However, due to computing time constraints, the search for acceptable models (more specifically in the current modified version 1 of the program) does not cover the model space extensively and, as a result of this, the final set of models does not depart considerably from the starting model.

A more recent version of the program (version 2) fits the tensor elements directly instead of using apparent resistivities and phases. Moreover, it runs up to 100 iterations, with the same number (50) of random models for each iteration as for version 1. Inversions using the two latter versions have indicated equivalent results and competitive computational times due to the improved programming optimization of version 2.

The Monte Carlo- Hedgehog inversion scheme (version 1) has also been adapted by the author to handle the near- source problem faced in Italy. In this particular problem, the transmitter- receiver distance (d) (in the Italian case, the distance between the DC railway and the measuring site) is also a parameter to be determined during modelling. Hence, the model incorporates the additional parameter d which is then randomly modified in a manner identical to that for h and ρ in Eq. (7.24), i.e. $d'_k=d_k\ 10^{r_l}$. The forward routine is written by Weidelt and described briefly in section 7.3.3.

7.4 1D models for Asiago

Despite the evidence provided by the dimensionality indicators (presented in Chapter 6) that the Asiago region is strictly two-dimensional, a predominant 1D feature was shown to hold in this area. Therefore, 1D modelling can be useful both for tracing the most salient geoelectrical structures and for serving as a starting point for 2D modelling. Due to data limitation and possible 2D effects, 1D inversion has been applied not only to the rotationally invariant curves (specifically, ρ_{i2} (Eq. 4.36)), but also to both the E pol and H pol directions. This course of action was found to be fruitful as it provided a cross check on the models derived from any particular direction or invariant. There is, in fact, no general standard procedure on this matter. For instance, various investigators (e.g. Rooney and Hutton, 1977, Jones and Hutton, 1979, Stanley, 1984) fitted 1D models to the major response curves by assuming these to be less distorted by near- surface inhomogeneities than the minor curves. Based on identical arguments (i.e. low level of distortion), Adam et al. (1982) chose the minor response curves for interpreting the deep conductive structure beneath the Pannonian basin. The use of average curves (provided by one of the rotationally invariant curves (Eqs. 4.36 and 4.37)) has been reported by other authors (e.g. Jodicke et al., 1983; Hutton et al., 1987).

As an initial step in this study, the same starting model was used for all sites and each distinct inversion scheme. This starting model was then conveniently modified to allow for the specific features of each site and to refine and optimize the resolution of the model parameters. As expected from both the linearized scheme and from the Monte Carlo- Hedgehog method of random search, the choice of starting model has considerable influence on the final model. These schemes tend to home in on the nearest minimum in the model parameter space. This is not necessarily the absolute minimum. As an example, Figs. 7.1(a)-(b) show the models for site Granezza (rotationally invariant responses) obtained with the Jupp and Vozoff code for 2 distinct starting models of 4 layers. The resulting models are different in some aspects. Figs. 7.2(a)-(b) illustrate the effect of the starting model on the final models derived by application of the Monte Carlo- Hedgehog algorithm. Again, two distinct final models (or more appropriately, ranges of models in

1D MODELS 2ND ORDER MARQUADT SITE GRANEZZA 452A

(a)

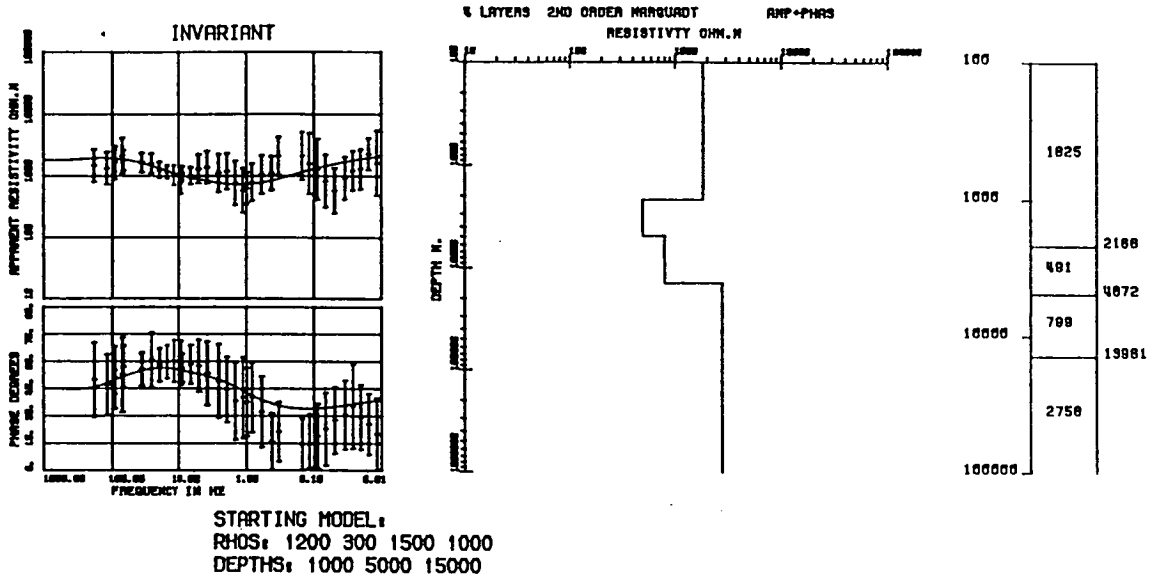

STARTING MODEL:
RHOS: 1200 300 1500 1000
DEPTHS: 1000 5000 15000

(b)

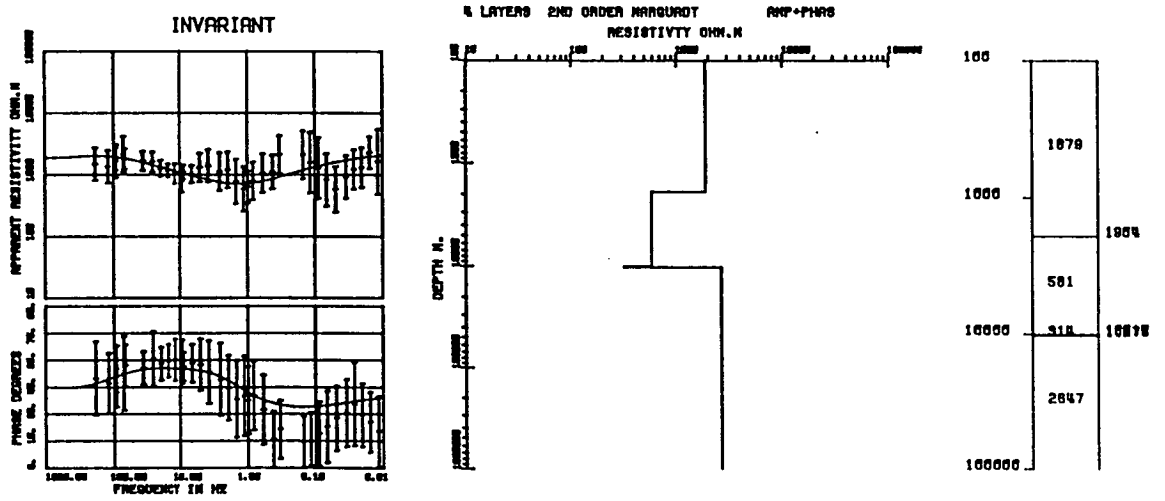

STARTING MODEL
RHOS: 1200 300 25 1000
DEPTHS: 1000 5000 7000

Fig. 7.1- Example of the influence of the starting model on the final solution of the 1D inversion using the 2nd order Marquadt scheme. Models for the rotationally invariant response- site Granezza, considering two distinct starting models (resistivities in Ωm and depths in m). Both amplitude and phase (shown in the left hand side of the Fig.) are used in the inversion, whose results are given either graphically (center of the Fig.) or by resistivity and depth values at the right hand side of the Fig.

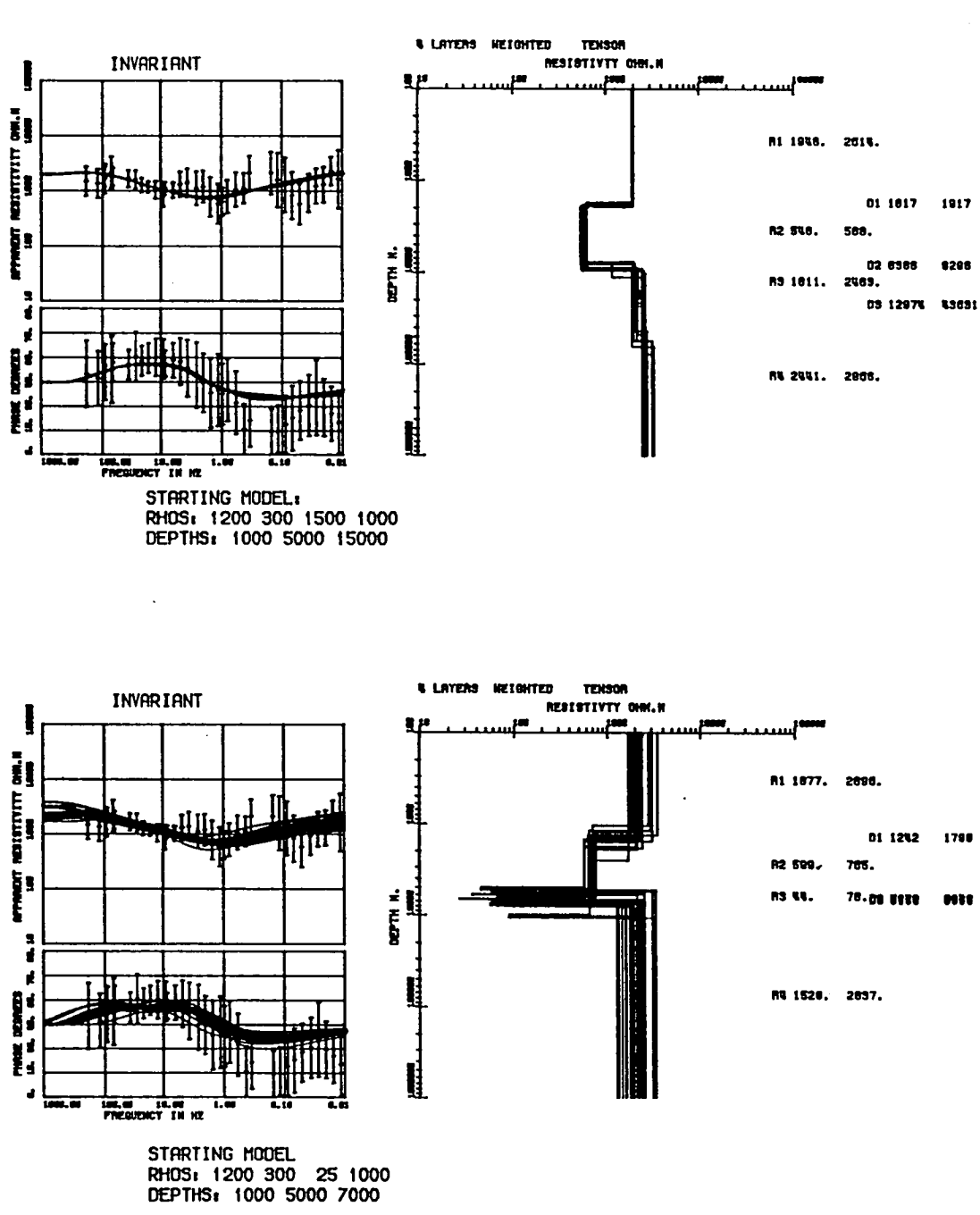

Fig. 7.2- Example of the influence of the starting model on the final solution of the 1D inversion using the Monte Carlo scheme. Models for the rotationally invariant response- site Granezza, considering two distinct starting models (the same ones of Fig. 7.1). The 5 best models are shown (center of the Fig.) along with the range of resistivity values (Ωm) and depths (m) (± 1 standard deviation) at the right hand side of the Fig.

Fig. 7.3(a)-(h)- 1D model results (rotationally invariant responses) for all the sites in the Asiago area.
Top- 1D model results using the weighted 2^{nd} order Marquadt scheme with the Bostick transformation values (points with vertical and horizontal error bars). Units and layout as in Fig. 7.1.
Bottom- 1D model results using Monte Carlo scheme. Plots of the 5 best models and range of resistivity and depths (± 1 standard deviation) given in the same units and layout as in Fig. 7.2.

1D MODELS SITE MANDRIELLE 456A

(a)

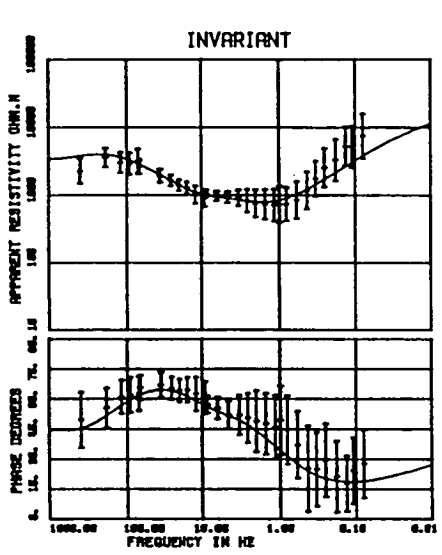

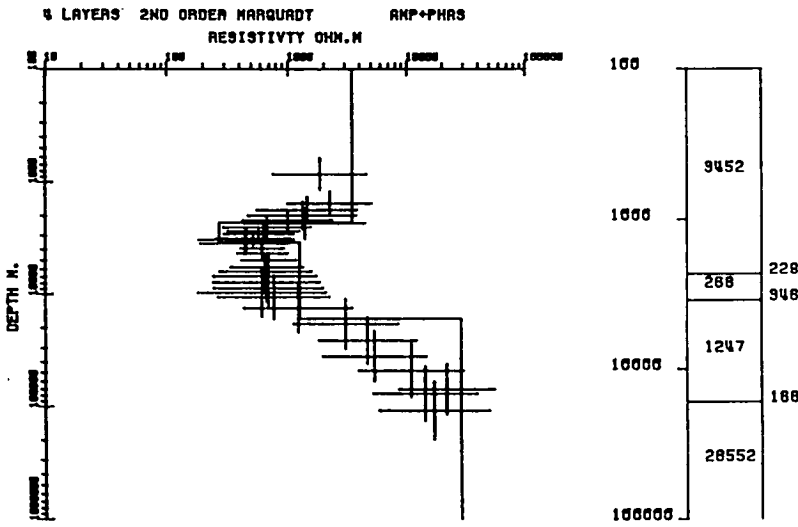

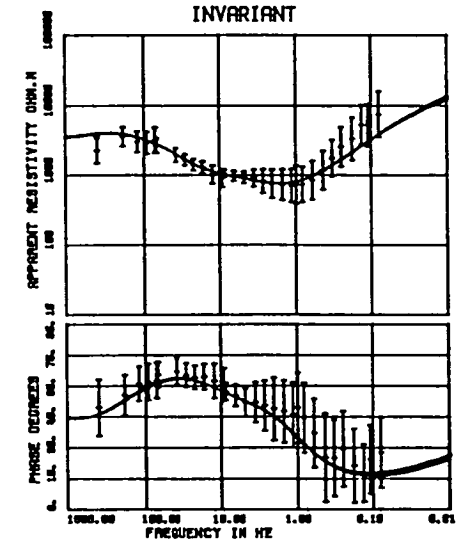

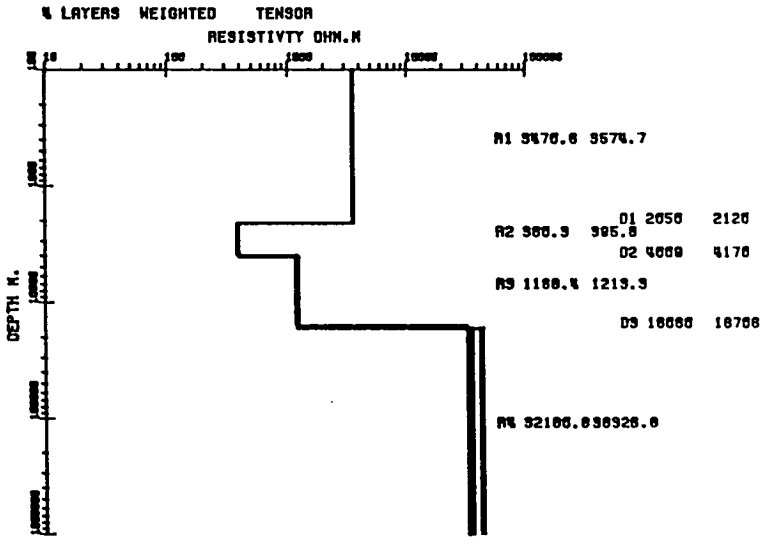

1D MODELS SITE C. MULO 454A

(b)

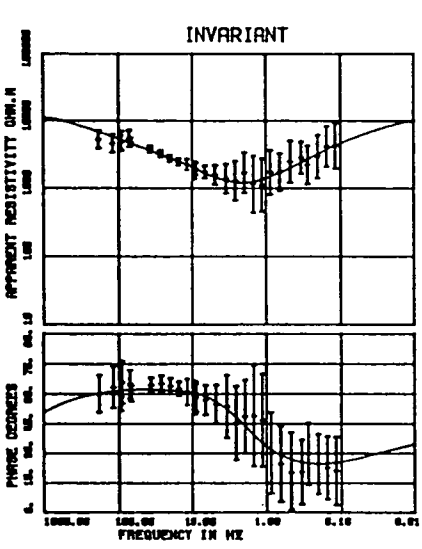

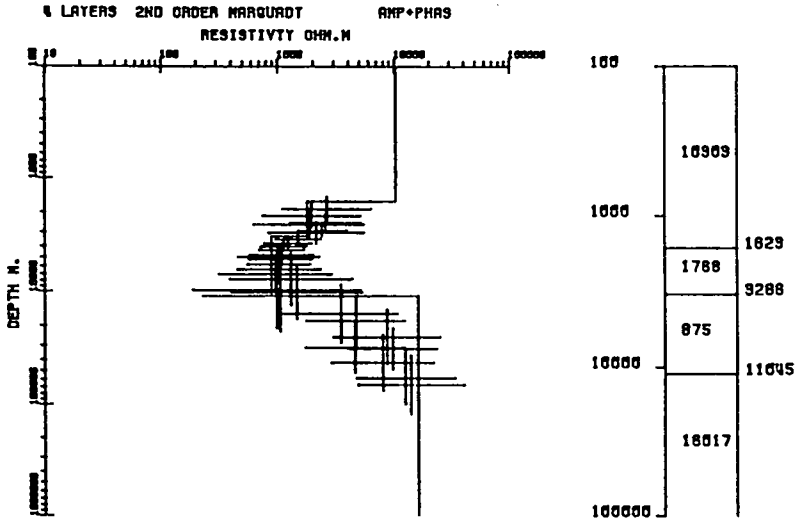

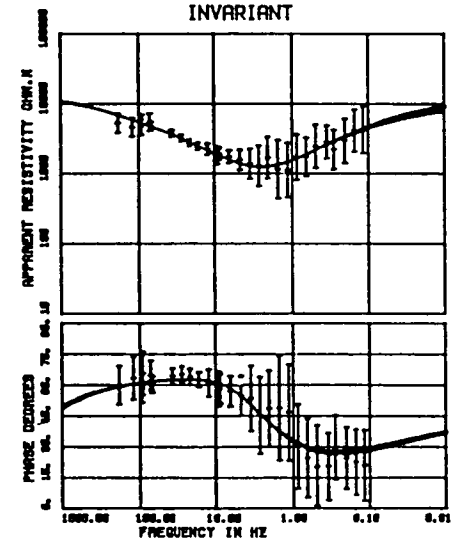

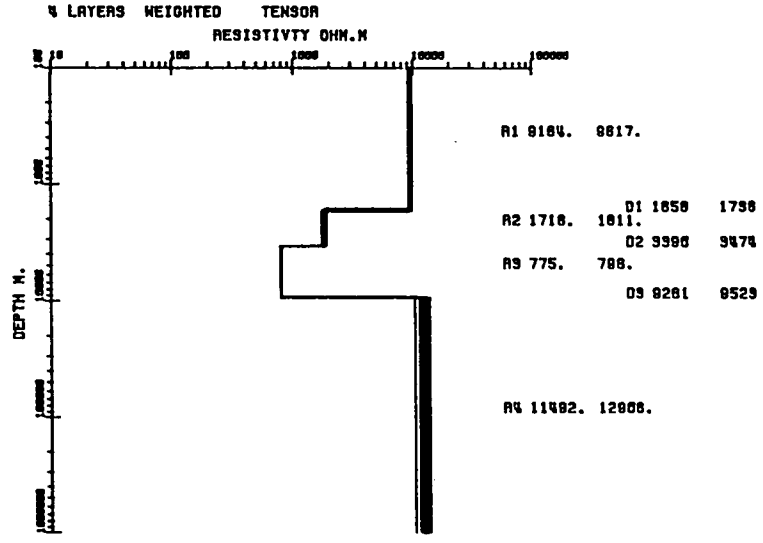

1D MODELS SITE LONGARA 455A

(c)

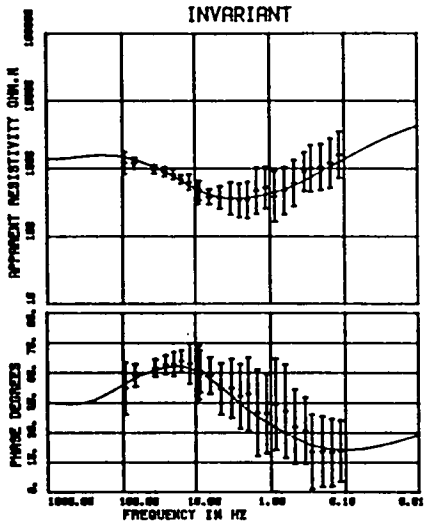

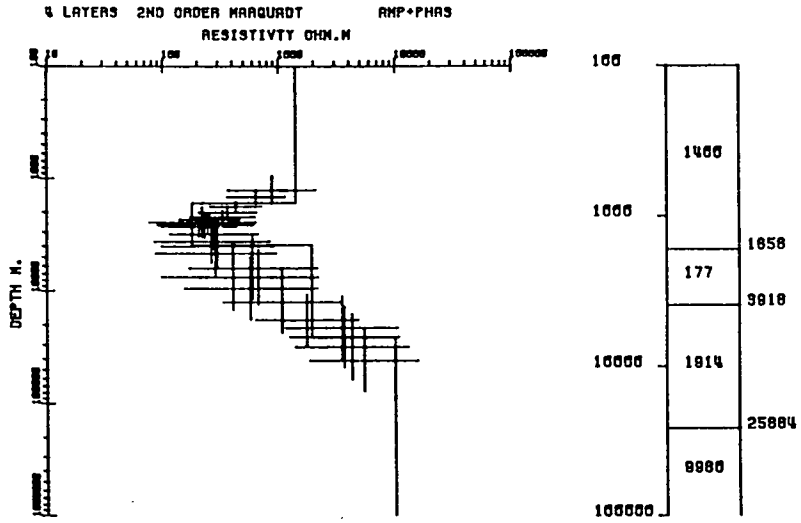

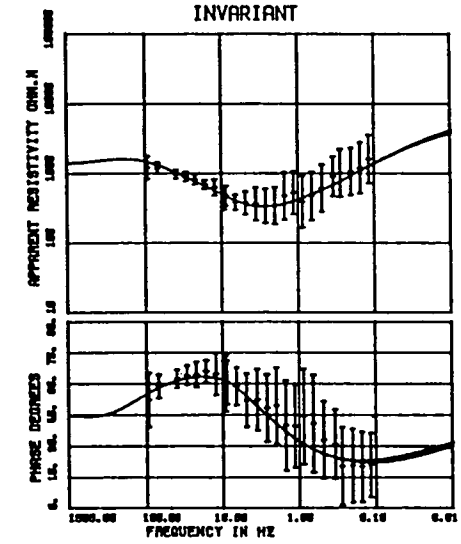

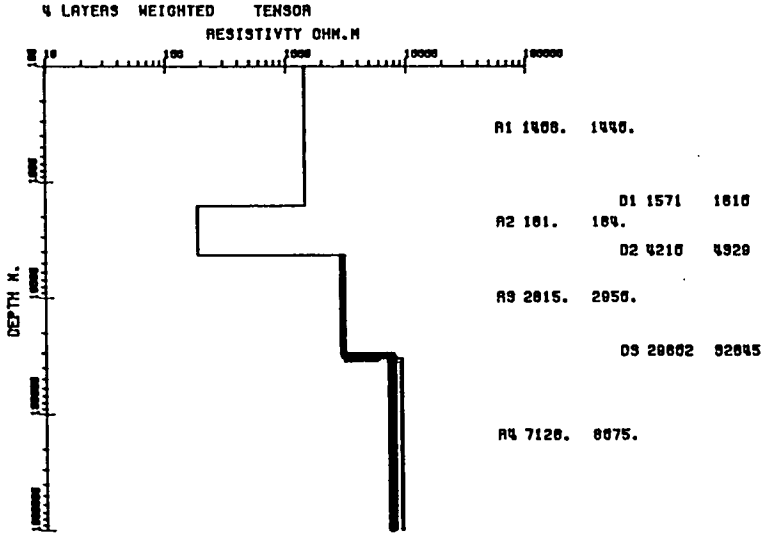

1D MODELS SITE V. DI NOS 690A

(d)

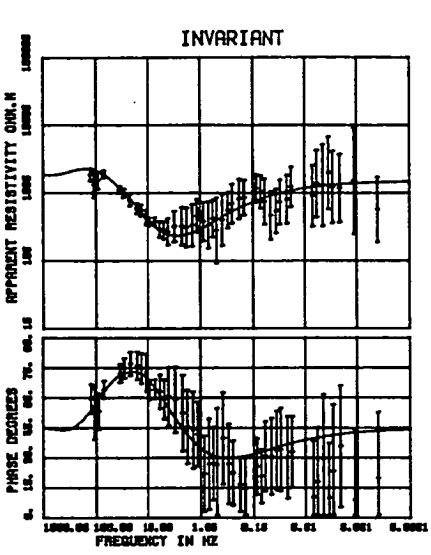

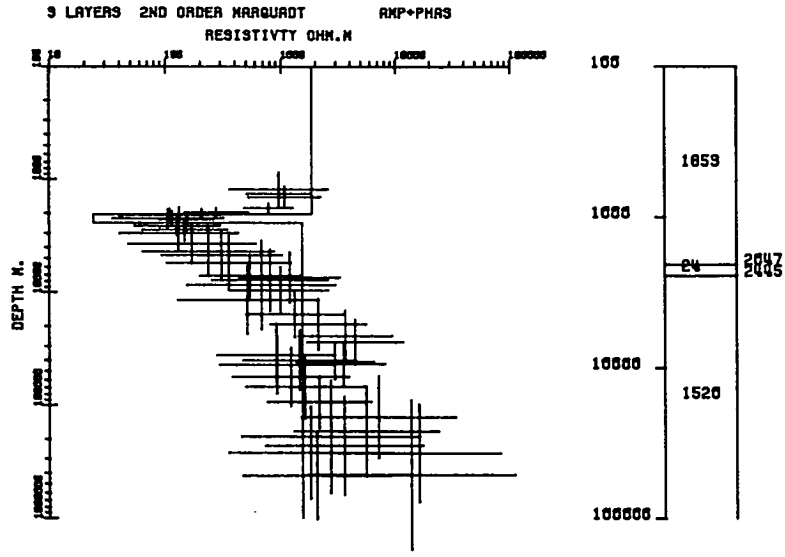

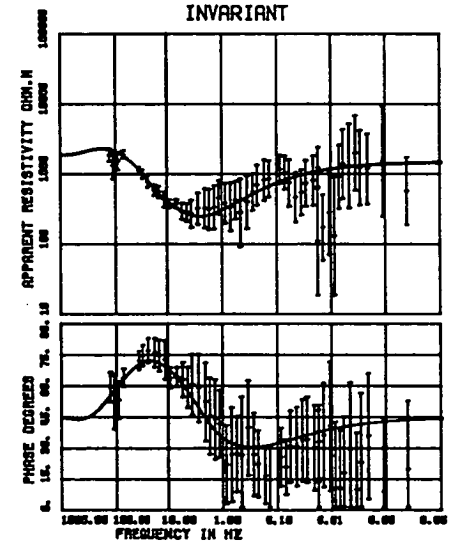

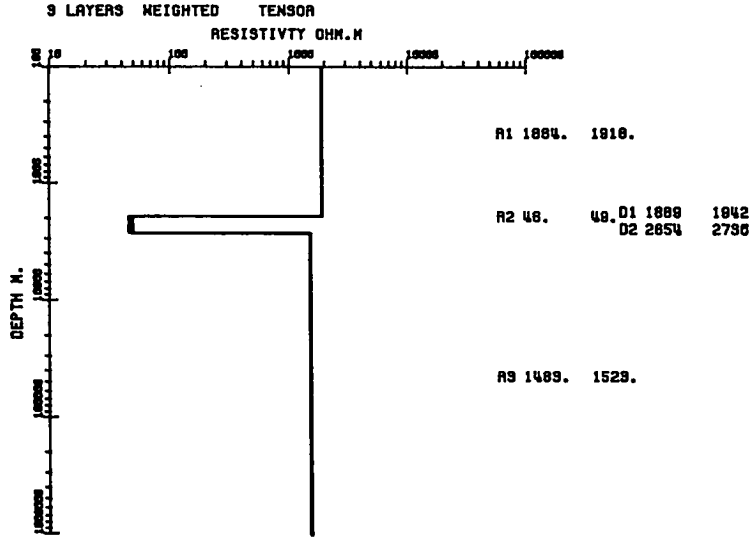

1D MODELS SITE C.S. ANTONIO 450A

(e)

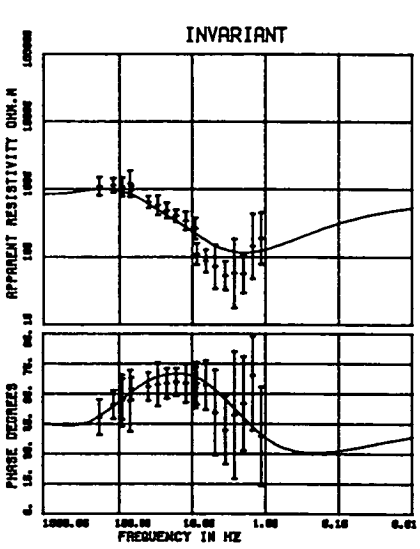

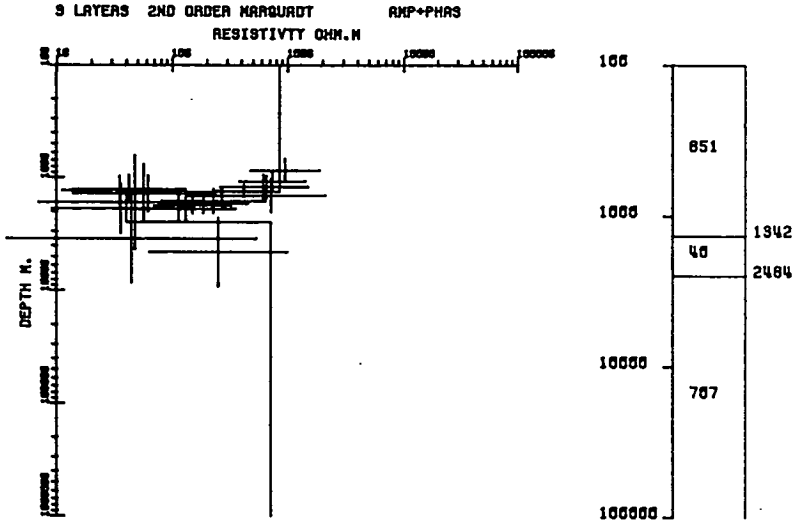

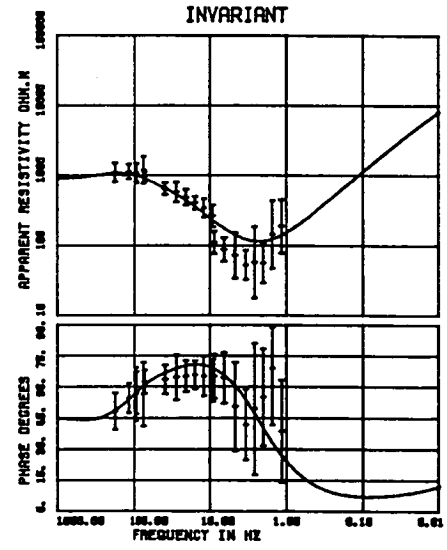

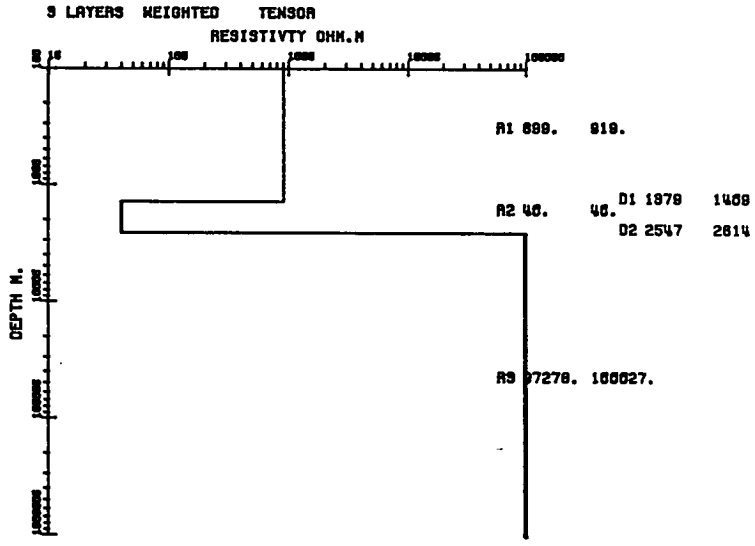

1D MODELS SITE OBSERVATORIO 451A

(f)

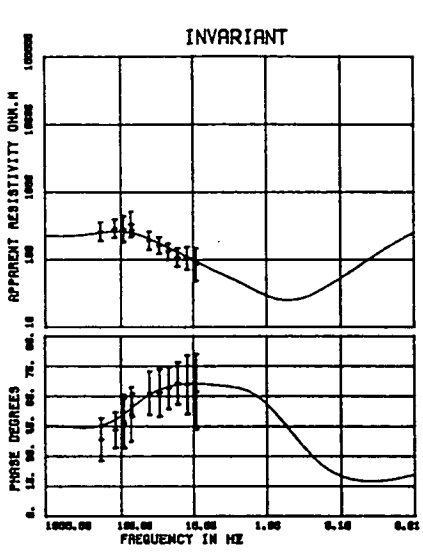

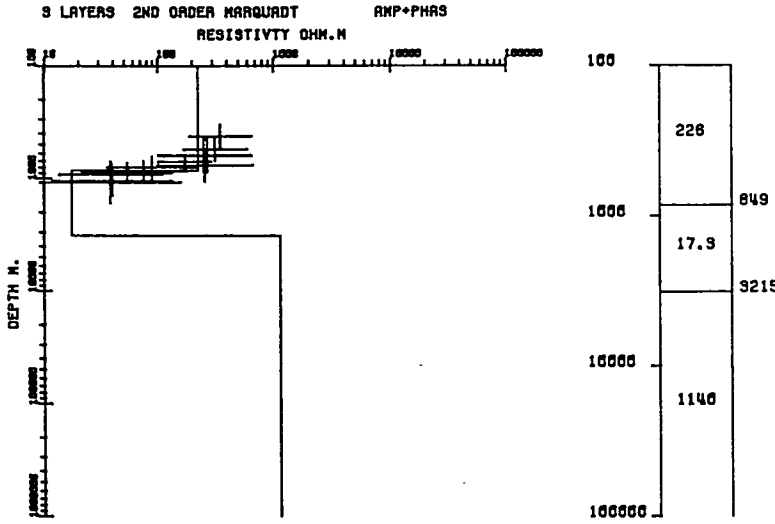

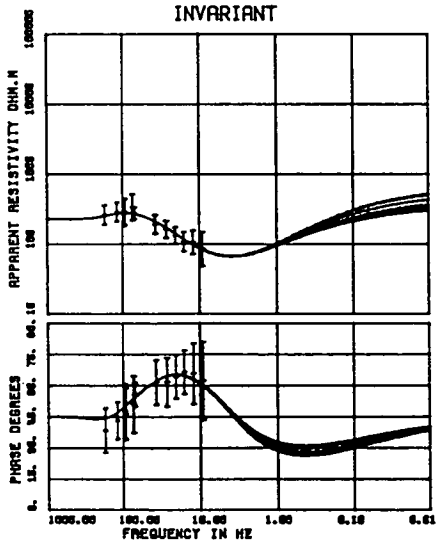

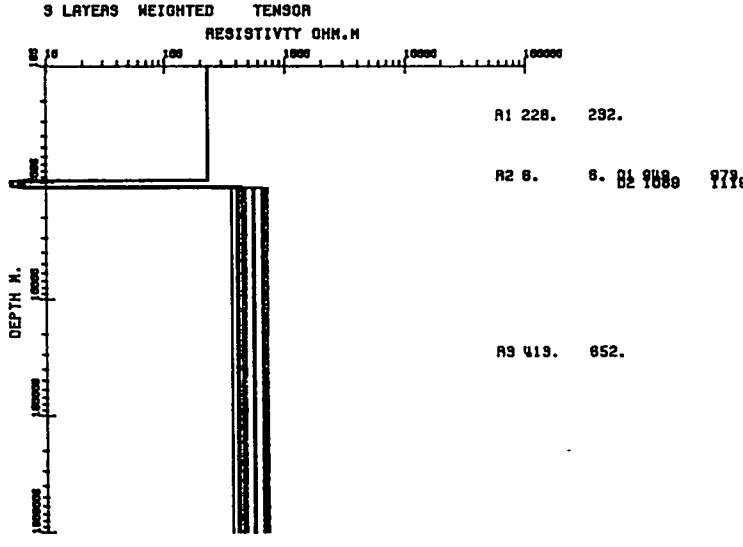

1D MODELS SITE AVE 453A

(g)

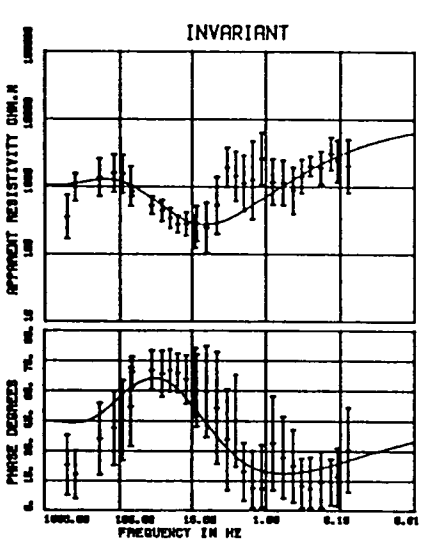

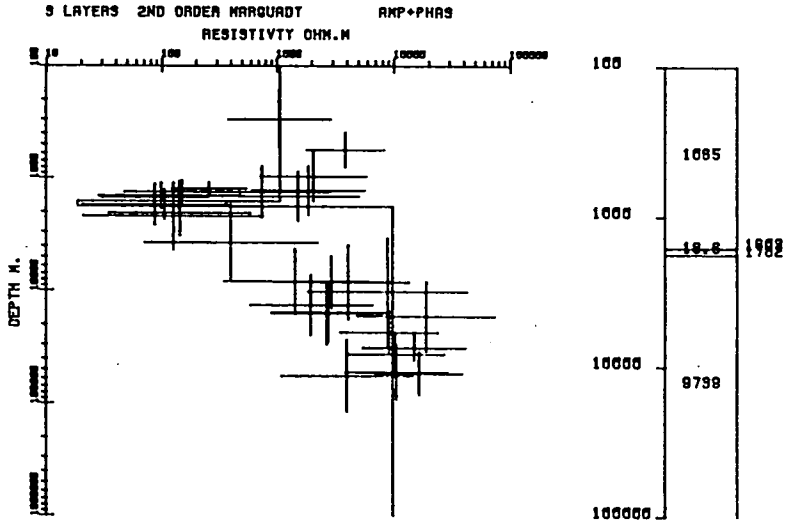

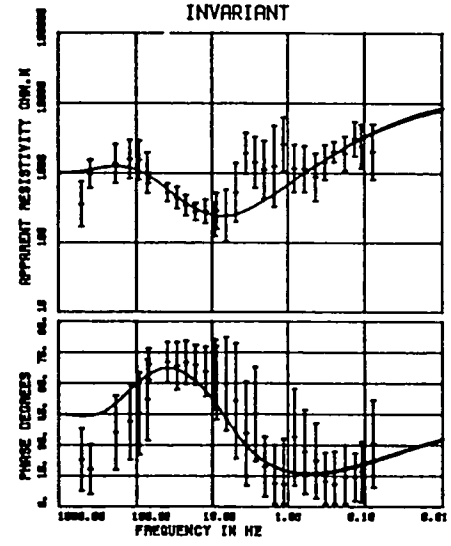

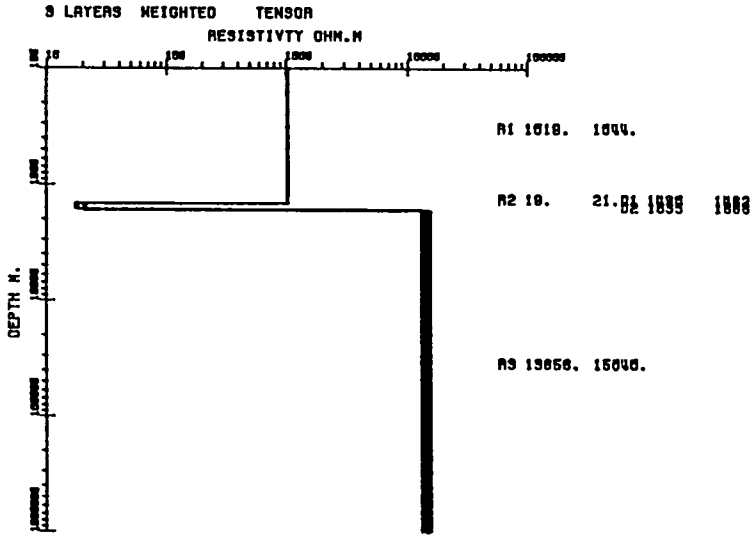

1D MODELS SITE GRANEZZA 452A

(h)

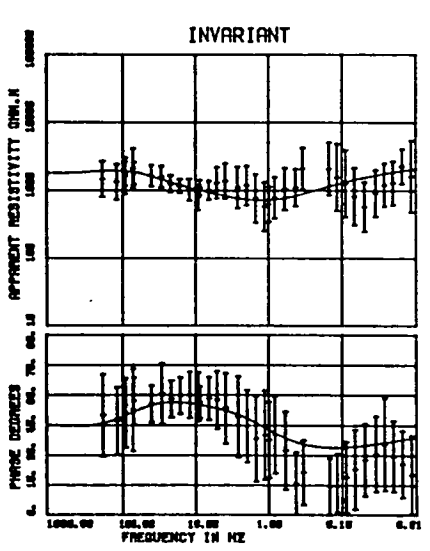

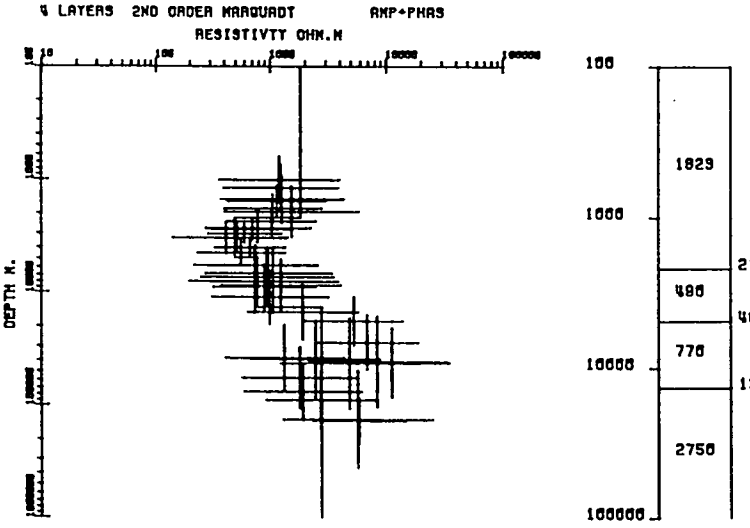

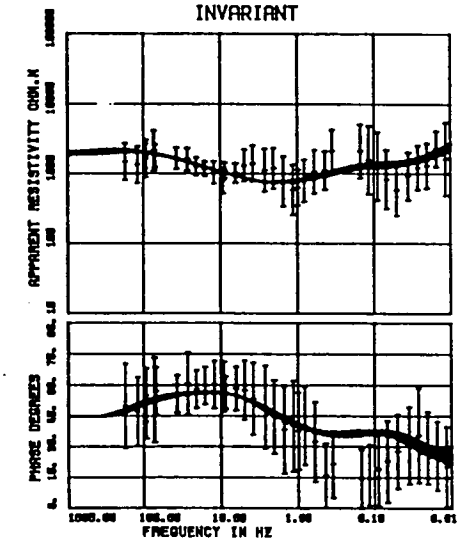

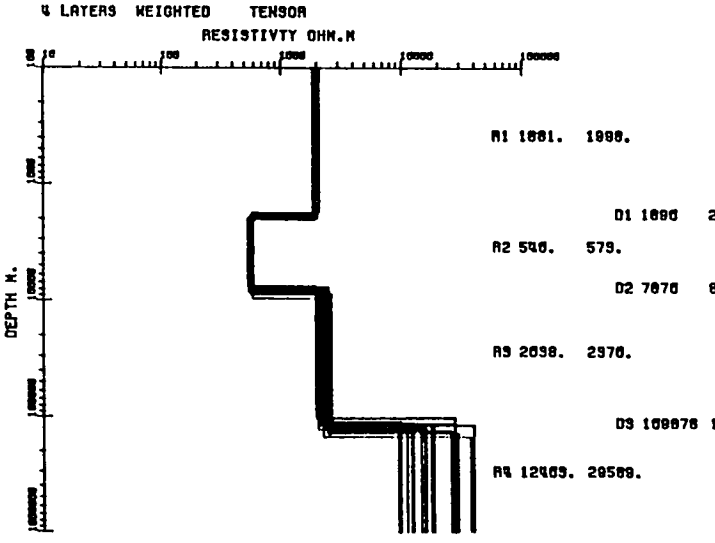

this case) are obtained. They are, however, in reasonable agreement with the models obtained with the Jupp and Vozoff code. Nonetheless, careful analysis and examination of the various models generated has proven effective in circumventing the inherent ambiguity of these schemes. The results of the 1D inversion for all sites (rotationally invariant) are shown in Figs. 7.3(a)-(h). They consist of plots presenting the Bostick transformation and the second order Marquadt 1D inversion results (top), and the Monte Carlo- Hedgehog 1D inversion (bottom). The values R_i and D_i are ± 1 standard deviation of 20 best models of resistivity and depth parameters, respectively. The models consist of 3 or 4 layers, as shown in Figs. 7.3; the computed responses fit the data reasonably well and are in overall good agreement at each site. Where noisy responses are present, there are minor differences between the results. The computing time required by the Jupp and Vozoff code is about 30 times less than that for the Monte Carlo- Hedgehog code, with typical running times of 90s for the Monte Carlo against 3s for the Jupp and Vozoff code (7 iterations on average) using an Amdahl 470 V/8 machine (EMAS). The Bostick transformations are also in fair agreement with both inversion schemes, except in the more resistive layers (depth to resistive interface poorly defined). The approximate transformations are known to be poor estimators in such a situation (Hyong and Berdichevsky, 1984; Schmucker, 1987). Nevertheless, bearing this limitation in mind, or perhaps modifying the transformations to overcome it (e.g. Hyong and Berdichevsky, 1984), the use of such transformations is highly recommended on account of their great simplicity and their relative effectiveness compared to more sophisticated inversion schemes.

An accompanying set of tables which summarize the parameter sensitivity analysis (performed by the Jupp and Vozoff code) for all the sites is provided in Appendix A. One example of this evaluation is given also in Tab. 7.1(a) where data sets from MAN (see also Fig. 7.3(a)) is modelled by a four layers structure. The V matrix is thus a 7 x 7 matrix, the first four rows containing the parameter space vector corresponding to 4 resistivity values and the last three rows to 3 depth values. The total number of parameters is therefore 7 and the number of effective parameters (the summation of all damping factors t_k, k=1,7) is 6.966. Hence, it can also be concluded that all parameters are relevant and well resolved. By using **V** and **t** (Eq. 7.17), the

Tab. 7.1(a)–(b) Summary the of relevant parameters for two sites in the Asiago area using the weighted 2^{nd} order Marquadt scheme (rotationally invariant response curves)

SUMMARY 1D RESULTS WEIGHTED 2ND ORDER MARQUADT
N.ITALY MANDRIELLE 456A INVARIANT (a)

NORMALIZED SINGULAR VALUES OF JACOBIAN

0.100E+01 0.446E+00 0.342E+00 0.284E+00 0.785E-01 0.432E-01 0.237E-01

NUMBER OF EFFECTIVE PARAMETERS: 6.966

SCALE FACTOR : 0.2009180E+00

DAMPING FACTORS (1.0 PERCENT LEVEL)

0.100E+01 0.100E+01 0.100E+01 0.100E+01 0.100E+01 0.997E+00 0.969E+00

PARAMETER SPACE EIGENVECTORS (V MATRIX)

1	0.019	-0.213	0.454	-0.862	0.040	-0.014	-0.058
2	0.324	0.058	-0.124	0.002	0.243	-0.172	-0.887
3	0.134	0.449	0.387	0.073	-0.744	0.162	-0.211
4	0.002	0.036	0.071	0.035	0.299	0.944	-0.108
5	0.732	-0.558	0.221	0.253	-0.102	0.045	0.164
6	-0.581	-0.539	0.374	0.334	-0.114	-0.020	-0.326
7	-0.053	-0.382	-0.659	-0.273	-0.522	0.224	-0.140

LAYER RESISTIVITIES

I	RO(I)	BOUND(1)	BOUND(2)	DAMPING
1	3452.2847	2311.1548	5156.8437	0.0001
2	268.3025	29.8017	2415.5076	0.0241
3	1246.7634	370.6240	4194.0547	0.0016
4	28552.1133	6275.8867	129897.5625	0.0029

LAYER DEPTHS (TO BASE)

I	Z(I)	BOUND(1)	BOUND(2)	DAMPING
1	2295.2998	1227.3479	4292.5078	0.0008
2	3465.4160	1324.8040	9064.8164	0.0032
3	16601.4961	5745.9219	47966.1055	0.0008

SUMMARY 1D RESULTS WEIGHTED 2ND ORDER MARQUADT (b)
N.ITALY C.MULO 454A INVARIANT

NORMALIZED SINGULAR VALUES OF JACOBIAN

0.100E+01 0.897E+00 0.593E+00 0.268E+00 0.119E+00 0.106E+00 0.143E-01

NUMBER OF EFFECTIVE PARAMETERS: 6.809

SCALE FACTOR : 0.9864545E-01

DAMPING FACTORS (1.0 PERCENT LEVEL)

0.100E+01 0.100E+01 0.100E+01 0.100E+01 0.100E+01 0.100E+01 0.809E+00

PARAMETER SPACE EIGENVECTORS (V MATRIX)

1	0.001	0.251	0.303	-0.436	-0.500	0.520	0.367
2	-0.156	0.469	-0.156	0.300	0.223	-0.195	0.744
3	-0.660	-0.132	-0.292	-0.633	0.125	-0.208	0.047
4	-0.075	-0.022	0.066	0.120	-0.742	-0.651	0.015
5	-0.116	0.768	0.309	-0.130	0.144	-0.181	-0.481
6	-0.268	0.256	-0.651	0.312	-0.336	0.390	-0.277
7	0.670	0.212	-0.524	-0.437	-0.016	-0.199	0.027

LAYER RESISTIVITIES

I	RO(I)	BOUND(1)	BOUND(2)	DAMPING
1	10303.4023	393.3833	269864.1875	0.0236
2	1767.5122	13.9735	223573.1875	0.1008
3	874.9719	340.3010	2249.7014	0.0004
4	16017.0312	3915.2761	65524.1836	0.0001

LAYER DEPTHS (TO BASE)

I	Z(I)	BOUND(1)	BOUND(2)	DAMPING
1	1622.7883	63.1245	41718.2070	0.0408
2	3286.1843	262.6001	41123.3828	0.0133
3	11044.6641	5464.4219	22323.4102	0.0001

individual contribution of each element of **V** can be assessed. The most important parameters can be also given either singly or in terms of products and ratios of the various parameters (Jupp and Vozoff, 1975a,b; Ilkisik and Jones, 1984). The most important parameters for this site are RO(4), RO(2), RO(1), RO(3) and Z(1)/Z(2). The bounds are coarse errors which are calculated as a function of **V**, the singular values of the Jacobian **J** and the residual errors in the data at 1% numerical convergence. These bounds are not representative of model variance as in the Monte Carlo case. Consider as a second example, the site OBS (Fig. 7.3(f) and Tab. 7.1(b)). A 3 layer model has been fitted so that the total number of parameters is 5. As the number of effective parameters is 3.014, it is evident that 2 of the parameters are not important. By inspection of the matrix **V** and by using Eq. 7.17, it can be concluded that both the resistivity of the third layer RO(3) and its depth Z(2) are not well resolved. As a further indication, their contribution to the final solution has been heavily damped (damping equal 0.9998 and 0.9790, respectively). Note that the bounds associated with these parameters are very close to the parameter values themselves, as the unimportant parameters are not changed much by the algorithm. Lack of information is the reason for the the poor resolution in this case since data for OBS is available only for frequencies higher than 10Hz and a 3 layer model can only be justified by the general conductivity pattern exhibited in the region. Nevertheless, any interpretation must embody this uncertainty. Appendix B contains the 1D model results for all sites obtained by the Monte Carlo- Hedgehog and the weighted second order Marquadt inversion codes for both the E pol and H pol directions.

Inversion using the Occam technique has been undertaken by assigning the same conductivity value to all layers of the starting model. The models obtained with the Occam technique (invariant, E pol and H pol)- Appendix C- are again in good agreement with those obtained with all the other inversion schemes used in this study. Convergence was achieved after about 4 iterations on average and computing times were only slightly longer than those for the Jupp and Vozoff code for most sets of data. However, convergence problems occurred with bad data (e.g. E pol direction for site C.S. Antonio), and this increased computer time substantially. The influence of the starting model on the final model derived by the application of the

(a) Bostick

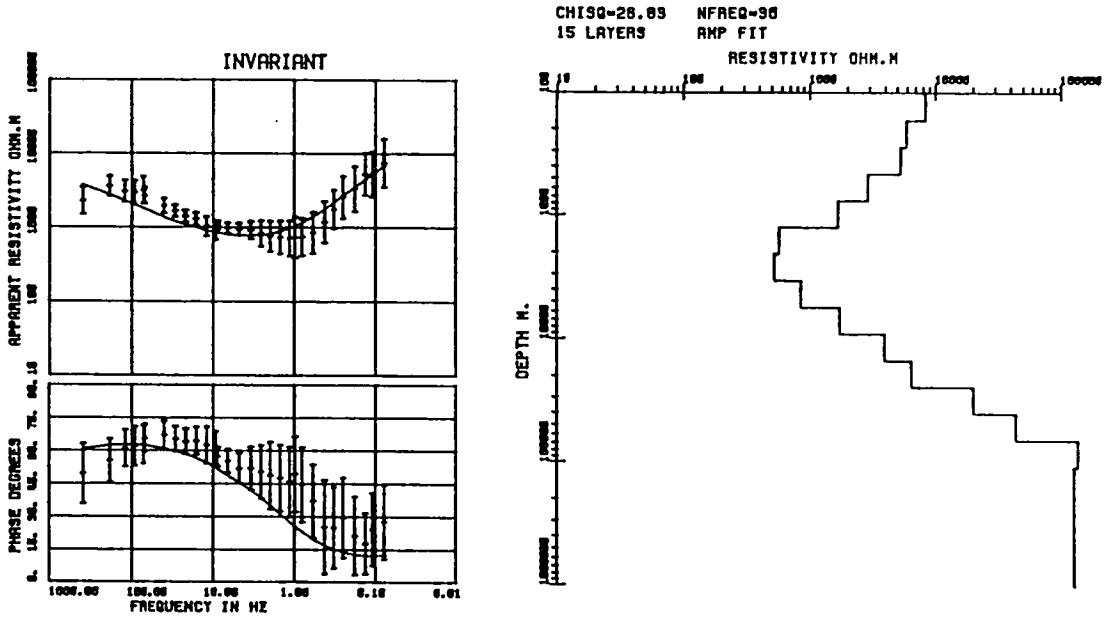

(b) 600 ohm-m halfspace

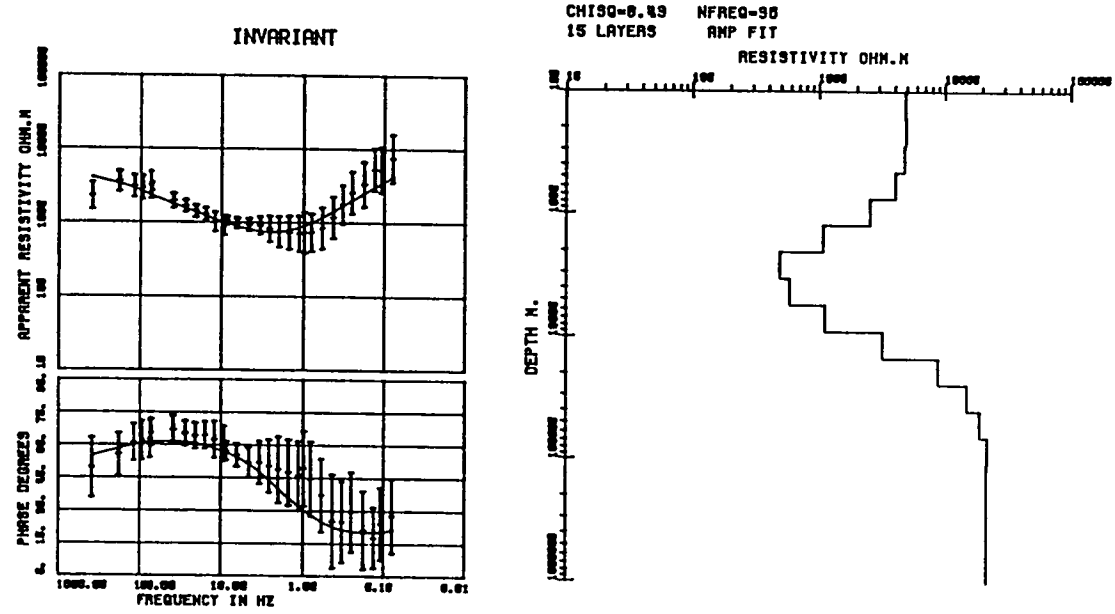

Fig. 7.4- Example of the influence of the starting model in the final solution of the 1D inversion using the Occam scheme. Models for the rotationally invariant- site Mandrielle considering as starting models:
(a)- Bostick transformation values
(b)- Constant resistivity value (600 Ωm) assigned for all layers

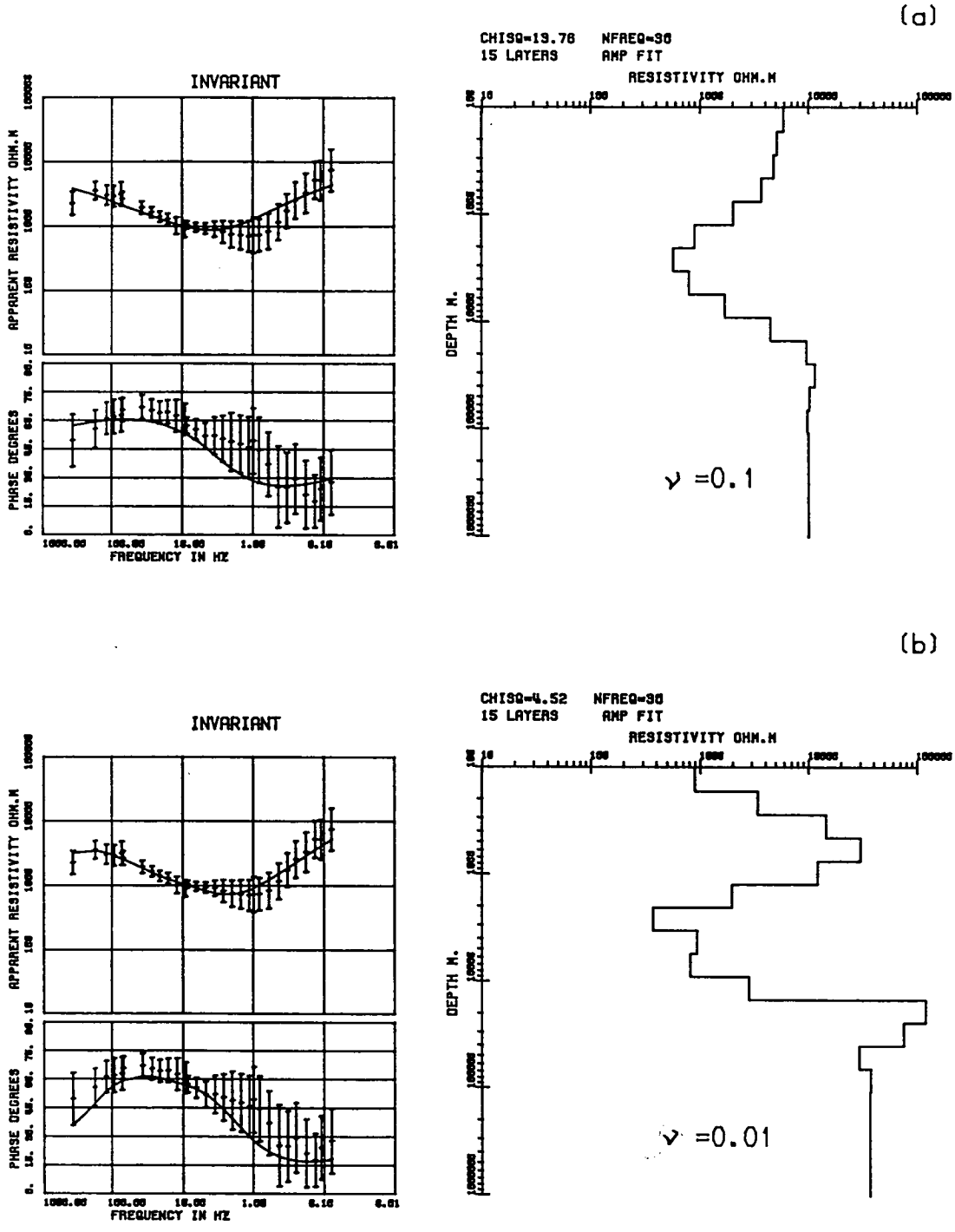

Fig. 7.5- Example of the influence of the Lagrange multiplier (μ) in the final solution of the 1D inversion using the Occam scheme.
(a)- ν = 0.1
(b)- ν = 0.01

Occam algorithm was also examined the results for one site (invariant response for Mandrielle) are shown in Fig. 7.4(a)-(b). Fig. 7.4(a) shows the models when using the Bostick transformation as the starting model and Fig. 7.4(b), the model resulting from a starting model of 600Ωm has been assumed for all layers (i.e. a halfspace model). While both inversions exhibit the same pattern, the associated resistivity values are not quite the same and there is a lower misfit for the halfspace starting model (χ^2=8.43). These results suggest that the minimum in the parameter space is not unique (see section 7.3.3). As an important parameter influencing the final solution, the choice of the Lagrange multiplier ν (not chosen by a linear search in the implemented code) is set by a compromise between smoothness and acceptable fitting. To illustrate this point, the results for the same site Mandrielle (invariant responses) are compared for 2 distinct values of ν (Fig. 7.5(a)-(b)). It can be observed that the higher value of ν (ν=0.1)- Fig. 7.5(a) expectedly produces a smoother Earth model (higher value of misfit- χ^2=13.76) than that obtained with ν=0.01 (χ^2= 4.52). Note that the same ν=0.1 was used for both inversions illustrated in Figs. 7.4. Note also that the χ^2 for the various sites (and polarizations) are well within $\chi^2 < n + \sqrt{2n}$ (n- number of data points) for the Occam inversion, indicating that it is possible to interpret these sites with an one- dimensional conductivity distribution (Parker, 1980; Hobbs, 1987).

The 1D models obtained using Jupp and Vozoff code have combined to form a composite 2D section for the invariant, E pol and H pol responses as shown in the Figs. 7.6-7.8, respectively. The Asiago profile is presented from North to South -the reader is referred to Tab 3.2 for a list of all sites in this region. Figs. 7.9, 7.10 and 7.11 represent composite 2D sections for the invariant, the E pol and the H pol responses, taking account of all the inversion schemes used in this study. The vertical boundaries at shallow and deep depths in Figs. 7.9, 7.10 and 7.11 are to some extent arbitrary (e.g. not always assumed halfway between 2 sites) due to the natural limitation imposed by a discrete set of measurements made at the surface. The resistivity values assigned in these Figs. represent average values from the different models. Notwithstanding varying resistivities and depths for the different sets of response curve (invariant, E pol and H pol), a common feature in all the composite sections presented is a conductive structure at

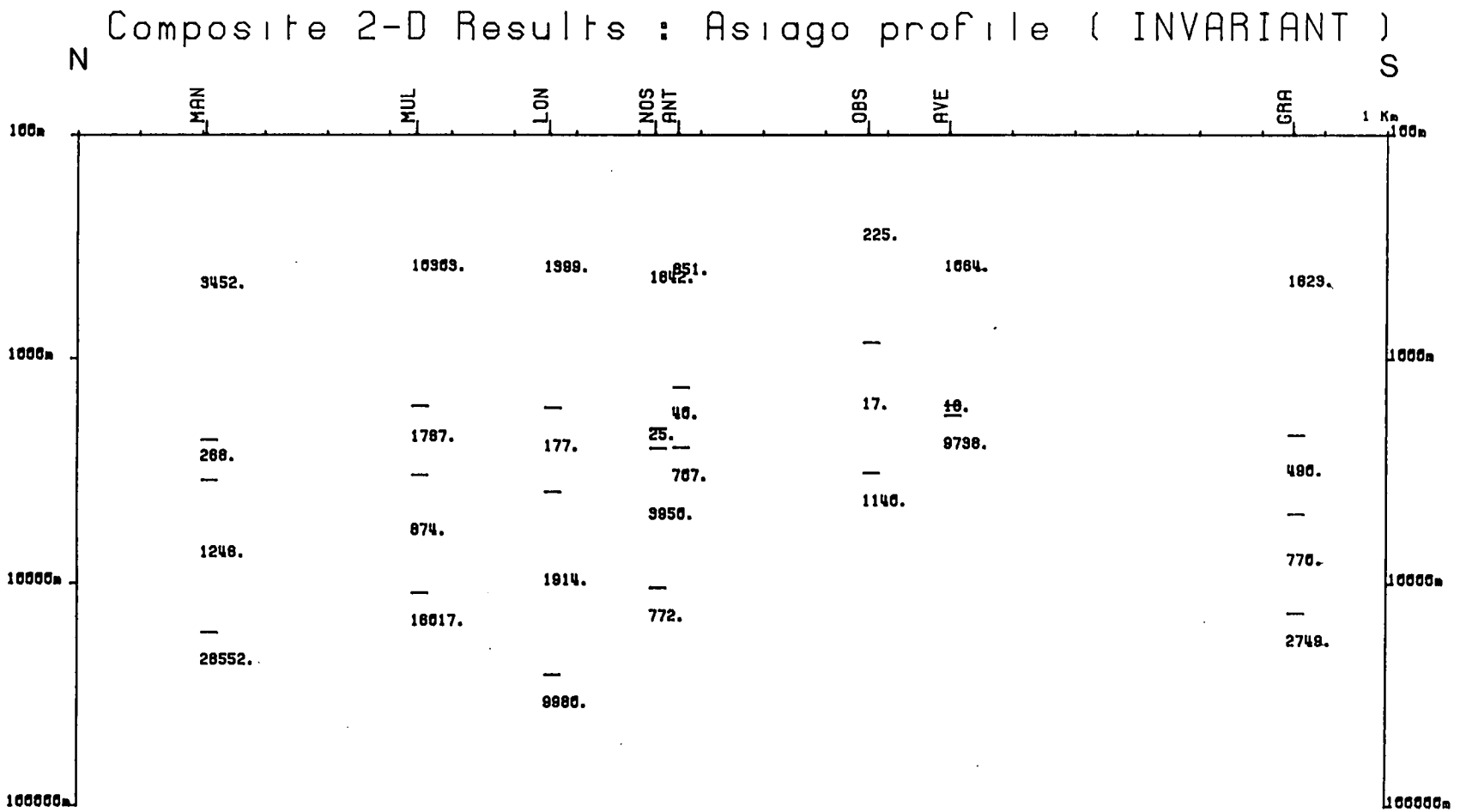

Fig. 7.6- Composite 2D section for the rotationally invariant responses considering all sites in the Asiago area using the 2nd order Marquadt scheme.

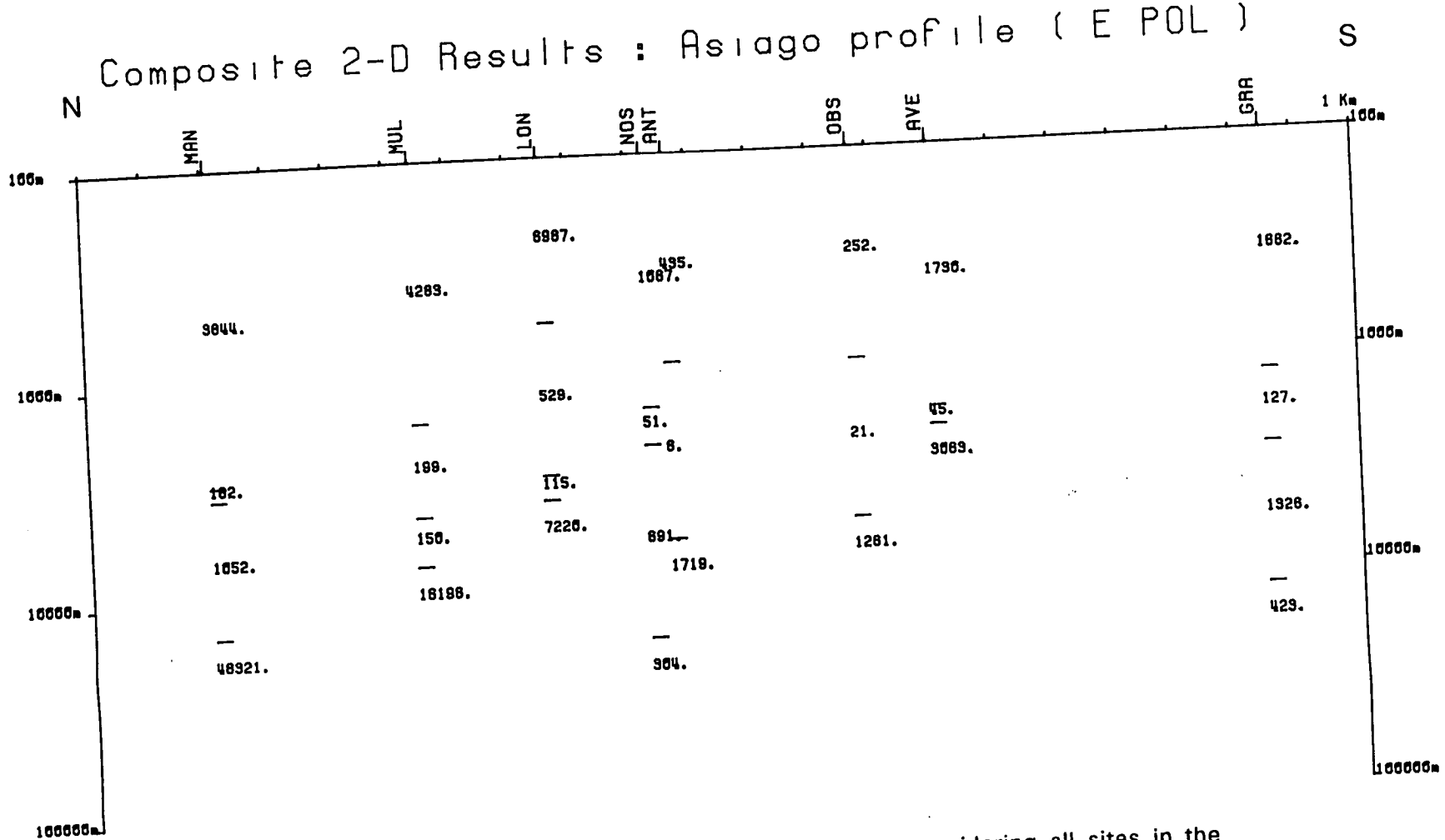

Fig. 7.7- Composite 2D section for the E pol response curves considering all sites in the Asiago area using the 2nd order Marquadt scheme.

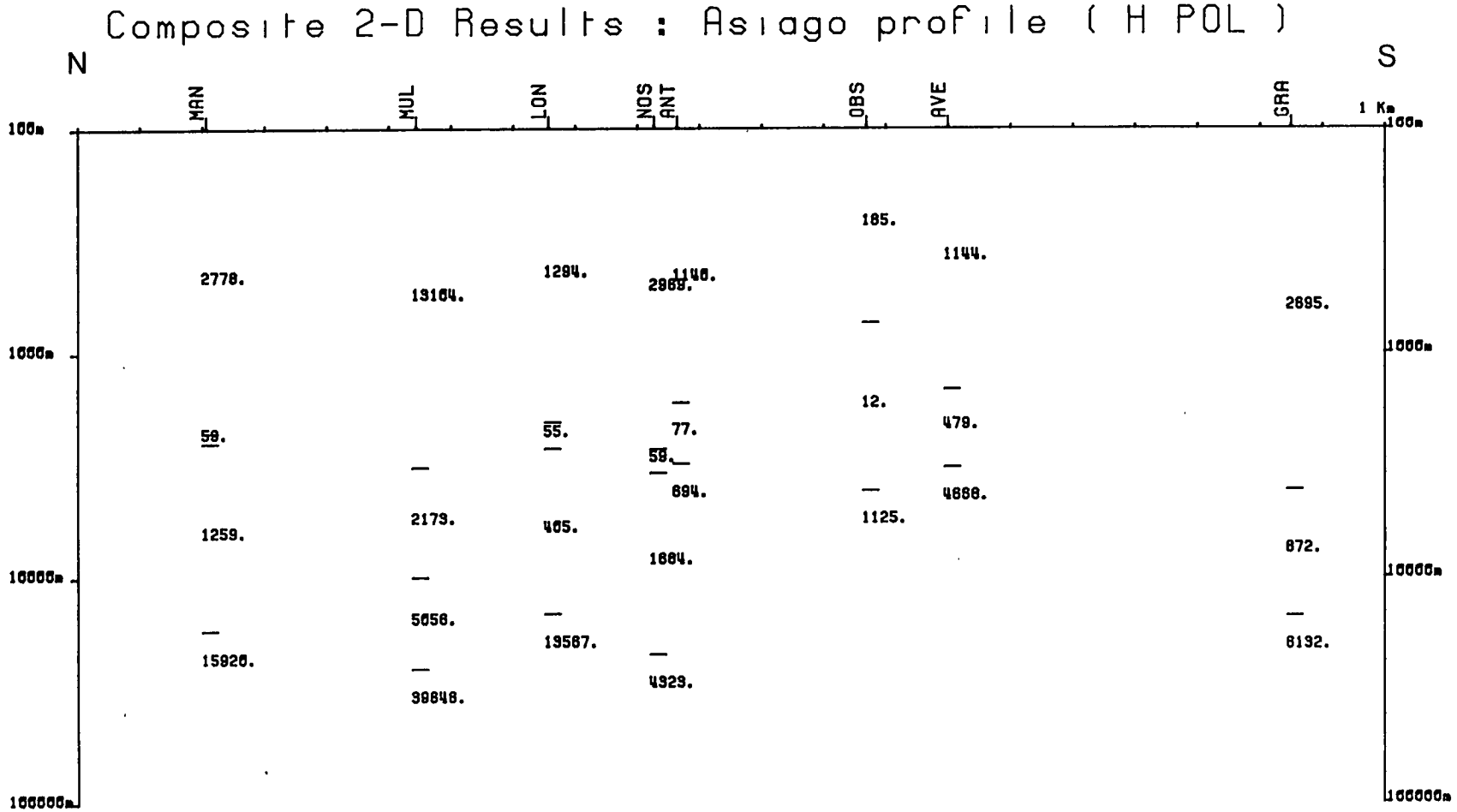

Fig. 7.8- Composite 2D section for the H pol response curves considering all sites in the Asiago area using the 2nd order Marquadt scheme.

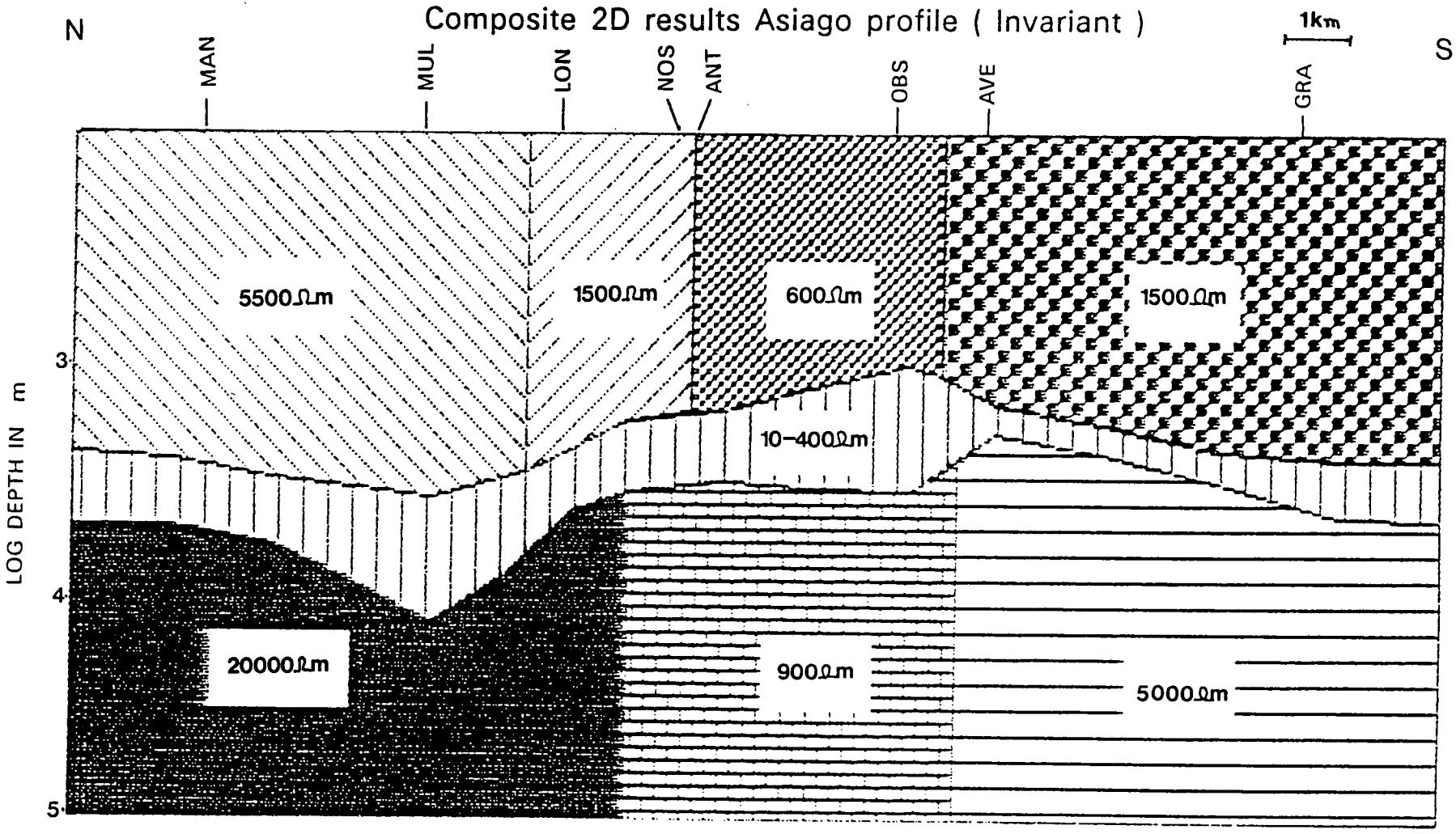

Fig. 7.9- Composite 2D section for the rotationally invariant response curves considering all sites in the Asiago area and all described inversion schemes.

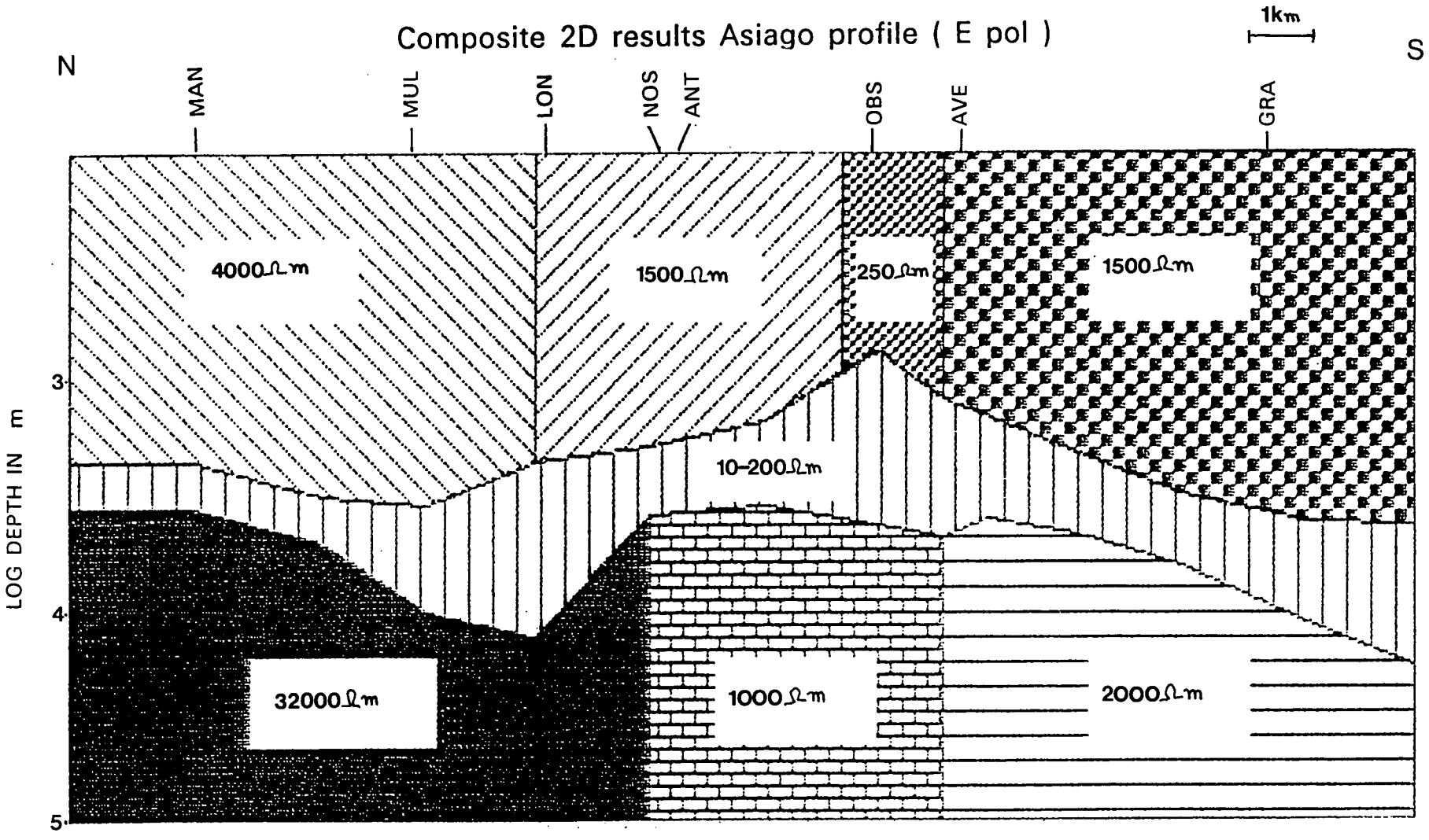

Fig. 7.10- Composite 2D section for the E pol response curves considering both all sites in the Asiago area and all described inversion schemes.

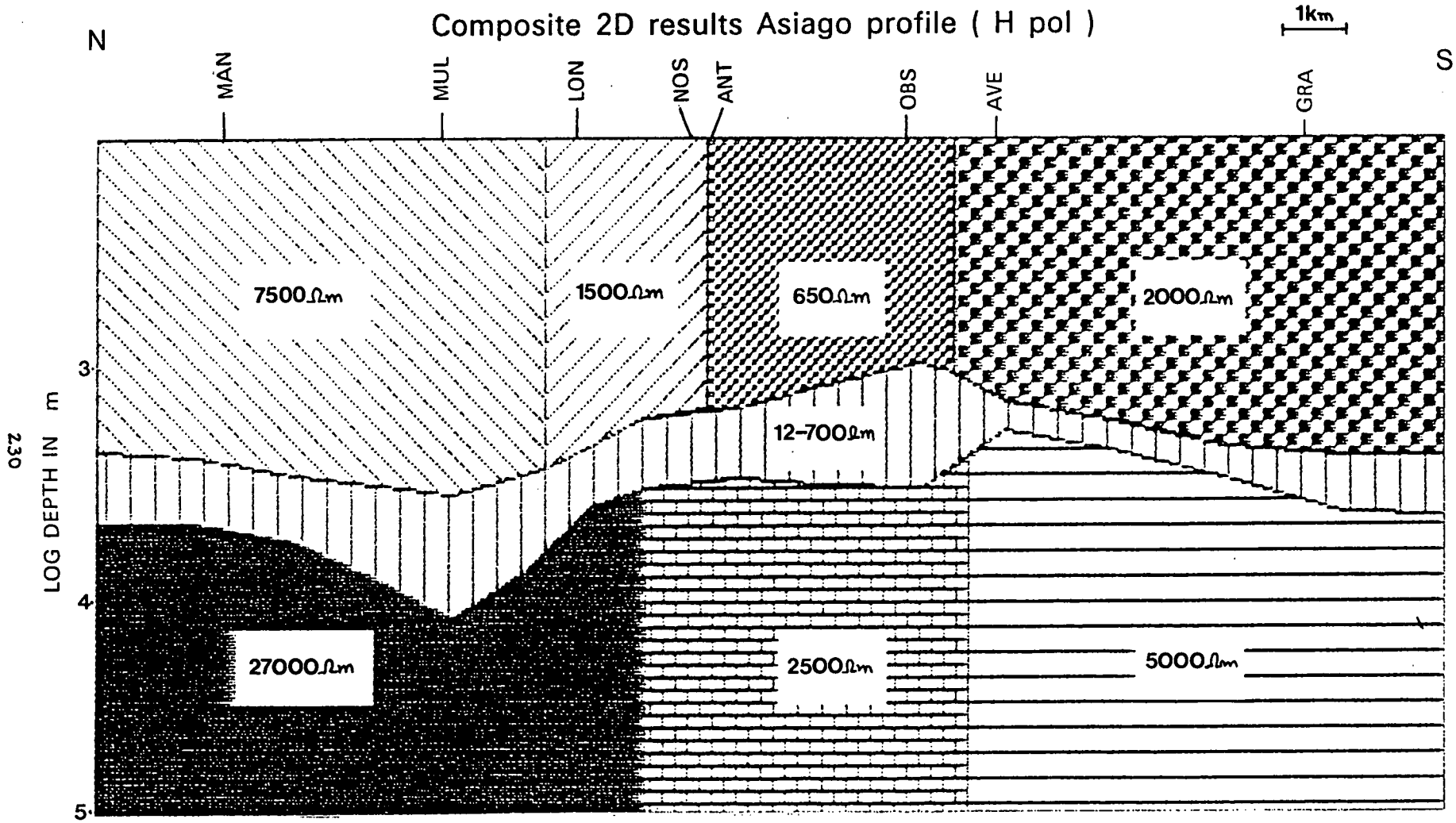

Fig. 7.11- Composite 2D section for the H pol response curves considering both all sites in the Asiago area and all described inversion schemes.

approximately 1.5-9Km along the whole profile. This feature, which appears to be more conductive at the centre of the profile, may be of tectonic origin and might be associated with the compressional effects observed in the vicinity of the subduction zone in the Alps (Laubscher, 1983). Further speculations about this conductive structure and possible tectonic implications are presented in Chapter 8.

7.5 2D studies

7.5.1 The 2D inversion algorithm

The 2D inversion was performed by using the algorithm described by Jupp and Vozoff (1977). This 2D inversion scheme is strongly related to their 1D counterpart which has been described in detail earlier in this Chapter. The main difference between the two inversion schemes is concerned with the distinct nature of the forward routines. As already stated in Chapter 2, no general analytical solution is available for the 2D problem and therefore the solution has to be obtained numerically. For that purpose, in the 2D scheme adopted in this study, the Earth is discretized using a mesh of rectangular elements. Field values are then associated with each node of the mesh and the equations governing the E-pol and H-pol cases are reduced to a discrete representation by the finite difference method. The boundary conditions are distinct for each polarization case, as already discussed in Chapter 2. In this scheme, the Earth- air interface does not need to be flat so that approximate 2D topographies can easily be incorporated into the inversion. The mesh must extend into the air for the E-pol case, but may be terminated at the highest topographic point for the H- pol case. Unlike in the 1D code, where the model parameter vector **x** comprises layer resisitivities and depths, in the 2D inversion **x** signifies blocks with initially assigned resistivities. An appropriate mesh design is important in obtaining accurate results with this code, and for that matter, any other reported code. Suggestions for mesh design can be found in the works by Muller and Losecke (1975), Doucet and Ngoc (1984) and Wannamaker et al. (1985). The 'rules of thumb' presented in this last paper have been followed as closely as possible in this study and are as follows:

(1)- Dimension change from one element to the next kept within a factor between 3 and 5;

(2)- Near boundaries, the element dimensions were chosen to be a fraction of the skin depth δ (say $\delta/3$ to $\delta/4$) in the block where the element resides;

(3)- Each single resistivity block was no less than 3 elements wide and 2 elements thick;

(4)- Element dimensions increased to the order of δ of the block when located at distances of 2 to 3δ's away from any variation in conductivity;

(5)- Vertical mesh boundaries extended 3 to 6 δ's away from the nearest 2D structure;

(6)- The bottom mesh boundary was set at 3 to 6 δ's in the background conductivity from the air- earth interface.

The program incorporates an automatic mesh subdivision scheme described by Madden (1973). For each frequency, this scheme ensures that the local discretization error is kept within some specified level. The inversion can be performed either independently for E-pol and H-pol cases or simultaneously. Large discrepancies between the individual and the simultaneous inversions suggest strong anisotropy or perhaps dominant 3D effects.

7.5.2 Topographic effect in the Italian Alps

The distortion of electromagnetic fields due to topography is an additional problem in the interpretation of MT data. It can be included in the more general class of surface inhomogeneities, for which a recent review has been published by Menvielle and Szarka (1986), and a collection of various types of distortions on sounding curves can be found in Berdichevsky and Dmitriev (1976). Several authors have reported investigations of the effect of topography by a number of techniques. The distortion of DC telluric fields due to a simple topographic feature has been determined by means of conformal mapping by Thayer (1975), Harinarayana and Sarma (1982), Harinarayana (1986). Two-dimensional approximations of various topographies have been studied using Rayleigh scattering theory for modelling a smooth cosinusoidal hill (Reddig and Jiracek, 1984), transmission elements and network analogies (e.g. Ku et al., 1973), and the finite element method (Wannamaker et al., 1985, 1986).

In this study, Alpine topography in the area surveyed (basically Cavalese, Asiago and surrounding valleys) has been approximated by a simple two- dimensional model which accounts only for the main features. Fig. 7.12

shows the assumed resistivity structure (the grid structure) and the actual location of four sites in the Asiago area. This assumed structure is a simplified composite 2D section derived from the 1D models. Provided that a reasonable resemblance to the actual Earth structure in the region is preserved, the adopted conductivity structure is not important insofar as only a qualitative assessment is of interest at this stage. The results of forward modelling (frequency range 10^{-2} - 10^{2} Hz) for this conductivity structure assuming either the presence of the topography or a flat Earth (resistivity map given in Fig. 7.13) are shown for all the 4 observational sites in Figs. 7.14 and 7.15. Comparison of the E and H- pol responses with and without topography indicates some differences which are perhaps better quantified in Figs. 7.16 and 7.17, in which the ratios (amplitude and phase) between the responses are plotted as a function of frequency. It can be seen that both polarizations are affected by topography and that the differences perceived are more pronounced at the lower frequencies. For the sites examined, the deviation in the values is always within 10 per cent of the flat responses. However, as no extra computational cost or difficulties are involved, this simplified topographic feature was incorporated in the 2D inversion carried out for this region.

7.5.3 2D results – Asiago area

The adequate determination of the two modes of induction (E pol and H pol) plays an important role on 2D studies. The simple rotation to a specified azimuth (e.g. 76^{0} NE in this study) does not solve the 90^{0} ambiguity already discussed in Chapter 4. Along a profile, the E pol responses are expected to exhibit a smoother pattern when compared to the H pol responses. This smoothness criterion for selecting the E pol responses which has been adopted by some authors (e.g. Schwarz et al., 1984) is based on physical principles; in the E pol mode of induction (unlike in the H pol mode) the current flux is parallel to the strike direction and is continuous at conductivity boundaries. However, actual data is not purely 2D and is often corrupted by noise and/or surface distortions. In such more realistic situations, the use of this criterion may be rather unsatisfactory, as it was in the Asiago data. Nevertheless, based on the same physical principles, the E pol and H pol responses for the site MUL (Fig. 6.2(b)) were verified to be inconsistent with the responses observed at adjacent sites. The site MUL,

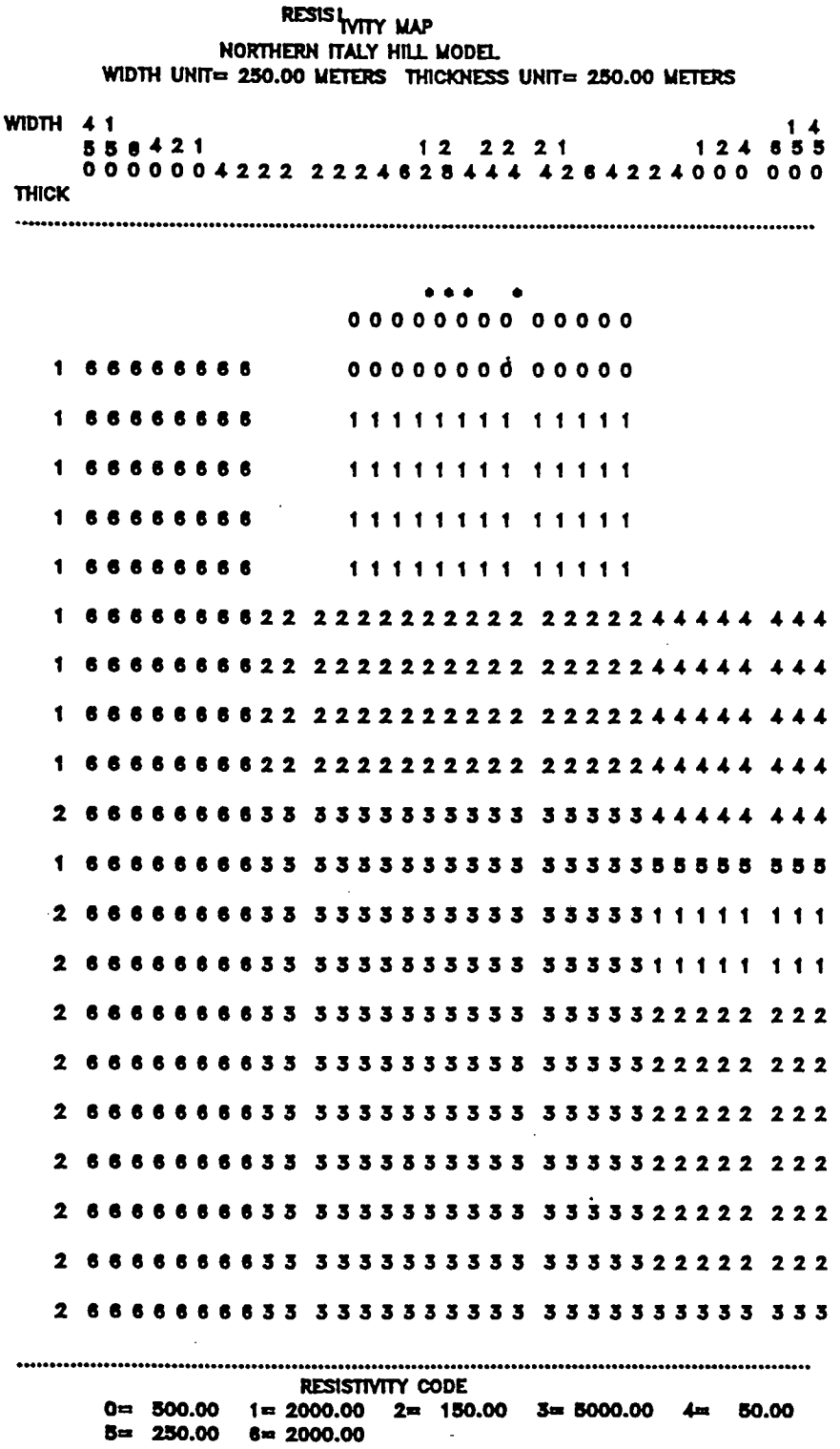

Fig. 7.12- Resistivity map of Nothern Italy, including simplified topography. The site locations at the top of the topography are indicated by asterisks. The numbers in the grid are codes for the resistivity (Ωm) values shown at the bottom of the Fig. Widths and thicknesses of the grid are given at the top and left hand side of the Fig., respectively.

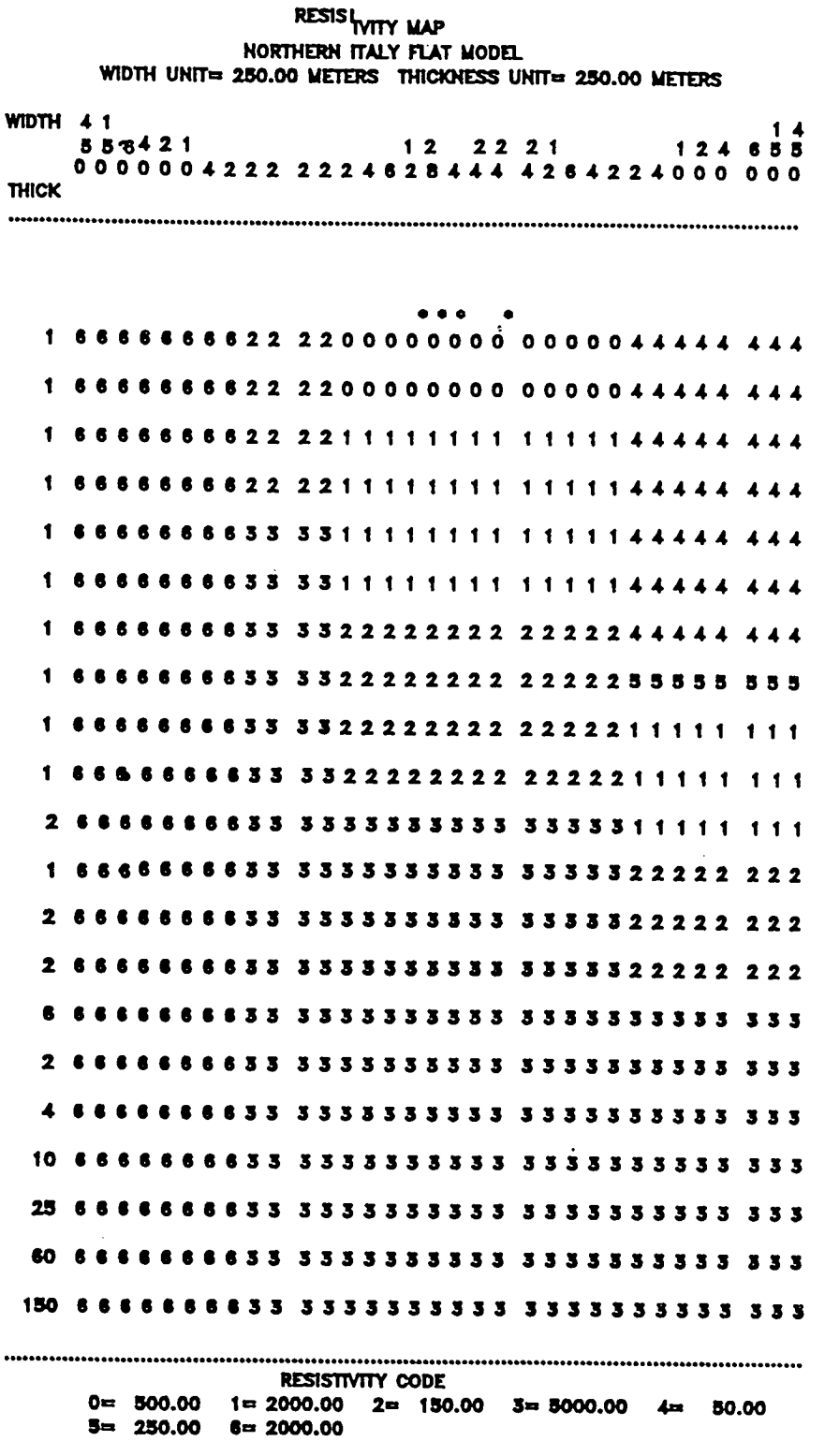

Fig. 7.13– Resistivity map of Northern Italy, neglecting topographic feature. Remainder information as in Fig. 7.12.

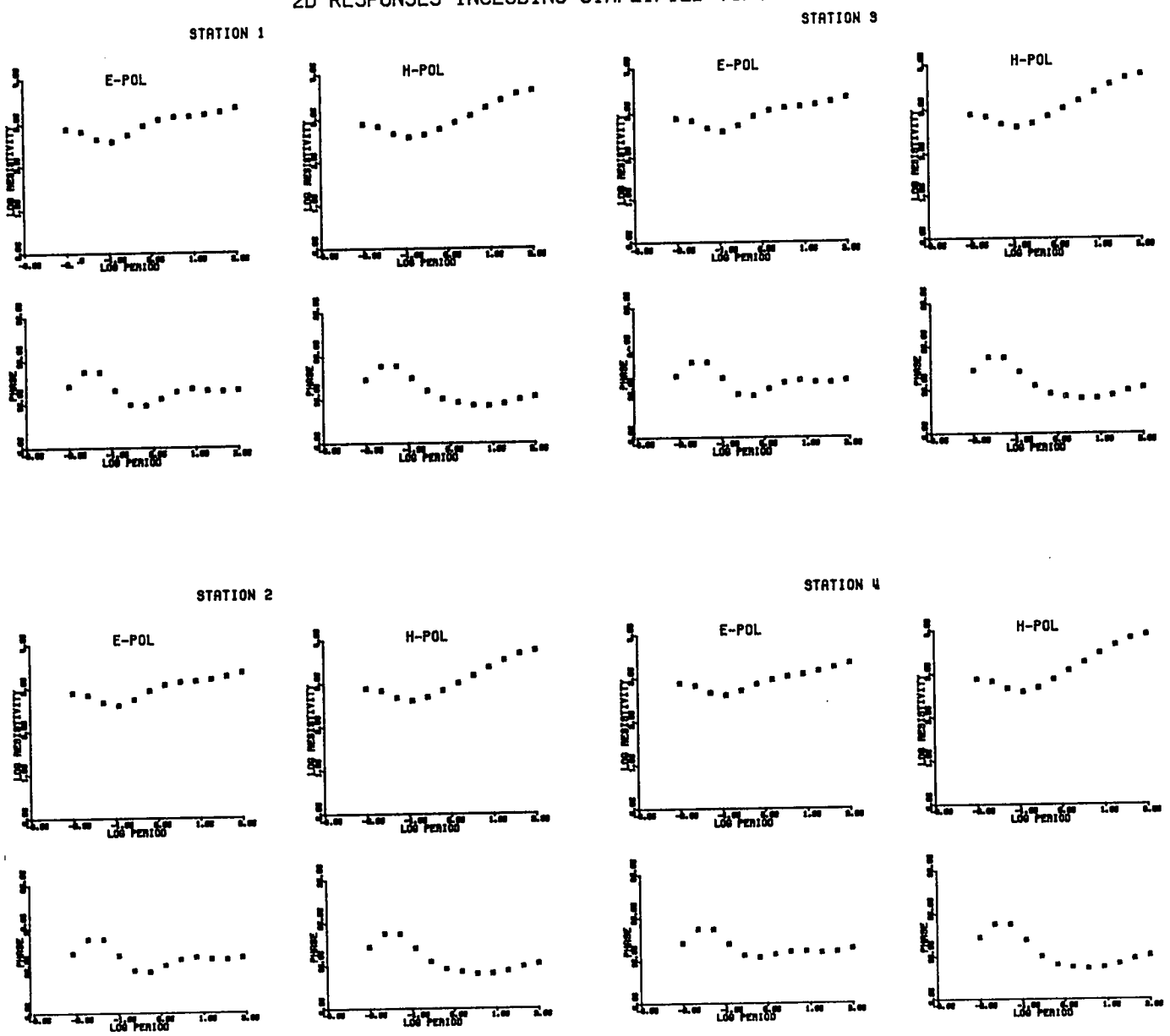

Fig. 7.14- E and H pol theoretical responses (amplitude and phase) for 4 sites in the Asiago

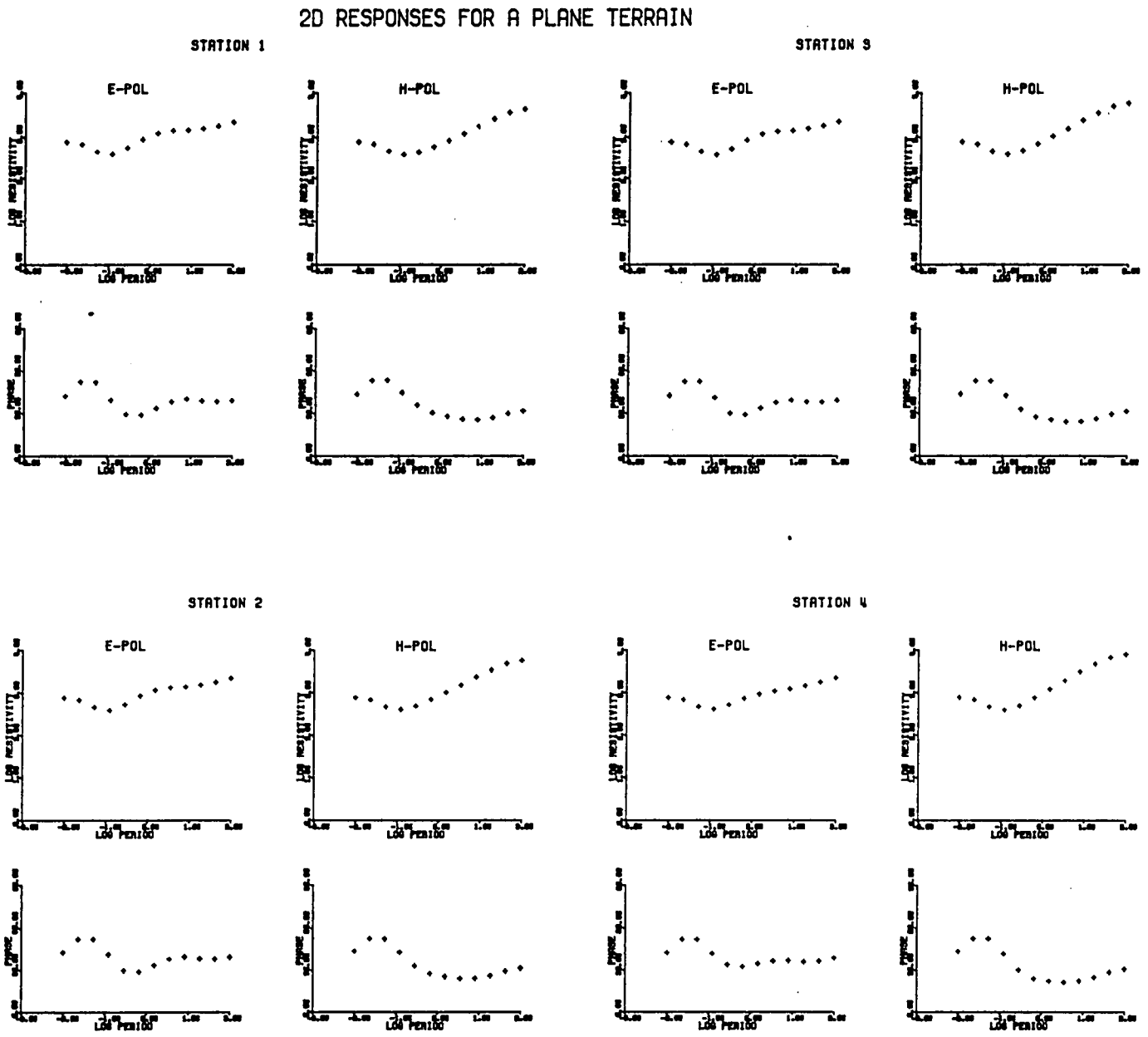

Fig. 7.15- E and H pol theoretical responses (amplitude and phase) for 4 sites, when the

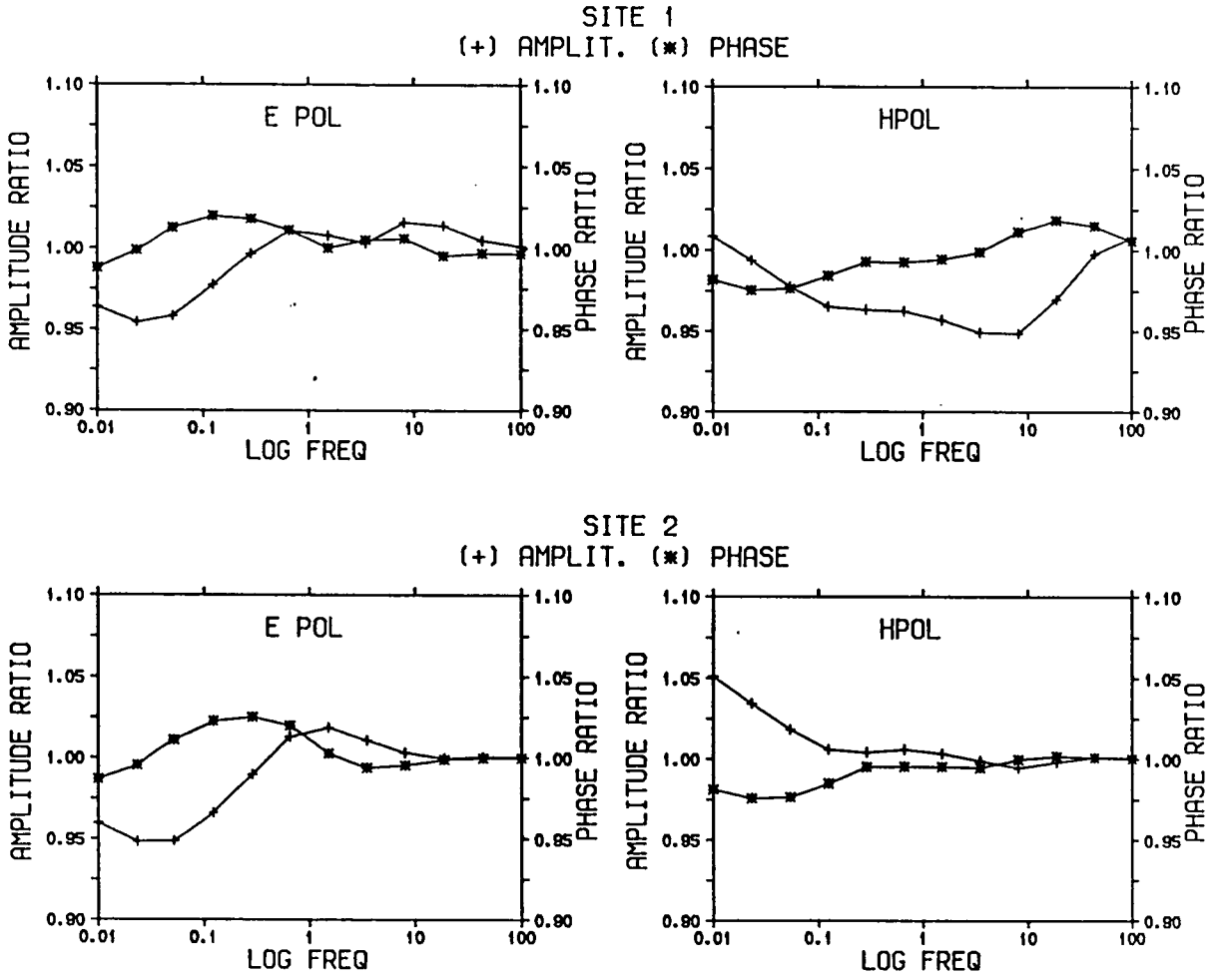

Fig. 7.16- Ratio of the responses topography model/flat model for sites 1 and 2 (E and H- pol cases).

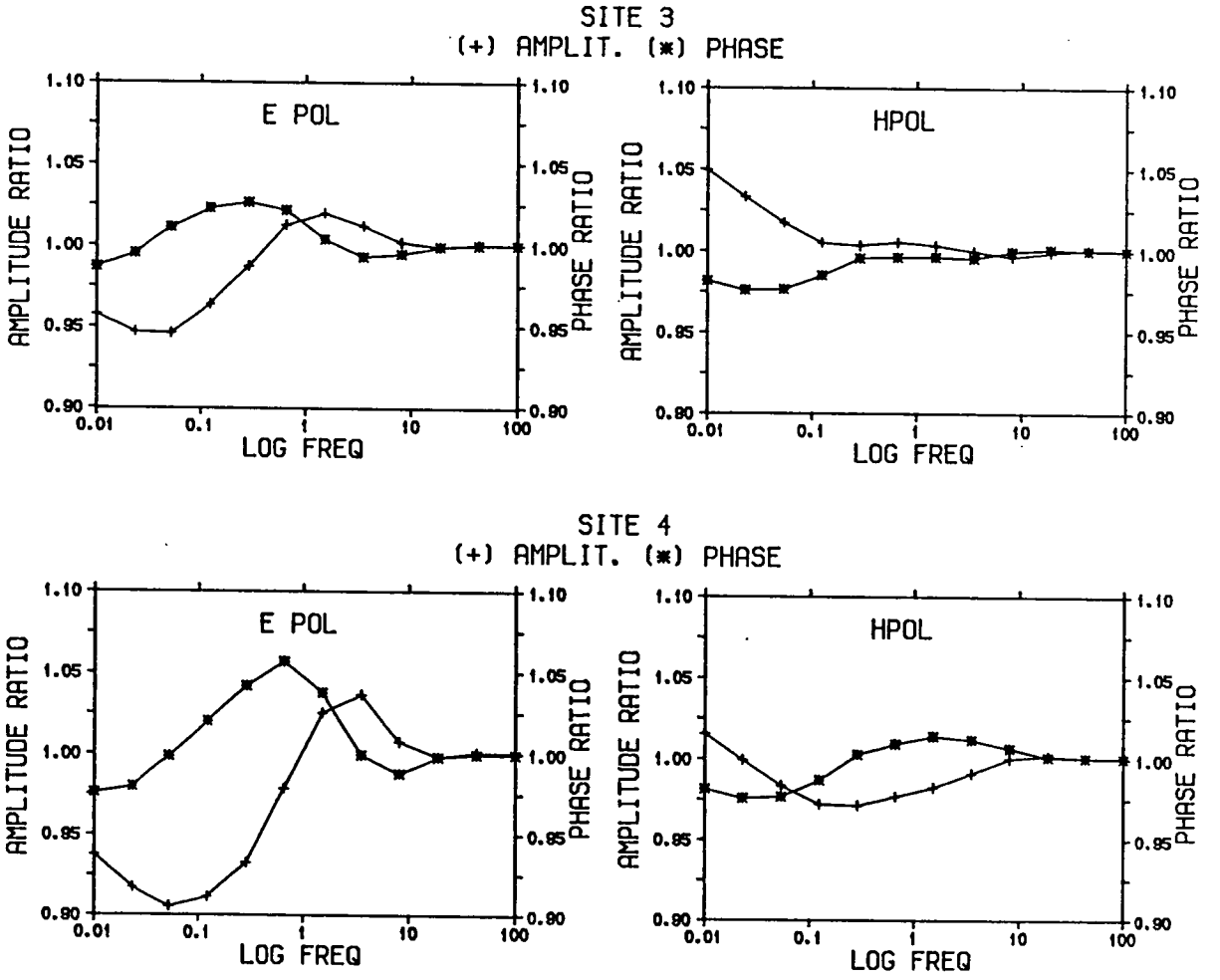

Fig. 7.17- Ratio of the responses topography model/flat model for sites 3 and 4 (E and H pol cases).

apparently lying on the resistive side of a vertical interface, should exhibit H pol response with higher apparent resistivity values than those for the E pol response (see for instance Vozoff, 1972). Thus, the E pol and H pol curves for MUL were interchanged. The 1D model results for this site also observed this change. Whether the apparently more resistive nature of the Earth structure surrounding MUL is founded by geological features or is merely due to near surface distortions is an interesting question. This point is further discussed in Chapter 8.

The starting model for the 2D inversion in the Asiago region -Fig. 7.18- is based on the results obtained with the compilation of 1D results. Some features were added after a number of inversions in order to improve the fit between field data and model. The inversion was performed for 13 frequencies in the range $4x10^{-4}$- 10^{2} Hz. A total of 10 resistivity blocks was used and the initial values are listed in Fig. 7.18. By making the reasonable assumption that the Earth tends to be more electrically homogeneous at greater depths, the responses for the periods higher than about 300s at the site NOS were added to those at adjacent sites (ANT and OBS) when carrying the inversion. A summary of the 2D inversion results (both polarizations undertaken simultaneously) required 10 iterations, is given in Tab. 7.2. An analysis of this Tab., similar to the one described for the 1D studies, indicates that all the resistivity blocks were well resolved. Note that the resistivity blocks beyond the Asiago profile (blocks 4 and 5) were kept fixed, so that their effect on the final model is minimized (i.e. damped). The overall fit of this model to the data (Figs. 7.19(a)-(d)) is reasonable. In these Figs., the E and H pol data and model responses are shown as a function of the period. The poor fit site MAN (Fig. 7.19(a)- top), which might well be due either to lateral effects of the Alpine orogeny or simply to remnant noise as indicated by the steep slope of the apparent resistivity curves in both polarizations. Further discussion of this model is presented in Chapter 8. Seeking additional elements for a more complete analysis of the resulting 2D model (Fig. 7.20), it seems worthwhile to consider other 2D models obtained independently for the E pol and H pol directions. The starting model for both E and H pol was the same as the one used for the simultaneous inversion of both directions. The 'resistivity map' in both cases was therefore the one given in Fig. 7.18. The final inversion results are summarized in the Tabs. 7.3 and 7.4, for the E pol (6

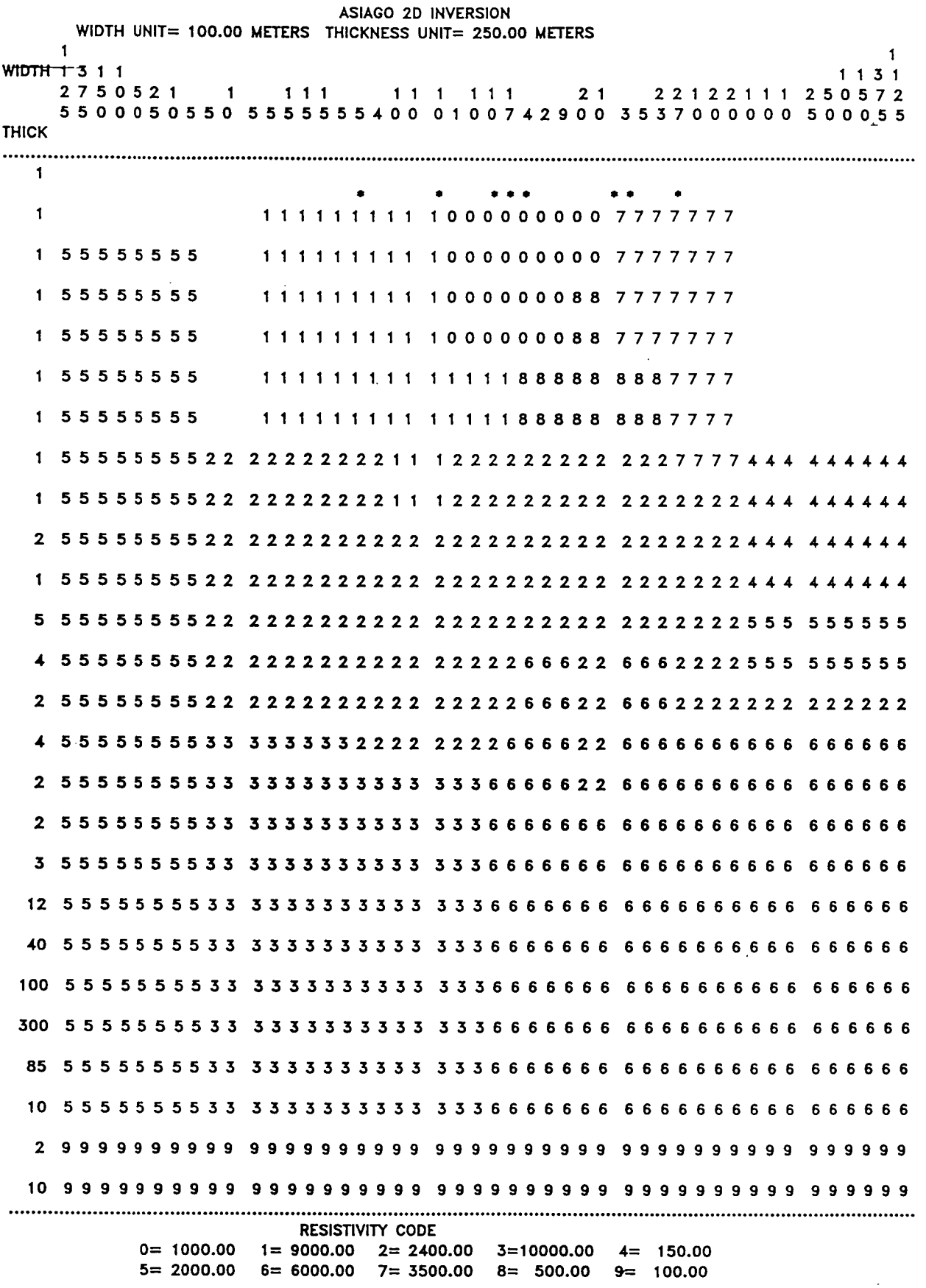

Fig. 7.18- Resistivity map of Asiago area used as starting model for the 2D inversion . See legend of Fig. 7.12 for additional information.

SUMMARY 2D RESULTS SIMULTANEOUS INVERSION BOTH POLARIZATIONS
ASIAGO REGION

NORMALIZED SINGULAR VALUES OF JACOBIAN

0.100E+01 0.560E+00 0.431E+00 0.355E+00 0.311E+00
0.244E+00 0.182E+00 0.138E+00 0.158E-07 0.152E-07

SCALE FACTOR : 0.5557931E+00

DAMPING FACTORS (1.000 PERCENT LEVEL)

0.100E+01 0.100E+01 0.100E+01 0.100E+01 0.100E+01
0.100E+01 0.100E+01 0.100E+01 0.000E+00 0.000E+00

PARAMETER SPACE EIGENVECTORS (V MATRIX)

1	0.295	-0.700	0.370	-0.073	0.123	-0.207	0.472	-0.017	0.000	0.000
2	-0.211	0.401	-0.247	-0.070	0.082	-0.506	0.671	0.126	0.000	0.000
3	0.873	0.424	0.052	0.194	0.089	-0.059	0.019	-0.076	0.000	0.000
4	0.161	-0.098	-0.106	-0.068	-0.086	-0.032	-0.131	0.961	0.000	0.000
5	0.000	0.000	0.000	0.000	0.000	0.000	0.000	0.000	-0.960	-0.282
6	0.000	0.000	0.000	0.000	0.000	0.000	0.000	0.000	-0.282	0.960
7	0.223	-0.005	-0.186	-0.736	-0.589	0.015	0.041	-0.157	0.000	0.000
8	-0.018	0.112	0.045	0.122	-0.147	0.794	0.552	0.116	0.000	0.000
9	0.066	0.013	-0.216	-0.538	0.771	0.254	-0.025	0.002	0.000	0.000
10	0.159	-0.384	-0.839	0.318	-0.029	0.032	0.056	-0.130	0.000	0.000

FINAL BLOCK RESISTIVITIES

I	RO(I)	BOUND(1)	BOUND(2)	DAMPING
1	1027.5281	913.0180	1156.3999	0.0000
2	11892.2275	10180.8242	13891.3193	0.0000
3	294.5896	276.7093	313.6252	0.0000
4	38388.8711	32724.9199	45033.1250	0.0000
5	150.0000	150.0000	150.0000	1.0000
6	2000.0002	2000.0002	2000.0002	1.0000
7	1104.5614	990.5338	1231.7156	0.0000
8	2447.8845	2109.3440	2840.7593	0.0000
9	95.3666	85.9526	105.8117	0.0000
10	1596.7784	1455.2640	1752.0541	0.0000

Tab. 7.2- Summary of results 2D inversion for simultaneous inversion of both polarizations.

Fig. 7.19(a)-(d)- Fitting model data for all sites in the Asiago area. Both polarizations undertaken simultaneously.

ASIAGO 2D RESULTS - SIMULTANEOUS E AND H POL

(a)

STATION 1

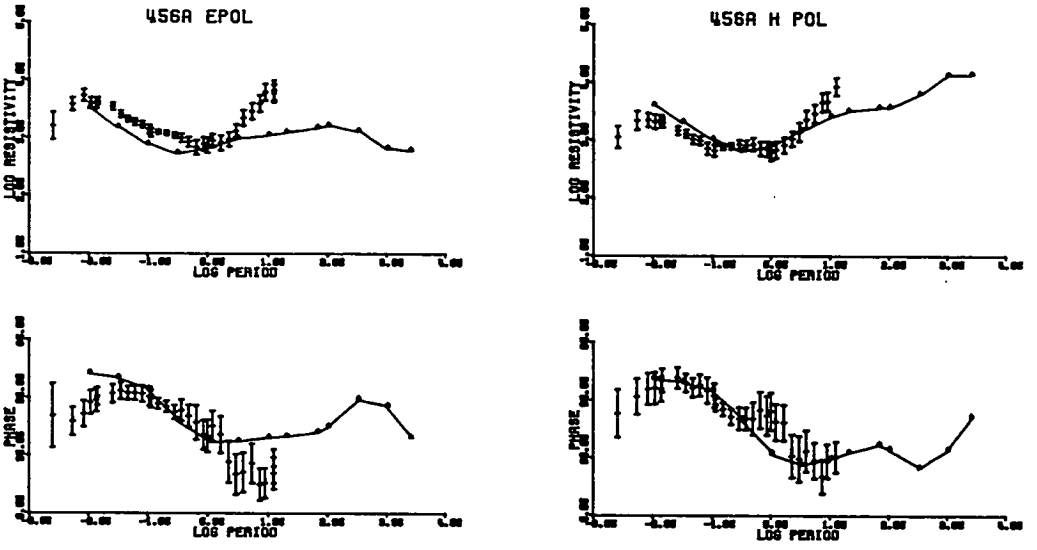

STATION 2

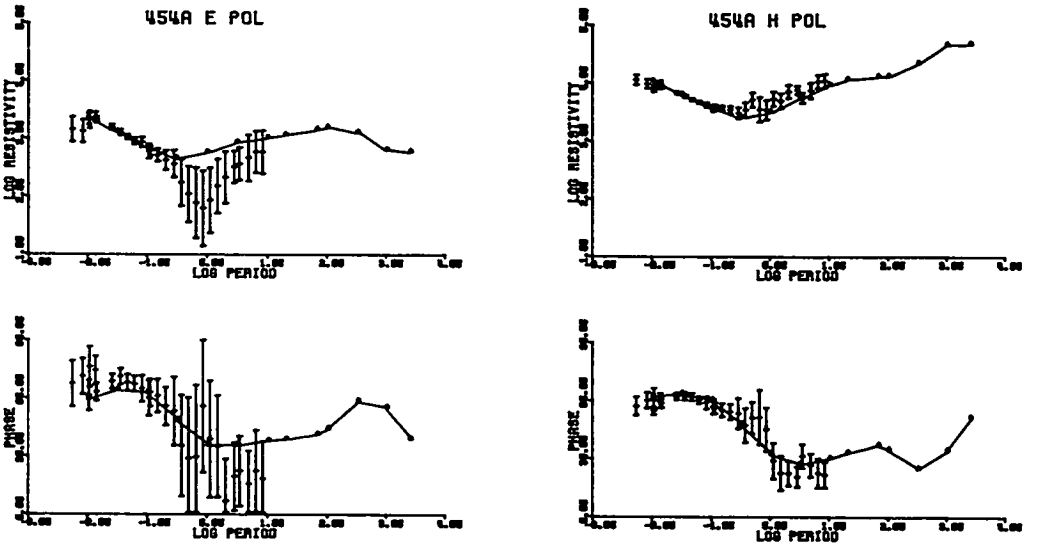

ASIAGO 2D RESULTS - SIMULTANEOUS E AND H POL

STATION 3 **(b)**

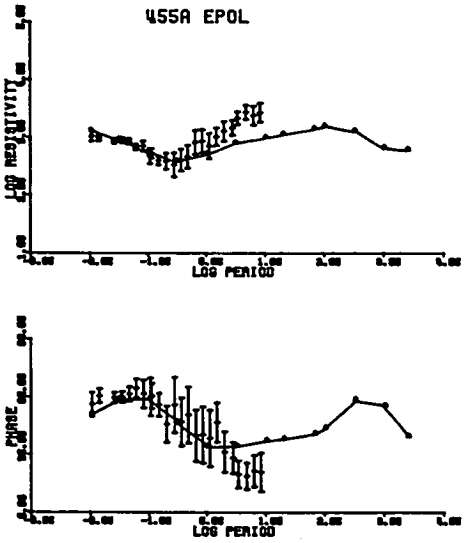

STATION 4

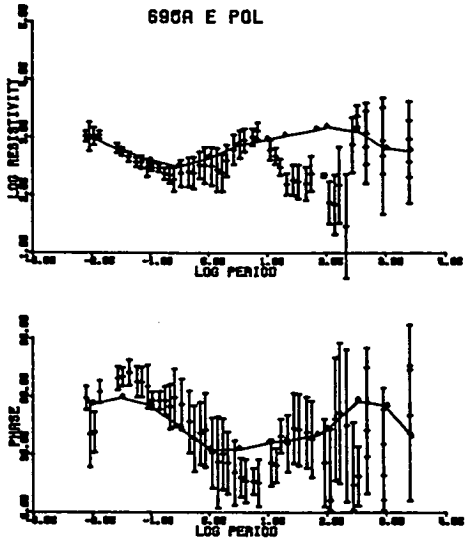

ASIAGO 2D RESULTS - SIMULTANEOUS E AND H POL

STATION 5 **(c)**

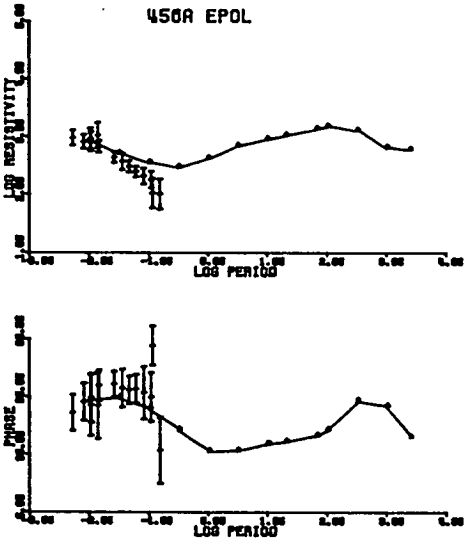

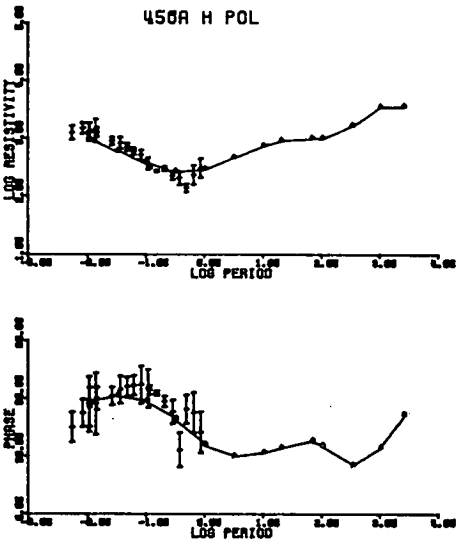

STATION 6

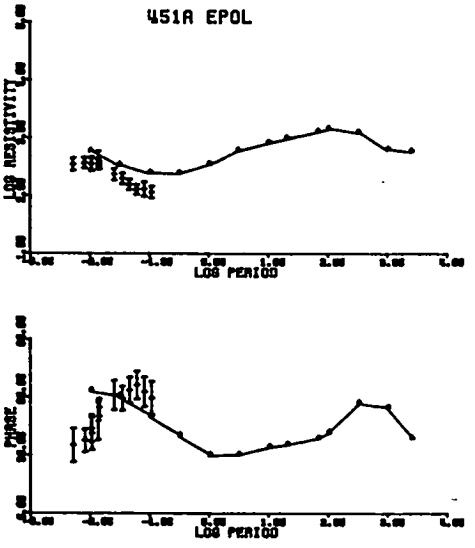

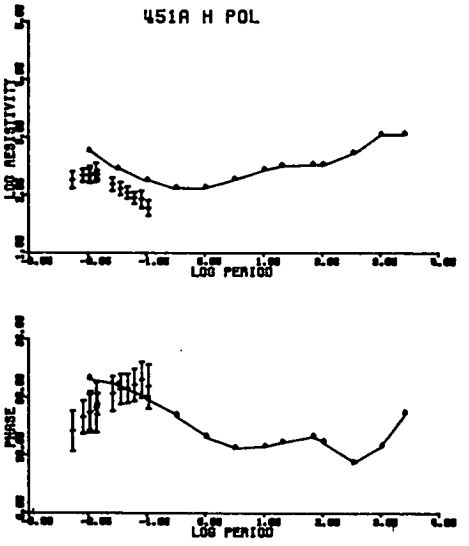

ASIAGO 2D RESULTS - SIMULTANEOUS E AND H POL

STATION 7 (d)

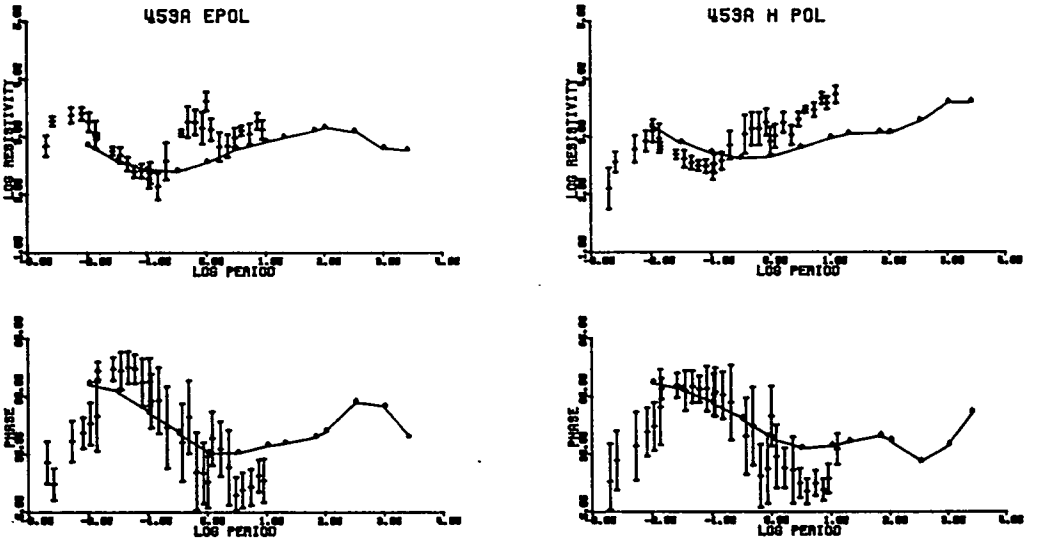

STATION 8

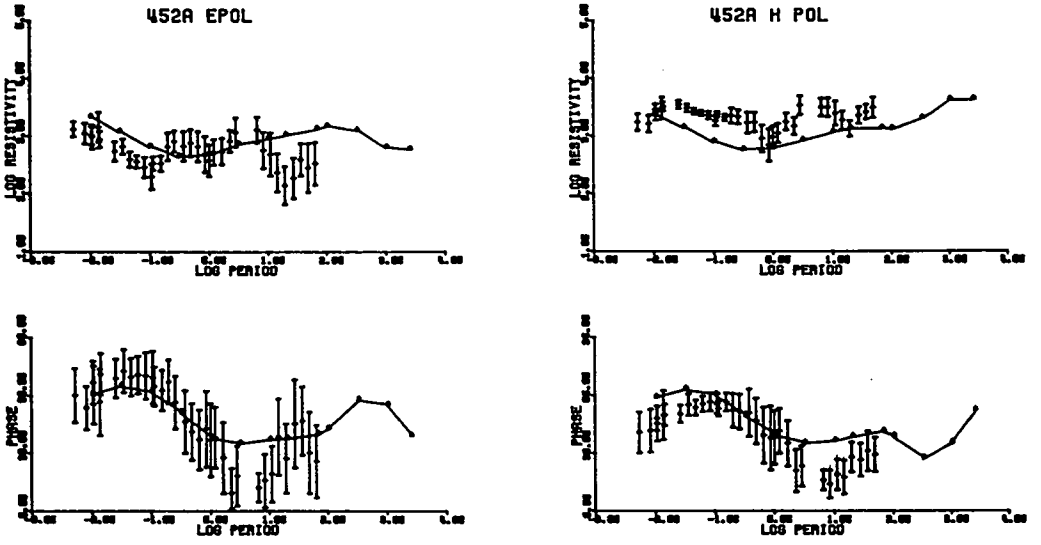

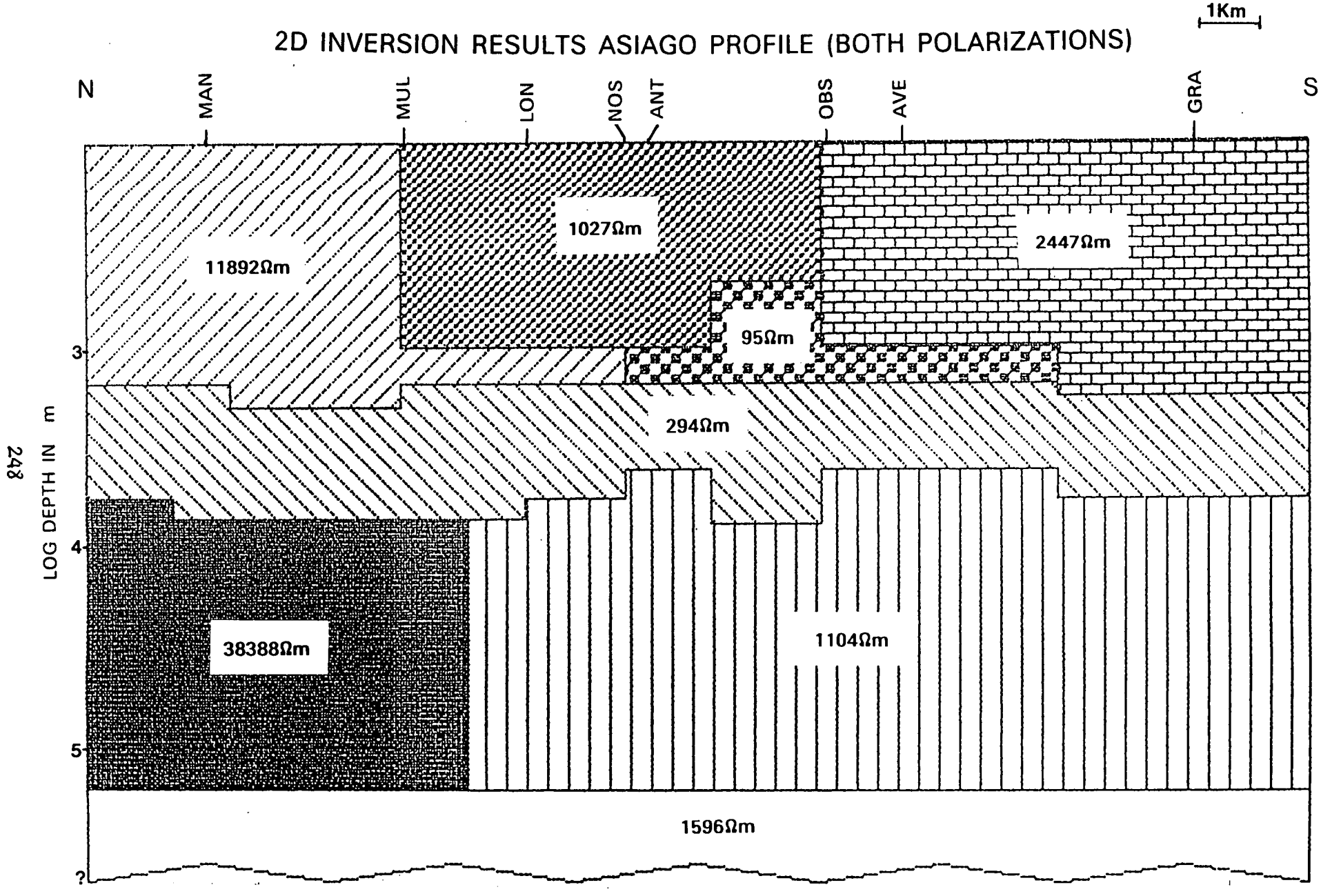

Fig. 7.20– 2D model results for the Asiago area. Both polarizations simultaneously inverted.

Fig. 7.21(a)–(d)– Fitting model/data for all sites in the Asiago area. Inversion for both polarizations undertaken independently.

ASIAGO 2D RESULTS - INDEPENDENT E AND H POL

(a)

STATION 1

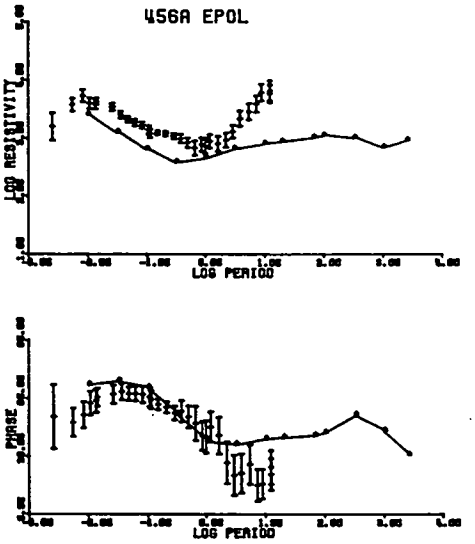

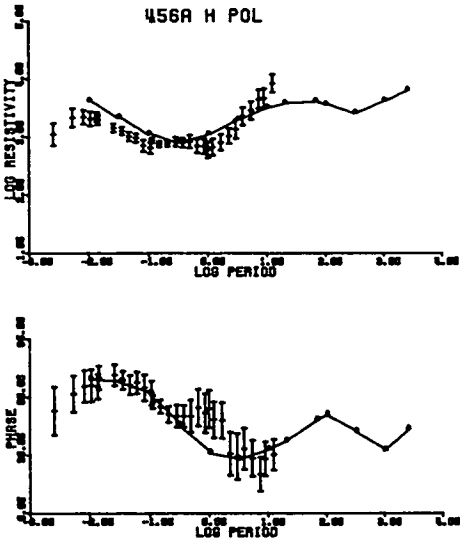

STATION 2

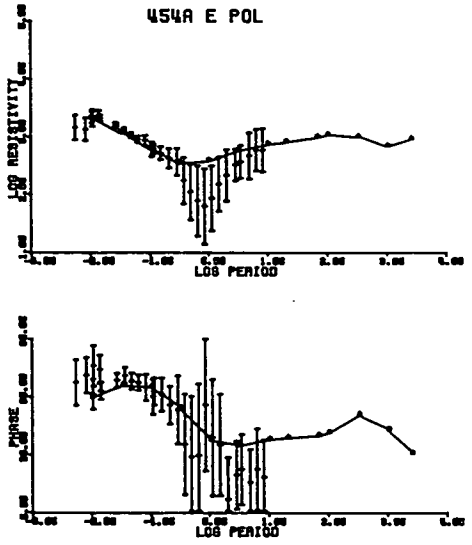

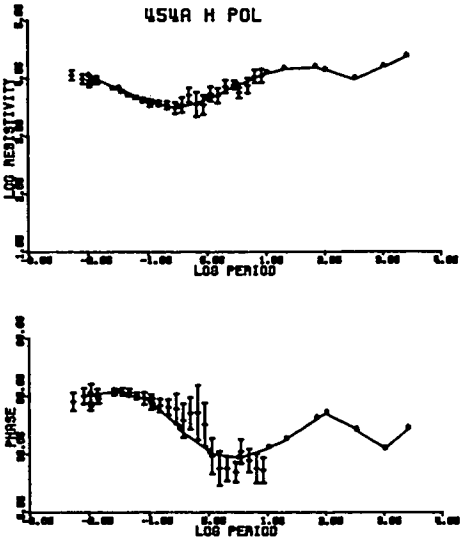

ASIAGO 2D RESULTS - INDEPENDENT E AND H POL

(b)

STATION 3

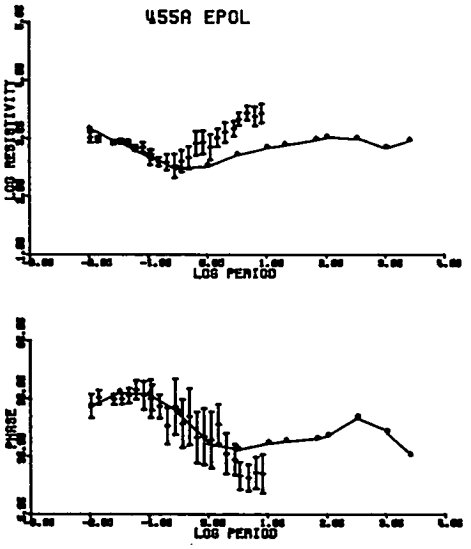

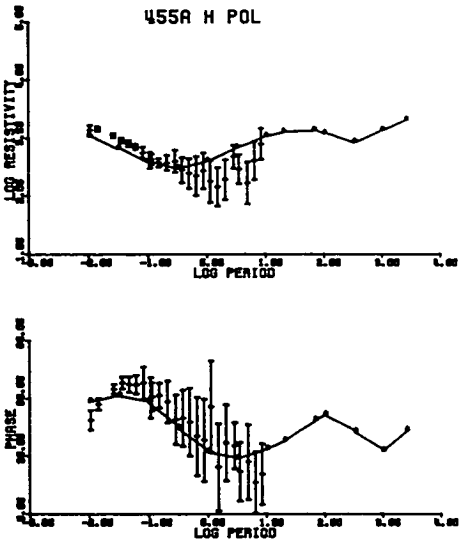

STATION 4

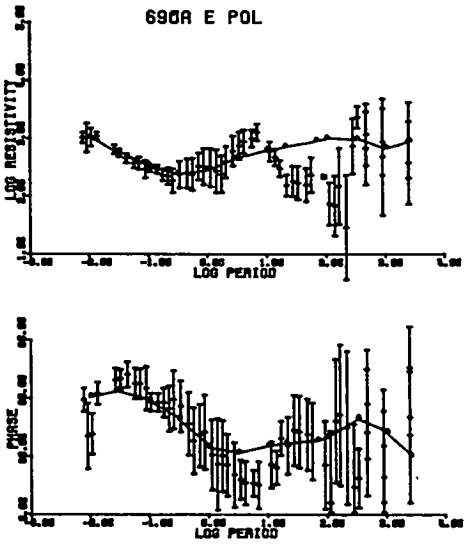

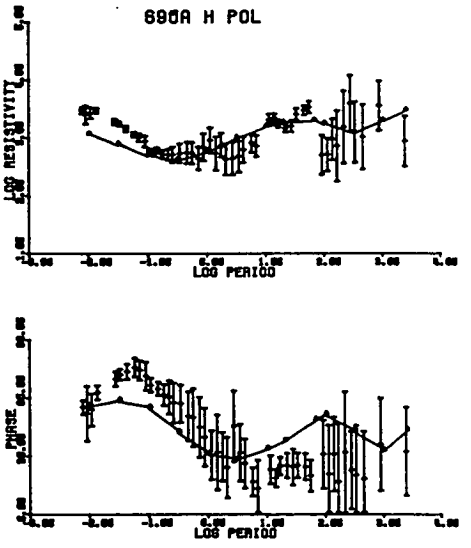

ASIAGO 2D RESULTS - INDEPENDENT E AND H POL

(c)

STATION 5

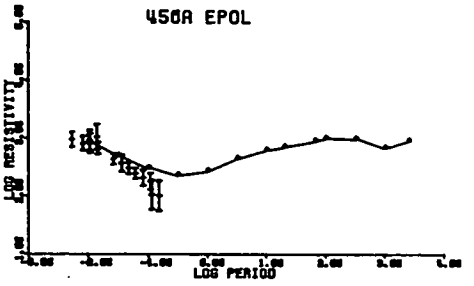

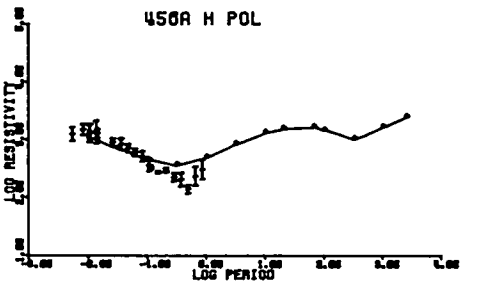

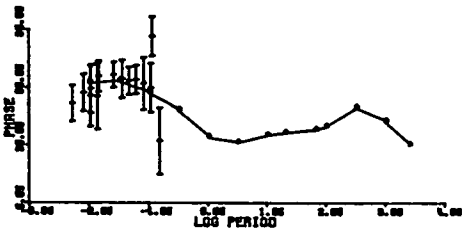

STATION 6

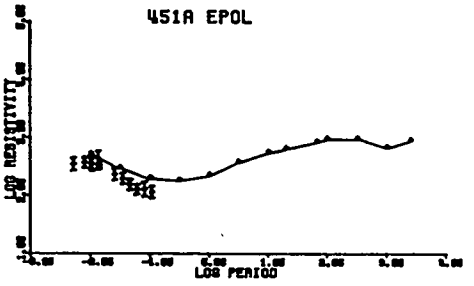

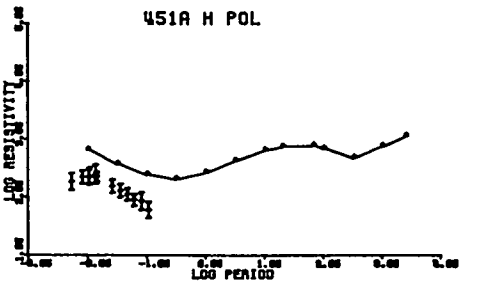

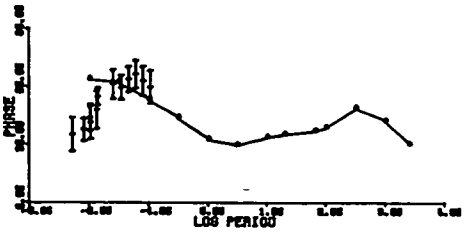

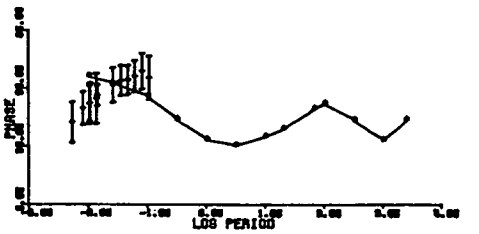

ASIAGO 2D RESULTS - INDEPENDENT E AND H POL

(d)

STATION 7

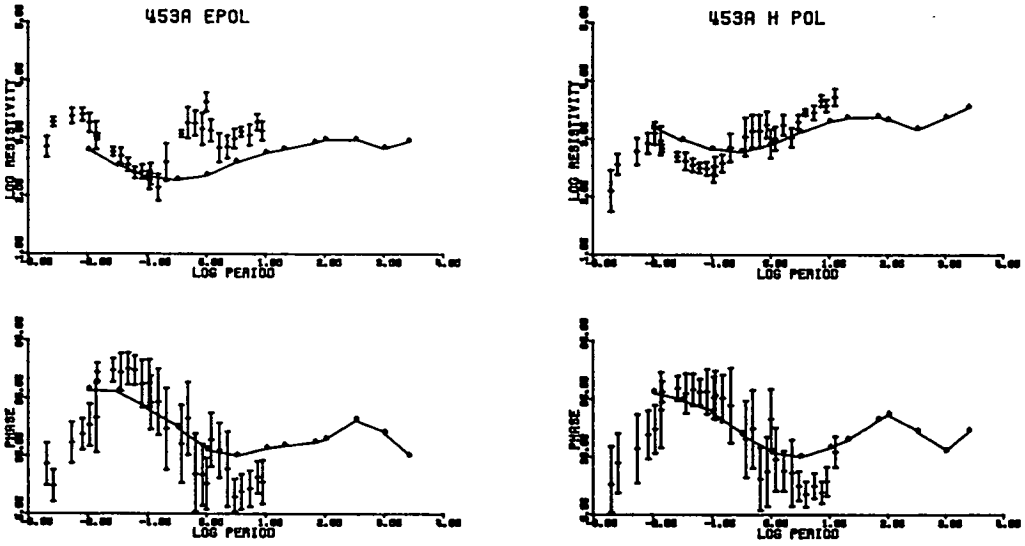

STATION 8

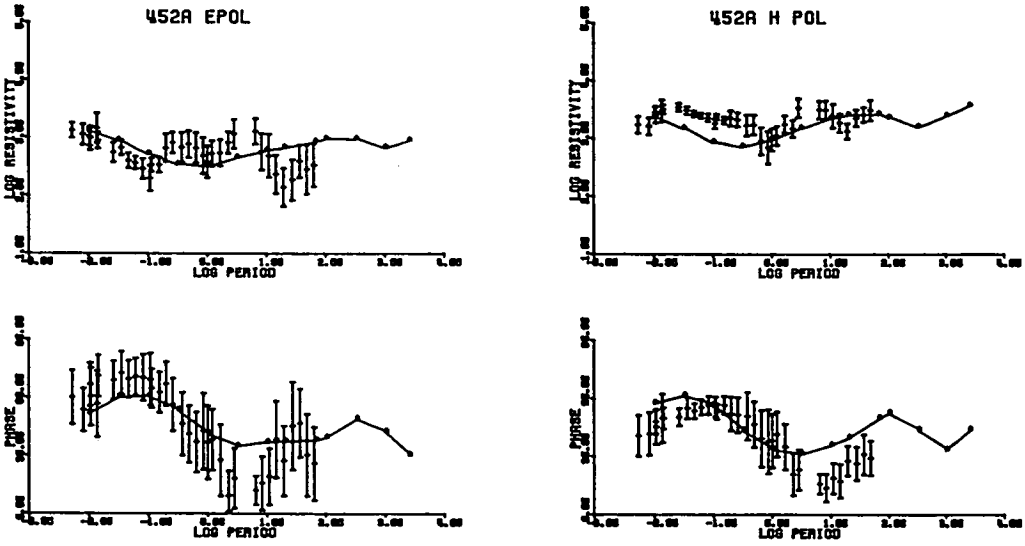

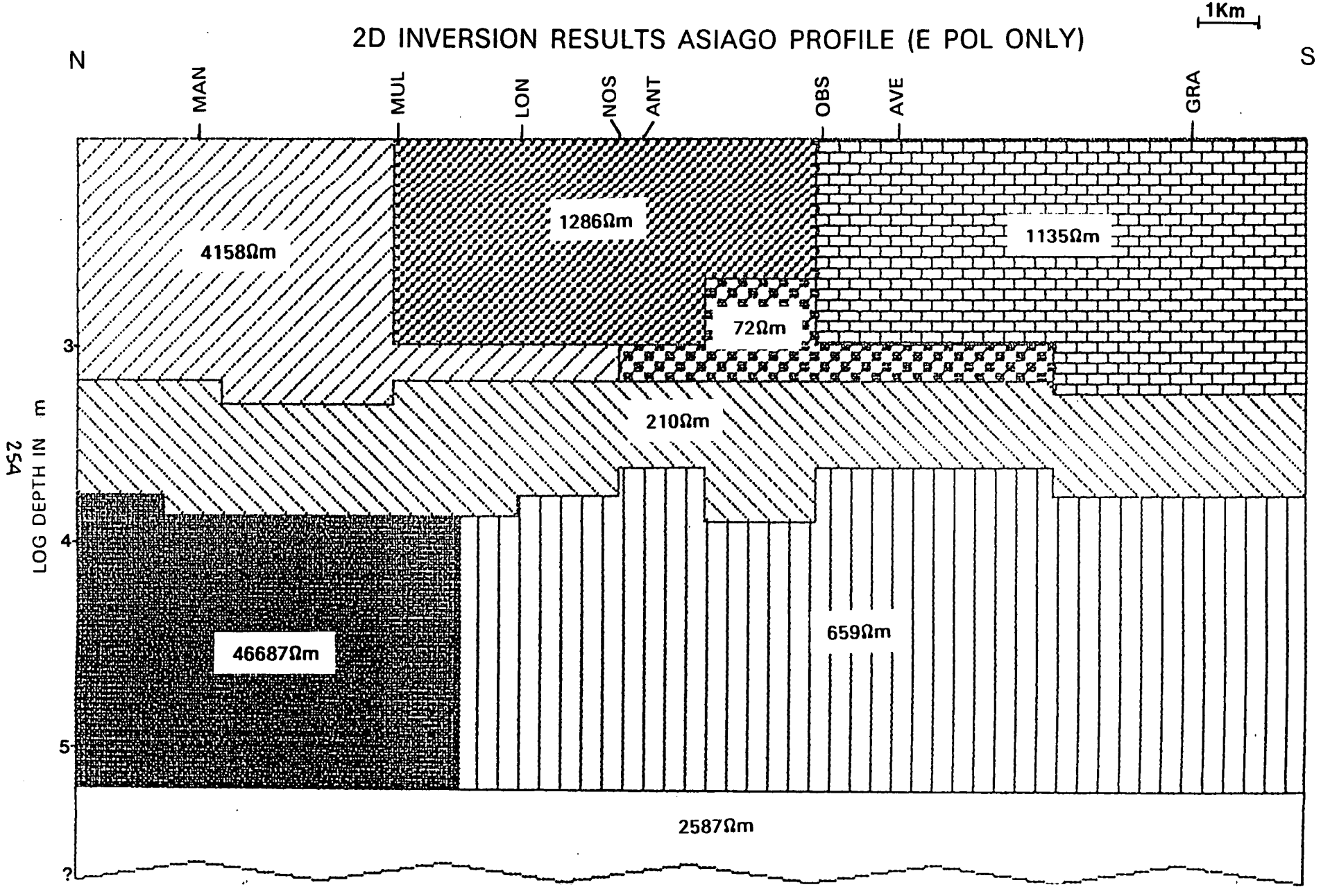

Fig. 7.22- 2D model results for the Asiago area. E pol inversion results only.

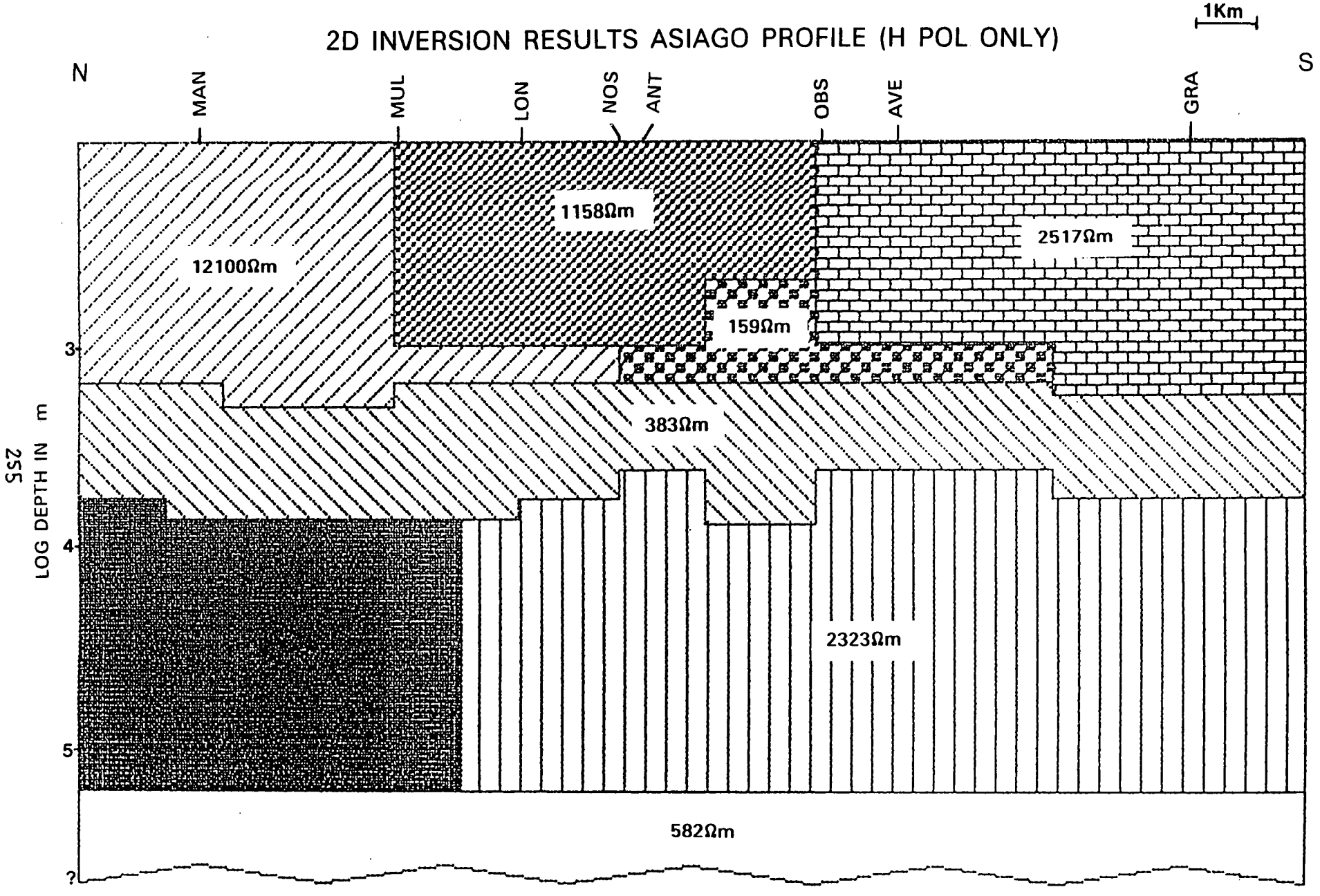

Fig. 7.23– 2D model results for the Asiago area. H pol inversion results only.

SUMMARY 2D RESULTS INDEPENDENT INVERSION E POL
ASIAGO REGION

NORMALIZED SINGULAR VALUES OF JACOBIAN

0.100E+01 0.704E+00 0.604E+00 0.399E+00 0.348E+00
0.297E+00 0.149E+00 0.214E−02 0.308E−07 0.277E−07

SCALE FACTOR : 0.3821268E+00

DAMPING FACTORS (1.000 PERCENT LEVEL)

0.100E+01 0.100E+01 0.100E+01 0.100E+01 0.100E+01
0.100E+01 0.100E+01 0.209E−02 0.000E+00 0.000E+00

PARAMETER SPACE EIGENVECTORS (V MATRIX)

1 0.007−0.001 0.004−0.194 0.966−0.094 0.141 0.000 0.000 0.000
2 0.000 0.000−0.001−0.033 0.136−0.024−0.990 0.000 0.000 0.000
3 −0.948 0.102−0.200 0.218 0.053 0.017 0.000−0.002 0.000 0.000
4 −0.003−0.001 0.002 0.001 0.001 0.000 0.000 1.000 0.000 0.000
5 0.000 0.000 0.000 0.000 0.000 0.000 0.000 0.000−0.898−0.439
6 0.000 0.000 0.000 0.000 0.000 0.000 0.000 0.000−0.439 0.898
7 −0.247−0.372 0.891−0.079−0.019−0.006−0.001−0.003 0.000 0.000
8 −0.008 0.002−0.005−0.134 0.071 0.988−0.009 0.000 0.000 0.000
9 −0.199 0.043−0.126−0.943−0.200−0.115 0.007 0.001 0.000 0.000
10 −0.015−0.922−0.388 0.012 0.003 0.001 0.000 0.000 0.000 0.000

FINAL BLOCK RESISTIVITIES

I	RO(I)	BOUND(1)	BOUND(2)	DAMPING
1	1286.0636	1141.7577	1448.6083	0.0001
2	4158.0552	3442.0840	5022.9521	0.0002
3	210.1525	198.4862	222.5046	0.0014
4	46687.1641	45489.6328	47916.2188	0.9899
5	149.9990	149.9990	149.9990	1.0000
6	2000.0002	1999.9998	2000.0007	1.0000
7	659.4229	617.1871	704.5488	0.0018
8	1135.9065	1024.3171	1259.6525	0.0001
9	72.8776	65.9020	80.5915	0.0008
10	2587.4412	2455.1021	2726.9138	0.0002

Tab. 7.3- Summary of results of 2D inversion for the E pol direction.

SUMMARY 2D RESULTS INDEPENDENT INVERSION H POL
ASIAGO REGION

NORMALIZED SINGULAR VALUES OF JACOBIAN

0.100E+01 0.568E+00 0.406E+00 0.282E+00 0.252E+00
0.191E+00 0.147E+00 0.116E+00 0.136E−07 0.128E−07

SCALE FACTOR : 0.6965790E+00

DAMPING FACTORS (1.000 PERCENT LEVEL)

0.100E+01 0.100E+01 0.100E+01 0.100E+01 0.100E+01
0.100E+01 0.100E+01 0.100E+01 0.000E+00 0.000E+00

PARAMETER SPACE EIGENVECTORS (V MATRIX)

1 0.361−0.651 0.335−0.144 0.179−0.053−0.526−0.026 0.000 0.000
2 −0.247 0.409−0.308−0.244 0.392 0.058−0.678−0.001 0.000 0.000
3 0.822 0.501 0.044 0.087 0.149−0.197 0.021−0.039 0.000 0.000
4 0.201−0.035−0.153−0.099−0.090 0.437−0.006 0.852 0.000 0.000
5 0.000 0.000 0.000 0.000 0.000 0.000 0.000 0.000 0.542 0.841
6 0.000 0.000 0.000 0.000 0.000 0.000 0.000 0.000 0.841−0.542
7 0.190 0.092 0.016−0.455−0.368 0.636−0.015−0.456 0.000 0.000
8 −0.025 0.156 0.085 0.443−0.707−0.088−0.512 0.046 0.000 0.000
9 0.031−0.028−0.203−0.661−0.384−0.593 0.029 0.142 0.000 0.000
10 0.233−0.350−0.848 0.249−0.033 0.014−0.018−0.204 0.000 0.000

FINAL BLOCK RESISTIVITIES

I	RO(I)	BOUND(1)	BOUND(2)	DAMPING
1	1158.0325	1037.9045	1292.0641	0.0000
2	12100.2793	10623.3848	13782.4961	0.0000
3	383.2718	360.7211	407.2322	0.0000
4	22727.5898	19396.2754	26631.0586	0.0000
5	150.0000	150.0000	150.0000	1.0000
6	2000.0002	2000.0002	2000.0002	1.0000
7	2323.9072	1988.9255	2715.3076	0.0000
8	2517.1487	2205.0471	2873.4250	0.0000
9	159.7153	140.4004	181.6874	0.0000
10	582.6967	535.3005	634.2894	0.0000

Tab. 7.4− Summary of results of 2D inversion for the H pol direction.

iterations) and the H pol (4 iterations) cases, respectively. Like in the simultaneous inversion, the resistivity blocks are well resolved, with the exception of the block assigned with the code '3' for the E pol case which has been heavily damped (Tab. 7.3). The fits between data and models are shown in combined plots in Figs. 7.21(a)-(d). Note that a slight improvement in the fit is achieved when compared with the results for the simultaneous inversion (Figs. 7.19(a)-(d)), especially for sites MUL (Figs. 7.19(a)- 7.21(a)- bottom) and GRA (Figs. 7.19(d)- 7.21(d)- bottom). The resulting 2D models for the E pol and H pol directions are shown in Figs. 7.22 and 7.23, respectively. As observed from Tabs. 7.2, 7.3 and 7.4 (or from Figs. 7.20, 7.22 and 7.23), for any individual block, each of the resulting resistivity values in the simultaneous inversion case (Tab. 7.2) tends to lie between the resulting resistivity values obtained by inverting the two polarizations independently. It is possible that some of the observed discrepancies between the block resistivity values for the 3 models are associated with either anisotropy or 3D effects, occurring singly or in combination. Anisotropy can be either microscopic (i.e. related to the rock fabric itself) or macroscopic, a fairly attractive explanation for the nappe structure exhibited in the Alps. Three-dimensional effects seem to be less important in this area, as suggested by the dimensionality study presented in Chapter 6. However, a full assessment of these conjectures is limited by the small quantity of the MT soundings in this area. In addition, it is not evident that the same block structure should hold for the 3 inversion models, a fact which is further enhanced by the inherent non-unique character of the 2D inversion procedure. Among a number of 2D models which were found to produce a reasonable fit with the measured data, the models presented here were selected on the grounds of simplicity and of constraints imposed by the available geological information, as discussed in Chapter 8. Computing times for the 2D inversion exceeded 3 hours CPU on a VAX/8500 machine.

7.6 Near- source modelling for Cavalese and Po Valley soundings

With the assumptions provided in section 5.5 , modelling of the data sets most affected by the Italian DC railway network was undertaken. A horizontal electric dipole source was chosen to emulate the electromagnetic

signals arising from the leakage to the ground of the DC railway current. As already reported earlier in this Chapter, both the Monte Carlo- Hedgehog and the Occam techniques were adapted for the near- source modelling studies presented in this section.

The modelling study also assumes a layered Earth and is restricted to the major response curves. The latter restriction is justified by the fact that the major curves, unlike the E pol or H pol modes of induction (refer to discussion at the beginning of section 7.5.3), are always associated with the preferred direction of current flow in the Earth; they are therefore expected to be dominated by the effect of the artificial signals. The azimuths for the major ($\pm$ 90^0 ambiguity- note that the azimuths in the Cavalese area have their directions either coinciding with the shortest line to the DC railway track or at right angles to it (see Fig. 5.17)) are thus aligned with the hypothetical direction of the horizontal dipole source and thus only the radial component is required. Due to computing time constraints, a specific modelling procedure was followed. Indeed, since the near- source forward routine involves a great number of calculations, its computing time is considerably higher than that required for the natural MT problem. As a result, when the intrinsically slow Monte Carlo- Hedgehog technique was initially applied to the data sets, the number of layers was limited to 3. With this constraint, a range of models associated with distinct estimations of the distance between the sounding location and the dipole source (DS) was obtained for each site. Typical running times were of the order of 1300s CPU on EMAS. The next step was the application of the Occam inversion in which a fixed DS was assumed (i.e. the average of the DS's obtained by the Monte Carlo- Hedgehog models) and the starting model was also derived from the Monte Carlo models. The models using the Occam technique were limited to a maximum of 6 layers, due again to computing time requirements which in this case were typically around 500s CPU.

As an example, Fig. 7.24 illustrates the model results for site 460 (VAR) using the Monte Carlo- Hedgehog technique. The Occam results for all sites in the Cavalese area are summarized in the Figs. 7.25(a)-(d). Note that due to the assumed small number of layers the usual smoothness of the Occam models was not observed in this study (γ=1 was used throughout). Taking in account all the uncertainties involved in this modelling study, the agreement

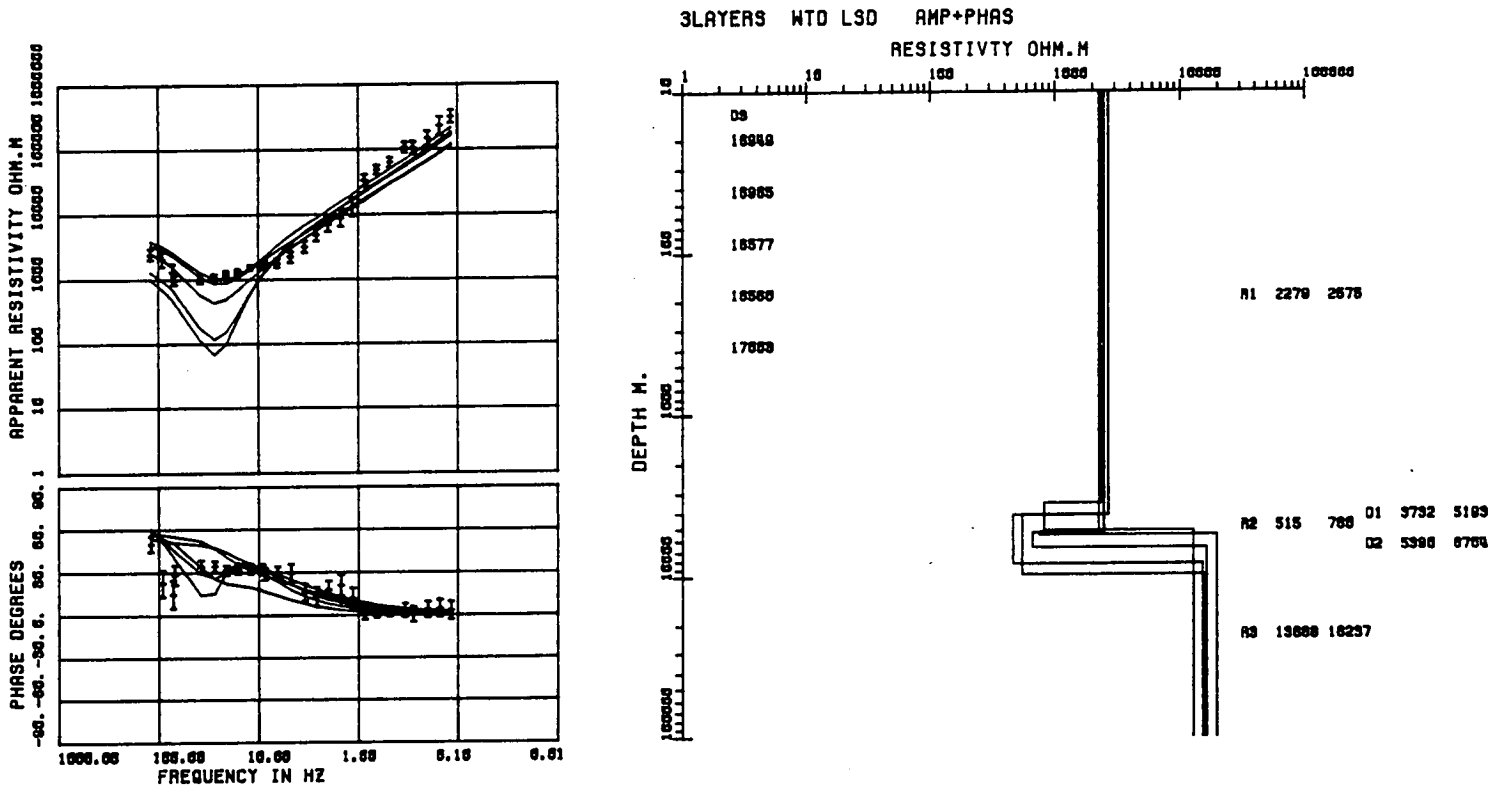

Fig. 7.24- Near- source modelling for the major response curve- site VAR using the Monte Carlo-Hedgehog scheme and assuming a horizontal electric dipole as source. DS is the sounding location - source distance for the five selected 3-layered models fitting app. resistivity and phase (indicated by 'AMP+PHAS'). Error bars are used as weights during inversion (WTD LSD).

Fig. 7.25- Occam models for the major response curves assuming a horizontal electric dipole source for the sites LAV (a), VAR (b), MAS (c) and MAG (d). Ancillary information comprises the misfit (CHISQ), the number of data points (NFREQ), the sounding location- dipole source distance (DS). The fit was performed by using both the app. resistivity and phase information (AMP + PHASE FIT).

OCCAM MODEL FOR SITE 463A MAJOR

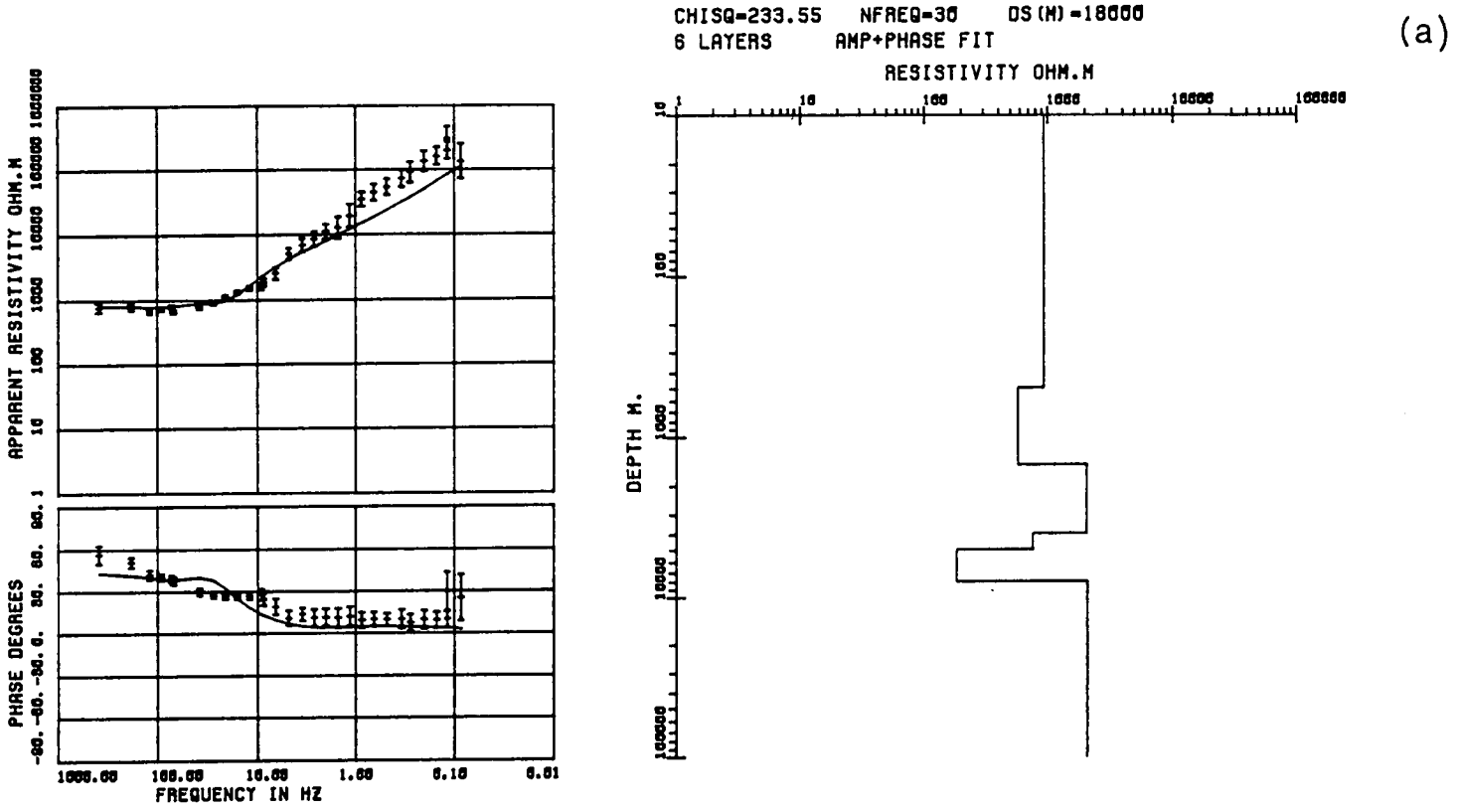

OCCAM MODEL FOR SITE 460A MAJOR

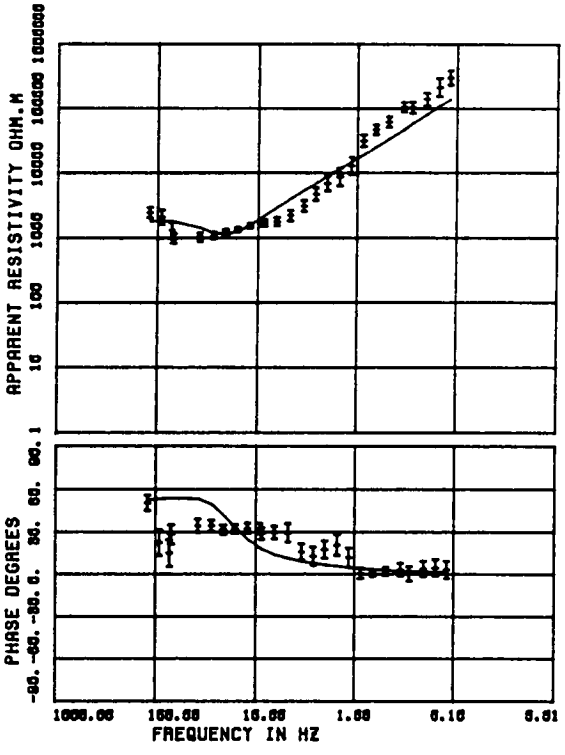

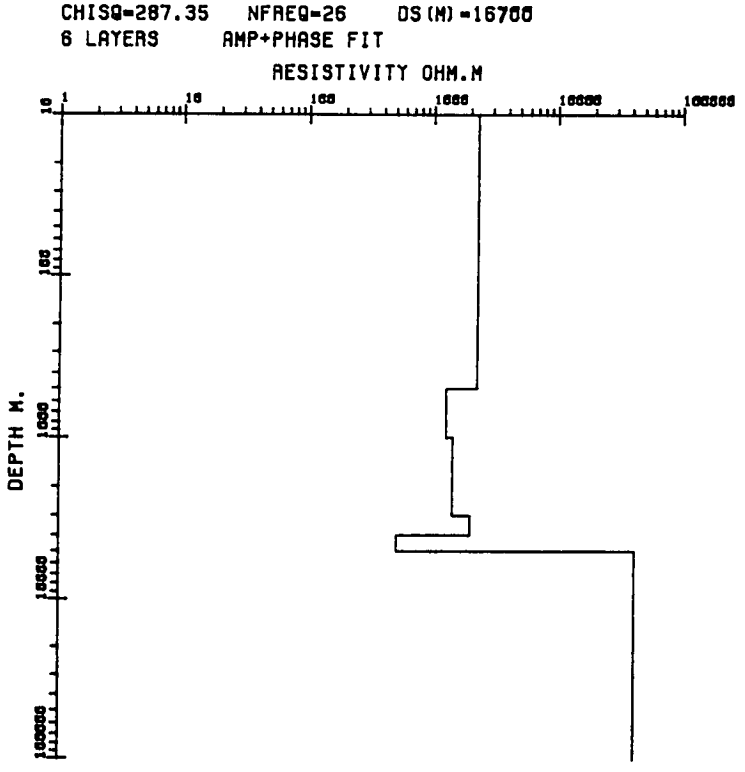

(b)

OCCAM MODEL FOR SITE 461A MAJOR

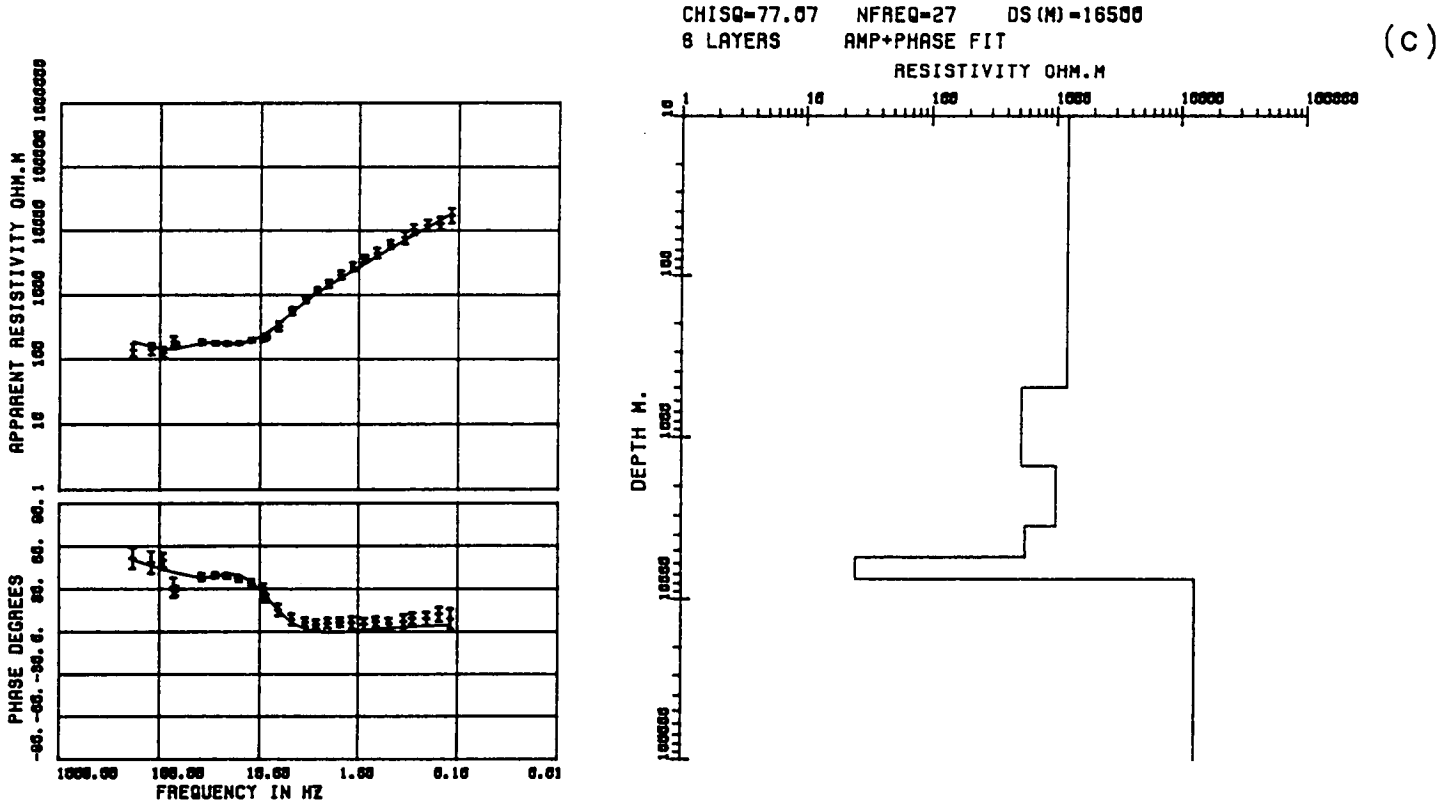

(C)

OCCAM MODEL FOR SITE 462A MAJOR

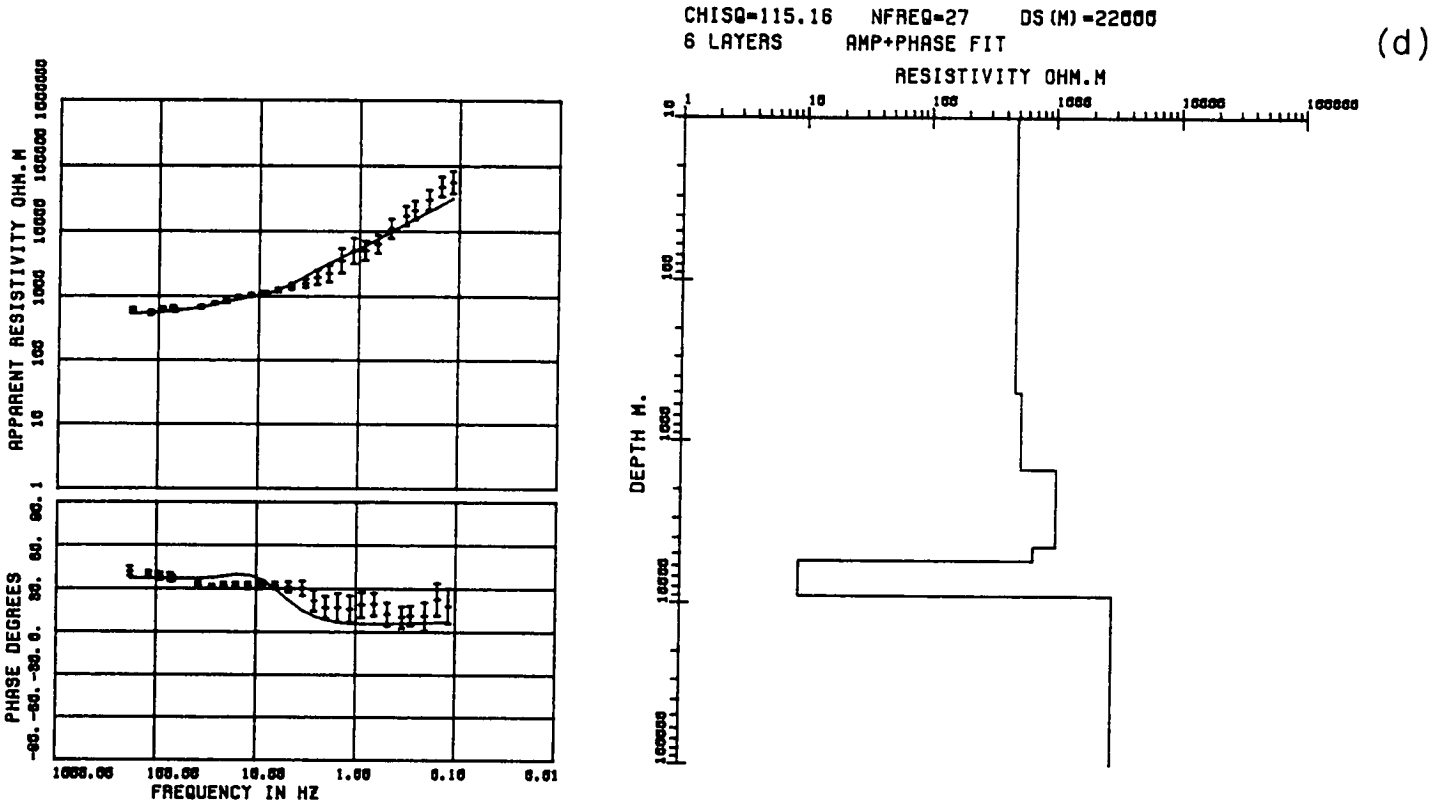

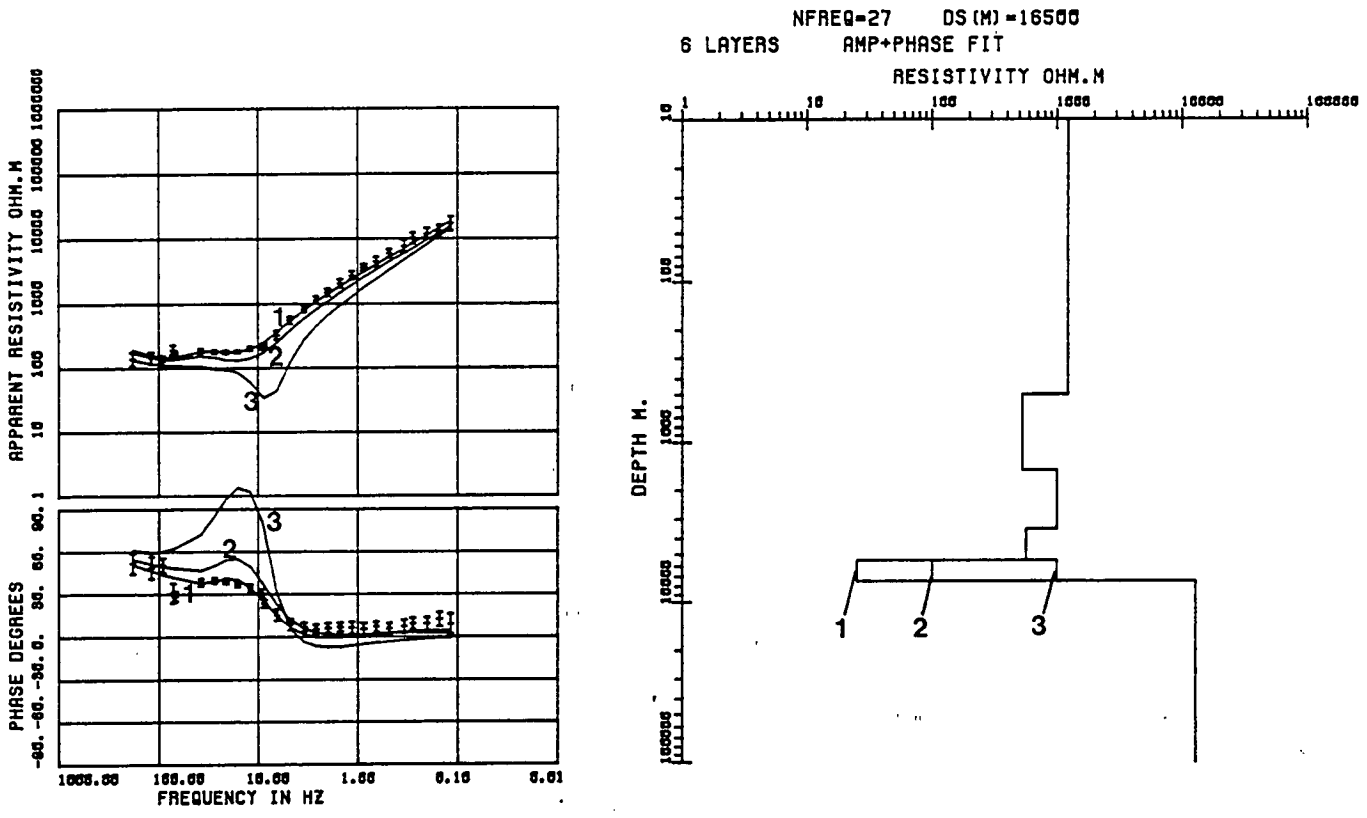

Fig. 7.26- Influence of the low resistivity layer on the fitting- site MAS (see Fig. 7.25(c)). Model 1- low resistivity layer = 25Ωm; Model 2- low resistivity layer = 100Ωm; Model 3- 'low resistivity layer' = 1500Ωm.

between data and models is quite satisfactory. The common feature in all the models for the Cavalese area is a conductive layer at depths of 3.5–7.5 Km approximately. These results are in reasonable accordance with the Asiago profile, and the sounding sites– noise source distances are all compatible with the expected distances to the railway track (see Fig. 5.17). Non– uniqueness of the inversion for active MT is well known and therefore the resolution of the parameters involved in the models is an important problem. Unfortunately though, neither the Monte Carlo– Hedgehog nor the Occam inversion scheme provides the means for an effective analysis of the parameter resolution. Of particular interest in the models for the Cavalese area is the conductive layer depicted by all models. The influence of this conductor on the resulting models was assessed by changing its resistivity value and keeping all the other parameters fixed. This analysis for the best fitting model, i.e. site MAS– Fig. 7.25(c), is summarized in Fig. 7.26 in which model 1 corresponds to the best fitting model (resistivity = 25Ωm), model 2 is associated with a layer of 100Ωm and for model 3 a resistivity of 1500Ωm was assigned. A similar pattern resulted at all other sites. Nevertheless, it is not digressive to reckon that completely different models, i.e. not containing any salient conductive features, might possibly exhibit fits similar to the ones presented in this study. An example of a reasonably good fit is given by a halfspace model for the site (Fig. 7.27(a)). A second example is shown in Fig. 7.27(b) for the site MAS. In this case a 3–layered model which consists of a resistive layer of 800Ωm intercalating two less resistive ones (compare with model of Fig. 5.25(c)) fits the data reasonably well. However, for the depths probed by this study, and considering both the relative proximity of the Asiago profile and the large scale of the Alpine orogeny, there is no reason to believe that the geoelectrical structure in the Cavalese area should be very dissimilar to that observed in Asiago. Hence, the presence of the conductive zone at depths 3.5–7.5Km attributed to the Cavalese area is supported both on grounds of 'fit' and on the accordance with the Asiago profile. However, the preliminary nature of these Cavalese models must not be ignored and only a very speculative interpretation is justifiable in this region.

Figs. 7.28(a)–(b) show the Po Valley model results derived from both the Monte Carlo– Hedgehog and the Occam techniques, respectively. The fit is satisfactory and the estimated distance is virtually the shortest line linking

the Vicenza- Padua railway sector and the sounding location. The Po Valley is characterized by a thick sedimentary layer and therefore the crystalline basement is expected to be at greater depths than those observed in the mountainous environments of Asiago and Cavalese. Being an isolated sounding little comment can be made about the MAT model except the fact that it is plausible.

Fig. 7.27- Examples of alternative models (horizontal electric dipole source) for two sites in the Cavalese area.
(a)- Halfspace model (1500Ωm) for site VAR.
(b)- 3- layered model for site MAS.
The sounding location- dipole source distances DS are the same ones considered in the models for these sites shown in Figs. 7.25.

HALFSPACE MODEL DIP. SOURCE SITE 460A MAJOR

CHISQ=313.18 NFREQ=26 DS(M)=16700

(a)

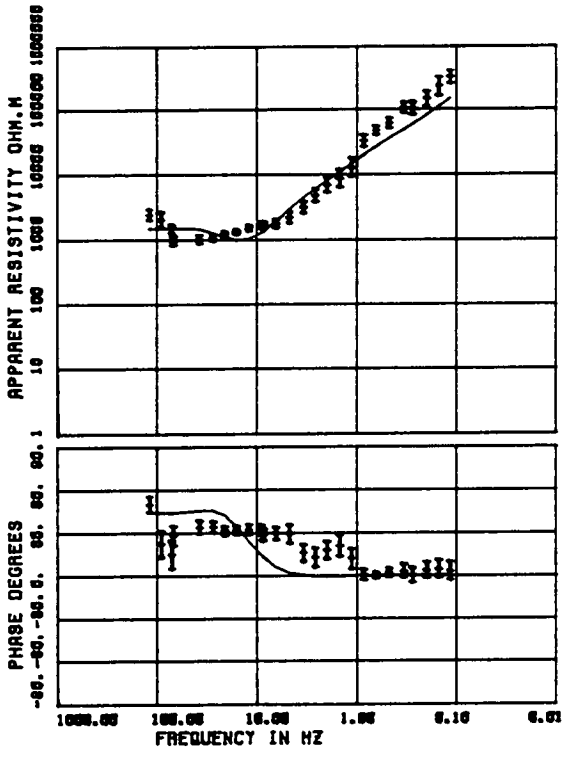

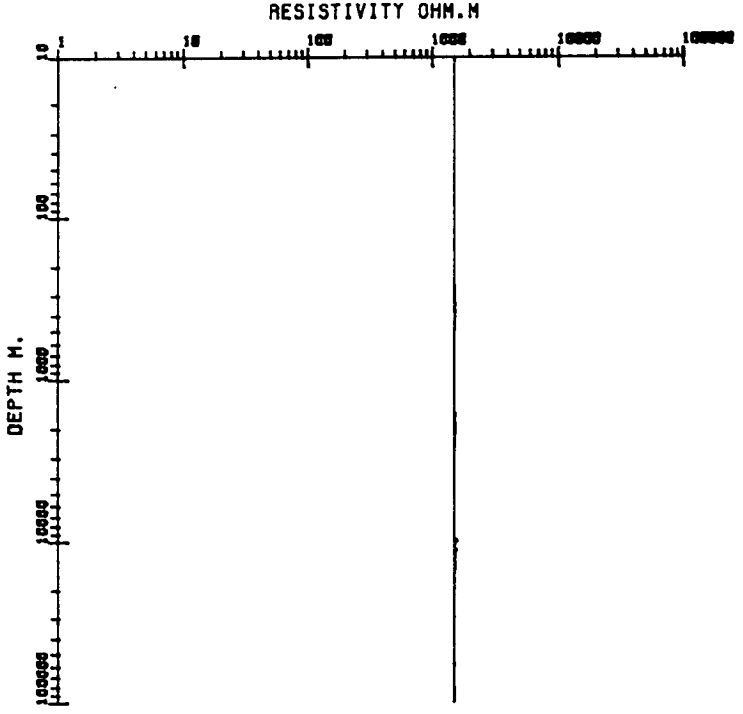

FORW. MODEL DIP. SOURCE SITE 461A MAJOR

CHISQ=346.79 NFREQ=27 DS(M)=16500

(b)

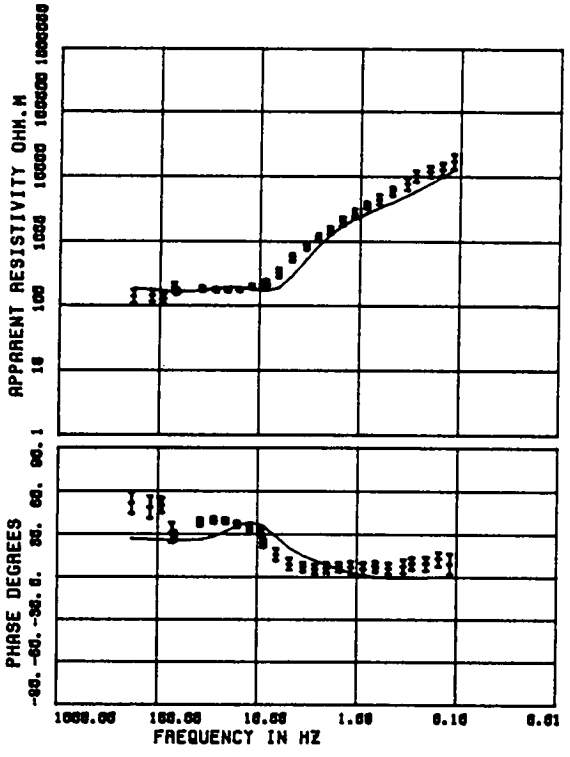

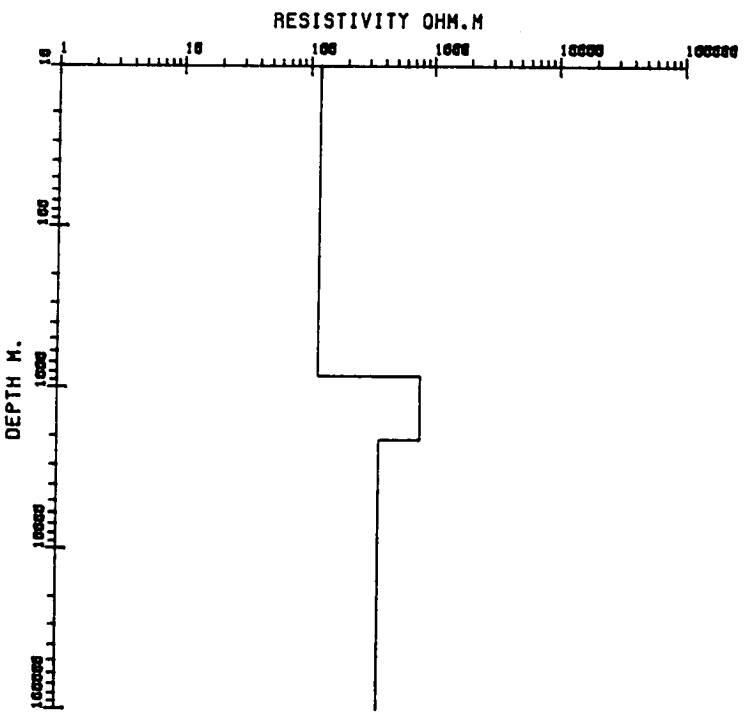

Fig. 7.28- Near- source modelling (horizontal electric dipole source) for the major response curve - Po Valley site.
(a)Monte- Carlo- Hedgehog models. See captions of Fig. 7.24.
(b)Occam model. See captions of Fig. 7.25.

DIPOLE MODEL FOR SITE 692A MAJOR

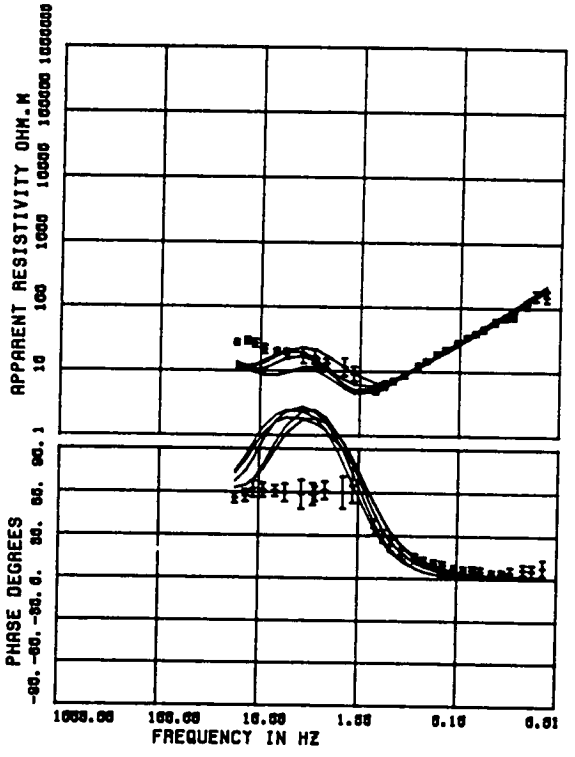

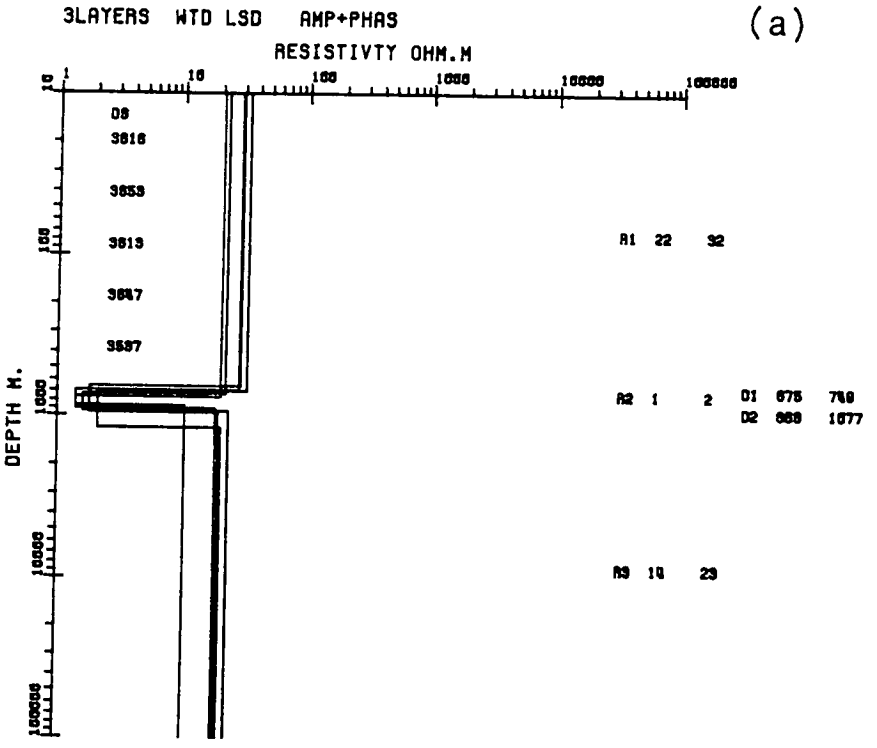

(a)

OCCAM MODEL FOR SITE 692A MAJOR

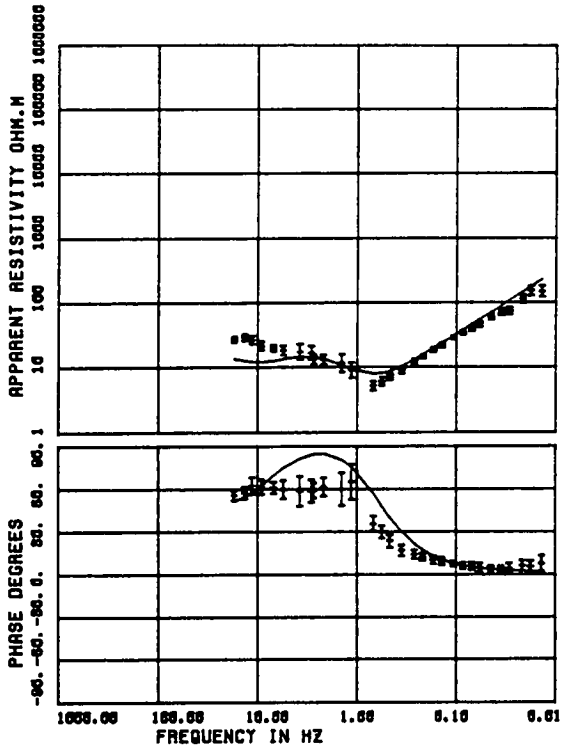

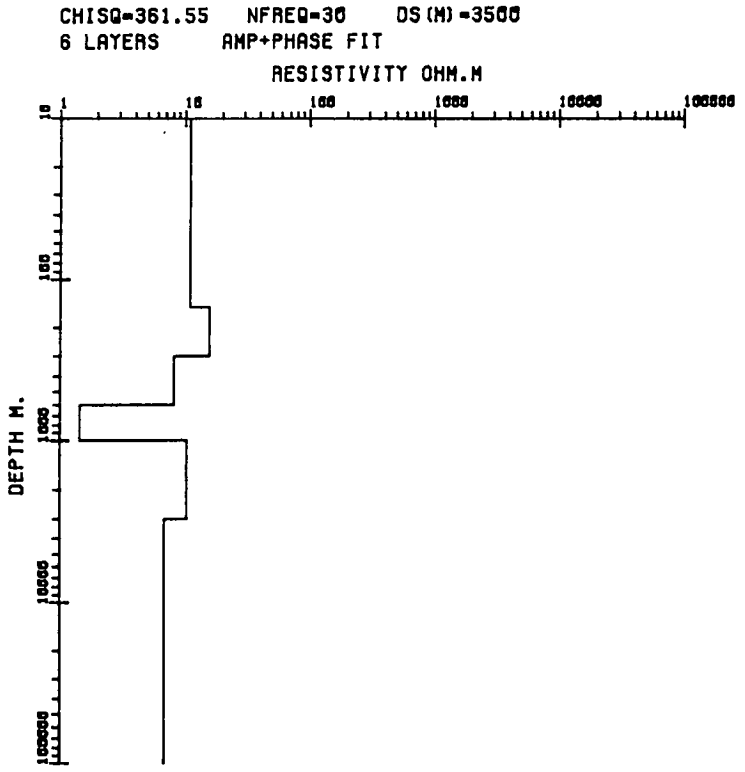

(b)

CHAPTER 8

INTERPRETATION AND CONCLUSIONS

8.1 Comparison of 1D and 2D model results- Asiago area

The 1D geoelectrical model results for the Asiago area were presented in Chapter 7 and summarized in the Figs. 7.9, 7.10 and 7.11 for the rotationally invariant, the E pol and the H pol curves, respectively. In the 1D modelling study, the distinct response curves yielded three geoelectrical models which reveal similar features; the most salient of them is the conductive structure at depths of approximately 1.5-9 Km across the entire profile.

The 2D models were also presented in Chapter 7 and shown in Figs. 7.20, 7.22 and 7.23 for the E and H pol directions inverted simultaneously, the inversion for E pol direction only and the inversion for the H pol only, respectively. In this latter case, the aim of the generation of three distinct models was the assessment of anisotropic effects. As discussed in Chapter 7, such effects are expected to be present in the complexly folded Alpine belt.

Comparison between the 1D and 2D model results will be restricted here to the composite section derived from the rotationally invariant response curves (Fig. 7.9) and the 2D inversion model obtained by simultaneously inverting the E pol and H pol directions. This restriction does not imply any loss of generality. 1D models derived from the rotationally invariant response curves are increasingly gaining acceptance among MT workers, as exemplified in recent investigations (e.g. Hutton et al., 1986, Livelybrooks, 1986, etc.) and has been shown to be less distorted by surface inhomogeneities than other response curves (Ingham, 1988). 2D modelling is always based on the simultaneous fitting (either by inversion or trial and error procedure) of the E and H pol directions.

While the main conductive pattern is preserved in both geoelectrical models shown in Figs. 7.9 and 7.20, some additional features are clearly evident in the 2D model results and are enumerated below.

(i)- The uppermost layer observed in the northernmost part of the profile extends underneath the uppermost layer observed at the centre of the profile.

(ii)- A relatively conductive structure (95Ωm) extending from ANT up to about

midway between AVE and GRA exists above the less conductive structure (294Ωm) which underlies the entire profile.

(iii)- The geoelectric structure at greater depths (i.e. in the range 10- 145Km), consists of two blocks of resistivities 38388Ωm (northermost sector) and 1104Ωm in the remaining part of the profile. Both blocks overlie a layer (of unresolved thickness) of resistivity equals to 1596Ωm.

These additional features were required during the inversion process in order to improve the fit between mathematical model and measured data (illustrated in Figs. 7.21(a)-(d)). The 2D geoelectrical model is thus regarded as more complete than the geoelectrical section derived from 1D models and its most prominent features are discussed in detail in section 8.2, where additional supporting geological and geophysical information is also provided.

8.2 Interpretation of the Asiago 2D geoelectrical model

More than one 2D geoelectrical model can be shown to fit satisfactorily the response curves measured in the Asiago profile; the 2D problem is highly non-unique. However, the preferred 2D model (Fig. 7.20) has parameters which are all well resolved (Tab 7.2) and is shown, in the discussion below, to be in good agreement with other geological and geophysical information. Therefore, any other realistic 2D model for the same data should not differ considerably from this chosen model, i.e. the important features should be virtually the same.

8.2.1 The uppermost layer- surface distortions or truly geological features

The uppermost layer of the 2D geoelectrical model (Fig. 7.20) is is divided into 3 distinct resistive bodies. Whether they truly represent the actual geoelectric structure in the profile is not easily assessed, due to likely occurring near surface distortions. One common type of surface distortion is the so-called 'static- shift' (e.g. Jones, 1987a,b), particularly frequent in regions of highly resistive surficial layers. Static- shift of an apparent resistivity curve is a 3D effect caused by an erroneous measurement of the pertinent horizontal component of the electric field. As a result, the H pol apparent resistivity curves may be offset either downwards or upwards by an unknown amount, with the phase curves remaining unaffected. The E pol

curves are not statically- shifted because no charges are generated within the Earth in this mode of induction. Typically, MT soundings statically- shifted display parallel apparent resistivity response curves (for all or part of the frequency range covered) and nearly identical phase curves. By inspecting the E pol and H pol sounding curves observed at MUL (Fig. 6.2(b)), one might be tempted to immediately conclude that static shift is present at this site. If that is the case at MUL, unless some a priori assumption is made, no solution for the static shift problem in MT is possible because there always remains an irresolvable static- shift factor (Larsen, 1977). The static- shift problem is tackled, more commonly among Soviet investigators, by modelling some sort of 'averaged response curve' representing the various sounding curves of a particular region (e.g. Berdichevsky et al., 1980, Krasnobayeva et al., 1981, Vanyan et al., 1983). Another- perhaps more effective- way may be provided by increasing gradually the distance between each pair of electrodes in an attempt to assess the dimension of the distortion. Novel techniques such as the electromagnetic array profiling - EMAP technique (e.g. Bostick, 1986; Word et al., 1986), in which several pairs of electrodes are deployed simultaneously, may thus offer the correct answer to the static- shift problem.

However, paleogeographic evolution and stratigraphic studies of the Venetian platform (Channel et al., 1979; Ferrari, 1982) suggest a period of main dolomitization (upper Triassic) in the entire platform, followed by calcareous facies (northernmost sector of the profile, i.e. sites MAN and MUL only) during the lower Jurassic, and pelagic carbonatic sedimentation. The latter is represented by the Ammonitico Veronese Formation (occurred mainly in the southernmost sector, i.e. site GRA, Middle Jurassic times) and the Biancone Formation observed at the centre of the profile (upper Jurassic). Therefore, the three distinct surficial geoelectric zones seem to correlate with the three distinct sedimentary depositional processes occurred in the area. The resistivity values associated with each of the three structures arise perhaps from the combination of a common component (the main dolomitization) and the three differentiated sedimentation processes.

Additionally, the gravimetric- seismic model shown in Fig. 8.1 (Italian Explosion Seismology Group, 1978) suggests the existence of a relatively light uppermost layer (density equals 2.55 g/cm^3) thinning towards the north of

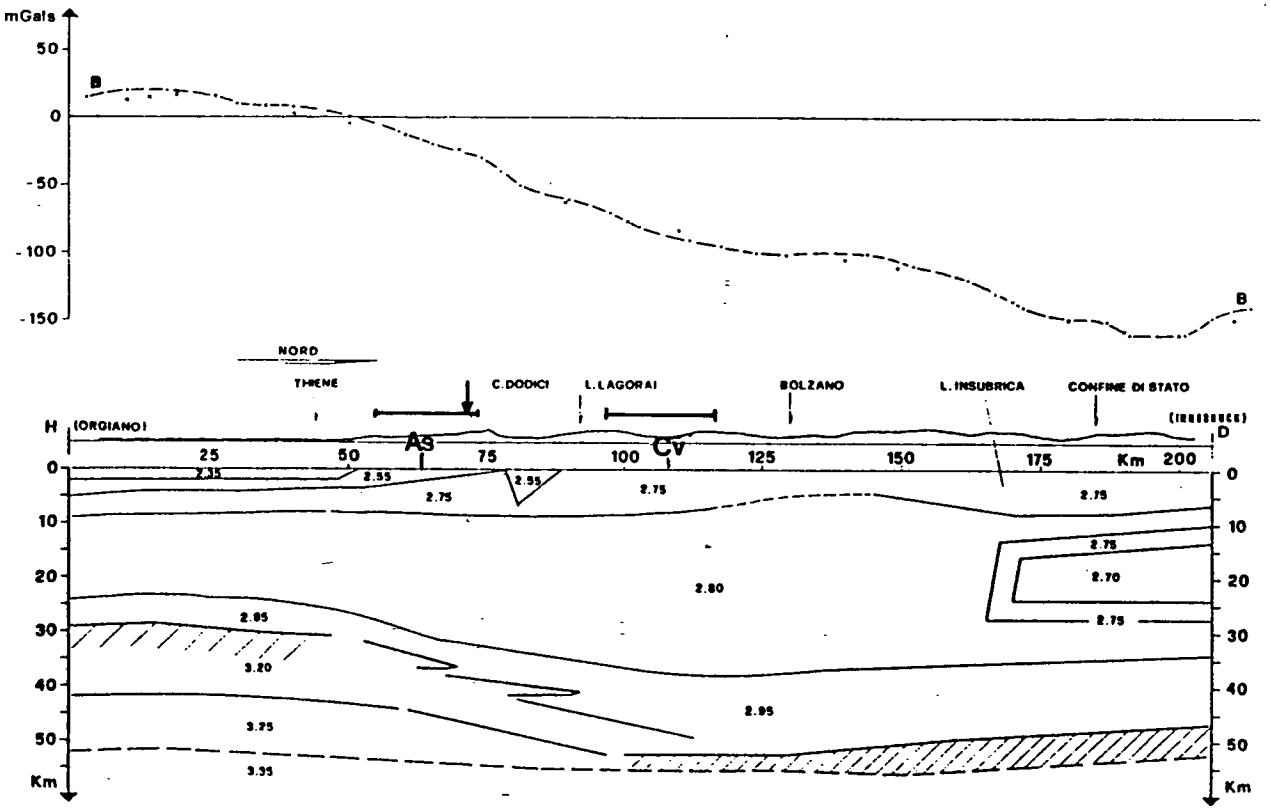

Fig. 8.1- Gravimetric- seismic model of a profile crossing the region surveyed in this study (both Asiago (As) and Cavalese (Cv) profiles are assigned in the Fig.). Observed and computed Bouguer anomaly values using the assigned densities (g/cm^3). The depth information is based on seismic refraction studies (Italian Explosion Seismology Group, 1978). The site MUL is indicated by an arrow in the Fig.

Asiago, i.e. towards the site MUL. The change in density may thus be correlated with the observed conductivity constrast. In fact, the calcareous facies deposits were not very extensive (Channel et al., 1982) and the observed conductivity in the northermost sector is predominantly due to the dolomitization process, which might also be reflected in the gravimetric-seismic model. However, one must bear in mind that gravimetric models are also known to be very non-unique. Moreover, the large scale involved in this particular seismic- gravimetric model (≈ 20Km average resolution- given by the spacing of gravimetric observations shown in Fig. 8.1) preclude a more accurate comparison. Anyhow, given these additional geological and geophysical evidence, the resistivity values obtained for the uppermost layer can be regarded as physically meaningful.

8.2.2 The crustal conductivity anomaly

Crustal electrical conductivity anomalies (CA) have been more often observed at greater depth intervals (say between 10 and 35Km (Shankland and Ander, 1983)) than the one observed in the Asiago profile, roughly between 1.5 and 9Km. Nevertheless, such apparent Earth's characteristic is basically a result of the low frequency range covered by most studies in past decades. Indeed, the range of depth intervals seems to exhibit wider variation than that reported by Shankland and Ander (1983) and shallower CA were found in various geological environments, and in particular in tectonically active areas (see Adam (1987) for a number of cases).

The relatively shallow CA observed in the Asiago profile (situated in a mountainous environment) must be explained in the framework of the plates collisional process which culminated with the formation of the Alps. A very extensive region, illustrated in the generalized cross- section of Fig. 8.2 (Laubscher, 1983), was involved in great compressional forces. Despite the complexity of the Alpine orogeny already discussed in Chapter 1, and the 3D (or even 4D) character of it, the generalized cross section is meant to picture the most prominent aspects involved in such orogenesis. The Asiago profile, with its hypothetical centre assigned in Fig. 8.2, is within the orogenic realm and therefore the tectonic features observed (see Fig. 6.1) can possibly be related to the 'wedge- like' effects developing composite shear zones (shear-induced folds, thrusts, decollements). Asiago area has suffered marine transgression followed then by uplift due to isostatic adjustment processes-

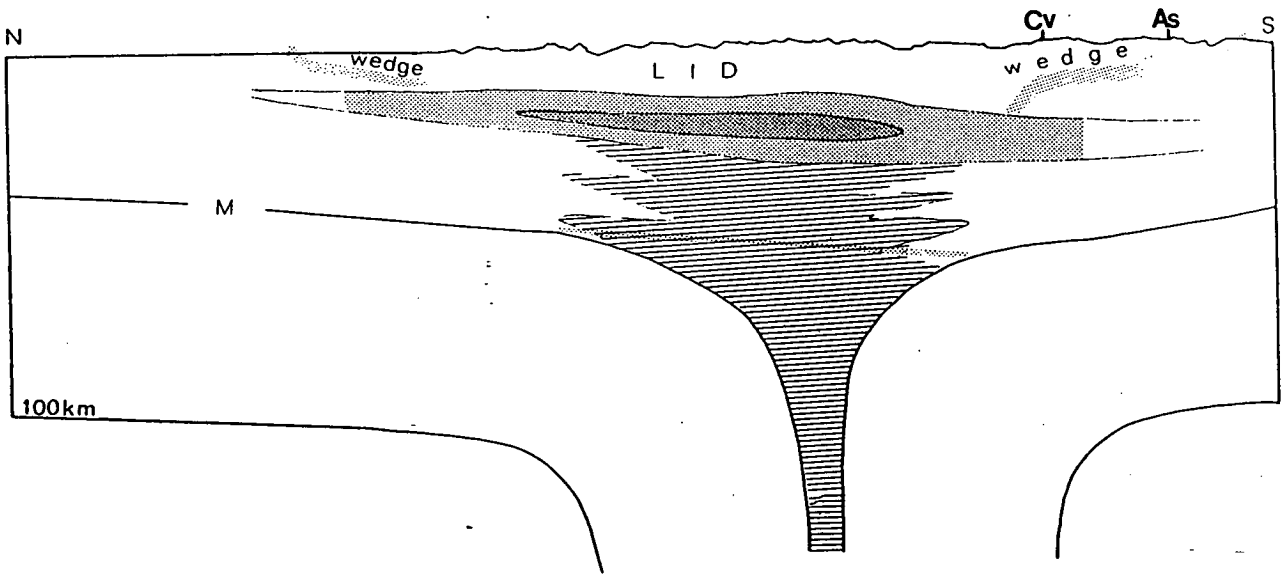

Fig. 8.2- Generalized 2D cross- section of the Alpine orogeny. The lid of the continental collision zone and its frontal edges. The presence of velocity inversions, particularly a low velocity channel is assigned by shading; darker shading indicates v_p less than 5.6Km/s. The hypothetical locations of Asiago (As) and Cavalese (Cv) are assigned in the Fig. (after Laubscher, 1983).

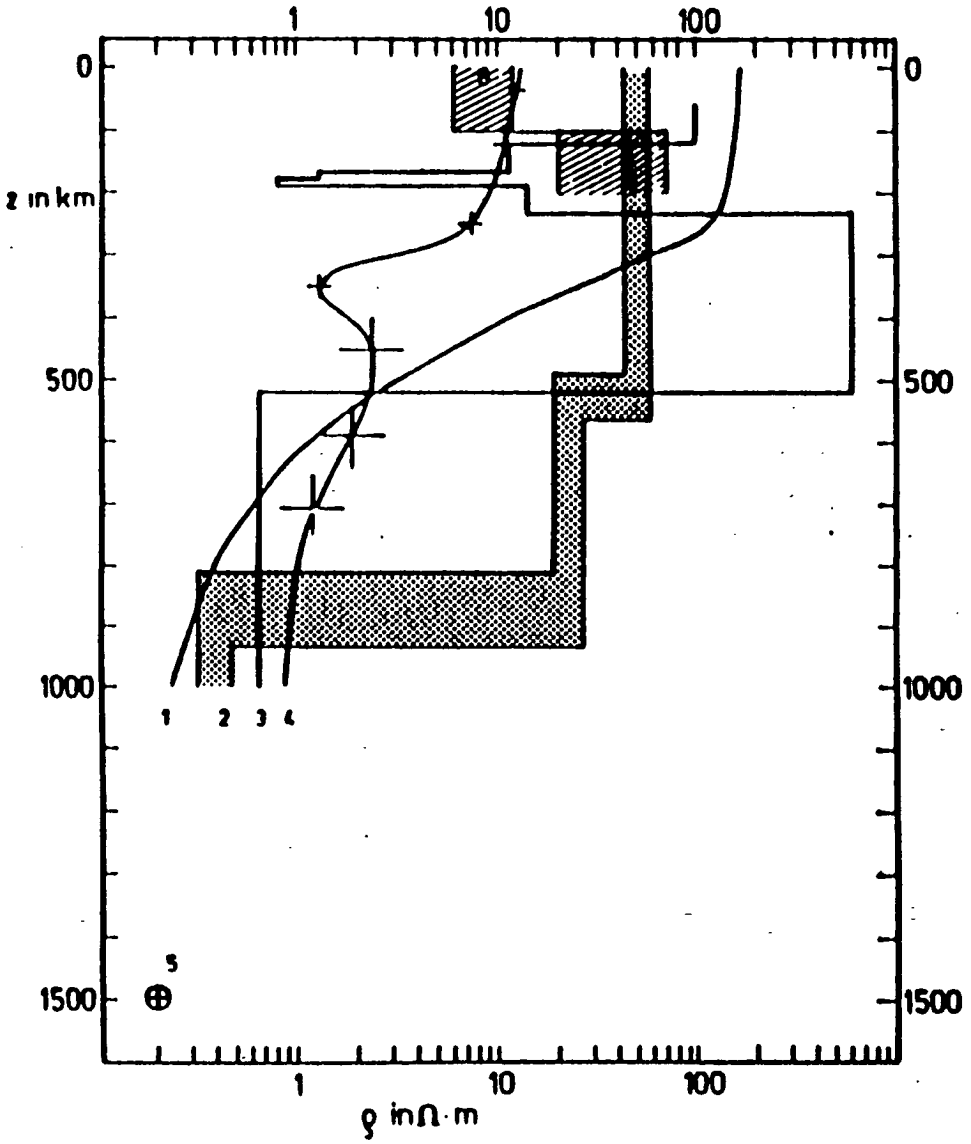

Fig. 8.3- Electrical resistivity of crust and upper mantle as determined by EM induction studies. (1) Banks (1972); (2) Schmucker (1974); (3) Tucson model, Larsen (1977); (4) Hawaii model, Larsen (1975); (5) Isikara (1977); (6) Poehls and Von Herzen (1976) (reproduced from Haak, 1980).

the present mountain chain (Altopiano dei Setti Comuni- Asiago is the central 'Comuni') thus resulting.

The material composing the crustal anomaly is associated with the sedimentary sequence which occurred during Permo-Triassic times. This sequence is constituted basically of a detrital formation (middle and upper Permian) and the series argillaceous- arenaceous, calcareous- marnose and conglomerates ending prior to the beginning of the main dolomitization already referred to. The physical mechanisms determining the conductivity values observed in this upper crust anomaly must also be addressed. As already discussed in Chapter 1, a variety of causes may be responsible for CA at crustal depths. In considering the Asiago case, some possible causes of low resistivities can be excluded on physical (and other information) grounds. Partial melting is frequently invoked in tectonically active regions, but the shallow depths involved and the absence of geothermal sources in the Asiago region result in this mechanism being summarily discarded. Metallic conduction (i.e. free electron conduction) may also be found responsible for anomalously conductive zones in the crust. However, mineralization zones seems to be well mapped in the Alps (Windley, 1977) and Asiago is not included. Graphite is not known to occur in this area either. Moreover, the two former materials would have resulted in even lower resistivity values (Haak and Hutton, 1986) than the one assigned by the 2D model.

The favoured cause ascribed to the CA observed in Asiago is thus the commonest physical mechanism associated with crustal conductivity anomalies: water content in the crust (Jiracek et al., 1983; Haak and Hutton, 1986). Considering the marine transgression process which occurred in the region, it seems reasonable to expect that brine has been retained in pores, cracks and voids. Additionally, the highly conductive structure described in (ii)- section 8.1 (see also Fig. 7.20) is possibly associated with the tectonic features observed at the surface- the synclinals of Gallio and Granezza. Its more conductive nature (compared to the crustal conductivity anomaly along the entire profile) is perhaps due to a higher water content, caused by frequently occurring incursion of near- surface waters into faults (Kerrich et al, 1984).

Considering now the Cavalese model results, the arguments provided in the interpretation of CA observed in the Asiago profile should also hold for

Cavalese. Thus, it seems natural to assign the presence of water as the physical mechanism responsible for the low conductivity values observed at depths 3- 8Km approximately (Figs. 7.25(a)-(d)). However, as previously discussed, in view of the inherent uncertanties of the active MT modelling attempted for Cavalese, the latter statement can only be rated as speculative.

8.2.3 The geoelectric structure at greater depths

The crystalline basement in the 2D geoelectrical model is represented by 2 blocks of rather distinct resistivity values (38388Ωm and 1104Ωm, see Fig. 7.20). The Moho discontinuity in the region, determined by seismic refraction studies at about 35Km depth (Italian Explosion Seismology Group, 1981), has no analogue in the 2D geoelectrical model. The same holds for the recently suggested existence of two crust-mantle like boundaries in the Southern Alps (Giese, 1985). However, this is not surprising as the Moho discontinuity is not necessarily an electrical boundary.

What can be tentatively regarded as the lithosphere- asthenosphere interface- the upper boundary of a layer of unusually high resistivity value (1594Ωm) at 145Km depth, was obtained after analysing the model resolution for a considerable number of depths in various inversion trials. It may be argued that the resistivity value at depths commonly associated with the asthenosphere (by definition, a highly conductive region) are higher than for most regions in the world. But lateral conductivity variations in the upper mantle are very often observed, as reviewed by Roberts (1983). For instance, Larsen (1977) has found resistivity values over 700Ωm for depths between 250Km and 500Km in Tuckson- Arizona (see Fig. 8.3 for a list of resistivity models of crust and upper mantle determined by other EM induction studies). The high resistivity values at great depths (in particular the northermost lithospheric block of this Alpine profile) may be resultant of (1) remnant noise on the response curves or (2) the Alpine orogeny itself.

The noise problem in the Italian data has been extensively considered in this study and assumption (1) seems attractive and less questionable. However, it seems worthwhile to analyse some of the aspects implied by (2). The low gravimetric (-160mgal Bouguer gravimetric anomaly) along the axis of the Alps is well known (Morelli, 1975, 1985; Kissling et al, 1983) and it implies light crustal material subducted into typically mantle depths (≃ 55Km). Under this light material, the existence of an anomalously dense and cold slab lying

along the axis of the Alps is well supported by two recent studies (Kissling et al., 1983; Schwendener and St. Mueller, 1985). Additionally, dehydration processes common to subduction zones, are also known to have occurred in the Alps. The combination of all these geophysical data form a perfect setting for a deep rooted anomalously resistive structure along the axis of the Alps. Therefore, it is plausible that lateral effects may extend as far as the Asiago region. The Cavalese results also suggested highly resistive layers at depths >9km and thus offer limited support to the above argument. However, the evidence provided by the 2D geoelectrical model is handicapped by the limited length of the Asiago profile when compared to the dimensions involved in the Alpine orogeny. In summary, whether these peculiar aspects of the geoelectrical model for the area of the Southern Alps covered in this study provide a true representation of the actual conductivity structure cannot, at this stage, be proposed with great confidence. Nevertheless, they are sufficiently novel as to invite further investigation.

8.3 Summary and recommendations

Cultural noise was found to be a major problem for the effective implementation of electromagnetic studies in the Italian Alps. While the best solution to the noise problem is to avoid it in the first place, it is clear that in highly urbanized areas cultural noise is unavoidable.

In this study, several practical processing techniques have been shown to alleviate the noise problem and, in a number of cases to produce interpretable response curves. The results of this study suggest that whenever EM surveys are to be undertaken in noisy environments, the use of standard processing techniques may be inadequate. Besides, as demonstrated for the Italian data, the incorporation of a simple delay- line filter in the data acquisition system can deal more efficiently with noise of a regular character, e.g. from the power lines. Ideally, such a filtering operation (accomplished by either software or hardware) should be 'intelligent' in the sense that it is able to trace the dominant noise frequency exactly in any particular section of recorded data. In most countries minor but nonetheless relevant fluctuations in the mains network frequency are often observed. The application of robust techniques for in- field processing of MT data is also strongly recommended

in noisy environments. Studies in which the Italian data is processed by means of the robust technique proposed by Rousseeuw (1984) are under way at the present time and will be reported in a future paper.

With reference to the modelling studies, the use of several 1D inversion schemes has proven beneficial as it lends increased credibility to the interpretation based on models resulting from a consensus. The 2D model presented in this study was much influenced by the 1D model results. Although not comprehensively covered by this study, the conductivity structure of the studied sector of the Southern Alps is in many respects in reasonable accordance with other available geophysical and geological information. Nevertheless, in line with the discussion presented earlier in this Chapter, the highly resistive deep structure suggested by the geoelectrical model should not be considered summarily implausible nor confidently accepted as factual. Further investigation is urged in order to clarify this interesting point.

The Cavalese area has been shown completely unsuitable for natural MT studies. It is possible that only active MT can produce satisfactory results, but it must be remembered that only shallow information can be obtained by currently available equipment. Alternatively, the use of the DC railway network as a geophysical exploratory tool seems feasible as demonstrated by the embryonic attempt made in this study. However, a more systematic analysis of the DC railway signal in Italy is essential. The exact location of the points along the track where currents leak to ground occur, and the actual physical characteristics and geometry of this source (e.g. a horizontal electric dipole source was assumed in this study) are the main questions to be answered. As far as inversion of active MT data are concerned, there is still a great deal to be achieved. Better assessment of the non-uniqueness of the models and a clear knowledge of the maximum depths probed are required.

REFERENCES

Abramovici, F. and Baumgarten, J., 1985. The Backus- Gilbert theory for piecewise continuous structures with variable discontinuity levels and its application to the magnetotelluric inverse problem. Geophys. J. R. astr. Soc. 81, 347-362.

Abramovici, F. and Shoham, Y., 1977. Inversion of anisotropic magnetotelluric data. Geophys. J. Roy. astr. Soc., 50, 55-74.

Adam, A., 1987. Are there two types of conductivity anomaly (CA) caused by fluid in the crust ? Phys. Earth Planet. Int. 45, 209-215.

Adam, A., Szarka, L., Vero, J., Wallner, A. and Gutdeutsch, R., 1986. Magnetotellurics (MT) in mountains: noise, topographic and crustal inhomogeneities effects. Phys. Earth Planet. Int. 42: 165-177.

Akaike, H. 1969a. Fitting autoregressive models for prediction. Ann. Inst. Statist. Math. 21: 243-247.

Akaike, H., 1969b. Power spectrum estimation through autoregressive model fitting. Ann. Inst. Stat. Math. 21: 407-419.

Akaike, H., 1976. Canonical correlation analysis of time series and the use of an information criterion. In 'System identification- advances and case studies.' Editors: R.K. Mehra and D.G. Laniotis. Academic Press, New York, 27-96.

Anderson, W.L., 1979. Numerical integration of related Hankel transforms of order 0 and 1 by adaptative digital filtering. Geophysics 44, 1287-1305.

Anderson, W.L., 1982. Fast Hankel transforms using related and lagged convolutions. ACM Trans. Math. Software 8, 34-368.

Backus, G. and Gilbert, F., 1967. Numerical application of a formalism for geophysical inverse problems, Geophys. J.R. astr. Soc., 13, 247-276.

Bailey, R.C. ,1970. Inversion of the geomagnetic induction problem. Proc. Roy. Soc. 315, 185-194.

Bailey, R.C. and Edwards, R.N., 1976. The effect of source field polarisation on geomagnetic anomalies in the British Isles, Geophys. J.R. astr. Soc., 45, 97-104.

Bailey, R.C., Edwards, R.N., Garland, G.D., Kurtz, R. and Pitcher, D.H., 1974. Electrical conductivity studies over a tectonically active area in Eastern Canada. J. Geomag. Geoelectr., 26, 125-146.

Banks, R.J., 1969. Geomagnetic variations and the electrical conductivity of the upper mantle. Geophys. J.R. astr. Soc. 17, 457-487.

Banks, R. J. , 1973. Data processing and interpretation in geomagnetic deep sounding. Phys. Earth Plan. Inter. 7, 339-348.

Barrodale, I. and Erickson, R.E., 1980. Algorithms for least squares linear prediction and maximum entropy spectral analysis, Parts I and II, Geophysics, 45, 3:420-446.

Beamish, D., 1986. Geoelectric structural dimensions from magnetotelluric data: methods of estimation, old and new. Geophysics, 51, 6: 1298-1309.

Bendat, J.S. and Piersol, A.G., 1971. Random data: Analysis and measurements procedures. Wiley- Interscience. New York.

Bennet, D.J. and Lilley, F.E.M., 1972. An array experiment with magnetic variometers near the coasts of South- east Australia. Geophys. J. R. astr. Soc. 29: 49-64.

Bentley, C.R., 1973. Error estimation in two-dimensional magnetotelluric analysis. Phys. Earth Planet. Int., 7, 423.

Berdichevsky, M.N. and Dmitriev, V.I., 1976. Distortion of magnetic and electrical methods by surface lateral inhomogeneities. Acta. Geod. Geophys. Mont. Acad. Sci. Hungary, 11, 447-483.

Berdichevsky, M.N., Vanyan, L.L., Kuznetsov, V.A., Levadney, V.T., Mandelvavm M.M., Nechaeva G.P., Okulesky B.A., Shilovsky P.P. and Shpak, I.P., 1980. Geoelectric model of the Baikal region. Phys. Earth Plant. Intr., 22, 1-11.

Berdichevsky, M.N. and Zhdanov, M.S., 1984. Advanced theory of deep geomagnetic sounding. In Methods in Geochemistry and Geophysics, 19, 408pp.

Best, M.E., Duncan, P., Jacobs, F.J. and Scheen, W.L., 1985. Numerical modelling of the electromagnetic response of three-dimensional conductors in a layered earth. Geophysics 50, 665-676.

Blackman, R.B. and Tukey, J.W., 1958. The measurement of power spectra. Dover Publ., New York.

Bostick, F.X. (Jr.), 1977. A simple and almost exact method of MT analysis. In 'Workshop on electrical methods in geothermal exploration', U.S. Geol. Surv., pp. contract No. 14080001-8-359.

Bostick, F.X., 1986. Electromagnetic array profiling. Contributed paper at the 56th SEG, Houston- Texas.

Bostick, F.X. and Smith, H.W., 1962. Investigations of large scale inhomogeneities in the Earth by the magnetotelluric method. Proc. Inst. Radio Engineers 50, 2339-2346.

Brasse, H. and Junge, A., 1984. The influence of geomagnetic variations on pipelines and an application for large- scale magnetotelluric depth sounding. J. Geophys. 55, 31-36.

Brewitt-Taylor, C.R. and Weaver, J.T., 1976. On the finite difference solution of two-dimensional induction problems. Geophys. J. R. astr. Soc., 47: 375-396.

Brewitt- Taylor, C.R. and Weaver, J.T. , 1986. A computer program for the solution of electromagnetic induction problems. Depart. Phys., University of Victoria, Canada.

Brewitt-Taylor, C.R., Johns, P.B., 1980. Diakoptic solution of induction problems. J. Geomag. Geoelectr., 32, Suppl. I: SI73-SI78.

Burg, J.P., 1967. Maximum entropy spectral analysis. 37th Ann. Int. Meet. Soc. Explor. Geophys., Ohlahoma City.

Burg. J.P., 1972. The relationship between maximum entropy spectra and maximum likelihood spectra. Geophysics, 37, 375-

Burg, J.P., 1975. Maximum entropy spectral analysis. Ph.D. thesis, Stanford University.

Cagniard, L., 1953. Basic theory of the magnetotelluric method of geophysical prospecting, Geophysics, 18, 605-635.

Campbell, W.H., 1987. Introduction to Electrical properties of the Earth's Mantle. PAGEOPH, 125, 193-204.

Cantwell, T., 1960. Detection and analysis of low frequency magnetotelluric signals, Ph.D. Thesis, Dept. Geology & Geophysics, M.I.T. Cambridge, Massachusetts.

Carter, G.C., Knapp, C.H. and Nuttal, A.H., 1973. Estimation of the magnitude squared coherence function via overlapped Fast Fourier Transform processing. IEEE Trans. Audio Electroacoust. AU-21, 4: 337-344.

Chaize, L. and Lavergne, M., 1970. Signal et bruit en magnetotellurique. Geophys. Prosp. 18: 64-87.

Channel, J.E.T., D'Argenio, B. and Horvath, F., 1979. Adria, the African Promontory. In: Mesozoic Mediterranean Paleogeography. Earth Sc. Rev. 15, 213-292.

Chave, A.D. and Booker, J.R., 1987. Electromagnetic induction studies. Rev. of Geophys., 25, 5: 989- 1003.

Chave, A.D., Thomson, D.J. and Ander, M.E., 1987. On the Robust estimation of power spectra, coherences and transfer functions., J.G.R., 92, B1, 633-648.

Coggon, J.H., 1971. Electromagnetic and electrical modeling by the finite element method, Geophysics, 36, 132-155.

Constable, S.C., Parker, R.L. and Constable, C.G., 1987. Occam's inversion: A practical algorithm for generating smooth models from electromagnetic sounding data. Geophysics, 52, 289-300.

Cooley, J.W. and Tukey, J.W., 1965. An algorithm for the machine calculation of complex Fourier series. Math. Comput., 19, 297-301.

COPROD, 1979. Comparative study of methods of deriving the conductivity profile within the earth from one-dimensional magnetotelluric data- organised by A.G.Jones, Report, 1-11.

Cox, C.S., Filloux, J.H. and Larsen, J.C., 1970. Electromagnetic studies of ocean currents and electrical conductivity below the ocean floor. In The Sea, A. Maxwell (Ed.) John Willey and Sons Inc.

Cox, C.S., Constable, S.C., Chave, A.D. and Webb, S.C., 1986. Controlled-source electromagnetic sounding of the oceanic lithosphere. Nature, 320, 6057: 52-54.

D'Erceville, I. and Kunetz, E., 1962. The effect of a fault on the earth's natural electromagnetic field, Geophysics, 27, 651-665.

De Zanche, V., Frascari, F.R.S., Grandesso, P. and Semenza, E., 1981. Foglio 37-Bassano del Grappa. In A. Castelarini: Carta tettonica delli Alpi meriodionali (scala 1:200000). Pubbl. n. 441 Progetto Finalizzato geodinamica (S.P.5), C.N.R., Bologna.

Das, U.C. and Verma, S.K., 1982. Electromagnetic response of an arbitrary shaped three dimensional conductor in a layered earth-numerical results. Geophys. J. Roy. astr. Soc., 69, 55-66.

Dawes, G.J.K., 1980. Computer program library. Internal publication, Dept., of Geophysics, Univ. of Edinburgh. U.K.

Dawes, G.J.K., 1984. Short period automatic magnetotelluric (SPAM) system in A broadband tensorial magnetotelluric study in Travave-Radiocondili geothermal Field. Final report, by V.R.S. Hutton et al. EEC Report Series. EUR A2-031-UK.

Dawes G.J.K., 1985. Magnetotelluric feasibility study Island of Milos - Greece., Final report, EN-3G-0008-UK (H).

Dawson, T.W., 1983. E- polarization induction in two thin sheets. g Geophys. J.R. astr. Soc. 73, 83-107.

Dekker, D.L., 1983. A magnetotelluric survey of the Bowen Basin. Ph.D. thesis, University of Queensland, Australia.

Devlin, T. ,1984. A broadband electromagnetic induction study of the Travale geothermal field, Italy, Ph.D. thesis, Edinburgh University.

Dietrich, V.J., 1984. Evolution of the Eastern Alps: the traditional concept and modern plate tectonics. Annales Geophys., 2, 2: 155-160.

Ding- yi, W., Wei, S. and Kang Kun, T., 1982. A note on MESA and spectral analysis of the hundred year geomagnetic data at Zo-se. Geophys. J. R. astr. Soc. 71, 275-283.

Dosso, H.W., 1966. Analogue model measurements for electromagnetic variations near vertical faults and dykes. Can. J. Earth Phys. 3, 287-303.

Dosso, H.W. and Nienaber, W., 1986. A laboratory electromagnetic model study of the Juan de Fuca Plate region. Phys. Earth Planet. Inter., 43: 34-46.

Dosso, H.W., Nienaber, W. and Parkinson, W.D., 1985. An analogue model study of electromagnetic induction in the Tasmania region. Phys. Earth Plan. Int. 39, 118-133.

Doucet, D. and Ngoc, P.V., 1984. Generalisation et optimalisation de la methode das differences finies pour la modelisation en magnetotellurique (MT). Geophys. Prosp. 32, 292-316.

Dupis, A., Iliceto, V. and Norinelli, A., 1972. Deep structural investigation by the magnetotelluric nethod in the area of the Berici- Euganean ridge.

Edwards, R.N., Law, L.K. and White, A., 1971. Geomagnetic variations in the British Isles and their relation to electrical currents in the ocean and shallow seas, Phil. Trans. Roy. Soc. Lond., No. 1204, 270, 289-323.

Egbert ,G.D. and Booker, J.R. , 1986. Robust estimation of geomagnetic transfer functions. Geophys. J. R. astr. Soc. 87, 173-194.

Eggers, D.E., 1982. An eigenstate formulation of magnetotelluric tensor. Geophys. 47,8: 1204-1214.

Ernst, T., 1981. A comparison of two methods of the transfer function calculation using the least-squares criterion in time and frequency domain. Publ. Inst. Geophys. Pol. Acad. Sci., G-2(143), 13-24.

Etheridge, M.A., V.J. Wall, R.H. Vernon, 1983. The role of the fluid phase during regional metamorphism and deformation. J. metamorphic Geol., 1: 205-226.

Everett, J.E. and Hyndman, R.D., 1967a. Geomagnetic variations and electrical conductivity structure in S.W. Australia, Phys. Earth. Planet. Int., 1, 24-34.

Everett, J.E. and Hyndman, R.D., 1967b. Magneto-telluric investigations in South-Western Australia, Phys. Earth. Planet. Int., 1, 49-54.

Ferrari, A., 1982. Note stratigrafiche sull'area veneto trentina (dal Triassico sup. ao Cretacico) In: A. Castellarin e G.B. Vai (a cura di), Guida alla geologia del Sudalpino centro-orientale. Guida Geol. Reg. S.G.I., 59-66, Bologna.

Filloux, J.H., 1977. Ocean floor magnetotelluric sounding over North Central Pacific. Nature 169, 297-301.

Fischer, G., 1982. Magnetotelluric observational techniques on land. Geophys. Surv. 4: 373-393.

Fischer, G. and Le Quang, B.V., 1981. An analytic one dimensional magnetotelluric inversion scheme. Geophys. J. Roy. astr. Soc., 67, 257-278.

Fitton, J.G. and Hughes, D.J., 1970. Volcanism and plate tectonics in the British Ordovician, Earth. Plan. Sci. Lett., 8, 223-228.

Fontes, S.L., Harinarayana, T., Dawes, G.W.K. and Hutton, V.R.S., 1987. Processing of noisy magnetotelluric data using digital filters and additional data selection criteria (to appear in Phys. Earth Planet. Int.).

Fontes, S.L. and Figueiredo, I., 1980. Comparacao espectral do campo geomagnetico em observatorios da America do Sul. Anais do XXXI Cong. Bras. Geol., Sta Catarina, Brasil.

Fontes, S.L. and Figueiredo, I., 1981. Analise espectral dos valores medios mensais do campo geomagnetico em Vassouras (Brasil), e Pilar, Trelew e La Quiaca (Argentina). 33ª Reun. Anual Soc. Bras. Progr. Cienc. (SBPC), Salvador, Brasil.

Fowler, R.A., Kolick, B.J. and Elliot, R.D., 1967. Polarization analysis of natural and artificially induced geomagnetic micropulsations. J. Geophys. Res. 72, 2871- 2883.

Fraser-Smith, A.C., 1981. Effects of man on geomagnetic activity and pulsations. Adv. Space Res. 1: 455-466.

Galson, D.A. and St Mueller, 1986. An introduction to the European geotraverse project: first results and present plans. Tectonophys. 126, 1-30.

Gamble, T.D., Goubau, W.M. and Clarke, J. 1979a. Magnetotellurics with a remote reference. Geophysics, 44, 1: 53-68.

Gamble, T.D., Goubau, W.M. and Clarke, J., 1979b. Error analysis for remote reference magnetotellurics. Geophysics. 47, 6: 932-937.

Gatto, G.O., Grandesso, P., Sarti, M. and Semenza, E., 1981. Foglio 22- Feltre. In A. Castellarin. Carta tettonica delli Alpi Meridionali (scala 1:200000), 85-90. Pubb 441., Progetto Finalizzato Geodinamica (S.P.5) C.N.R., Bologna.

Goldstein, M.A. and Strangway, D.W., 1975. Audio frequency magnetotellurics with a ground electric dipole source. Geophysics 40, 4: 669-683.

Giese, P., 1985. The structure of the upper lithosphere between the Ligurian sea and the Southern Alps. Part B: the consolidated crust and the uppermost mantle. Proceed. 2nd Workshop on the European geotraverse Project (EGT) (D.A. Galson and St. Mueller eds.), 143-154.

Gomes-Trevino, E., 1987. Should the electric line be straight in magnetotelluric surveys? Geophys. Prosp. 35, 920-923.

Goubau, W.M., Gamble, T.D. and Clarke, J., 1978. Magnetotellurics data analysis: removal of bias. Geophysics 43, 6: 1157-1166.

Goubau, W.M., Maxton, P.M., Koch, R.H., Clarke, J., 1984. Noise correlation lengths in remote reference magnetotellurics. Geophysics, 49, 4: 433-438.

Gough, D.I., 1986. Seismic reflectors, conductivity, water, and stress in the continental crust. Nature, 323: 143-144.

Gundel, A., 1977. Estimation of transfer function with reduced bias in geomagnetic induction studies. Acta Geod. Geophys. Mont. Acad. Sci. Hung. 12 (1-3), 345-352.

Haak, V. and Hutton, V.R.S., 1986. Electrical resistivity of continental lower crust; The nature of the lower continental crust, Geological Society special publication no. 24, 35-49.

Hampel, F.R., Ronchetti, E.M., Rousseeuw, P.J. and Stahel, W.A., 1986. Robust statistics- the approach based on influence functions. John Wiley and Sons, 502pp.

Harinarayana, T. and Sarma, S.V.S., 1982. Topographic effects on telluric measurements. Pageoph, 120, 778, 783.

Harinarayana, T., 1986. Distortion of telluric field mesurements near a hill using conformal mapping method. 8th Worshop on Electromagnetic Induction in the Earth and Moon, Neuchatel.

Harris, F.J., 1978. On the use of windows for harmonic analysis with discrete Fourier transform. Proc. IEEE 66, 11:51-83.

Heinrich, B. and Junge, A., 1984. The influence of geomagnetic variations on pipelines and an application for large-scale magnetotelluric depth sounding. J. of Geophys. 55. 31-36.

Herman, J.R., 1979. Electromagnetic ambients and man-made noise. Multi-volume EMC encyclopedia, vol. 3, Don White Consultants Inc., Virginia.

Hermance, J.F., 1973. Processing of magnetotelluric data. Phys. Earth Plan. Int., 7: 349-364.

Hermance, J.F., 1982. The assymptotic response of three dimensional basin offsets to magnetotelluric fields at long periods: The effect of current channeling Gephysics, 47, 1562-1573.

Hermance, J.F., 1983. Electromagnetic induction studies. Rev. Geophys. Space Phys. 21, 652-665.

Hermance, J.F. and Grillot, L.R., 1974. Constraints on temperature beneath Iceland from magnetotelluric data. Phys. Earth Planet. Int. 8, 1-12.

Hermance, J.F. and Pedersen, J., 1980. Deep structure of the Rio Grande rift: a magnetotelluric interpretation. J. Geophys. Res. 85: 3899-3912.

Hill, E.R.G., 1987. A magnetotelluric study in the Moine Thrust region of Northern Scotland. Ph.D. thesis, Univ. of Edinburgh, 197pp.

Hjelt, S.E., 1986. Regional studies in the 80's. 8th Workshop on Electromagnetic induction in the Earth and Moon. Neuchatel, Review papers, 1-25.

Hobbs, B.A., 1975. Analytical solutions to global and local problems of electromagnetic induction in the Earth. Phys. Earth and Pla. inter., 10, 250-261.

Hobbs, B.A., 1982. Automatic model finding for the one-dimensional magnetotelluric problem. Geophys. J. R. astr. Soc. 68, 253-264.

Hobbs, B.A. ,1987. Conductivity profiles from global data. PAGEOPH, 125, 2/3: 393-407.

Hohmann, G.W., 1971. Electromagnetic scattering by conductors in the earth near a line source of current. Geophysics, 36, 101-131.

Hohmann, G.W., 1983. Three- dimensional EM modeling. Geophys. Surveys 6, 27-53.

Hoogervorst, G.H.T.C., 1979. Geological information from fluctuating earth currents. Geophys. Prosp. 27: 214-232.

Hutton, V.R.S., 1976. The electrical conductivity of the Earth and planets. Rep. Prog. Phys. 39: 487-572.

Hutton, V.R.S., Dawes, G.J.K., Devlin, T. and Roberts, R., 1984. A broadband tensorial magnetotelluric study in the Travale- Radicondoli geothermal field - EEC report series. Contract no. EG-A2-031 U.K. Final report.

Hutton, V.R.S., Dawes, G.J.K, Ingham, M.R., Kirkwood, S. and Mbipom, E.W., 1981. Recent studies of time variations of natural electromagnetic studies in Scotland. Phys. Earth Plan. Int. 24, 66-87.

Hutton, V.R.S., Gough, D.I., Dawes, G.J.K. and Travassos, 1987. Magnetotelluric soundings in the Canadian Rocky mountains. Geophys. J. R. astr. Soc., 90, 245-263.

Hyong, L.V.Z. and Berdichevsky, M.N., 1984. Generalization of Schmucker method for interpreting MT sounding. Izvestiya 20, 162-166.

Ilkisik, O.M. and Jones, A.G., 1984. Statistical evaluation of MT and AMT methods applied to a basalt covered area in the Southeastern Anatolia, Turkey. Geophys. Prosp 32, 706-724.

Isikara, A.M., 1977. Solar cycle controlled variation of the geomagnetic field. Acta Geodaet. Geophys. et Montanist. Acad. Sci. Hung. 12: 397-405.

Italian Explosion Seismology Group, 1978. Preliminary interpretation of the profile HD across the Eastern Alps. Boll. Geof. teor. ed appl. XX, 79, 287-302.

Italian Explosion Seismology Group, 1981. Crust and mantle structures in the Southern Alps from deep seismic wave depression analysis. Boll. Geof. teor. ed appl. XIII, 92, 297-330.

Ingham, M.R., 1988. The use of invariant impedances in magnetotelluric interpretation. Geophysical Journal, 92,1, 165-169.

Jackson, D.D., 1972. Interpretation of insufficient and inconsistent data. Geophys. J. R. astr. Soc. ,28, 97-109.

Jackson, D.D., 1973. Marginal solutions to quasi-linear inverse problems in geophysics: The Edgehod Method. Geophys. J. R. astr. Soc., 35, 121-136.

Jacobs, J.A., 1970. Geomagnetic micropulsations, Springer-Verlag, New York.

Jenkins, G.M. and Watts, D.G., 1968. Spectral analysis and its applications. Holden- Day.

Jiracek, G.R., Gustafson, E.P. and Mitchell, P.S. , 1983. Magnetotelluric results opposing magma origin of crustal conductors in the Rio Grande rift. Tectonophysics 94, 299-326.

Jiracek, G.R., Rodi, W.L. and Vanyan, L.L., 1986. Implications of magnetotelluric modelling for the deep crustal conductor in the Rio Grande Rift. Phys. Earth Plan. Int., in press.

Jodicke, H., Untiedt, J., Oglemann, W., Schulte, L. and Wagenitz, V., 1983. Electrical conductivity structure of the crust and upper mantle beneath the Rhenish Massif, Plateaus uplift (edited by K. Fuchs et al), Springer-Verlag, Berlin, 288-302.

Jones, A.G., 1977. Geomagnetic induction studies in Southern Scotland. Ph.D. thesis, University of Edinburgh.

Jones, A.G., 1979. On the difference between polarization and coherence. J. Geophys. 45, 223-229. fields by conductivity anomalies, Geophys. J. R. astr. Soc., 20, 317-334.

Jones, A.G., 1987a. MT and reflection: an essential combination. Geophys. J. R. astr. Soc., 89, 7-18.

Jones, A.G. and Hutton, V.R.S., 1979. A multi-station magnetotelluric study in Southern Scotland. II- Monte Carlo inversion of the data and its geophysical and tectonic implications. Geophys. J. Roy. astr. Soc., 56, 351-368.

Jones, A.G., 1987b. Static shift of magnetotelluric data and its removal in a sedimentary basin environment. (submitted to Geophysics)

Jones, A.G., 1983. On the equivalence of the Niblett and Bostick transformations in the magnetotelluric method. J. Geophys., 53, 72-73.

Jones, F.W. and Kelly, A.M., 1966. Man-made telluric micropulsations. Can. J. Phys. 44: 3025-3031.

Johnston, M.J.S., 1987. Tectonomagnetism and Tectonoelectricity. Rev. of geophys. 25, 5: 983-988.

Jones, F.W., 1973. Induction in laterally non- uniform conductors: theory and numerical models. Phys. Earth Planet. Int. 7, 282-293.

Jones, F.W. and Pascoe, L.J., 1971. A general computer program to determine the penetration of alternating electric currents in a two- dimensional model of a region of uniform conductivity with an embedded inhomogeneity. Geophys. J. R. astr. Soc. 24, 3-30.

Jupp, D.L.B., 1978. Estimation of magnetotelluric impedance functions. Phys. Earth Planet. Int. 17: 75-82.

Jupp, D.L.B. and Vozoff, K., 1975. Stable iterative methods for the inversion of geophysical data. Geophys. J. R. astr. Soc., 42: 957-976.

Jupp, D.L.B. and Vozoff, K., 1976. Discussion on: 'The magnetotelluric method in the exploration of sedimentary basins by Keeva Vozoff (1972), Geophysics, 41, 325-328.

Jupp, D.L.B. and Vozoff, K., 1977. Two-dimensional magnetotelluric inversion. Geophys. J. R. astr. Soc., 50: 333-352.

Kaikkonen, P., 1977. A finite element program package for eletromagnetic modeling. J. Geophys., 43: 179-192.

Kaikkonen, P., 1983. Two- dimensional finite element modelling in magnetotellurics. In 'The development of the deep geolectric model of the Baltic shield. Part I- Numerical methods. (Hjelt, S.E. and Vanyan, L.L. eds.) Dep. of Geophysics, Univ. of Oulu, report 7.

Kanasewich, E.R., 1985. Time sequence analysis in Geophysics. Third edition. Univ. of Alberta Press., 480pp.

Kao, D.W., Rankin, D., 1977. Enhancement of signal-to-noise ratio in magnetotelluric data. Geophysics, 42, 1: 103-110.

Kao, D., Orr, D., 1982. Magnetotelluric studies in the Market Weighton area of eastern England. Geophys. J. R. astr. Soc., 70: 323-327.

Kaufman, A.A. and Keller, G., 1981. The magnetotelluric sounding method. Elsevier, 595pp.

Keller, G.V. and Frichkneckt, 1970. Electrical methods in geophysical prospecting. Pergamon Press, Oxford.

Keilis-Borok, V.I. and Yanoskaya, T.B., 1967. Inverse problems in seismology. (structural review). Geophys. J. R. astr. Soc. 13, 223-234.

Kerrich, R., La Tour, T.E. and Willmore, L., 1984. Fluid participation in deep fault zones: evidences from geological, geochemical and $^{18}O/^{16}O$ relations. J. Geophys. Res. 89,B6, 4331-4343.

Kissling, E., St. Mueller and Werner, D., 1983. Gravity anomalies, seismic structure and geothermal history of the Central Alps. Annal. Geophysicae 1, 1: 37-46.

Kleiner,B. and Graedel, T.E., 1980. Exploratory data analysis in geophysical sciences. Rev. Geophys. Space. Phys. 18, 3; 699-717.

Kovaleskiy, I.V., Mikerina, N.V., Novysh, V.V. and Gorodnicheva, O.P., 1961. Distribution of the earth currents from an electrified railroad in the Southern Urals. Geomag. Aeron., 1, 5: 723-726.

Krasnobaya, A.G., D'Yakonov, B.P., Astaf'yev, P.F., Batalova, O.V., Vishnev, V.S., Gavrilova, I.E., Zhuravleva, P.B. and Kirillov, S.K., 1981. Electromagnetic experiments on the Baltic shield. Izvestiya Earth Phys. 17, 439-444.

Kroger, P., Michell, H.J. and Elsner, R., 1983. Comparison of errors in local and reference estimates of the magnetotelluric impedance tensor. J. Geophys. 52, 97-105.

Kisak, E. and Silvester, P., 1975. A finite element program package for magnetotelluric modelling. Comput. Phys. Comm. 10, 421-433.

Ku, C.C., Hsieh, M.S. and Lim, S.H., 1973. The topographic effect in electromagnetic fields. Can. J. Earth Sci. 10: 645-650.

Lambert, I.B. and Wyllie, P.J., 1970. Melting in the deep crust and upper mantle and the nature of the low velocity layer. Phys. Earth Planet. Int. 3, 316-322.

Lanczos, C., 1958. Linear systems in self-adjoint form. Am. math. Montlhly, 65, 665-679.

Lanczos, C., 1961. Linear differential operators. p124. D. Van Nostrand, London.

Larsen, J.C., 1975. Low frequency (0.1-6.0 cpd) electromagnetic study of deep mantle electrical conductivity beneath the Hawaiian Islands. Geophys. J. R. Astron. Soc. 43, 17-43.

Larsen, J.C., 1977. Removal of local surface conductivity effects from low frequency mantle response curves. Acta Geod., Geophys. Mont. Acad. Sci. Hung., 12(1-3): 183-186.

Larsen, J.C., 1980. Electromagnetic response functions from interrupted and noisy data. J. Geomag. Geoelect. 32, Suppl I: 89-103.

Larsen, J.C., 1981. A new technique for layered earth magnetotelluric inversion. Geophysics, 46, 9: 1247-1257.

Laubscher, H.P., 1974a. Evoluzione e struttura delle Alpi. Le Science (ed. ital. of Scientific American) 72, August.

Laubscher, H.P. ,1974b. The tectonics of subduction in the Alpine system. memorie della Societa geologica Italiana, Vol XIII, suppl. 2, 275-283.

Laubscher, H.P., 1983. Detachment, shear and compression in the Central Alps. In 'Tectonics of mountains chains'. (R. Hatcher ed.), Geol. Soc. Amer. mem. 158, 191-211.

Laubscher, H.P., 1985. The tectonics of the Western and Southern Alps: correlation between surface observations and deep structure. Proceed. 2nd Workshop on the European Geotraverse (EGT) Project. Europ. Sci. Found. 9, 93-102.

Laubscher, H. P. and Bernoulli, D., 1982. History and deformation of the Alps. In 'Mountain building processes'. (K.J. Hsu ed.), Academic Press, 169-180.

Levinson, H., 1947. The Wiener RMS error criterion in filter design and prediction. J. Math. Physic. 25, 261-278.

Lienert, B.R., 1980. The effect of source field polarisation on estimates of the magnetotelluric impedance tensor. Geophys., 45, 1803-1812.

Lines, L.R. and Jones, F.W., 1973. The perturbation of alternating geomagnetic fields by three-dimensional island structures, Geophys. J.R. astr. Soc., 32, 133-154.

Lines, L.R. and Treitel, S., 1984. Tutorial: A review of least squares inversion and its application to geophysical problems. Geophys. Prospec. 32, 159-186.

Linington, R.E., 1974. The magnetic field disturbances caused by DC electrical railways. Prospezioni Archeolog. 9: 9-20.

Livelybrooks,D.W., 1986. Modelling earth resistivity structure for MT data: a comparison of rotationally- invariant and conventional earth response functions. Contributed paper at 'Fall AGU', San Francisco- USA.

Macbain, J.A. and Bednar, J.B., 1986. Existence and uniqueness properties of the one-dimensional magnetotellurics problem. J. Math. Phys. 27, 645-649.

Macnae, J.C. and Lamontagne, Y. and West, G.F., 1985. Noise processing techniques for time- domain EM systems. Geophysics 49, 7: 934-948.

Madden, T.R., 1972. Transmission systems and network analogies to geophysical forward and inverse problems. Tech. Rep. no. 72-3, Dept. of Earth and Planetary Sciences, MIT.

Marchisio, G.B. and Parker, R.L., 1984. Exact nonlinear inversion of electromagnetic soundings. EOS 64, 692.

Marple, L., 1980. A new autoregressive spectrum analysis algorithm: IEEE Trans. Acoust. Speech and Signal Proc., ASSP, 28, 441-455.

Marquardt, D.W., 1963. An algorithm for least squares estimation of non-linear parameters, J. Geophys. Res., 67, 1907-1918.

McMechan, G.A. and Barrodale I., 1985. Processing of electromagnetic data in the time domain. Geophys. J. Roy. astr. Soc., 81, 277-293.

Mckerrow, W.S., Leggett, J.K. and Eales, M.H. 1977. Imbricate thrust model of the Southern Uplands of Scotland. Nature, 267,237-239.

McKirdy, D.M. and Weaver, 1984. Induction in a thin sheet of variable conductance at the surface of a stratified Earth, I. Two- dimensional theory. Geophys. J. R. astr. Soc. 78, 93-103.

Mckirdy, D.McA., Weaver, J.T. and Dawson, T.J. 1985. Induction in a thin sheet of variable conductance at the surface of a stratified earth-II. Three dimensional theory. Geophys. J. Roy. astr. Soc., 80, 177-194.

Menvielle, M. and Szarka, L., 1986. Distortions of electromagnetic fields: topographic and man- made. Rev. pap. 8th Worshop on Electromagnetic Induction in the Earth and Moon, Neuchatel.

Mikerina, I.A., 1962. Study of interference at the Voyeykovo magnetic observatory. Geomag. Aeron. 2(6), 941-944.

Morelli, C., 1975. The gravity map of Italy. In: Structural model of Italy. L. Ogniben, M. Parroto and A. Praturton (eds.). Quaderno de la Ricerca Scientifica , 90, CNR, 427-449.

Morelli, C., 1985. Regional gravity anomalies in the area of the southern segment. Proceedings of the 2nd workshop on the European Geotraverse (EGT) Project- The southern segment. D.A. Galson and St. Mueller (eds.), Eur. Sc. Found., 53-58.

Muller W. and Losecke W., 1975. Accelerating convergence techniques and grid spacing problems in two dimensional magnetotelluric modelling. Geophys. J. Roy. astr. Soc., 41, 185-191.

Nabetani S., Rankin D., 1969. An inverse method of magnetotelluric analysis for a multilayered Earth. Geophys. 34, 75-86.

Niblett, E.R. and Sayn-Wittgenstein, C., 1960. Variations in electrical conductivity with depth by the magneto-telluric method, Geophysics, 25, 998-1008.

Nienaber, W., Dosso, H.W., Law, L.K., Jones, F.M. and Ramaswamy, V., 1979. An analogue model study of electromagnetic induction in the Vancouver Island region. J. Geomagn. Geolectr. 31, 115-132.

Nobes, D.C., 1986. The inclusion of anisotropy in Maxwell's equations. Geophys. J.R. astr. Soc. 85, 655-662.

Oldenburgh, D.W., 1979. One-dimensional inversion of natural source magnetotelluric observations. Geophysics, 44, 7: 1218-1244.

Oldenburgh, D.W., Whittall, K.P. and Parker R.L., 1984. Inversion of ocean bottom magnetotelluric data revisited. J. Geophys. Res., 89, 1829-1833.

Olhoeft, G.R., 1981. Electric properties of granites with implications for the lower crust. J. Geophys. Res. 86, 931-936.

Park, J. and Chave, A.D., 1984. On the estimation of magnetotelluric response functions using the singular value decomposition. Geophys. J. R. astr. Soc., 77: 683-709.

Park, S.K., 1985. Distortion of magnetotelluric sounding curves by three dimensional structures. Geophysics 50, 785-797.

Park, S.K., Orange, A.S. and Madden, T.R., 1983. Effects of three- dimensional structures on magnetotelluric sounding curves. Geophysics 48, 10: 1402-1405.

Parker, R.L. 1980. The inverse problem of electromagnetic inversion: existence and construction of solutions based on incomplete data. J. Geophys. Res. 85, 4421- 4428.

Parker, R.L., 1983. The magnetotelluric inverse problem. Geophys. Surv., 6: 5-25.

Parker, R.L., 1977. Understanding inverse theory. Ann. Rev. Earth Planet. Sci., 5: 35-64.

Parker, R.L., 1970. The inverse problem of electrical conductivity in the mantle, Geophys. J. R. astr. Soc., 22, 121-138.

Parkinson, W.D., 1962. The influence of continents and oceans on geomagnetic variations, Geophys. J. R. astr. Soc., 6, 441-449.

Parkinson, W.D., 1983. Introduction to Geomagnetism. Scottish Academic Press, Edinburgh, 438pp.

Parzen, E., 1976. Some recent advances in time series modelling. IEEE Trans. Automat. Control AC-19, 720-723.

Petiau, G. and Dupis, A. , 1980. Noise, temperature coefficient and long time stability of electrodes for telluric observations. Geophys. Prosp., 28, 792-804.

Pedersen, L.B., Svennekjaer, M., 1984. Extremal bias coupling in magnetotellurics. Geophysics, 49, 11: 1968-1978.

Pedersen, L.B., 1982. The magnetotelluric impedance tensor - its random and bias errors. Geophys. Prosp., 30: 188-210.

Pedersen, L.B., 1986. Some aspects of magnetotelluric field procedures. 8th Workshop on Electromagnetic Induction in the Earth ana Moon. Neuchatel.

Poehls, K.A. and Von Herzen, 1976. Electrical resistivity structure beneath the north-west Atlantic ocean. Geophys. J. R. Astr. Soc. 47: 331-346.

Price, A.T., 1950. Electromagnetic induction in a semi-infinite conductor with a plane boundary, Quart. J. Mech. Appl. Maths., 3, 385-410.

Price, A.T., 1962. The theory of magnetotelluric fields when the source field is considered, J. Geophys. Res., 67, 1907.

Price, A.J., 1963. A note on the interpretation of the magnetic variations and magnetotelluric data. J. Geomag. Geoelec., 15, 4, 241-248.

Pridmore, D.F., Hohmann, G.W., Ward, S.H. and Sill, W.R., 1981. Investigation of finite element modelling for electrical and electromagnetic data in three dimensions. Geophysics, 44, 1009-1024.

Progetto Finalizzato Geodinamica, 1982. Evoluzione neotettonica deli' Italia Nord- Orientale. Memorie di Scienze Geologiche, Univ. di Padova, vol XXXV, 335-376.

Raiche, A.P., 1974. An integral equation approach to three dimensional modelling. Geophys. J. Roy. Soc., 36, 363-376.

Rankin, D., 1962. The magnetotelluric effect of a dike. Geophysics, 27: 666-676.

Ranganayaki, R.P., 1984. An interpretive analysis of magnetotelluric data. Geophys., 49, 1730-1748.

Ranganayaki, R.P. and Madden, T.R., 1980. Generalized thin sheet analysis in magnetotellurics: an extension of Price's analysis. Geophys. J. R. astr. Soc. 60, 445-457.

Reddig, R.P. and Jiracek, 1984. Topographic modelling and correction in magnetotellurics. Extended abstract to the 54th SEG, Atlanta, USA.

Reddy, I.K. and Rankin, D., 1972. On the interpretation of magnetotelluric data in the plains of Alberta. Can. J. Earth Sci., 9, 514-527.

Reddy, I.K. and Rankin, D., 1973. Magnetotelluric response of a two-dimensional sloping contact by finite element method, Pure Appl. Geophysics, 105, 847.

Reddy, I.K. and Rankin, D., 1975. Magnetotelluric response of laterally inhomogeneous and anisotropic media. Geophys. 40, 6: 1035-1045.

Reddy, I.K., Rankin, D. and Phillips, R.J., 1977. Three- dimensional modelling in magnetotelluric and magnetic variational sounding. Geophys. J.R. astr. Soc. 51, 313-325.

Richmond, A.D. and Baumjohann, W., 1983. Three dimensional analysis of magnetometer array data. J. Geophys. 54, 138-156.

Rikitake, T. 1975, A model of the Geoelectric structure beneath Japan, J.G.G., 27, 233-244.

Roberts, R., 1983. Electromagnetic evidence for lateral inhomogeneities within the Earth's upper mantle. Phys. Earth Plan. Int. 33, 198- 212.

Robinson, E.R., 1964. Recursive decomposition of stochastic processes. In H.O. Wold (editor), Econometric model Building, North- Holland, Amsterdam, pp. 111-168.

Robinson, E.R., 1967. Statistical communication and detection. Hafner, new York, N.Y. 362pp.

Rokityansky, I.I., 1982. Geoelectromagnetic investigation of the Earth's crust and mantle. Springer-Verlag, Berlin, 381pp.

Rooney, D. and Hutton, V.R.S., 1977. A magnetotelluric and magnetovariational study of the Gregory Rift Valley, Kenya, Geophys. J. Roy. Soc, 51, 91-119.

Rooney, D., 1976. Magnetotelluric measurements across the Kenyan Rift Valley. Ph. D. thesis, Univ. of Edinburgh, U.K., 206pp.

Rousseeuw, P.J., 1984. Least median of squares regression. J. Am. Statist. Assoc. 79, 871-880.

Rousseeuw, P.J. and Leroy, A.M., 1987. Robust regression and outlier detection. John Wiley and Sons, 314pp.

Russell, B., 1946. History of western philosophy: George and Unswin, Ltd. (cited by Constable et al ,1987)

Sandberg, S.K. and Hohmann, 1982. Controlled- source audiomagnetotellurics in geothermal exploration. Geophysics, 47, 1: 100-116.

Saito, T., 1969. Geomagnetic pulsations. Space Sci. Rev. 10, 320-412.

Schmucker, U., 1970. Anomalies of geomagnetic variations in the southwestern United States, J. Geomag. Geoelec., 15, 193-221.

Schmucker, U., 1974. Erdmagnetische Tiefensondierung mit Langperioschen Variationen. Prot. Koll. Erdmagn. Tiefensondierung, Grafrath, pp.313-343.

Schmucker, U., 1987. Substitute conductors for electromagnetic response estimates. PAGEOPH 125, 2/3: 341-367.

Schnegg, P.A. and Fischer, G., 1984. A new pulsed audiomagnetotelluric technique. J. Geophys. 55: 191-198.

Schnegg, P.-A., Le Quang, B. and Fischer, G. 1980. Management and processing of MT data in the field with a microprocessor. 5th Workshop on Electromagnetic Induction in the Earth and Moon. Istanbul.

Schnegg, P.-A., Fischer, G., Fontes, S.L, Hutton, V.R.S. and Finzi, E., 1986. The effect of DC railways on MT measurements in Northen Italy. 8th Workshop on Electromagnetic Induction in the Earth and Moon. Neuchatel.

Schwarz, G., Haak, V., Martinez,E., Bannister,J., 1984. The electrical conductivity of the Andean crust in northern Chile and Southern Bolivia as inferred from magnetotelluric measurements. J. Geophys., 55: 169-178.

Schwendner, H. and St. Mueller, 1985. New evidence of a density anomaly in the upper mantle below the Southern Alps. Proceedings of the secondworkshop on the European Geotraverse (EGT) Project- The southern segment. D.A. Galson and St. Mueller (eds.), Eur. Sc. Found., 115-120.

Shankland, T.J., Ander, M.E., 1983. Electrical conductivity, temperatures, and fluids in the lower crust. J. Geophys. Res., 88, B11: 9475-9484.

Shankland, T.J., O'Connell, R.J. and Waff, H.S., 1981. Partial melting and electrical conductivity anomalies for the upper mantle. Rev. Geophys., 19, 394-406.

Silvia, M.T. and Robinson, E.R., 1979. Deconvolution of geophysical time series in the exploration for oil and natural gas. Elsevier, Amsterdam, 251pp.

Silvester P. and Haslam C.R.S., 1972. Magnetotelluric modelling by the finite element method. Geophys. pros. 20, 872-891.

Sims, W.E., Bostick, F.X. Jr., 1969. Methods of magnetotelluric analysis. Tech. Rep. 58, Univ. of Texas at Austin.

Sims, W.E., Bostick, F.X. Jr., and Smith, H.W., 1971. The estimation of magnetotelluric impedance tensor elements from measured data. Geophysics, 36, 5: 938-942.

Sommerfeld, A., 1964. Partial differential equations in physics: New York, Academic Press Inc.

Smith, B.D. and Ward, S.H., 1974. On the computation of polarisation ellipse parameters. Geophys., 36, 938-942.

Smith, J.T. and Booker, J.R., 1986. MT inversion for minimum structure. Geophysics, in press.

Smith and Shano, 1971. An improved Marquadt procedure for nonlinear regressions. Tectonometrics 13, 67-75.

Srivastava, S.P., 1965. Method of interpretation of magneto-telluric data when source field is considered, J. Geophys. Res., 70, 945-954.

Stanley, W.D., 1984. Tectonic study of Cascade Range and Columbia Plateau in Washington State based upon magnetotelluric soundings. J. Geophys. Res. 89,B6, 4447-4460.

Sternberg B.K., Washburne, J.C. and Anderson, R.G., 1985. Investigation of MT static shift correction methods. Contributed paper at 55th SEG, held in Houston, Texas on 2-6 Nov.

Stodt, J.A., 1983. Noise analysis for conventional and remote reference magnetotelluric data. Ph. D. thesis, The University of Utah.

Strangway, D.W., Swift, C.M.(Jr.) and Holmer, R.C., 1973. The application of audiofrequency magnetotellurics (AMT) to mineral exploration. Geophysics, 38, 1159-1175.

Sule P.O., 1985. A broad band magnetotelluric investigation in Southeast Scotland. Ph.D. thesis, University of Edinburgh, 302pp.

Swift, C.M., 1967. A magneto-telluric investigation of an electrical conductivity anomaly in the south-western United States, Ph.D. Thesis, Department of Geology & Geophysics, M.I.T., Cambridge, Massachusetts.

Swift, C.M., 1971. Theoretical magnetotelluric and Turan response from two-dimensional inhomogeneities, Geophysics, 36, 38-52.

Szarka, L., 1983. Exploration of high resistivity basement using electric and magnetic fields of quasi-static point sources. Geophys. Prospect. 31, 829-839.

Thayer, R.E., 1975. Topographic distortion of telluric currents: a simple calculation. Geophysics, 40, 1: 91-95.

Tikhonov, A.N., 1950. On investigation of electrical characteristics of deep strata of Earth's crust (in Russian). Dokl. Akad. Nauk. SSSR, 73: 295-297 (cited by Rokityansky, 1982).

Ting, S.C., G.W. Hohmann, 1981. Integral equation of the three-dimensional magnetotelluric response. Geophysics, 46, 2: 182-197.

Travassos, J.M., 1987. Investigations of the Analysis and Modelling of Magnetotelluric data. Ph.D. thesis, University of Ediburgh, 219pp.

Twomey, S., 1977. Introduction to the mathematics of inversion in remote sensing. In Developments in Geomathematics 3, Elsevier, 243pp.

Ulrych, T.J. and Clayton, R.W., 1976. Time series modelling and maximum entropy. Phys. Earth Planet. Int. 12: 188-200.

Valiant, M.J., 1976. N.E.R.C. (Natural Environmental Research Council) geologger technical handbook, IGS magnetic observatory, Hartland.

Vasseur, G. and Weidelt, P., 1977. Bimodel electromagnetic induction in non-uniform thin sheets with an application to the northern pyrenean induction anomaly. Geophys. J. Roy. astr. Soc. 51, 669-690.

Vozoff, K., 1972. The magnetotelluric method in the exploration of sedimentary basins. Geophysics, 37, 1: 98-141.

Vozoff, K. and Jupp, D.L.B., 1975. Joint inversion of geophysical data, Geophys. J.R. astr. Soc., 42, 977-999.

Wait, J.R., 1954. On the relationship between telluric currents and the earth's magnetic field, Geophysics, 19, 281-289.

Wannamaker, P.E., Hohmann, G.W. and Ward, S.W., 1984. Magnetotelluric responses of three dimensional bodies in layered earths. Geophysics 49, 1517-1533.

Wannamaker, P.E., Stodt, J.A. and Rijo, L., 1986. Two-dimensional topographic responses in magnetotellurics modelled using finite elements. Geophysics, 51, 11: 2131-2144.

Wannamaker, P.E., Hohmann, G.W., San Filipo, W.A., 1984. Electromagnetic modelling of three dimensional bodies in layered earths using integral equations. Geophysics, 49, 60-74.

Wannamaker, P.E., Stodt, J.A. and Rijo, L., 1985. Finite element program for solution of magnetotelluric responses of two dimensional earth resistivity structure, Program documentation, Univ. of Utah., Research Institute Report ESL- 158.

Wannamaker, P.E., Stodt, J.A. and Rijo, L., 1987. A stable finite element solution for two dimensional magnetotelluric modelling. Geophys. J. R. astr. Soc. 88, 277-296.

Ward, S.H., 1983. controlled source electrical method for deep exploration. Geophys. Surv. 6, 137-152.

Weaver, J.T., 1963. The electromagnetic field within a discontinuous conductor with reference to geomagnetic pulsations near a coastline. Can. J. Phys. 41, 484-495.

Weaver, J.T., C.R. Brewitt-Taylor, 1978. Improved boundary conditions for the numerical solution of E-polarization problems in geomagnetic induction. Geophys. J. R. astr. Soc., 54: 309-317.

Weaver, J.T., 1973. Induction in a layered plane earth by uniform and non-uniform source fields. Phys. Earth Plant. Int., 7, 266-281.

Weidelt, P., 1975. Eletromagnetic induction in three-dimensional structures. J. Geophys., 41: 85-109.

Weidelt, P., 1972. The inversion problem of Geomagnetic induction, Zeitschrift fur Geophysik, 38, 257-289.

Weidelt P., 1986. Discrete frequency inequalities for magnetotelluric impedances of one-dimensional conductors. J. Geophys., 59, 171-176.

White, R.E., 1973. The estimation of signal spectra and related quantities by means of the multiple coherence function. Geophys. Prosp. 21: 660-703.

Windley, B.F., 1977. The Evolving continents. John Wiley and Sons, 385pp.

Wiggins, R.A. Miller, S.P., 1972. New noise-reduction technique applied to long period oscillations from the Alaskan earthquake. Bull. Seismol. Soc. Am. 62: 471-479.

Wieladek, R. and Ernst, T., 1977. Application of method of least squares to determining impulse reponses and transfer functions. Publ. Inst. Geophys. Pol. Acad. Sci., G-1(110), 3-12.

Word, D.R., Smith, H.W. and Bostick, F.X. Jr., 1971. Crustal investigations by the magnetotelluric tensor impedance method. In Heacock, J.G. (Ed). The structure and physical properties of the Earth's crust. Am. Geophys. Union Geophys. Monograph 4, 145-167.

Yanagihara, K., 1979. Magnetic field disturbance produced by electric railway. Mem. Kakioka Magnetic Observatory 38: 17-36.

Yegorov, I.V., Chernyak, E.L., Palshin, N.A., Demidova, T.A. and Kaikkonen, P., 1983. Numerical thin sheet modelling of the telluric field distortions by the hybrid technique, I. Theory and an example for the Baltic Shield. Phys. Earth Planet. Int. 33, 56-63.

Zhang, P., Roberts, R.G. and Pedersen, L.B., 1987. Magnetotelluric strike rules. Geophysics 52, 3:267-278.

Zhdanov, M.S. and Golubev, N.G., 1983. Use of finite functions method for the solution of the 2D problem. J. Geomag. Geoelectr. 35, 747-766.

Appendix A– Summary of the parameter sensitivity analysis (1D models using the 2nd order Marquadt scheme) for all the sites in the Asiago area. The analysis includes the models for the rotationally invariant , the E pol and the H pol response curves.

SUMMARY 1D RESULTS WEIGHTED 2ND ORDER MARQUADT
N.ITALY LONGARA 455A INVARIANT

NORMALIZED SINGULAR VALUES OF JACOBIAN

0.100E+01 0.753E+00 0.415E+00 0.214E+00 0.126E+00 0.558E-01 0.275E-01

NUMBER OF EFFECTIVE PARAMETERS: 6.982

SCALE FACTOR : 0.1525497E+00

DAMPING FACTORS (1.0 PERCENT LEVEL)

0.100E+01 0.100E+01 0.100E+01 0.100E+01 0.100E+01 0.999E+00 0.983E+00

PARAMETER SPACE EIGENVECTORS (V MATRIX)

1	0.080	-0.302	0.888	-0.145	0.303	-0.034	0.016
2	0.542	0.155	-0.287	-0.204	0.735	-0.122	0.057
3	0.097	0.116	0.110	0.680	0.008	-0.580	0.408
4	-0.004	0.001	0.004	0.169	0.112	0.689	0.696
5	0.627	-0.674	-0.150	0.114	-0.336	0.055	-0.022
6	-0.544	-0.645	-0.306	0.058	0.403	-0.153	0.072
7	-0.026	-0.035	-0.046	-0.656	-0.281	-0.383	0.583

LAYER RESISTIVITIES

I	RO(I)	BOUND(1)	BOUND(2)	DAMPING
1	1399.8459	891.3872	2198.3357	0.0000
2	177.0211	78.3612	399.8979	0.0001
3	1914.4983	291.5100	12573.5078	0.0032
4	9980.0312	777.9941	128022.8125	0.0088

LAYER DEPTHS (TO BASE)

I	Z(I)	BOUND(1)	BOUND(2)	DAMPING
1	1657.7913	1057.4971	2598.8455	0.0000
2	3917.5037	1914.1455	8017.5898	0.0001
3	25884.2148	2938.8015	227981.5625	0.0060

SUMMARY 1D RESULTS WEIGHTED 2ND ORDER MARQUADT
N.ITALY V. DI NOS 690A INVARIANT

NORMALIZED SINGULAR VALUES OF JACOBIAN

0.100E+01 0.235E+00 0.116E+00 0.112E+00 0.227E-01 0.578E-02 0.673E-03

NUMBER OF EFFECTIVE PARAMETERS: 5.064

SCALE FACTOR : 0.4792118E+00

DAMPING FACTORS (1.0 PERCENT LEVEL)

0.100E+01 0.100E+01 0.100E+01 0.100E+01 0.964E+00 0.100E+00 0.205E-04

PARAMETER SPACE EIGENVECTORS (V MATRIX)

1	0.020	-0.029	0.377	0.924	0.030	-0.049	0.003
2	-0.146	-0.028	-0.024	-0.043	0.091	-0.976	0.121
3	-0.008	-0.011	0.010	0.002	-0.135	0.110	0.985
4	-0.012	-0.021	0.922	-0.379	0.076	0.004	0.001
5	-0.650	0.755	0.023	0.032	-0.016	0.071	-0.007
6	0.745	0.653	0.022	-0.011	-0.016	-0.129	0.025
7	-0.014	-0.027	0.078	-0.006	-0.983	-0.106	-0.124

LAYER RESISTIVITIES

I	RO(I)	BOUND(1)	BOUND(2)	DAMPING
1	1842.2087	1383.3735	2453.2295	0.0013
2	25.7372	16.3718	40.4601	0.7952
3	3950.7812	3355.0088	4652.3477	0.8685
4	772.9080	568.7212	1050.4033	0.0003

LAYER DEPTHS (TO BASE)

I	Z(I)	BOUND(1)	BOUND(2)	DAMPING
1	2042.3796	1791.3506	2328.5859	0.0026
2	2506.5471	2177.7178	2885.0286	0.0086
3	10492.5742	4152.4414	26513.0859	0.0488

SUMMARY 1D RESULTS WEIGHTED 2ND ORDER MARQUADT
N.ITALY S. ANTONIO 450A INVARIANT

NORMALIZED SINGULAR VALUES OF JACOBIAN

0.100E+01 0.667E+00 0.538E+00 0.136E+00 0.294E-01

NUMBER OF EFFECTIVE PARAMETERS: 4.987

SCALE FACTOR : 0.1906872E+00

DAMPING FACTORS (1.0 PERCENT LEVEL)

0.100E+01 0.100E+01 0.100E+01 0.100E+01 0.987E+00

PARAMETER SPACE EIGENVECTORS (V MATRIX)

1	0.012	-0.324	0.938	-0.125	0.010
2	-0.235	0.388	0.018	-0.886	0.093
3	0.000	0.039	0.019	0.122	0.992
4	-0.963	-0.209	-0.039	0.162	-0.011
5	0.128	-0.836	-0.344	-0.398	0.088

LAYER RESISTIVITIES

I	RO(I)	BOUND(1)	BOUND(2)	DAMPING
1	851.3687	708.6011	1022.9006	0.0000
2	39.8250	22.9880	68.9939	0.0001
3	707.0359	117.1829	4265.9766	0.0130

LAYER DEPTHS (TO BASE)

I	Z(I)	BOUND(1)	BOUND(2)	DAMPING
1	1341.9683	1151.6938	1563.6782	0.0000
2	2483.8542	1641.3669	3758.7761	0.0001

SUMMARY 1D RESULTS WEIGHTED 2ND ORDER MARQUADT
N.ITALY OBSERVATORIO 451A INVARIANT

NORMALIZED SINGULAR VALUES OF JACOBIAN

0.100E+01 0.853E+00 0.157E+00 0.344E−02 0.302E−04

NUMBER OF EFFECTIVE PARAMETERS: 3.014

SCALE FACTOR : 0.2074382E+00

DAMPING FACTORS (1.0 PERCENT LEVEL)

0.100E+01 0.100E+01 0.100E+01 0.139E−01 0.000E+00

PARAMETER SPACE EIGENVECTORS (V MATRIX)

1	0.169	0.980	0.101	−0.001	0.000
2	−0.153	−0.075	0.985	−0.016	0.000
3	0.000	0.000	0.000	0.008	1.000
4	−0.974	0.182	−0.137	0.002	0.000
5	0.001	0.000	−0.016	−1.000	0.008

LAYER RESISTIVITIES

I	RO(I)	BOUND(1)	BOUND(2)	DAMPING
1	225.9845	205.5268	248.4785	0.0000
2	17.2787	12.5702	23.7509	0.0001
3	1140.1777	1138.3071	1142.0510	0.9998

LAYER DEPTHS (TO BASE)

I	Z(I)	BOUND(1)	BOUND(2)	DAMPING
1	848.6562	768.0918	937.6707	0.0000
2	3215.3696	2635.3628	3923.0276	0.9790

SUMMARY 1D RESULTS WEIGHTED 2ND ORDER MARQUADT
N.ITALY AVE 453A INVARIANT

NORMALIZED SINGULAR VALUES OF JACOBIAN

0.100E+01 0.734E-01 0.514E-01 0.165E-01 0.406E-03

NUMBER OF EFFECTIVE PARAMETERS: 3.878

SCALE FACTOR : 0.1466648E+01

DAMPING FACTORS (1.0 PERCENT LEVEL)

0.100E+01 0.100E+01 0.999E+00 0.880E+00 0.271E-05

PARAMETER SPACE EIGENVECTORS (V MATRIX)

1	0.000	-0.068	-0.997	-0.033	0.005
2	-0.075	0.015	0.005	-0.008	0.997
3	-0.011	0.036	-0.035	0.999	0.007
4	-0.664	-0.745	0.050	0.022	-0.039
5	0.744	-0.663	0.045	0.033	0.066

LAYER RESISTIVITIES

I	RO(I)	BOUND(1)	BOUND(2)	DAMPING
1	1064.8594	916.1616	1237.6912	0.0016
2	18.5612	18.4572	18.6659	0.9227
3	9738.7148	6712.4687	14129.3047	0.1195

LAYER DEPTHS (TO BASE)

I	Z(I)	BOUND(1)	BOUND(2)	DAMPING
1	1603.2078	1467.7722	1751.1401	0.0010
2	1782.4224	1637.8547	1939.7502	0.0025

SUMMARY 1D RESULTS WEIGHTED 2ND ORDER MARQUADT
N.ITALY GRANEZZI 452A INVARIANT

NORMALIZED SINGULAR VALUES OF JACOBIAN

0.100E+01 0.780E+00 0.605E+00 0.360E+00 0.269E+00 0.122E+00 0.429E-01

NUMBER OF EFFECTIVE PARAMETERS: 6.997

SCALE FACTOR : 0.8154082E-01

DAMPING FACTORS (1.0 PERCENT LEVEL)

0.100E+01 0.100E+01 0.100E+01 0.100E+01 0.100E+01 0.100E+01 0.997E+00

PARAMETER SPACE EIGENVECTORS (V MATRIX)

1	0.564	-0.722	0.329	-0.183	0.124	-0.051	0.020
2	0.441	0.481	-0.132	-0.339	0.418	-0.440	0.269
3	0.107	0.328	0.562	-0.224	-0.270	0.489	0.451
4	0.034	0.110	0.345	0.678	0.622	0.142	0.037
5	0.678	0.176	-0.374	0.400	-0.350	0.268	-0.124
6	-0.090	-0.227	-0.144	0.372	-0.247	-0.343	0.776
7	-0.078	-0.212	-0.528	-0.210	0.408	0.596	0.325

LAYER RESISTIVITIES

I	RO(I)	BOUND(1)	BOUND(2)	DAMPING
1	1823.1025	1132.5786	2934.6328	0.0000
2	490.0256	92.1464	2605.9094	0.0002
3	770.3611	89.5334	6628.3203	0.0006
4	2749.6301	1172.0837	6450.4453	0.0000

LAYER DEPTHS (TO BASE)

I	Z(I)	BOUND(1)	BOUND(2)	DAMPING
1	2172.0190	719.9839	6552.4570	0.0000
2	4884.5859	276.9724	86142.7500	0.0018
3	13526.8203	1961.1060	93301.8750	0.0003

SUMMARY 1D RESULTS WEIGHTED 2ND ORDER MARQUADT
N.ITALY 456A EPOL

NORMALIZED SINGULAR VALUES OF JACOBIAN

0.100E+01 0.260E+00 0.181E+00 0.135E+00 0.417E−01 0.226E−01 0.168E−02

NUMBER OF EFFECTIVE PARAMETERS: 5.961

SCALE FACTOR : 0.4050403E+00

DAMPING FACTORS (1.0 PERCENT LEVEL)

0.100E+01 0.100E+01 0.100E+01 0.100E+01 0.997E+00 0.963E+00 0.790E−03

PARAMETER SPACE EIGENVECTORS (V MATRIX)

1 0.002−0.039 0.674−0.736 0.050 0.005 0.008
2 0.113−0.006−0.029−0.011 0.045 0.018 0.992
3 0.105 0.569 0.017−0.069−0.796−0.160 0.030
4 0.002 0.054 0.023 0.028 0.233−0.970 0.008
5 0.739−0.268 0.441 0.411−0.118−0.020−0.063
6 −0.653−0.152 0.521 0.470−0.214−0.035 0.105
7 −0.052−0.760−0.280−0.251−0.498−0.176 0.016

LAYER RESISTIVITIES

I	RO(I)	BOUND(1)	BOUND(2)	DAMPING
1	3844.4614	2950.8093	5008.7539	0.0001
2	162.2411	151.8388	173.3561	0.8728
3	1052.3914	517.1519	2141.5901	0.0035
4	48321.2969	14990.3984	155762.8750	0.0347

LAYER DEPTHS (TO BASE)

I	Z(I)	BOUND(1)	BOUND(2)	DAMPING
1	2860.5435	2183.1863	3748.0579	0.0020
2	3309.5447	2329.3401	4702.2266	0.0057
3	14086.6641	7458.6797	26604.4375	0.0021

SUMMARY 1D RESULTS WEIGHTED 2ND ORDER MARQUADT
N.ITALY 454A E POL

NORMALIZED SINGULAR VALUES OF JACOBIAN

0.100E+01 0.593E+00 0.363E+00 0.190E+00 0.662E-01 0.278E-01 0.124E-01

NUMBER OF EFFECTIVE PARAMETERS: 6.687

SCALE FACTOR : 0.1587707E+00

DAMPING FACTORS (1.0 PERCENT LEVEL)

0.100E+01 0.100E+01 0.100E+01 0.100E+01 0.999E+00 0.983E+00 0.704E+00

PARAMETER SPACE EIGENVECTORS (V MATRIX)

1	0.070	-0.050	0.585	-0.804	0.053	-0.003	-0.016
2	0.259	0.216	-0.765	-0.541	0.080	-0.006	-0.031
3	0.016	0.370	0.073	0.008	-0.582	-0.051	-0.718
4	0.002	0.035	0.011	0.014	0.122	0.980	-0.149
5	0.961	-0.119	0.149	0.197	-0.040	0.004	0.010
6	-0.004	0.133	-0.011	-0.079	-0.727	0.185	0.643
7	-0.063	-0.883	-0.211	-0.122	-0.327	0.043	-0.218

LAYER RESISTIVITIES

I	RO(I)	BOUND(1)	BOUND(2)	DAMPING
1	4283.1680	2613.8958	7018.4609	0.0001
2	198.7068	114.4712	344.9285	0.0002
3	149.9428	5.6059	4010.5945	0.1399
4	16195.5586	940.7434	278817.8125	0.0216

LAYER DEPTHS (TO BASE)

I	Z(I)	BOUND(1)	BOUND(2)	DAMPING
1	1585.3721	1236.5710	2032.5596	0.0000
2	4274.4766	136.8380	133523.8750	0.1112
3	7200.6523	1848.1575	28054.6367	0.0122

SUMMARY 1D RESULTS WEIGHTED 2ND ORDER MARQUADT
N.ITALY 455A EPOL

NORMALIZED SINGULAR VALUES OF JACOBIAN

0.100E+01 0.287E+00 0.179E+00 0.713E−01 0.595E−01 0.334E−02 0.104E−02

NUMBER OF EFFECTIVE PARAMETERS: 5.011

SCALE FACTOR : 0.3643583E+00

DAMPING FACTORS (1.0 PERCENT LEVEL)

0.100E+01 0.100E+01 0.100E+01 0.100E+01 0.999E+00 0.123E−01 0.119E−03

PARAMETER SPACE EIGENVECTORS (V MATRIX)

1	0.002	−0.054	0.060	−0.136	0.078	0.612	0.771
2	−0.069	−0.820	−0.169	0.472	−0.260	0.009	0.059
3	−0.196	0.015	−0.021	−0.065	0.008	−0.770	0.602
4	−0.045	−0.001	0.100	0.500	0.859	−0.018	0.008
5	0.010	−0.559	0.395	−0.632	0.321	−0.083	−0.148
6	−0.532	−0.053	−0.742	−0.296	0.234	0.102	−0.102
7	0.819	−0.093	−0.501	−0.133	0.175	−0.119	0.084

LAYER RESISTIVITIES

I	RO(I)	BOUND(1)	BOUND(2)	DAMPING
1	6987.1914	5912.5781	8257.1133	0.8233
2	529.3899	351.7627	796.7122	0.0019
3	115.1427	102.3025	129.5943	0.7914
4	7220.1367	3936.1768	13243.9102	0.0009

LAYER DEPTHS (TO BASE)

I	Z(I)	BOUND(1)	BOUND(2)	DAMPING
1	569.6179	340.5312	952.8181	0.0148
2	2897.2112	2009.5066	4177.0586	0.0105
3	3752.9797	2916.8772	4828.7422	0.0106

SUMMARY 1D RESULTS WEIGHTED 2ND ORDER MARQUADT
N.ITALY 690A E POL

NORMALIZED SINGULAR VALUES OF JACOBIAN

0.100E+01 0.426E+00 0.233E+00 0.197E+00 0.953E−01 0.410E−01 0.261E−01

NUMBER OF EFFECTIVE PARAMETERS: 6.975

SCALE FACTOR : 0.1790525E+00

DAMPING FACTORS (1.0 PERCENT LEVEL)

0.100E+01 0.100E+01 0.100E+01 0.100E+01 0.100E+01 0.996E+00 0.979E+00

PARAMETER SPACE EIGENVECTORS (V MATRIX)

1 0.021−0.107 0.973−0.166 0.069 0.062 0.077
2 −0.297 0.049−0.094−0.020 0.123 0.463 0.819
3 −0.081 0.107 0.115 0.282−0.739−0.464 0.357
4 −0.016 0.022 0.118 0.837 0.493−0.192 0.062
5 −0.634−0.754−0.046 0.028−0.042−0.092−0.132
6 0.709−0.637−0.090 0.088−0.077 0.078 0.254
7 −0.025 0.026 0.087 0.428−0.428 0.718−0.331

LAYER RESISTIVITIES

I	RO(I)	BOUND(1)	BOUND(2)	DAMPING
1	1067.1133	596.8918	1907.7666	0.0001
2	51.1722	4.3292	604.8628	0.0150
3	691.5676	99.4708	4808.0977	0.0035
4	304.0342	117.5807	786.1558	0.0002

LAYER DEPTHS (TO BASE)

I	Z(I)	BOUND(1)	BOUND(2)	DAMPING
1	1469.9802	824.4028	2621.0994	0.0004
2	2199.2119	936.6228	5163.7969	0.0014
3	16706.8633	2114.1531	132024.1250	0.0042

SUMMARY 1D RESULTS WEIGTHED 2ND ORDER MARQUADT
N.ITALY 450A EPOL

NORMALIZED SINGULAR VALUES OF JACOBIAN

0.100E+01 0.412E+00 0.178E+00 0.610E−03 0.170E−05

NUMBER OF EFFECTIVE PARAMETERS: 3.000

SCALE FACTOR : 0.2390798E+00

DAMPING FACTORS (1.0 PERCENT LEVEL)

0.100E+01 0.100E+01 0.100E+01 0.139E−04 0.000E+00

PARAMETER SPACE EIGENVECTORS (V MATRIX)

1	0.054	−0.977	0.209	0.000	0.000
2	−0.090	0.203	0.975	0.000	0.000
3	0.000	0.000	0.000	−0.003	1.000
4	−0.995	−0.071	−0.077	0.000	0.000
5	0.000	0.000	0.000	1.000	0.003

LAYER RESISTIVITIES

I	RO(I)	BOUND(1)	BOUND(2)	DAMPING
1	435.0178	374.3582	505.5061	0.0000
2	6.3350	4.9191	8.1583	0.0000
3	1719.5071	1719.5020	1719.5120	1.0000

LAYER DEPTHS (TO BASE)

I	Z(I)	BOUND(1)	BOUND(2)	DAMPING
1	917.0474	857.8206	980.3630	0.0000
2	6001.6133	5995.8633	6007.3633	0.9999

SUMMARY 1D RESULTS WEIGTHED 2ND ORDER MARQUADT
N.ITALY 451A EPOL

NORMALIZED SINGULAR VALUES OF JACOBIAN

0.100E+01 0.711E+00 0.141E+00 0.108E−03 0.959E−06

NUMBER OF EFFECTIVE PARAMETERS: 3.000

SCALE FACTOR : 0.2204443E+00

DAMPING FACTORS (1.0 PERCENT LEVEL)

0.100E+01 0.100E+01 0.100E+01 0.137E−07 0.000E+00

PARAMETER SPACE EIGENVECTORS (V MATRIX)

1	0.006 0.995 0.098 0.000 0.000
2	0.153−0.098 0.983 0.000 0.000
3	0.000 0.000 0.000−0.006−1.000
4	0.988 0.009−0.153 0.000 0.000
5	0.000 0.000 0.000 1.000−0.006

LAYER RESISTIVITIES

I	RO(I)	BOUND(1)	BOUND(2)	DAMPING
1	252.1828	229.2336	277.4294	0.0000
2	21.5010	15.4568	29.9086	0.0000
3	1261.5959	1261.5959	1261.5959	1.0000

LAYER DEPTHS (TO BASE)

I	Z(I)	BOUND(1)	BOUND(2)	DAMPING
1	950.0583	864.3184	1044.3035	0.0000
2	5153.6562	5152.9062	5154.4023	0.9996

SUMMARY 1D RESULTS WEIGHTED 2ND ORDER MARQUADT
N.ITALY 453A EPOL

NORMALIZED SINGULAR VALUES OF JACOBIAN

0.100E+01 0.149E+00 0.106E+00 0.478E−01 0.319E−02

NUMBER OF EFFECTIVE PARAMETERS: 4.008

SCALE FACTOR : 0.6986493E+00

DAMPING FACTORS (1.0 PERCENT LEVEL)

0.100E+01 0.100E+01 0.100E+01 0.998E+00 0.102E−01

PARAMETER SPACE EIGENVECTORS (V MATRIX)

1	0.005	0.043	0.998	−0.044	0.020
2	−0.141	0.017	−0.021	−0.025	0.989
3	−0.032	0.077	0.040	0.995	0.020
4	−0.642	−0.761	0.040	0.038	−0.077
5	0.753	−0.642	0.025	0.071	0.120

LAYER RESISTIVITIES

I	RO(I)	BOUND(1)	BOUND(2)	DAMPING
1	1730.5869	1484.4675	2017.5117	0.0003
2	45.5910	42.9630	48.3797	0.8543
3	3063.5679	2243.2000	4183.9531	0.0021

LAYER DEPTHS (TO BASE)

I	Z(I)	BOUND(1)	BOUND(2)	DAMPING
1	1644.2725	1484.2024	1821.6057	0.0030
2	2000.7356	1806.0774	2216.3738	0.0073

SUMMARY 1D RESULTS WEIGHTED 2ND ORDER MARQUADT
N.ITALY 452A EPOL

NORMALIZED SINGULAR VALUES OF JACOBIAN

0.100E+01 0.616E+00 0.301E+00 0.218E+00 0.122E+00 0.972E-01 0.263E-01

NUMBER OF EFFECTIVE PARAMETERS: 6.979

SCALE FACTOR : 0.1526614E+00

DAMPING FACTORS (1.0 PERCENT LEVEL)

0.100E+01 0.100E+01 0.100E+01 0.100E+01 0.100E+01 0.100E+01 0.980E+00

PARAMETER SPACE EIGENVECTORS (V MATRIX)

1	0.023	-0.167	0.938	-0.086	0.223	-0.183	0.032
2	0.514	0.087	-0.253	-0.072	0.565	-0.567	0.136
3	0.083	0.087	0.065	0.171	-0.367	-0.112	0.897
4	0.007	0.014	0.037	0.818	0.449	0.351	0.067
5	0.553	-0.781	-0.061	0.044	-0.202	0.192	-0.038
6	-0.649	-0.588	-0.208	0.039	0.213	-0.338	0.169
7	0.039	0.042	0.060	0.535	-0.456	-0.598	-0.376

LAYER RESISTIVITIES

I	RO(I)	BOUND(1)	BOUND(2)	DAMPING
1	1662.8455	941.1099	2938.0784	0.0000
2	127.5567	40.9175	397.6462	0.0004
3	1326.4111	104.5374	16830.0078	0.0164
4	423.8809	172.8476	1039.4995	0.0001

LAYER DEPTHS (TO BASE)

I	Z(I)	BOUND(1)	BOUND(2)	DAMPING
1	1276.2688	793.4985	2052.7595	0.0000
2	2796.2559	1117.8579	6994.6680	0.0006
3	12442.2852	2172.7876	71249.6875	0.0029

SUMMARY 1D RESULTS WEIGHTED 2ND ORDER MARQUADT
N.ITALY 456A H POL

NORMALIZED SINGULAR VALUES OF JACOBIAN

0.100E+01 0.107E+00 0.842E-01 0.639E-01 0.220E-01 0.122E-01 0.548E-03

NUMBER OF EFFECTIVE PARAMETERS: 5.648

SCALE FACTOR : 0.8402414E+00

DAMPING FACTORS (1.0 PERCENT LEVEL)

0.100E+01 0.100E+01 0.100E+01 0.999E+00 0.959E+00 0.690E+00 0.899E-05

PARAMETER SPACE EIGENVECTORS (V MATRIX)

1	0.002	-0.149	0.264	-0.952	0.049	0.009	0.007
2	0.077	0.009	-0.013	0.004	0.021	0.015	0.997
3	0.043	0.425	0.500	0.033	-0.713	-0.241	0.018
4	0.000	0.043	0.099	0.033	0.404	-0.908	0.006
5	0.700	-0.605	0.320	0.180	-0.080	-0.023	-0.043
6	-0.708	-0.568	0.354	0.180	-0.112	-0.031	0.067
7	-0.009	-0.326	-0.666	-0.165	-0.554	-0.340	0.012

LAYER RESISTIVITIES

I	RO(I)	BOUND(1)	BOUND(2)	DAMPING
1	2778.6956	2137.8010	3611.7244	0.0007
2	59.8055	58.2909	61.3593	0.9180
3	1259.5366	653.0356	2429.3191	0.0365
4	15920.4648	6839.4492	37058.7109	0.2547

LAYER DEPTHS (TO BASE)

I	Z(I)	BOUND(1)	BOUND(2)	DAMPING
1	2266.7876	1834.6016	2800.7854	0.0014
2	2518.3818	1991.5808	3184.5288	0.0031
3	17072.9297	8670.5625	33617.7500	0.0438

SUMMARY 1D RESULTS WEIGHTED 2ND ORDER MARQUADT
N.ITALY 454A H POL

NORMALIZED SINGULAR VALUES OF JACOBIAN

0.100E+01 0.676E+00 0.456E+00 0.286E+00 0.152E+00 0.100E+00 0.294E-01

NUMBER OF EFFECTIVE PARAMETERS: 6.987

SCALE FACTOR : 0.1127606E+00

DAMPING FACTORS (1.0 PERCENT LEVEL)

0.100E+01 0.100E+01 0.100E+01 0.100E+01 0.100E+01 0.100E+01 0.987E+00

PARAMETER SPACE EIGENVECTORS (V MATRIX)

1	0.194	-0.358	0.582	-0.634	0.298	0.056	0.033
2	0.590	0.450	-0.428	-0.249	0.432	0.109	0.080
3	0.089	0.349	0.375	0.121	-0.227	0.140	0.802
4	0.018	0.073	0.131	0.166	0.330	-0.907	0.132
5	0.761	-0.427	0.035	0.340	-0.335	-0.081	-0.047
6	-0.125	-0.475	-0.163	0.407	0.601	0.281	0.356
7	-0.105	-0.366	-0.541	-0.461	-0.301	-0.238	0.450

LAYER RESISTIVITIES

I	RO(I)	BOUND(1)	BOUND(2)	DAMPING
1	13104.3750	6537.6211	26267.1367	0.0000
2	2173.5317	921.3660	5127.4297	0.0001
3	5056.5859	304.3196	84020.3125	0.0085
4	39646.9180	9064.1055	173417.8125	0.0003

LAYER DEPTHS (TO BASE)

I	Z(I)	BOUND(1)	BOUND(2)	DAMPING
1	3229.9629	1700.4194	6135.3437	0.0000
2	9982.6992	1507.8276	66091.2500	0.0017
3	25142.9961	3297.7224	191699.0000	0.0027

SUMMARY 1D RESULTS WEIGHTED 2ND ORDER MARQUADT
N.ITALY 455A H POL

NORMALIZED SINGULAR VALUES OF JACOBIAN

0.100E+01 0.440E+00 0.300E+00 0.213E+00 0.507E−01 0.138E−01 0.111E−01

NUMBER OF EFFECTIVE PARAMETERS: 6.390

SCALE FACTOR : 0.2772632E+00

DAMPING FACTORS (1.0 PERCENT LEVEL)

0.100E+01 0.100E+01 0.100E+01 0.100E+01 0.998E+00 0.786E+00 0.606E+00

PARAMETER SPACE EIGENVECTORS (V MATRIX)

1	0.061	−0.283	0.942	−0.155	0.041	−0.044	0.023
2	−0.206	0.089	−0.024	−0.039	0.172	−0.844	0.453
3	−0.067	0.151	0.170	0.574	−0.766	−0.074	0.151
4	0.001	0.002	0.005	0.055	0.164	0.489	0.855
5	−0.792	−0.586	−0.107	0.063	−0.042	0.097	−0.049
6	0.567	−0.735	−0.234	0.192	−0.065	−0.175	0.104
7	0.024	−0.066	−0.127	−0.775	−0.591	−0.004	0.166

LAYER RESISTIVITIES

I	RO(I)	BOUND(1)	BOUND(2)	DAMPING
1	1294.0869	932.5471	1795.7920	0.0005
2	55.7554	3.5138	884.7075	0.2270
3	405.6084	131.6757	1249.4192	0.0092
4	13567.9258	820.2065	224441.7500	0.3323

LAYER DEPTHS (TO BASE)

I	Z(I)	BOUND(1)	BOUND(2)	DAMPING
1	2028.2219	1327.5269	3098.7571	0.0026
2	2659.1807	1255.8914	5630.4531	0.0093
3	14395.0820	5803.4219	35706.2187	0.0093

SUMMARY 1D RESULTS WEIGHTED 2ND ORDER MARQUADT
N.ITALY 690A H POL

NORMALIZED SINGULAR VALUES OF JACOBIAN

0.100E+01 0.276E+00 0.147E+00 0.906E−01 0.468E−01 0.126E−01 0.809E−02

NUMBER OF EFFECTIVE PARAMETERS: 6.015

SCALE FACTOR : 0.3474486E+00

DAMPING FACTORS (1.0 PERCENT LEVEL)

0.100E+01 0.100E+01 0.100E+01 0.100E+01 0.998E+00 0.718E+00 0.300E+00

PARAMETER SPACE EIGENVECTORS (V MATRIX)

1	0.024	−0.024	0.990	−0.114	0.050	−0.046	0.036
2	−0.177	−0.031	−0.061	−0.032	0.074	−0.657	0.725
3	−0.056	−0.072	0.089	0.455	−0.682	0.371	0.417
4	−0.020	−0.022	0.062	0.788	0.605	0.076	0.042
5	−0.652	0.752	0.041	0.010	−0.015	0.066	−0.062
6	0.734	0.654	0.000	0.073	−0.045	−0.088	0.136
7	0.023	0.023	−0.054	−0.390	0.398	0.641	0.524

LAYER RESISTIVITIES

I	RO(I)	BOUND(1)	BOUND(2)	DAMPING
1	2969.5972	2036.9482	4329.2734	0.0011
2	59.0332	8.6179	404.3821	0.4415
3	1684.5049	326.3162	8695.7227	0.1207
4	4323.5859	1931.0554	9680.4023	0.0031

LAYER DEPTHS (TO BASE)

I	Z(I)	BOUND(1)	BOUND(2)	DAMPING
1	2677.1326	2001.0127	3581.7053	0.0028
2	3414.6501	2223.9585	5242.8281	0.0103
3	21736.9609	2972.4692	158957.1875	0.2586

SUMMARY 1D RESULTS WEIGHTED 2ND ORDER MARQUADT
N.ITALY 450A H POL

NORMALIZED SINGULAR VALUES OF JACOBIAN

0.100E+01 0.708E+00 0.381E+00 0.105E+00 0.394E-01

NUMBER OF EFFECTIVE PARAMETERS: 4.996

SCALE FACTOR : 0.1971018E+00

DAMPING FACTORS (1.0 PERCENT LEVEL)

0.100E+01 0.100E+01 0.100E+01 0.100E+01 0.996E+00

PARAMETER SPACE EIGENVECTORS (V MATRIX)

1	0.000	0.209	-0.972	0.108	0.025
2	-0.431	-0.217	0.053	0.844	0.226
3	-0.011	-0.070	-0.021	-0.279	0.958
4	-0.784	0.559	0.091	-0.252	-0.039
5	0.447	0.769	0.210	0.367	0.173

LAYER RESISTIVITIES

I	RO(I)	BOUND(1)	BOUND(2)	DAMPING
1	1140.2495	907.3125	1432.9890	0.0000
2	77.4577	36.8423	162.8479	0.0003
3	694.3665	176.1646	2736.8987	0.0038

LAYER DEPTHS (TO BASE)

I	Z(I)	BOUND(1)	BOUND(2)	DAMPING
1	1666.4238	1279.6721	2170.0620	0.0000
2	3112.7332	1879.0149	5156.4805	0.0001

SUMMARY 1D RESULTS WEIGHTED 2ND ORDER MARQUADT
N.ITALY 453A H POL

NORMALIZED SINGULAR VALUES OF JACOBIAN

0.100E+01 0.418E+00 0.287E+00 0.186E+00 0.356E−01

NUMBER OF EFFECTIVE PARAMETERS: 4.994

SCALE FACTOR : 0.1593952E+00

DAMPING FACTORS (1.0 PERCENT LEVEL)

0.100E+01 0.100E+01 0.100E+01 0.100E+01 0.994E+00

PARAMETER SPACE EIGENVECTORS (V MATRIX)

1	0.142	−0.913	0.237	−0.290	0.076
2	0.524	−0.032	−0.256	0.342	0.736
3	0.196	0.172	0.913	0.310	0.042
4	0.256	−0.281	−0.207	0.686	−0.585
5	−0.775	−0.239	0.032	0.482	0.329

LAYER RESISTIVITIES

I	RO(I)	BOUND(1)	BOUND(2)	DAMPING
1	1144.5857	745.7498	1756.7236	0.0000
2	479.1511	107.2411	2140.8381	0.0033
3	4668.6211	3078.2722	7080.6016	0.0000

LAYER DEPTHS (TO BASE)

I	Z(I)	BOUND(1)	BOUND(2)	DAMPING
1	1451.3755	372.9539	5648.1250	0.0021
2	3231.9607	1408.8037	7414.4922	0.0007

SUMMARY 1D RESULTS WEIGHTED 2ND ORDER MARQUADT
N.ITALY 452A H POL

NORMALIZED SINGULAR VALUES OF JACOBIAN

0.100E+01 0.924E+00 0.538E+00 0.267E+00 0.192E+00

NUMBER OF EFFECTIVE PARAMETERS: 5.000

SCALE FACTOR : 0.9294820E-01

DAMPING FACTORS (1.0 PERCENT LEVEL)

0.100E+01 0.100E+01 0.100E+01 0.100E+01 0.100E+01

PARAMETER SPACE EIGENVECTORS (V MATRIX)

1	0.633	−0.741	0.194	0.077	0.080
2	0.515	0.504	−0.140	0.422	0.533
3	0.122	0.125	0.211	−0.834	0.479
4	0.380	0.045	−0.786	−0.338	−0.350
5	−0.419	−0.423	−0.529	0.085	0.598

LAYER RESISTIVITIES

I	RO(I)	BOUND(1)	BOUND(2)	DAMPING
1	2695.7610	2059.7063	3528.2344	0.0000
2	872.8010	473.8914	1607.5022	0.0000
3	6132.8359	3122.7058	12044.5781	0.0000

LAYER DEPTHS (TO BASE)

I	Z(I)	BOUND(1)	BOUND(2)	DAMPING
1	4093.5396	2396.3003	6992.8906	0.0000
2	14848.8008	8399.0625	26251.3555	0.0000

Appendix B- 1D models (E pol and H pol curves) for all the sites in the Asiago area.
(a)- 2^{nd} order Marquadt scheme.
(b)- Monte Carlo- Hedgehog scheme.

1D MODELS SITE MANDRIELLE 156A

(a)

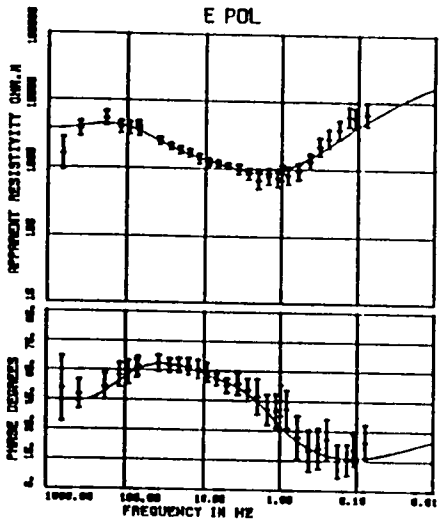

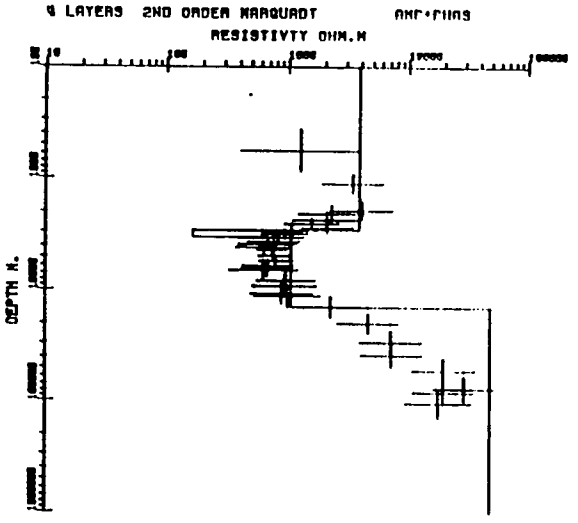

(b)

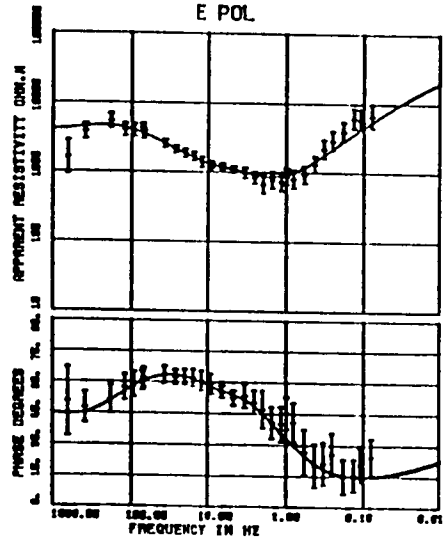

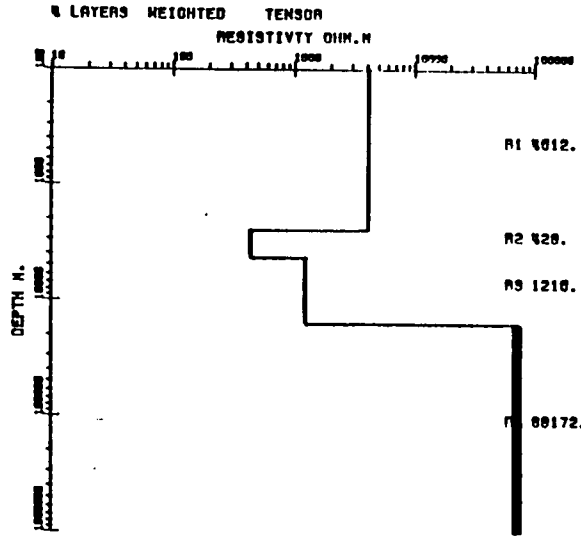

1D MODELS SITE MANDRIELLE 456A

(a)

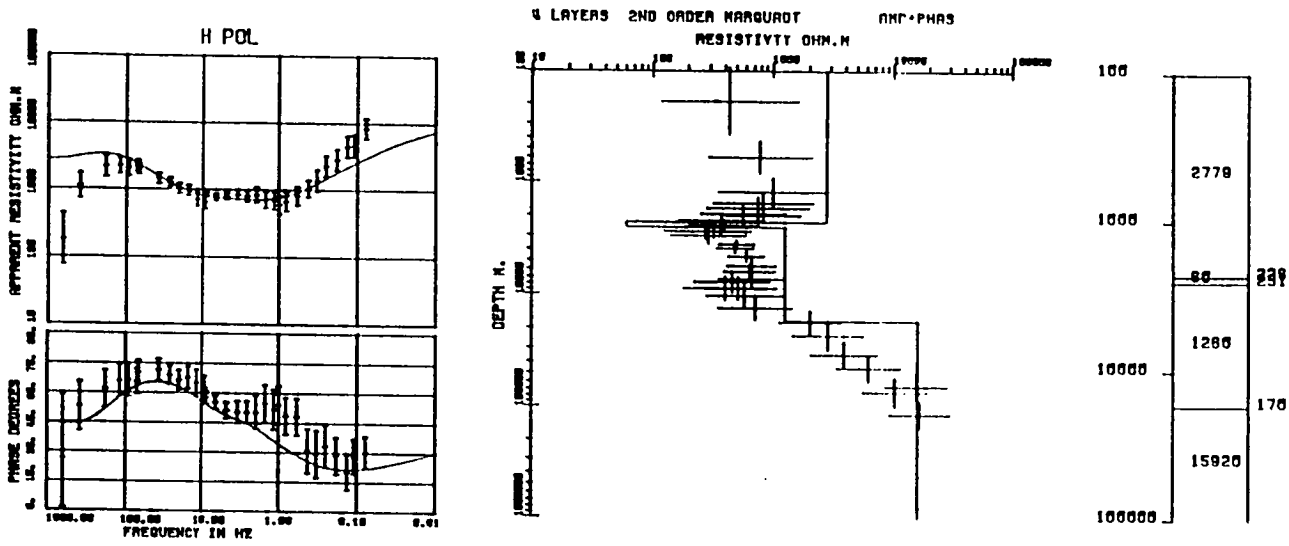

(b)

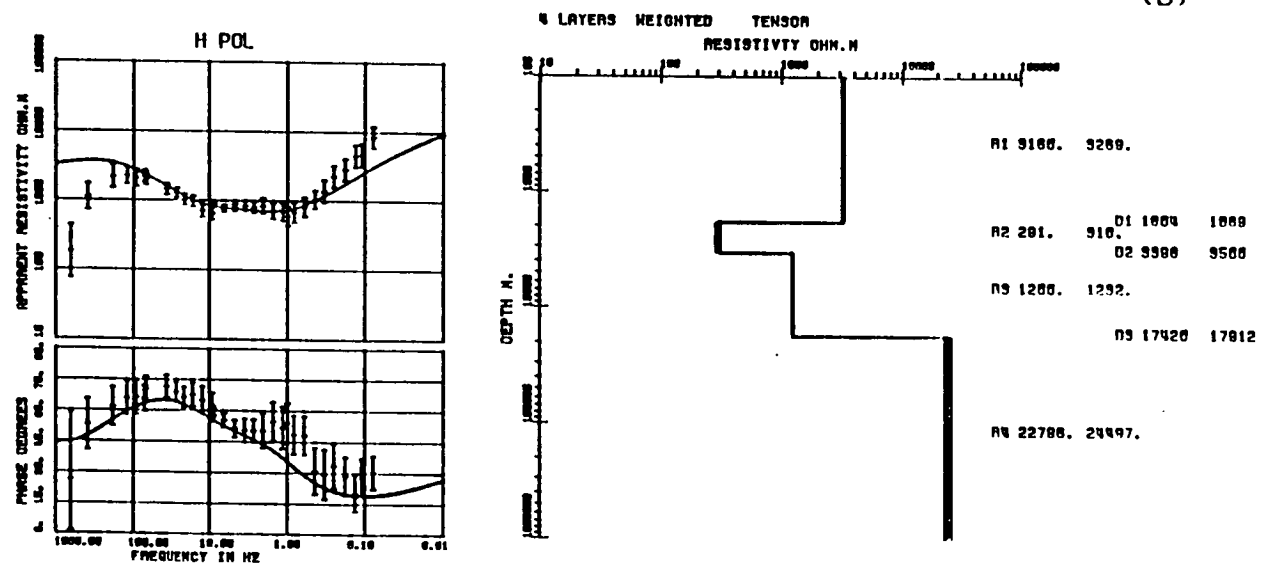

1D MODELS SITE C. MULO 454A

(a)

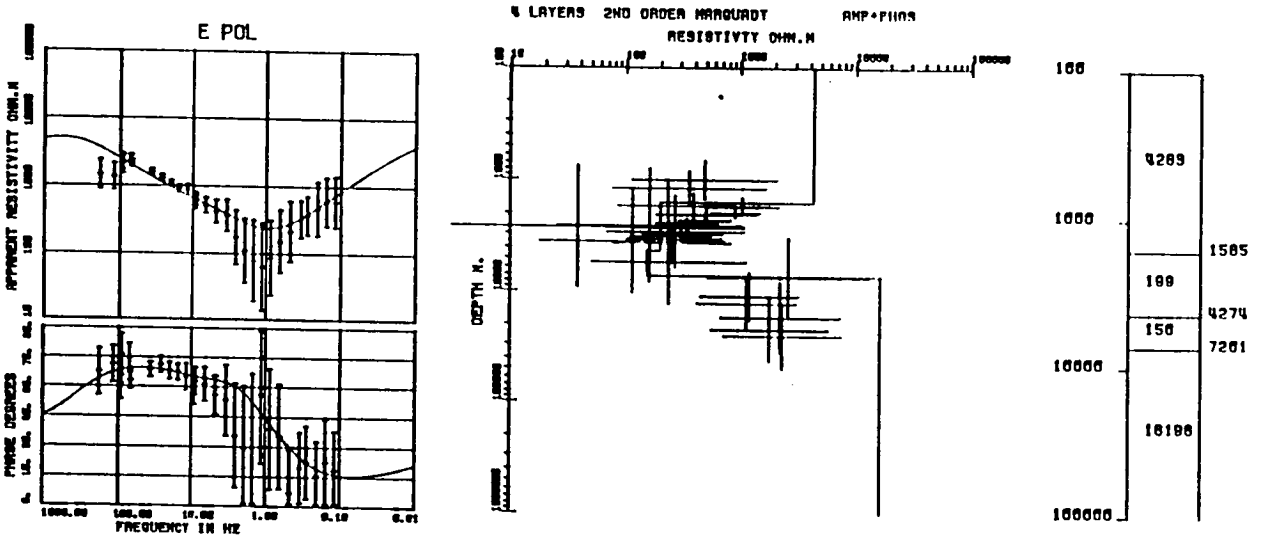

(b)

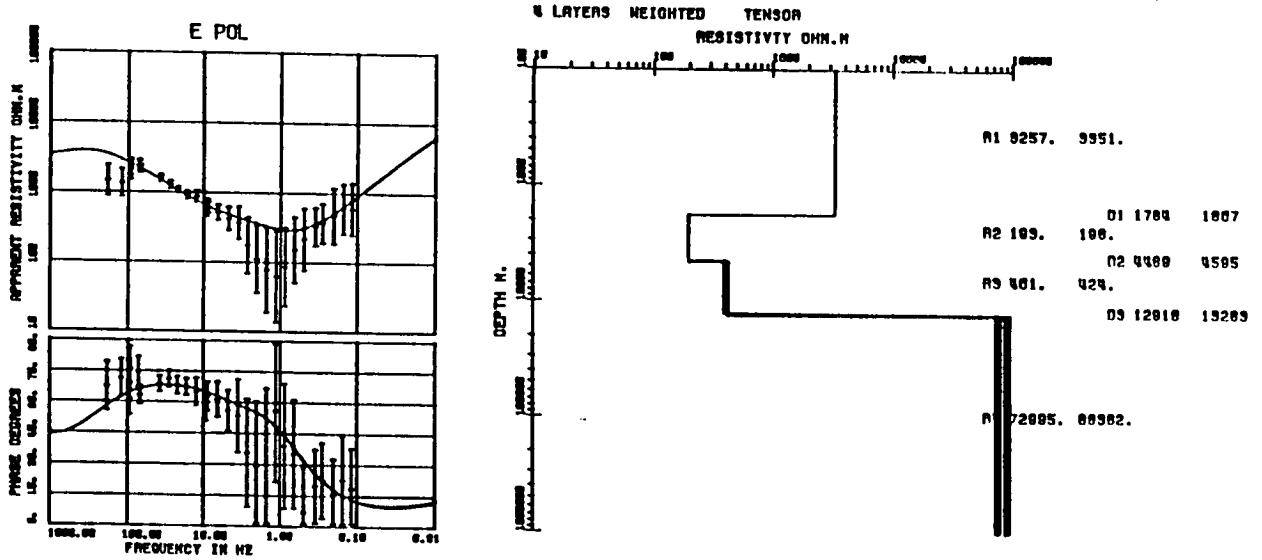

1D MODELS SITE C. MULO 454A

(a)

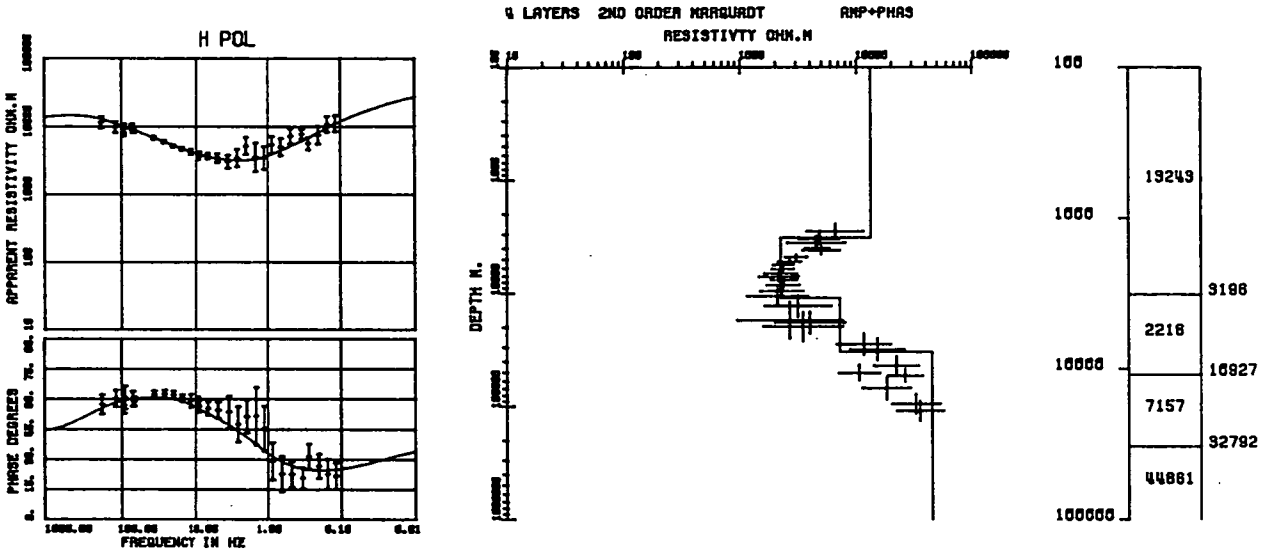

(b)

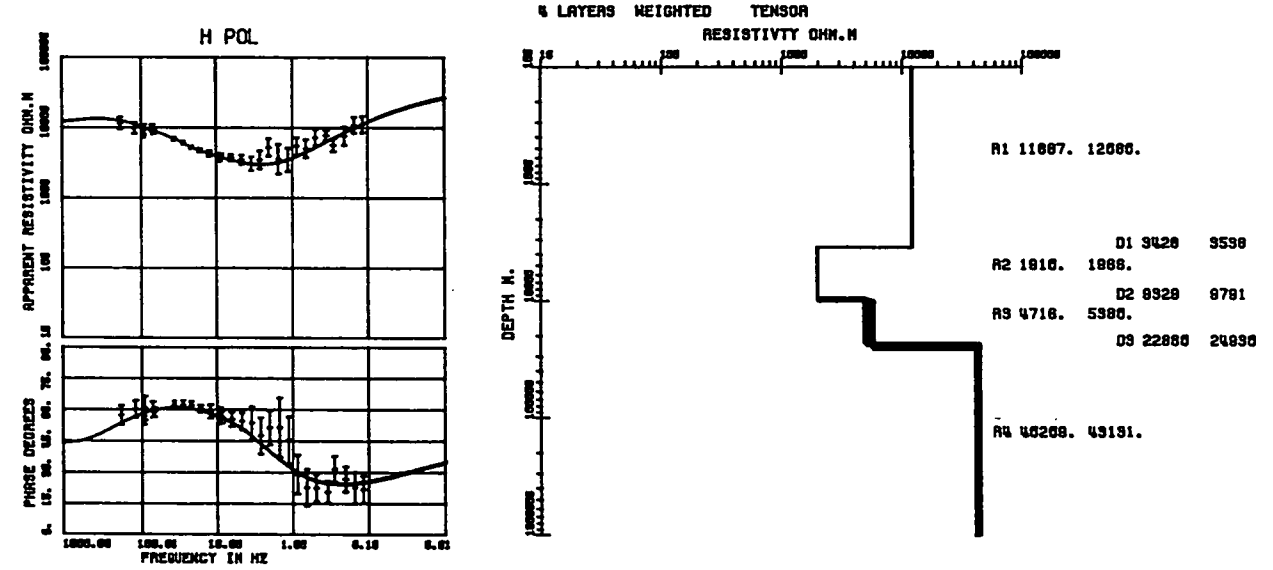

1D MODELS SITE LONGARA 455A

(a)

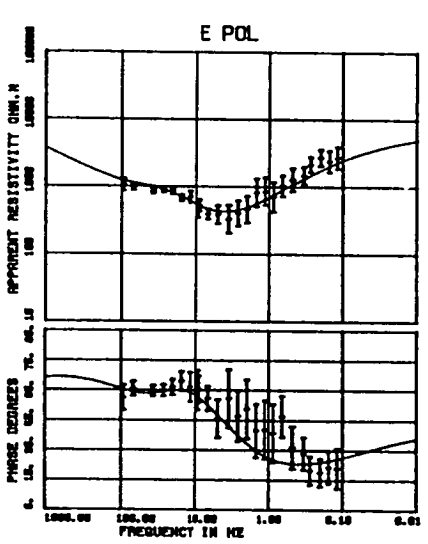

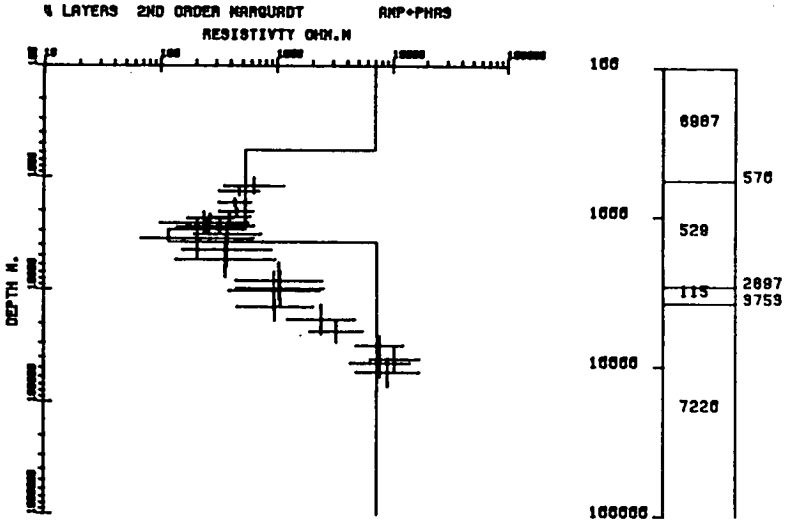

(b)

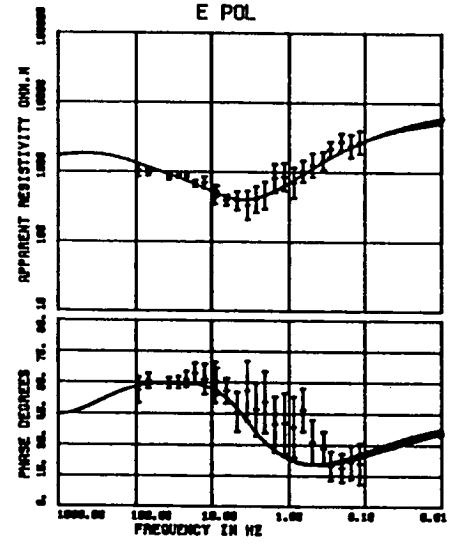

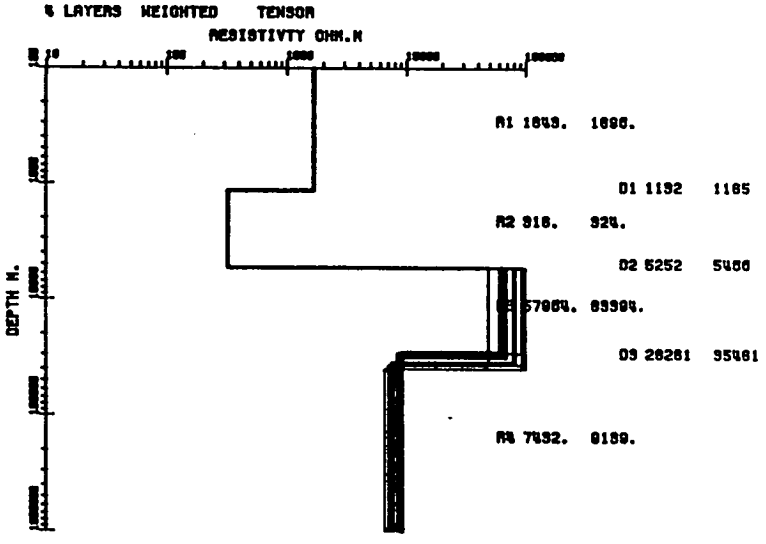

1D MODELS SITE LONGARA 455A

(a)

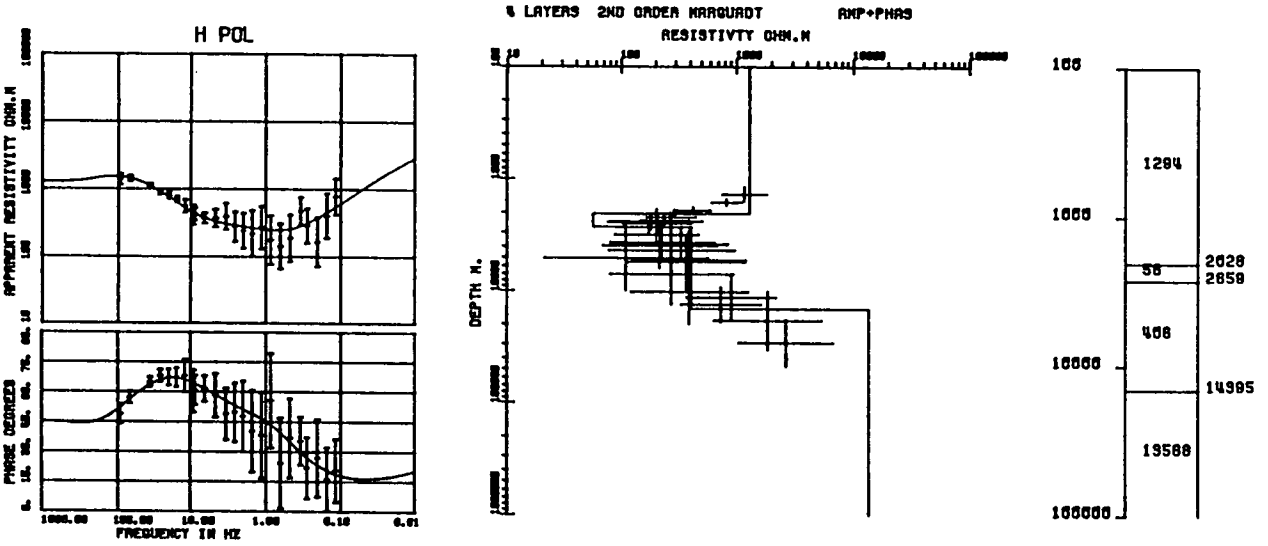

(b)

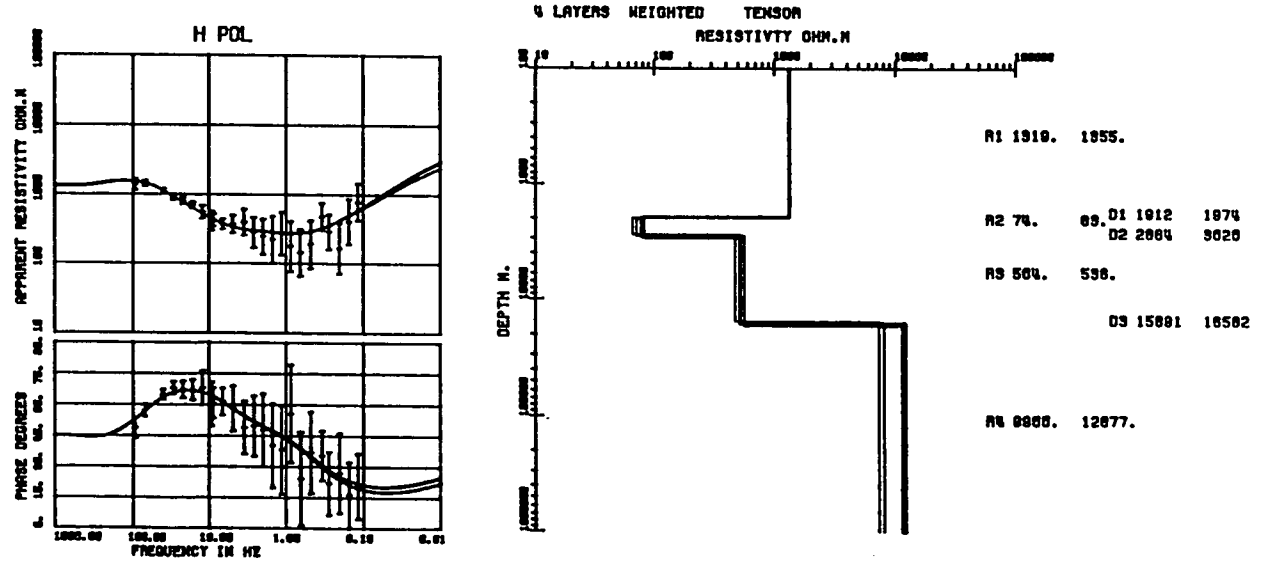

1D MODELS SITE V. DI NOS 690A

(a)

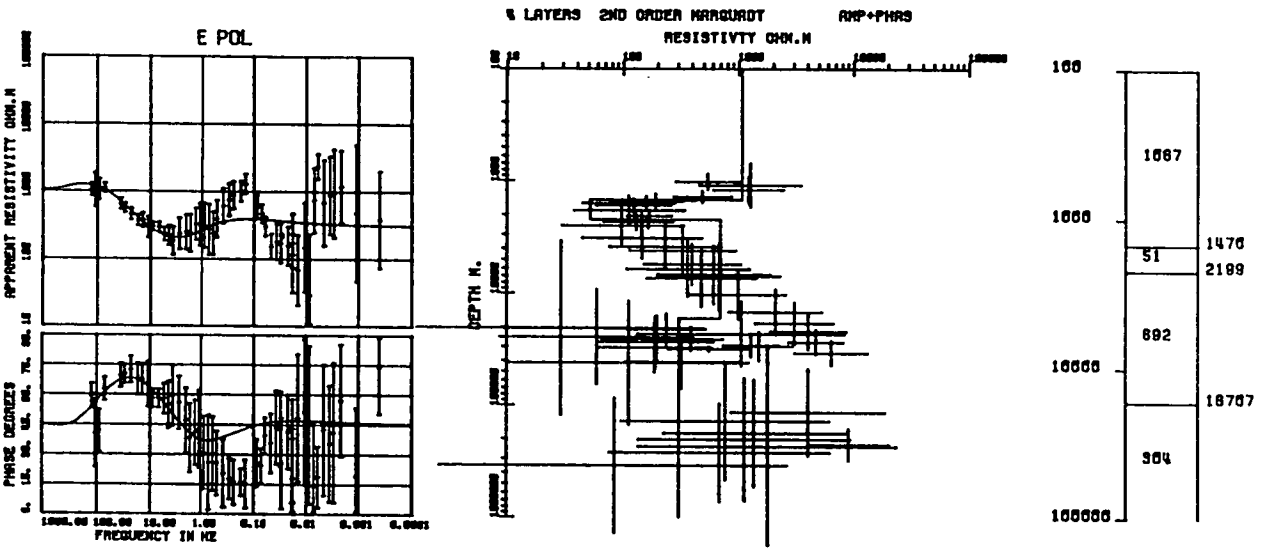

(b)

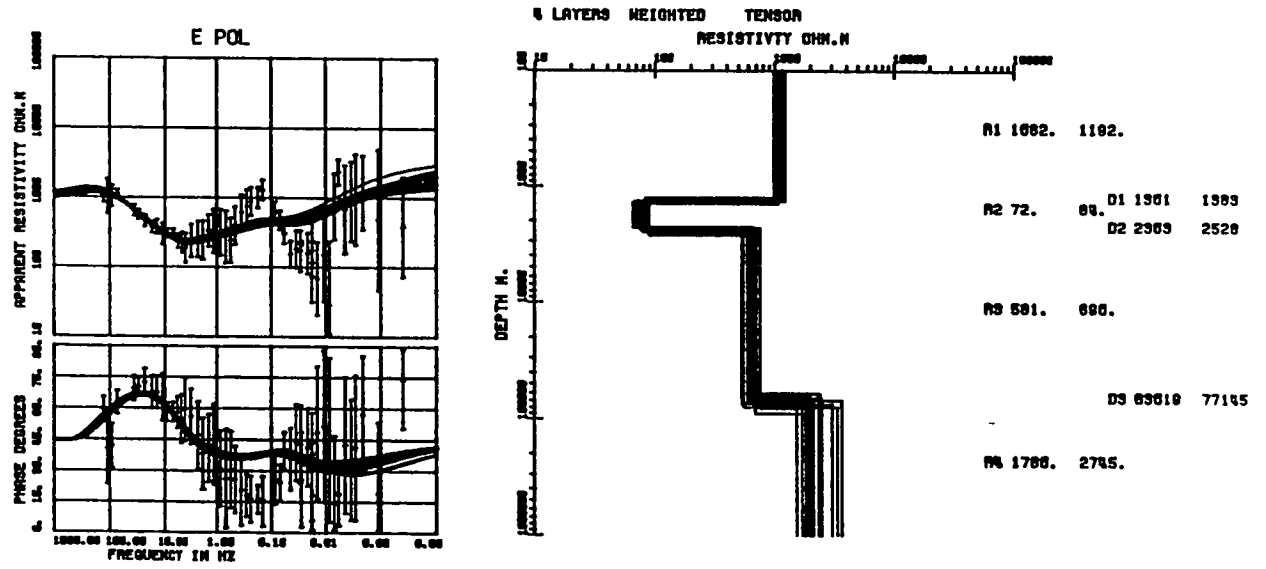

1D MODELS SITE V. DI NOS 690A

(a)

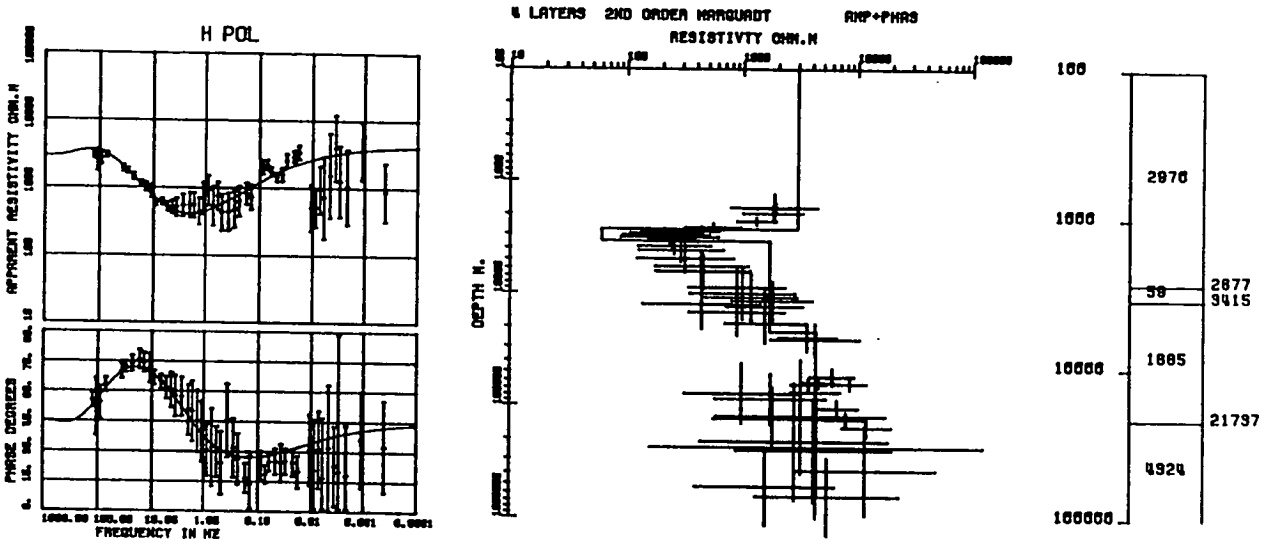

(b)

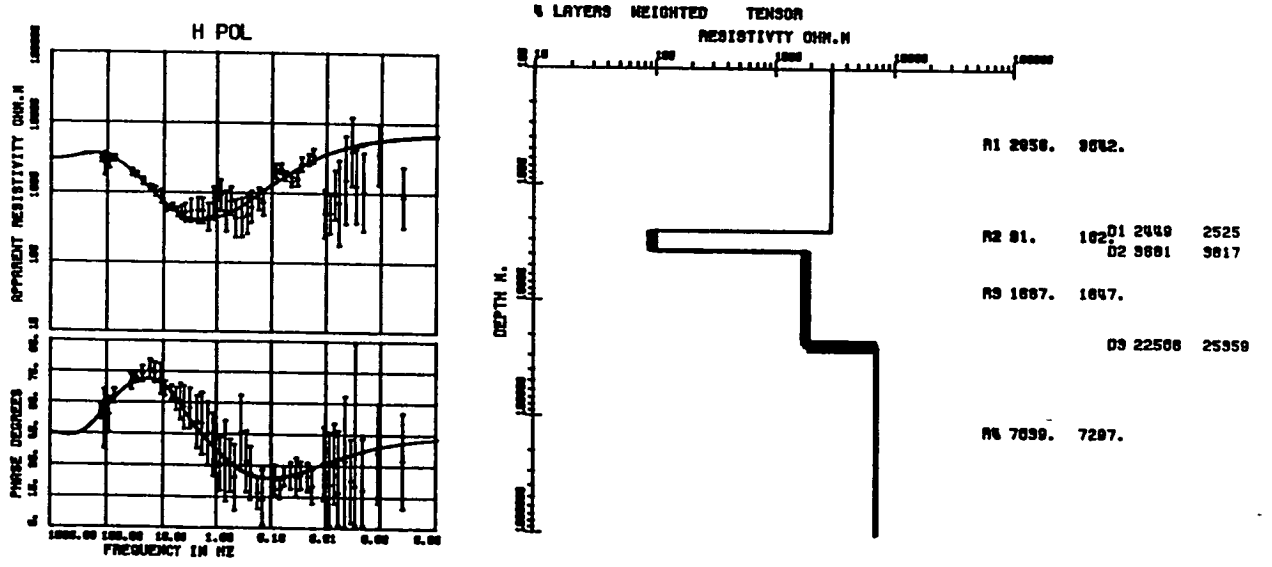

1D MODELS SITE C.S. ANTONIO 450A

(a)

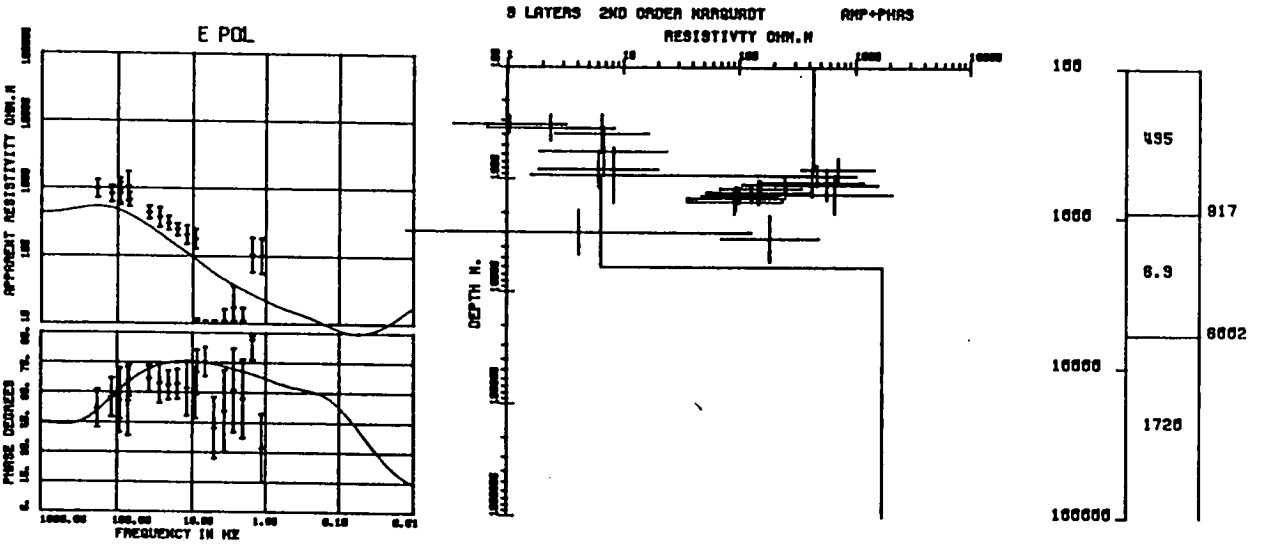

(b)

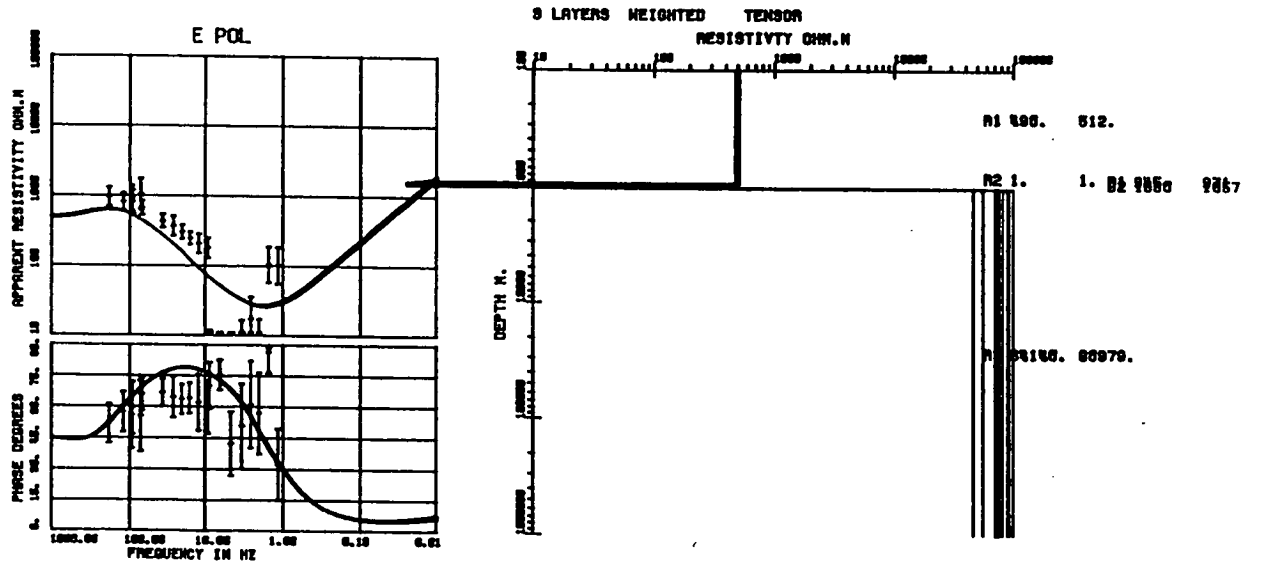

1D MODELS SITE C.S. ANTONIO 450A

(a)

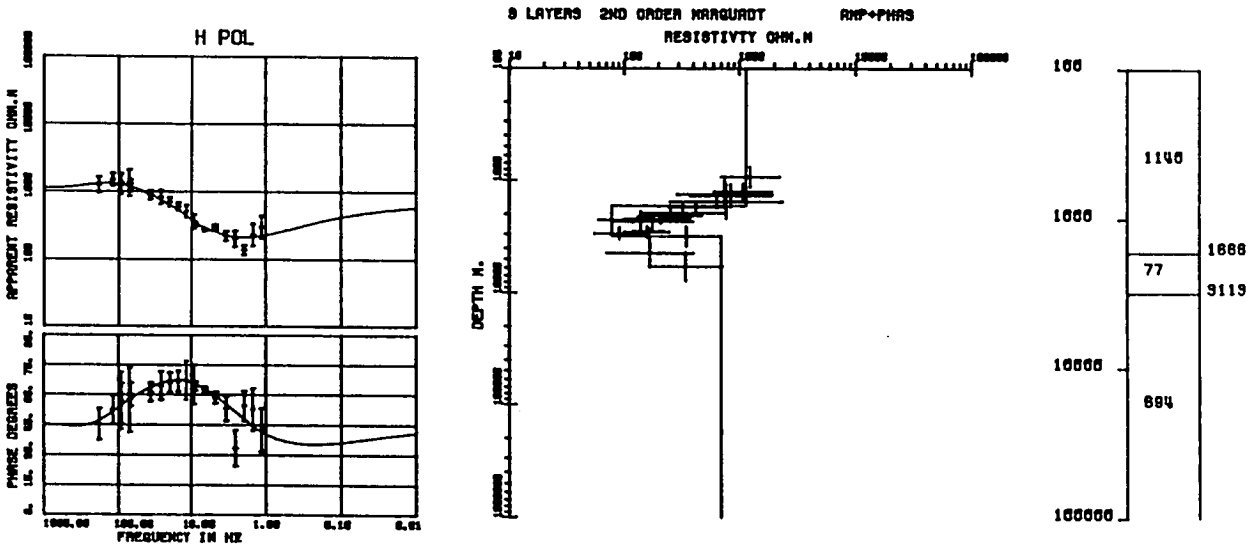

(b)

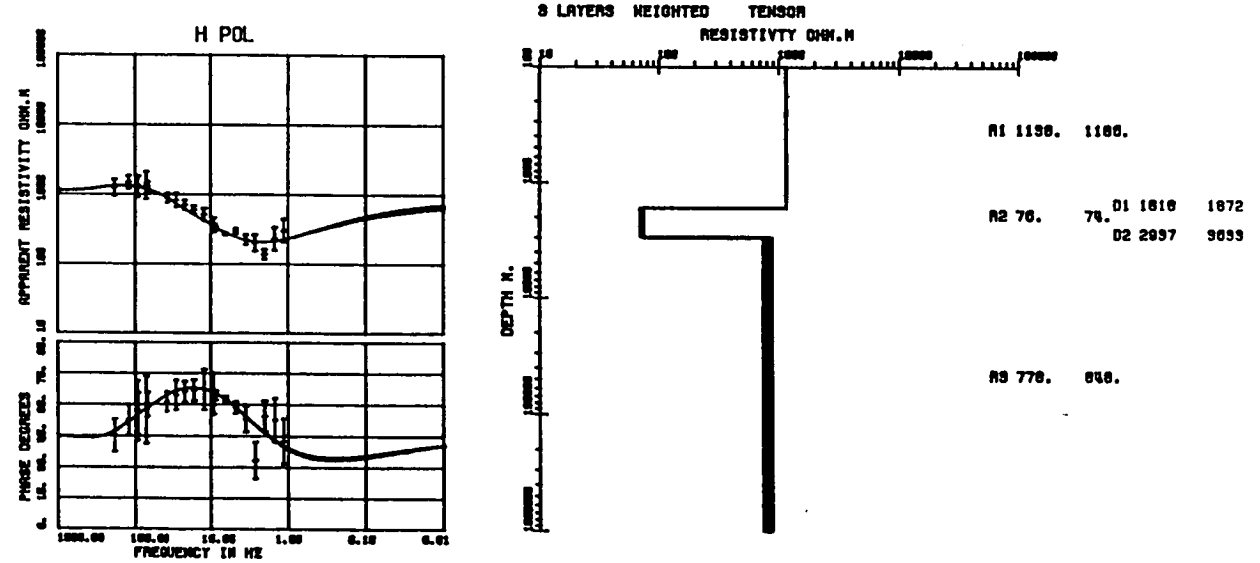

1D MODELS SITE OBSERVATORIO 451A

(a)

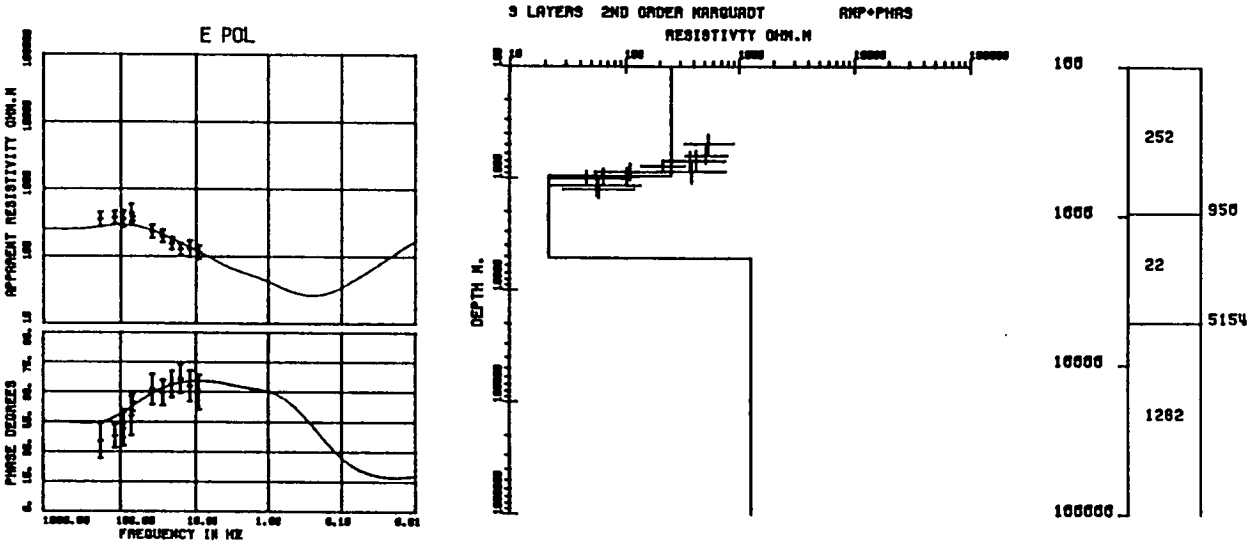

(b)

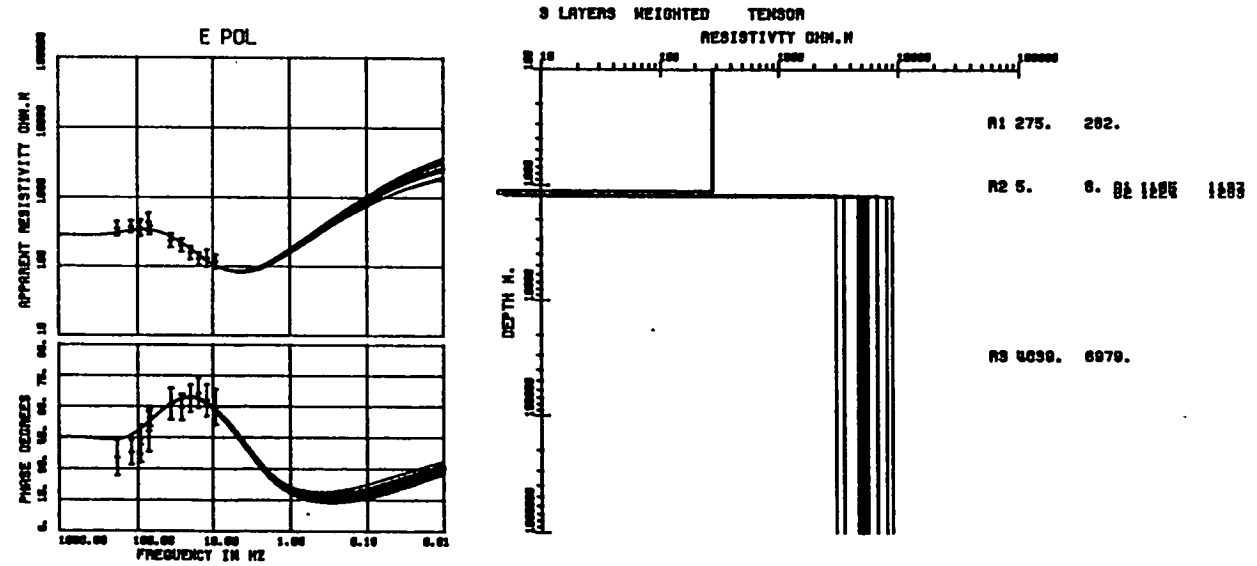

1D MODELS SITE OBSERVATORIO 451A

(a)

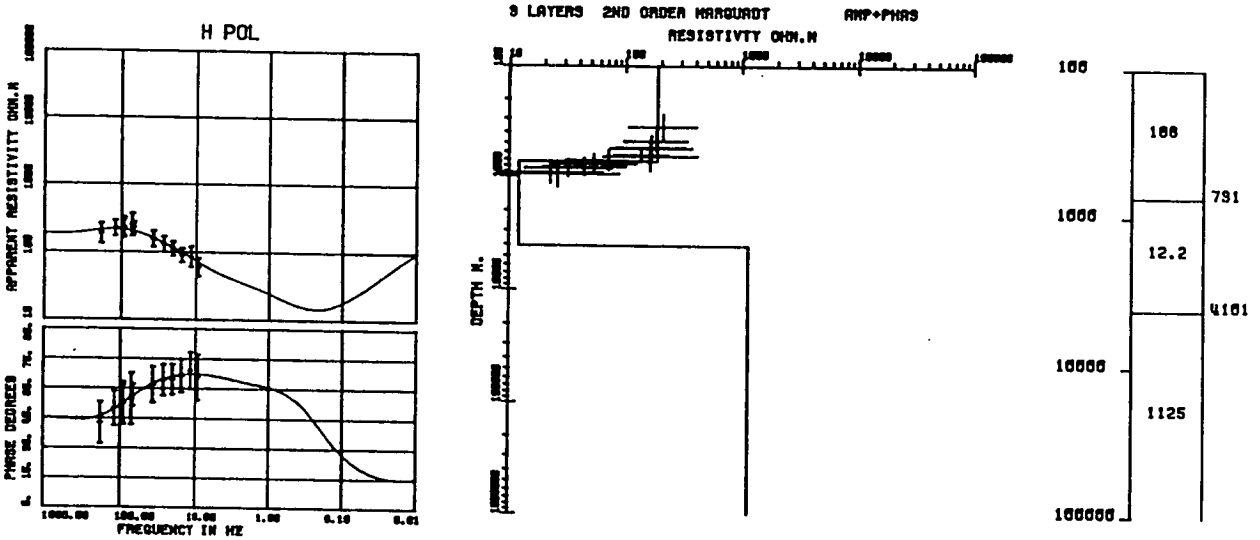

(b)

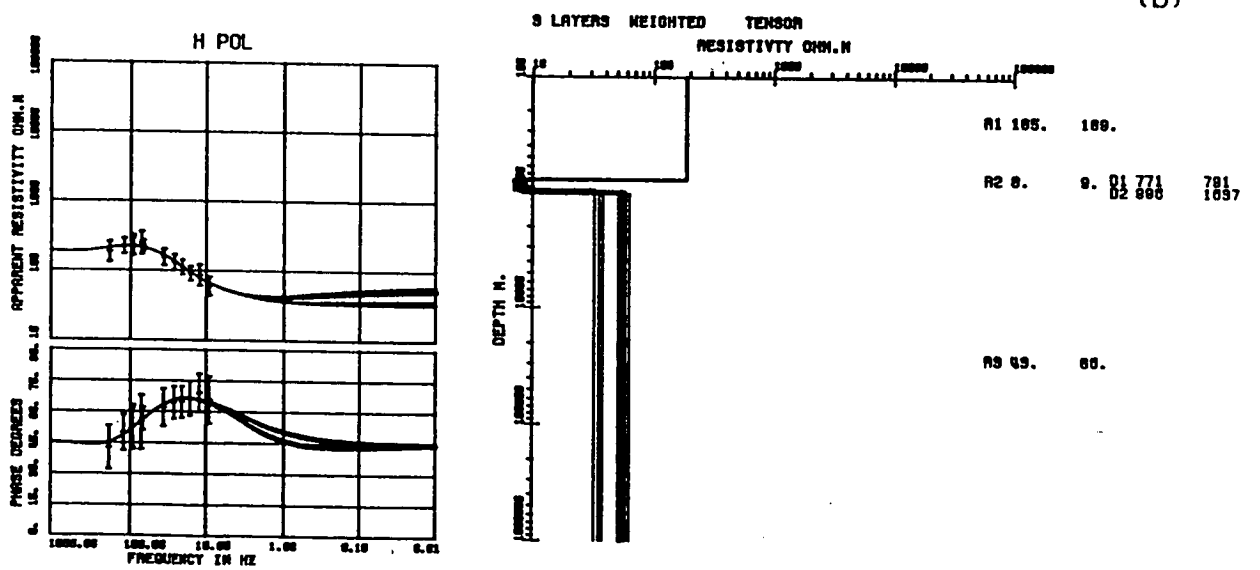

1D MODELS SITE AVE 453A

(a)

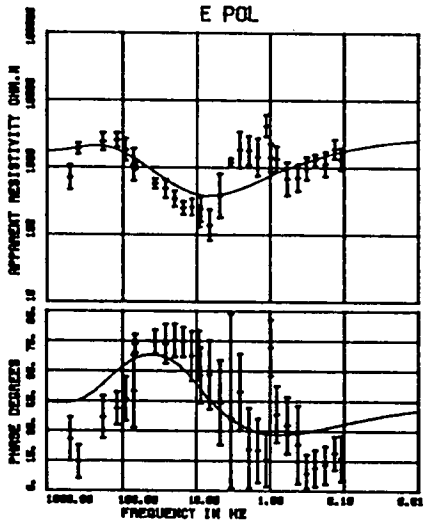

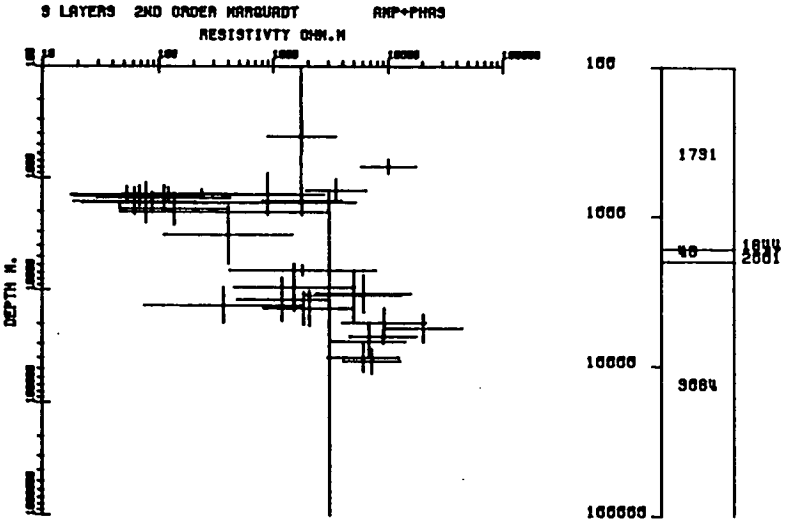

(b)

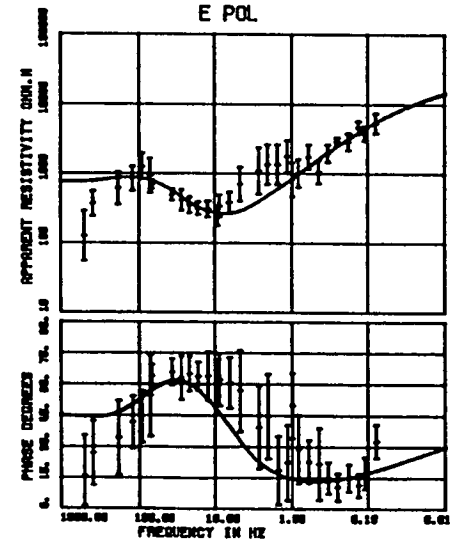

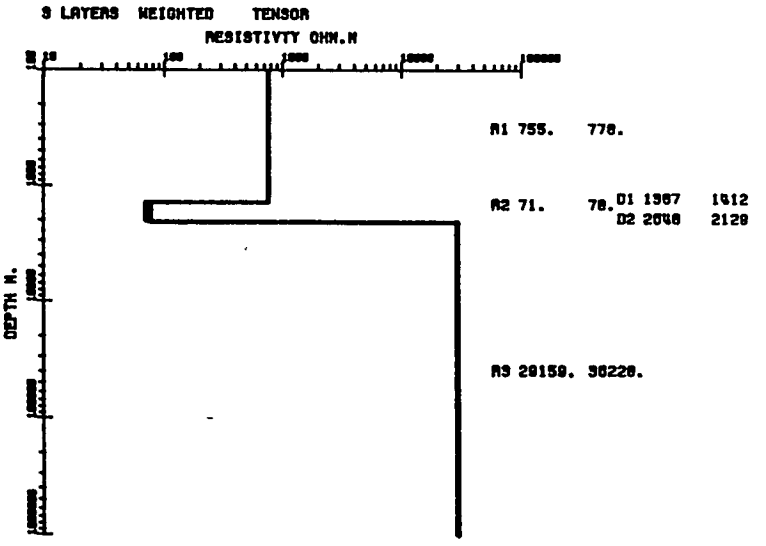

1D MODELS SITE GRANEZZA 452A

(a)

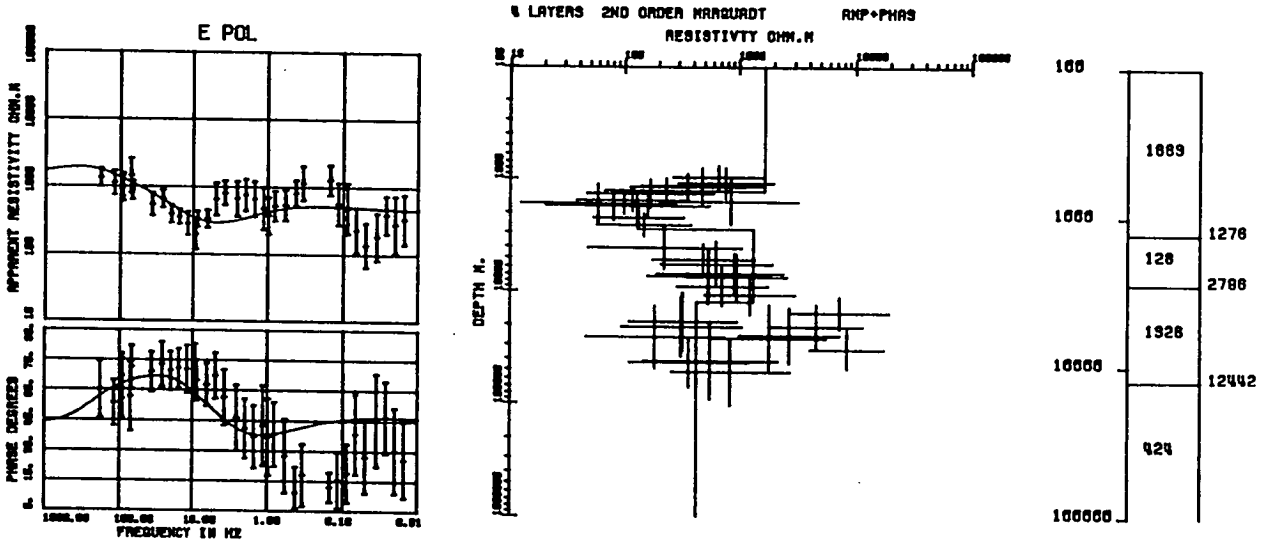

(b)

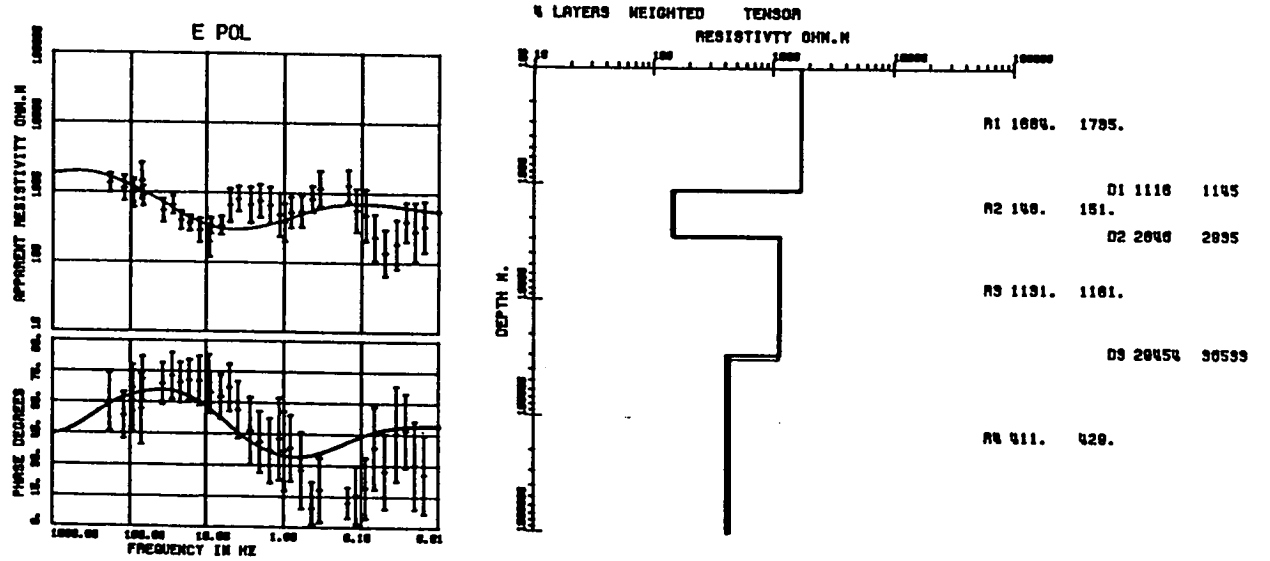

1D MODELS SITE GRANEZZA 452A

(a)

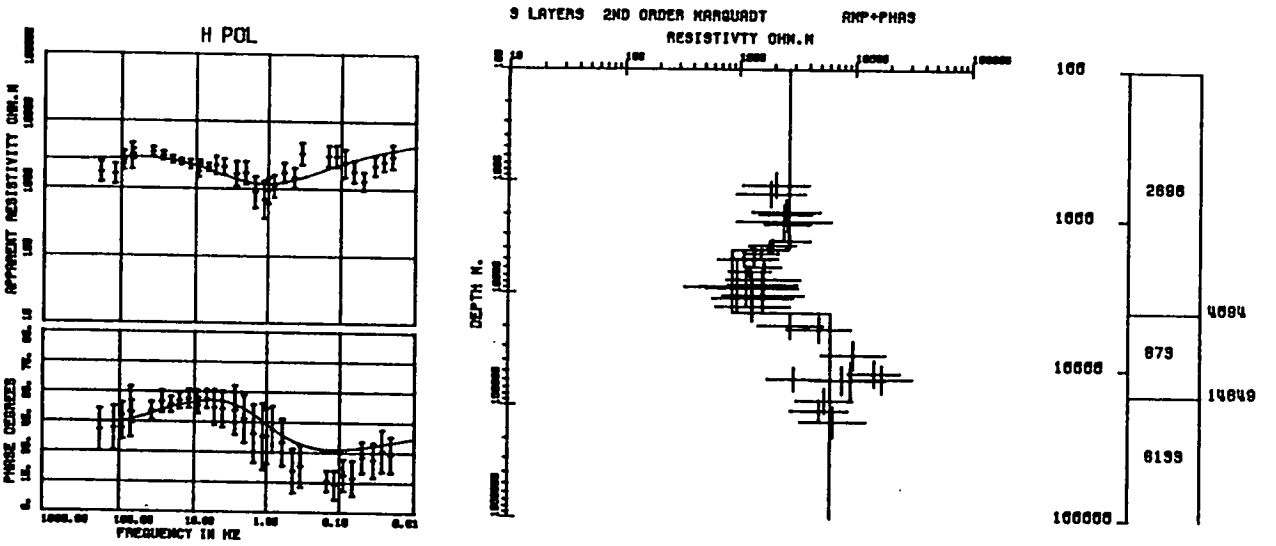

(b)

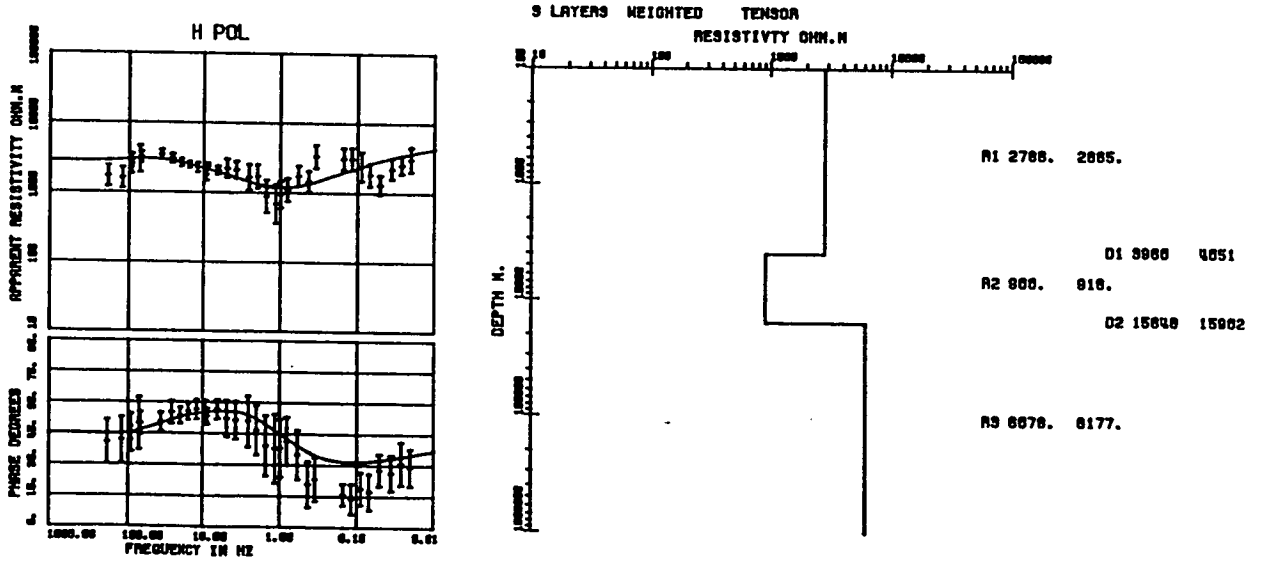

Appendix C– Occam models (rotationally invariant, E pol and H pol curves) for all the sites in the Asiago area.

OCCAM MODEL SITE MANDRIELLE 456A

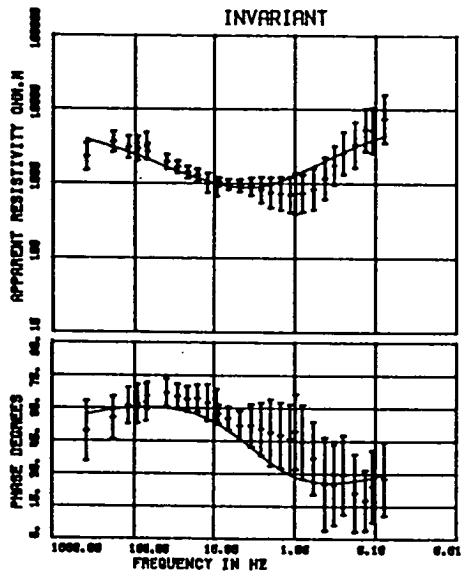

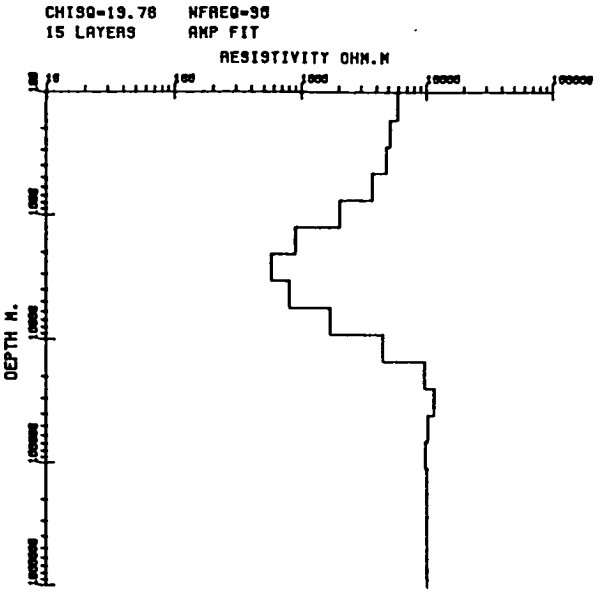

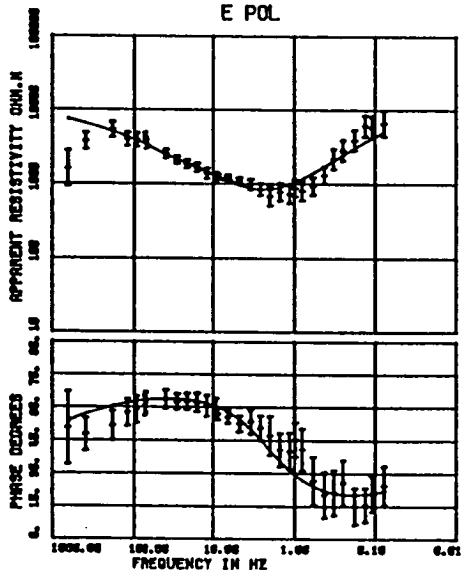

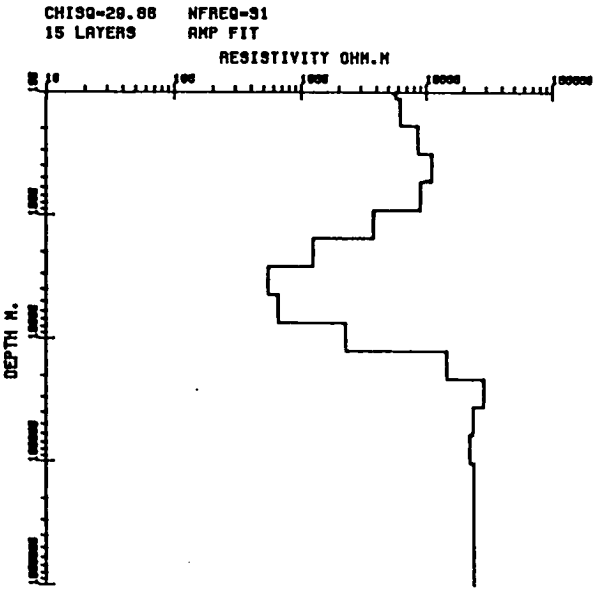

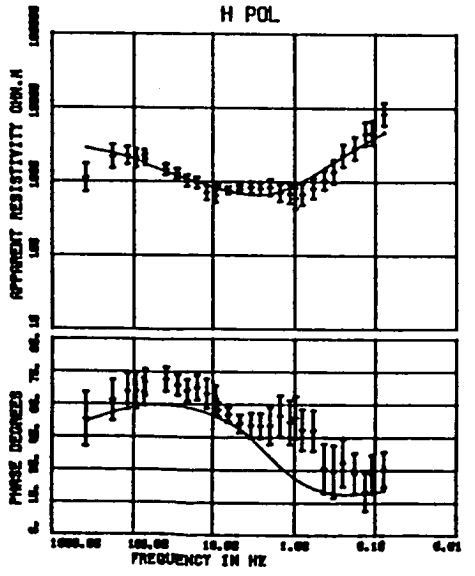

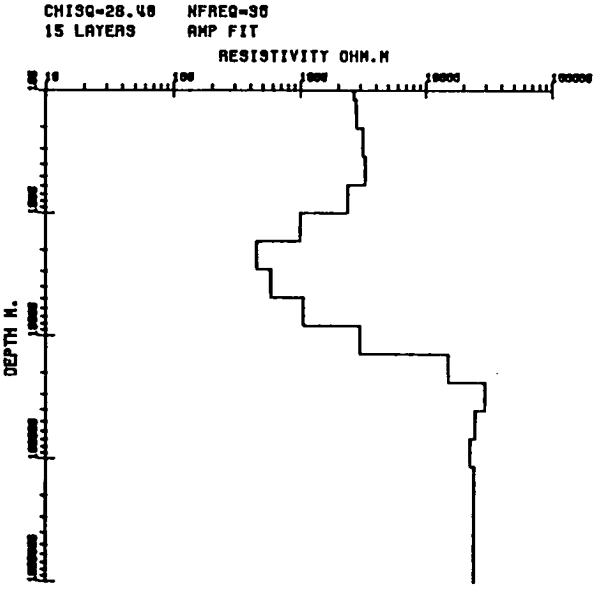

OCCAM MODEL SITE C. MULO 454A

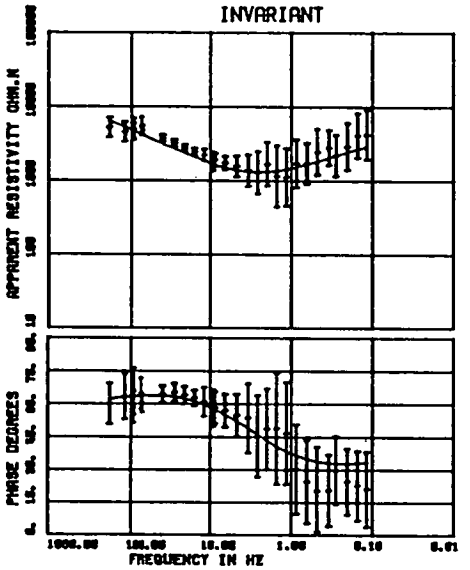

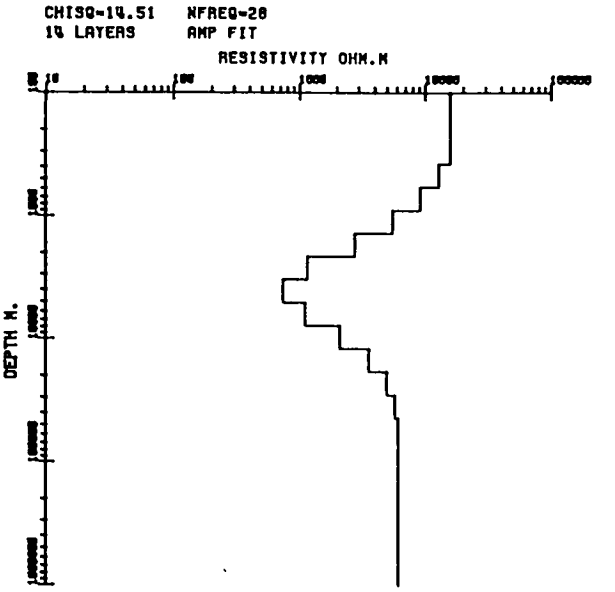

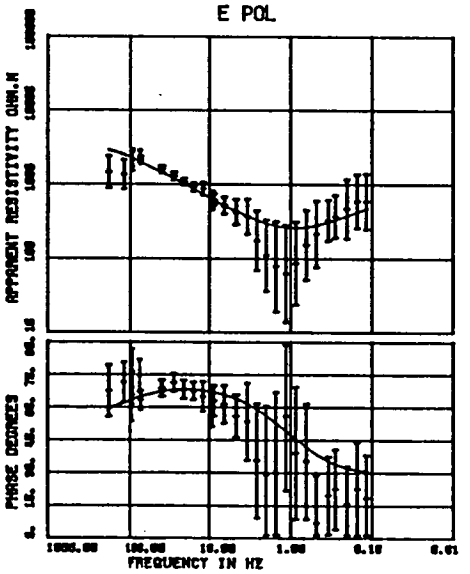

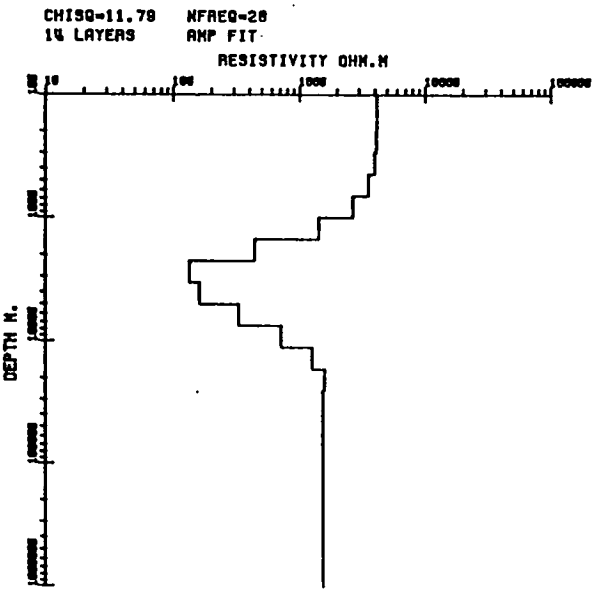

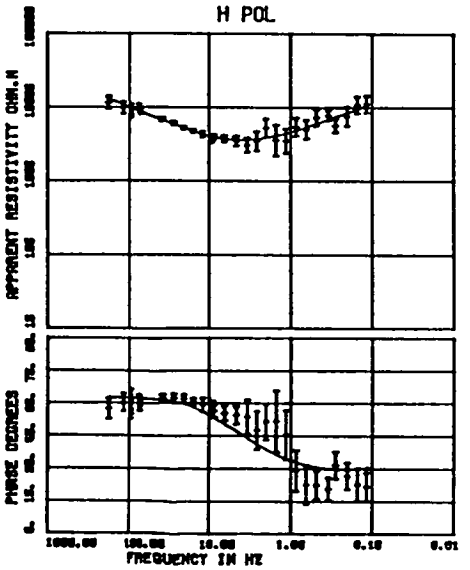

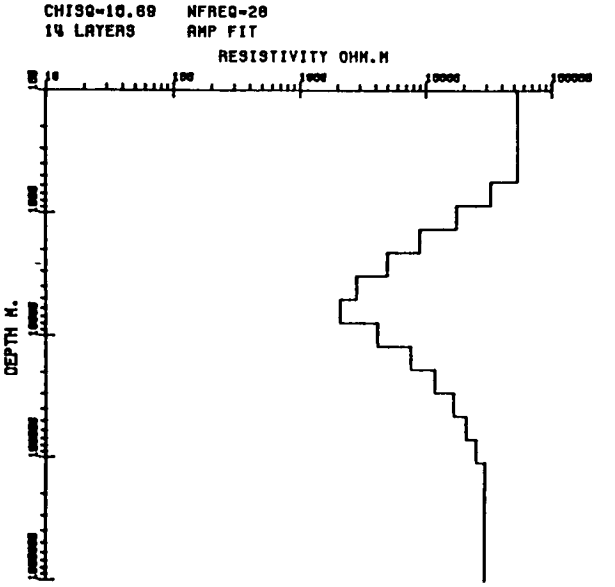

OCCAM MODEL SITE LONGARA 455A

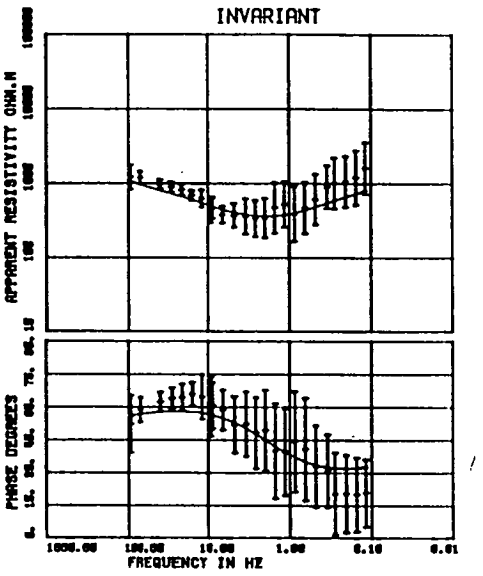

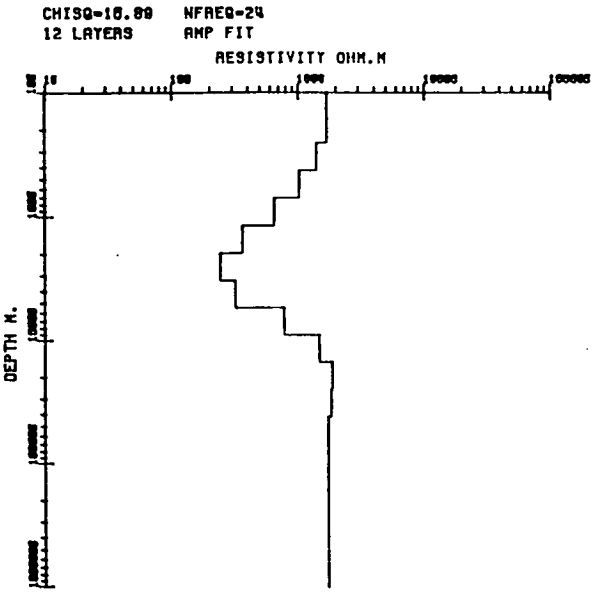

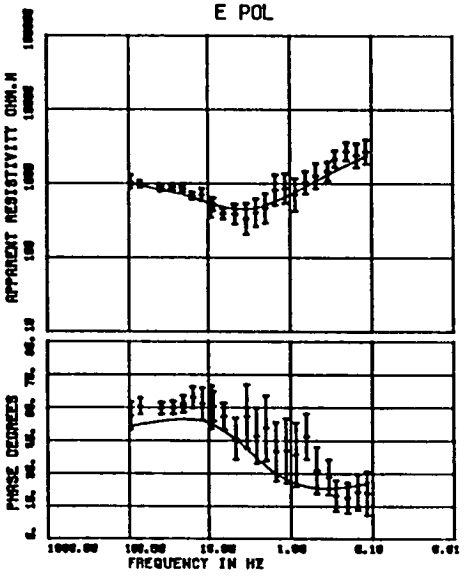

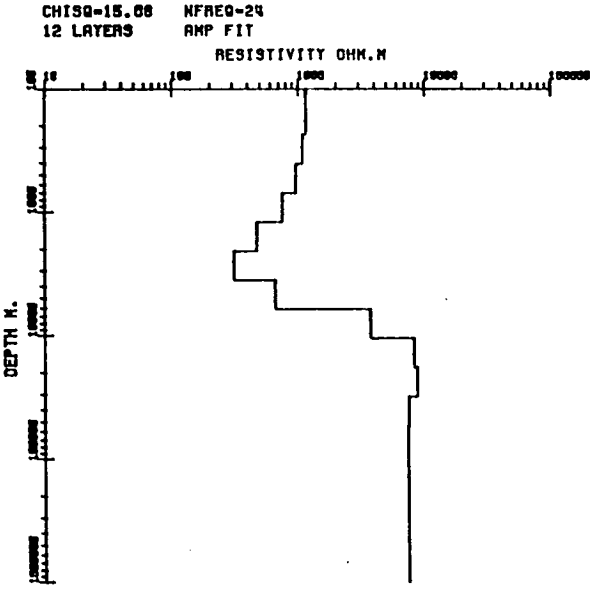

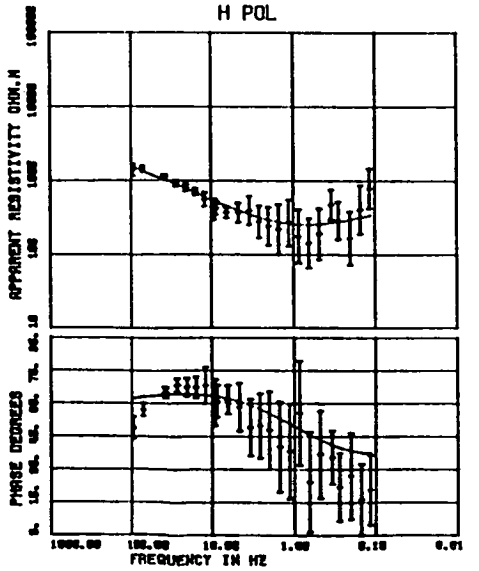

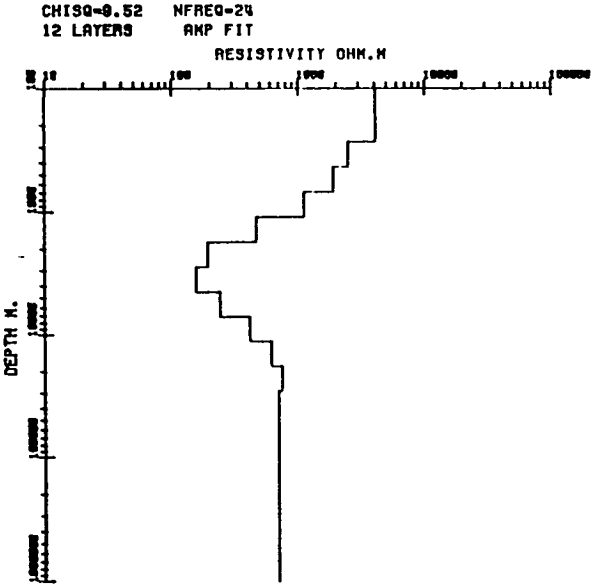

OCCAM MODEL SITE V. DI NOS 690A

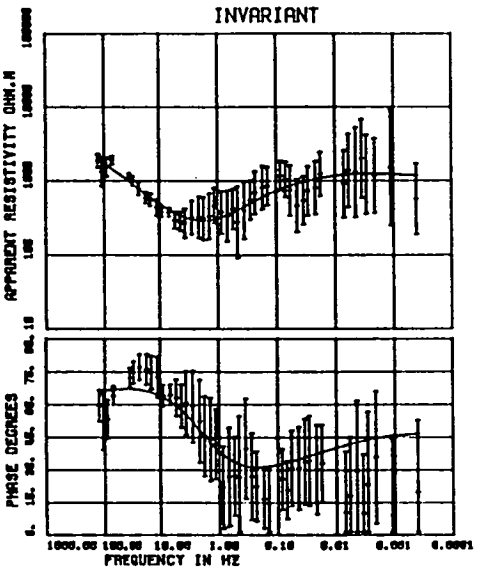

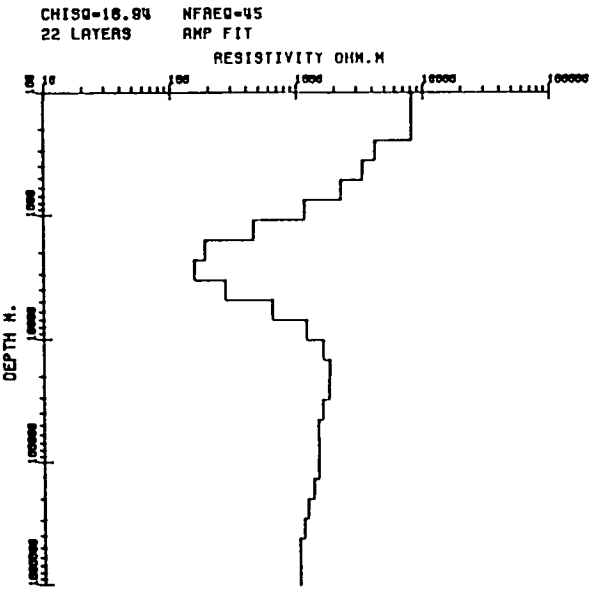

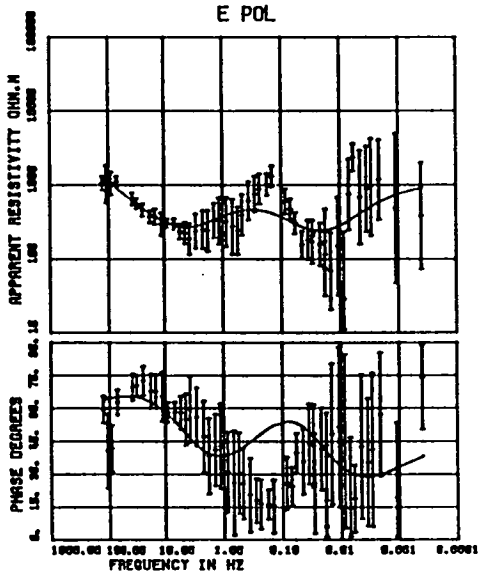

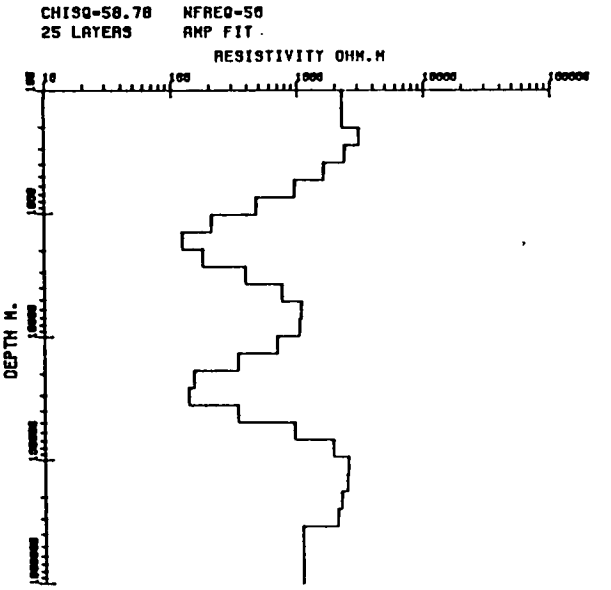

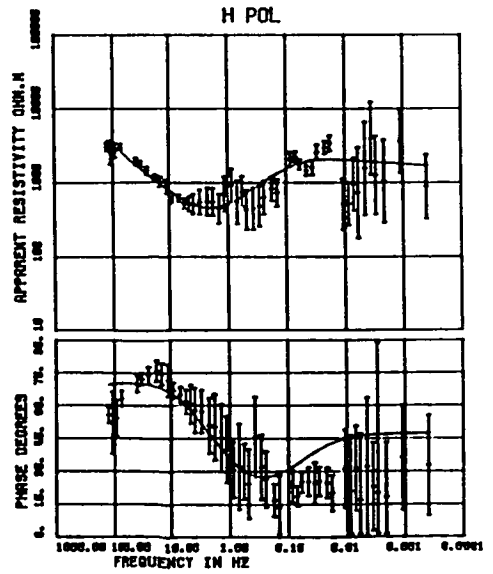

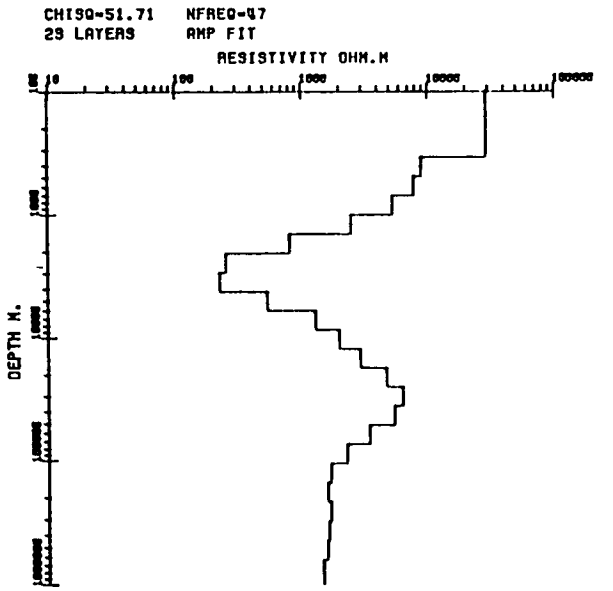

OCCAM MODEL SITE C.S. ANTONIO 450A

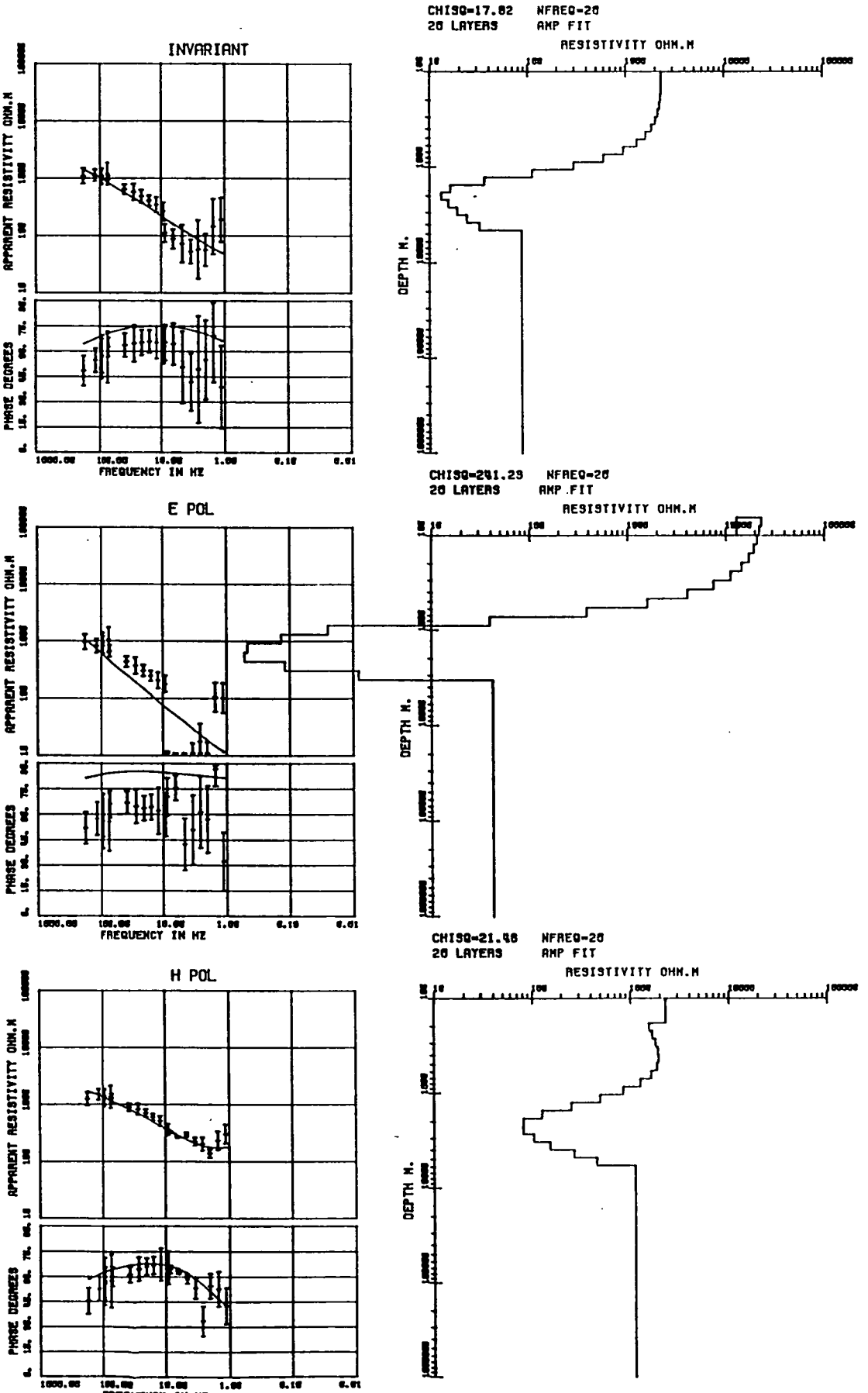

OCCAM MODEL SITE OBSERVATORIO 451A

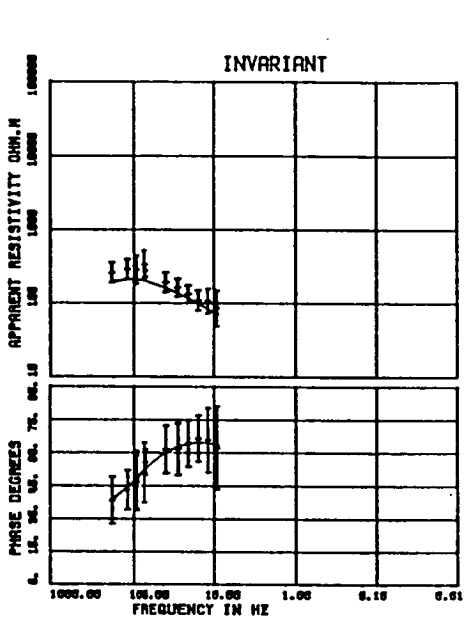

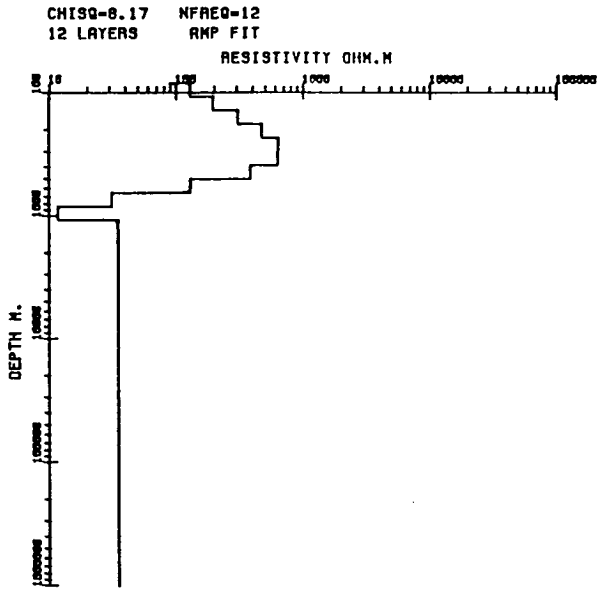

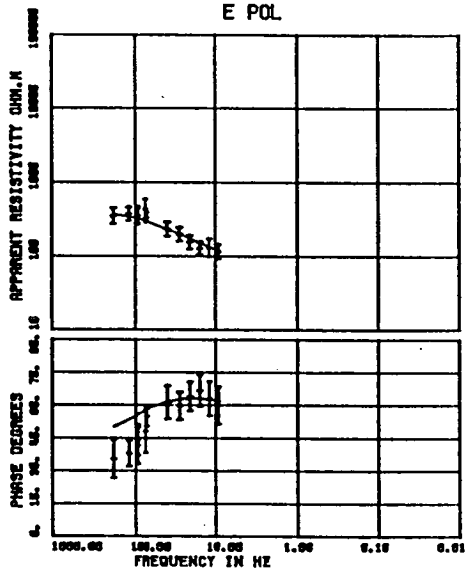

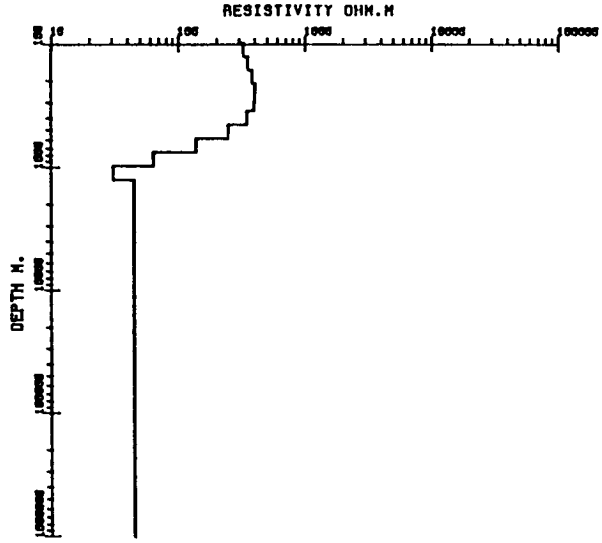

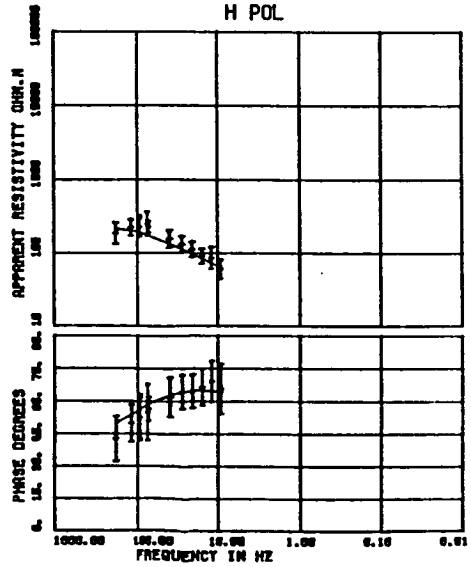

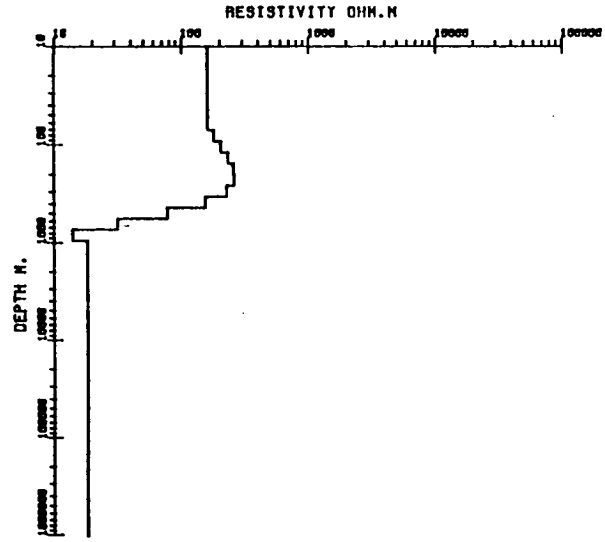

OCCAM MODEL SITE AVE 453A

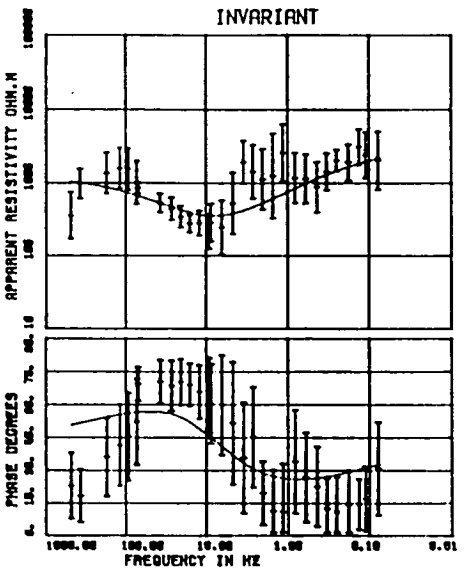

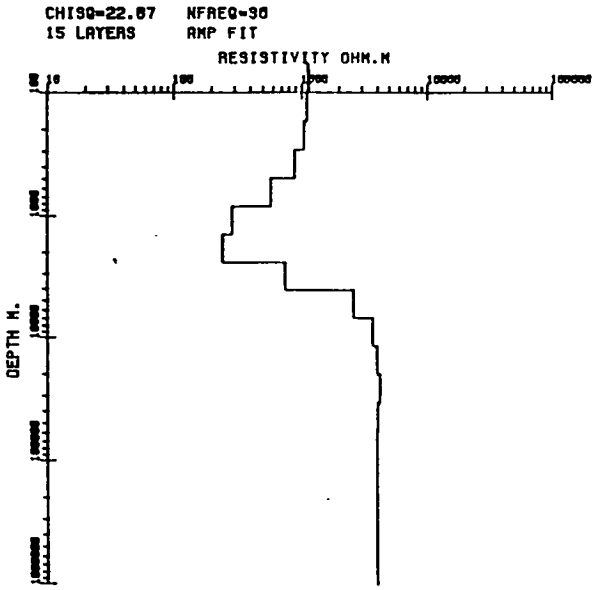

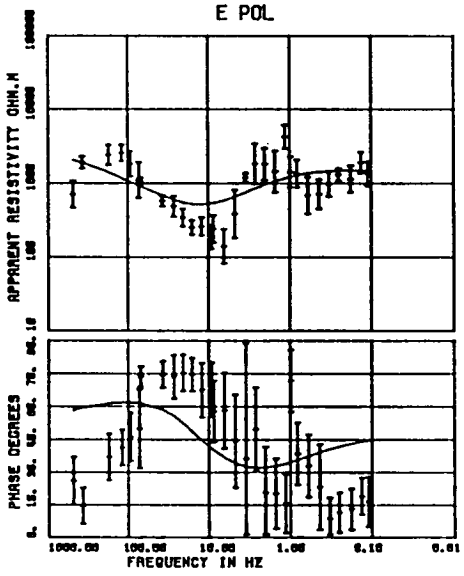

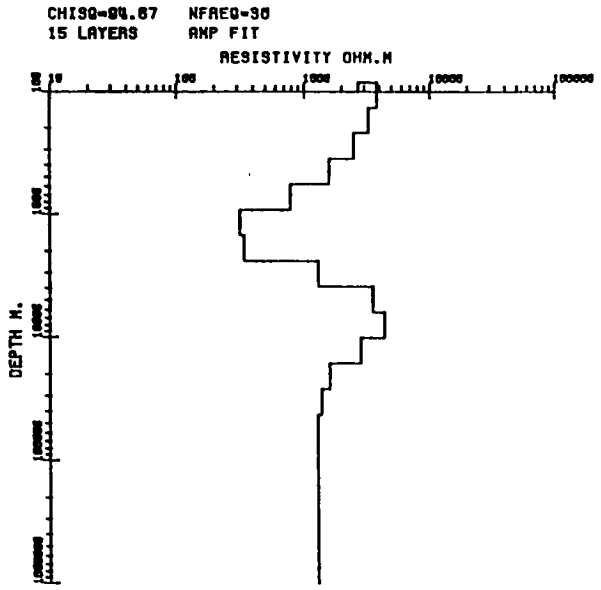

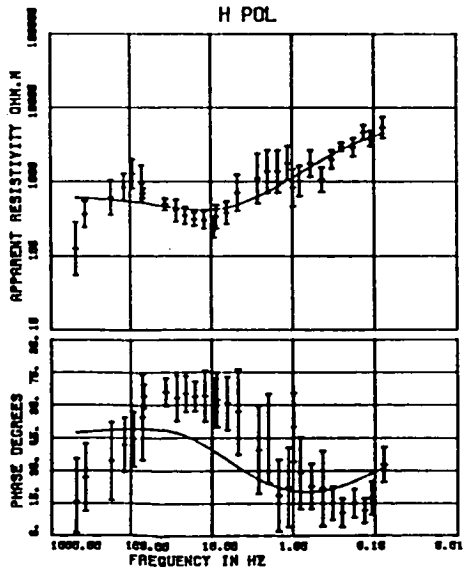

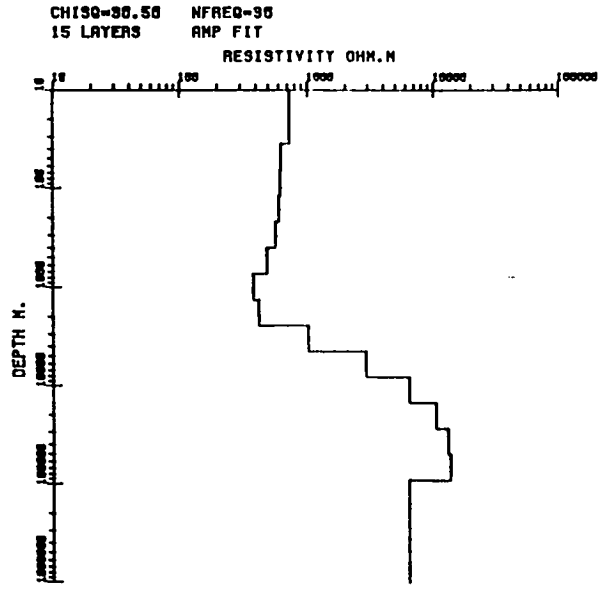

OCCAM MODEL SITE GRANEZZA 452A